BENZOTHIADIAZOLE-BASED ORGANIC MATERIALS FOR ELECTRONIC APPLICATIONS

Ph.D. THESIS

by

AMBIKA PATHAK

DEPARTMENT OF CHEMISTRY
INDIAN INSTITUTE OF TECHNOLOGY ROORKEE
ROORKEE-247667 (INDIA)
MAY, 2019

BENZOTHIADIAZOLE-BASED ORGANIC MATERIALS FOR ELECTRONIC APPLICATIONS

A THESIS

*Submitted in partial fulfilment of the
requirements for the award of the degree*

of

DOCTOR OF PHILOSOPHY

in

CHEMISTRY

by

AMBIKA PATHAK

**DEPARTMENT OF CHEMISTRY
INDIAN INSTITUTE OF TECHNOLOGY ROORKEE
ROORKEE–247667 (INDIA)
MAY, 2019**

INDIAN INSTITUTE OF TECHNOLOGY ROORKEE
ROORKEE

CANDIDATE'S DECLARATION

I hereby certify that the work which is being presented in the thesis entitled "**BENZOTHIADIAZOLE BASED ORGANIC MATERIALS FOR ELECTRONIC APPLICATIONS**" in partial fulfilment of the requirement for the award of the Degree of Doctor of Philosophy and submitted in the Department of Chemistry of the Indian Institute of Technology Roorkee, Roorkee is an authentic record of my own work carried out during a period from July, 2014 to May, 2019 under the supervision of Dr. K. R. Justin Thomas, Professor, Department of Chemistry, Indian Institute of Technology Roorkee, Roorkee.

The matter presented in this report has not been submitted by me for the award of any other of this or any other institution.

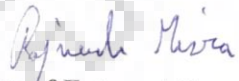Dated   (AMBIKA PATHAK)

This is to certify that the above statement made by the candidate is correct to the best of my knowledge.

(K. R. JUSTIN THOMAS)
Supervisor

The Ph. D. Viva-Voce Examination of Ms AMBIKA PATHAK Research Scholar, has been held on 8 August 2019.

Chairperson, SRC   Signature of External Examiner

This is to certify that the student has made all the corrections in the thesis

(K. R. JUSTIN THOMAS)
Supervisor   Head of the Department

Dated:

i

ACKNOWLEDGEMENTS

Ambika Pathak

Abstract

Among the molecular building blocks used in the organic electronic materials, benzothiadiazole is found to be efficient moiety. Benzothiadiazole showed strong electron withdrawing capability due to existence of two imine groups. This property improves the distribution of donor electrons and broadens the absorption spectra into the NIR region. It also acts as low band chromophore and narrows the band gap of the molecule. This ensures the efficient light-harvesting ability and facile charge transport in device. In this thesis, we extensively investigated the design, synthesis and optoelectronic applications of benzothiadiazole-based functional materials. The thesis contains seven chapters. The first chapter presents the aim and scope for the work on benzothiadiazole derivatives and its scope for utility in optoelectronic applications such as organic light emitting diodes (OLEDs) and dye sensitized solar cell (DSSCs). The second chapter describes the literature background related to synthesis, physicochemical, thermal, electrochemical characterization and electronic applications of benzothiadiazole-based compounds used as sensitizer in DSSCs and as luminescent materials in OLEDs.
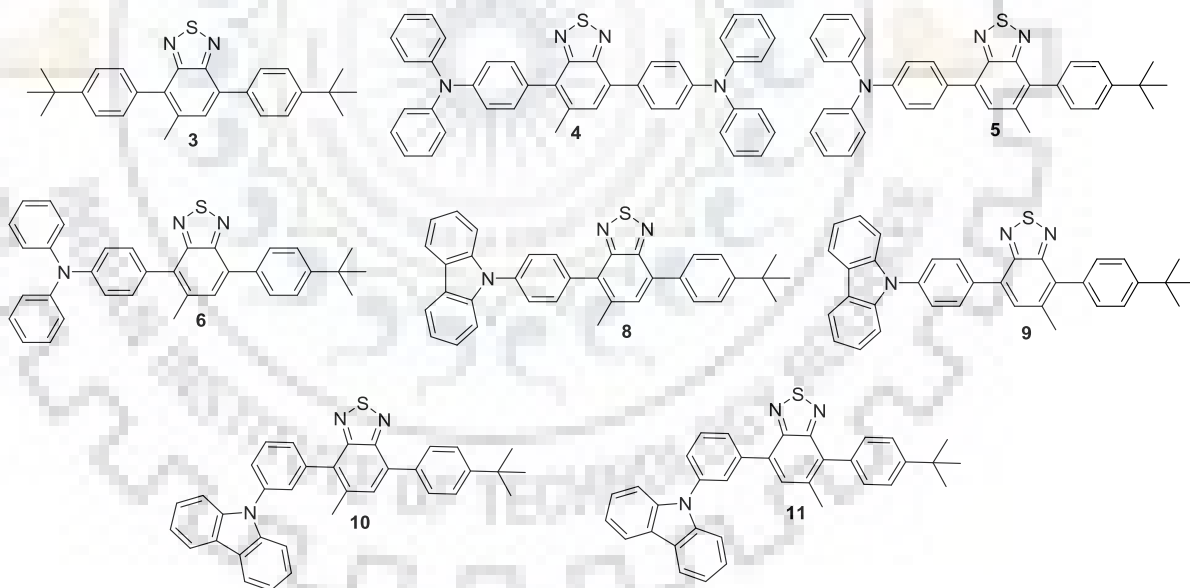
In chapter 3, a series of 5-methylbenzo[d][1,2,3]thiadiazole (MBTD)-based derivatives have been synthesized using palladium catalyzed Suzuki-Miyaura coupling reaction in moderate to good yields. The selective Suzuki coupling reactions resulted in eight regioisomers. The effect of methyl substitution on electronic absorption, emission, thermal, electrochemical and electroluminescent characteristics was studied in detail and compared with non-methylated benzothiadiazole derivatives. The dyes (**5** and **9**) containing methyl unit near *tert*-butylpheny

showed red-shifted absorption when compared to its analogous regioisomer(**6** and **8**) due to interrupted π-conjugation between donor and benzothiadiazole in later. The geometrical changes in the ground (non-planar) and excited (more planar) states manifested in the absorption and emission properties. All the dyes displayed positive solvatochromism in the emission spectra, whereas their absorption profiles are not affected with increase of polarity which indicates that dyes are non-polar in ground state. The dyes restrained the formation of molecular aggregates in the solid state. All of the compounds exhibited exceptional thermal stability attributable to the rigid (MBTD) building block. The compound containing disubstituted triphenylamine exhibited high lying HOMO in the series while the LUMO is stabilized in *tert*-butylpheny substituted compound. The electronic structure correlations are supported by density functional calculations. Solution processed multi-layered OLED device were fabricated employing these compounds either as host emitters or dopant emitters in suitable host matrix and exhibited green/yellowish green electroluminescence
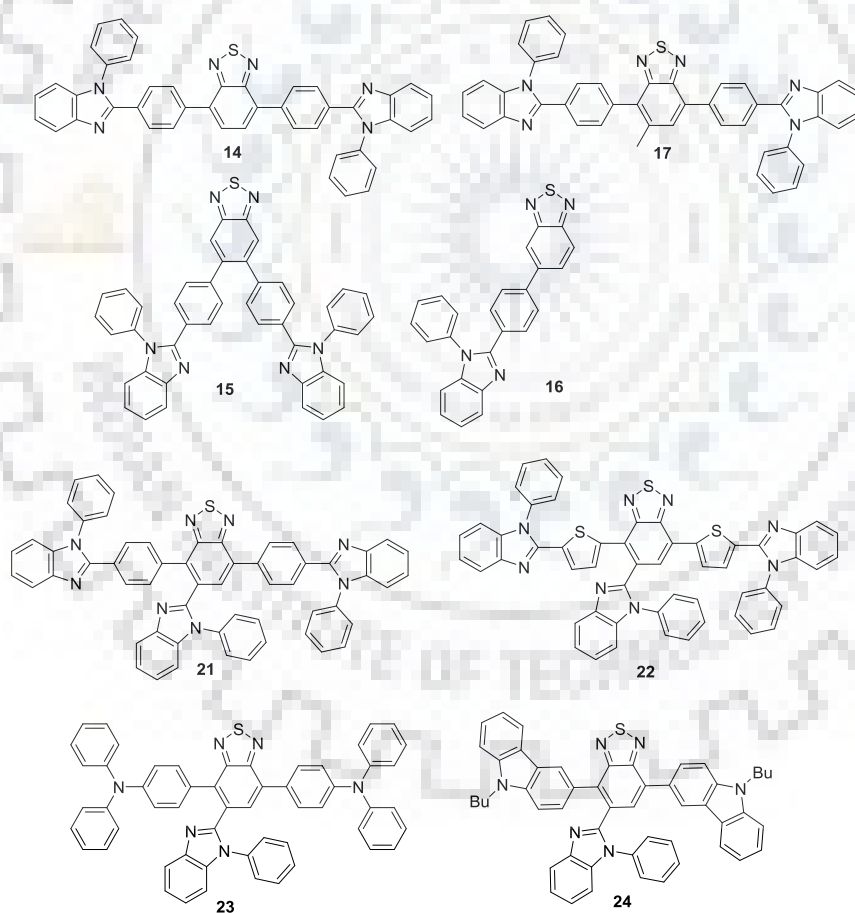
In chapter 4, we demonstrate the tuning of optical, electrochemical and electroluminescent properties in the benzimidazole-benzothiadiazole conjugates. Effect for functionalization if the nuclear propertion of benzothiadiazole was studied by synthesized 4,7- disubstituted and 5,6 substituted derivatives. The former has linear conjugation while the later offers "V" shaped

molecular structures. Additionally the effect of donor in the conjugation was also investigated. The introduction of *N*-phenylbenzimidazole unit is believed to impart rigidity to molecule and generate anti-aggregation property. Also it may have additional effects on the electron affinity and transporting properties. The effect of different substitution pattern on electronic absorption, emission, thermal, electrochemical and electroluminescent characteristics was studied in detail and compared with benzothiadiazole derivatives which lacks lateral substitution. Interestingly, the linear benzimidazole derivatives substituted at C4 and C7 of benzothiadiazole showed bathochromic shift when compared to its lateral substituted regioisomer with substitution at C5 and C6 position. Moreover the tri- benzimidazole substituted chromophore showed red shift when compared to substituted at C4 and C7. This suggests the lateral substituents may be participating in the conjugation. The dye containing lateral benzimidazole exhibits distinct HLCT nature with moderate quantum yield of 25-75%. The device with 5% dopant concentration exhibited satisfactory performance with violet, green, yellow and orange-red emission. The thiophene based compound (**22**) as orange-red emitter exhibited excellent performance in the series which is attributed to the utilization of both energies of LE and CT excitons (i.e., hybridized local and charge transfer (HLCT))
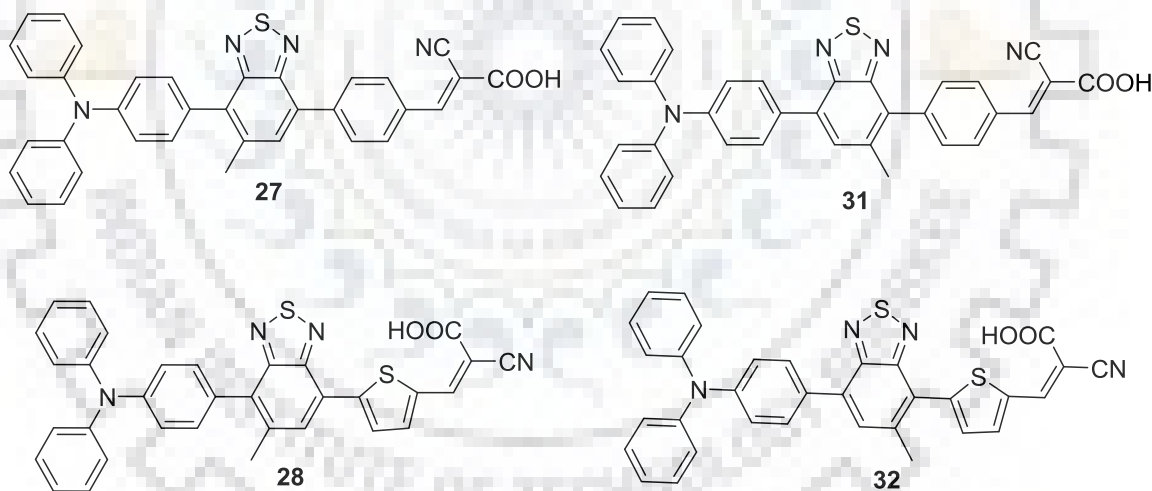
In chapter 5, we have designed and synthesized a series of compounds based on 5-methyl benzothiadiazole to demonstrate the variation of properties by changing the position of methyl group with respect to spacer for dye sensitized solar cell applications. The substitution of methyl group at C5 or C6 position leads to synthesis of two types of isomeric dyes. The compound containing methyl unit substituted near donor exhibited high molar extinction coefficient, strong light harvesting ability, and better photovoltaic performances compared to their congeners where methyl unit is positioned near acceptor. The compounds tethered with benzene or thiophene as spacer modulates the electronic communication, influencing light harvesting and in turn efficiency. Consequently, investigation of DSSCs performances under

standard global AM 1.5 solar conditions, the dyes containing methyl unit substituted near donor with thiophene as spacer exhibited two fold increment in power conversion efficiency (PCE) value upto 4.33% when compared to its congener (2.71%).
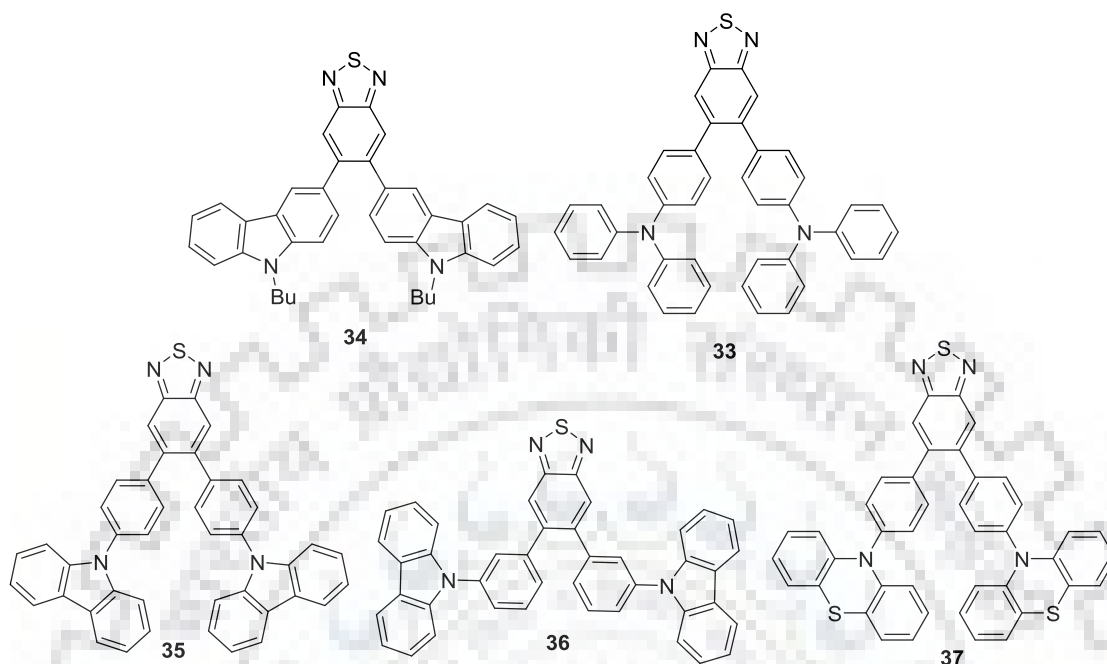
In chapter 6, a series of lateral 5, 6-substituted benzothiadiazole hybrids are presented. The effect of substitution at C5 and C6 position of benzothiadiazole nucleus have been analysed by photophysical, electrochemical, thermal and electroluminescence properties. The compound containing triphenylamine substitution (**33**) exhibited bathochromic shift in absorption spectra when compared to other derivatives. Among the carbazole containing dyes, simple modification of attachment with phenyl spacer (*para* and *meta*) *para* linked *N*-phenyl carbazole compound exhibited red shift in absorption and emission spectra due to extended π-conjugation. This work provides the photophysical, electrochemical insight into lateral functionalization with classical donor-acceptor energy pair in comparison with linear isomers.

In chapter 7, a summary of the work is presented critical analyses and established structure property correlation for new materials. Moreover, by considering recent developments, the scope for development of benzothiadiazole-based covalent organic framework (COF) materials is presented for optoelectronic applications.

Table of Contents

List of Figures

xx

List of Tables

xxii

List of Schemes

List of Abbreviations

OLED	Organic Light Emitting Diodes
OPV	Organic Photovoltaics
OFET	Organic Filed Effect Transistors
NLO	Non-Linear Optics
EL	Electroluminescence
$J_{SC}.[$	Short circuit current
V_{OC}	Open Circuit Voltage
HOMO	Highest Occupied Molecular Orbital
LUMO	Lowest Unoccupied Molecular Orbital
TEA	Triethylamine
HLCT	Hybridized Local And Charge Transfer
TOL	Toluene
THF	Tetrahydrofuran
DCM	Dichloromethane
DMF	Dimethylformamide
ACN	Acetonitrile
EtOAc	Ethylacetate
TCE	Trichloroethane
BuEt	Butylether
DCB	*m*-Diclorobenzene
TEA	Triethylamine
DEE	Diethyl ether
BTD	Benzothidiazole
HATCN	1,4,5,8,9,11-hexaazatriphenssylene-hexacarbonitrile
TAPC	1,1-bis[4-[*N, N*-di(ptolyl)amino]phenyl]cyclohexane
TCTA	tris(4-(9Hcarbazol-9-yl)phenyl)amine
B4PyMPM	4,6-bis[3,5-(dipyrid-4-yl)phenyl]-2-methylpyrimidine
$\varPhi_F$	Flourescence Quantum Yield
ICT	Intramolecular Charge Transfer
TGA	Thermogravimetric analysis
CV	Cyclic voltammetry

DPV	Differential pulse voltammetry
HTL	Hole Transport Layer
ETL	Electron Transport Layer
DFT	Density Functional Theory
TDDFT	Time-dependent density functional theory
AIE	Aggregation Induced Emission

List of Publications

[1] **Ambika Pathak**, K. R. Justin Thomas, Meenu Singh and Jwo-Huei Jou, Fine-Tuning of Photophysical and Electroluminescence Properties of Benzothiadiazole-Based Emitters by Methyl Substitution, *J. Org. Chem.* **2017**, *82*, 11512

[2] **Ambika Pathak**, Tina Tomer, K.R. Justin Thomas, Miao- Syuan Fan, Kuo-Chuan Ho, Fine tuning the absorption and photovoltaic properties of benzothiadiazole dyes by donor-acceptor interaction alternation via methyl position, *Electrochimica Acta* **2019**, 3*04*, 1-10

[3] Rajendra Kumar Konidena, K. R. Justin Thomas, **Ambika Pathak**, Deepak Kumar Dubey, Snehasis Sahoo, and Jwo-Huei Jou ,Tuning the Photophysical and Electroluminescence Properties in Asymmetrically Tetrasubstituted Bipolar Carbazoles by Functional Group Disposition, *ACS Appl. Mater. Interfaces* **2018**, *10*, 24013.
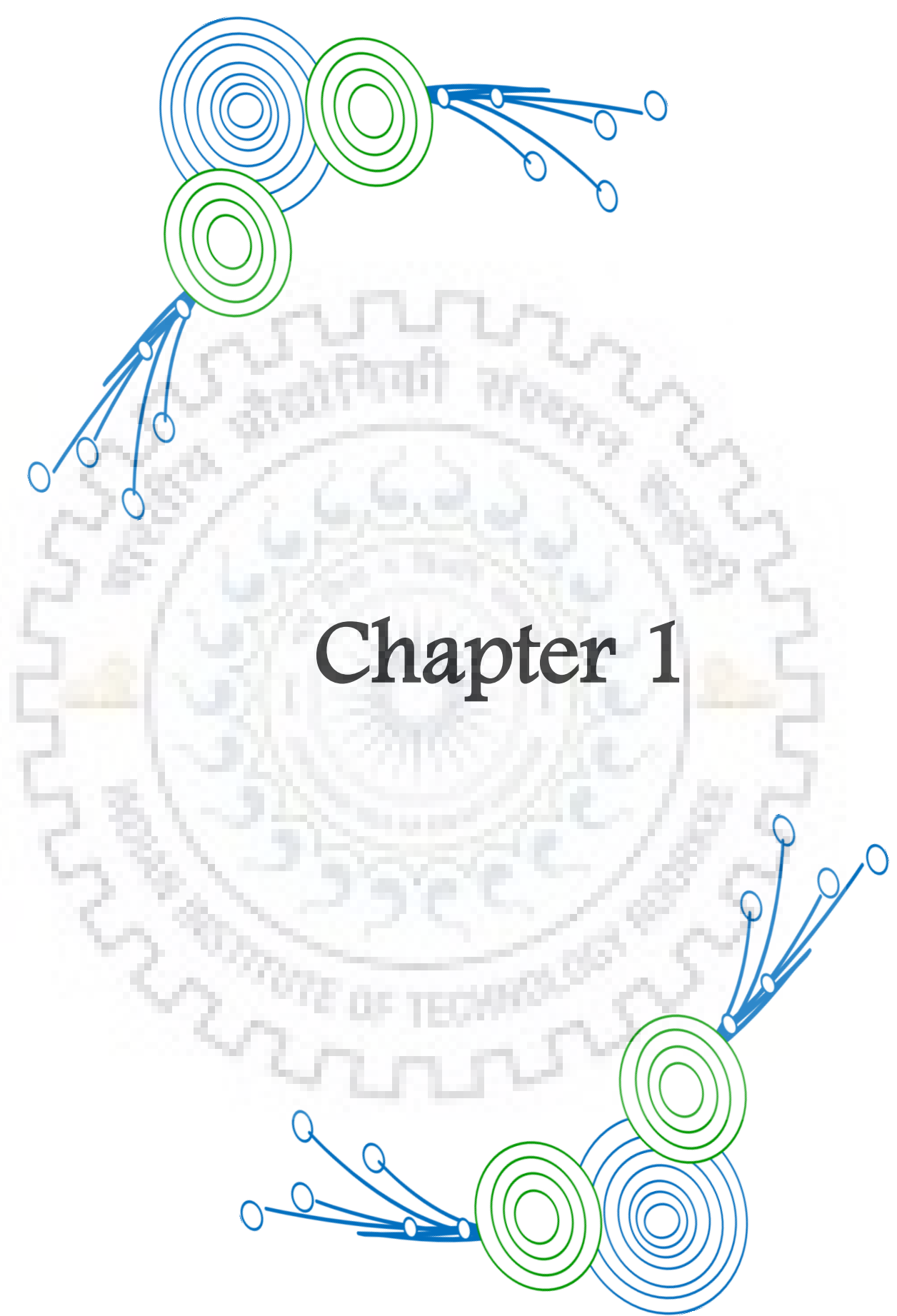
Chapter 1

Chapter 1

Benzothiadiazole-based organic materials for electronic applications: Aim and Scope

The small organic π-conjugates are attractive for application in various optoelectronic devices. [1] They offer fine pathways for chemical modification and functional alteration by employing simple structural changes. The field of organic optoelectronics have significantly developed which includes OLEDs, [2, 3] OPVs, [4] OFETs, [5] NLOs [6] and in molecular sensors.[7] Several strategies have been adopted to engineer the molecular framework which are necessary to boost the performance of these devices. In this thesis, we have discussed the molecular engineering of the dyes suitable for DSSCs and OLEDs. The structural modulation to donor, acceptor interaction by altering the conjugation in D-π-A framework allows to increase the molar extinction.[8] This presumably improves the solar light coverage of organic sensitizer and thus perceive broader IPCE spectra for DSSC. The structural modulation also effects the alignment of LUMO and HOMO energy levels which ensures efficient electron injection and dye regeneration. This works together effectively in enhancing the J_{SC}.[9] Similarly, to influence the V_{OC}, bulky units are suggested to be used which would preferably eliminate the π−π stacking interaction of sensitizers on the surface of nano-crystalline TiO_2. [10] Also, lowering the HOMO energy level of the dye is useful for effective dye regeneration and increases V_{OC} by reducing the charge recombination between the oxidized sensitizer and conduction band. [11]

Similarly OLED have drawn attention because of their application in high-resolution, full-color displays, backlights, and white lighting.[12] To further improve the device performances several strategies can be used including structural engineering. As for efficient OLED, the materials should facilitate (a) high internal quantum efficiency (b) low operating voltage (c) high light out-coupling efficiency. [13] The challenges are to optimize the organic material to be used as emissive layer in order to enhance the exciton utilization which eventually increases the efficiency. Thus it's required to choose the conformation which significantly drives the material for improved PLQE, thermal and morphological stability. Likewise, the thermal and morphological stability promotes the heat resistivity and durability to the materials and also gives homogeneous, isotropic for ease processiblity. This characteristic can be attained by substituting chromophores which may induce the twisting of structure. [14] Similarly, the introduction of bulky groups in non-linear fashion may also forbid the π-π

stacking which will supress the non-radiative decay. Moreover, the carrier injection efficiency can be improved by tuning HOMO-LUMO energy levels which is supported by introducing hole or electron affinity groups. [15]

Generally, the core structure of the materials influences the fundamental properties such as physiochemical, thermal and charge transport characteristics which eventually determines the performance of the device. In addition, the appended unit/peripheral chromophores helps to fine tune the functional properties further. Among the utilized heteroaromatic hydrocarbons, benzothiadiazole has been utilized as auxiliary acceptor in the structure employed in optoelectronic devices. [16] The molecule exhibits low band gap and enhance the light absorption and improves the light harvesting. It also provides rigid molecular structure, high electron affinity, good electron transporting ability. Eventually, these properties have elevated BTD unit to be applied as luminescent material in FOLED and sensitizer in the DSSCs. The chemical modification can be reformed by functionalization at 4 and 7 positions. [17] Recently, few materials based on the 4, 5 and 7 functionalization are reported which suggests different topological linking will be interesting and provides beneficial pathway to improve the fundamental properties of the materials to be used for electroluminescent and photovoltaic applications. [18, 19]

So here, in this thesis with the impact of above discussion we have chosen benzothiadiazole nuclei to explore its different functionalization, which has showed promising structure-property relationship in materials suitable for OLED and DSSC devices. The main theme of the work is conjugation inhibition by structural alteration to effect favourable functional tuning. Two general strategies were employed to restrict the emission in blue region, firstly the lateral functionalization at benzothiadiazole. This helps to retard the conjugation either by imposing nonplanarity or due to poor overlap of orbitals. Secondly, functionalization at C5 position of benzothiadiazole where, simple methyl substitution at C5 position was found to modulate the conjugation across the C4-C7 axis by steric twisting. Alternatively introduction of chromophores at C5 & C6 position led to new series of compound showing different properties from those resulting from C4 & C7 substitution. These set of compounds served as new models to evaluate the electronic conjugation via C5 & C6. Due to poor electronic interaction C5 & C6 substituted compound exhibited significantly blue shifted emission when compared to those of C4 & C7 analogs.

The structural diversity used in the thesis work is illustrated in Figure 1.1. Using the same methodologies but differing the chromophore we have obtained dyes useful for OLED and DSSC applications.
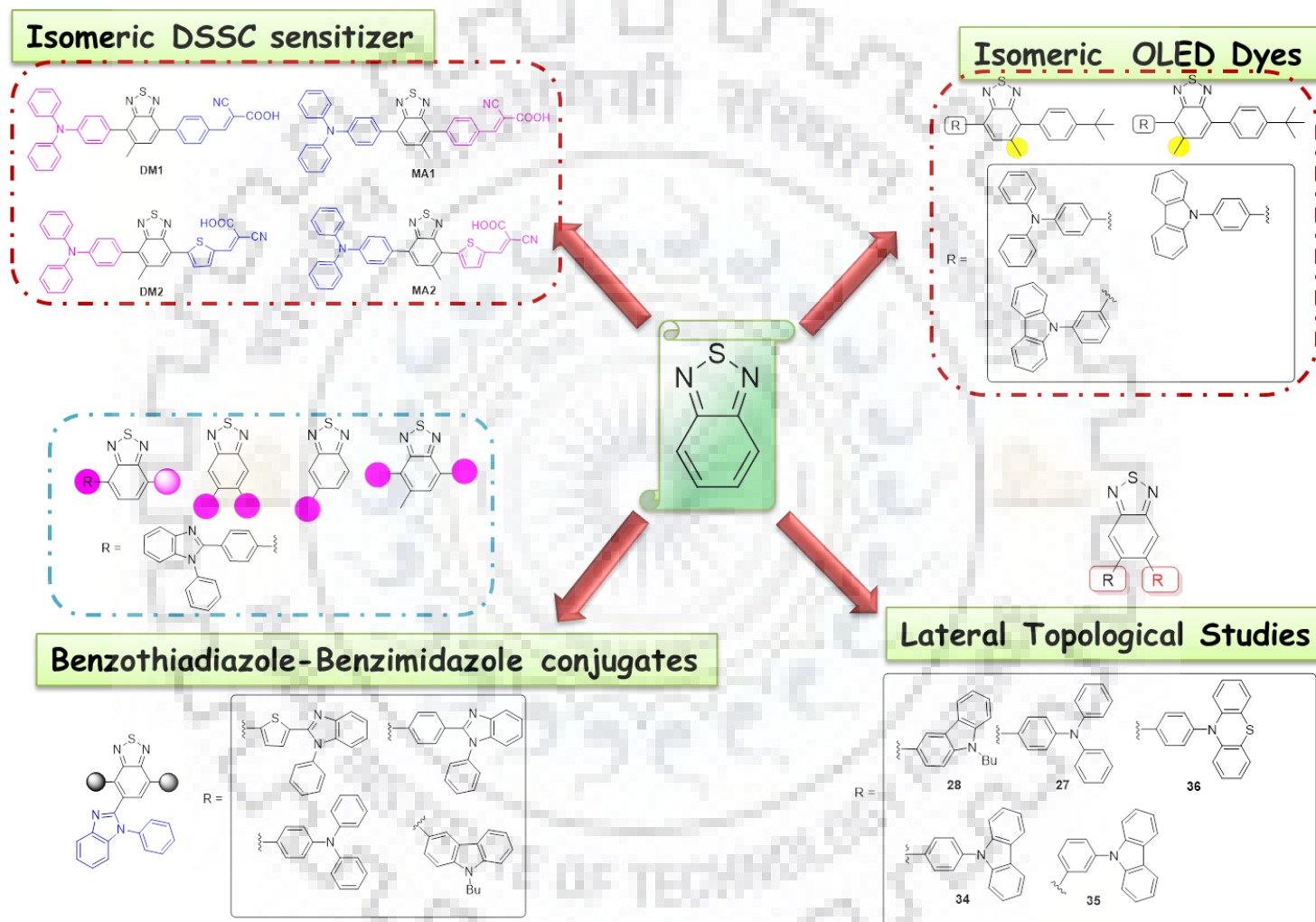
Figure 1.1 The proposed molecular structures at different functionalization of benzothiadiazole
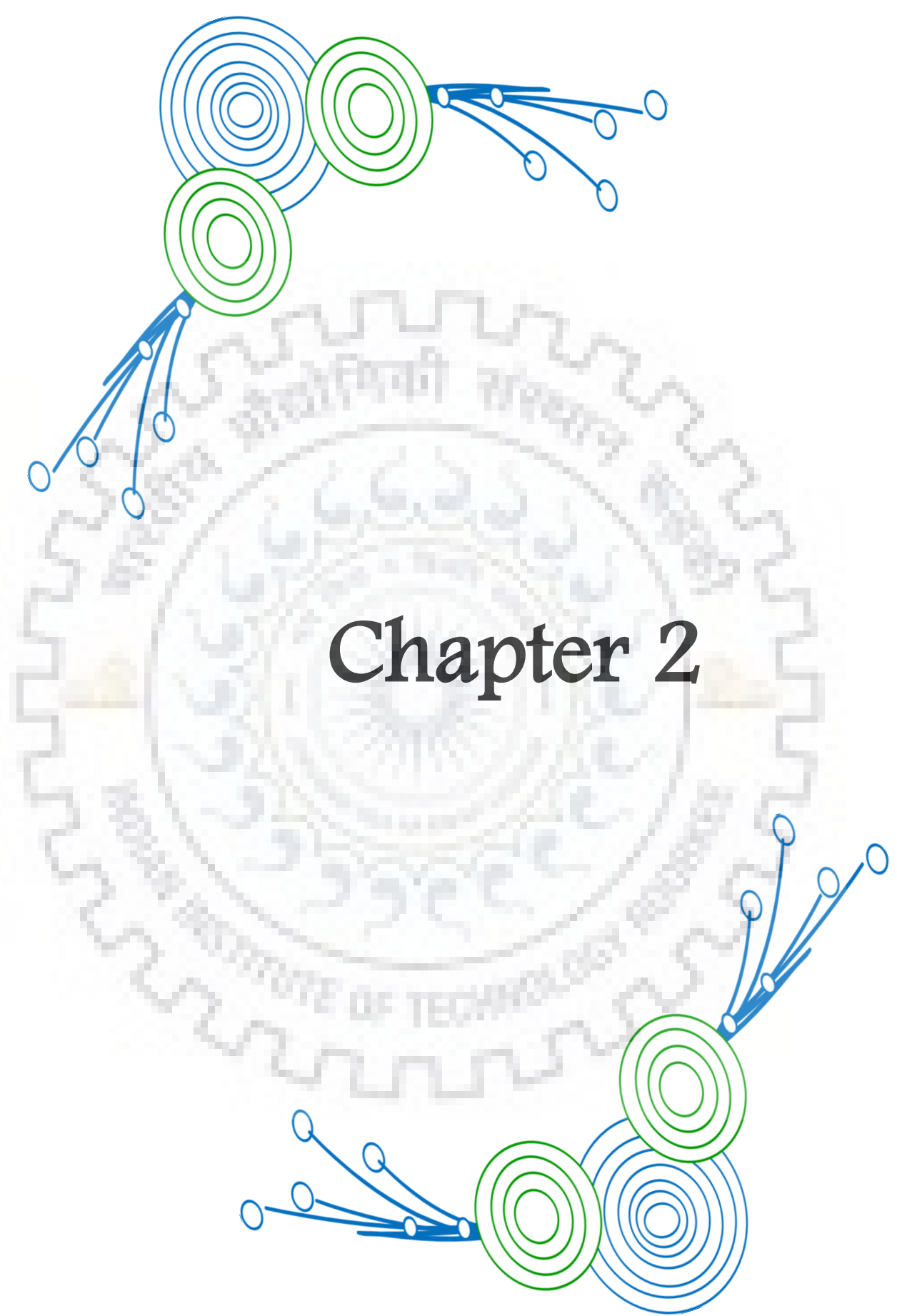
Chapter 2

Chapter 2

A Review: On Benzothiadiazole Derivatives for OLED and DSSC

2.1 Introduction

The π-conjugated framework plays an important role in the functional properties of the organic dyes due to its effective electronic communication across the molecular framework. Moreover, the incorporation of an auxillary acceptor provides the supplementary support to accept an electron in D-A'-π-A molecular configuration and enhances the conjugation and reduces the energy gap.[20] However, among the various auxillary acceptors (cyano, benzotriazole, quinoxaline, phthalimide, diketopyrrolopyrrole, thienopyrazine, thiazole, triazine, cyanovinyl, cyano- and fluoro-substituted phenyl) benzothiadiazole is considered to be one of the interesting core for practicing molecular engineering in various molecules suitable for electronic applications, such as OLEDs,[21] solar cells,[22] OFETs. [23] The structure of benzothiadiazole consists of 1,2,5-thiadiazole unit fused with benzene ring. (Figure 2. 1.) The thiadiazole unit consists of two nitrogen atoms at 2 and 5-positions of thiophene ring replacing its carbon atom. The electron withdrawing nitrogen of imine unit (–C=N–) impart electron deficient nature of the benzothiadiazole nucleus. Moreover, the π-conjugation builds up a facile electronic communication thus shifts the absorption spectrum to visible region.[24, 25] Some characteristics of benzothiadiazole that makes it one of the important classes of conjugated systems used in electronic applications are as follows.

1. The benzothiadiazole efficiently helps to reduce the energy gap which improves the photoabsorption response and ultimately results in better light-harvesting which improves the photovoltaic performance. [26]

2. It also improves sensitizer's photo-stability and helps to enhance the performance. [26]

3. Benzothiadiazole compounds are expected to afford well-ordered crystal structures as a result of their highly polarized properties. [27]

4. X-ray analyses suggest a quinoid character for benzothiadiazole ring, which favors the extension of delocalization to build up the intense colored compounds.
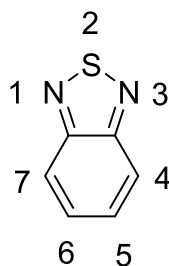
Figure 2.1. Structure of benzothiadiazole

In this chapter, we present a brief literature survey on the synthesis and application of benzothiadiazole derivatives in DSSCs and OLEDs. The synthesis of benzothiadiazole is commonly achieved by treating *ortho*-phenylenediamine with freshly distilled thionyl chloride using triethylamine (TEA) as base and dichloromethane as solvent.[28]
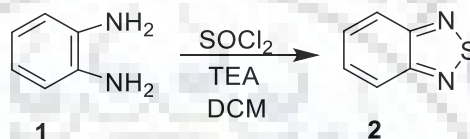
Scheme 2.1. Synthetic protocol for benzothiadiazole nuclei.

2.2. Synthesis of Multi-Substituted Benzothiadiazole

In general, the benzothiadiazole derivatives for functional materials are synthesized by following two step protocols, first the halogenation of hetro-aromatic components and second, the metal catalyzed cross coupling reactions. The benzothiadiazole molecule has been explored to mono-/di-/tri- and tetra substituted derivatives which effectively controls and tunes the functional properties such as photophysical, electrochemical and thermal stability. The conventional halogenation process on benzothiadiazole nuclei results substitution at mono (C4/C5) to tetra (C4, C5, C6, C7) position, which is discussed below.

2.2.1 Synthesis of Mono-Substituted Benzothiadiazole

Pilgram et al [28] reported synthesis of monosubstituted benzothiadiazole derivatives at C4 and C5 positions, where the 4-bromo-2,1,3-benzothiadiazole (**3**) synthesized with selective bromination (1.7 equiv. of benzothiadiazole (**2**) (Scheme 2.2) in the presence 48% hydrobromic acid, refluxed for 1h. However, to synthesize 5-bromo-2,1,3-benzothiadiazole (**7**), 2-nitroaniline (**4**) is treated by 1 equiv. of *N*-bromosuccinamide followed by reduction that results in 4-bromobenzene-1,2-diamine (**6**). Further, the intermediate **6** undergoes the condensation process as shown in Scheme 2.3 in the presence of thionyl chloride. These mono substituted derivatives are well established in literature for electronic and medicinal use.
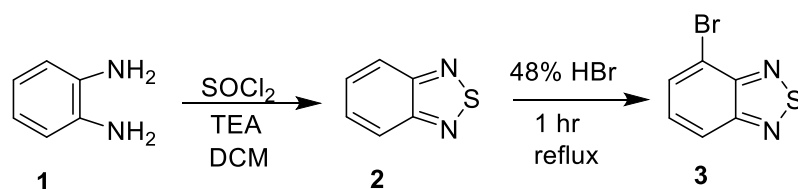
Scheme 2.2. Synthesis of 4-bromo-2,1,3-benzothiadiazole
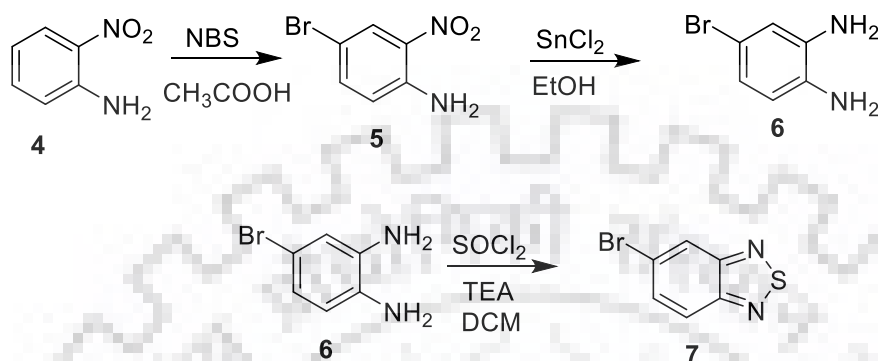
Scheme 2.3. Synthesis of 5-bromo-2,1,3-benzothiadiazole
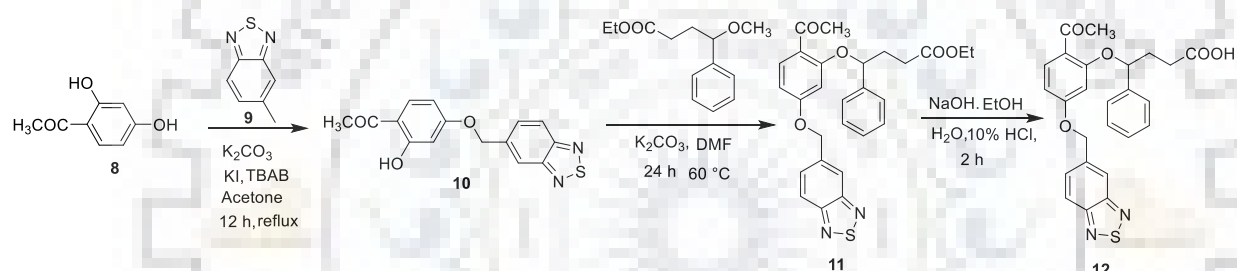
Scheme 2.4. Synthesis of mono-substituted benzothiadiazole derivative.

Cai et al achieved mono-substitution at C5 position by mono-condensation with 1-(2,4-dihydroxyphenyl)ethan-1-one (**8**) with suitable benzothiadiazole (**9**) followed by second condensation with ethyl 4-methoxy-4-phenylbutanoate that resulted intermediate ethyl 4-(2-acetyl-5-(benzo[*c*][1,2,5]thiadiazol-5-ylmethoxy)phenoxy)-4-phenylbutanoate (**11**) which on heating with 10% NaOH aqueous solution in ethanol resulted the mono-substituted benzothiadiazole. Further to neutralize the excess of base, 10% HCl was added.(Scheme 2.4) [29] Some of the mono-substituted benzothiadiazole derivatives are shown in Figure 2.2 where **M1**, a benzothiadiazole and quinoxiline hybrid which contains dithienylbenzothiadizole attached via C5 of benzothiadiazole unit. This derivative is used as the donor materials in polymer solar cells. [30] **M2,** a phenoxybutanoic acid derivative showed affinity for endothelin 1 receptors thus useful in testing anatagonist activity on the contraction of the rat thoracic aortic ring [29] Likewise **M3** and **M4** were designed to study compatibility of different synthetic protocols.
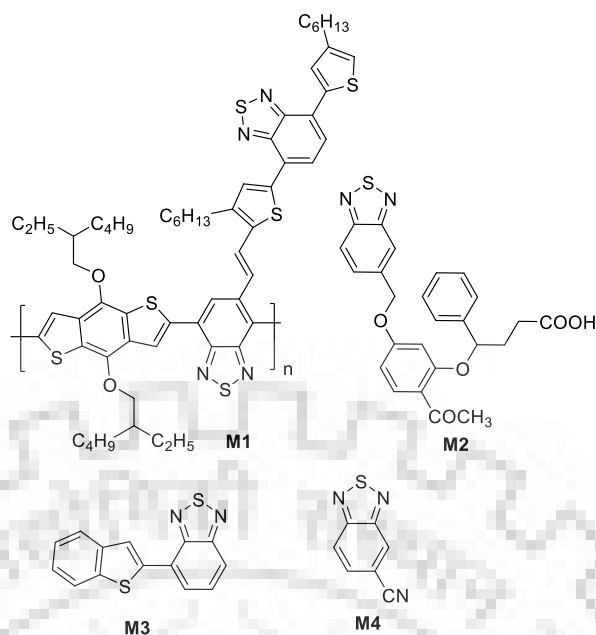
Figure 2.2. Mono-substituted benzothiadiazole derivatives.

2.2.2 Synthesis of Di-Substituted Benzothiadiazole

The di-bromination in high yield on highly nucleophilic 4,7–positions of benzothiadiazole can be accomplished using 2.0 equiv. of bromine in 48% HBr solution under reflux. (Scheme 2.5)
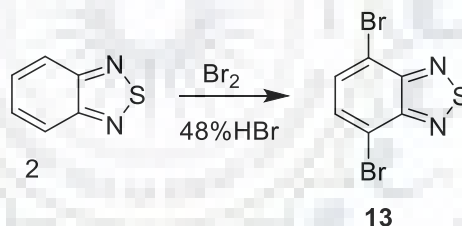
Scheme 2.5. Synthesis of 4,7-dibromo-2,1,3-benzothiadiazole

Further, to install bromine at 5,6-positions of benzothiadiazole unit, the tosylated diamine **14** is treated with 2.0 equiv. of bromine in dichloromethane. Subsequently, the intermediate underwent deprotection with H_2SO_4 to results 4,5-dibromobenzene-1,2-diamine (**15**). This on condensation with thionyl chloride yield 5,6-dibromo-2,1,3-benzothiadiazole as shown in scheme 2.6
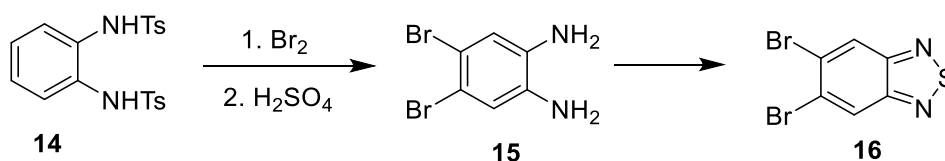
Scheme 2.6. Synthesis of 5,6-dibromo-2,1,3-benzothiadiazole[28]

To obtain methylated benzothiadiazole derivative, 5,6-dimethylbenzo[*c*][1,2,5]thiadiazole (**18**) was obtained by condensation of 4,5-dimethylbenzene-1,2-diamine with thionyl chloride in the presence of pyridine under reflux.(Scheme 2.7) [28]
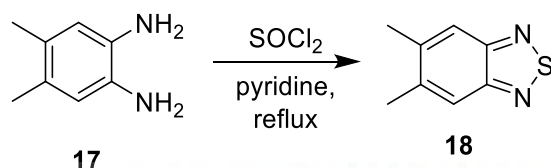
Scheme 2.7. Synthesis of 5,6-dimethyl-2,1,3-benzothiadiazole

2.2.3. Synthesis of Tri-Substituted Benzothiadiazole

Zhang et al [31, 32] designed tri-substituted benzothiadiazole derivatives at 4,5 6 position by following condensation of 4-methylbenzene-1,2-diamine (**19**) with thionyl chloride and further brominating at 4, 7 position as reported by Pilgram and coworkers.(Scheme 2.8)This benzothiadiazole derivatives has been used as chemosensors for mercury.
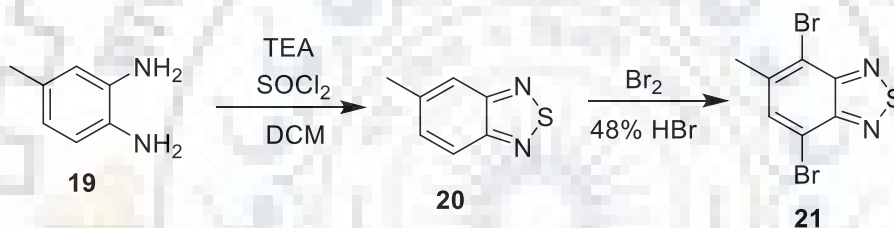
Scheme 2.8. Synthesis of 4,7-dibromo-5-methylbenzo[*c*][1,2,5]thiadiazole

Cho et al [18] demonstrated new protocol for iodinated derivatives of fluoro benzothiadiazoles (**23**) prepared by hydrogenation of precursor with Pd/C and hydrazine hydrate in absolute ethanol subsequent cyclization with SOCl$_2$ resulting mono-benzothiadiazole which undergoes di-iodination at 4,7 position by following Barker–Waters procedure which involve Ag$_2$SO$_4$ and I$_2$ in concentrated H$_2$SO$_4$ at 110 °C with good yield.
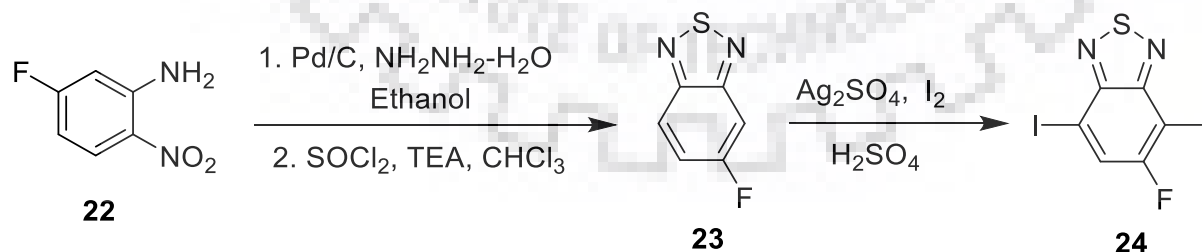
Scheme 2.9. Synthesis of 5-fluoro-4,7-diiodobenzo[*c*][1,2,5]thiadiazole
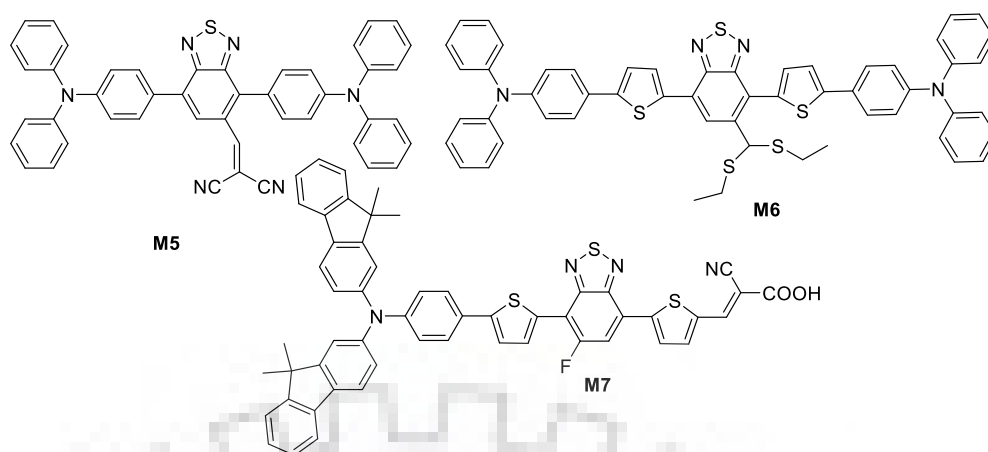
Figure 2.3. Representative structure of tri-substituted benzothiadiazole derivatives.

2.2.4. Synthesis of Tetra-Substituted Benzothiadiazoles

The fast addition of 4 eq of bromine to benzothidiazole in the presence of HBr resulted 4,5,6,7-tetrabromo-2,1,3-benzothiadiazole. Some of the tetra-substituted derivatives of benzothiadiazole which have been used in DSSC are shown in Figure 2.4 and discussed later in the chapter.[28]
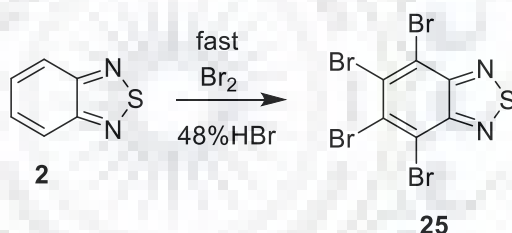
Scheme 2.10. Synthesis of perbromobenzo[*c*][1,2,5]thiadiazole
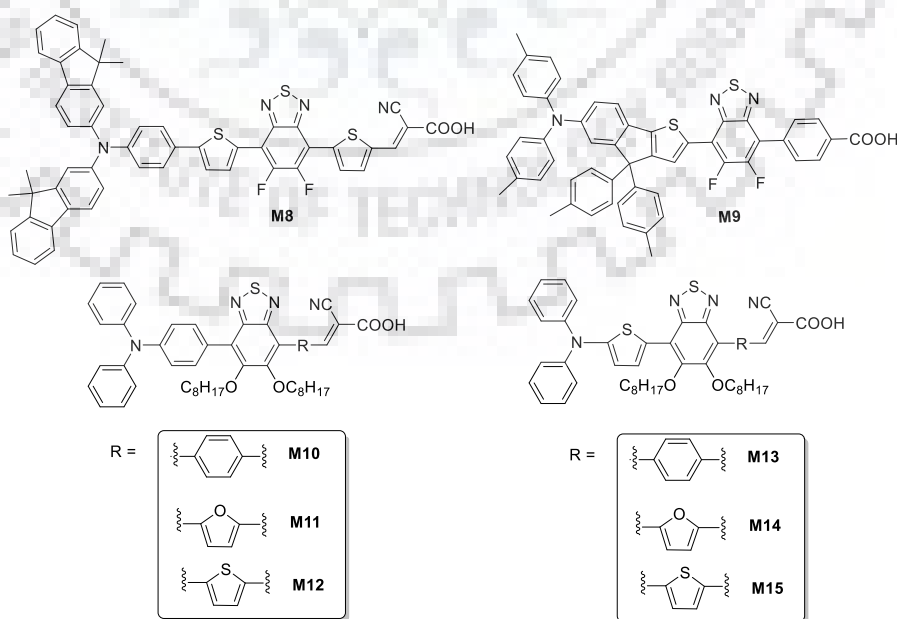
Figure 2.4. Representative structure of tetra-substituted benzothiadiazole derivatives.

11

2.3 Benzothiadiazole based small molecules in DSSC applications.

In 1991, Gratzel and coworkers developed sensitizers which played an key role in modulating DSSC performance.[33] In this review, we are representing the organic sensitizers which are designed to overcome the unfavorable processes and to improve photovoltaic performances. The introduction of metal free sensitizers have far stronger light-harvesting ability due to high molar extinction coefficients and are suitable for low-cost and environment friendly applications.[34] The molecules are engineered with the possibility to enhance π-conjugation which eventually shifts the absorption bands to longer wavelength covering up almost whole visible and near-infrared light regions to maximize the light-harvesting efficiency. Here, we will address how the benzothiadiazole nucleus contributes in designing the sensitizer for DSSCs application.

2.3.1 Benzothiadiazole Participation as Auxiliary Acceptor.

The introduction of additional acceptor is highly useful for improving the photophysical properties, stability, and photocurrent generation in light harvesting devices. Moreover, the benzothiadiazole unit participates well in regulating the HOMO-LUMO energy levels which facilitate electron injection and dye regeneration and consequently affect the capacity of organic sensitizers to harvest light in sensitized solar cells. [35] The improvements in solar cell performance by incorporating the benzothiadiazole as auxiliary acceptor have been documented well in the literature. Here, we critically analyze the prospects of benzothiadiazole moiety as an additional acceptor by comparing with the molecules which lack benzothiadiazole. (Figure 2.5) For example, Cai et al. [36] have reported **A1-2** and **B1-2**, by replacing thiophene in **A1-2** with benzothiadiazole results in **B1** and **B2,** respectively**.** The incorporation of benzothiadiazole lowered the band gap and extends the conjugation, which emphasize the bathochromic shift of **B1** and **B2** with 69 nm and 59 nm to their analogues demonstrate respectively. Further the device was fabricated using **B2** as sensitizer gave a short circuit current density of 14.81 mA cm^{-2}, an open circuit voltage of 0.688 V and *FF* of 0.69, corresponding to an overall efficiency of 7.03% under standard global AM 1.5 solar light condition
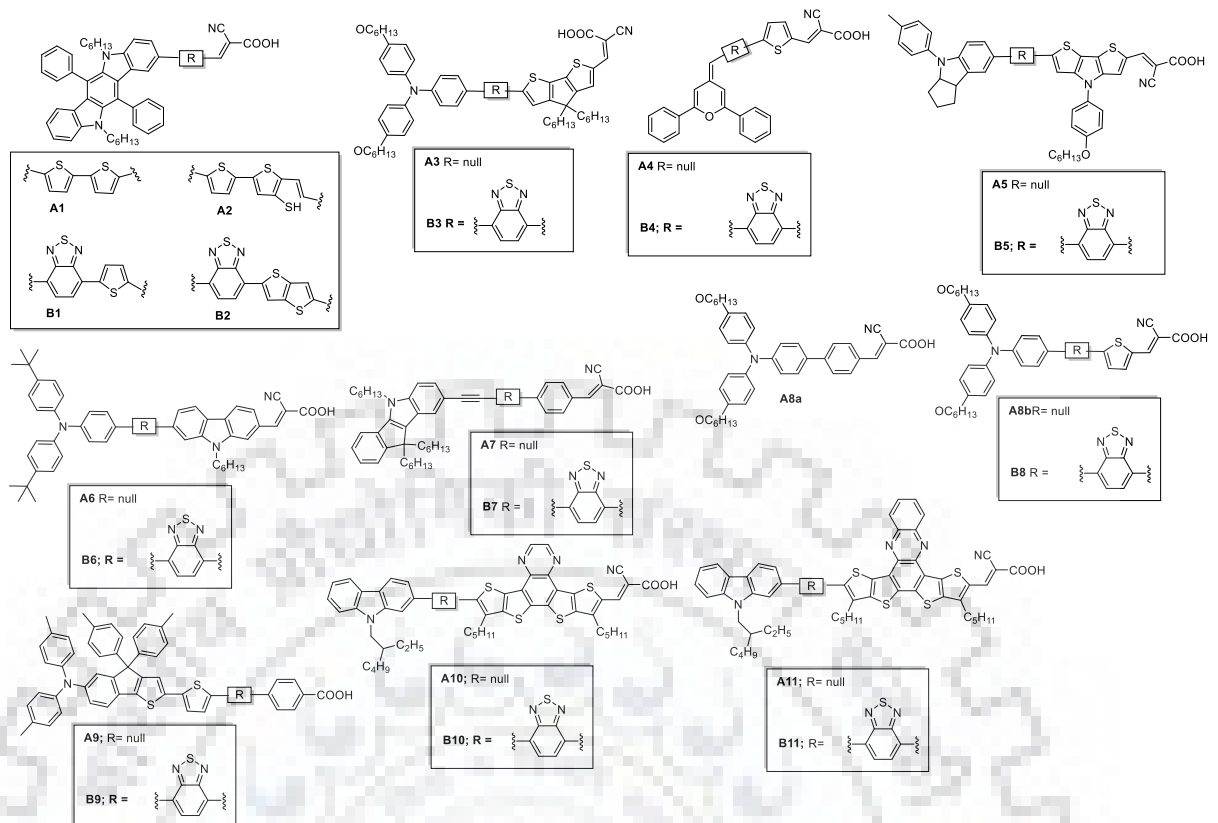
Figure 2.5. Some benzothiadiazole derivatives reported for DSSC applications.

Wang et al. [37] have reported a sensitizer containing a benzothiadizole–cyclopentadithiophene moiety as the spacer with triphenylamine as donor unit (**B3**) which showed red shift of 44 nm than **A3** (λ_{abs} = 512 nm). The obtained oxidation potential is significantly more positive than that of $[Co(bpy)3]^{2+/3+}$ (0.57 V *vs*. NHE) which extensively optimized the power conversion efficiency to 9.01% with a short circuit current density of 17.0 mA cm^2 and open circuit voltage of 0.749 V. In addition, aggregation in TiO$_2$ surface outcomes charge transfer between the monomers which restrict the electron injection kinetics and decrease the conversion efficiency. Thus, to analyze and reduce the phenomenon of aggregation in DSSC application structural evaluation has been carried out. [38] For example, Fan et al. [39] reported molecules **A4** and **B4** containing 2,6-diphenyl-4*H*-pyran donor unit, where **B4** containing benzothiadiazole exhibits red shift of 185 nm relative to **A4** dye. It also effectively lowers the LUMO to -2.96 eV via intramolecular charge transfer, relative to **A4** (-2.64 eV). The HOMO energy levels of both dyes are basically similar (5.10 eV) attributed to same electron donating unit. Xie et al. [40] have reported the dye **A5** and **B5,** where benzothiadiazole incorporation extended the conjugation and precisely reduced the band gap marking the better electronic communication, thus exhibited bathochromic shift of 15 nm. The device containing **B5** sensitizer gave a short circuit current density of 15.84 mA cm^{-2}, open circuit voltage of 660 mV and *FF* of 0.68, corresponding to an overall efficiency of 7.14%.

Duan et al. [41] have reported **A6** and **B6**, where incorporation of benzothiadiazole (**B6**) (λ_{abs} = 460 nm) has shown significant red shift of 22 nm as compared to **A6** (λ_{abs} = 438 nm). This promptly exhibited PCE of 6.76%, short circuit current density of 10.55 mA cm^{-2}, open circuit voltage of 900 mV and *FF* of 0.71. Yan et al. [42] have reported ethynylene linked dyes to introduce conjugation for facile electronic communication and three hexyl chains to suppress dye aggregation to prevent unfavorable recombination. The insertion of benzothiadiazole (**B7**) has shown 38 nm red shift when compared to **A7** (λ_{abs} = 419 nm) with power conversion efficiency of 7.99%, short circuit current density of 14.1 mA cm^{-2}, open circuit voltage of 0.829 V and *FF* of 68.4%.

Eom et al.[43] reported **A8a** and **A8b** dyes with D–π–A configuration and phenyl (λ_{abs} = 405 nm) and thiophene (λ_{abs} =443 nm) spacer which exhibited bathochromic shift to former ($\Delta\lambda_{abs}$ = 38 nm) attributable to the increase in planarity in molecular structure. Moreover, on introducing benzothiadiazole (**B8**) the extension of conjugation shifts to visible region and displayed better power conversion efficiency of 7.12%, with short circuit current density of 14.7 mA cm^{-2}, open circuit voltage of 653 mV and *FF* of 0.74%. Liu et al [44] have reported **A9** and **B9**, where benzothiadiazole substituted dye (**B9**) exhibited red shift of 78 nm when compared to **A9** and also reduced the band gap from 1.17 to 0.63 eV. The device containing dye **B9** showed PCE of 4.01%, short circuit current density of 8.98 mA cm^{-2}, open circuit voltage of 0.66 V and *FF* of 0.68. The efficiency further improved on addition of co-absorbent CDCA to 4.99%, with short circuit current density of 10.90 mA cm^{-2}, open circuit voltage of 0.66 V and *FF* of 0.69. Huang et al. [45] reported dyes containing quinoxalinedithienothiophene (**A10** and **B10**) and phenazinedithieno-thiophene (**A11** and **B11**) as spacer. Where, quinoxalinedithienothiophene derivatives (**A10** and **B10**) exhibited similar absorption profile among phenazinedithieno-thiophene derivatives, the benzothiadiazole containing dye (**B11**) exhibited hypsochromic shift when compared to **A11** in absorption spectra. Overall, **A11** based device exhibited photovoltaic performance with PCE up to 7.77%, an open circuit voltage of 0.692 V, short circuit current density of 15.6 mA cm^{-2} and *FF* of 72%. These data indicated that benzothiadiazole moiety is a promising auxiliary acceptor and its incorporation is useful in expanding the sensitizer absorption as well as the power conversion efficiency.

Table 2.1. Photophysical and electrochemical properties of the compounds **B1-B11**

Dye	λ_{abs} (nm) (ε (1x10^{-3} M^{-1} cm^{-1}))	λ_{em} (nm)	E_{0-0}[e] (eV)	E_{OX}[f] (V vs NHE)	E^*_{OX}[g] (V vs NHE)	HOMO (eV)	LUMO (eV)	$\lambda_{em}^{TiO_2}$ (nm)	E_{OX} (V)
A1[a]	453 (63.1)	-	2.01	0.85	-1.16	-	-	467	-
B1[a]	522 (56.3)	-	1.91	0.91	-1.00	-	-	517	-
A2[a]	464 (59.7)	-	2.02	0.86	-1.16	-	-	458	-
B2[a]	522 (59.5)	-	1.94	0.85	-1.09	-	-	514	-
A3	512(43.4)	561	2.03	1.02	-1.01	-	-	461	-
B3	556 (57.8)	688	1.95	1.09	-0.86	-	-	536	-
A4[d]	536	-	2.3	-	-	-	-	-	-
B4[d]	722	-	1.7	-	-	-	-	-	-
A5[d]	549 (50.16)	-	2.02	0.75	-1.27	-	-	461	-
B5[d]	563 (44.51)	-	1.83	0.81	-1.02	-	-	530	-
A6[b]	438 (36.1)	-	-	-	-	-5.17	-2.87	393	0.59
B6[b]	460 (35.6)	-	-	-	-	-5.18	-3.01	366, 456	0.60
A7[b]	419 (12.5)	-	2.26	-	-	-	-	420	1.08
B7[b]	468 (12.9)	-	2.17	-	-	-	-	462	1.13
A8a[a]	405 (22.46)	603	2.56	1.05	-1.50	-	-	-	-
A8b[a]	443 (27.07)	615	2.38	1.00	-1.38	-	-	-	-
B8[a]	392 (15.62) 514 (19.26)	729	2.03	1.00	-1.03	-	-	-	-
A9[d]	310 (32.32) 442 (64.41)	561	2.48	0.81	1.67	-	-	431	-
B9[d]	401 (26.81) 520 (23.00)	702	2.06	0.93	-1.13	-	-	516	-
A10[a]	543 (24.4)	-	2.28	-	-	-5.11	-2.83	616	0.76
B10[a]	545(28.6)	-	2.27	-	-	-5.13	-2.86	629	0.78
A11[a]	603 (16.9)	-	2.06	-	-	-5.07	-3.01	666	0.72
B11[a]	589(25.4)	-	2.10	-	-	-5.11	-3.01	662	0.76

[a] THF. [b] DCM. [c] CHCl$_3$ [d] DCM solution derived from CPCM-TDDFT/6-31+G(d,p) calculations [e] E_{0-0} was determined from the intersection of absorption and emission spectra [f] Ground state oxidation potentials of dyes on TiO$_2$ were measured with 0.1 M TBAPF$_6$ and a scan rate of 50 mV/s (calibrated

with Fc/Fc^{+3} as an external reference and converted to NHE by addition of 0.63 V) [g] Excited-state oxidation potentials were calculated according to E_{OX}-E_{0-0}.

Table 2.2. Photovoltaic properties of the compounds **B1-B11**

Dye	J_{SC} (mA cm^{-2})	V_{OC} (mV)	*FF* (%)	PCE (%)
A1[c]	12.28	754	67	6.24
B1[d]	11.57	707	68	5.55
A2[d]	9.40	644	68	4.11
B2[c]	14.81	688	69	7.03
A3[b]	11.81	768	72	6.53
A3+4.8μm	16.97	749	71	9.01
B3	15.24	786	67	7.99
B3+4.8μm	17.2	756	72	9.31
A5	7.88	640	68	3.44
B5	15.84	660	68	7.14
A6	7.52	950	71	5.03
B6	10.55	900	71	6.76
A7	10.4	843	65.8	5.74
B7	14.1	829	68.4	7.99
A8a[a]	9.20	744	75.59	5.18
A8b[a]	12.79	742	74.67	7.09
B8[a]	14.70	653	74.17	7.12
A9	8.35	670	68	3.82
A9+CDCA	8.16	720	72	4.23
B9	8.98	660	68	4.01
B9+CDCA	10.90	660	69	4.99
A10[a]	12.92	661	75.73	6.48
B10[a]	12.47	695	73.11	6.33
A11[a]	15.63	691	71.88	7.77
B11[a]	13.76	661	74.79	6.81

[a] Dipping solution: 0.3 mM dye solution (EtOH/THF = 2:1) with 20 mM CDCA. [b] The cell employed 7.0 μm TiO2 transparent without light scattering layers, the electrolyte solution was 0.2 M [Co(bpy)$_3$](PF$_6$)$_2$, 0.02 M [Co(bpy)$_3$](PF6)$_3$, 0.1 M LiClO$_4$ and 0.5 M 4-tert-butylpyridine in acetonitrile [c] CHCl$_3$-EtOH = 1:3 [d] -DMF(3:1)

2.3.2 Benzothiadiazole derivatives diversified with different donors and linkers
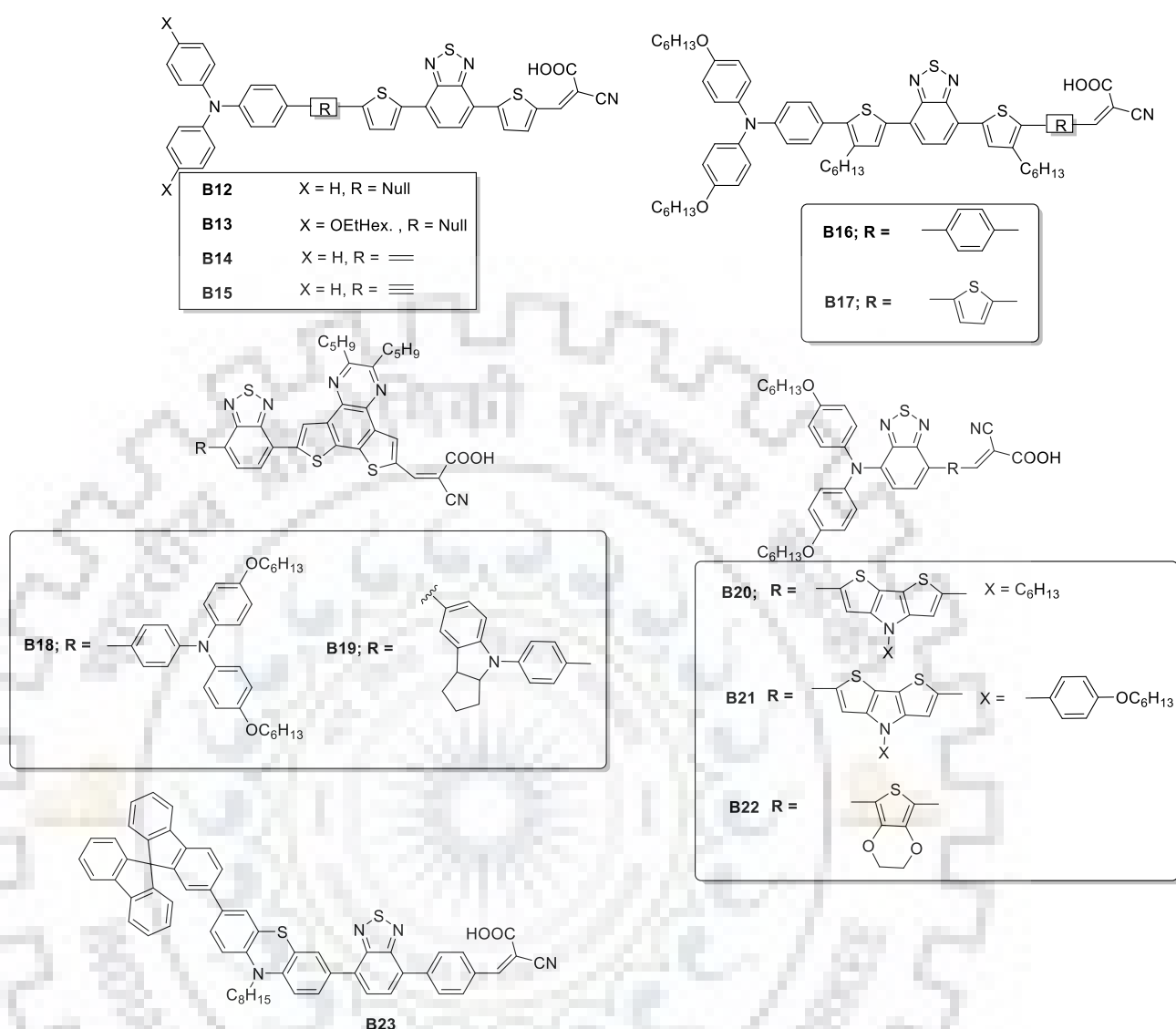
Figure 2.6. Structures of benzothiadiazole derivatives diversified with donors and spacers.

Furthermore, benzothiadiazole derivatives achieved structural property relationships on the basis of diverse donors and spacers as illustrated further in chapter and the effect of their configurations on photophysical, electrochemical and photovoltaic properties compiled in Table 2.3 and Table 2.4. Likewise, to show the influence of the configuration of sensitizers of different donors and linkers Lee et al. [46] reported series of π-conjugated dyes (**B12, B13, B14** and **B15**), comprising triphenylamine moieties as the electron donor bridged to benzothiadiazole moieties with single (**B12**) double (**B14**) and triple bond (**B15**). Due to poorer π-orbital overlap and mismatch in energy of the π-orbitals, **B15** showed blue shifted absorption than other derivatives. The **B13** has evolved the role of alkoxy group by preventing aggregation of dyes in TiO$_2$ film. Further the same has attained the maximum power conversion efficiency of 7.30% with short circuit current density of 17.9 mA cm^{-2}, open circuit voltage of 620 mV

17

and *FF* of 0.66. Similarly, Yegit et al. [47] introduced phenyl and thiophene unit in between thiophene and anchoring group. The dye showed red shift absorption with thiophene (**B17**) when compared to phenylene (**B16**) bridged dye attributable to facile electronic conjugation in former. However, because of the electron-rich thiophene bridge, LUMO level was elevated. The device containing **B17** sensitizer showed better photovoltaic performance with a short circuit current density of 11.15 mA cm^{-2}, a open circuit voltage of 580 mV, and an *FF* of 0.59, corresponding to an overall PCE of 3.81%. Huang et al. [48] reported dyes **B18** and **B19**, containing dipentyldithieno[3,2-f:2′,3′-*h*]quinoxaline (DPQ) as a π-spacer, which provide effective delocalization of the π-electrons and can facilitate the intramolecular charge transfer (ICT) of the dyes due to its planarity. The introduction of the two alkyl chains on the DPQ and two alkoxy chains on triphenylamine could increase the solubility of dyes, reduce the intermolecular aggregation, and restrict the charge recombination at the TiO_2 surface which can facilitate the ICT of the dyes. The dye **B18** with dihexyloxyl substituted triphenylamine exhibited hypso and hypochromic shift when compared to indoline derivative (**B19**) by 18 nm. The device containing **B19** showed better photovoltaic performance with a short circuit current density of 17.61. mA cm^{-2}, an open circuit voltage of 685 mV, and a *FF* of 0.59 corresponding power conversion efficiency of 7.12%. Li et al. [49] reported **B20-22**, employed with dithiophene and ethylenedioxythiophene as linker. The **B20** and **B21** have much higher molar extinction coefficients than **B22** attributable to better light harvesting ability of dithiophene moiety when compared to ethylenedioxythiophene. Moreover, the device containing **B21** as sensitizer exhibited photovoltaic performance with a short circuit current density of 17.96. mA cm^{-2}, a open circuit voltage of 809 mV, and an *FF* of 0.56, corresponding to an overall PCE of 8.14% using electrolyte composed of 0.25 M [Co(II)(phen)$_3$](PF6)$_2$, 0.05 M [Co(III)(-phen)$_3$](PF6)$_3$, 0.5 M TBP and 0.1 M LiTFSI in acetonitrile.

Jia et al. [50] reported **B23** by introducing bulky spirobiflourene unit onto phenothiazine moiety and also an alkyl chain in order to increase the solubility of the molecule. The dye exhibited absorbance maxima of 452 nm and the bulky group and chain helped in reducing recombination which resulted to electron life time value 41.9 ms. The longer lifetime corresponds to lower dark current thus suitable to exhibit better photovoltaic performance with a short circuit current density of 12.32. mA cm^{-2}, an open circuit voltage of 840 mV, and an *FF* of 64.63, corresponding to an overall PCE of 6.69%.
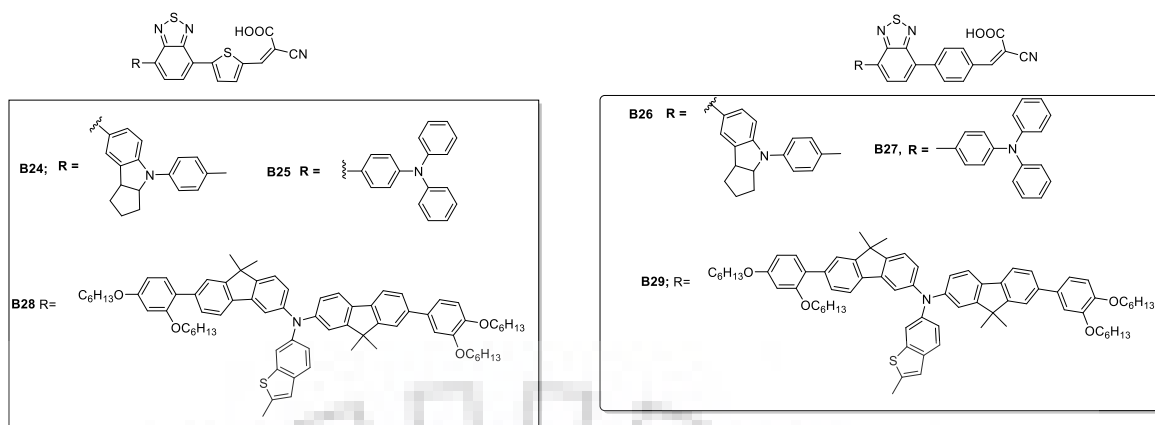
Figure 2.7. Structures of benzothiadiazole derivatives substituted with different donor units.

Further, to illustrate the effect of different donor unit on the D-A-π-A configuration Zhu et al. [51] proposed four molecules **B24-B27,** where indole derivatives (**B24** and **B26**) showed bathochromic shift of 36 and 41 nm when compared to triphenylamine derivatives (**B25** and **B27**) attributable to more auxochromic effect of indoline unit. Similarly, the thiophene spacer derivatives (**B24** and **B25)** which provides planarity to molecule and results in better electronic communication produces bathochromic shift when compared to non-planar phenyl spacer (**B26** and **B27**). The HOMO values of **B24** and **B26** are almost identical, about 0.67 V. While for **B25** and **B27**, it shifted to 0.95 V as the electron donating tendency decreased from indoline unit to triphenylamine unit. The incident-photon-conversion efficiency of **B26** reaches nearly 850 nm with a power conversion efficiency as high as 8.7% in liquid electrolyte and 6.6% in ionic-liquid electrolyte.

Seo et al.[52] reported two dyes **B28** and **B29**, by incorporating bulky donor dipentyldithieno[3,2-*f*:2′,3′-*h*]quinoxaline with a dialkoxyphenyl unit and a cyanoacrylic acid group as an anchoring group connected with benzothiadiazole thiophene and phenyl as π-bridges. The thiophene bridged dye (**B28**) exhibited bathochromic shift when compared to dye **B29**, the phenylene bridge. The device containing **B29** sensitizer showed better photovoltaic performance with a short circuit current density of 11.3 mA cm^{-2}, a open circuit voltage of 858 mV, and an *FF* of 74.1, corresponding to an overall conversion efficiency of 7.01. These molecules carrying the thiophene spacer proved potentially beneficial in enhancing the light harvesting capacity of sensitizer. The same group reported **B30** and **B31**[53], varying the spacer from thiophene to ethylenedioxythiophene, which participate in reducing the band gap from 2.12 to 2.05 V thus influencing redshifted absorption and emission bands. Further, the device containing **B30** sensitizer showed better photovoltaic performance with a short circuit current density of 14.3 mA cm^{-2}, a open circuit voltage of 0.58 V, and an *FF* of 0.72,

Figure 2.8. Structures of benzothiadiazole derivatives substituted with different donor units

Fernades et al [54] reported **B32**, which contains 5-hexyl-2,2′-bithienyl as donor in conjugation with benzothiadiazole thiophene and cyanoacrylic acid. On comparing, the dye **B32** with triphenylamine substituted **B25, B32** exhibited red shift in absorption when compared to **B25** attributable to the lower electron donating ability of *N,N* diphenylanilino group. The *N,N* diphenylanilino group contains nitrogen nonbonding lone pair that participate in partial delocalization of the conjugated phenyl units and is organized in a nonplanar fashion. The device containing **B32** as sensitizer exhibited better photovoltaic performance than **B25** with a short circuit current density of 9.36 mA cm^{-2}, a open circuit voltage of 0.63V, and an *FF* of 60.72, corresponding to an overall conversion efficiency of 4.51%. Further, the performance was improved to 5.22 % for the cell sensitized with **N719**. Likewise, Dall'Agnese et al [55] reported julolidine containing dye **B33**, which leads absorption spectrum to 368 nm in ethanol solution. The device containing **B33** dye exhibited photovoltaic performance with a short circuit current density of 9.36. mA cm^{-2}, a open circuit voltage of 0.296, and an *FF* of 0.55, corresponding to an overall conversion efficiency of 1.85% using electrolyte composition 0.7 M LiI + 0.05 M I$_2$.

Following the concept of a wide linkage probability of donor unit, research was carried out by Keerthi et al.[56] on carbazole substitution and reported **B34-B29** series of dyes. The dye **B37** and **B36** showed a redshift in absorption maxima by 15-20 nm when compared to **B35** and **B38** (461 nm-459 nm) due to directly linked carbazole at C2-position on benzothiadiazole nucleus facilitating the electronic communication.

Table 2.4. Photophysical and electrochemical properties of the compounds **B36-B43**

Dye	λ_{abs} (nm) (ε (1x10^{-3} M^{-1} cm^{-1}))	λ_{em} (nm)	E_{0-0}[b] (eV)	E_{OX}[c] (V *vs* NHE)	E^*_{OX}[d] (V *vs* NHE)	HOMO	LUMO	$\lambda_{em}^{TiO_2}$ (nm)
B36[a]	476 (26.10)	595	2.02	-	-	-5.47	-3.45	-
B37[a]	474 (25.71)	589	1.83	-	-	-5.29	-3.46	-
B38[a]	461 (11.02)	557	1.97	-	-	-5.41	-3.44	-
B39[a]	484 (26.20)	628	1.70	-	-	-5.24	-3.54	-
B16[f]	530 (16.18)	700	1.89	1.40	-	4.61	-3.21	-
B17[f]	545 (20.98)	720	1.81	1.66	-	4.61	-2.95	-
B18[h]	529(29.73)		1.97	1.07	-0.90	-	-	519
B19[h]	547(31.97)		1.94	1.00	-0.94	-	-	519
B20[f]	571 (59.0)		1.98	0.88	-1.10	-	-	-
B21[f]	567 (59.2)		1.94	0.90	-1.04	-	-	-
B22[f]	566 (39.0)		2.02	0.95	-1.07	-	-	-
B23[a]	452(8.2)	567	2.41	0.98	-1.43	-	-	-
B32	506(28.55)[i]	625[i]	2.15[j]			-4.74[j]	-2.59[j]	
B33	482(23.76)[i]	655[i]	2.50[j]			-5.11[j]	-2.61[j]	
B41	504(21)	-	2.04	-	-	5.50	3.55	-
B40[a]	541 (24.4)	-	1.86	-	-	5.122	3.256	-
B41[a]	526(40.3)	-	1.91	0.95	-1.00	-	-	526
B42[f]	562 (47.4)	-	2.00	0.94	-1.06	-	-	543
B43[f]	543(60.80)	-	2.01	0.79	-1.22	-	-	539

[a] THF. [b] E_{0-0} was determined from the intersection of absorption and emission spectra in THF.

[c] Ground state oxidation potentials of dyes on TiO$_2$ were measured in ACN with 0.1 M TBAPF$_6$ and a scan rate of 50 mV s1 (calibrated with Fc/Fc^{+3} as an external reference and converted to NHE by addition of 0.63 V).

[d] Excited-state oxidation potentials were calculated according to E_{OX}-E_{0-0}.

[e] DCM solution derived from CPCM-TDDFT/6-31+G(d,p) calculations

[f] DCM. [g] CHCl$_3$/CH$_3$OH = 4/1 ($\approx$10^{-5} M) [h] CHCl$_3$. [i] Ethanol [j] DMF
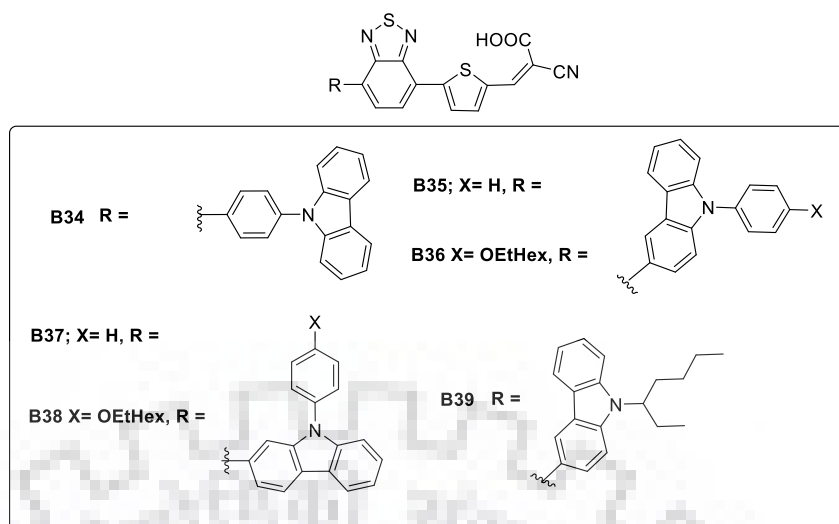
Figure 2.9. Structures of benzothiadiazole derivatives substituted with different donor units.

Similarly, linking benzothiadiazole at C3-position of carbazole donor unit as in **B35** and **B38**, hindered the charge transfer from donor to the acceptor. The overall PCE of these molecules are in the order of **B39** > **B37** > **B36** > **B34** > **B35** > **B38**, respectively. Where **B39** sensitizer showed better photovoltaic performance with a short circuit current density of 8.30 mA cm^{-2}, a open circuit voltage of 0.64 V, and an *FF* of 0.73, corresponding to an overall conversion efficiency of 3.8%.

Table 2.5. Photovoltaic properties of the compounds **B12-B43**

Dye	J_{SC} (mA cm^{-2})	V_{OC} (mV)	FF (%)	PCE (%)
B12[a](80mM)	15	580	65	5.72
B13[a]	17.9	520	66	7.30
B14[a]	10.6	540	59	3.37
B15[a]	13	560	63	4.55
B24[g]	11.9	650	68	5.3
B26[g]	12.9	600	68	5.3
B27[g]	9.5	690	75	4.9
B25[g]	11.2	600	75	5.0
B30[e]	12.2	580	68	4.82
B30(40mM)[e]	14.3	580	77	5.97
B31(0mM)[e]	10.8	550	66	3.93
B31(40mM)[e]	13.3	560	68	5.03
B28	8.08	801	71.7	4.64

B29	11.3	858	74.1	7.01
B34[a]	03.90	590	68.1	1.56
B35[a]	3.22	640	73.0	1.53
B36[a]	4.85	650	73.5	2.36
B37[a]	7.37	650	68.6	3.29
B38[a]	2.43	0.67	71.1	1.20
B39[a]	8.30	640	73.8	3.80
B16	8.55	600	62	3.16
B17	11.15	580	59	3.81
B18[h]	14.51	721	65	6.78
B19[h]	17.61	685	59	7.12
B20[f]	14.38	807	56	6.50
B21[f]	17.96	809	56	8.14
B22[f]	10.51	789	63	5.22
B23	12.32	840	64.63	6.69
B32	2.60	500	69	0.95
B32 +N719	5.51	580	74	2.49
B33	9.36	630	72	4.51
B33+N719	10.30	670	71	5.22
B40	8.35	517	69	1.15
B41	16.36	694	72	8.2
B42	20.28	724	68.26	10.02
B43	19.64	760	625	9.25

[a](EtOH/THF = 2:1) with 20 mM CDCA.Dipping solution: 0.3 mM dye solution EtOH/THF = 2:1) with 20 mM CDCA.[b] Irradiated light: AM 1.5G (100 mW cm^2); cell area tested with a metal mask:0.141 cm^{2}.[c] (CHCl3-EtOH = 1:3)[d] AV-DMF(v/v 3:1) [e] (CHCl$_3$-MeOH = 1:3)[f] Electrolyte E1: 0.25 M [Co(II)(phen)3](PF6)2, 0.05 M [Co(III)(phen)3](PF6)3, 0.5 M TBP and 0.1 M LiTFSI in acetonitrile[g] 0.3 mM , E1: 0.7 M LiI + 0.05 M I$_2$
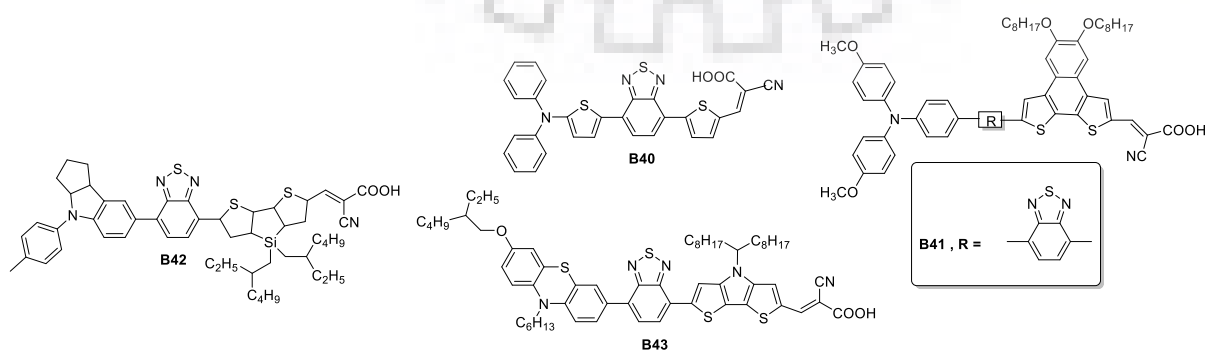
Figure 2.10. Structures of benzothiadiazole derivatives diversified in donors and spacers.

24

Velusamy et al. [57] reported **B40** by replacing benzene with thiophene in **B27**, here **B40** exhibited bathochromic shift when compared to **B27** ($\Delta\lambda_{abs}$ = 60 nm). The device containing dye **B27** exhibited photovoltaic performance with a short circuit current density of 10.44. mA cm^{-2}, a open circuit voltage of 0.546 V, and an *FF* of 0.66, corresponding to an overall conversion efficiency of 3.77%. Feng et al[58] reported **B41** dye embedded naphtho[2,1-*b*:3,4-*b*]dithiophene, showed promising optoelectronic properties. The device containing dye **B41** exhibited photovoltaic performance with a short circuit current density of 16.36. mA cm^{-2}, a open circuit voltage of 0.694 V, and an *FF* of 0.72, corresponding to an overall conversion efficiency of 8.2%. Gao et al. [59] reported dye **B42** containing 4-bis(2-ethylhexyl)- 4*H*-silolo[3,2-*b*:4,5-*b*]dithiophene (DTS), exhibited absorption maxima at 562 nm .The device containing dye **B42** exhibited photovoltaic performance with a short circuit current density of 20.28. mA cm^{-2}, a open circuit voltage of 0.724 V, and an *FF* of 0.68, corresponding to an overall conversion efficiency of 10.02%.Han et al[60] reported **B43** dye embedded with dithienopyrrole π-spacer with phenothiazine donor, exhibited bathochromic shift of 47 nm and low E_{0-0} of 2.01 eV when compared to dye which lacks benzothiadiazole with same configuration. This stands helpful for **B43** which showed photovoltaic performance with a short circuit current density of 19.46 mA cm^{-2}, a open circuit voltage of 0.760 V, and an *FF* of 0.62, corresponding to an overall conversion efficiency of 9.25%. In this way, the molecular design strategy helped to obtain suitable HOMO-LUMO energy level, to extend the conjugation which broaden the IPCE through the modification of optoelectronic and electrochemical properties of the organic sensitizers.

2.3.3 Benzothiadiazole derivatives with alkyl and alkoxy chains on linkers.

The photovoltaic performance in DSSCs applications faces unfavorable process of recombination due to aggregation which includes, recombination between the TiO$_2$ and positive charge center of oxidized dyes, and from TiO$_2$ to the electrolyte. These recombination one or another way reduces the overall power conversion efficiency. Thus to reduce such unwanted process alkyl or alkoxy chains are being incorporated which not only reduce the aggregation but also increase the electron lifetime by preventing the dark current. [61] It also improves open circuit voltage of the cell and reduces the reorganization energy of the dye, improves short circuit current density of the cell. The alkylated chains reported to increase the solubility and in some cases enhance the electron donating property of donor moiety. [62]

Kim et al. [63] reported dyes **B44** and **B45** dye containing 4,7-dithiophen-2-yl benzo[1,2,5]thiadiazoles with bis(9,9-dimethylfluorenyl)amine as the donor. The **B44** showed bathochromic shift of 66 nm when compared to the dye containing alkyl chain **B45**, the alkyl

chain twisted the facile electronic communication in **B45**. However photovoltaic performance of device containing **B44/B45** exhibited short circuit current density of 9.58/12.03 mA cm^{-2}, an open circuit voltage of 643/720 mV, and a *FF* of 75.54/76.19, corresponding to an overall conversion efficiency of 4.66/6.61%.
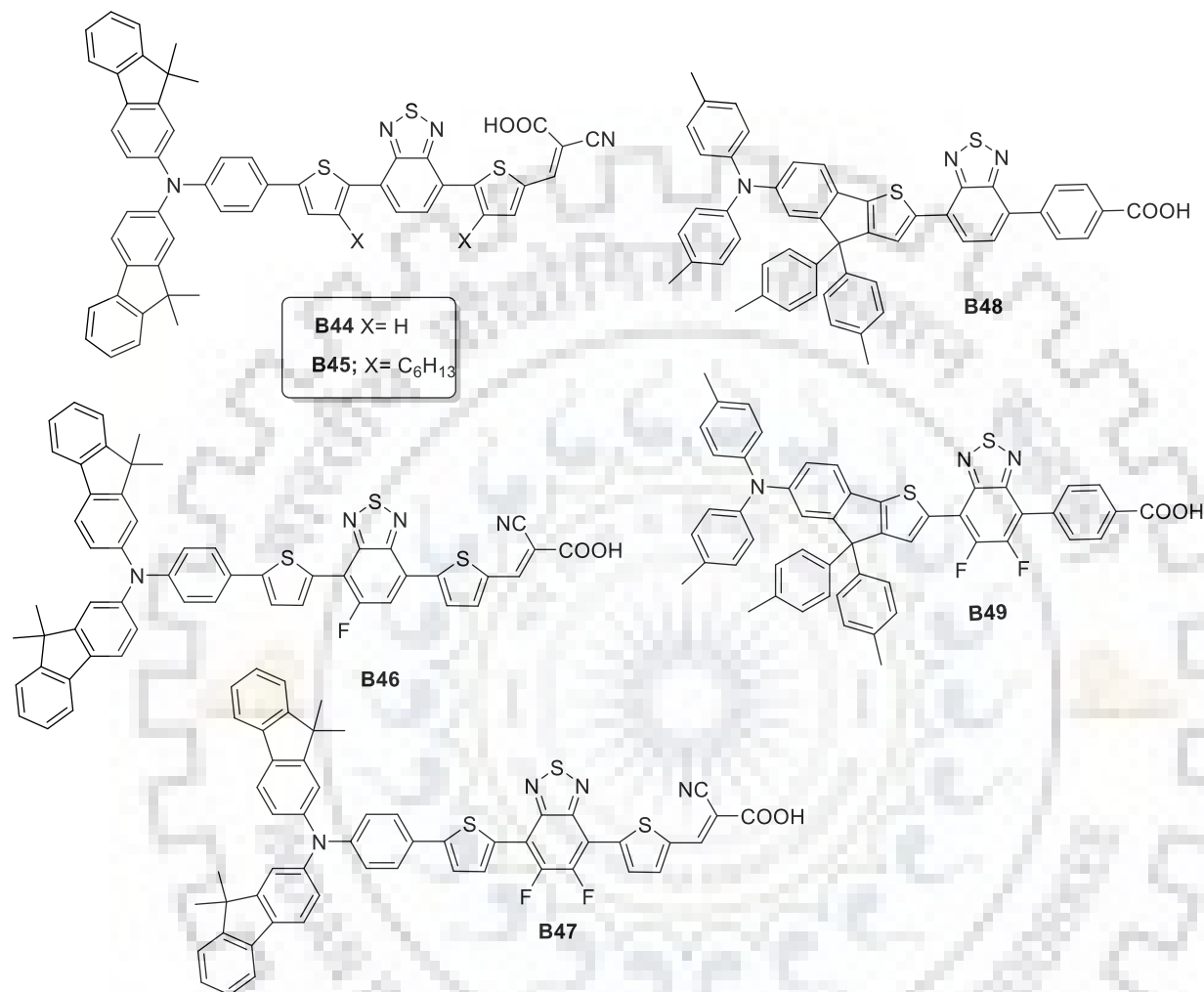
Figure 2.11. Flourene decorated benzothiadiazole derivatives for DSSCs.

The same group reported the dyes **B46** and **B47** introducing flourine unit on benzothiadiazole nuclei. The dyes varied on account of substitution of fluorine at C5 and C6 position of benzothiadiazole nucleus. Interestingly, **B46** mono-flouro derivative exhibited redshift absorptions of about 77 nm when compared to di-flouro derivative **B47**, probably due to steric hindrance in conjugation and electron withdrawing effect by fluorine unit, respectively. The device containing dye **B46/B47** exhibited photovoltaic performance with short circuit current density of 11.96/12.57 mA cm^{-2}, a open circuit voltage of 650/670 mV, and an *FF* of 68.20/69.83 corresponding to an overall conversion efficiency of 5.32/5.91% . The efficiency found to be two fold higher than the **B44**, thus supporting the effective role of fluorinated benzothiadiazole molecules.[64] Huang et al. [65] reported the dyes **B48** and **B49,**

where **B49** contains fluorine unit at C5 &C6 position of benzothiadiazole**.** Both the triphenylamine derivative contains indenothiophenene unit as the donor and thiophene spacer and benzoic acid as acceptor. The donor unit enhanced the light capturing ability and electron lifetime which presumably favors to deal with dark current. Moreover, fluoro-containing dye **B49** showed improved performance when compared to **B47** and **B48.** The dye **B49** exhibited high molar extinction coefficient with higher IPCE value at 450-600 nm and higher short circuit current density. The device containing **B49** showed the highest PCE of 7.91%, with the corresponding short circuit current density of 14.86 mA cm^{-2}, a open circuit voltage of 710 mV, and an FF of 75%.
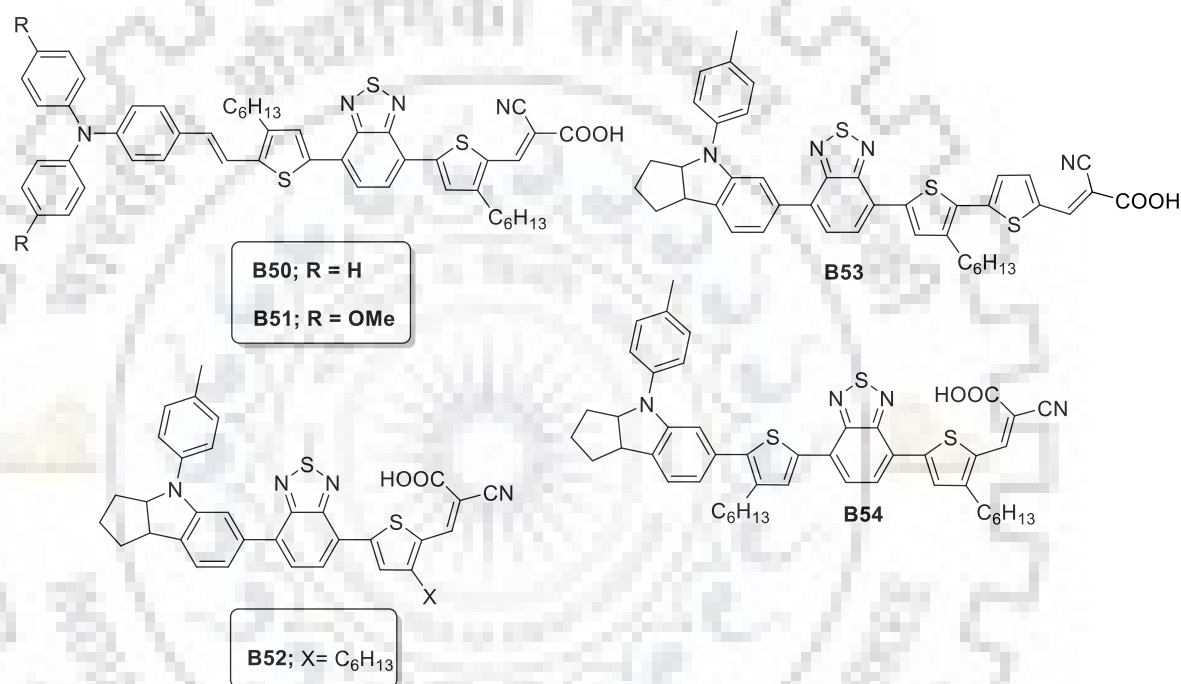
Figure 2.12. Benzothiadiazole derivatives with /without alkyl chains on linkers.

Similarly, Tang et al. [66] reported **B50** and **B51** by replacing fluorene based donor in **B45** dyes to vinyl linked triphenylamine derivative. However, **B51** showed bathochromic shift when compared to **B50** by 17 nm attributable to strong electron donating effect of alkoxy group. But the dye **B51** showed poor photovoltaic performance than **B50** probably because of its weaker driving force for dye regeneration and electron injection process. The device containing dye **B50/B51** exhibited short circuit current density of 16.46/11.94 mA cm^{-2}, an open circuit voltage of 545/555 mV, and a *FF* of 0.67/0.71, corresponding to an overall conversion efficiency of 6.04/4.68% respectively. Further, with the similar configuration Wu et al.[67] reported **B54** with indoline donor which showed bathochromic shift in absorption than **B45.** However, **B54** showed poor performance when compared to **B45** as the E$_{ox}$ (V *vs* NHE) for **B54** is 0.57 V resulting ΔG_{inj} is much closer to conduction band of TiO$_2$ that is kinetically not much

favorable. Meanwhile, **B52** dye favored to study progressive role of alkyl chain on comparing previous reported dye **B24.** The dye **B54** showed red shift of 11 nm compared to **B24.** In the case of **B54**, the redshift in absorption bands and onset is caused by an increase in the conjugation length of the donor part due to the incorporation of the additional hexyl thiophene subunit The device containing dyes **B52, B54** exhibited short circuit current density of 14.3/10.4 mA cm^{-2}, a open circuit voltage of 639/629 mV, and an *FF* of 0.75/0.71 corresponding to an overall conversion efficiency of 6.85/4.64 %, respectively. Further the same group reported **B53**[68] with additional thiophene toward anchoring unit in **B52**. It showed hypsochromic shift when compared to **B52** by 10 nm attributable to twisting which prevented the facile donor-acceptor conjugation. The dye **B53** with co-adsorbent CDCA exhibited short circuit current density of 18.00 mA cm^{-2}, a open circuit voltage of 696 mV, and an *FF* of 0.72 corresponding to an overall conversion efficiency of 9.04%. [EES2012-5_8261–8272]

Chou et al [69] reported new dipolar compounds **B55-59** containing 5,6-bis-hexyloxy-benzo[2,1,3]thiadiazole between the electron donating arylamine and the electron accepting 2-cyanoacrylic acid. On comparing dyes without hexyloxy chains, these dyes effectively suppress the dark currents and significantly improve the cell performance. The dye **B25** on comparing with hexyloxy substituted dyes **B55-59** has showed poor efficiency. The device containing the dye **B58** exhibited better photovoltaic performance with short circuit current density of 15 mA cm^{-2}, an open circuit voltage of 0.67 mV, and an *FF* of 0.66 corresponding to an overall conversion efficiency of 6.72% with effect of recombination resistance (285Ω) and charge transfer resistance (16.6Ω).
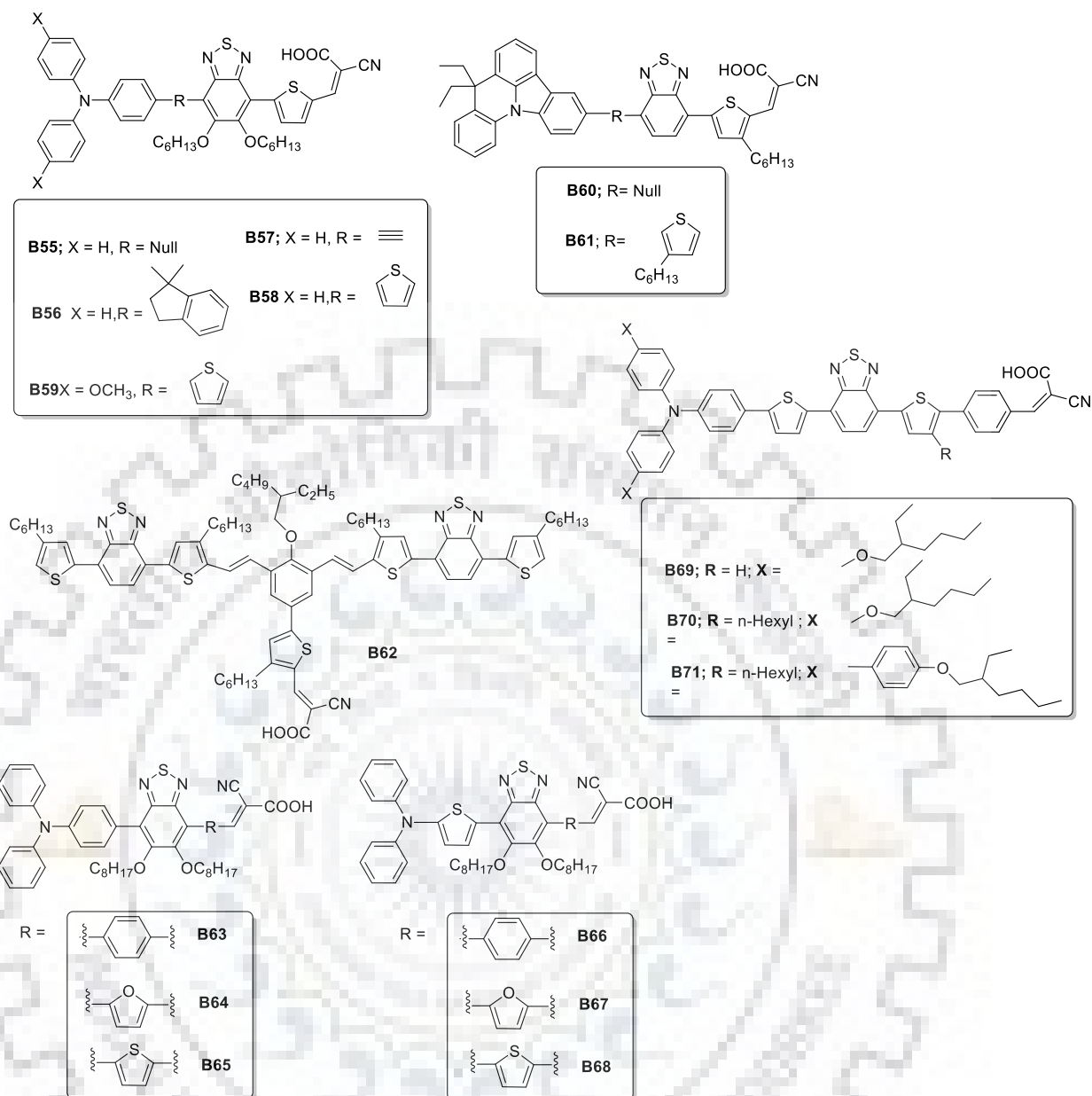
Figure 2.13. Comparisons of benzothiadiazole derivatives with /without alkyl and alkoxy chains on linkers.

Similarly, Hu et al. [70] reported dipolar compounds **B60-61** containing long alkyl chains grafted on a π-bridge between the electron donating 8,8-diethyl-8*H*-indolo[3,2,1]acridine and the electron accepting 2-cyanoacrylic acid. **B61** exhibited bathochromic shift by extending the conjugated system when compared to **B60** by 32 nm. The device containing dye **B60/B61** exhibited photovoltaic performance with short circuit current density of 9.71/11.82 mA cm^{-2}, an open circuit voltage of 712/682 mV, and a *FF* of 75/72 corresponding to an overall conversion efficiency of 5.20/5.82%. Furthermore, Wang et al [71] reported **B62** containing long alkyl chains grafted on a π-bridge. The **B62** exhibited 492 nm (46,450 M^{-1} cm^{-1}) and device showed photovoltaic performance with short circuit current density of 5.83 mA cm^{-2}, an

open circit voltage of 0.52 mV, and an *FF* of 0.72 corresponding to an overall conversion efficiency of 2.18%. However, the PCE value of **B62** is only 1.48% when CDCA is added. It indicates that the addition of CDCA has less effect on reducing the formation of aggregates because 4,7-bis-(4-hexylthiophen-2-yl)benzo[1,2,5] thiadiazole unit has enough alkyl chain.

To understand the effect of alkoxy unit on the performance of DSSC, Chen et al[72] reported the bis(octyloxy)benzo-[*c*][1,2,5]thiadiazole derivatives **B63-B65** based on D–A–π–A configuration. Where, the dye **B63** exhibited redshift in absorption when compared to dyes **B64** and **B65** with 40 and 45 nm, respectively. This can be explained by the fact that the replacement of the benzene moiety by thiophene or furan leads to enhancement in the coplanarity between the 5,6-bis(octyloxy)benzo[*c*][1,2,5]thiadiazole unit and the cyanoacetic anchoring moiety. The device containing dye **B65** exhibited photovoltaic performance with short circuit current densityof 10.20 mA cm^{-2}, a open circuit voltage of 658 mV, and an *FF* of 0.63 corresponding to an overall conversion efficiency of 4.24%. However, with coadsorbent CDCA (20 X 10^{-3} M) the device showed short circuit current density of 10.49 mA cm^{-2}, a open circuit voltage of 790 mV, and an *FF* of 0.73 corresponding to an overall conversion efficiency of 6.07%. Further the same group reported **B66-B68** [73] containing *N*,*N*-diphenylthiophen-2-amine as the donor based on similar D–A–π–A configuration. The dye **B66** exhibited redshift absorptions when compared to **B67** and **B68** of about 42 and 58 nm, respectively, for same reason. Further, on comparing the absorption maxima we observe this dye showed bathochromic shift to earlier reported **B63-B65**, arising due to the presence of *N*,*N*-diphenylthiophen-2-amine replacing phenyl. The device containing dye **B67** exhibited photovoltaic performance with short circuit current density of 16.88 mA cm^{-2}, an open circuit voltage of 662 mV, and an *FF* of 64.03 corresponding to an overall conversion efficiency of 7.16% with I/I$_3$. Moreover, a photoelectric conversion efficiency of 6.14% was obtained with short circuit current density of 11.35 mA cm^{-2}, a open circuit voltage of 0.760 V and an *FF* of 71.16% with the Co(II)/(III) electrolyte under standard global AM 1.5 solar conditions. Grisorio et al [74] reported **B69-B71** molecules based on D–A–π–A configuration containing the positioning an alkyl chain onto the π-spacer and increasing the bulkiness of the electron-donor. The dye **B69** (535 nm) exhibits bathochromic shift when compared to **B70** (527 nm) and **B71** (524 nm) by 8 and 11 nm, respectively. The dyes showed good molar extinction coefficient which leads to better light harvesting property. The dye assembled the efficiency by introducing CDCA as their power conversion efficiency increased from 4.1% to 8.6% in the case of **B69** (using 30 mM CDCA), from 5.1% to 9.5% in the case of **B70** (using 10 mM CDCA) and from 5.5% to 9.8% in the case of **B71** (using 10 mM CDCA

Table 2.6. Photophysical and electrochemical properties of the compounds **B44-B55**

Dye	λ_{abs} (nm) (ε (1×10^{-3} M^{-1} cm^{-1}))	λ_{em} (nm)	E_{0-0}[b] (eV)	E_{OX}[c] (V vs NHE)	E^*_{OX}[d] (V vs NHE)	HOMO (eV)	LUMO (eV)	λ_{em}^{TiO2} (nm)
B44[g]	534, (19.74), 374 (36.69)		1.93	0.98	-0.95	-	-	-
B45[g]	468 (19.29), 370 (72.00)		2.07	1.08	-0.99	-	-	-
B46[a]	329 (19.3), 538 (23.70)	752		0.83	-1.10	-	-	-
B47[a]	337 (115.2), 461 (42.90)	644		0.80	-1.41	-	-	-
B48[h]	374 (25.71), 532 (21.16)	692	2.03	0.94	-1.09	-	-	515
B49[h]	374 (34.53), 525 (30.86)	689	2.05	1.0	-1.05	-	-	520
B50[a]	393 (4.66), 557 (4.67)	-	1.86	-	-	-5.43	-3.57	390,587
B51[a]	400 (4.74), 574 (4.71)	-	1.55	-	-	-5.27	-3.72	404,608
B52[f]	547 (23.50)	-	2.06	0.67	-1.39	-	-	-
B53[f]	536 (20.80)	-	2.05	0.66	-1.39	-	-	-
B54[f]	557 (27.500)	-	1.85	0.57	-1.28	-	-	-
B55[a]	466 (20.1), 408 (13.7), 307 (22.6)	619	2.29	-	-	-5.71	-3.42	455

[a] Absorption and emission spectra were measured in THF. [b] E_{0-0} was determined from the intersection of absorption and emission spectra in THF. [c] Ground state oxidation potentials of dyes on TiO_2 were measured in ACN with 0.1 M TBAPF6 and a scan rateof 50 mV s1 (calibrated with Fc/Fc^{+3} as an external reference and converted to NHE by addition of 0.63 V). [d] Excited-state oxidation potentials were calculated according to E_{OX}-E_{0-0}. [f] Absorption and emission spectra were measured in DCM. [g] Absorption spectra were measured in ethanol solution. [h.] Absorption and emission spectra were measured in CHCl$_3$

Table 2.7. Photophysical and electrochemical properties of the compounds **B56-B71**

Dye	λ_{abs} (nm) (ε (1x10^{-3} M^{-1} cm^{-1}))	λ_{em} (nm)	E_{0-0}[b] (eV)	E_{OX}[c] (V vs NHE)	$E*_{OX}$[d] (V vs NHE)	HOMO (eV)	LUMO (eV)	λ_{em}^{TiO2} (nm)
B56[a]	454 (39.6), 345 (46.0), 310(sh)	614	2.33	-	-	-5.59	-3.26	441
B57[a]	478 (37.4), 344 (36.3), 298 (25.2)	577	2.31	-	-	-5.73	-3.42	460
B58[a]	501 (25.5), 371 (27.6), 346(sh)	631	2.17	-	-	-5.56	-3.39	489
B59[a]	536 (30. 7), 422 (sh), 309 (28.3)	-	1.98			-5.38	-3.40	518
B60[a]	478	-	2.08	1.15	-0.93	-	-	484
B61[a]	510	-	1.93	1.10	-0.83	-	-	512
B62[h]	387 (51.00), (46.045)	492	2.23	1.19	-1.04	-	-	397
B63[f]	423	-	2.49	0.99	-1.50	-	-	412
B64[f]	463	-	2.22	1.0	-1.22	-	-	457
B65[f]	468	-	2.23	1.01	-1.22	-	-	457
B66[f]	483 (10.1)	-	2.11	0.71	-1.40	-	-	467
B67[f]	525 (18.2)	-	1.90	0.72	-1.18	-	-	508
B68[f]	531 (13.4)	-	1.92	0.71	-1.21	-	-	506
B69	378 (41.6), (38.3)	535	-	-	-	5.04	3.24	-
B70	370 (33.6), (27.9)	527	-	-	-	5.02	3.15	-
B71	354 (48.6), (30.10)	524	-	-	-	5.24	3.17	-

[a] Absorption and emission spectra were measured in THF. [b] E_{0-0} was determined from the intersection of absorption and emission spectra in THF. [c] Ground state oxidation potentials of dyes on TiO_2 were measured in ACN with 0.1 M TBAPF6 and a scan rateof 50 mV s1 (calibrated with Fc/Fc^{+3} as an external reference and converted to NHE by addition of 0.63 V). [d] Excited-state oxidation potentials were calculated according to E_{OX}-E_{0-0}. [f] Absorption and emission spectra were measured in DCM. [h] Absorption and emission spectra were measured in CHCl$_3$

Table 2.8. Photovoltaic properties of the compounds **B44-B71**

Dye	J_{SC} (mA cm^{-2})	V_{OC} (mV)	*FF* (%)	PCE (%)
B44	9.58	643	75.54	4.66
B45	12.03	720	76.19	6.61
B46	11.96	650	68.20	5.32
B47	12.57	67	69.83	5.91
B48	12.48	690	73	6.29
B49	14.86	710	75	7.91
B50	16.46	545	0.67	6.04
B51	11.94	555	0.71	4.68
B52[e]	14.3	639	0.75	6.85
B52[f]	15.00	672	0.77	7.76
B52[f]**+DCA**	14.15	673	0.76	7.23
B53	17.26	692	0.64	7.63
B53 +CDCA	18.28	689	0.71	8.99
B54[e]	10.4	629	0.71	4.64
B55[g]	12	680	0.68	5.57
B56[g]	11.3	680	0.69	5.34
B57[g]	12.7	700	0.70	6.22
B58	15.2	670	0.66	6.72
B59[g]	11.9	670	0.68	5.36
B60[a]	9.71	712	0.75	5.20
B61[a]	11.82	682	0.72	5.82
B62	5.83	520	0.72	2.18
B62+CDCA	3.71	590	0..67	1.48
B63	6.54	768	0.67	3.37
B63+10CDCA	6.62	794	0.76	3.97
B63+20CDCA	6.67	796	0.74	3.93
B64	9.14	638	0.64	3.71
B64+10CDCA	10.03	729	0.68	4.95
B64+20CDCA	9.23	757	0.74	5.20
B65	10.20	658	0.63	4.24
B65+10CDCA	11.53	748	0.60	5.18

B65+20CDCA	10.49	790	0.73	6.07
B66 [f]	15.05	686	64.53	6.66
B67 [f]	16.88	662	64.03	7.16
B68 [f]	15.37	629	64.02	6.19
B69	9.0	666	0.69	4.14
B69+CDCA(30mM)	18.11	663	0.72	8.64
B70	11.16	693	0.66	5.11
B70+CDCA(10mM)	19.76	704	0.68	9.49
B71	11.54	714	0.67	5.49
B71+CDCA(10mM)	19.80	721	0.68	9.77

[a] Dipping solution: 0.3 mM dye solution (EtOH/THF = 2:1) with 20 mM CDCA. [b] Irradiated light: AM 1.5G (100 mW cm^2); cell area tested with a metal mask:0.141 cm^2.

[c] (CHCl3-EtOH = 1:3) [d] AV-DMF(v/v 3:1) [e] 8 μm transparent and 4 μm scattering

[f] 12 μm transparent and 4 μm scattering [g] Experiments were conducted using TiO_2 photoelectrodes with approximately 18 mm thickness and 0.25 cm^2 working area on the FTO (15 U sq^1) substrates

2.3.4. Isomeric Derivatives of Benzothiadiazole
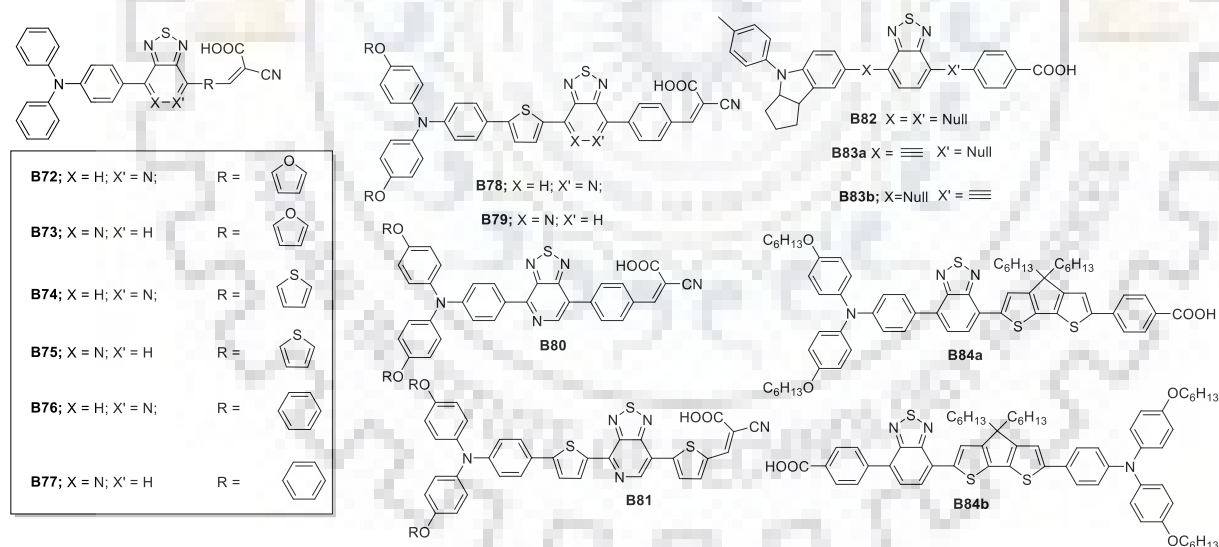
Figure 2.14. Structures of benzothiadiazole-based isomeric derivatives.

To establish the structure property relationship, Chaurasia et al [75] reported D–A–π–A configured isomeric dyes **B72, B74, B76, B78** and **B73, B75, B77, B80, B81** based on position of pyridine nitrogen distal or proximal to donor moiety respectively. The dyes **B77** & **B79** exhibited least aggregation of 26 and 27 nm, respectively on TiO_2 adsorption on comparison with solution, which stimulates these for effectively improving photovoltaic performances. Interestingly, the device containing **B77**/**B79** exhibited photovoltaic performance with short

circuit current density of 9.47/7.15 mA cm^{-2}, an open circuit voltage of 600/610 mV, and an *FF* of 68/70 corresponding to an overall conversion efficiency of 3.87/3.06 %. The efficiency improved to 4.24 % on addition of CDCA with short circuit current density of 10.01, open circuit voltage of 610 and a *FF* of 69.The efficiency is two fold higher than their respective isomers **B76** & **B78**.

Table 2.9. Photophysical and electrochemical properties of the compounds **B72-B83**

Dye	λ_{abs} (nm) (ε (1x10^{-3} M^{-1} cm^{-1}))	λ_{em} (nm)	E_{0-0} [b](eV)	E_{OX}[c] (V *vs* NHE)	$E*_{OX}$[d] (V *vs* NHE)	HOMO (eV)	LUMO (eV)	λ_{em}^{TiO2} (nm)	E_{OX}
B72	522,398,310	-	1.90	-	-	5.76	3.86	485	0.56
B73	536,386,316	674	2.03	-	-	5.78	3.75	508	0.57
B74	548,414,310	749	1.91	-	-	5.76	3.85	502	0.56
B75	546,410,306	710	1.96	-	-	5.83	3.87	502	0.62
B76	498,358,308	693	2.10	-	-	5.76	3.66	472	0.56
B77	497,356,308	675	2.13	-	-	5.79	3.66	470	0.58
B78	526,360	-	1.89	-	-	5.62	3.73	488	0.42
B79	518,352	715	2.00	-	-	5.67	3.67	492	0.46
B80	525,356,314	-	1.88	-	-	5.48	3.60	463	0.28, 1.06
B81	580,370	-	1.73	-	-	5.31	3.58	538	0.23, 0.84
B82[f]	484 (19.90)	-	2.17	0.87	-1.30	-	-	462	
B83a[f]	482 (22.30)	-	2.18	0.91	-1.27	-	-	453	
B83b[f]	508 (25.70)	-	2.07	0.88	-1.19	-	-	474	

Similarly, Song et al [76] reported B82-84, for the systematic positional study of ethynyl group at D-A-π-A configuration. It was found that inserting an ethynyl unit to the side of the anchoring group (**B83b**) showed a higher molar extinction coefficient with a red shift in the absorption band. Interestingly, **B83a** and **B83b** displayed a better photovoltaic performance when compared to **B82**. However, the device containing **B83b** exhibited better photovoltaic performance with a short circuit current density of 13.44. mA cm^{-2}, an open circuit voltage of 786 V, and an *FF* of 0.67, corresponding to an overall conversion efficiency of 7.13%. Following similar isomeric strategy Wang et al.[77] reported the cyclopentadithiophene benzothiadiazole containing dyes **84a** and **84b** on the basis of switching the position of anchoring group. The sensitizers 84b have established the breakthrough among metal free organic sensitizer with overall conversion efficiency of 12.7%.

Table 2.10. Photovoltaic properties of the compounds **B72-B84**

Dye	J_{SC} (mA cm^{-2})	V_{OC} (mV)	*FF* (%)	PCE (%)
B72	0.72	0.45	0.59	0.19
B73	2.41	0.52	0.65	0.82
B74	2.67	0.48	0.61	0.78
B75	3.35	0.52	0.67	1.16
B76	7.06	0.57	0.72	2.88
B77	9.47	0.60	0.68	3.87
B77+30mM	10.01	0.61	0.69	4.24
B78	2.89	0.56	0.65	1.06
B79	7.15	0.61	0.70	3.06
B80	3.18	0.55	0.72	1.26
B81	2.18	0.51	0.62	0.69
B82	12.61	728	0.66	6.12
B83a	13.22	695	0.68	6.28
B83b	13.44	786	0.67	7.13
B84a	1.94	828	0.78	10.0
B84a+C239	2.34	796	0.77	11.5
B84b	2.15	765	0.75	9.6
B84b+C239	2.30	847	0.78	12.7

2.3.5 The influential role of anchoring unit on benzothiadiazole derivatives
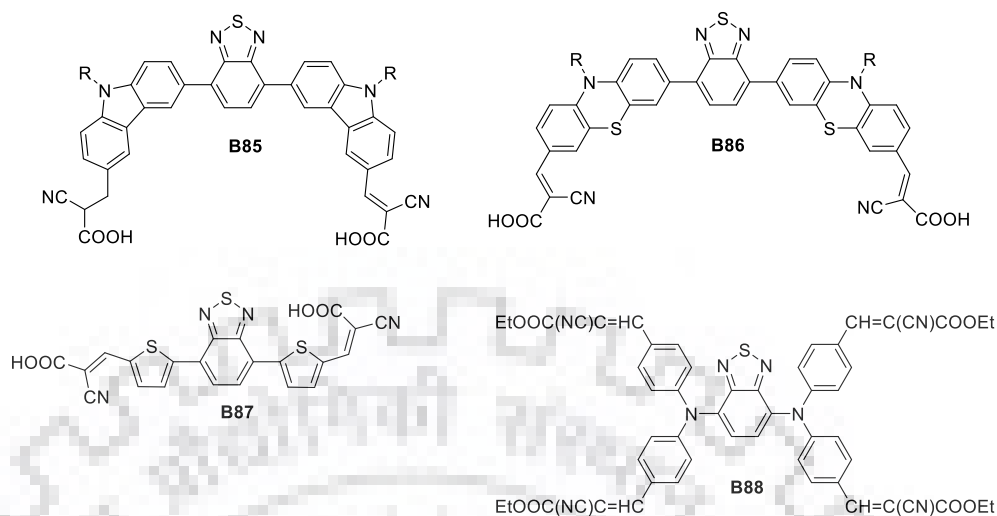
Figure 2.15. Di-anchoring and directly linked benzothiadiazole derivatives.

In designing the sensitizer, like other components anchoring unit also plays an essential role. The emphasis is mainly on the covering the broad absorption spectral range and light harvesting ability, achieved by extending conjugation. [78] The D-A interaction allows the dye adsorption on TiO_2 surface. The structural factors such as incorporation of two or more anchoring and donor groups help to strengthen the adsorption on the TiO_2 surface, improve the light absorbing ability, suppress the charge recombination, increase in electronic communication, enhance binding strength and improve overall performance of DSSCs. [78] Murali et al [79] reported A-D-π-D-A configured bent molecules **B85** and **B86,** where **B86** consisting of carbazole and phenothiazine moieties as electron donors with 2,1,3 benzothiadiazole as a π-linker with two end-anchoring groups. The dye **B86** exhibited bathochromic shift when compared to **B85** dye with 31 nm attributable to electron donating property of phenothiazine when compared to carbazole. Meanwhile, this resulted in high HOMO level (0.62 V *vs.* NHE). Under standard global AM 1.5 solar conditions, the **B86** sensitized solar cells exhibited a short circuit current density of 13.1 mA cm^{-2}, an open circuit voltage of 730 mV, a *FF* of 0.72, corresponding to an overall conversion efficiency of 6.87%. Mikroyannidis et al [80] reported bianchoring configured **B87,** which showed absorption maximum at 455 nm when recorded in THF. The device containing **B87** as sensitizer exhibited a short circuit current density of 7.72 mA cm^{-2}, an open circuit voltage of 0.65 V, a FF of 0.45, corresponding to an overall conversion efficiency of 2.42%. Shah et al. [81] reported **B88** the tetra-substituted anchoring group which showed absorption maxima at 545 nm and poor

photovoltaic performance with a short circuit current density of 0.23. mA cm^{-2}, a V_{OC} of 330 mV, and an *FF* of 0.38, corresponding to an overall conversion efficiency of 0.03%.
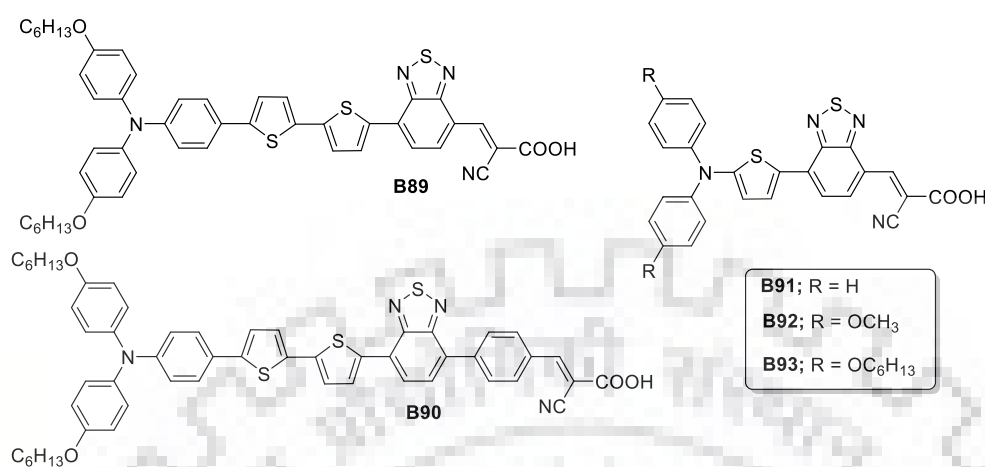
Figure 2.16. Di-anchoring and directly linked benzothiadiazole derivatives.

The linkage of anchoring group directly on benzothiadiazole nuclei shows significant impact on the performance of DSSC. For example, Haid et al [82] reported the dyes **B89** and **B90** containing triphenylamine as donor, oligothiophene as both donor and π-bridge, and benzothiadiazole/cyanoacrylic acid as acceptor that can be anchored to the TiO₂ surface. The geometry of molecule brings forth the impact of the additional phenyl group on the photophysical and photovoltaic performance. The dye **B89** exhibit bathochromic shift of 55 nm compared to **B90** in absorption this attributes to interference of electronic delocalization by non-planar phenyl spacer. The device containing the dyes **B89/B90** exhibited a short circuit current density of 3.40/18.47 mA cm^{-2}, an open circuit voltage of 489/640 mV, a FF of 0.74/0.69, corresponding to an overall conversion efficiency of 1.24/8.21%. The insertion of the phenyl ring increased the efficiency by 6.5 times and blocks the back electron transfer of the charge separated state, thus slowing down recombination processes by over 5 times, while maintaining efficient electron injection from the excited dye into the TiO₂. Similarly, Lin et al [83] reported **B91, B92** and **B93** containing various diarylthienylamine donors and a cyanoacrylic acid acceptor bridged by 2,1,3-benzothiadiazole acceptor. The dye **B93** exhibited bathochromic shift when compared to **B91, B92** attributable to appended hexyloxy chain on donor moiety which induce donor-acceptor interaction. Moreover, **B93** exhibited a short circuit current density of 11.10 mA cm^{-2}, an open circuit voltage of 450 mV, a *FF* of 0.63, corresponding to an overall conversion efficiency of 3.16%.
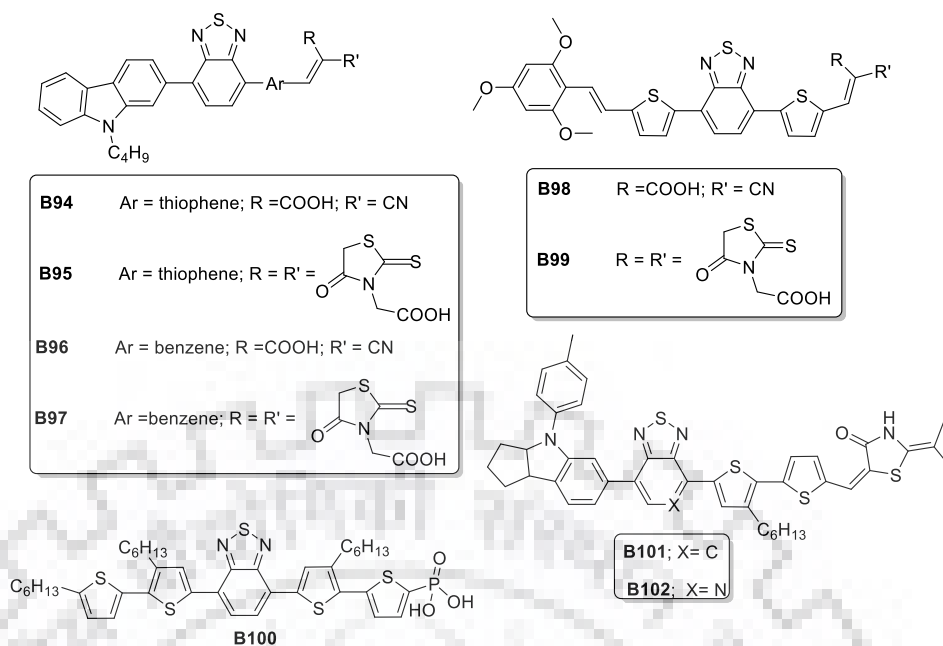
Figure.2.17. Structures of benzothiadiazole derivatives with different anchoring groups.

The anchoring groups are chemical substituent which enables the adsorption of dyes on TiO_2 substrate which acts as means for electron injection to initiate the electrical circuit in a DSSCs. Han et al[84] reported **B94-103** to study the effect of anchoring groups through comparison of different π-bridges and acceptors. The dye with thiophene (**B94** and **B95**) exhibited red shift when compared to phenyl spacer derivatives (**B96** and **B97**). Moreover, the dyes with rhodanine acetic acid acceptor (**B95** and **B97**) exhibit bathochromic shift compared to cyanoacetic acid acceptor derivatives (**B94** and **B96**) attributes to better π-conjugation. However, the device containing the dye **B96** with benzene bridge and cyanoacetic acid acceptor showed the most efficient photoelectricity conversion efficiency and has the maximum power conversion efficiency of 5.40% with open circuit voltage of 710 mV, short circuit current density of 10.99 $mAcm^{-2}$, and *FF* of 0.71 under simulated AM 1.5 irradiation. By following the same idea the effect of anchoring group was investigated further, where Elmorsy et al [85] reported **B98** and **B99**, and encountered the similar behavior as above, **B99** exhibited bathochromic shift when compared to **B98** the acrylic acid anchoring derivative by 13 nm attributed to the greater conjugation of the 4-oxo-2-thioxothiazolidine ring compared with the cyanoacetic unit. The device containing dye **B98/B99** exhibited a short circuit current density of 15.27/8.7 mA cm^{-2}, a open circuit voltage of 0.61/0.56 V, a *FF* of 65.12/64.65, corresponding to an overall conversion efficiency of 6.03/3.2%.

Stadler et al. [86] reported **B100** oligothiophene with benzothiadiazole functionalized with phosphonic acid group for anchoring onto TiO_2 substrate exhibited absorption maxima at 504 nm in chloroform. The dye exhibited photovoltaic performance with a short circuit current

density of 13.4. mA cm^{-2}, an open circuit voltage of 700 mV, and an *FF* of 0.68, corresponding to an overall conversion efficiency of 6.40% using electrolyte composition 0.1 M LiI +. 0.5M TBP. Further, Islam et al.[87] demonstrated the consensitization of **B100** which has enhanced the efficiency from 6.40% to 7.7% with HSQ4 cis-configured squaraine rings oligothiophene with benzothiadiazole functionalized with phosphonic acid group for anchoring onto TiO$_2$ substrate exhibited absorbance maxima of 504 nm in chloroform. The dye exhibited photovoltaic performance with a short circuit current density of 18.09 mA cm^{-2}, a open circuit voltage of 0.58, and an *FF* of 0.73, corresponding to an overall conversion efficiency of 7.77 % using electrolyte composition 0.1 M LiI +. 0.5M TBP.

Table 2.11. Photophysical and electrochemical properties of the compounds **B85-B94**

Dye	λ_{abs} (nm) (ε (1x10^{-3} M^{-1} cm^{-1}))	λ_{em} (nm)	E_{0-0} [b](eV)	E_{OX}[c] (V *vs* NHE)	E^*_{OX}[d] (V *vs* NHE)	HOMO /LUMO	λ_{em}^{TiO2} (nm)
B85[a]	440(29.4)	560	2.36	0.91	-1.45	-	456
B86[a]	471(27.8)	592	2.18	0.62	-1.56	-	482
B87[d]	455	565	2.17	-	-	-5.45/-3.20	443
B88	545	-	1.29	-	-	-5.39/-4.10	-
B89[f]	395,570	681	1.60	-	-	-5.22/-3.62	-
B90[f]	392, 515	665	1.67	-	-	-5.14/-3.47	-
B91[f]	613	-	1.74	1.02	-0.72	-	513
B92[f]	650	-	1.65	0.87	-0.78	-	548
B93[f]	654	-	1.64	0.87	-0.77	-	547
B94[g]	486	593	2.28	-	-	-5.5[a]/-3.27	463

[a] Absorption and emission spectra were measured in DMF. [b]E_{0-0} was determined from the intersection of absorption and emission spectra in THF. [d] Absorption and emission spectra were measured in THF. [c] Ground state oxidation potentials of dyes on TiO$_2$ were measured in ACN with 0.1 M TBAPF6 and scan rate of 50 mV s1 (calibrated with Fc/Fc^{+3} as an external reference and converted to NHE by addition of 0.63 V). [d] Excited-state oxidation potentials were calculated according to E_{OX}-E_{0-0}. [f] Absorption and

emission spectra were measured in DCM.[g] Absorption spectra were measured in CH_3OH: $CHCl_3$ cosolvent (1:10).

Table 2.12. Photophysical and electrochemical properties of the compounds **B95-B102**

Dye	λ_{abs} (nm) (ε (1×10^{-3} M^{-1} cm^{-1}))	λ_{em} (nm)	E_{0-0} [b](eV)	E_{OX}[c] (V *vs* NHE)	E^*_{OX}[d] (V *vs* NHE)	HOMO /LUMO	λ_{em}^{TiO2} (nm)
B95	507	596	2.19	-	-	-5.4[a]/-3.23	480
B96	441	568	2.47	-	-	-5.5[a]/-3.06	391
B97 [g]	446	572	2.46	-	-	-5.4[a]/-3.03	397
B98 [a]	382,545	700	1.93	-	-	-5.47/-3.54	-
B99 [a]	368,558	708	1.89	-	-	-5.49/-3.54	-
B100	504 (21)	-	2.04			-5.50/-3.55	-
B101[f]	538 (35.3)		1.94	0.70	-1.24	-	-
B102[f]	582 (31.5)		1.78	0.68	-1.10	-	-

[a] Absorption and emission spectra were measured in DMF. [b] E_{0-0} was determined from the intersection of absorption and emission spectra in THF. [d] Absorption and emission spectra were measured in THF. [c] Ground state oxidation potentials of dyes on TiO_2 were measured in ACN with 0.1 M TBAPF6 and ascan rate of 50 mV s1 (calibrated with Fc/Fc^{+3} as an external reference and converted to NHE byaddition of 0.63 V). [d] Excited-state oxidation potentials were calculated according to E_{OX}-E_{0-0}. [e] DCM solution derived from CPCM-TDDFT/6-31+G(d,p) calculations [f] Absorption and emission spectra were measured in DCM.

Conversely, later **B53** was grafted with 2-(1,1-dicyanomethylene)rhodanine (DCRD) anchoring group and reported as **B101**, they both showed similar absorption maxima with interesting electroluminescence properties. Moreover, the dye **B102** designed with incorporation of pyridine unit which increased the electron withdrawing nature thus reduced the HOMO LUMO band gap compared to other derivatives, which enhances the facile electronic conjugation. The dye **B102** exhibited bathochromic shift compared to dye which lacks benzothiadiazole unit and **B101** with 78 nm and 44 nm, respectively. The device containing dye

B101 exhibited photovoltaic performance with short circuit current density of 16.73 mA cm^{-2}, a open circuit voltage of 5071 mV, and an *FF* of 0.71 corresponding to an overall conversion efficiency of 8.53% with coadsorbent CDCA (10×10^{-3} M).[[88]

From the above discussion, it is clear that the presence of benzothiadiazole as an auxiliary acceptor in improving the photophysical, electrochemical and light harvesting capacity of sensitizer. The benzothiadiazole derivatives excelled as sensitizer with promising efficiency of 9.04 and 13% in the solar cells with iodine and cobalt redox electrolytes, respectively. In general, the indoline-benzothiadiazole and cyclopentadithiophene-benzothiadiazole based derivatives have approached to benchmark efficiency. Thus, benzothiadiazole containing molecules can be extensively implemented for commercial applications.

Table 2.13. Photovoltaic properties of the compounds **B85-B102**

Dye	J_{SC} (mA cm^{-2})	V_{OC} (mV)	*FF* (%)	PCE (%)
B85[a]	7.51	0.762	0.76	4.35
B86 [a]	13.1	0.728	0.72	6.87
B87[b]	7.72	0.65	0.45	2.42
B87[c]	10.34	0.71	0.51	3.6
B88	0.236	330	38	0.03
B89	3.40	489	0.74	1.24
B90	18.47	640	0.69	8.21
B91[e]	0.31	0.28	0.45	0.039
B91[f]	9.12	0.41	0.62	2.30
B92[e]	0.42	0.25	0.45	0.045
B92[f]	13.06	0.39	0.62	3.13
B93[e]	0.44	0.30	0.45	0.059
B93[f]	11.10	0.45	0.63	3.16
B94	12.08	0.61	0.69	5.07
B95	4.12	0.56	0.71	1.65
B96	10.99	0.71	0.69	5.40
B97	6.98	0.63	0.87	3.81
B98 (10mM)	15.27	0.61	65.12	6.03
B99 (10mM)	8.7	0.56	64.65	3.2
B100	13.4	700	68	6.40
B100+HSQ$_3$	17.21	611	67	7.05

B100+HSQ₄	18.09	580	73	7.77
B101+CDC A (10X10⁻³)	16.73	0.71	71.26	4.02
B102 +CDCA (10X10⁻³)	11.01	0.54	67.13	8.53

[a]The cell employed 4.8 mm transparent and 4.2 mm scattering TiO_2 layers, the electrolyte solution was 0.05 M I_2, 0.1 M LiI, 0.6 M DMPII, and 0.5 M TBP in acetonitrile. I-V measurements were performed under simulated AM 1.5G 1 sun illumination. The size of the electrode was 0.12 cm[2b]FTO/TiO_2-BTD/polymer electrolyte/PEDOT:PSS coated FTO [c]FTO/ZTO-BTD/polymer electrolyte/PEDOT:PSS coated FTO [e] The composition for the EL1 electrolyte is: 0.6 M 1-butyl-3-methylimidazoliumiodide (BMII), 0.05 M LiI, 0.03 M I_2, 0.5 M 4-tert-butylpyridine (TBP), and 0.1 Mguanidinium thiocyanate in a mixture of acetonitrile and valeronitrile (85/15, v/v). [f] The composition for the EL2 electrolyte is: 0.6 M 1,2-dimethyl-3-propylimidazolium iodide (DMPII), 0.05 M LiI, 0.03 M I_2 in acetonitrile

2.4 Benzothiadiazole Based Small Molecules in OLEDs

OLED is promising technology for future lighting, as OLEDs are self-illuminating, less power consuming and disposable, thus growing rapidly in the lighting market. Several remarkable properties like extremely thin, flexible, varying sizes and shapes, transparency like window and reflective like mirror made OLEDs much more attractive in the field of lighting technology. It is prominently used in high quality flat panel displays and lighting applications.[89] The organic molecules form the electroluminescent layer which undergoes organized molecular engineering resulting in intense electroluminescence, which preferably improves the performance of OLED. Interestingly, tuning of molecules with different chromophoric units transcends the material to display gamut of colors.[90] The full color display consists of red, blue and green light emitting materials. Likewise, the benzothiadiazole based bipolar molecules explored the wide range of green to red regions in organic materials as emitters. [91]

2.4.1 Benzothiadiazole Based Red Emitters.

The emitters with long wavelength, high brightness and good color fidelity, are in great demand. Therefore, to design red emitting materials with standard red CIE coordinates (0.67, 0.33), the molecules are required to possess elongated conjugation or strong charge transfer character. Similarly, when a strongly conjugated benzothiadiazole moiety is introduced, which

allows the molecule to narrow the molecular band gap, thus strategically fulfils the designing for red emitters.

However, the red emitting dyes faced serious problem of concentration quenching of electroluminescence because of their polarity and inherent tendency to aggregate via π-π interaction. [92] So to cope up the adverse effect of non-radiative decay doping was adopted which provides the balanced charge transport and restriction of recombination zone in emitting layer. Some of the molecules, however, are designed to omit doping in order to show better performance. Figure 2.18 shows some of the examples of red emitting benzothiadiazole derivatives.
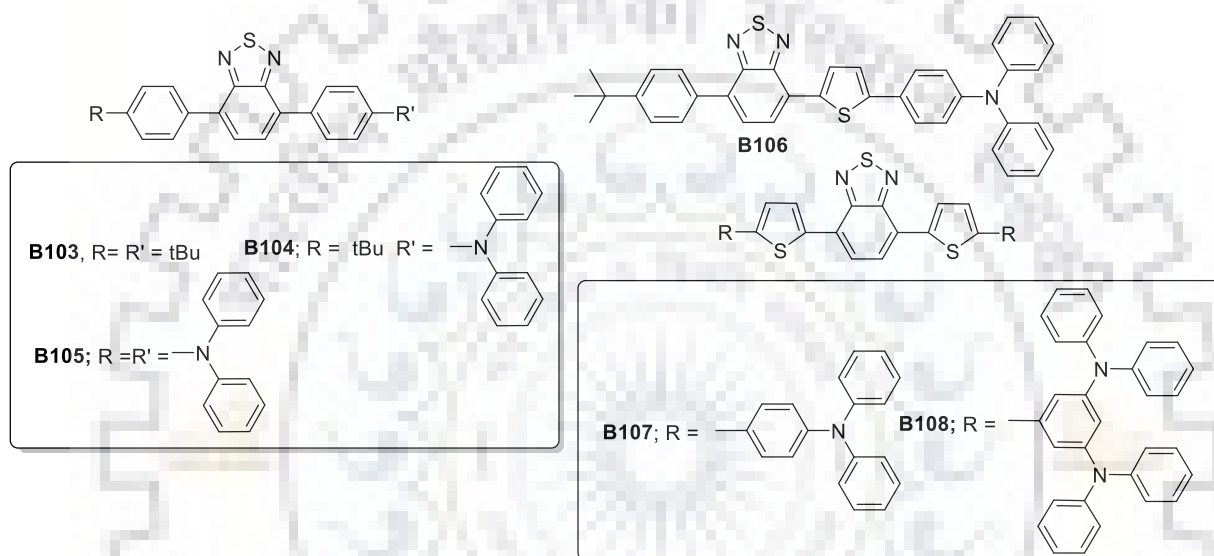
Figure 2.18. Benzothiadiazole conjugates as red emitters.

Thomas et al [93] reported bipolar red emitting materials containing benzothiadiazole with pheripheral substitution of diarylamine and *tert* butyl phenyl (**B103-B108**). The molecules **B103-B108** exhibit remarkable thermal decomposition temperature of 405, 410, 460, 428 °C, respectively attributable to their rigid and bulky substitution of triphenylamine derivatives. The device configured with ITO/**B105, B106, B108** (40nm)/TPBI (40nm)/Mg/Ag showed much improved electroluminescent characteristics with turn-on voltage of 2.5/3.2/3.0 V, maximum current efficiency of 4.4/0.91/2.0 cd A^{-1} maximum luminescence of 31807 /8087/9138 cd m^{-2}, respectively.

In order to suppress aggregation and emphasize on improving luminescence, the degree of functionality has been increased which also participate well in enhancing thermal and morphological stability. Thus, Huang et al. [94] reported **B109** and **B110** based on double end-capped 4,7-di(thiophen-2-yl)-2,1,3-benzothiadiazole and 4,7-di(4-hexylthiophen-2-yl)-2,1,3-benzothiadiazole, respectively. They showed attractive thermal stabilities with high decomposition temperatures over 400 °C. The double-layered devices with configuration

[ITO/PEDOT:PSS/PVK/**B109**:MEHPPV (80:20)/Ba/Al] and [ITO/PEDOT:PSS/PVK/**B110**:P-PPV(64:36)/Ba/Al] showed electroluminescent characteristics with low turn-on voltage of 3.8 V and EQE of 2.1 % (890 cdm^{-2}) with CIE coordinates (0.69, 0.30) for **B109**; and turn on voltage of 4.3 V and EQE of 1.82% with brightness of 1960 cdm^{-2} higher than that of **B109** (CIE = 0.65, 0.34) for **B110**.

Table 2.14. Device performance of OLEDs fabricated using **B103-B108**

Dye	λ_{max} (nm)	λ_{em} (nm) $\Phi_F{}^a$ (%)	Turn-on voltage	EQE (%)	Current efficiency	Maximum luminance	λ_{EL} (nm)
	DCM	DCM	(V)		(cdA^{-1})	(cdm^{-2})	
B103	389	512 (51)	-	-	-	-	-
B104	436	630 (75)	-	-	-	-	-
B105	459	639 (78)	2.5	2.1	4.4	31807	602
B106	472	665 (27)	3.2	0.99	0.91	8087	640
B107	529	695 (14)	-	-	-	-	-
B108	489	632 (50)	3.0	1.7	2.0	9138	626

^{a} Flourescence quantum yields

^{b}ITO/**B103-B108** (40nm)/TPBI (40nm)/Mg:Ag

^{c}At 100 mA cm^{-2}

Table 2.15. Device performance of OLEDs fabricated using **B109 and B110**

Dye	λ_{max} (nm)	λ_{em} (nm), Film $\Phi_F{}^a$ (%)	HOMO^b /LUMO	Turn-on voltage	EQE (%)	Maximum luminance	λ_{EL} (nm)	CIE
	DCM	DCM		(V)		(cd m^{-2})		
B109	512	627,655 672 (0.93)	-5.12/-3.06	3.8	2.1	890	635	(0.69, 0.30)
B110	486	613,656 630 (0.58)	-5.36/-3.18	4.3	1.8	1960	637	(0.65, 0.34)

^{a}Quantum yields were measured in DCM (1.0×10^{-6} mol L^{-1}) using rhodamine B in ethanol as the reference (φr) 0.64. ^{b}Derived from onset oxidation voltages using Ag/AgCl as reference electrode and ferrocene as internal standard. ^{c}ITO/PEDOT:PSS/PVK/**B110**:P-PPV(64:36)/Ba/Al.
^{d}At 1 cd m^{-2}

Due to better visual sensitivity, the current efficiency of **B110** was 1.23 cd A^{-1} with respect to 0.37 cd A^{-1} of **B109** while their external device efficiencies were very close under the same current. Further the same group reported **B110** as emitter and fabricated with different

45

architecture , where the device with configuration MoO_3 (HIL) 6 nm/NPB (HTL) 100 nm/130 nm/Alq_3 (ETL) 30 nm/LiF(1.5 nm) /Al(200 nm) exhibited better performance with turn on voltage of 2.9 V, current efficiency of 3 cd A^{-1} , however at a current density of 19 mA cm^{-2} it showed , turn-on voltage 6.9 V, current efficiency of 2.2 cd A^{-1} and luminescence of 402 cd m^{-2}. [95] Moreover, the same group introduced **B111** by replacing *n*-hexyl substituent with 4-*sec*-butoxyphenyl which enhanced the thermal stability and amorphous morphology with transition glass temperature (T_g) of 137.8° C higher than earlier reported for **B110** (82.8° C). The dyes have been fabricated with configuration ITO/PEDOT:PSS (50 nm)/**B111** (45 nm)/Ba (4 nm)/Al (120 nm) and ITO/PEDOT:PSS (50 nm)/PVK (40 nm)/ **B111** (45 nm)/Ba (4 nm)/Al(120 nm). The dye with two layered configuration of device with PVK which acts as electron-blocking/hole-transporting layer showed four fold increase of the current efficiency up to 2.1 cd A^{-1}, corresponding to EQE of 2.74 % and CIE coordinates (0.64, 0.35). [96]

Table 2.16. Device performance of OLEDs fabricated using **B110**

Dye	λ_{max} (nm) DCM	λ_{em} (nm), Φ_F^a (%) DCM	HOMO/ LUMO[b]	Turn-on voltage (V)	Current efficiency (cd A^{-1})	Maximum luminance (cd m^{-2})	λ_{EL} (nm)
B110	486	613 (0.58)	-5.4/ -3.2	6.7[c]/6.9d[c] /7.5[e]	2[c] /2.2[d] /1.6[e]	379[c] /402[d] /309[e]	630

[a]rhodamine B in ethanol.

[b]cyclic voltammetry in DCM/ACN (5:1) in the presence of *n*-Bu_4NPF_6 as electrolyte, using Ag/AgCl as the reference electrode and ferrocene as an internal standard.

[c]**D1** = MoO_3 (HIL) 6 nm/NPB(HTL) 70 nm / 130 nm / Alq3 (ETL) 30 nm / LiF(1.5 nm) /Al(200 nm)

[d]**D2** = MoO_3 (HIL) 6 nm/NPB(HTL) 100 nm / 130 nm / Alq3 (ETL) 30 nm / LiF(1.5 nm) /Al(200 nm)

[e]**D3** = MoO_3 (HIL) 6 nm/NPB(HTL) 100 nm / 130 nm / BCP(HBL)10 nm/Alq_3 (ETL) 20 nm / LiF(1.5 nm) /Al(200 nm) [f]At 19 mA cm^{-2}

Table 2.17. Device performance of OLEDs fabricated using **B111**

Dye	λ_{max} (nm) DCM	λ_{em} (nm) Φ_F^a (%) DCM	Film	Turn-on voltage (V)	EQE (%)	Current efficiency(cd A^{-1})	Maximum luminance (cd m^{-2})	λ_{EL} (nm)	CIE
B111	491	609 (0.44)	622 (0.6)	-	2.74	2.1	-	632	(0.64, 0.35)

[a]ITO/PEDOT:PSS(50 nm)/PVK(40 nm)/ **B111** (45 nm)/Ba (4 nm)/Al(120 nm) [b]At 1 cd m^{-2}
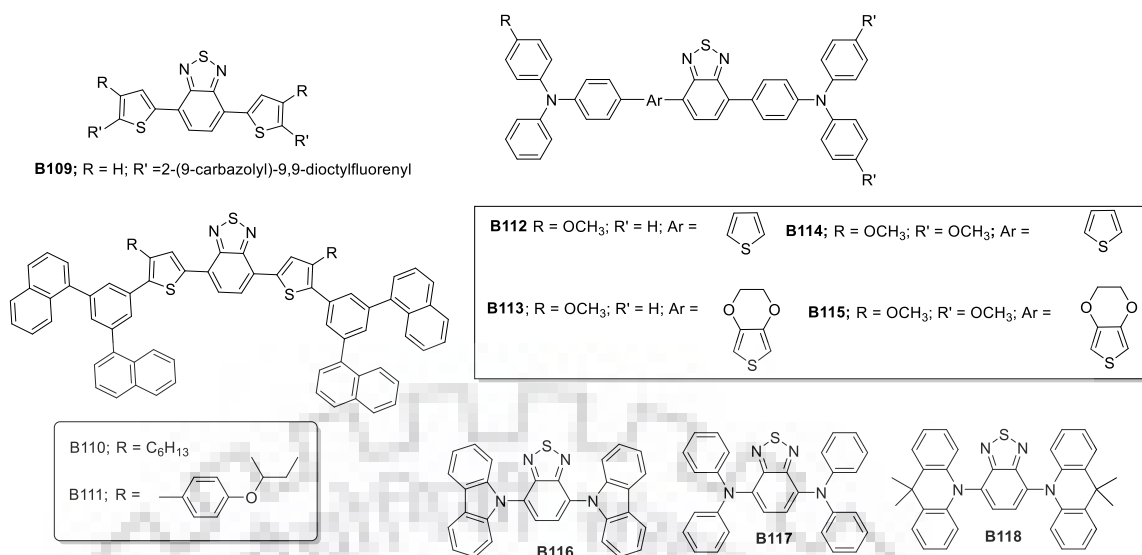
Figure 2.19. Benzothiadiazole derivatives incorporated with different donors.

Table 2.18. Device performance of OLEDs fabricated using **B113-B115**

Dye	λ_{max} (nm)	λ_{em} (nm) $\Phi_F{}^a$(%)	Turn-on voltage[c] (V)	Power efficiency (lm W^{-1})	Current efficiency (cd A^{-1})	Maximum luminance (cd m^{-2})	λ_{EL} (nm)	CIE
	TOL	TOL						
B113	519	640 (37)	4.5[a]/6.5	1.62[a]/0.80[b]	3.10[a]/2.29[b]	6115[a]/2792[b]	636	(0.64, 0.33)
B114	511	630 (49)	4.5[a]/6.5[b]	3.14[a]/1.15[b]	5.50[a]/3.83	10800[a] /5393[b]	624	(0.63, 0.35)
B115	529	650 (31)	5.0[a]/6.5[b]	0.87[a]/0.57[b]	2.05[a]/1.71[b]	3395[a]/2193[b]	652[b]	(0.65, 0.32)

[a]ITO/PEDOT:PSS/ **B113-B115**/Ca/Al [b]ITO/PEDOT:PSS/ **B113-B115**/PF-EP/LiF/Al

[c]At 1.0 cd m^{-2}

Chen et al [97] reported benzothiadiaozle derivatives **B112**, **B113, B114** and **B115** as red dopant units with polyfluorene acting as blue host. The different electron donating ability of the donor unit constructed the dopant/host system. The device with configuration ITO/PEDOT:PSS/**B113-B115**/Ca/Al showed saturated red emission at 636 nm with a luminous efficiency of 2.29 cd A^{-1} and CIE of (0.64, 0.33) for **B113.** Similarly, **B114** exhibited pure red emission at 624 nm with a luminous efficiency of 3.83 cd A^{-1} and CIE of (0.63, 0.35) for respectively. Furthermore, the configuration was modified by introducing PF-EP (Ethanol solublephosphonate-functionalized polyfluorene) as an additional electron injection layer. The device with configuration (ITO/PEDOT:PSS/**B113-B115**/PF-EP/LiF/Al) showed high

performance with maximum current efficiencies of 5.50 cd A^{-1} and CIE of (0.62, 0.35) for **B114**, 3.10 cd A^{-1} and CIE of (0.63, 0.33) for **B113**, respectively.

Table 2.19. Device performance of OLEDs fabricated using **B116-B118**

Dye	λ_{max} (nm) TOL	λ_{em} (nm) TOL	Film / $\Phi_F{}^a$ (%)	Turn-on voltage (V)	Power efficiency (lm W^{-1})	Current efficiency (cd A^{-1})	Maximum luminance (cd m^{-2})	λ_{EL} (nm)
B116	455	559	578/ 0.54	-	-	-		-
B117	482	638	636/ 0.57	3.7	10.8	11	2980	636
B118	510	648	661/ 0.27	-	-	-		-

^{a}PL quantum yields in neat films.

^{b}ITO/MoO3 (8 nm)/TAPC(50 nm)/mCP (10 nm)/3 wt% **B117**:CBP (20 nm)/TmPyPB(40 nm)/LiF/Al

^{c}At 100 cd m^{-2}

Table 2.20. Device performance of OLEDs fabricated using **B119** and **B120**

Dye	λ_{em} (nm) $\Phi_F{}^c$(%) DCM	Turn-on voltage (V)	Power efficiency (lmW^{-1})	Maximum current efficiency (cdA^{-1})	Maximum luminance (cdm^{-2})	λ_{EL} (nm)	CIE
B119^a	536 (0.84)	3.5	4.1	5.7	6901	534	(0.34,0.62)
B120^a	611 (0.62)	3.0	0.3	0.5	2210	628	(0.62,0.38)
B119^b	-	2.5	20.7	31.6	9226	534	(0.34,0.61)
B120^b	-	7.5	2.3	7.2	1136	628	(0.62,0.36)

^{a}ITO/PEDOT:PSS/ **B119**or **B120** (spin-coating)/Ba(10 nm)/Al(100 nm)

^{b}ITO/PEDOT:PSS/ **B119** or **B120** (spin-coating)/ TPBi(30–60 nm)/LiF(0.5 nm)/Al(100 nm)

^{c}Measured in an integrated sphere in DCM

Ni et al [98] reported D–A–D structured molecules, **B116, B117, B118** with different electron donating group**.** All the molecules showed high thermal stability with decomposition temperature of 389 °C for **B117**, 340 °C for **B116**, 381 °C for **B118**. The device configured as ITO/MoO3 (8 nm)/TAPC(50 nm)/mCP (10 nm)/3 wt% **B118**:CBP (20 nm)/TmPyPB(40

nm)/LiF/Al exhibited maximum external quantum efficiency of 8.8% at a maximum luminance of 2980 cd m^{-2} with the emission peak at 636 nm.
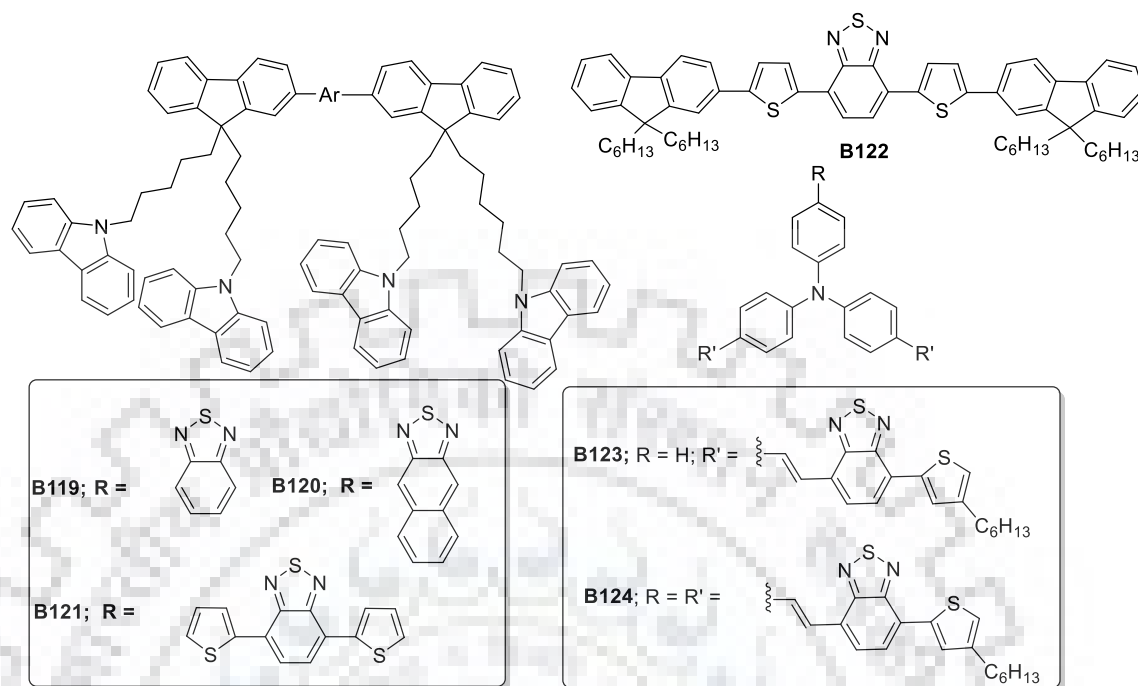
Figure 2.20. Benzothiadiazole derivatives containing peripheral functionalities.

Furthermore, to tune the emissive properties of organic materials Zhang et al [99] reported **B119** benzothiadiazole derivatives with four alkyl-linked peripheral carbazole groups. Interestingly on replacing benzothiadiazole to napthobenzothiadiazole unit (**B120**) the dye showed spectral shift to red region and displayed **B120** as red emitter. The carbazole attachments induce the dyes to be more thermally stable (~ 400 °C) and amorphous with glass transition temperature (T$_g$) of 85 °C and 89 °C for **B119** and **B120** respectively**.** The dyes are configured with ITO/PEDOT:PSS/**B119** or **B120** (spin-coating)/Ba(10 nm)/Al(100 nm) structure. The **B119** based device showed a maximum electroluminescence around 534 nm with the CIE coordinates of (0.34, 0.62) and the **B120** exhibited a maximum electroluminescence at 628 nm and CIE coordinates of (0.62, 0.38). The dyes fabricated with double layered device with configuration ITO/PEDOT:PSS/ **B119** or **B120** (spin-coating)/TPBi (30–60 nm)/LiF(0.5 nm)/Al(100 nm). Here, **B119** exhibited a maximum brightness of 9226 cd m^{-2}, current efficiency of 31.6 cd A^{-1} and power efficiency of 20.7 lm W^{-1} and **B120** also significantly improved the performance with a maximum brightness of 1136 cd m^{-2}, luminous efficiency of 7.2 cd A^{-1} and power efficiency of 2.3 lm W^{-1}. Consequently, Wang et al [100] tuned the green emitting dye **B119** to be employed as red emitter by introducing dithienylbenzothiadiazole unit resulting in **B121.** The peripheral carbazole attachment in the

dye attributes to its high thermal and morphology stability with T_d of 486 °C and T_g of 90 °C. The dyes were fabricated as emitter in device architecture of ITO/PEDOT (80 nm)/**B121** (45 nm)/LiF (0.5 nm)/Al (120 nm) which exhibits a maximum luminance efficiency of 0.10 cd A^{-1}, corresponding to an external quantum efficiency of 0.27% twice of dye **B122** (0.10 %).This may be due to the introduction of carbazole groups which increases the hole injection and transport ability and results significant improvement of the electroluminescent performance of **B121.** On introducing hole blocking layer TPBi the device showed improved external quantum efficiency to 0.93% with a maximum luminance of 932 cd m^{-2}, a maximum current efficiency of 0.22 cd A^{-1}.

Table 2.21. Device performance of OLEDs fabricated using **B121-B122**

Dye	λ_{max} (nm) THF	λ_{em} (nm) THF	Film	Turn-on voltage (V)	EQE (%)	Current efficiency (cdA^{-1})	Maximum luminance (cdm^{-2})	λ_{EL} (nm)	CIE
B121[a]	510	603	643	6.0	0.27	0.10	45	652	(0.65, 0.33)
B121[b]	-	-	-	4.0	0.93	0.22	932		(0.70 0.30)
B122[a]	510	618	637	5.5	0.10	0.05	81	668	(0.69, 0.31)

[a]ITO/PEDOT (80 nm)/**B121** (45 nm)/LiF (0.5 nm)/ Al (120 nm)
[b]ITO/PEDOT/**B121**/(TPBi)/LiF (0.5 nm)/Al (100 nm)

Table 2.22. Device performance of OLEDs fabricated using **B123** and **B124**

Dye	λ_{em} (nm) Film	Turn-on voltage (V)	Current efficiency (cd A^{-1})	Maximum luminance (cd m^{-2})	λ_{EL} (nm)	CIE
B123[a]	646	2.9	0.235	1855	628	(0.64,0.30)
B124[a]	657	2.2	0.53	7278	640	(0.66,0.28)
B123[b]	646	2.2	0.53	3186	642	(0.64,0.29)
B124[b]	657	2.0	0.91	7794	649	(0.64,0.29)

[a]Device A. ITO/PEDOT:PSS (30 nm)/ PVK (30 nm)/ **B123-B124** (60 nm)/Ca(10 nm)/Al(120 nm),
[b]Device B. ITO/PEDOT:PSS (30 nm)/ PVK:poly-TPD (1:1) (30 nm)/ **B123-B124** (60 nm)/Ca(10 nm)/Al(120 nm),

The molecule's substitution pattern influence thermal and morphological stability and also optical band gap. For example, Jing et al [101] reported dyes containing triphenylamine as core and attached with benzothiadiazole-(4-hexyl)thiophene peripherally The dyes are peripherally attached with two benzothiadiazole-(4-hexyl)thiophene unit named as **B123** and **B124** contains three arms of benzothiadiazole-(4-hexyl)thiophene units. The dyes showed pure red-emission peaked at 646 and 657 nm, respectively. The **B124** exhibited as red emitter with a higher maximum luminance of 7794 cdm^{-2} and a maximum current efficiency of 0.91 cdA^{-1}.
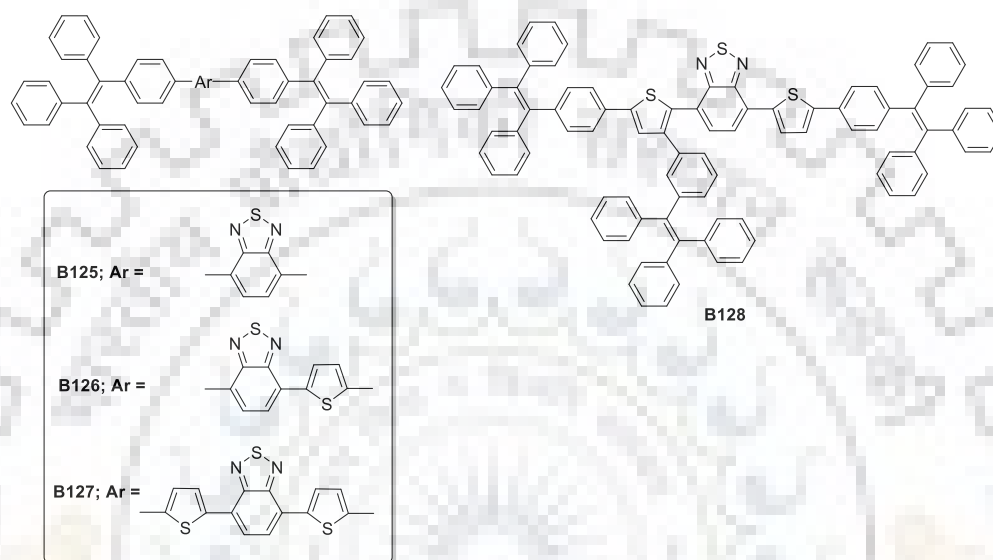
Figure 2.21. Benzothiadiazole-tetraphenylethylene conjugates.

Table 2.23. Device performance of OLEDs fabricated using **B125- B127**

Dye	λ_{max} (nm) THF	λ_{em} (nm) THF	$\Phi_F{}^a$(%) Film	Turn-on voltage (V)	EQE (%)	Current efficiency (cd A^{-1})	Maximum luminance (cd m^{-2})	λ_{EL} (nm)
B125	418	538 (61)	539 (89)	3.9	1.5	5.2	13540	540
B126	464	592 (37)	600 (55)	5.4	3.1	6.4	8330	592
B127	510	623 (25)	661	4.4	1.0	0.4	1640	668

^{a}ITO/NPB (60 nm)/**B125-B127** (20 nm)/TPBi (10 nm)/Alq3 (30 nm)/LiF (1 nm)/Al (100 nm).

^{b}At 1 cd m^{-2}

Moreover, the non-planar moiety has also showed the high influence on thermal and morphological stability and participates well in increasing the conjugation. Zhao et al [102] reported tetraphenylethylene substituted heterocyclic dyes (**B125, B126, B127**). The molecules

51

are highly thermal and morphologically stable with decomposition temperature in the range of 429–495 °C and glass-transition temperatures at 130–221 °C. The T_d and T_g are higher than the dyes with similar core and triphenylamine end-cappers (**B130** and **B131**). The devices made as ITO/NPB (60 nm)/**B125-B127** (20 nm)/TPBi (10 nm)/Alq$_3$ (30 nm)/LiF (1 nm)/Al (100 nm) where NPB work as hole transporting, TPBi as hole-blocking and Alq$_3$ as electron-transporting layers, respectively. The device based on **B125** showed a maximum luminescence of 13540 cd m^{-2}, a maximum current efficiency of 5.2 cd A^{-1}, and a maximum external quantum efficiency of 1.5%. The device of **B126** exhibited better performance radiating orange-red electroluminescence with EQE of 3.1% (8330 cd m^{-2}, 6.4 cd A^{-1}) which are much higher than the values attained by most non-doped fluorescent red OLEDs where **B127** exhibits red electroluminescence at 668 nm, with maximum brightness of 1640 cd m^{-2} and EQE of 1.0%.

Further, the same group reported **B128** by attaching laterally an additional tetraphenylethylene unit to the **B127** core to explore the phenomenon of aggregation induced emission more effectively. The steric effect lowered the molecular conjugation however enhanced the thermal and morphological stability (T_d = 465 °C and T_g = 174 °C) when compared to reported **B127**. The molecule fabricated as emitter in ITO/NPB (60 nm)/**B128** (20 nm)/TPBi (40 nm)/LiF (1 nm)/Al (100 nm) where NPB works as hole transporting layer and TPBi as electron transporting layer. The configuration showed red luminophore with CIE of (0.67, 0.32) emissions at 650 nm, and high brightness of 3750 cd m^{-2} and EQE of 3.7%. Moreover, the nanoparticles of **B128** are presented as promising fluorescent visualizers for cellular imaging with low cytotoxicity.[103]

Table 2.24. Device performance of OLEDs fabricated using **B128**

Dye	λ_{max} (nm)	λ_{em} (nm) $\Phi_F{}^a$(%)	Film	Turn-on voltage (V)	EQE (%)	Current efficiency (cd A^{-1})	Maximum luminance (cd m^{-2})	λ_{EL} (nm)	CIE
	THF	THF							
B128	490	620 (18)	646	4.2	3.7	2.4	3750	650	(0.67, 0.32).

^{a} rhodamine B

^{b}ITO/NPB (60 nm)/**B128** (20 nm)/TPBi (40 nm)/LiF (1 nm)/Al (100 nm)
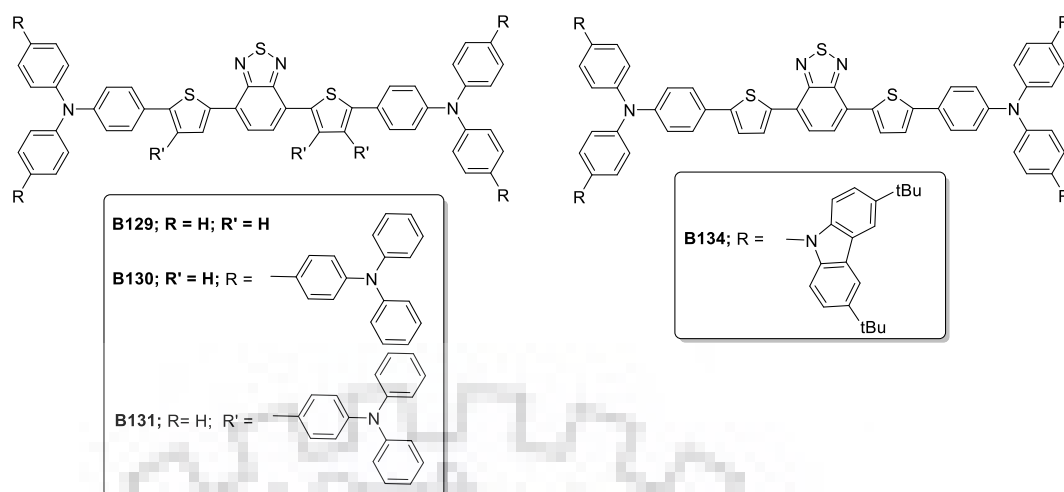
Figure 2.22. Multi-substituted benzothiadiazole derivatives.

Table 2.25. Device performance of OLEDs fabricated using **B129- B131**

Dye	λ_{max} (nm)	λ_{em} (nm)	Film	Turn-on voltage	Current density	Current efficiency	Maximum luminance	λ_{EL} (nm)	CIE
	DCM			(V)	(mA cm^{-2})	(cd A^{-1})	(cd m^{-2})		
B129	528	643	670	3.0/5.8	826	6.25	16827	656	(0.67, 0.33)
B130	503	641	646	3.2/4.6	995	4.22	17716	662	(0.66, 0.33)
B131	540	650	651	3.3/6.4	935	1.79	6552	675	(0.69, 0.31)

[a]ITO/PEDOT:PSS/**B129-B131**/BCP/LiF:Al.

[b]At 1 cd m^{-2}

[c]At 100 cd m^{-2}

The introduction of bulky group favors the thermal and morphological stability and renders the aggregations by avoiding π-π stacking. Likewise, Thangthong et al [104] reported **B129, B130, B131** containing triphenylamine units substituted at different positions which helps to tune up the emission to pure red. The bulky substitution also helps in reducing luminance quenching by preventing aggregation of the planar conjugated core as well as improves the hole transporting capability, thermal stability and solubility of the molecule. This robust design results high thermal stability for **B129** (365 °C), **B130** (370 °C), **B131** (430 °C), and high T$_g$ in the range of 156-176 °C which provides good morphology for materials. Fabricating these materials with configuration ITO/PEDOT:PSS/**B130-B131** (spin coating)/BCP/LiF:Al resulted an improved performance as BCP layer balances the charge injection and increase the

53

probability of electron holes recombination at EML layer. The device showed excellent luminance efficiency of 6.25 cd A^{-1} and a pure red emission with CIE coordinates of (0.67, 0.33).
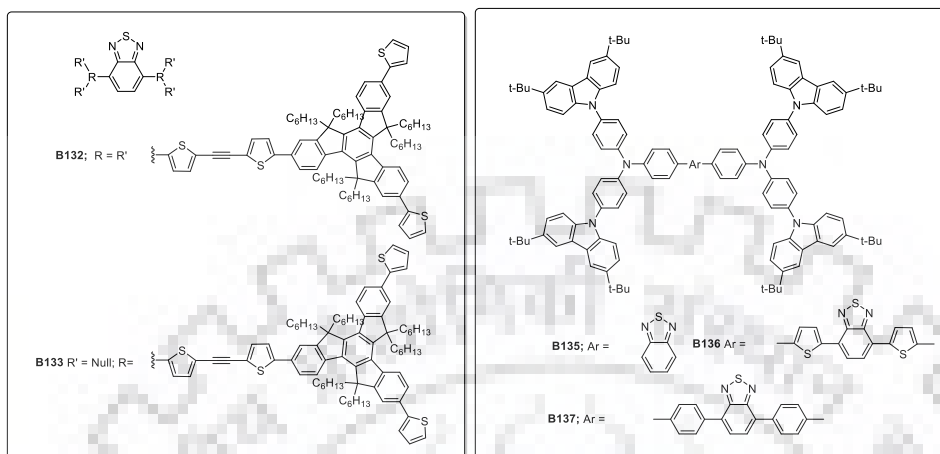
Figure 2.23. Benzothiadiazole substituted star shaped molecules.

Table 2.26. Device performance of OLEDs fabricated using **B132- B133**

Dye	λ_{max} (nm) DCM	Film	λ_{em} (nm) $\Phi_F{}^a$(%) DCM	Film	Turn-on voltage (V)	Current efficiency (cd A^{-1})	Maximum luminance (cd m^{-2})	λ_{EL} (nm)
B132	398	518	631 (25)	638	9.1	1.07	1290	630
B133	509	522	631 (25)	643	3.2	0.11	2260	635

^{a}rhodamine B as the standard, Φ_{PL}=0.65 in ethanol

^{b}ITO/PEDOT (30 nm)/EML(**B132-B133**)/Ca (15 nm)/Al (150 nm).

The designing of benzothiadiazole based dendrimer molecules helps to tune the emissive ability by selecting the core and employing the type of generations of the dendrons. It reduces the crystallization and retains emissive ability of a fluorescent core in the solid state, as well as improves the amorphous stability and solubility of the material.[105] Wang et al [106] reported π-conjugated red emitting dendrimer **B132** and **B133,** containing truxene as the branch. The emission intensity for **B132** was two times higher than for **B133** which results more light harvesting significantly better for red emitting materials. The emission maxima red-shifted by 12 nm for **B133** and 7 nm for **B132** in film when compared to solution this suggest that intermolecular aggregation suppressed by the dendritic structure. The device with configuration ITO/PEDOT (30 nm)/EML(**B133** or **B132**)/Ca (15 nm)/Al (150 nm) structured. Here, **B132** exhibits good performance with the emission maxima at about 630 nm, a turn on voltage of 9.1

V, maximum luminescence of 1290 cdm^{-2}, and maximum current efficiency of 1.07 cdA^{-1}. However, **B133** exhibits a turn on voltage of 3.2 V with a higher luminescence maxima of 2260 cdm^{-2}, and a lower maximum current efficiency of 0.11 cd/A. Benzothiadiazole based dendrimers are also reported by Khanasa et al,[107] where they introduced bis(3,6-di-*tert*-butylcarbazol-9-ylphenyl)aniline as an end-capping group to di(thiophen-2-yl)benzothiadiazole as core (**B134).** The bulky end capping helps to suppress aggregation-caused fluorescence quenching of the planar conjugated core as well as increase the hole transporting capability, thermal stability (T$_d$ = 339 °C and T$_g$ = 255 °C) and solubility of the molecule. A simple double layer device of ITO/PEDOT:PSS/**B134** (spin-coating)/BCP(40nm)/LiF(0.5 nm)/Al(150 nm) was fabricated which exhibited a high luminescence maxima of 12325 cd m^{-2} at 15.2 V, a maximum current efficiency of 3.97 cd A^{-1}, and a low turn on voltage of 2.2 V. Further they reported a series of bis(3,6-di-*tert*-butylcarbazol-9-ylphenyl)aniline end-capped oligoarylenes namely, **B135, B136** The dyes showed high T$_g$ value of 243-255 °C and the dye **B136** showed high T$_d$ value of 368 °C than that of other dyes **B135** (330 °C) and **B134** (339 °C) that prone the dyes for more thermal stability for effective OLED performance. The dyes fabricated in device with the structure of ITO/PEDOT:PSS/**B135-B136** (spin-coating)/BCP(40 nm)/LiF(0.5 nm)/Al(150 nm). The dyes exhibited different range of emission with **B135** (orange emission) and **B136** (yellow emission) as EML. It showed better performance in terms of maximum brightness (32817−47497 cd m^{-2}) and maximum current efficiency (4.17−5.19 cd A^{-1}), while the **B134**-based spin-coating double-layer device exhibits slightly lower performance (12325 cd m^{-2}, 3.97 cd A^{-1}) with excellent red color purity (CIE = 0.66, 0.33) and low device turn-on voltage of 2.2 V. [108]

Table 2.27. Device performance of OLEDs fabricated using **B134**

Dye	λ_{max} (nm)	λ_{em} (nm)	Film	Turn-on voltage (V)	Current density (mA cm^{-2})	Current efficiency (cd A^{-1})	Maximum luminance (cd m^{-2})	λ_{EL} (nm)	CIE
	DCM								
B134	528	640	644	2.2/4.7	1009	3.97	12325	653	(0.66, 0.33)

[a]ITO/PEDOT:PSS/B134(spin-coating)/BCP(40nm)/LiF(0.5 nm)/Al(150 nm)

[b]At 1 cd m^{-2}

[c]At 100 cd m^{-2}

Table 2.28. Device performance of OLEDs fabricated using **B135- B136**

Dye	λ_{max} (nm)	λ_{em} (nm)	Film	Turn-on voltage (V)	Current efficiency (cd A^{-1})	Maximum luminance (cd m^{-2})	λ_{EL} (nm)	CIE
		DCM						
B134	528	640	644	2.7/5.7	1.53	4523	625	(0.65, 0.33)
B135	462	600	601	2.9/4.9	2.46	5212/	586	(0.52, 0.46)
B136	422	513	528	2.4/4.7	3.85	7851	553	(0.43, 0.55)

^{a}ITO/PEDOT:PSS/ **B134-B136** (spin-coating)/LiF(0.5 nm):Al(150nm)

^{b}At 1 cd m^{-2} ^{c}At 100 cd m^{-2}
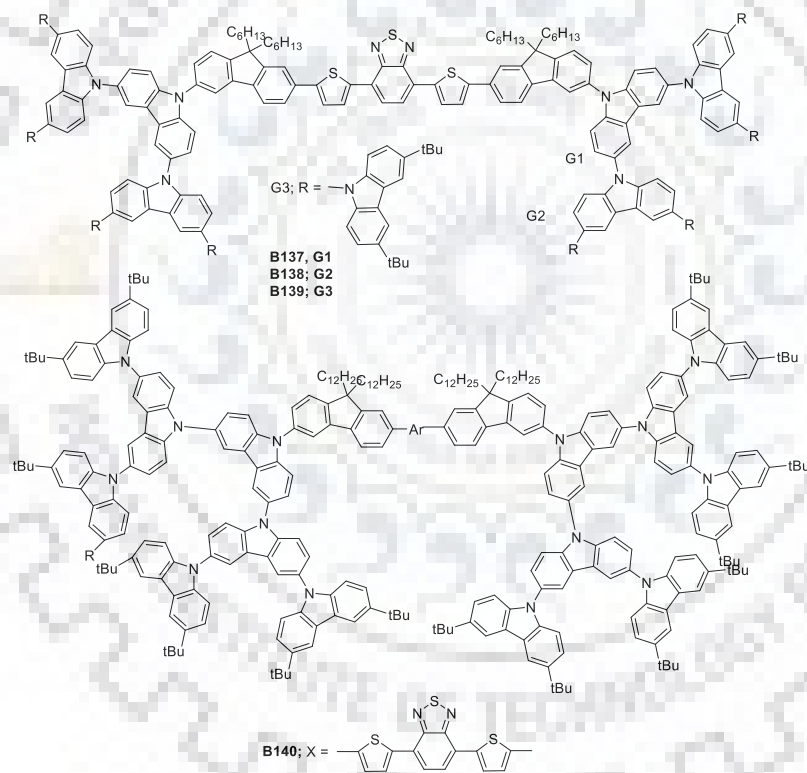
Figure 2.24. Carbazole decorated benzothiadiazole derivatives.

Further, Prachumrak et al [109] reported the carbazole dendrimer with benzothiadiazole as sole core **B137**, **B138** and **B139** which showed thermal decomposition in the range of 326-378 °C and glass transition temperatures in the range of 115-283° C. The devices fabricated in configuration ITO/PEDOT−PSS/**B137-B139** (spin coating) (30 nm)/BCP (40 nm)/LiF (0.5 nm)/Al (150 nm) exhibited stable red color around 622−645 nm, with high luminance

efficiencies (upto 4.80 cd A^{-1} at 1.2 mA cm^{-2}) and CIE coordinates of (0.65, 0.33), which are close to the pure red color.

Table 2.29. Device performance of OLEDs fabricated using **B137-B139**

Dye	λ_{max} (nm) DCM	λ_{em} (nm) $\Phi_F{}^a$(%) DCM	Film	Turn-on voltage (V)	EQE (%)	Current efficiency (cd A^{-1})	Maximum luminance (cd m^{-2})	λ_{EL} (nm)	CIE
B137	513	611 (0.39)	630	4.4/7.6		1.16	2106	645	(0.65, 0.33)
B138	514	608 (0.15)	625	4.4/6.4		2.75	3354	622	(0.63, 0.36)
B139	514	606 (0.10)	616	4.5/7.2		4.80	4655	622	(0.63, 0.35)

^{a}Measured in DCM using coumarin 6 as a standard

^{b}ITO/PEDOT−PSS/**B137-B139**(spin coating)/ BCP(40nm)/LiF(0.5 nm)/Al(150 nm)

^{c}At 1 cd m^{-2}

^{d}At 100 cd m^{-2}

Table 2.30. Device performance of OLEDs fabricated using **B140.**

Dye	λ_{max} (nm)	λ_{em} (nm) $\Phi_F{}^a$(%) DCM	Film	Turn-on voltage (V)	Current density (mA cm^{-2})	Current efficiency (cd A^{-1})	Maximum luminance (cd m^{-2})	λ_{EL} (nm)	CIE
B140	513	606, (0.10)	614	3.6	320	4.93	5584	622	(0.63, 0.36)

^{a}Measured in DCM with quinine sulfate as a standard

^{b} ITO/PEDOT:PSS/**B140** (spin-coating) (40 nm)/BCP(40 nm)/LiF (0.5 nm):Al (150 nm)

Furthermore, they replaced hexyl chain of the dye **B139** to dodecane resulting **B140.** Interestingly, it has shown similar absorption and emission spectra as observed for the dye **B139.** However, on using the dye **B140** as emitter with the double layered structure of ITO/PEDOT:PSS/**B140** (spin-coating) (40 nm)/BCP(40 nm)/LiF (0.5 nm):Al (150 nm), the device showed better performance compared to dye **B139** with the same configuration. The

device exhibited maximum luminescence up to 5584 cd m^{-2} at 14.4 V, high current efficiency of 4.93 cd A^{-1}, and low turn on voltage of 3.6 V.[110]
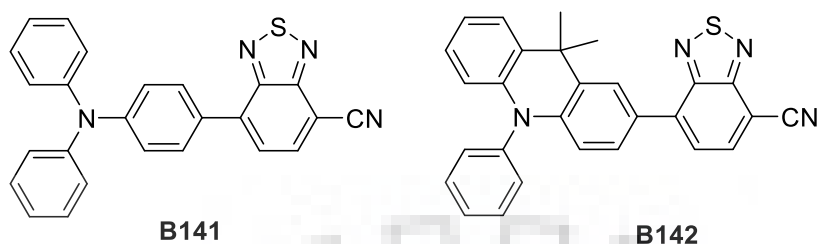
Figure 2.25. Cyano integrated benzothiadiazole derivatives.

Recently Wang et al. have developed cyano containing BTD derivative based on D-A-A configuration (**B141, B142**). The dye **B141** and **B142** consists of TPA and acridine unit as donor substituent respectively. Both the dyes in solid state exhibited red emission over 660 nm. The acridine unit not only supported the dye **B142** to exhibit red shift in absorption and emission with high PLQY but also helpful in enhancing thermal decomposition above 300°C and glass transition temperatures of 86° C. Thus when dye **B141** and **B142** fabricated in configuration ITO/ HATCN / TAPC / TCTA / CBP: 25 wt% 4CzIPN: 0.5 wt% **B141** and **B142** (spin-coating) (40 nm)/ B4PyMPM (50 nm)/LiF (0.5 nm):Al (150 nm) exhibited stable red color around 595 nm, with high current efficiencies (upto 35.5 cd A^{-1}) and increased EQE of 15.8%. [111]

Table 2.31. Device performance of OLEDs fabricated using **B141-B142.**

Dye	λ_{max} (nm) [a]	λ_{em} (nm) Φ_F[a](%)[a] DCM	Turn-on voltage (V)	Maximum EQE (%)	Current efficiency (cd WA^{-1})	λ_{EL} (nm)
[b]**B141**	505	667,	3.5	10.3	27.5	580
[c]**B141**	-	-	3.6	9.5	23.5	587
[b] **B142**	511	669	3.4	15.8	35.5	595
[c] **B142**	-	-	3.5	11.4	21.5	603

[a]Measured in DCM with quinine sulfate as a standard

[b] ITO/ HATCN / TAPC / TCTA / CBP: 25 wt% 4CzIPN: 0.5 wt% **B141** and **B142** (spin-coating) (40 nm)/ B4PyMPM (50 nm)/LiF (0.5 nm):Al (150 nm)

c ITO/ HATCN / TAPC / TCTA / CBP: 25 wt% 4CzIPN: 1 wt% **B141** and **B142** (spin-coating) (40 nm)/ B4PyMPM (50 nm)/LiF (0.5 nm):Al (150 nm)

2.4.2 Benzothiadiazole Based Green Emitter.

It is commonly accepted that the benzothiadiazole unit absorption capability of the material to red region due to conjugation. Thus, an appropriate structural tuning is required to restrict the absorption of such molecules in green region.
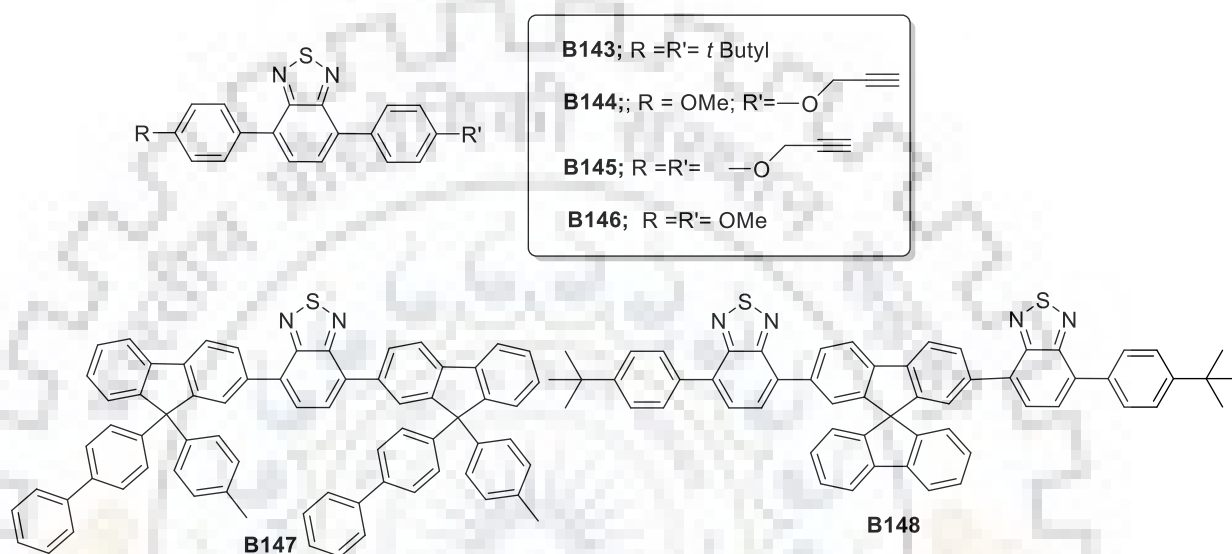
Figure 2.26. Benzothiadiazole-fluorene derivatives as green emitters.

Several proceedings were conducted to optimize the green region. Such as, Omar et al [112] reported benzothiadiazole (**B143**-**B146**), and fluorene derivatives as green emitters (**B147** and **B148**). The dyes **B144**, **B145**, and **B146** produced strong green electrogenerated chemiluminescence in non-aqueous solutions. This electrogenerated chemiluminescence could be seen by the naked eye, even in the presence of light. The fluorene derivatives, **B147** and **B148** also produce bright, easily observable electrogenerated chemiluminescence. The electrogenerated chemiluminescence quantum efficiencies of the series, compared to that of 9,10-diphenylanthrace, was estimated to range from 0.05 to 7%. This series shows rare green photoluminescence (490-556 nm) with high photoluminescence quantum efficiency in solution 5 to 90%.

Further, they incorporated **B147** in device with structure ITO/DPAInT2/DPAInF/TCTA/**B147**/Alq$_3$/LiF/Al which displayed impressive device characteristics such as maximum external quantum efficiency of 3.7% (12.9 cd A^{-1}) and maximum brightness at 168000 cd m^{-2}. [113]

Table 2.32. Photophysical, electrochemical and electrogenerated chemiluminescence properties of the compounds **B143-B148**.

Dye	λ_{max} (nm)	λ_{em} (nm), $\Phi_F{}^a$ (%)	$\lambda_{max}{}^{ECL}$ (nm)	E_{0-0} (V)	E_{ox} (eV)	HOMO/LUMO (V)
	ACN	ACN				
B143	388	512 (5)	518	3.04	1.64, 1.83	-6.02/-2.93
B144	404	546 (5.5)	560	2.77	1.37, 1.49	-5.75/-2.93
B145	400	542 (5.2)	556	2.80	1.42, 1.54	-5.79/-2.92
B146	406	556 (7.0)	555	2.75	1.33, 1.45	-5.71/-2.92
B147	412	544 (90)	548	2.85	1.46, 1.61	-5.84/-2.89
B148	417	535(75)	536	2.87	1.43, 1.56	-5.81/-2.88

[a] Quantum yield calculated relative to the fluorescein in solution.

Table 2.33. Device performance of OLEDs fabricated using **B147**

Dye	λ_{max} (nm)		λ_{em} (nm)		EQE (%)	Turn-on voltage (V)	Power efficiency (lm W^{-1})	Current efficiency (cd A^{-1})	Maximum luminance (cd m^{-2})
	DCM	Film	DCM	Film					
B147[a]	415	421	525	544	2.6	2	9	8.6	40700
B147[b]	-	-	-	-	3	2.5	7.7	10	122000
B147[c]	-	-	-	-	3.3	2	11.2	11.4	64000
B147[d]	-	-	-	-	3.7	2.5	11	3.7	168000

[a]Device 1. ITO/PEDOT (20 nm)/ NPB (20 nm)/ TCTA (10 nm)/**B147** (30 nm)/ LiF (0.5 nm)/Al (150 nm)

[b]Device 2. ITO/ PEDOT (20 nm)/ NPB (20 nm)/ TCTA (10 nm)/**B147** (30 nm)/ Alq$_3$ (30 nm)/LiF (0.5 nm)/Al (150 nm)

[c]Device 3. ITO/DPAInT2 (20 nm)/ DPAInF (20 nm)/TCTA (10 nm)/**B147** (30 nm)/ LiF (0.5 nm)/Al (150 nm)

[d]Device 4. ITO/ DPAInT2 (20 nm)/ DPAInF (20 nm)/TCTA (10 nm)/**B147** (30 nm)/ Alq$_3$ (30 nm)/LiF (0.5 nm)/Al (150nm)
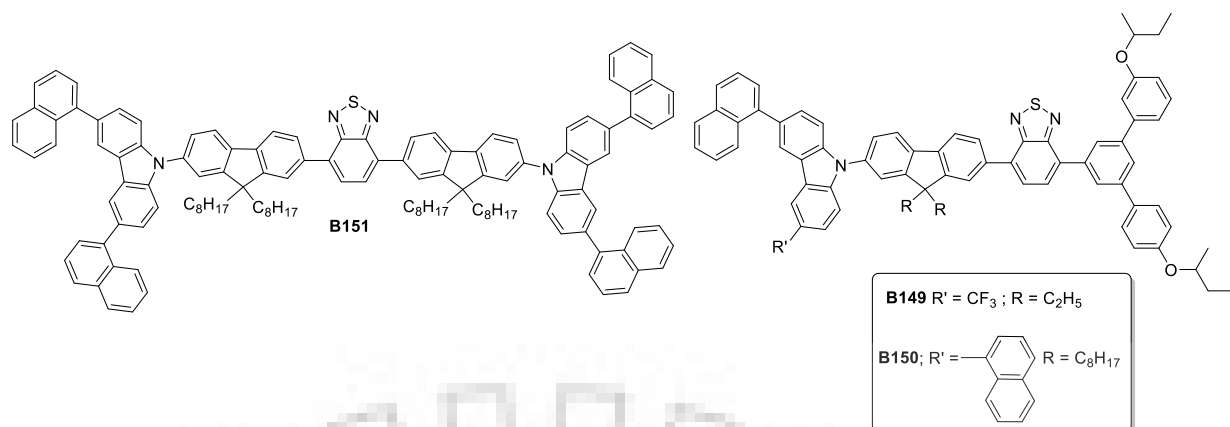
Figure 2.27. Napthyl substituted benzothiadiazole derivatives for OLED

Table 2.34. Device performance of OLEDs fabricated using **B149- B150.**

Dye	λ_{max} (nm)		λ_{em} (nm), $\Phi_F{}^a$ (%)		EQE (%)	Current efficiency (cd A^{-1})	Maximum luminance (cd m^{-2})	CIE (x,y)
	p-Xylene	Solid	*p*-Xylene	Solid				
149	300,400	301,413	500 (0.58)	521(0.51)	3.7	7.5	1308	(0.33,0.57)
150	302,408	285,413	504(0.67)^a	518(0.72)	2.6	10.6	1228	(0.34,0.58)

ITO/PEDOT:PSS/**B149-B150**/Ba/Al

Li et al reported asymmetrical carbazolyl and dendron substituted BTD derivatives **B149** and **B150.** The asymmetrical substitution helps dyes to achieve good thermal and morphology stability with T_g of 130 °C and ~95 °C for **B149** and **B150** respectively. The dyes fabricated as green emitter following configuration ITO/PEDOT:PSS/**B149-B150**/Ba/Al exhibited maximum EQE of 3.7/2.6% with maximum luminance of 1308 and 1228 cd/m^2[17]

Table 2.35. Device performance of OLEDs fabricated using **B151**

Dye	λ_{max} (nm)		λ_{em} (nm), $\Phi_F{}^a$ (%)		Turn-on voltage (V)	Current efficiency (cd A^{-1})	λ_{EL} (nm)	CIE (x,y)
	p-Xylene	Solid	*p*-Xylene	Solid				
B151	300,400	301,413	500(0.58)	521(0.51)	4.5	11.7	532	(0.34, 0.58)

^{a} p-xylene using quinine bisulfate in 0.1 N H$_2$SO$_4$ (r = 0.54).

ITO/PEDOT:PSS(50 nm)/PVK(40 nm)/ **B151**(45nm)/TPBI(30nm)/LiF(1.5 nm)/Al(200 nm).

Furthermore, they reported benzothiadiazole derivatives **B149-B151** and they showed good performance with green fluorescent emission where **B149** exhibited 519 nm and 536 nm in drop cast thin film that showed yellow-green light emission. In device ITO/PEDOT:PSS(50 nm)/PVK(40 nm)/**B149–B151**(45nm)/ETL(30 nm)/LiF(1.5 nm)/Al(200 nm) the dye **B149**

showed better performance with maximum current efficiency of 14.3 cd A^{-1} with CIE coordinates (0.38, 0.59). At 20 and 100 mA cm^{-2}, luminescence efficiency of 11.1 and 8.7 cd A^{-1}, respectively. [114]

Table 2.36. Device performance of OLEDs fabricated using **B152- B153**

Dye	λ_{max} (nm) DCM	λ_{em} (nm) DCM	Turn-on voltage (V)	Current efficiency (cd A^{-1})	Maximum luminance (cd m^{-2})	EQE (%)
B152[a]	346, 425	549	4.43	1.22	3720	0.34
B153[a]	365, 420	546	4.18	1.69	15958	0.47
B152	-	-	6.16	1.74	6724	0.48
B153[b]	-	-	4.18	1.71	20388	0.47

ITO/PEDOT-PSS/**B152-153**/Ca/Al [a]room temp [B100 °C]
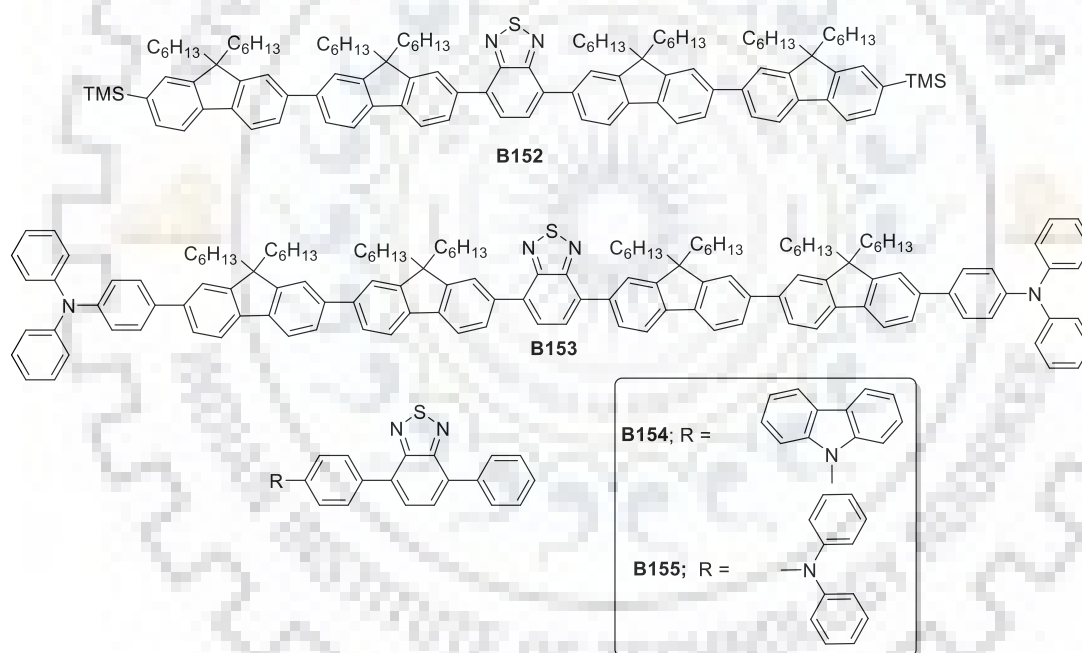
Figure 2.28. Benzothiadiazole-flourene derivatives as green emitters

The same group reported **B152** and **B153** by extending the bifluorene arms of **B149** where **B152** contains trimethylsilyl end groups. Moreover, the dye **B153** has added complexity with triphenylamine units end-capping the oligomer. The capping manifested the thermal stability with thermal decomposition temperature of 428 and 406 °C for **B152** and **B153,** respectively. Both dyes exhibit a emission peak at 556 nm and a shoulder at 598 nm. The CIE coordination are as (0.42, 0.56) and (0.43, 0.55), respectively. The unannealed **B152** device exhibited a highest luminance of 3720 cd m^{-2} at 10.2 V with a maximum current efficiency of 1.22 cd A^{-1}

at 9.0V and a maximum EQE of 0.34%. However, the dye **B153** incorporated device exhibited a highest luminance of 15958 cd m^{-2} at a bias voltage of 9.36 V.[115]

Table 2.37. Device performance of OLEDs fabricated using **B154- B155**

Dye	λ_{max} (nm)	λ_{em} (nm)		Power Efficiency (lm W^{-1})	EQE (%)	Current efficiency (cd A^{-1})	λ_{EL} (nm)	CIE
	DCM	DCM	Film					
B154	394	527		16.38	6.95	23.99	538	(0.34,0.60)
B155	437	587		7.18	3.80	8.84	588	(0.55,0.45)

ITO/PEDOT:PSS(40nm)/NPB (40 nm)/**B154** (20 nm) or **B155** (30 nm)/TPBi (40 nm)/LiF/Al.

Wang et al [116] reported two benzothiadiazole derivatives with triphenylamine (**B153**) and N-phenyl carbazole (**B154**) as donor that has tuned the molecule to exhibit green to orange emission respectively and thermaly and morpholoical stable with thermal decomposition temperature of 340°C and 391°C, respectively. Moreover, the non-doped OLED of **B154** with device ITO/PEDOT:PSS (40 nm)/NPB (40 nm)/**B154** (20 nm) or **B155** (30 nm)/ TPBi (40 nm)/LiF/Al. exhibited an excellent performance with a green emission and CIE coordinate of (0.34, 0.60). It showed a maximum current efficiency of 23.99 cd A^{-1}, and a EQE of 6.95% was achieved through hybridization of local and charge-transfer (CT) state (HLCT) and "hot exciton", in which the former is responsible for high PL efficiency while the latter contributes to high exciton utilization.
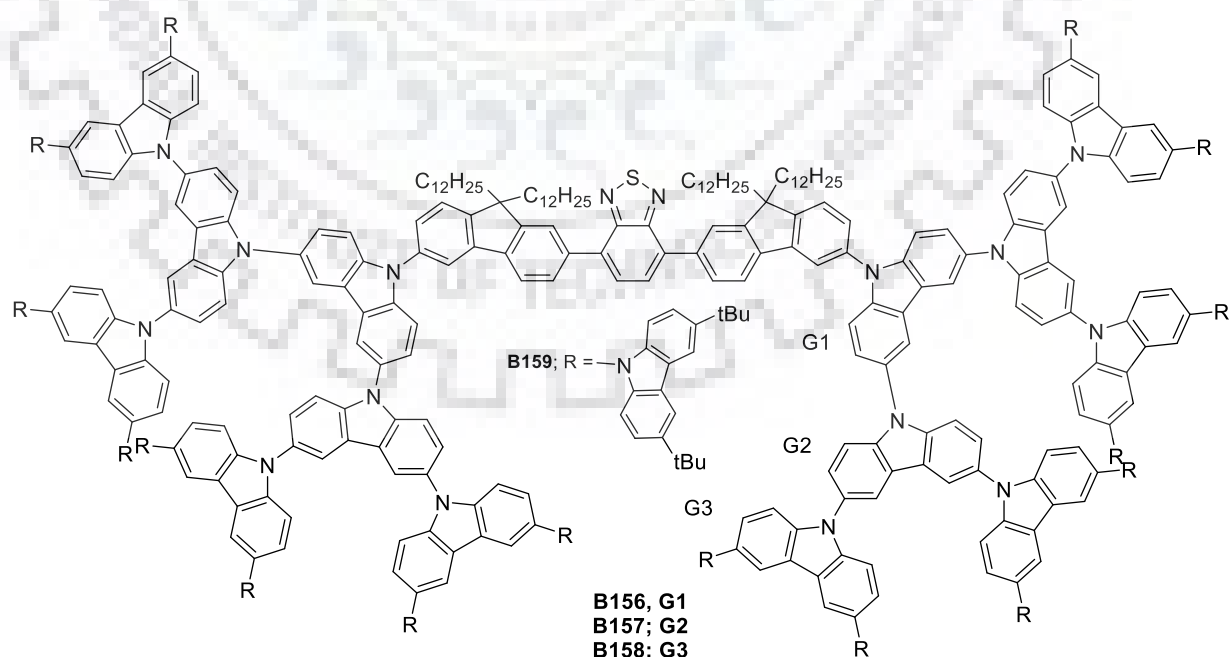
Figure 2.29 Benzothiadiazole-carbazole derivatives as green emitters

Furthermore, the same group reported benzothiadiazole cored carbazole dendrimer as green emitting materials **B156-159,** which showed high thermal stability with T_{5d} around 321 °C to glass transition temperatures (T_g) ranging from 142 to 364 °C, indicating highly stable amorphous material. Among green emitters The **B158-B159** based green OLEDs are the two best performing devices among all these analogues. These devices exhibit maximum luminescence up to 8521/2079 cd m^{-2} at 14.4 V, high current efficiency of 9.12/10.01 cd A^{-1}, and turn on voltage of 4.0 V. [117]

Table 2.38. Device performance of OLEDs fabricated using **B156-159**

Dye	λ_{em}(nm);		Turn-on voltage (V)	Current density (mA cm^{-2})	Current efficiency (cd A^{-1})	Maximum luminance (cd m^{-2})	λ_{EL} (nm)	CIE
	DCM	Film Φ_F^a (%)						
B156	540	539 (0.18)	4.2/8.0	231	0.21	472	540	(0.37, 0.59)
B157	534	529 (0.13)	4.1/6.1	245	2.19	4328	525	(0.31, 0.62)
B158	530	523 (0.09)	4.0/6.0	391	9.12	8521	521	(0.27, 0.62)
B159	528	514 (0.05)	4.0/6.9	224	10.01	2079	509	(0.22, 0.56)

^{a}Measured in DCM with quinine sulfate as a standard.

^{b}ITO/PEDOT:PSS/**B156-159** (spin-coating) (40 nm)/BCP (40 nm)/LiF (0.5 nm):Al (150 nm)

^{c}At 1 cd m^{-2}

^{d}At 100 cd m^{-2}
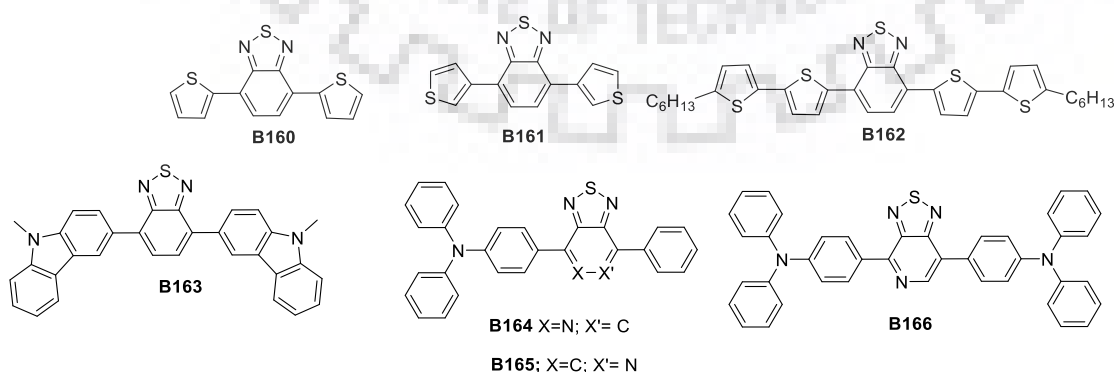
Figure 2.30. Benzothiadiazole derivatives used as orange yellow emitters

Wang et al [118] reported two isomers based on linking of thiophene unit to benzothiadiazole. The dye **B160** (4,7-di(thiophen-2-yl)benzo[*c*][1,2,5] thiadiazole), linked with C2 position of thiophene while **B161** (4,7-di(thiophen-3-yl)benzo[*c*][1,2,5] thiadiazole), linked with C3 position to benzothiadiazole. The isomeric dyes exhibited a good morphology and thermal stability (~265 °C). The device fabricated with configuration ITO/MoO$_3$ (5 nm)/TAPC (20 nm)/**B160-166** (30 nm)/Bphen (30 nm)/LiF (1 nm)/Al (100 nm), where the dye **B160** showed a low turn-on voltage (2.45 V) with a maximum luminance of 1825 cdm^{-2}and a slight red-shift of electroluminescence (26 nm). The performance of dye **B160** attributed to its higher HOMO and lower LUMO level which facilitates efficient hole and electron injection, respectively compared to the dye **B161**.

Table 2.39. Device performance of OLEDs fabricated using **B160** and **B161**

Dye	λ_{max} (nm)	λ_{em} (nm), Φ_F(%)		Turn-on voltage (V)	Current efficiency (cd A^{-1})	λ_{EL} (nm)	HOMO/ LUMO
	DCM	DCM	Film				
B160	445	558 (13.2)	584 (7.2)	2.45	0.65	610	-5.5/-3.4
B161	414	518 (13.4)	540 (6.7)	4.10	0.55	593	-5.8/-3.3

ITO/MoO$_3$ (5 nm)/TAPC (20 nm)/**B160** or **B161** (30 nm)/Bphen (30 nm)/LiF (1 nm)/Al (100 nm)

Mroz et al [119] reported benzothiadiazole derivatives **B160** and **B162** as guest for polybenzofulvene host materials. The device with configuration ITO/PEDOT:PSS/EL/Ca/Al fabricated with blends of **B160** and **B162** exhibited yellow and red emission, respectively. It also reduced micro aggregation with quantum yield of 85% for **B160** blend which outstands the standard poly(*N*-vinylcarbazole) with quantum yield of 50%. Wu et al [120] reported carbazole substituted **B163** which showed glass transition temperature around 106 °C which excelled as good morphological stability and high thermal stability too with decomposition temp at 330 °C. The device demonstrated orange-yellow light with maximum electroluminescence at 608 nm. The EQE increases with increasing current density and levels off at 0.34% with a slight decrease at higher current densities. These results demonstrate that amorphous mixtures are suitable materials for OLED. Jiang et al [121] reported, **B166** and the two positional isomers **B164**, **B165** defined by proximal and distal positions of donor triphenylamine unit to *N* of pyridine core, respectively. The dye **B164** exhibits ~10 nm red shift when compared to **B165** and all the compounds showed high thermal stability around 306-367 °C. The dye **B166**

showed relatively better performance with deep red emission, maximum external quantum efficiency of 3.87%, (12 000 cd m^{-2})

It is concluded that benzothiadiazole derivatives featuring carbazole and fluorene showed bright green emission in OLED with maximum luminescence of 16800 cdm^{-2}. However, the development of green emitting benzothiadiazole are still challenging and more structural diversity by functional group disposition is required to understand the structure-property relationship.

Table 2.40. Device performance of OLEDs fabricated using **B164- B166**

Dye	λ_{max} (nm) DCM	λ_{em} (nm) DCM	Turn-on voltage (V)	Power efficiency (lm W^{-1})	Current efficiency (cd A^{-1})	Maximum luminance (cd m^{-2})	λ_{EL} (nm)	EQE (%)
B164	480	658	4.3	2.10	3.72	7060	608	2.89
B165	470	672	4.3	2.28	3.89	7730	616	3.36
B166	507	670	3.4	1.85	2.16	10 550	644	3.87

ITO (95 nm)/HATCN (5 nm)/NPB (40 nm/TCTA (5 nm)/MADN: (7 wt%) **B164-166** (20 nm)/TPBI (40 nm)/LiF (1 nm)/Al (90 nm); Calculated with a luminance of 1 cd m^{-2}

2.5 Summary and Outlook

In summary, in this chapter we presented brief review on structure-property relationship of benzothiadiazole based functional materials in DSSCs and OLEDs. Benzothiadiazole and its derivatives have been found as promising building blocks in constructing molecular materials for DSSC (sensitizer) and OLED applications as dopant in polymer hosts, fluorescent emitters, HLCT emitters and TADF emitters. The linear π-conjugation owing to structural extension of in 4,7-substitution generally led to red-emitting molecules. Presence of additional bulky chromophores provides the rigidity that enhances the thermal stability and also sterically impedes the conjugation. Several benzothiadiazole derivatives such as indoline–benzothidiazole and cyclopentadithiophene-benzothiadiazole conjugates excelled in DSSC with efficiency greater than 12.8%. Similarly, several benzothiadiazole-based emitters showed promising efficiency (15.8%) due to hybridization of LE and CT states.

However, designing of benzothiadiazole-based molecules with HLCT, TADF emission is challenging. It was observed that the functionalization on 4,7-positions extended the linear π-conjugation, however functionalization at 5,6 positions of BTD system remain unexplored. Similarly, wealth of information about the benzothiadiazole derivatives exhibiting red emission is available but the realization of green or blue emission from benzothiadiazole derivatives is

challenging. With an extensive research of the structure-property relationship via diverse functionalization of mono-, di-, tri-substituted derivatives, we attempted to solve these challenges in our work. Further, we also attempted to investigate structural alternations required to achieve specific red, green and blue emitters with benzothiadiazole core. Despite these efforts, we feel that there are many opportunities remain unexplored in the field of benzothiadiazole chemistry.
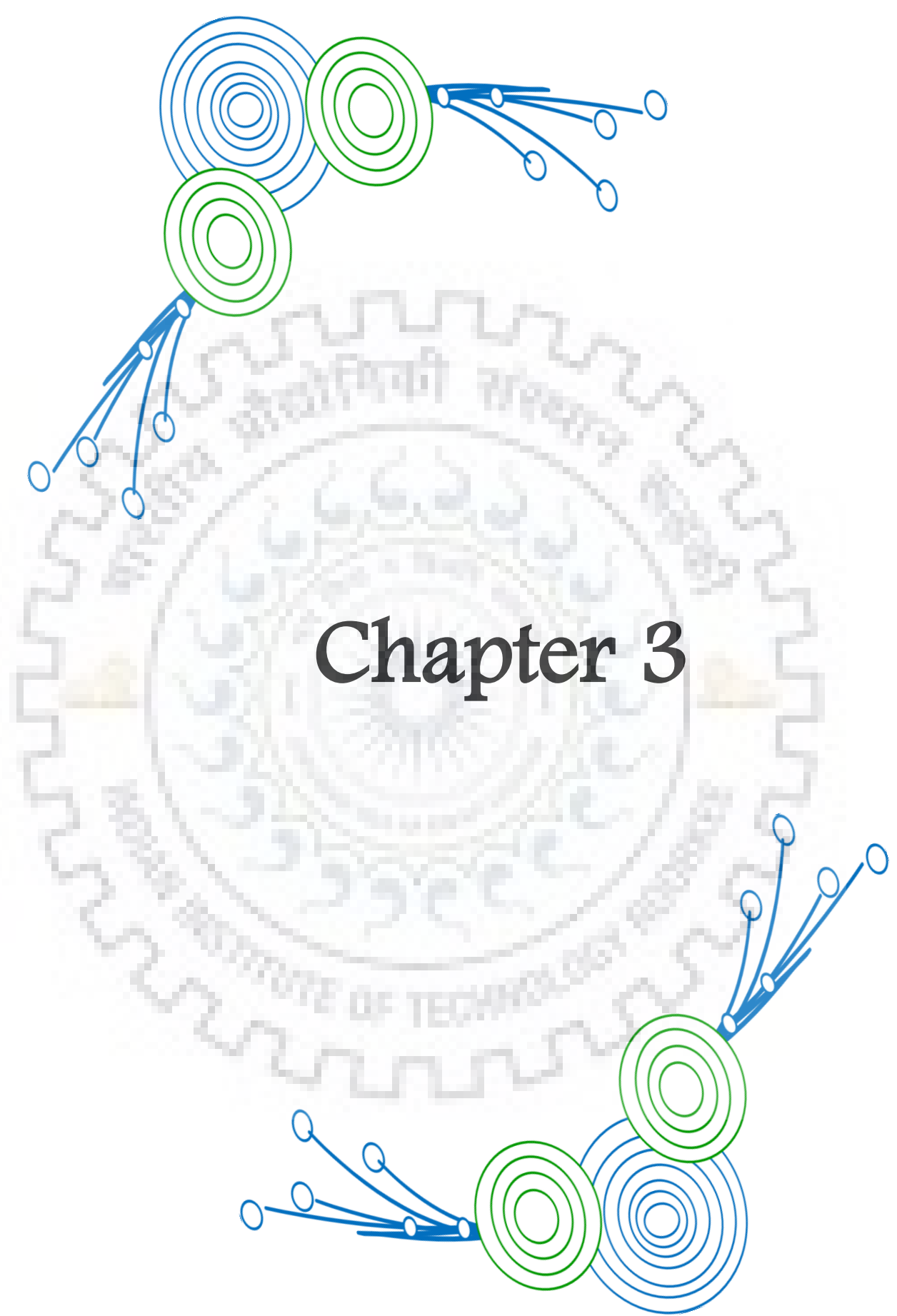
Chapter 3

Chapter 3

Methyl Substitution as a Facile Approach to Fine Tune Photophysical and Electroluminescence Properties of Benzothiadiazole-Based Emitters
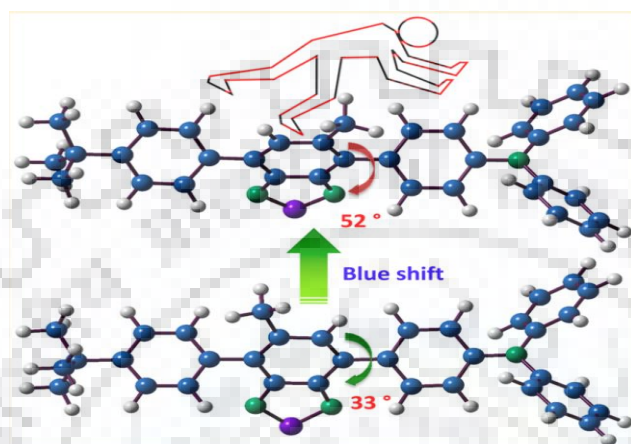
3.1 Introduction

Study of structure-property relationship of organic π-conjugated materials has drawn immense interest in recent years due to the potential utility of organic semiconductors in electronic devices such as OLEDs,[123] OPVs,[124] OFETs, [125] NLO, [126] and sensors. [127] Among the devices, OLEDs are attractive due to their practical application in solid state lightning sources and flat panel displays. Among the variety of organic material configurations (small molecules, [128] and polymers[129]) exploited for application in OLED, small molecules dominate due to their well organized molecular structure, versatile control on functional properties by structural alternations with simple chemical modifications, reproducible synthetic protocols, easy purification methods and capability to be processed both in solution and vacuum deposition methods. [130] Small molecules featuring bipolar Donor-Acceptor (D-A) arrangement are widely explored due their built in bifunctional qualities. [131] The D-A design is adopted mainly due to its tunable emission characteristics, balanced charge transport and promising thermal characteristics which are beneficial to promote the device performance in a desired fashion. [130, 131,132]

In dipolar compounds, the donor-acceptor interaction mainly determines the functional efficacy. Nature of donor and acceptor and the geometry of the linker used to tether donor and acceptor are important factors which affect the functional outcome in such compounds. In general, the planar arrangement of aromatic segments in organic materials leads to π-aggregates

in solid state, which severely affects device parameters. On the other hand, it has been found that the moderate π-π interaction is necessary for better charge hopping in the device. These drawbacks are often overcome by the introduction of rigid chromophores with twisted molecular geometry or alkyl units at specific positions in the molecular framework which can prevent severe π-π stacking interactions in the solid state. This avoids aggregation-induced fluorescence quenching while allowing moderate π-interaction which enhances thermal stability, solubility and device parameters. [132,133]

As discussed in Chapter 2 , BTD is an promising building block in the construction of functional materials for optoelectronic devices due to its high electron affinity, rigid molecular structure and ability to tune the absorption/emission wavelength to near infrared region. [17, 20] Thomas et al[93] reported red emitting materials by modifying C4 & C7 positions of BTD with arylamine or phenyl units for OLED and achieved decent device performance with EQE close to 2.1%. Besides, in recent years the investigation on structure-property relationship of regioisomers is highly demanding due to their significant changes in the physicochemical, thermal, and carrier transport properties by simple structural alterations.[134, 135] For instance, Jiang et al [24] reported nitrogen modified BTD core ([1,2,5]thiadiazolo[3,4-*c*]pyridine (PT)) substituted with triphenylamine and phenyl units on C4 & C7 positions which results in two asymmetric regioisomers such as proximal **L5** (*N*,*N*-diphenyl-4-(7-phenyl-[1,2,5]thiadiazolo[3,4-*c*]pyridin-4-yl) aniline) and distal **L6** (*N*,*N*-diphenyl-4-(4-phenyl-[1,2,5]thiadiazolo[3,4-*c*]pyridin-7-yl)aniline), on the ground of orientation of the nitrogen with respect to the donor triphenylamine. They investigated the role of twist angle and freedom of rotation on photophysical properties and the device performance of the materials. The **L6** based device showed red-emission with EQE of 3.36% and CIE ~(0.67, 0.33).

In this chapter, we demonstrate a simple strategy to tune the optical, electrochemical and electroluminescet properties of the BTD dyes by introducing methyl group on BTD nucleus. [136,137] We developed a series of methyl-BTD-based green/greenish yellow emitting materials by substituting with triphenylamine/*N*-phenylcarbazole/*tert*-butylphenyl units on its C4 & C7 positions [20, 98, 107, 138-139] (Figure 3.2). The selective Suzuki coupling reactions resulted in regioisomers **5** & **6, 8** & **9, 10** & **11**. The effect of methyl substitution on electronic absorption, emission, thermal, electrochemical and electroluminescent characteristics was studied in detail and compared with non-methylated BTD derivatives. [15] Interestingly, the dye **5, 9** and **11** showed red-shifted absorption when compared to its regioisomer **6, 8** and **10** due to interrupted π-conjugation between triphenylamine/ *N*-phenylcarbazole and BTD dictated by methyl unit at C5. Thus, the methyl group on BTD nucleus acted as a gateway to modulate

the electronic communication with the donor depending on its position relative to the donor. When the methyl group is close to the donor it affected the coplanarity between the donor and BTD units and reduced the donor-acceptor interaction. The geometrical changes in the ground (non-planar) and excited (more planar) states manifested in the absorption and emission properties. The dyes displayed positive solvatochromism in the emission spectra indicative of more pronounced ICT in the excited state. The dye **4** exhibited high lying HOMO in the series while the LUMO is stabilized in **3**. The electronic structure correlations are supported by density functional calculations
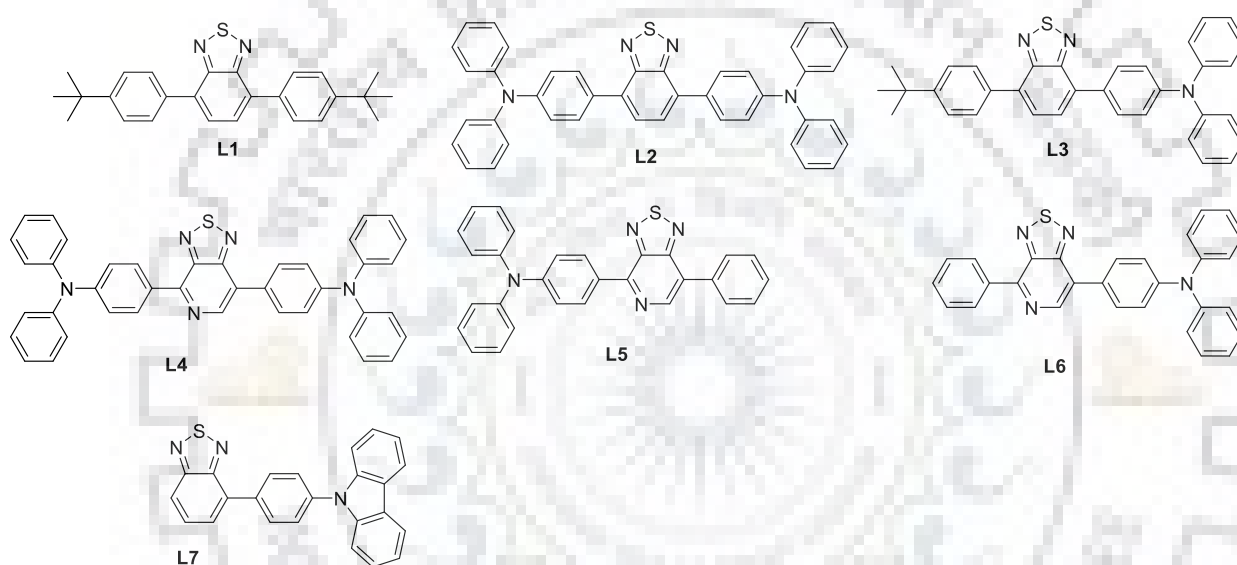
Figure 3.1 Structures of the related dyes.
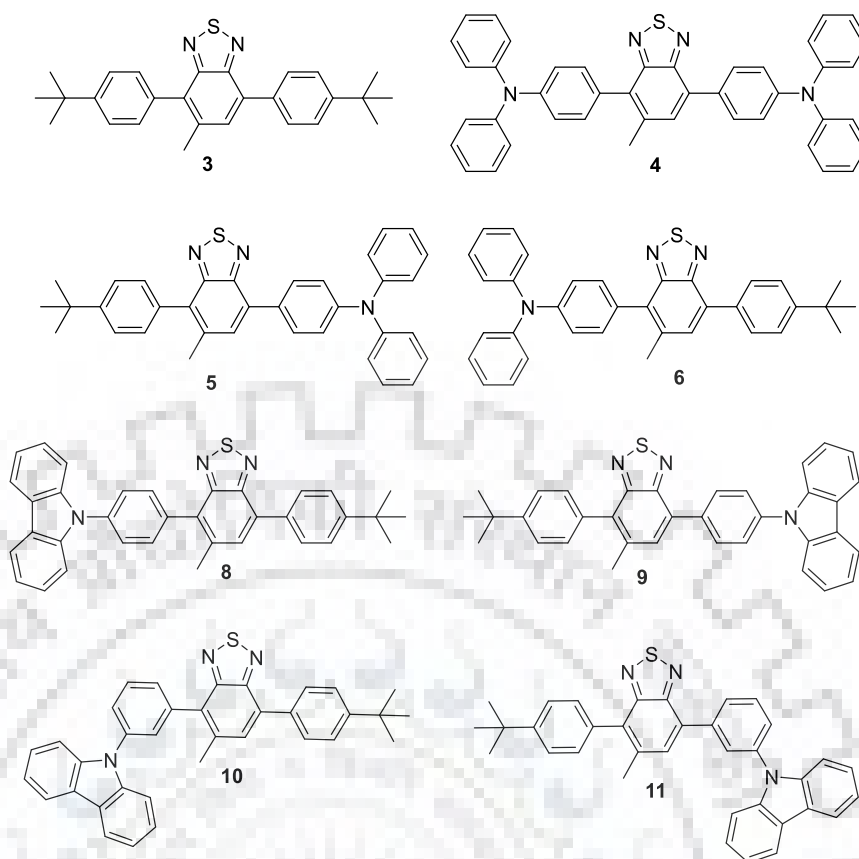
Figure 3.2 Structures of the target dyes.
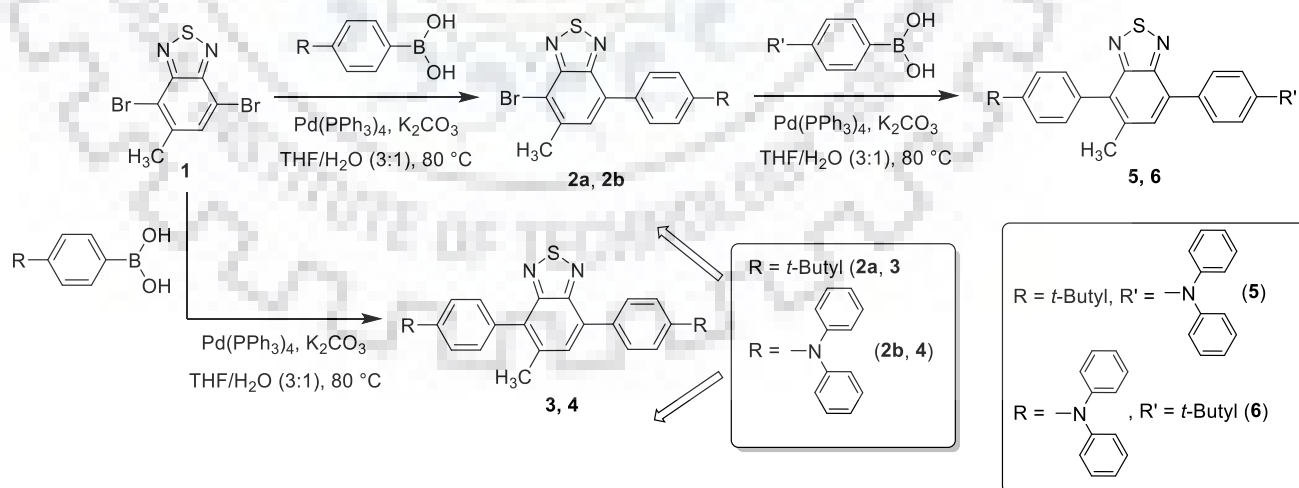
Scheme 3.1 Synthetic protocol of the dyes, **3-6.**
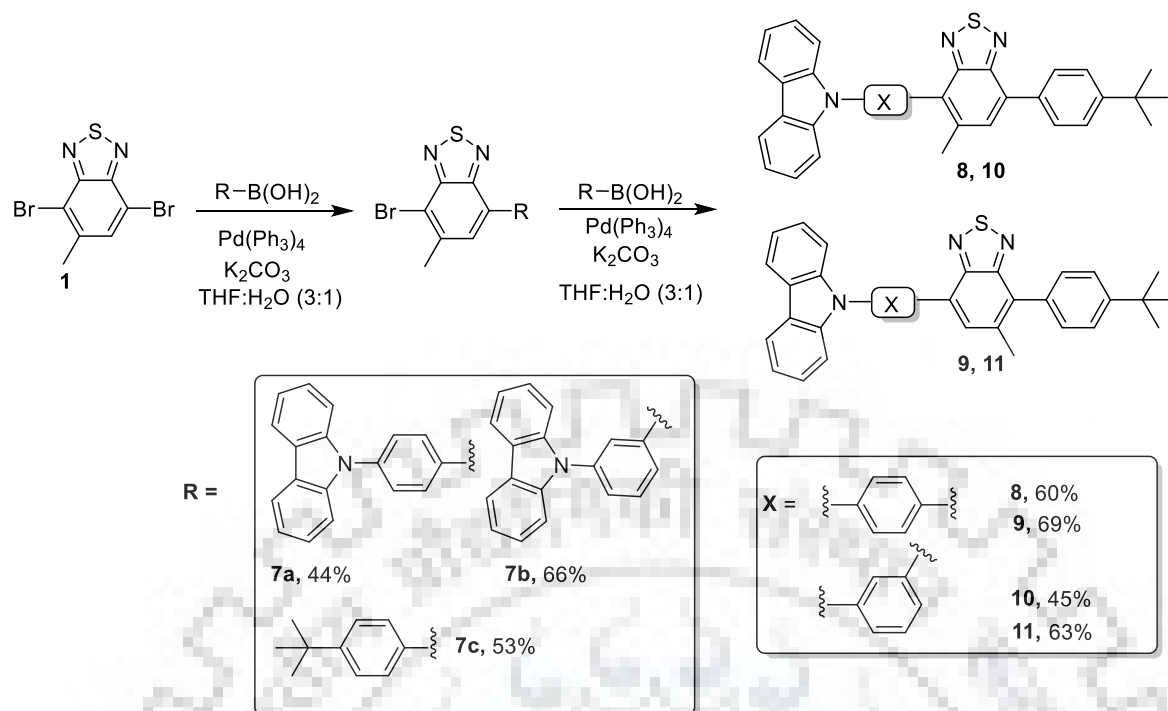
Scheme 3.2 Synthetic protocol of the dyes **8-11**

3.2 Results and Discussion

3.2.1 Synthesis and Characterization

The starting material 4,7-dibromo-5-methylbenzo[*c*][1,2,5]thiadiazole (**1**) was synthesized from 4-bromobenzene-1,2-diamine by following a procedure reported in literature. [28] Syntheses of the isomeric dyes **5, 8, 10** and **6, 9, 11** which show variation in the position of methyl group on the benzothiadiazole nucleus, were accomplished by a two-step protocol (Schemes 1 and 2) by reverting the sequence of reagents. In the first step, the intermediates 4-bromo-7-(4-*tert* butylphenyl)-5-methylbenzo[*c*][1,2,5]thiadiazole (**2a),** 4-(7-bromo-6 methylbenzo[*c*][1,2,5]thiadiazol-4-yl)-*N,N*-diphenylaniline (**2b), 7a** and **7b** were synthesized by treating **1** with stoichiometric amount of respective aryl boronic acids under Suzuki coupling conditions.[140] Finally, the intermediates **2a** ,**2b, 7a** and **7b** were converted to the target dyes **5, 9, 11, 6, 8** & **10** by treating them with triphenylamine, *meta* or *para N*-phenylcarbazole and the *tert*-butylphenyl boronic acids. The isomeric dyes **5** & **6, 8** & **9, 10** & **11** were obtained by two fold Suzuki coupling reaction of **1** with respective aryl boronic acids. The structures of the dyes were established by ¹H, ¹³C NMR, HRMS spectra and elemental analyses. In addition, molecular structure of **2a** was confirmed by single crystal X-ray diffraction analysis (Figure 3.3, Table 3.3). This reveals that the first Suzuki-coupling reaction on **1** deliver aryl unit at C7 position. The selective formation of C7 substituted derivatives **2a,**

2b, 7a and **7b** from **1** is due to the steric inhibition for reaction at C4 because of methyl group at C5. Also, the reactivity preference can also be rationalized by electronic effects. [141] Electron releasing effect of methyl group on C5 may reduce the electrophilic nature of C4 which is *ortho-* to C5. Thus, the first step of Suzuki coupling reaction, i.e. oxidative addition is preferred at relatively electron deficient site (C7). [142] All the dyes (**3-11**) are green, yellow, or orange solids and soluble in common organic solvents such as TOL, THF, DCM, DMF, ACN, TEA, DEE but insoluble in alcohol.
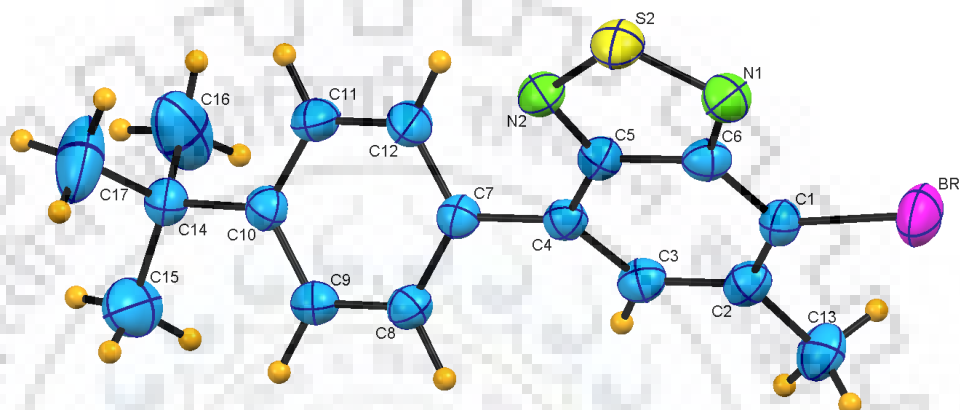
Figure 3.3 Molecular structure of **2a.** (50% thermal ellipsoids shown)

3.2.2. Photophysical properties

The photophysical properties of the dyes were investigated by absorption and fluorescence spectroscopy. The absorption spectra of the compounds recorded in DCM are displayed in Figure 3.4 and the relevant data compiled in Table 3.1. All the compounds showed absorption profile in the range 240-500 nm. The higher energy peak observed below ~340 nm is assigned to the multiple localized π-π* electronic transitions originating from chromophores such as phenyl, triphenylamine, *N*-phenylcarbazole and benzothiadiazole, [143, 144, 110] which is merged together in most of the dyes. As per literature bands at lower wavelength ~250 nm would be associated with π-π* transition of carbazole and ~300 nm attributable to π-π* transition of benzothiadiazole unit.[110, 117] The absorption appearing in the wavelength range, 365-432 nm is invariably present in all the compounds and assigned to the intramolecular charge transfer transition from the appended chromophores to MBTD acceptor.

Moreover, as per the nature of chromophores, their position of attachment and chromophore density exhibited significant influence on the absorption wavelength and molar extinction coefficients of the dyes. Thus, the triphenylamine substituted derivatives (**4-6**) exhibited bathochromic shift (~26-67 nm) when compared to phenyl and *N*- phenylcarbazole derivatives (**3, 8, 9, 10, 11**) attributable to the extended conjugation by triphenylamine unit.[134] Among

75

the triphenylamine derivatives, **4** possess most red-shifted ($\Delta\lambda$ = 30 nm) absorption owing to the presence of two triphenylamine units which extend the conjugation in the orbitals contributing to the electronic transition (*vide supra*). Interestingly, among the mono-triphenylamine functionalized isomers (**5 & 6**), **5** displays red-shift in (~16 nm) absorption, which is attributed to the changes in the planarity. The optimized geometries of the dyes are shown in Figure 3.6. The dihedral angle between the triphenylamine and BTD units for **6** is significantly larger (52.07°) than that in the isomer **5** (33.37°). This large twisting, originating due to methyl unit at C5, retards effective electronic interaction between the chromophores. Moreover among *N*-phenylcarbazole derivatives, *para* substituted derivatives showed bathochromic shift over *meta* derivatives which indicates the presence of better donor-acceptor interaction in the former. [135] However, *N*-phenyl carbazole derivatives do not show effects attributable to the presence of methyl group. It may be possibly due to reduced ICT arising from weak donor strength and tilting of carbazole. Overall, it suggests that C5 methyl plays significant role in the absorption properties due to steric interaction.

It is also interesting to compare the absorption parameters of **3-6** dyes with BTD derivatives (**L1-L3**) which lack methyl group. [93] Generally, the present dyes (**3-6**) show blue shift in absorption with lower molar extinction coefficients than **L1**-**L3**. The unsymmetrical dyes **5** and **6** show more blue shift than the symmetrical dyes **3** and **4** when compared to the corresponding non-methylated dyes (**L1**-**L3**). Particularly, **6** exhibited drastic blue shift than that of **5** when compared to **L3**. This points out that the disturbance in the interaction of triphenylamine unit with BTD is more significantly affecting absorption features. The molar extinction coefficient for the longer wavelength absorption in these dyes assumes the order **6** $<$ **5** $<$ **4** $<$ **3,** which further confirms the role of methyl group in altering the transition dipole of the electronic excitation. Interestingly, order of molar extinction coefficient for the UV-absorption is reversed for the dyes **5 & 6**. This indicates that inhibition of visible absorption and permission of UV absorption are modulated by methyl substituent. Moreover, the *para N-* phenylcarbazole derivative **9 & 8** showed similar absorption profile to structurally similar compound **L7** (381 nm) which contains *para N*-phenylcarbazole and benzothiadiazole unit. [145] This probably indicates that electronic communication is less favorable between *para N-* phenylcarbazole and MBTD unit in the present dyes and does not get altered on methyl introduction. [146]
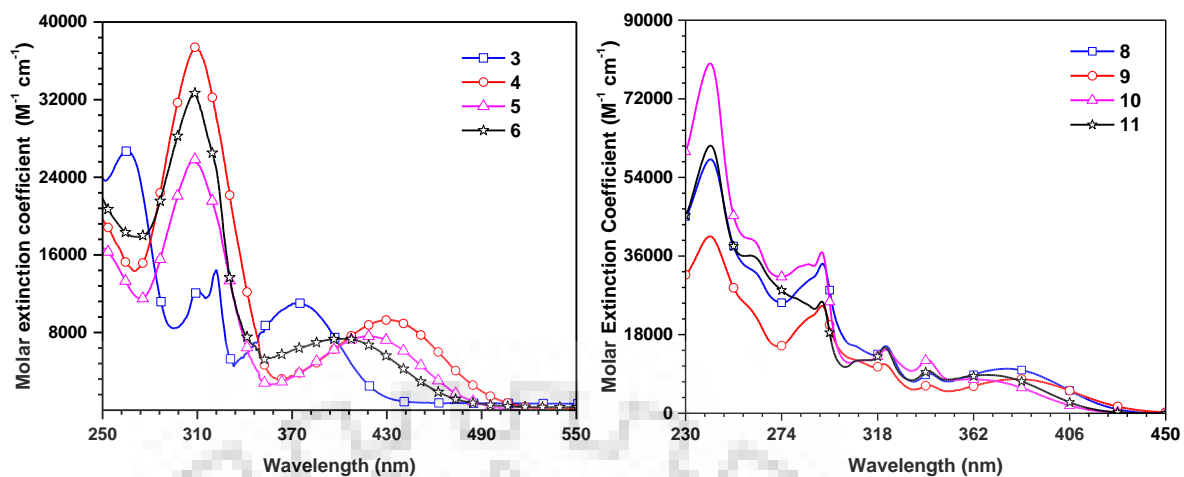
Figure 3.4. Absorption spectra of the dyes recorded in DCM.
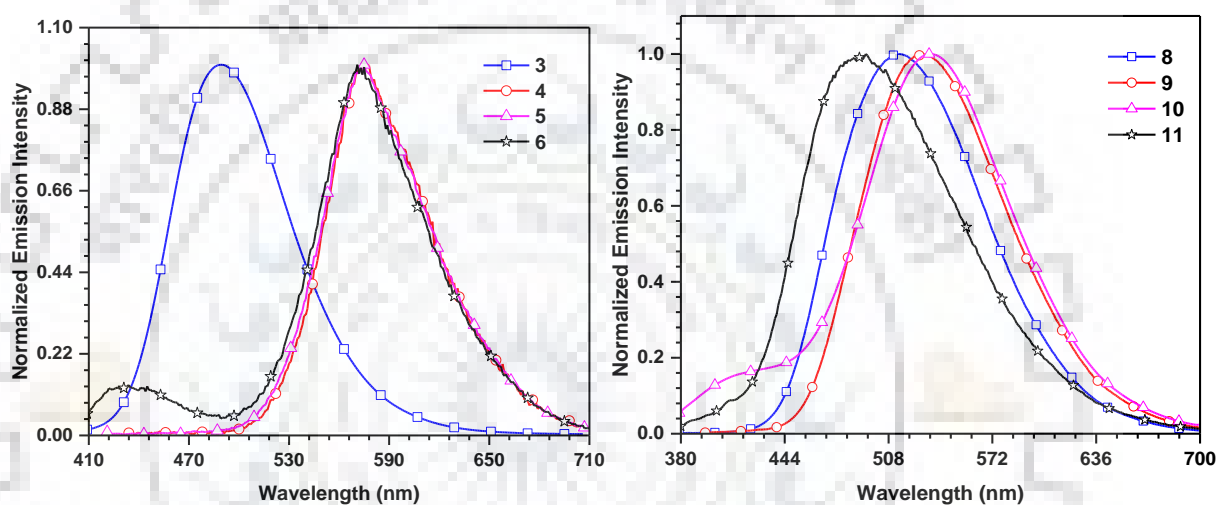
Figure 3.5. Emission spectra of the dyes recorded in DCM.
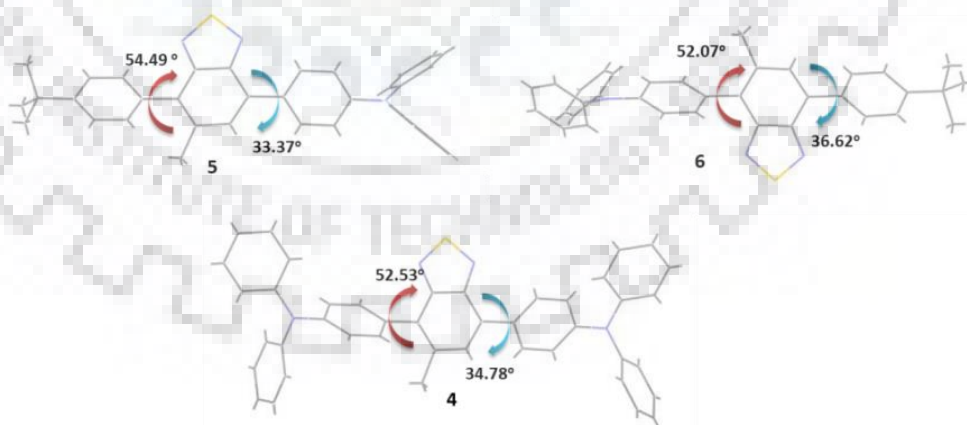
Figure 3.6. Variation of dihedral angles in the B3LYP/6-31G(d,p) optimized geometries of **4**, **5** and **6.**

77

Table 3.1 Optical properties of the dyes

Dye	λ_{abs} (nm) ($\varepsilon_{max} \times 10^3$ (M^{-1} cm^{-1}))[a]	λ_{em} (nm)[a] (Φ_f)[b]	Stokes shift (cm^{-1})	λ_{em} (nm)[c]
3	376 (11.04), 322 (14.48), 311 (12.34)	489 (0.14)	6146	472
4	432 (9.30), 309 (37.40)	577 (0.21)	5817	555
5	418 (7.63), 308 (25.87)	575 (0.19)	6532	547
6	402 (7.36), 309 (32.66)	571 (0.18)	7362	547
8	241 (58.15), 261 (sh), 293 (34.36), 322 (15.40), 341 (9.01), 377 (10. 19)	514	7070	506
9	241 (40.55), 260 (sh), 293 (24.59), 321 (11.29), 342 (6.41), 381 (7.85)	528	7307	495
10	241 (80.17), 261 (sh), 293 (36.87), 322 (14.56), 341(12.26), 365 (7.72)	534	9051	477
11	241 (61.30), 261 (sh), 292 (25.57), 321 (15.09), 341(9.63), 368 (8.77)	498	5852	488

[a] Measured in DCM solution. [b] Absolute quantum yields determined using a calibrated integrated sphere system. [c] Measured for spin cast film from TOL. [d] Estimated from DFT (B3LYP/6 31G(d,p)) calculation.

The emission spectra recorded for the compounds in DCM are shown in Figure 3.5 and corresponding data listed in Table 3.1. In general, the dyes emit green (**3, 8, 9, 10, 11**) or orange color (**4-6**). Similar to absorption characteristics, the triphenylamine derivatives (**4-6**) displayed red-shifted emission when compared to phenyl and *N*-phenylcarbazole derivatives (**3, 8, 9, 10, 11**) suggesting an extended conjugation involving triphenylamine unit in the former compounds. Interestingly, the dyes **4-6** showed similar emission profile indicating the emission originating from similar electronic excited state. Since the dyes **4-6** possess BTD and triphenylamine unit, it is speculated that the emission originates from the ICT state involving these two chromophores. Among *N*-phenylcarbazole derivatives, the profile follows the order **10 > 9 > 8 > 11.** Further**,** the Stokes shift is observed in similar order which indicates the dyes undergone structural reorganization during excitation from ground to the excited state. The Stokes shifts of the triphenylamine dyes follow the order, **4 < 5 < 6**. The larger Stokes shift observed for **6** when compared to its regioisomer, **5**, points that **6** is undergoing significant structural reorganization due to larger twisting between BTD and triphenylamine units. Similar to absorption, the dyes **3-6**, exhibited blue shift in emission when compared to their corresponding non-methylated dyes (**L1-L3**).

Further, to understand the interaction of dyes with solvent in ground and excited state, solvatochromic study was performed with different solvents. The absorption and emission spectral variation observed due to solvent polarity is displayed in Figures 3.7 and 3.8. It is observed that all compounds displayed solvent insensitive absorption spectra. This clearly points that the ground states of dyes are non-polar in nature and displays no solvent selective association/interaction. However, in the emission spectra, the compounds exhibit positive solvatochromism, i.e. the emission maxima progressively increases on increasing solvent polarity (Figure 3.8). This permits us to make a conclusion that these dyes are selectively stabilized by polar solvents in excited state due to enhanced polarization. Emission shift to longer wavelength for the dyes in the polar solvents may arise due to following reasons, (a) structural reorganization and/or (b) stabilization in polar solvents due to photo-induced ICT. This is further confirmed by comparing the Stokes shifts for the compounds in non-polar (TOL) and polar solvent (ACN). The estimated emission shift ($\Delta\lambda$) between the solvents (λ_{ACN}-λ_{TOL}) for dyes lies in range of 19-86 nm and assumes the order **10** (86 nm).> **9** (53 nm) **8** (43 nm) > **6** (42 nm) > **5** (34 nm) > **11** (25 nm) >**4** (23 nm) > **3** (19 nm). Large Stokes shift and decrement of quantum yield in polar solvents cannot originate from structural changes alone, ICT may be the reason for poor quantum yields observed in **4-6**. [147,148] More drastic effects for **10** supports the above hypothesis where planarization of the molecule may facilitate charge transfer between *N*-phenylcarbazole and BTD.
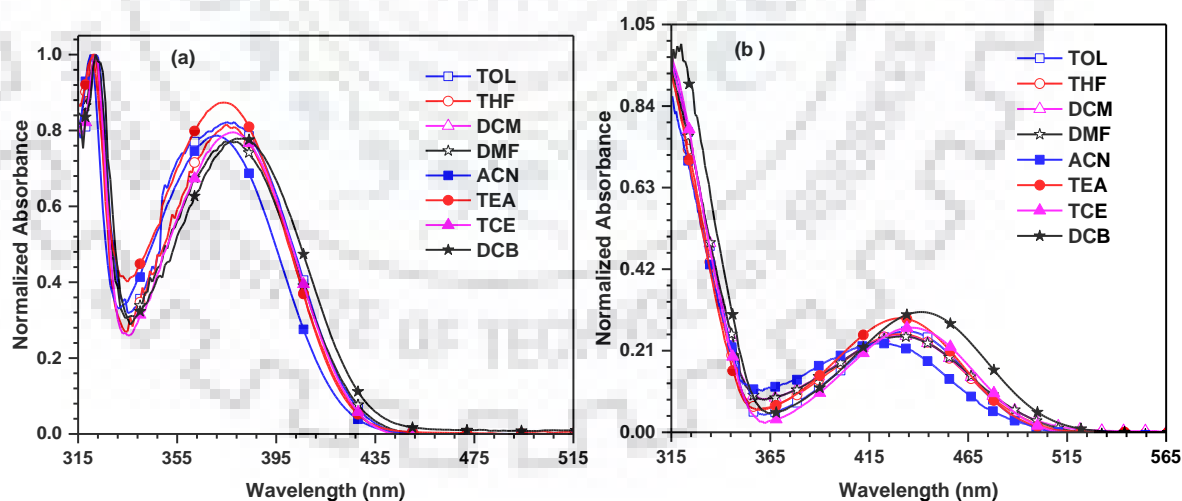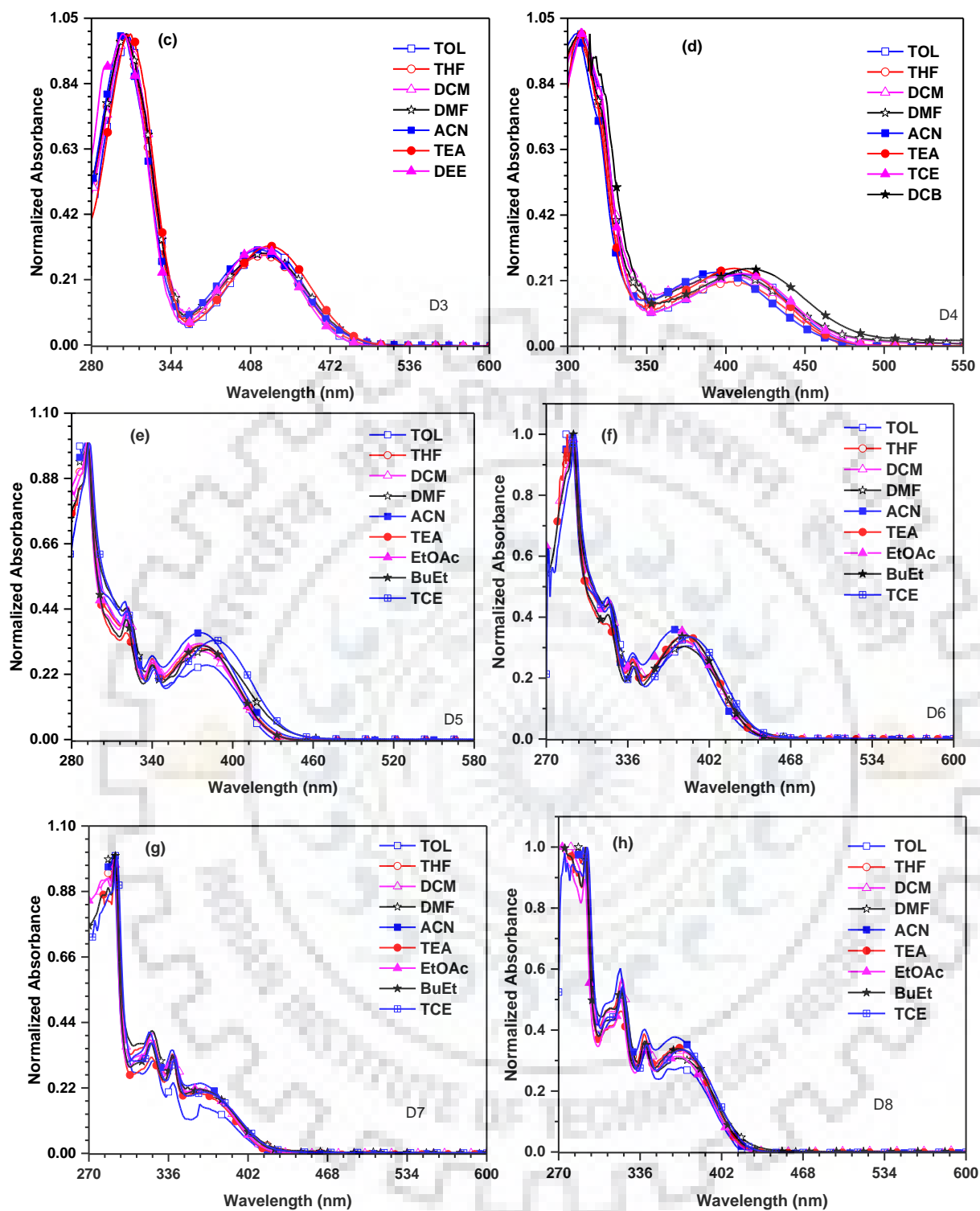
Figure 3.7. Absorption spectra of the dyes recorded in different solvents a) **3** b) **4** c) **5** d) **6** e) **8** f) **9** g) **10** h) **11**
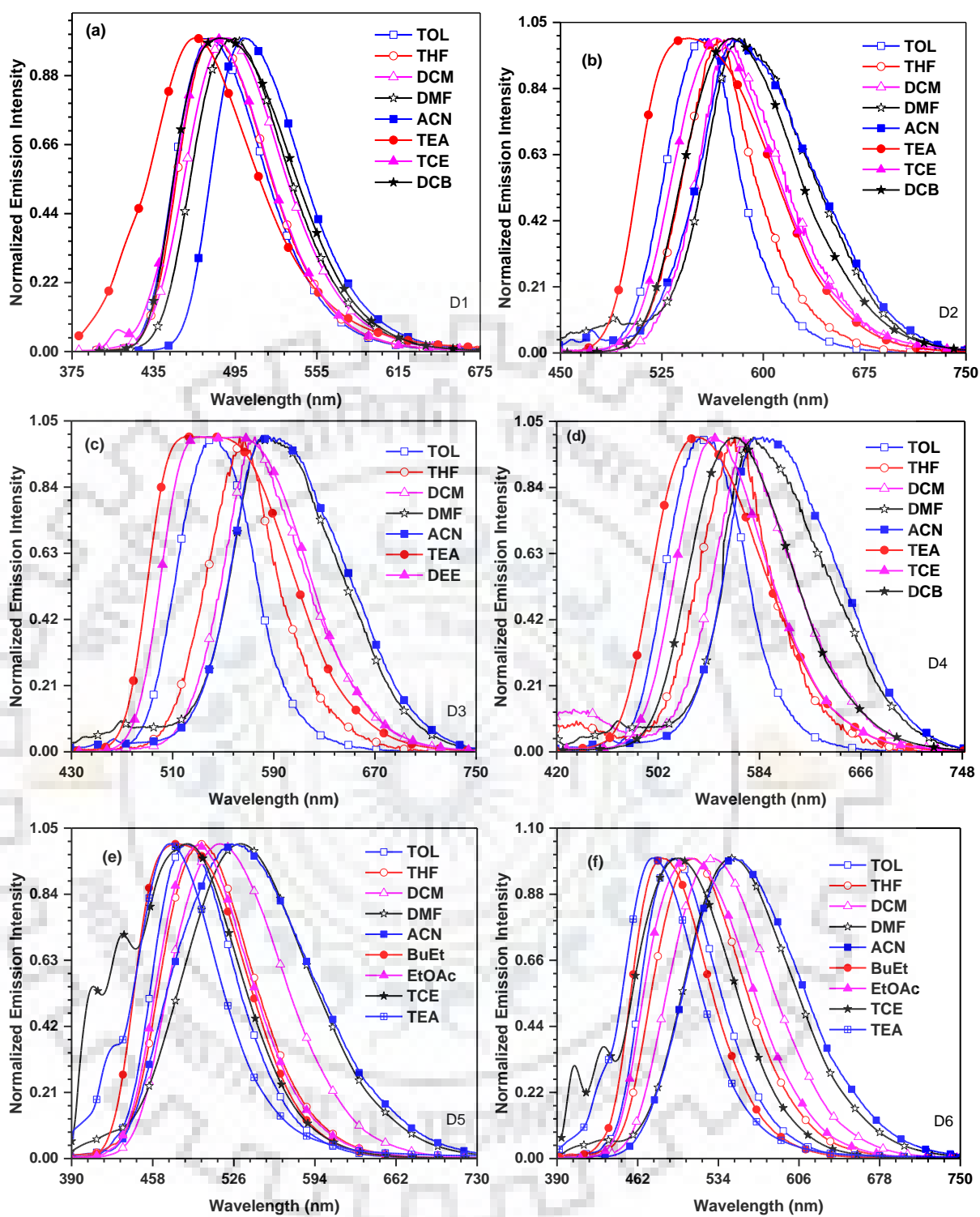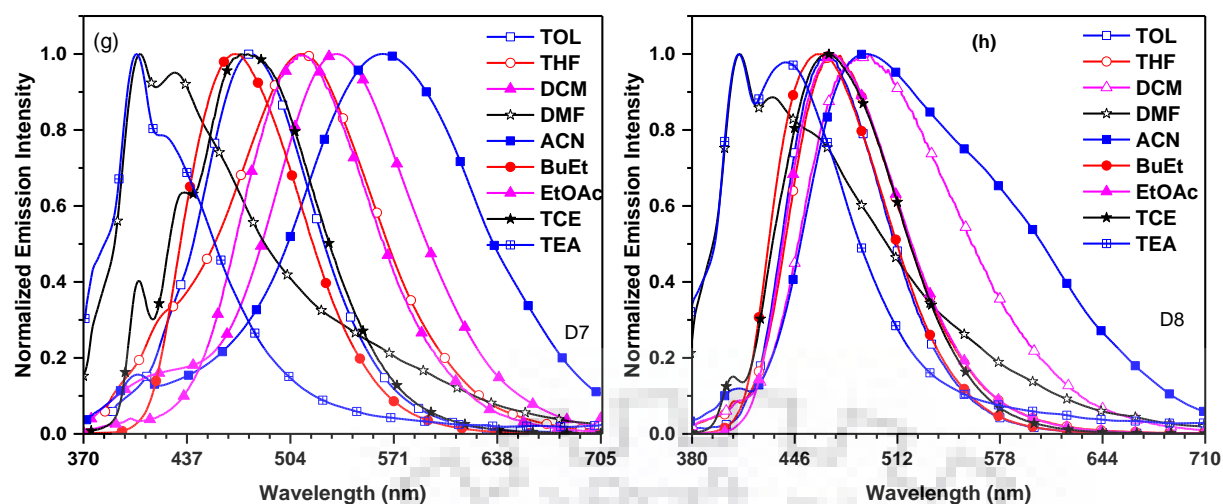
Figure 3.8 Emission spectra of the dyes recorded in different solvents a) **3** b) **4** c) **5** d) **6** e) **8** f) **9** g) **10** h) **11**

Furthermore, the dipole moment of the excited state was evaluated from the slope of a plot of the Stokes shift (v_a–v_f) versus the solvent polarity function f, using the Lippert–Mataga equation.[149] The isomeric dyes exhibited two independent slopes of the fitted line suggesting the presence of two distinct excited-states. [149] (Figure 3.9). Moreover, the isomeric dyes **5, 6, 8, 9** and **11** exhibited dipole moments μ_e, ≤ 9.06D in solvents with low polarity and ≥24.45 D in solvents with high polarity. The usual excited-state, which is a LE-like state, can be attributed to small μ_e of low polarity, while large μ_e of high polarity should be treated as a CT-like state. The inter-crossed coupling of LE and CT excited state in moderate polar environment channels the hybridized local and charge-transfer (HLCT) state. Where, the LE dominates the luminescence of the HLCT state in low-polarity solvents. In addition, as the solvent polarity increases, the CT part in HLCT state gradually decreases owing to the strong interaction between the solvent medium and the excited state of CT (large dipole point) to influence the decay transition of HLCT state, resulting in an inter-crossed character of LE and CT states.[150]
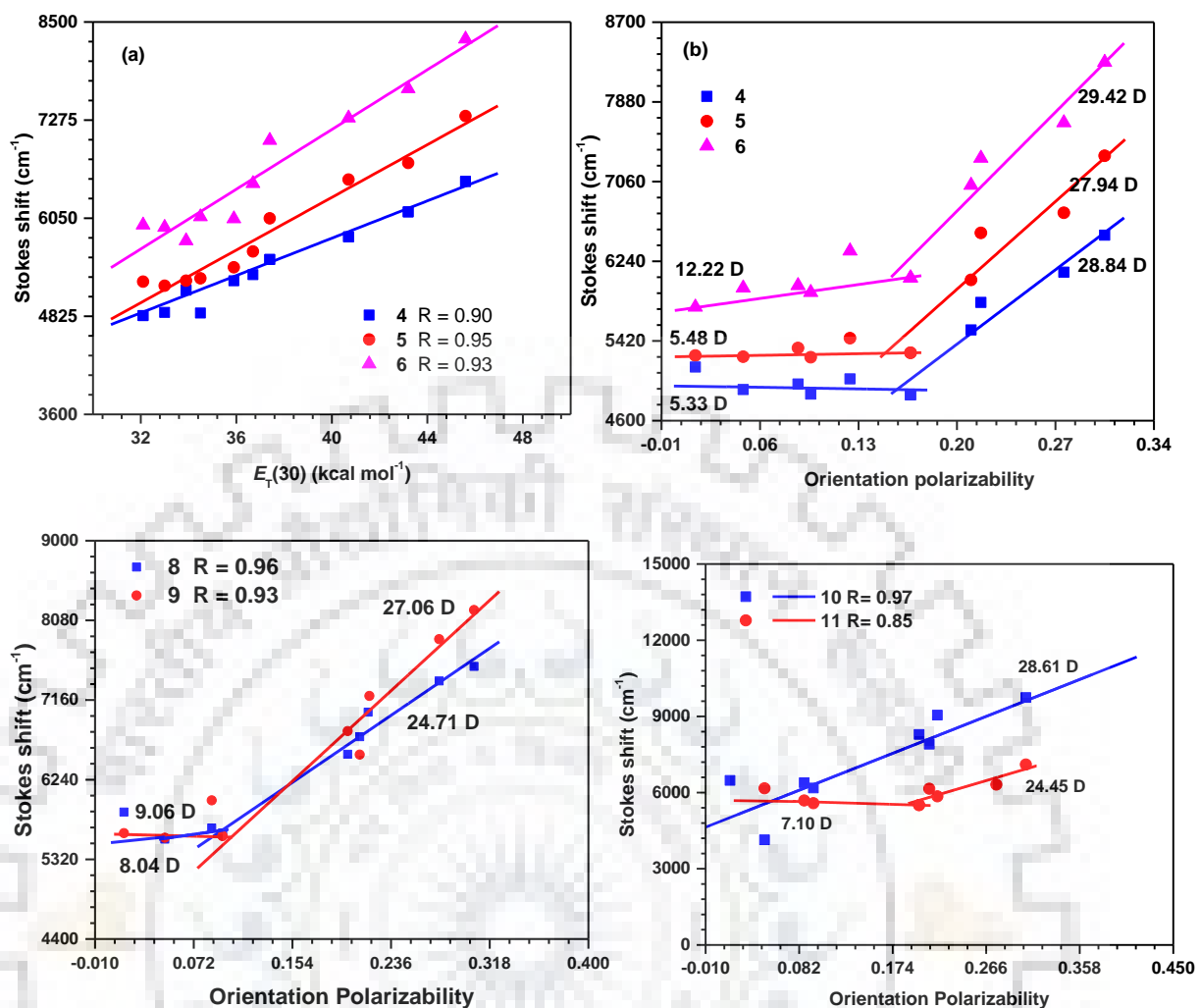
Figure 3.9. Correlation between the Stokes shift and solvent parameter, $E_T(30)$ (a) and correlation plot of *v vs* Δf (b, c and d)
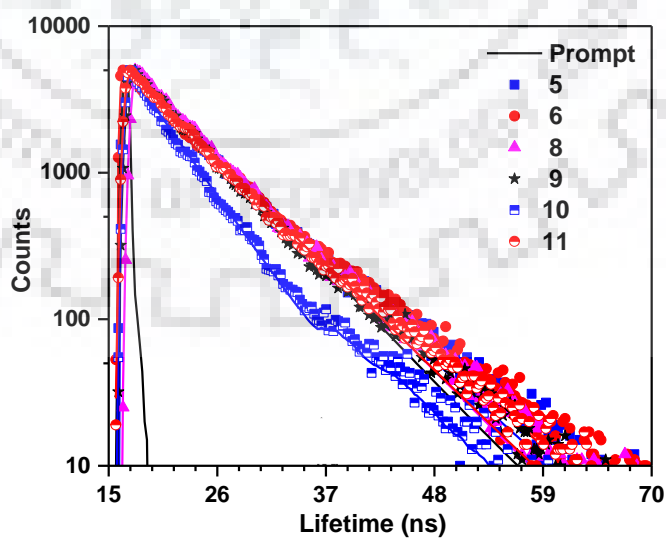
Figure 3.10 Time-resolved fluorescence decay profiles for the dyes in dichloromethane solution

83

Further, single-exponential lifetimes of 6.9, 7.2, 6.3, 6.1, 4.5 and 6.5 ns are acquired for the isomeric dyes **5, 6, 8, 9, 10** and **11**, respectively, which show the inter-crossed LE and CT are formed as one hybridized state not two separated state, as called a hybridized local and charge-transfer state, and shown in Figure 3.10. Furthermore, the radiative rate constant (k_r) and the non-radiative rate constant (k_{nr}) were calculated by using the following relations: $k_r = \Phi_f/\tau_f$ and $k_{nr} = (1 - \Phi_f)/\tau_f$. The similar radiative rate constant $k_r \sim 2.4\text{-}2.9 \times 10^7$ sec^{-1} were observed for the isomeric dyes, which arise from comparable oscillator strength (*vide infra*). However, the non-radiative rate constant (k_{nr}) calculated shows a trend, **10 > 11 > 9 > 8 > 6 > 5** attributable to larger twist angles between donor and acceptor segments. This allows us to suppose that radiationless relaxation processes compete with fluorescence where compound **10** attains highest k_{nr} value (19.3×10^7 sec^{-1}) this may be due to methyl unit at C5 position near *meta N*-pheny carbazole donor unit which coherently impedes the interaction whereas the TPA derivatives (**5, 6**) aided in suppressing the non-radiative process.

The emission spectra recorded for the drop-cast thin films of the dyes are displayed in Figure 3.11. For **4-6** and **9-10** compounds in thin film exhibited a broad emission profile in close resemblance to those observed in TOL solutions. This probably indicates that the dielectric constants for the solid films of the dyes are approximately close to that in corresponding TOL solution and solid state is devoid of aggregation while **8** and **11** dyes showed *H*-type aggregation This indicates the importance of methyl unit in **4-6** and **9-10** dyes in inhibiting aggregation in solid state. [151] Interestingly, all three isomers **5**-**6**, **8-9** and **10-11** exhibited similar emission pattern in solid state suggesting the excited state is similar for both, which may arise due to planarization in the excited state.
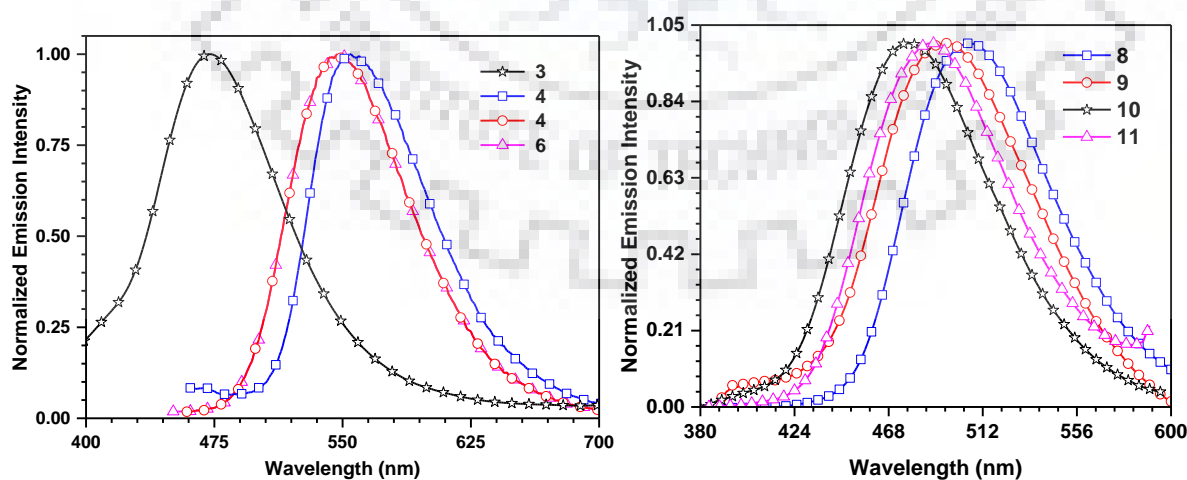
Figure 3.11. Emission spectra of the drop-cast thin films of the dyes.

Table 3.2. Photophysical properties of the dyes

Dye	τ^a (ns)	$\Phi_F{}^b$	$k_r{}^c$ (10^7 s^{-1})	$k_{nr}{}^d$ (10^7 s^{-1})
5	6.89	0.19	2.7	11.0
6	7.22	0.18	2.9	13.0
8	6.3	0.16	2.5	13.3
9	6.17	0.18	2.9	13.3
10	4.55	0.12	2.6	19.3
11	6.49	0.10	1.5	13.9

$^a\tau$ = fluorescence lifetime decay ^{b}Absolute quantum yields determined with a calibrated integrating sphere system. ^{c} Radiative decay rates (k_r) calculated using Φ_F/ τ. ^{d}Non-radiative decay rate (k_{nr}) calculated using $\Phi_F = k_r/(k_r + k_{nr})$.

Table 3.3. Emission data of the dyes recorded in various solvents

Dye	λ_{em} (nm)								$\Delta\lambda$ ($\lambda_{TOL}-\lambda_{DMF}$) (nm)	Stokes shift (cm^{-1})							
	TOL	DCM	THF	ACN	TEA	TCE	DCB	DMF		TOL	DCM	THF	ACN	TEA	TCE	DCB	DMF
3	476	489	477	504	466	481	485	495	19	5801	6146	5845	7186	5350	5665	5767	6253
4	559	577	566	578	546	566	577	582	23	5152	5817	5534	6508	4833	5268	5345	6128
5	546	575	563	469(sh), 586	544	551	566	463(sh), 580	34	5270	6532	6048	7325	5258	5436	5697	6739
6	537	427(sh), 571	439(sh), 564	439(sh), 461(sh), 585	534	545	564	448, 477(sh), 579	42	5768	7301	7022	8287	5965	6042	6483	7666
8	489	514	501	525	473	487	-	532	36	5866	7070	6636	7548	5454	5782	-	7381
9	493	528	510	548	476	499	-	546	55	5623	7307	6570	8348	5170	6002	-	7863
10	478	534	511	564	403, 431	476	-	429	86	6477	9051	7903	9742	4141	6389	-	4314
11	465	498	469	491	410, 440	467	-	432	26	5522	5852	6151	7106	61667	5687	-	6314

Table 3.4 Crystal data and structure refinement for **2a**

Empirical formula	L17 H17 Br N2 S
Formula weight	361.29
Temperature	296(2) K
Wavelength	0.71073 Å
Crystal system	Monoclinic,
Space group	C 2/c
Unit cell dimensions	a = 18.6401(12) Å a = 90°
	b = 14.9843(10) Å b = 112.356(3)°
	c = 12.6094(9) Å g = 90°
Volume	3257.2(4) Å^3
z	8
Density (calculated)	1.474 Mg/m^3
Absorption coefficient	2.647 mm^{-1}
F(000)	1472
Crystal size	None
Theta range for data collection	1.801 to 28.326°
Index ranges	-24<=h<=21, -19<=k<=19, -16<=l<=16
Reflections collected	24989
Independent reflections	4057 [R(int) = 0.0546]
Completeness to theta = 25.242°	100.0 %
Absorption correction	None
Refinement method	Full-matrix least-squares on F^2
Data / restraints / parameters	4057 / 0 / 201
Goodness-of-fit on F^2	0.987
Final R indices [I>2sigma(I)]	R1 = 0.0434, wR2 = 0.1067
R indices (all data)	R1 = 0.1207, wR2 = 0.1435
Extinction coefficient	n/a
Largest diff. peak and hole	0.450 and -0.385 e. Å^{-3}

Table 3.5 Thermal and electrochemical data of the dyes

Dye	T_{onset} (°C)[a]	E_{ox} (V)[b]	HOMO (eV)[c]	LUMO (eV)[d]	E_{0-0} (eV)[e]
3	308	1.12	-5.92	-3.02	2.90
4	445	0.52	-5.32	-2.53	2.79
5	395	0.50	-5.30	-2.84	2.46
6	369	0.49	-5.29	-2.78	2.51
8	394	0.87	-5.67	-2. 77	2.90
9	374	0.87	-5.67	-2.84	2.83
10	436	0.88	-5.68	-2.46	3.22
11	375	0.88	-5.68	-2. 59	3.09

[a] Temperature corresponding to 10% weight loss. [b] Measured for 0.1 mM dichloromethane solutions and the potentials are quoted with reference to ferrocene internal standard. [c] HOMO = -(4.8 + E_{ox}). [d] LUMO = HOMO – E_{0-0}. [e] Optical band gap obtained from the intersection of absorption and emission spectra

3.2.3 Thermal properties

Thermal stability of the compounds was examined by thermogravimetric analysis (TGA) under N_2 atmosphere at a heating rate of 10 °C/min. All the dyes exhibited excellent thermal stability with high thermal decomposition temperature (T_d) in the range 308-445 °C. (Figure 3.12) The onset decomposition temperatures corresponding to the 10% weight loss (T_{onset}) are above 369 °C.(Table 3.5) The triphenylamine and carbazole containing dyes (**4-6 & 8-11**) exhibited higher T_d when compared to **3**. As the carbazole functionalization adds up thermal robustness due to rigid molecular structure to the dyes. Since the isomeric dyes (**5 & 6, 8 & 9, 10 & 11**) possess same molecular weight the difference in thermal stability may arise from variation in geometrical orientations. It is probable that in **5,** a more planar arrangement between BTD and triphenylamine units helps to achieve ordered structure in solid state. The compounds containing planar fragments are reported to exhibit pronounced thermal stability.[152] Interestingly, dyes **8** and **10** exhibits better thermal stability when compared to its isomers **9** and **11.** Further on comparison with non-methylated BTD derivatives (**L1-L3**), MBTD derivatives exhibited enhanced thermal stability which supports the effective influence of methyl on the rigidity and thermal stability of molecules.
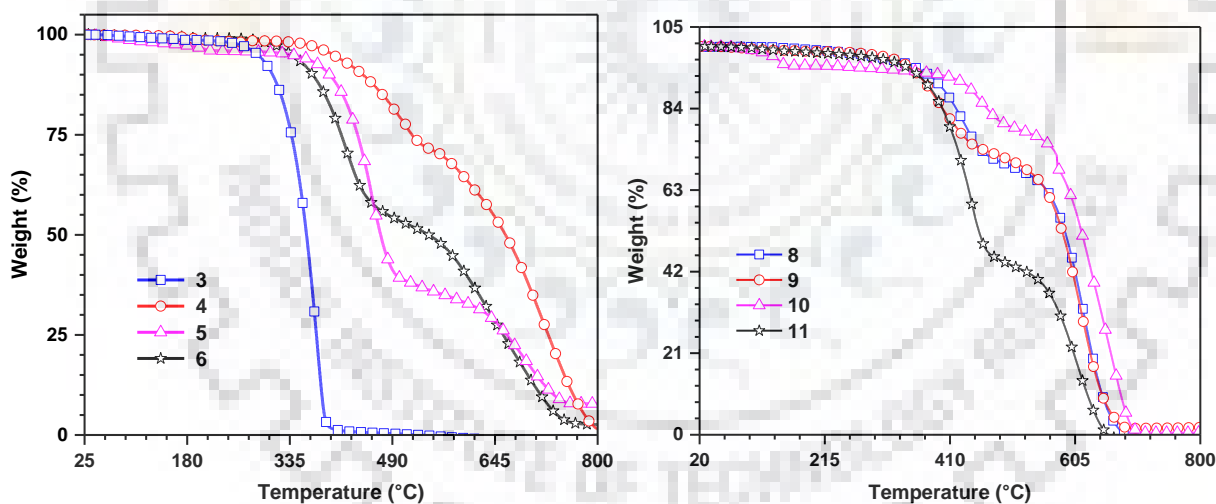
Figure 3.12. Thermogravimetric plots of the dyes.

3.2.4 Electrochemical properties

To investigate the redox propensity of the compounds cyclic voltammetric studies were conducted for the dyes in DCM solution. All the triphenylamine containing dyes (**4, 5** and **6**) exhibited a quasi-reversible oxidation, (Figure 3.13) attributable to the removal of electron from triphenylamine unit while *N*-phenlcarbazole containg dyes (**8-11**) exhibits irreversible oxidation

attributed to oxidation of carbazole moiety. The oxidation potential of **4-6** dye are lower than that of **3, 8, 9, 10, 11** which further supports the involvement of electron rich triphenylamine in oxidation. The HOMO and LUMO energy levels of the materials are very crucial parameters for the understanding of charge transport kinetics in the molecular layers. The HOMO energy levels of the compounds (Table 3.5.) were calculated using oxidation potential of the dyes with reference to ferrocene HOMO energy (4.8 eV) which falls in the range 5.29-5.68 eV. The energies of lowest unoccupied molecular orbital (LUMO) were estimated by subtracting the band gap (E_{0-0}) from the HOMO values where the band gaps of the compounds were obtained from the optical edge.
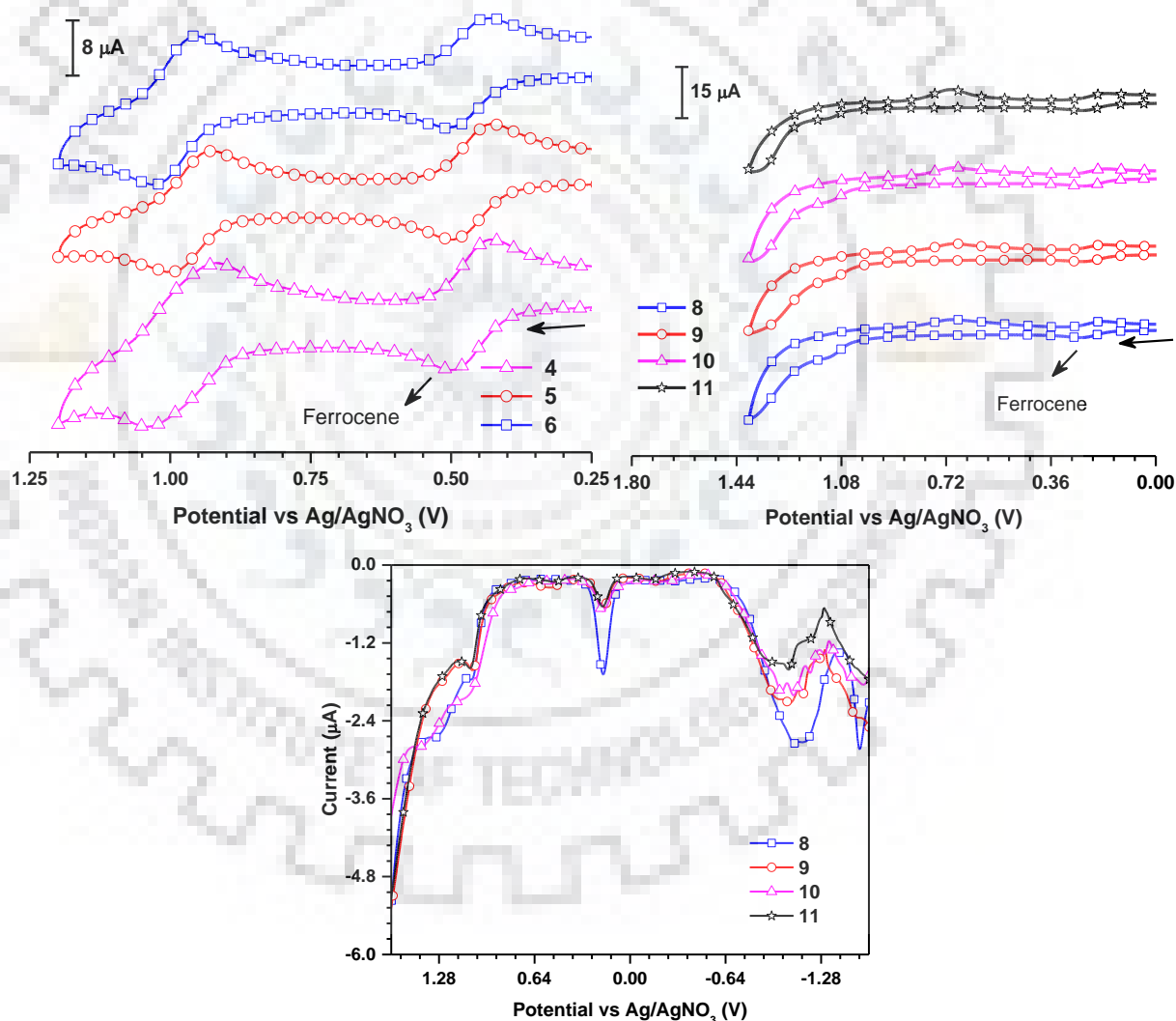
Figure 3.13. Cyclic voltammograms and Differential Pulse Voltammogram of the dyes recorded in DCM a) triphenylamine based dyes (**4-6)** and b) carbazole based dyes (**8-11)**

The presence of TPA, an electron donating group upshifts the HOMO & LUMO energy level of **4-6** dyes when compared to **8- 11** dyes showing the difference of electron richness between TPA and *N*-phenylcarbazole. Further, among the isomers the E_{0-0} of **5, 9 and 11** is smaller than **6, 8 and 10** which participates in keeping conjugation effects more facile in absorption profile as described before (*vide supra*).
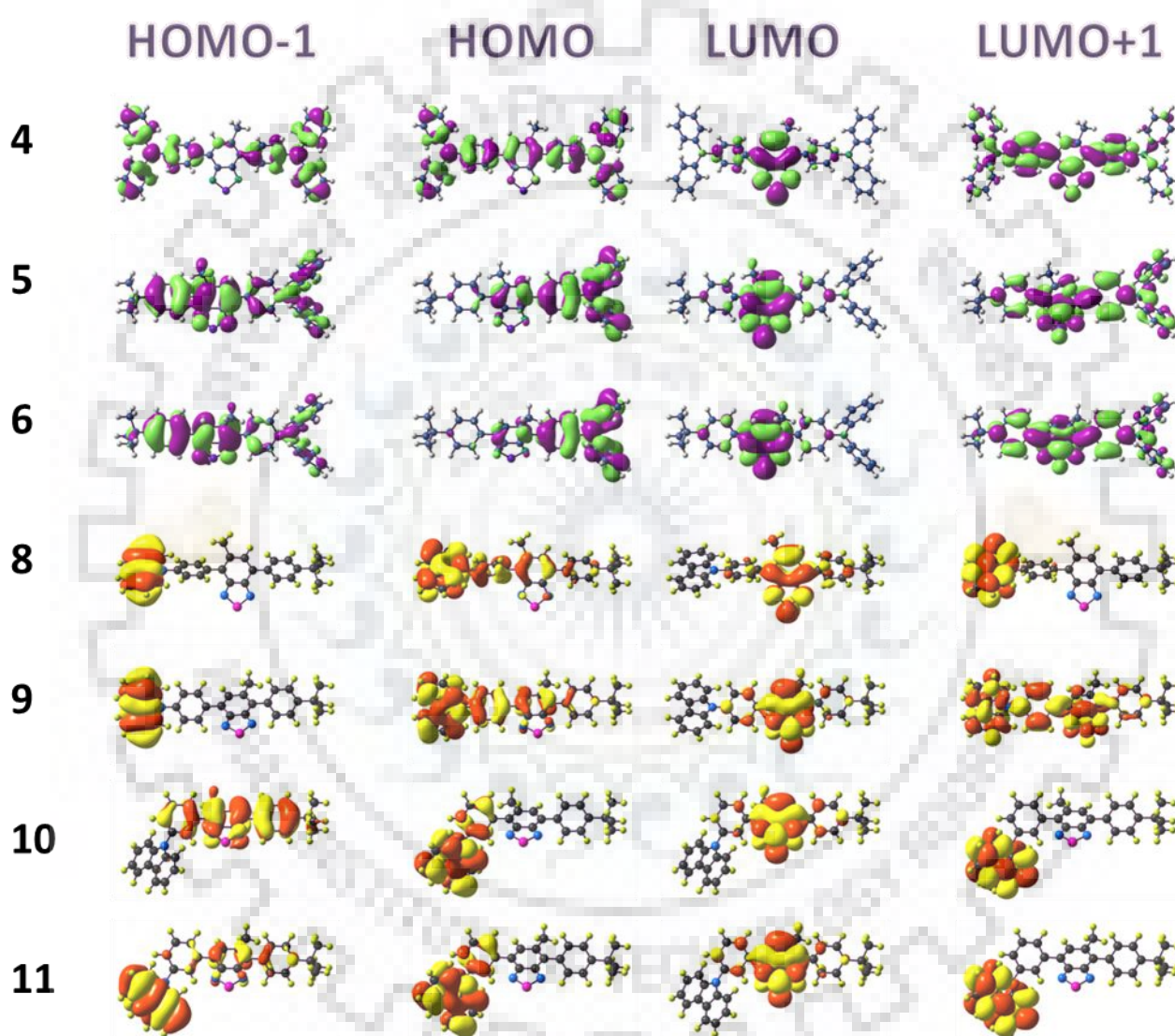
Figure 3.14. Composition of frontier molecular orbitals of the compounds **4-11.**

3.2.5 Theoretical investigations

To further unravel the electronic structure of the dyes, DFT calculation was performed as implemented in Gaussian 09 program package. [153] The computed absorption wavelengths, their oscillator strengths (*f*) and orbital contributions for the most-appropriate transitions of the

compounds are listed in Table 3.5. The optimized geometries of the dyes showed variations attributable to the presence of methyl group on BTD nucleus as described earlier. (Figure 3.3). The HOMOs of **4-6, 8-9** are generally delocalized over the triphenylamine/*N*-phenylcarbazole and benzene of BTD unit (Figure 3.14), while BTD exclusively participated in constructing the LUMOs. This indicates an appreciable charge transfer from the triphenylamine/N-phenylcarbazole donor to BTD acceptor for the visible wavelength absorption. However in **10** & **11,** HOMOs are restricted to *N*-phenylcarbazole while BTD absolutely participated in constructing the LUMOs. In **3**, HOMO is on the phenyl rings in the conjugation path very similar to the HOMO in **5** & **6**. The absorption in **3** is mainly originates π-π* type. Further, on comparing isomers, **5** & **6**, in **5** the HOMO is mainly localized on triphenylamine unit and spread upto BTD. However, in **6**, the HOMO is located on triphenylamine unit and relatively less contributed by BTD unit due to the large dihedral angle between BTD and triphenylamine induced by methyl unit. The similar organization of frontier orbitals has been observed in **8** & **9** dyes, this corroborates the observation of blue shift in absorption for **6**, **8** dyes when compared to **5**, **9** dyes. Interestingly, no such effect is observed in **10** and **11** dyes as the *meta* positioning breaking the link for electronic communication thus methyl role is not much manifested. This corroborates to blue shift in absorption for *meta* linked dyes when compared to *para* substituted dyes

3.2.6 Electroluminescence Characteristics

To assess the electroluminescence performance of the materials two type of OLED devices I, II and III were fabricated with multilayer configuration. The compounds were employed either as host emitters (device I) or dopants emitters (device II) in TCTA host and (device III) in CBP host with different concentrations (1 or 3 or 5wt %). The device configuration is ITO/PEDOT:PSS/**4-11**/TPBi/LiF/Al for device I, ITO/PEDOT:PSS/TCTA:**4-6**/TPBi/LiF/Al for device II and ITO/PEDOT:PSS/CBP:**8-11**/TPBi/LiF/Al for device III. Here, poly(3,4-ethylenedioxythiophene)-poly(styrenesulfonate) (PEDOT:PSS) served as hole injection layer, 1,3,5-tris(*N*-phenylbenzimidazol-2-yl)- benzene (TPBi) functioned as electron transporting layer (ETM) and hole blocking layer. The emitting layers were sandwiched between ITO anode and Al cathode. An additional electron injection layer (LiF) was also used. For the doped devices, tris(4-carbazoyl-9-ylphenyl)amine (TCTA) and 4,4′-Bis(*N*-carbazolyl)-1,1′-biphenyl (CBP) was used as host material as it possessed suitable HOMO and LUMO to ensure efficient charge trapping by new dyes. The energy level alignment for the compounds used in the devices is depicted in Figure 3.15

Table 3.6 Computed absorption wavelengths and their oscillator strengths (*f*) of dyes.

Dye	λ_{abs} (nm)	*f*	Assignment (%)
4	430.0	0.66	HOMO→LUMO (90%)
	295.3	1.22	HOMO→LUMO+1 (72%)
	272.3	0.73	HOMO-7→LUMO (24%), HOMO-1→LUMO+6 (19%), HOMO→LUMO+6 (20%)
5	417.8	0.51	HOMO-1→LUMO (10%), HOMO→LUMO (87%)
	289.8	0.77	HOMO→LUMO+1 (82%)
	275.9	0.24	HOMO-6→LUMO (70%), HOMO-2→LUMO (11%)
	272.7	0.29	HOMO→LUMO+3 (90%)
6	408.6	0.43	HOMO-1→LUMO (15%), HOMO→LUMO (83%)
	287.0	0.78	HOMO →LUMO+1 (70%), HOMO→LUMO+4 (19%)
	275.0	0.29	HOMO-6→LUMO (38%), HOMO-5→LUMO (28%), HOMO-2→LUMO (12%)
	272.4	0.31	HOMO→LUMO+3 (92%)
8	376.84	0.5013	HOMO-2→LUMO (49%), HOMO→LUMO (48%)
	281.21	0.1202	HOMO→LUMO+1 (82%) HOMO-2→LUMO+1 (7%), HOMO-1→LUMO+6 (7%)
	276.02	0.2577	HOMO-6→LUMO (48%), HOMO-4→LUMO (12%), HOMO-3→LUMO (27%) HOMO-2→LUMO+7 (3%)
9	380.02	0.525	HOMO-2→LUMO (36%), HOMO→LUMO (62%)
	281.53	0.1323	HOMO→LUMO+1 (34%), HOMO→LUMO+2 (47%) HOMO-2→LUMO+1 (2%), HOMO-2→LUMO+2 (6%), HOMO-1→LUMO+6 (7%)
	277.33	0.1949	HOMO-6→LUMO (66%), HOMO-3→LUMO (24%) HOMO-2→LUMO+7 (2%)
10	367.1	0.4353	HOMO-1→LUMO (96%) HOMO-2→LUMO (2%)
		0.2391	HOMO-6→LUMO (43%), HOMO-3→LUMO (31%) H-7→LUMO (3%), HOMO-5→LUMO (7%), HOMO-4→LUMO (7%), HOMO-1→LUMO+4 (2%), HOMO-1→LUMO+7 (4%)
11	366.14	0.4187	HOMO-2→LUMO (77%), HOMO-1→LUMO (15%) HOMO→LUMO (5%)
	278.15	0.1051	HOMO-6→LUMO (35%), HOMO-3→LUMO (52%) HOMO-5→LUMO (2%), HOMO→LUMO+1 (4%)

From this, it is evident that the hole and electron injection into emissive layer is facile and does not involve retarding energy barrier. Current density–voltage–luminescence (I–V–L) plots of the diodes are shown in Figure 3.16 and the key parameters listed in Table 3.7. Relatively, device I exhibited high current densities for dyes **4-6** and low operating voltages than device II and III. However, device I showed poor luminance when compared to corresponding doped device (Device II and III). It indicates the leakage of charge carriers at the interface of respective electrodes

without formation of excitons in emitting layer for device I. [154] The failure of non-doped device (device I) is attributed to the large hole injection barrier (> 0.42 eV) when compared to electron injection barrier (> 0.14 eV), which would impede the charge transport balance in the molecular layers.
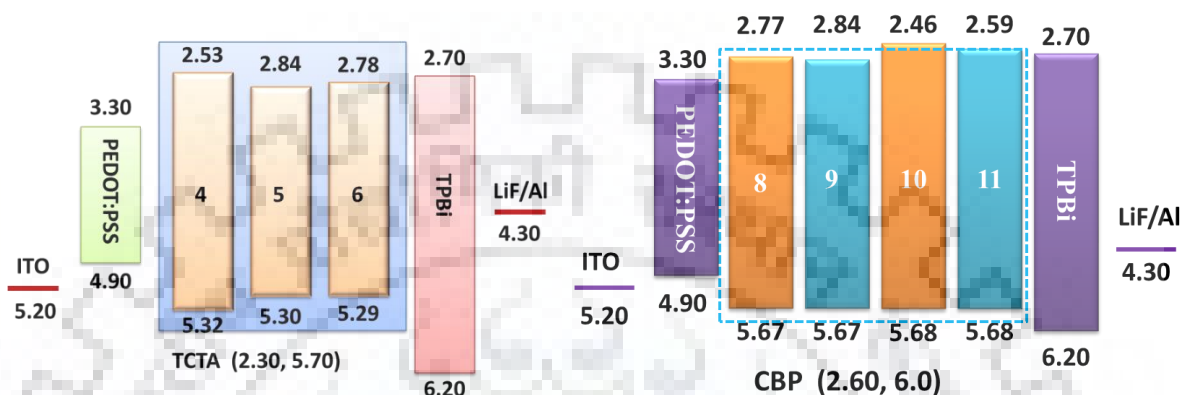
Figure 3.15 Energy-level diagram of the materials used for the fabrication of OLED devices (all values are in eV with respect to vacuum level).

Therefore, to boost the EL performance of the compounds, we employed them as dopant emitters in TCTA and CBP host matrix with different weight ratios (1 wt%, 3wt% and 5 wt %). It is noted that the current densities of doped device reduced with dramatic enhancement in the brightness. This can be explained as follows, the main charge carriers in device II is TCTA and in device III is CBP, which can guarantee balanced charge transport and restriction of recombination zone in emitting layer. Secondly, the well matched energy levels of host with guest can effectively trap the electronically generated excitons by guest emitters, which ensure the electroluminescence originate from guest. I-V characteristic of the doped devices, irrespective of dopant concentration remained same further confirming the charge carrier as host. [154] Drop in luminance at high current density is characteristic of charges leaking to electrode without recombining to form excitons in the emitter layer or exciton formation at the electrode/interface. [154,155] Such excitons may be quenched at the electrode without emission. [156, 157] The diodes with 3 and 5 wt% dyes exhibited excellent performance in the **8-11** and **4-6** series respectively with maximum luminescence, current efficiency, power efficiency and EQE.
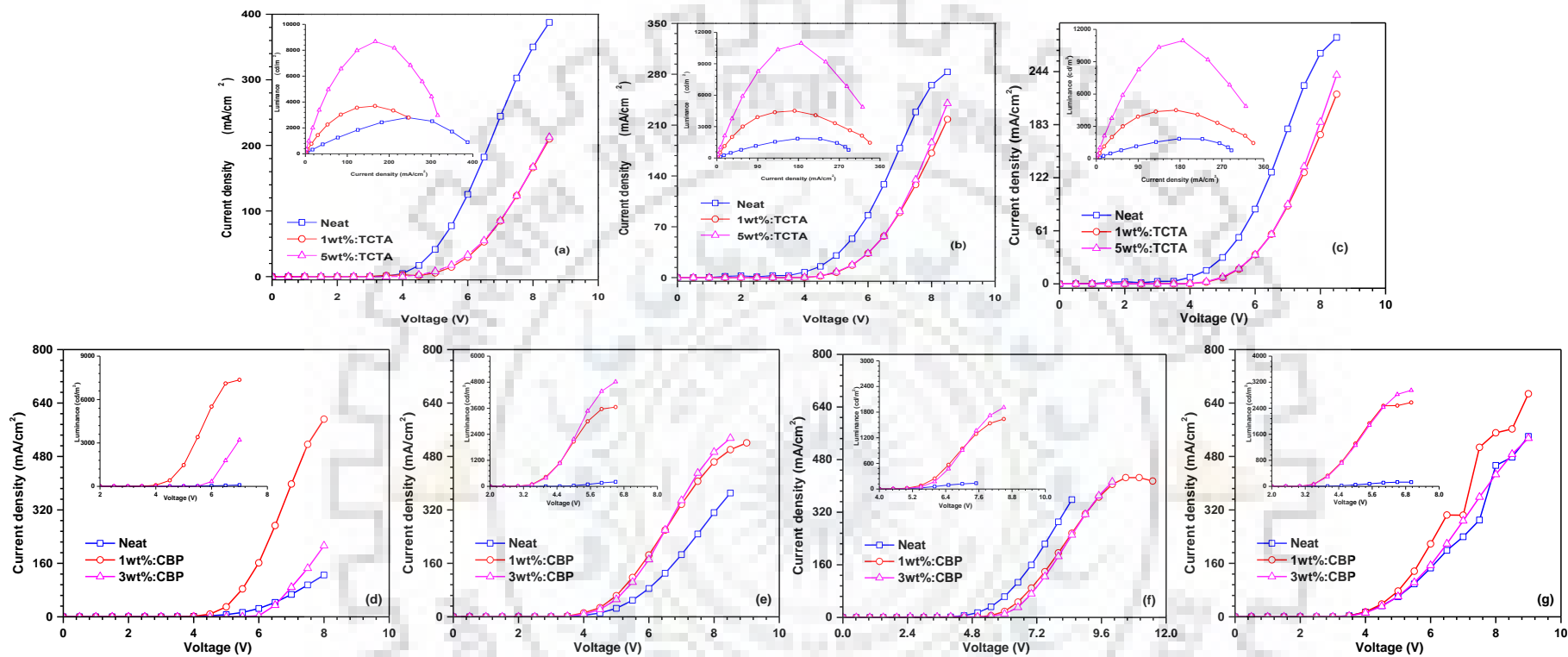
Figure 3.16 Current density–voltage (I–V) and luminance–current density (L–I) plots of the diodes of(a) **4,** (b) **5** (c) **6** (d) **8**(e) **9**(f) **10**(g) **11**
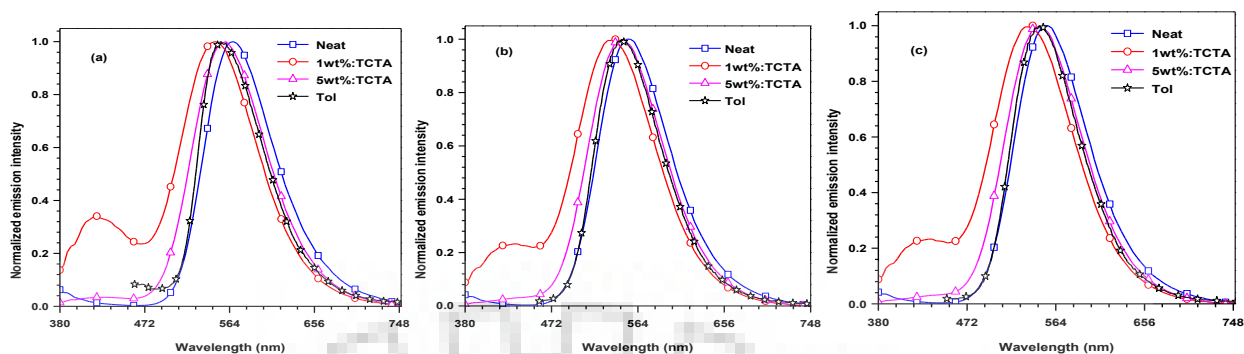
Figure 3.17 Comparison of EL and PL spectra of (a) **4**, (b) **5** and (c) **6.**
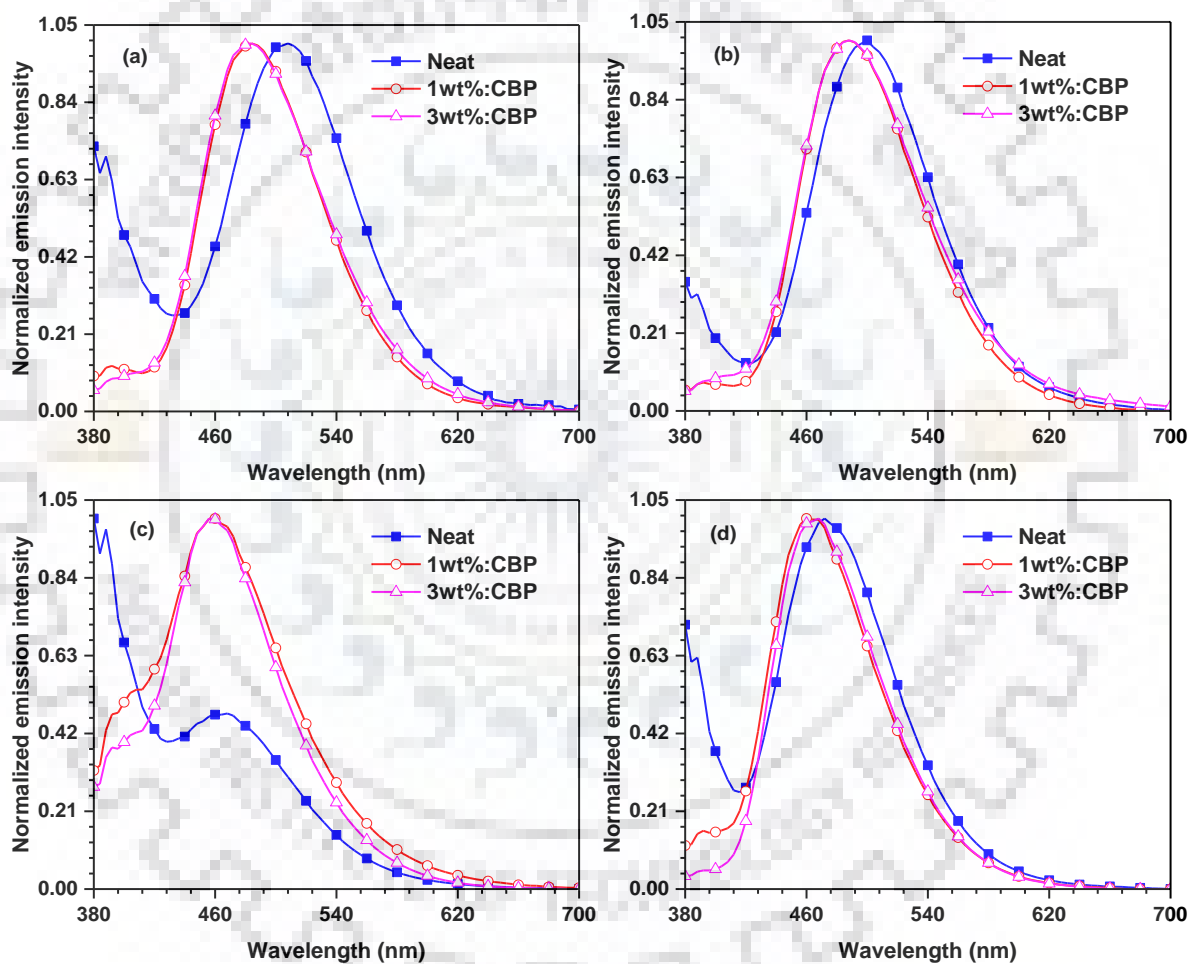
Figure 3.18 EL spectra of the diodes in different doping concentrations (a) **8**, (b) **9** (c) **10** and (d) **11.**

The EL spectra of the devices are shown in Figures 3.17 and 3.18 The EL profiles of devices doped with **4-6** are displayed close resembling (>556 nm) that observed in solid film and in toluene. However **8** and **11** only displayed resemblance in toluene solution. This clearly suggests

95

the recombination occurs in the emitting layer and excitons transferred effectively to the dopant. At low concentration of dopant (1%) a higher energy shoulder is observed at ~420 nm attributable to the TCTA/CBP emission. [154, 158] This suggests incomplete energy trapping at low dye concentration. Interestingly, with increasing the dopant concentration the EL maxima and color coordinates showed negligible change indicating stability for EL even at high doping concentration. Overall the device based on **5** with 5 wt% dopant concentration exhibited excellent performance in the series with L_{max} of 10960 cdm^{-2}, η_c of 15.7 cdA^{-1}, η_p of 12.1 lmW^{-1} and EQE of 4.6%. This is attributed to its low lying LUMO and efficient trapping of generated excitons in TCTA host due to its well aligned energy levels with the host matrix.

Table 3.7 Electroluminescence characteristics of the dyes

Dye	Conc. (wt%)[a]	Driving Voltage[b] (V)	Power Efficiency[b] (lm W^{-1})	Current Efficiency[b] (cd A^{-1})	EQE[b] (%)	CIE[b]	Max. luminescence (cd m^{-2})	EL max. (FWHM) (nm)
4	Neat	4.0/5.3	1.4/1.0	1.8/1.7	0.6/0.5	(0.48, 0.51)/(0.47, 0.52)	2797	568 (88)
	1	4.5/5.7	4.3/2.9	6.2/5.1	2.1/1.8	(0.35, 0.48)/(0.34, 0.47)	3692	548 (91)
	5	4.1/5.0	11.6/7.8	15.0/12.5	4.5/3.8	(0.42, 0.54)/(0.42, 0.53)	8675	560 (93)
5	Neat	3.8/5.9	1.0/0.7	1.2/1.4	0.4/0.4	(0.43, 0.55)/(0.42, 0.56)	2040	556 (89)
	1	4.3/5.4	5.9/4.0	8.0/6.8	2.6/2.3	(0.32, 0.50)/(0.31, 0.49)	4502	540 (91)
	5	4.1/5.0	12.1/8.5	15.7/13.5	4.6/3.9	(0.38, 0.56)/(0.38, 0.56)	10960	548 (92)
6	Neat	4.6/6.8	1.2/0.8	1.7/1.7	0.5/0.5	(0.40, 0.57)/(0.38, 0.57)	1675	556 (89)
	1	4.3/5.1	10.9/5.7	15.2/9.2	4.8/3.0	(0.30, 0.52)/(0.29, 0.49)	4361	540 (91)
	5	4.1/5.0	10.9/8.5	14.1/13.6	4.1/4.0	(0.36, 0.56)/(0.34, 0.55)	8447	548 (92)
8	1	-	4.1/3.3	5.2/5.0	2.5/2.6	(0.18, 0.31)/ (0.17, 0.3)	7359	484 (92)
	3	-	3.3/4.0	5.9/7.8	2.8/4	(0.18, 0.31)/ (0.18, 0.3)	4939	484 (92)
9	1	-	3.7/2.8	4.2/3.9	1.9/2	(0.18, 0.34)/ (0.18, 0.32)	3653	488 (94)
	3	-	4.8/3.4	5.4/4.8	2.4/2.3	(0.20, 0.35)/ (0.19, 0.33)	4821	488 (94)
10	1	-	0.8/0.5	1.4/1.0	1.1/0.9	(0.17, 0.19)/ (0.17, 0.18)	1639	456 (112)
	3	-	0.8/0.5	1.5/1.2	1.1/1.0	(0.16, 0.18)/ (0.16, 0.17)	1911	456 (87)
11	1	-	2.1/1.2	2.4/1.8	1.7/1.5	(0.16, 0.19)/ (0.16, 0.18)	2578	460 (83)
	3	-	2.2/1.4	2.5/2.2	1.7/1.6	(0.15, 0.2)/ (0.16, 0.19)	2951	460 (81)

[a] concentration of dye for doped devices (device II) [b] value at 100/1000 cd/m^2

3.3. Conclusions

In conclusion, we have synthesized a series of methyl substituted benzothiadiazole containing derivatives featuring triarylamine and *N*-phenylcarbazole by Suzuki coupling reaction protocol. The methyl substitution on BTD nucleus helped us to obtain three pairs of positional isomers **5** & **6, 8** & **9, 10** & **11** by changing the sequence of Suzuki coupling reagents. The structure-function relationships of the dyes were studied systematically and compared with the non-methylated BTD derivatives (**L1-L3**). The triphenylamine substituted derivatives (**4, 5** & **6**) showed red-shifted absorption/emission profiles when compared to 4- *tert*-butyl phenyl (**3**) and *N*-phenylcarbazole analogue (**8-11**). Among the positional isomers, **5** exhibited bathochromic shift when compared to **6** due to steric hindrance on triphenylamine by methyl unit, which probably led to twisted arrangement hampering conjugation. However, among *N*-phenylcarbazole derivatives, *para* linked exhibited bathochromic shift to *meta* analogs due to presence of better electronic communication. The absorption profiles of the dyes are insensitive to the solvent polarity suggestive of non-polar ground state. However, the dyes exhibited positive solvatochromism in emission indicating a polar excited state involving significant structural and electronic reorganizations. **5** displayed higher thermal stability than its isomer **6**, attributable to the more planar arrangement of BTD and triphenylamine units in former.. Electrochemical studies showed HOMO/LUMO shift to high level in triphenylamine derivatives (**4, 5** & **6**) compared to 4- *tert*-butyl phenyl (**3**) and *N*-phenylcarbazole analogue (**8-11**). Further, the dyes were applied in solution processable multilayer OLEDs either as host emitters or as dopant emitters. The doped devices exhibited green or yellowish green electroluminescence with CIE of $0.36 \leq x \leq 0.43$, $0.54 \leq y \leq 0.56$ and superior luminance. The device fabricated with isomer **5** exhibited better performance in the series attributable to well-aligned energy levels which resulted in EQE of 4.6% (15.7cd A^{-1}) and L$_{max}$ of 10960 cd m^{-2} with 5 wt% dopant concentration.

3.4. Experimental Section

3.4.1. General Methods

All chemicals bought from commercial source and used as received without further purification. The solvents have been dried and distilled with standard distillation set up to be used for synthesis and analytical assay. For purification of the compounds column chromatography has been used with silica gel (100-200 mesh) as the stationary phase. The

NMR spectral data (^{1}H and ^{13}C) has been collected on JEOL 400 MHz NMR spectrometer in $CDCl_3$, with TMS (0.00 ppm) as internal standard, to calibrate the chemical shift values. Mass spectral (HRMS) data were recorded on ESI TOF high resolution mass spectrometer. Elemental analyses for carbon, hydrogen and nitrogen were performed on a Vario EL III microanalyzer. Optical measurement such as absorption and emission has been conducted at room temperature on Cary 100 UV-vis spectrophotometer and Shimadzu spectrofluorimeter, respectively Absolute quantum yield were recorded by a calibrated integrating sphere connected to the spectrofluorimeter. Cyclic voltammetric (CV) and differential pulse voltammetric (DPV) experiments were performed by using an electrochemical analyzer with a conventional three-electrode configuration consisting of a glassy carbon working electrode, platinum auxiliary electrode, and a non-aqueous $Ag/AgNO_3$ reference electrode. The potential are quoted against ferrocene internal standard. The measurements were performed at room temperature in 1×10^{-4} M dichloromethane solution and using 0.1M tetrabutylammonium perchlorate as a supporting electrolyte Thermogravimetric analysis (TGA) was performed under nitrogen atmosphere at heating rate of 10 °C /min. All the reactions were performed under a nitrogen atmosphere unless mentioned specifically.

3.4.2. Theoretical computations

All the theoretical computations were performed with the Gaussian 09 program package. [153] The ground-state geometries were fully optimized without any symmetry constrains at the density functional theory (DFT) level with Becke's three parameters hybrid functional and Lee, Yang and Parr's correlational functional B3LYP and MPW1K using the 6-31G(d,p) basis set on all atoms. [158,159] Vibrational analyses on the optimized structures were performed to confirm the optimized structures belonging to minima. The oscillator strengths and excitation energies for the lowest singlet transitions at the optimized geometry in the ground state were obtained by TD-DFT calculations by using the same basis set and MPW1K functional. [160]

3.4.3. X-ray Crystal Structure Determination

Crystals of the compounds **2a** suitable for X-ray data collection were grown from dichloromethane/hexanes mixture. X-ray data of **2a** was collected on a CCD diffractometer using Mo Kα (λ = 0.71073). The data were corrected for Lorentz and polarization effects. A total of 24989 reflections were measured out of which 4057 were observed [I>2 σ(I)] for maximum theta 28.326° at room temperature. The structures were solved by direct methods using SHELXS-97 and refined by full-matrix least squares refinement methods based on F^2, using SHELXL-2014/7. All non-hydrogen atoms were refined anisotropically. All hydrogen

atoms were fixed geometrically with their U_{iso} values 1.2 times of the phenylene and methylene carbons and 1.5 times of the methyl carbons. All calculations were performed using Bruker SHELXTL package. A final refinement of 201 parameters gave R1 = 0.0434, wR2 = 0.1067 for the observed data and R1 = 0.1207, wR2 = 0.1435 for all data. Crystal data refinement conditions and experimental details are tabulated in Table 2.

3.4.4. OLED device fabrication

The electroluminescent devices were fabricated using a pre-cleaned glass substrate deposited with indium tin oxide (ITO) (thickness: 125 nm) as an anode, poly(3,4-ethylene-dioxythiophene)–poly(styrenesulfonate) (PEDOT:PSS, thickness: 35 nm) as a hole-injection layer (HIL), an emissive layer (EML), TPBi as an electron-transport layer (ETL) (thickness: 35 nm), lithium fluoride (LiF) as an electron-injection layer (EIL, thickness: 0.7 nm), and an Al layer as a cathode (thickness: 150 nm). At first, the aqueous solution of PEDOT: PSS was spin-coated at 4000 rpm for 20 s to form a 35 nm HIL layer. Dyes **4**, **5** and **6** were doped in tris(4-carbazoyl-9-ylphenyl)amine (TCTA) and **8**, **9, 10** and **11** doped in 4,4′-Bis(*N*-carbazolyl)-1,1′-biphenyl (CBP) deposited by spin-coating at 2500 rpm for 20 s and served as an emissive layer. After that, the TPBi layer was coated onto it. Finally, LiF and the Al cathode were thermally evaporated at 1.0×10^{-5} Torr.

3.4.5. Synthesis

4-Bromo-7-(4-*tert*-butylphenyl)-5-methylbenzo[*c*][1,2,5]thiadiazole (2a). A mixture of 4,7 –dibromo-5-methylbenzo[*c*][1,2,5]thiadiaole (0.40 g, 1.29 mmol), 4-*tert*-butylphenylboronic acid (0.21 g ,1.16 mmol), K_2CO_3 (0.53 g, 3.87 mmol), Pd(PPh₃)₄ (3 mol%) and THF:H₂O (3:1) was heated at 80°C under nitrogen atmosphere. After completion of the reaction, it was poured into ice water and extracted with chloroform. The combined organic layer was thoroughly washed with water and dried over anhydrous Na_2SO_4, filtered organic extract was evaporated to obtain orange residue, which was purified by column chromatography on silica gel using hexanes/chloroform (1:1) as eluant. Pale yellow solid (0.30 g, 65%); mp 108−112 °C; [1] H NMR (400 MHz, CDCl₃, δ ppm): 7.82 (d, *J* = 8.0 Hz, 2H), 7.95 (s, 1H), 7.55 (d, *J* = 8.0 Hz, 2H), 2.60 (s, 3H), 1.38 (s, 9H); [13] C NMR (100 MHz, CDCl₃, δ ppm): 154.6, 152.1, 151.9, 139.9, 133.7, 132.8, 131.2, 128.9, 125.8, 113.2; 34.8, 31.4, 23.0; HRMS (ESI-TOF) *m/z*: [M]$^+$ Calcd for $C_{17}H_{17}BrN_2S$ 360.0290, found 360.0293; Anal. Calcd for $C_{17}H_{17}BrN_2S$: C, 56.51; H, 4.74; N, 7.75; S, 8.87. Found: C, 56.51; H, 4.52; N, 7.58; S, 8.73.

4-(7-Bromo-6-methylbenzo[*c*][1,2,5]thiadiazol-4-yl)-*N,N*-diphenylaniline (2b) It was obtained from 4,7–dibromo-5-methylbenzo[*c*][1,2,5]thiadiaole (0.31 g, 1 mmol), 4-

(diphenylamino)phenylboronic acid (0.43 g, 1.5 mmol) by following the procedure described above for **2a**. Orange solid (0.30 g, 58%); mp 187−190 °C; ^{1}H NMR (400 MHz, CDCl$_3$, δ ppm): 7.79 (d, J = 6.0 Hz, 2H), 7.56 (s, 1H), 7.29− 7.24 (m, 4H), 7.19−7.03 (m, 8H), 2.65 (s, 3H); ^{13}C NMR (100 MHz, CDCl$_3$, δ ppm): 154.5, 151.8, 148.3, 147.3, 139.9, 132.2, 130.5, 129.8, 129.7, 129.3, 124.9, 123.4, 122.7, 112.6, 22.9; HRMS (ESI-TOF) *m/z*: [M+H]$^+$ Calcd for C$_{25}$H$_{19}$BrN$_3$S 472.0399, found 472.0403; Anal. Calcd for C$_{25}$H$_{18}$BrN$_3$S: C, 63.56; H, 3.84; N, 8.90; S, 6.79. Found: C 63.50; H, 3.79; N, 8.80; S, 6.69.

4,7-Bis(4-(*tert*-butyl)phenyl)-5-methylbenzo[*c*][1,2,5]thiadiazole (3) It was obtained from 4,7-dibromo-5-methylbenzo[*c*][1,2,5]thiadiazole (0.20 g, 0.64 mmol) and 4-*tert*-butyl phenyl boronic acid (0.25 g, 1.4 mmol) by following a procedure described above for **2a**. Pale green solid (0.18 g, 67%); mp 188−192 °C; ^{1}H NMR (400 MHz, CDCl$_3$, δ ppm): 7.89 (d, J = 8.0 Hz, 2H), 7.65 (s, 1H), 7.56 (t, J = 8.0 Hz, 4H), 7.41 (d, J = 8.0 Hz, 2H), 2.47 (s, 3H), 1.40 (s, 18H); ^{13}C NMR (100 MHz, CDCl$_3$, δ ppm): 156.0, 152.5, 151.3, 150.5, 136.7, 134.5, 133.8, 132.2, 131.9, 131.5, 129.7, 128.8, 125.6, 34.7, 31.4, 20.4; HRMS (ESI-TOF) *m/z*: [M+H]$^+$ Calcd for C$_{27}$H$_{31}$N$_2$S 415.2202, found 415.2206; Anal. Calcd for C$_{27}$H$_{30}$N$_2$S: C, 78.22; H, 7.29; N, 6.76; S, 7.73. Found: C, 78.13; H, 7.20; N, 6.63; S, 7.60

4,4'-(5-Methylbenzo[*c*][1,2,5]thiadiazole-4,7-diyl)bis(*N,N*-diphenylaniline) (4) It was obtained from 4,7-dibromo-5-methylbenzo[*c*][1,2,5]thiadiazole (0.20 g, 0.64 mmol) and 4-(diphenyl amino) phenyl boronic acid (0.40 g, 1.40 mmol) by following a procedure described above for **2a.** Orange solid (0.26 g, 65%); mp 268−272 °C; ^{1}H NMR (400 MHz, CDCl$_3$, δ ppm): 7.85 (d, J = 8.0 Hz, 2H), 7.63 (s, 1H), 7.35 (d, J = 8.0 Hz, 2H), 7.31−7.27 (m, 8H),7.22−7.18 (m, 12 H), 7.08−7.04 (m, 4H) 2.51 (s, 3H); ^{13}C NMR (100 MHz, CDCl$_3$, δ ppm): 156.1, 152.4, 147.9, 147.5, 147.5, 147.2, 136.7, 131.5, 131.0, 130.9, 129.8, 129.3, 124.9, 124.8, 123.2, 123.2, 122.9, 122.4, 20.6; HRMS (ESI-TOF) m/z: [M+H]$^+$ Calcd for C$_{43}$H$_{33}$N$_4$S 637.2420, found 637.2414; Anal. Calcd for C$_{43}$H$_{32}$N$_4$S: C, 81.10; H, 5.07; N, 8.80; S, 5.03. Found: C, 81.13; H, 5.00; N, 8.83; S, 4.98.

4-(7-(4-(*tert*-Butyl)phenyl)-6-methylbenzo[*c*][1,2,5]thiadiazol-4-yl)-*N,N*-diphenylaniline (5) It was obtained from **2b** (0.30 g, 0.60 mmol) and 4-*tert*-butyl phenyl boronic acid (0.12 g, 0.66 mmol) by following a procedure described above for **2a**. Pale yellow solid, (0.28 g, 89%); mp 214−217 °C; ^{1}H NMR (400 MHz, CDCl$_3$, δ ppm): 7.86 (d, J = 8.0 Hz, 2H), 7.63 (s, 1H), 7.55 (d, J = 8.0 Hz, 2H), 7.41 (d, J = 8.0 Hz, 2H), 7.36−7.28 (m, 4H), 7.22−7.20 (m, 6H),7.08 (t, J = 8.0 Hz, 2H) 2.51 (s, 3H), 1.40 (s, 9H); ^{13}C NMR (100 MHz, CDCl$_3$, δ ppm): 156.2, 152.4, 150.6, 148.0, 147.6, 136.9, 133.9, 131.9, 131.5, 131.3, 131.0, 129.9, 129.8, 129.4, 125.3, 124.9, 123.3, 123.1, 34.8, 31.5, 20.6; HRMS (ESI-TOF) m/z: [M]$^+$ Calcd for C$_{35}$H$_{31}$N$_3$S 525.2233,

found 525.2230; Anal. Calcd for $C_{35}H_{31}N_3S$: C, 79.96; H, 5.94; N, 7.99; S, 6.10. Found: C, 79.93; H, 5.80; N, 7.83; S, 6.10

N-(4-(7-(4-*tert*-Butylphenyl)-5-methylbenzo[*c*][1,2,5]thiadiazol-4-yl)phenyl)-N-phenylbenzenamine (6). It was obtained from **2a** (0.30 g, 0.83 mmol) and 4-(diphenyl amino) phenyl boronic acid (0.26 g, 0.91 mmol) by following a Suzuki reaction condition procedure as described above for **2a**. Pale yellow solid (0.14 g, 32 %); mp 192−197 °C; ^{1}H NMR (400 MHz, CDCl$_3$, δ ppm): 7.89 (d, J = 8.0 Hz, 2H), 7.65 (s, 1H), 7.57 (d, J = 8.0 Hz, 2H), 7.35(d, J = 8.0 Hz, 2H), 7.32−7.28 (m, 4H), 7.22−7.19 (m, 6H), 7.08 (t, J = 8.0 Hz, 2H) 2.51 (s, 3H), 1.40 (s, 9H); ^{13}C NMR (100 MHz, CDCl$_3$, δ ppm): 156.0, 152.5, 151.3, 147.6, 147.2, 136.7, 134.5, 132.2, 131.96, 131.2, 131.0, 130.2, 129.3, 128.8, 125.6, 124.9, 123.2, 122.3, 34.7, 31.3, 20.6; HRMS (ESI-TOF) m/z: [M]$^+$ Calcd for $C_{35}H_{31}N_3S$ 525.2233, found 525.2230; Anal. Calcd for $C_{35}H_{31}N_3S$: C, 79.96; H, 5.94; N, 7.99; S, 6.10. Found: C, 79.33; H, 5.80; N, 7.87; S, 6.09.

7-(4-(9*H*-Carbazol-9-yl)phenyl)-4-bromo-5-methylbenzo[*c*][1,2,5]thiadiazole (7a) It was obtained from 4,7–dibromo-5-methylbenzo[*c*][1,2,5]thiadiaole (0.30 g, 0.97 mmol), (4-(9*H*-carbazol-9-yl)phenyl)boronic acid (0.30 g, 1.07 mmol) by following the procedure described above for **2a**. Pale green (0.20 g, 44%); mp 160-165°C; ^{1}H NMR (400 MHz, CDCl$_3$, δ ppm): 8.18 -8.15 (m, 4H), 7.76 -7.73 (m, 3H), 7.53 (t, J = 8 Hz, 2H), 7.46-7.44 (m, 2H), 7.32 (t, J = 8 Hz, 2H), 2.73(s, 3H); ^{13}C NMR (100 MHz, CDCl$_3$, δ ppm): 154.5, 151.8, 148.3, 147.3, 139.9, 132.2, 130.5, 129.8, 129.7, 129.4, 124.9, 123.4, 122.7, 112.6, 22.9.

7-(3-(9*H*-Carbazol-9-yl)phenyl)-4-bromo-5-methylbenzo[*c*][1,2,5]thiadiazole (7b) It was obtained from 4,7–dibromo-5-methylbenzo[*c*][1,2,5]thiadiaole (0.40 g, 1.29mmol), (3-(9*H*-carbazol-9-yl)phenyl)boronic acid (0.33 g, 1.16 mmol) by following the procedure described above for **2a**. Pale green (0.40 g, 66%); mp 123-126°C; ^{1}H NMR (400 MHz, CDCl$_3$, δ ppm): 8.18 -8.14 (m, 3H), 8.00 (d, J = 8 Hz, 1H), 7.76 (t, J = 8 Hz, 2H), 7.68 (s, 1H) 7.58 (d, J = 8 Hz, 2H), 7.44 (t, J = 8 Hz, 2H), 7.31 (t, J = 8 Hz, 2H), 2.68 (s, 3H); ^{13}C NMR (100 MHz, CDCl$_3$, δ ppm): 153.4, 151.5, 140.6, 140.4, 139.8, 138.2, 135.2, 131.5, 130.1, 127.8, 127.7, 126.8, 125.9, 123.4, 120.3, 119.6, 114.2, 112.5, 109.8, 109.7.

4-(4-(9*H*-Carbazol-9-yl)phenyl)-7-(4-(*tert*-butyl)phenyl)-5-methylbenzo[*c*][1,2,5]thiadiazole (8) It was obtained from 4-bromo-7-(4-(*tert*-butyl)phenyl)-5-methylbenzo[*c*][1,2,5]thiadiazole (0.30 g, 0.83 mmol), (4-(9*H*-carbazol-9-yl)phenyl)boronic acid (0.35 g, 1.2 mmol) by following the procedure described above for **2a**. Green (0.26 g, 60%); mp 235-237°C; ^{1}H NMR (400 MHz, CDCl$_3$, δ ppm): 8. (d, J = 8 Hz, 2H), 7.93(d, J = 8 Hz, 2H), 7.76 -7.72 (m, 5H), 7.62-7.59 (m, 4H), 7.46 (t, J = 8 Hz, 2H), 7.32 (t, J = 8 Hz, 2H),

2.59 (s, 3H), 1.41 (s, 9H); ^{13}C NMR (100 MHz, CDCl$_3$, δ ppm):155.8, 152.2, 151.5, 140.7, 131.8, 131.7, 128.8, 126.6, 125.9, 125.71, 123.4, 120.0, 110.0, 34.7, 31.35, 20.57.

4-(3-(9*H*-Carbazol-9-yl)phenyl)-7-(4-(*tert*-butyl)phenyl)-5-methylbenzo[*c*][1,2,5]thiadiazole (10) It was obtained from 4-bromo-7-(4-(*tert*-butyl)phenyl)-5-methylbenzo[*c*][1,2,5]thiadiazole (0.20 g, 0.55 mmol), (3-(9*H*-carbazol-9-yl)phenyl)boronic acid (0.19 g, 0.65 mmol) by following the procedure described above for **2a**. Yellow (0.10 g, 35%); mp 126-128 °C; ^{1}H NMR (400 MHz, CDCl$_3$, δ ppm): 8.22 (s, 1H) 8.16 (t, *J* = 8 Hz, 3H), 8.10 (d, *J* = 8 Hz, 1H)7.81 -7.67 (m, 4H),7.63-7.59 (m, 2H),7.46-7.41(m, 3H),7.33-7.32 (m, 3H), 2.60 (s, 3H), 1.56 (s, 9H); ^{13}C NMR (100 MHz, CDCl$_3$, δ ppm):150.8, 148.9, 143.0,140.7, 140.7, 138.4, 137.3, 137.39, 135.0, 132.2, 130.4, 130.0, 129.7, 129.0, 128.0, 127.7, 126.6, 125.9, 123.4, 120.3, 120.0, 115.4, 109.8, 34.7, 31.4, 20.5

4-(7-(4-(*tert*-butyl)phenyl)-6-methylbenzo[*c*][1,2,5]thiadiazol-4-yl)-*N,N*-diphenylaniline (9) It was obtained from 7-(4-(9*H*-Carbazol-9-yl)phenyl)-4-bromo-5-methylbenzo[*c*][1,2,5]thiadiazole (0.20 g, 0.42 mmol), 4-(*tert*-butyl)phenyl)boronic acid (0.08 g, 0.46 mmol) by following the procedure described above for **2a**. Pale green (0.15 g, 69%); mp 189-192°C; ^{1}H NMR (400 MHz, CDCl$_3$, δ ppm): 8.23 (d, *J* = 8 Hz, 2H), 8.17 (d, *J* = 8 Hz, 2H), 7.79 -7.73 (m, 3H),7.59-7.53 (m, 4H),7.46-7.43(m, 4H),7.32 (t, *J* = 8 Hz, 2H), 2.54(s, 3H), 1.45(s, 9H); ^{13}C NMR (100 MHz, CDCl$_3$, δ ppm):150.7, 140.7, 136.7, 132.4, 130.5, 129.7, 127.0, 125.9, 125.3, 123.4, 120.1, 120.0, 109.9, 77.0, 34.7, 31.3, 20.5.

7-(3-(9H-Carbazol-9-yl)phenyl)-4-(4-(*tert*-butyl)phenyl)-5-methylbenzo[*c*][1,2,5]thiadiazole (11) It was obtained from 7-(3-(9*H*-carbazol-9-yl)phenyl)-4-bromo-5-methylbenzo[*c*][1,2,5]thiadiazole (0.40 g, 0.45 mmol), 4-(*tert*-butyl)phenyl)boronic acid (0.15 g, 0.85 mmol) by following the procedure described above for **2a**. Pale Yellow (0.28 g, 63%); mp 123-125 °C; ^{1}H NMR (400 MHz, CDCl$_3$, δ ppm): 8.18 -8.15 (m, 4H), 7.76 -7.73 (m, 3H),7.53 (t, *J* = 8 Hz, 2H),7.46-7.44(m, 2H),7.32 (t, *J* = 8 Hz, 2H), 2.73(s, 3H); ^{13}C NMR (100 MHz, CDCl$_3$, δ ppm):150.7, 132.3, 130.0, 129.6, 127.9, 127.7, 126.5, 125.9, 125.2, 120.30, 119.9, 109.9, 34.7, 31.4, 20.4.
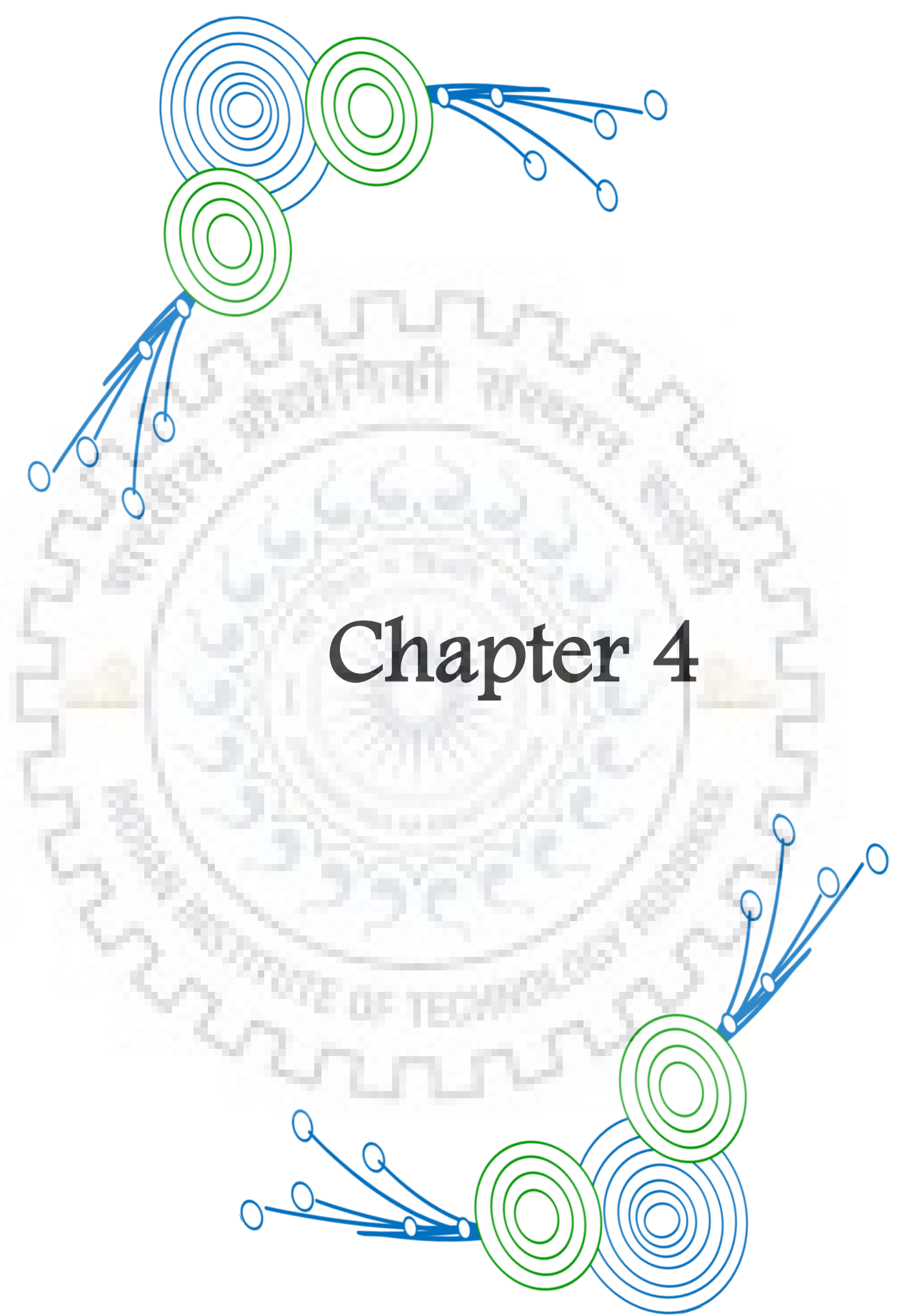
Chapter 4

Chapter 4

Synthesis and Characterization of Benzothiadiazole-Benzimidazole Conjugates
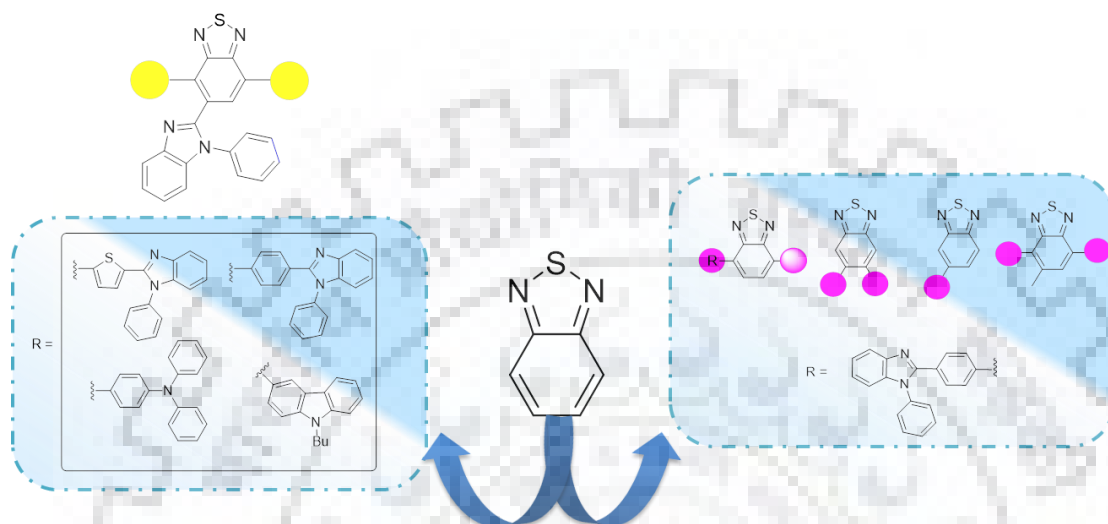
4.1 Introduction

The flexibility in designing the molecule has accelerated the wide scope to explore the structure-property relationship of organic π-conjugated materials. Such verstality in designs owes promising application in electronic devices such as OLEDs, [161, 162] OPVs, [163, 164, 165] OFETs, [166, 167] NLO and sensors.[168, 169] Among the devices, OLEDs has attained firm position in optoelectronic fields as this technology introduced solid state lightning sources and flat panel displays.[170] But still more strategies are required to improve the electroluminescence efficiency. One of the major problems with the conjugated organic materials is the aggregation state in the solid. It is found that non-linear molecules reduce the intermolecular aggregation by suppressing π−π stacking and enhance solid-state fluorescence. [171, 172] Among the class of π-conjugates BTD nuclei has attaracted wide attention due to its high electron affinity and rigidity.[16, 23] BTD derivatives are found to exist generally green or red color depending upon the nature of conjugation. However blue emitting BTD derivatives are elusive.[173-175] The orange-red emitters have to possess high rigidity in molecular structure to suppress non-radiative internal conversion process directed by low energy gap and strong charge transfer for long-wavelength emissions. [95, 176-180] Interestingly, till now only

few examples of benzothiadiazole unit capable of constructing orange-to-red emitters with high efficiency are reported. For example, Ni et al[98] reported D–A–D structured 4,7-bis(9,9-dimethylacridin-10(9*H*)-yl) benzo[*c*][1,2,5]thiadiazole red TADF material, which exhibited maximum external quantum efficiency of 8.8% at a maximum luminance of 1.06 cd m^{-2} with the emission peak at 636 nm. Wang et al [111] reported D-A-A structured orange-red TADF emitter which showed high external quantum efficiency of 10% and 11% with 0.5 wt% dopant concentration based device.

In this chapter, we report two sets of benzimidazole-benzothiadiazole conjugates (Type1 and 2) to tune the optical, electrochemical and electroluminescet properties. Here, the benzothiadiaozle unit is introduced as electron accepting core to design the gamut of emitters from blue to red region, in virtue of its bulky conjugated structure and excellent electron-accepting ability. The Type1 series deals with different functionalization of benzimidazole unit on benzothiadiazole nuclei and named according to substitution, are as follows **14, 15, 16** and **17**. Whereas, the Type2 series consists of **21, 22, 23** and **24** where benzimidazole unit is substituted at lateral position followed by substitution of triphenylamine, carbazole and phenyl-benzimidazole chromophores at C4 and C7 positions of benzothiadiazole nuclei. The introduction of *N*-phenylbenzimidazole unit measured to impart rigidity to the molecule and helps in reducing aggregation propensity. Also improves electron-transporting ability to the resulting materials and facilitate electron injection. The effect of different substitution pattern on electronic absorption, emission, thermal, electrochemical and electroluminescent characteristics was studied in detail and compared with BTD derivatives which lacks lateral substitution. Interestingly, the linear benzimidazole derivative **14** showed bathochromic shift when compared to its lateral substituted regioisomer **15.** Moreover the lateral substituted BI chromophore derivative **21** showed red shift when compared to **14.** This suggests the lateral substitution may be participating in extending the conjugation. The dye **23** and **24** exhibited high lying HOMO in the series while **21** and **22** showed low lying LUMO in series**.** The dye **21 22, 23** and **24** exhibits distinct HLCT excited state with moderate quantum yield of 25-75%. The device with 5% dopant concentration exhibited satisfactorily performance with green, yellow and orange-red emission. The dye **22** as orange-red emitter exhibited excellent performance in the series with maximum luminance of 9032 cdm^{-2}, maximum current efficiency of 8.5 cdA^{-1}, maximum power efficiency of 5.1 lmW^{-1} , CIE coordinates of (0.55, 0.44) and EQE of 9.1%. This is attributed to the utilization of both energies of LE and CT excitons (i.e. HLCT).[181-182]
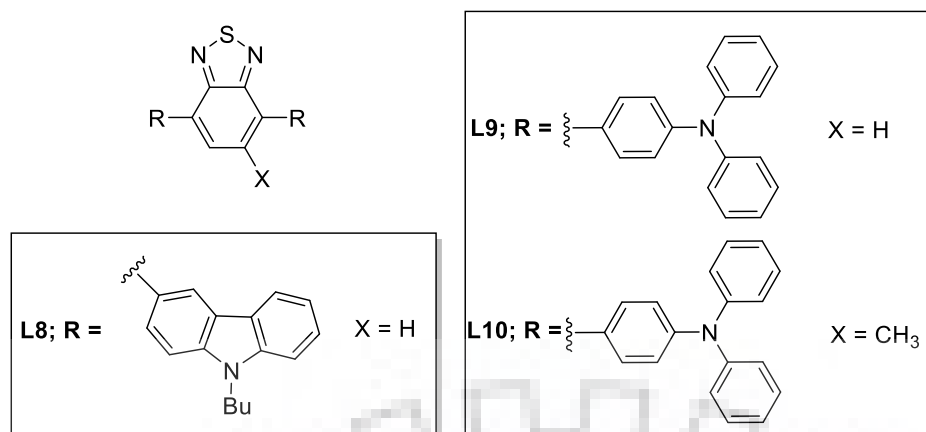
Figure 4.1 Structures of the related dyes.
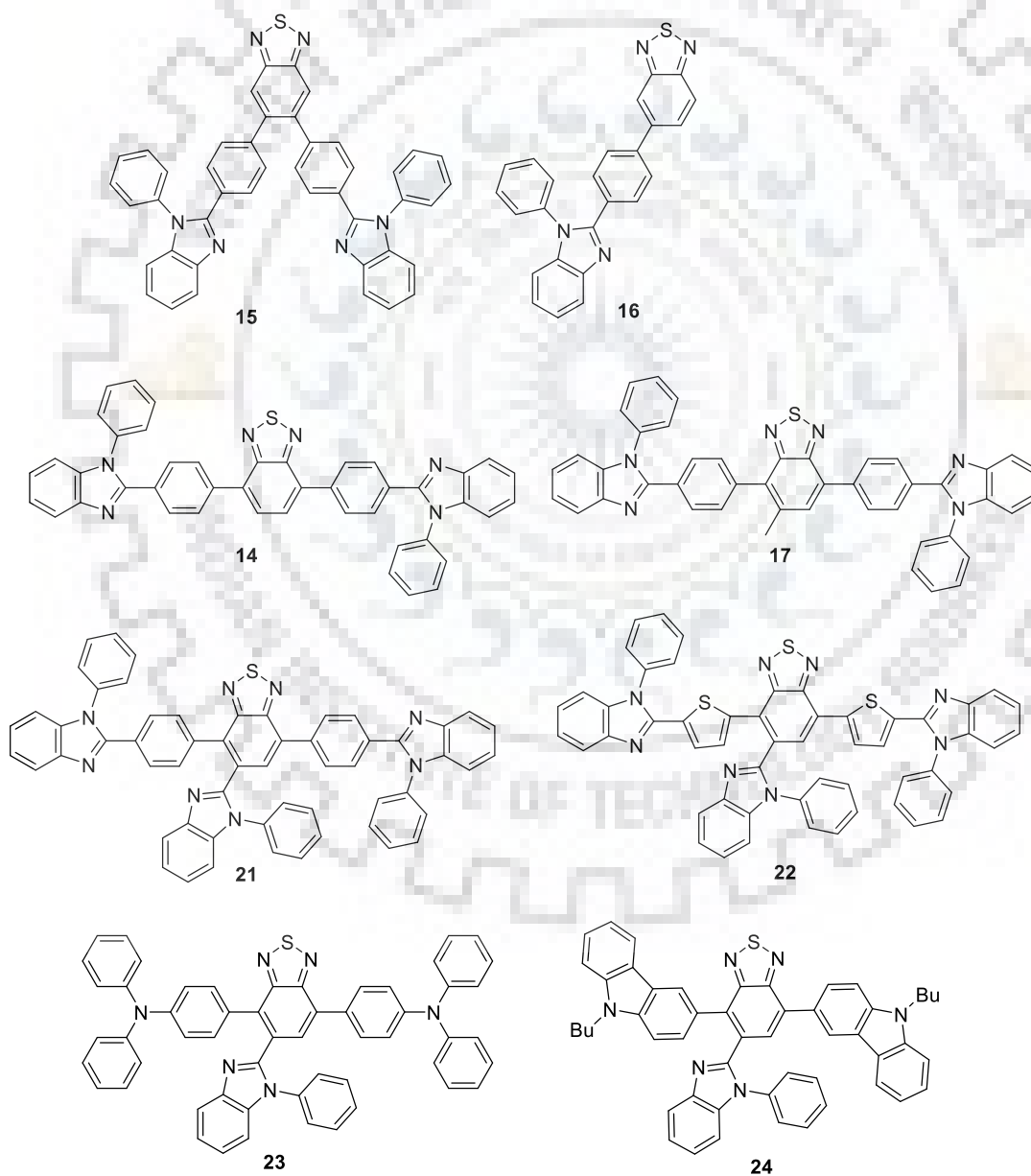
Figure 4.2 Structures of the target dyes.

4.2 Results and Discussion

4.2.1 Synthesis and Characterization

The starting materials of Type 1 dyes, the mono or di-bromo derivatives of benzothiadiazole (**1**) was synthesized by following a procedure reported in literature.[28] Syntheses of the dyes **14, 15, 16** and **17** which showed variation in the position of benzimidazole group on the benzothiadiazole nucleus, were accomplished by a two-step protocol. (Scheme 4.1). The first step includes the synthesis of aldehyde intermediates **13a, 13b, 13c** and **13d** by treating the respective bromo derivatives with stoichiometric amount of arylaldehyde boronic acids under Suzuki coupling conditions. Finally, the intermediates **13a, 13b, 13c** and **13d** were converted to the target dyes **14, 15, 16** and **17**by treating them with *N1*-phenylbenzene-1,2-diamine under condensation.
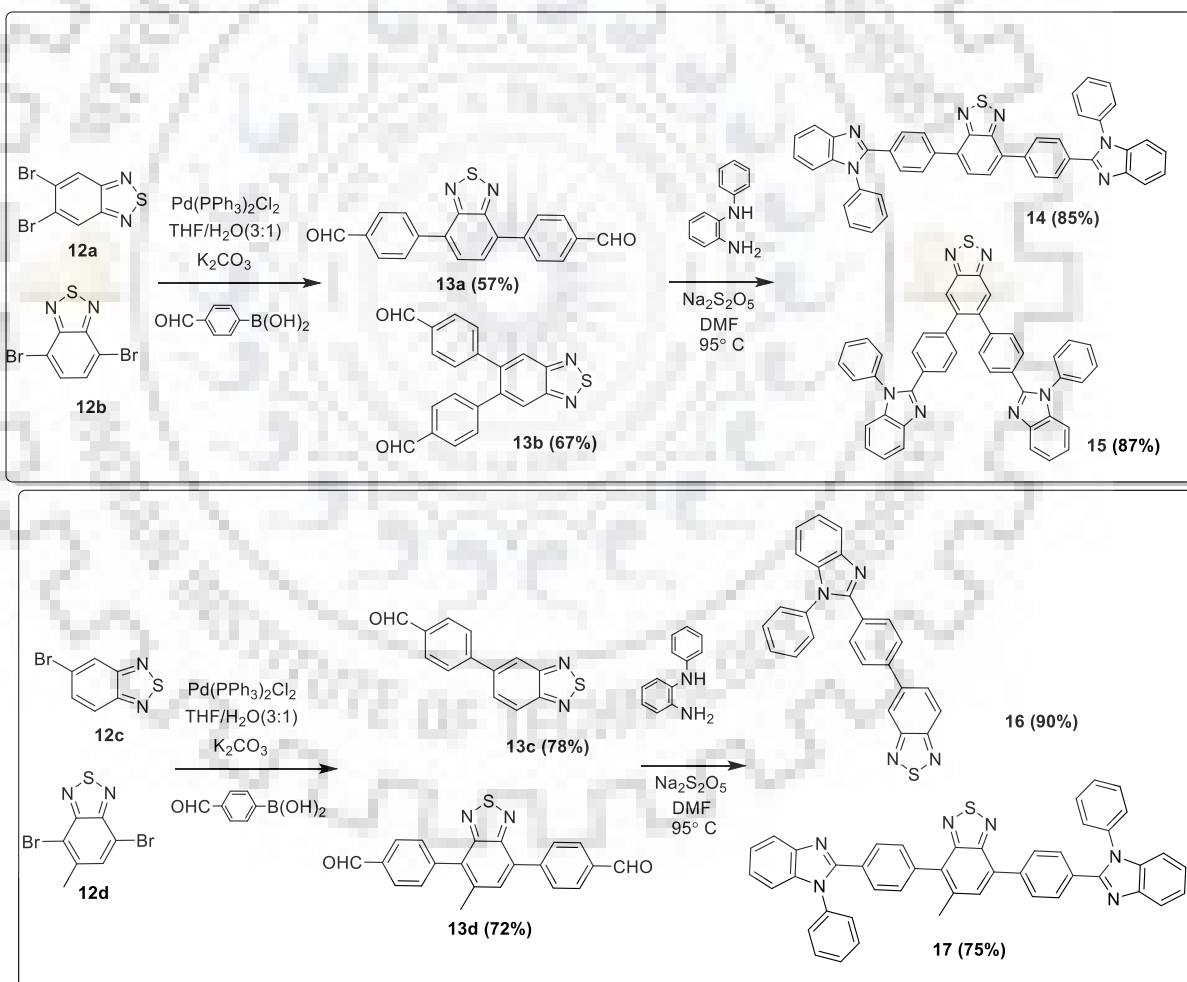
Scheme 4.1 Synthetic protocol of the dyes **14, 15, 16** and **17**.
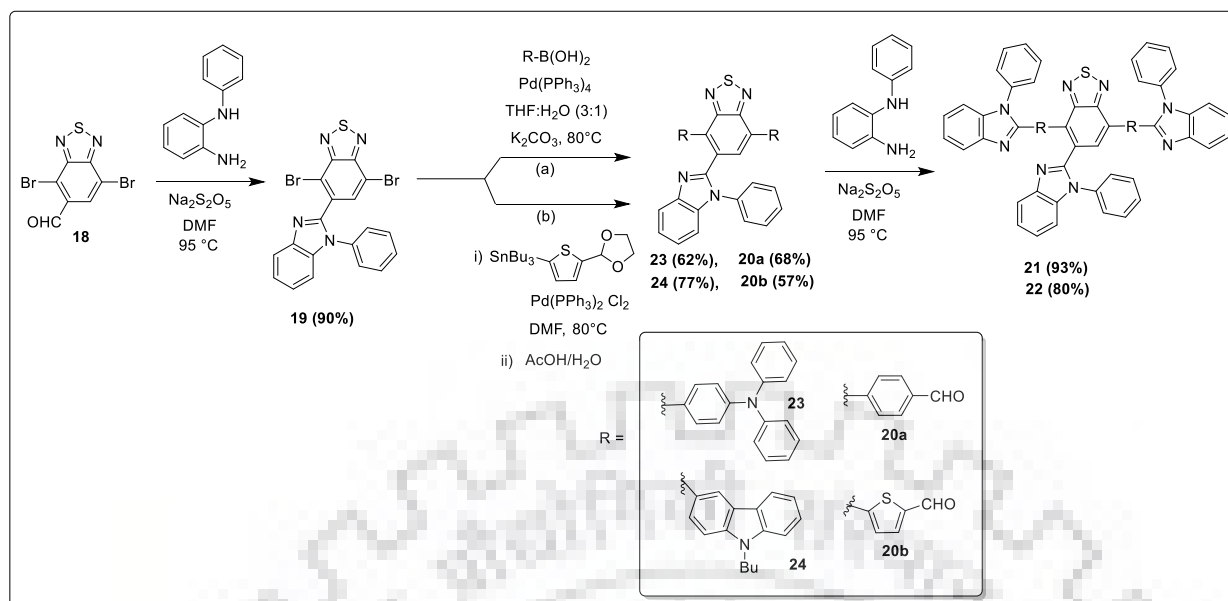
Scheme 4.2 Synthetic protocol of the dyes **21, 22, 23 and 24**.

Moreover, the starting material for Type 2 dyes, the 4,7-dibromobenzo[*c*][1,2,5]thiadiazole-5-carbaldehyde (**18**) was synthesized from 4,7-dibromo-5-methylbenzo[*c*][1,2,5]thiadiazole by following a procedure reported in literature.[28] The syntheses of the dyes **23-24** and dialdehyde intermediate (**20a, 20b**) were accomplished by following Pd catalysed Suzuki/Stille reaction condition (Scheme 4.2) with respective aryl boronic acids/stannylene reagents. Then the resulting aldehyde intermediates **20a** and **20b** were converted to target dyes **21** and **22** by treating them with *N1*-phenylbenzene-1,2-diamine under condensation condition used to prepare intermediate 4,7-dibromo-5-(1-phenyl-1*H*-benzo[*d*]imidazole-2-yl)benzo[*c*][1,2,5]thiadiazole (**19**). The structures of the intermediates and the target dyes were fully characterized and confirmed by ^{1}H, ^{13}C NMR, HRMS spectra. All the dyes (**14, 15, 16, 17, 21, 22, 23** and **24**) are pale green, green, orange, or red solids and soluble in common organic solvents such as TOL, THF, DCM, DMF, ACN.

4.2.2. Photophysical properties

The photophysical properties of the dyes were investigated by absorption and fluorescence spectroscopy. The absorption spectra of the compounds measured in DCM are displayed in Figure 4.3 and the relevant data summarized in Table 4.1. All the compounds showed two prominent absorption peaks in the range 260-560 nm. The higher energy peak is assigned to the multiple localized π-π* electronic transitions originating from chromophores such as phenyl-benzimidazole, triphenylamine, carbazole and benzothiadiazole whilst the longer wavelength absorption in the range of 350-560 nm is invariably present in all the compounds and probably originates from the delocalized π-π* transition from the conjugation segment comprising

benzothiadiazole and benzimidazole units in **14, 15, 16, 17, 21** and **22.** However, for the dyes **23** and **24** the origin of longer absorption wavelength may be assigned to the intramolecular charge transfer transition from the subjoined donor unit to BTD acceptor. [183]

Interesting structure-property relationship is observed in the absorption profile, on substitution of benzimidazole (BI) chromophore at different positions (C4, C5, C6, C7) affects absorption wavelength and led to the trend, **22 > 21 > 14** > **17 > 16 > 15** this is attributed to auxochromic effect enhancing the conjugative delocalization and steric manifestation at C5 and C6 in the molecule. [184, 185] In compound **14,** where BI unit is substituted linearly at C4 & C7 positions exhibited bathochromic shift (~ 49 nm) when compared to its analogous regioisomer **15,** where BI is present at C5 & C6 position. Furthermore, on comparing **14** dye with lateral substituted dyes (**17, 21** and **22**) the methyl substituted dye **17** showed hypsochromic shift of 20 nm attributed to steric interaction of lateral substitution hindering facile conjugation. However, the laterally substituted benzimidazole dye **21** showed similar absorption profile with higher molar extinction coefficient when compared to non-methylated **17,** this suggests the BI unit enhancing the orbital overlapping and increasing the π-π* delocalization.[186] Moreover, on comparing the mono- to di-substituted lateral dyes (**16** and **15**), the mono-substituted dye at C5 position of BTD nuclei (**16**) exhibited red shift of ~8 nm when compared to di-substituted dye at C5 and C6 positions (**15**). This may be attributed to lateral congestion at C5 and C6 positions disrupting the electronic communication. Likewise, on comparing among the laterally substituted benzimidazole-BTD derivatives, the backbone unit (**19**) of **21-22** and **23-24** series showed red shift to 1,2-diphenyl-1*H*-benzo[*d*]imidazole unit (326 nm), this suggests the lateral substitution may be participating in extending the conjugation. Nevertheless, on comparing among the molecules substituted by donor chromophore (**23 & 24**) **23,** the triphenylamine derivative exhibited bathochromic shift (22 nm) than the carbazole derivative (**24**) attributed to strong donor ability of former dye which extends the conjugation influencing absorption wavelength and molar extinction coefficients of the dyes. Moreover, among acceptor substituted dyes (**21** & **22**) the linearly appended benzimidazole unit with thiophene linker derivative (**22**) exhibited ~89 nm red shift when compared to phenyl derivatives (**21**) ascribed to planar configuration of thiophene that participates well in electronic communication when compared to non-planar phenyl unit. [10]
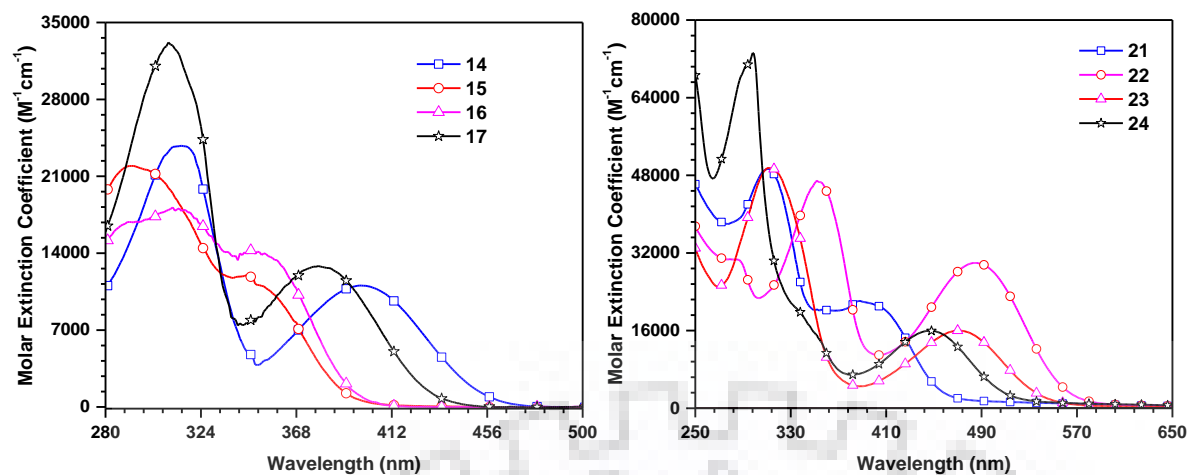
Figure 4.3 Absorption spectra of the dyes recorded in DCM.

Furthermore, on comparing the present dyes (**23** and **24**) with similar molecules reported in literature (**L8**, **L9** and **L10**). [93,187] The dye **23** and **24** showed bathochromic shift (~12 nm) and high molar extinction coefficient compared to literature reported analogues dyes which lacks lateral substitution (**L8** and **L9**), attributed to lateral benzimidazole unit which may be significantly participates in extending the conjugation. However the blue shift as observed in **L10** due to steric congestion in absorption profile is not much imposed on BI-BTD hybrids as lateral phenyl benzimidazole helped in increasing the π-conjugation. Thus, BI-BTD hybrids endowed the molecule to tune the emitting region and also outdo the aggregation for high photoluminescence efficiency.[188, 189]
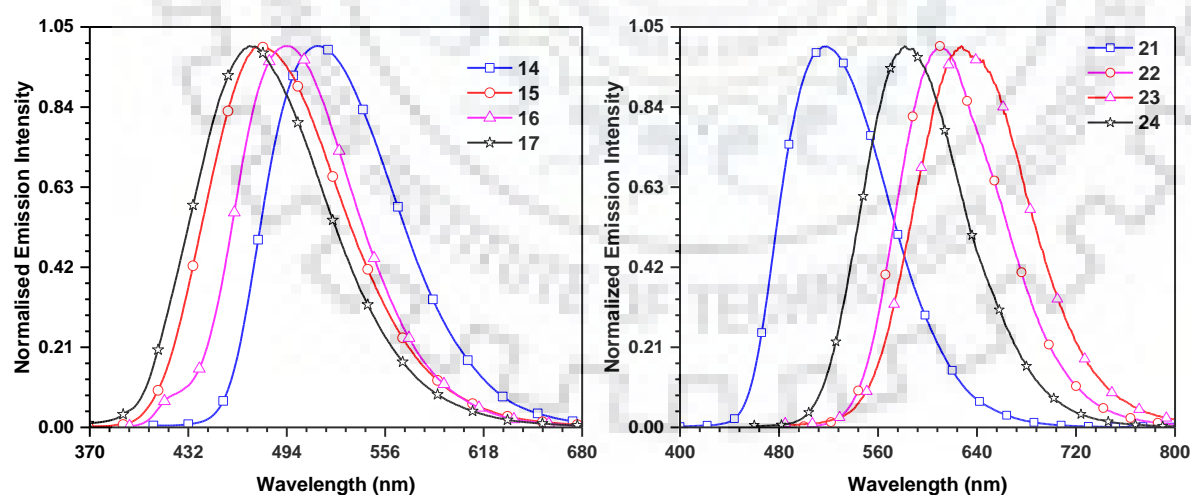
Figure 4.4 Emission spectra of the dyes recorded in DCM.

The emission spectra recorded for the compounds in DCM are shown in Figure 4.4 and corresponding data listed in Table 4.1.In general, the dyes emit blue (**15, 17**) green (**14, 16, 21**), yellow (**24**) or red colors (**22** and **23**). Similar to absorption characteristics, the linear derivatives (**14**) displayed red-shifted emission when compared to "V" shaped derivative (**15**)

112

suggesting an extended conjugation in the former compound. The non-methyl substituted dyes displayed bathochromic shift when compared to methylated **17** dyes.

Table 4.1 Optical properties of the dyes

Dye	λ_{abs} (nm) ($\varepsilon_{max} \times 10^3$ (M^{-1} cm^{-1}))[a]	λ_{em} (nm)[a] (Φ_f)[b]	Stokes shift (cm^{-1})	λ_{em} (nm)[c]
14	315 (25.03), 398 (12.30)	513 (0.55)	5632	521
15	292 (23.27), 345(13.33)	478 (0.30)	8065	447
16	311 (17.38), 353 (13.20)	493 (0.25)	7295	436
17	309 (31.71), 378 (11.41)	470 (0.58)	5178	441
21	311 (49.35), 396 (21.68)	515 (0.70)	5835	503
23	313 (49.54), 471 (16.01)	628 (0.44)	5308	592
22	352 (46.93), 485 (29.95)	610 (0.78)	4225	610
24	299 (73.16), 449 (15.95)	582 (0.52)	5090	567
L8	238,297, 437	576	5522	596
L9	309, 459	639	6137	-
L10	309 (37.40), 432 (9.30)	577 (0.21)	5817	555

[a] Measured in DCM solution. [b] Absolute quantum yields determined using a calibrated integrated sphere system. [c] Measured for spin cast film from TOL.

Moreover, mono-substituted **16** has showed bathochromic shift when compared to di-substituted lateral derivative **15** as observed in absorption profile ascribed to lateral congestion due BI unit. Similarly, the donor and acceptor appended chromophores at benzothiadiazole nuclei showed similar trends as observed in absorption profile. Among the dyes **23** and **24**, the triphenylamine derivative (**23**) displayed ~46 nm red-shifted emission when compared to carbazole derivative (**24**) suggesting an extended conjugation involving triphenylamine unit in the former compound. Similarly, the acceptor analogues follow the similar trend as in absorption profile (**22** > **21**). However, the dye **23** exhibited hypsochromic shift to **L9** (~11 nm), while the dye **24** showed similar emission to **L8,** this may be a result of steric interaction of bulky triphenylamine unit with the laterally substituted benzimidazole while no such hindrance observed in carbazole–benzimidazole unit. Further on comparison with methyl substituted dye **L10**, the **23** dye exhibited bathochromic shift (51 nm). The Stokes shifts of these dyes follow the order, **15** > **16** > **14** > **21** > **23** > **17** > **24** > **22**. The larger Stokes shift observed for the dye **15** when compared to its regioisomer **14**, indicates that the dye **15** underwent significant structural reorganization due to larger twisting of phenyl benzimidazole units at lateral position. Similarly, the larger Stokes shift observed for **21** and **23** when

compared to **22** and **24** possibly due to significant structural reorganization due to larger twisting between BTD and phenyl benzimidazole, triphenylamine units respectively in the excited state.

To understand further the interaction of dyes with solvent in ground and excited state, solvatochromic study was performed with different solvents. The absorption and emission spectral variation observed due to solvent polarity is displayed in Figures 4.5 and 4.6. It is observed that all compounds displayed solvent insensitive absorption spectra. This clearly points that the ground states of dyes are non-polar in nature and displays no solvent selective association/interaction. However, in the emission spectra, the compounds exhibit positive solvatochromism, i.e. the emission maxima progressively increases on increasing solvent polarity (Figure 4.6). This permits us to make a conclusion that these dyes are selectively stabilized by polar solvents in excited state due to enhanced polarization. However, this shifting of emission with polarity may arise due to following reasons, (a) structural reorganization and/or (b) stabilization in polar solvents due to photo-induced ICT. Interestingly, the donor appended dyes showed drastic emission shift ($\Delta\lambda$) from non-polar (TOL) to polar (DMF) solvent in the range of 37-67 nm and follows the order **23** (67 nm) >**24** (37nm).

This may be due to stabilization in polar solvents by photo-induced ICT that presumably be the reason for poor quantum yield of **23** (0.44) and **24** (0.52). Whilst the acceptor substituted derivatives followed the order **15** (85 nm) > **16** (67 nm)> **14** (23 nm) > **17** (19 nm).~ **21** (19 nm) >**22** (12 nm) the lower difference may be due to slight interaction of molecules with solvents which indicates absence of charge transfer. However, the shift in polarity in **15** and **16** arises due to redistribution of electron density in the excited state of the dyes due to structural reorganization in the excited state, confirmed by large Stokes shift of lateral substituted dyes. [190,191] Moreover, the reasonably larger Stokes shifts for organic luminescent materials are also beneficial for electroluminescent applications as it ensures the reduction of self-absorptions.[192]
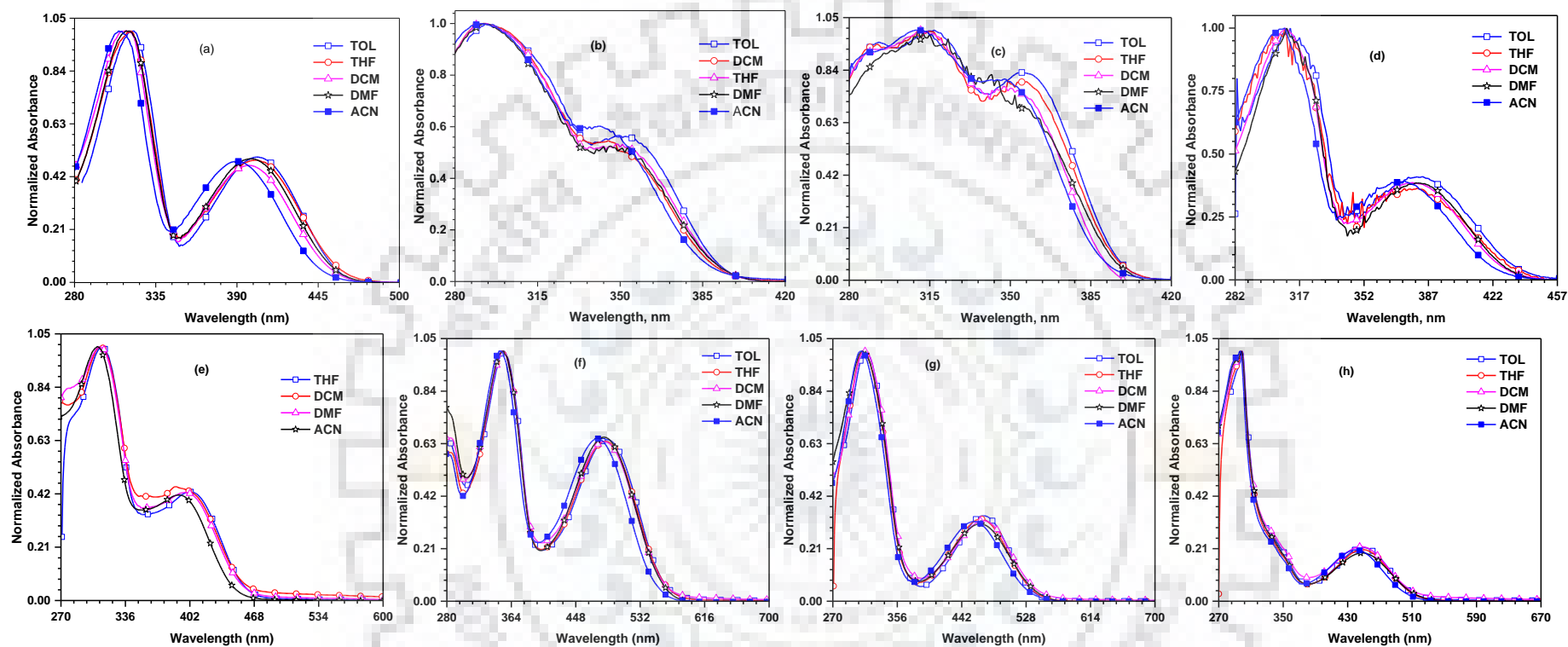
Figure 4.5 Normalized absorption spectra of the dyes recorded in different solvents a) **14** b) **15** c) **16** d) **17** e) **21** f) **22** g) **23** and h) **24**

Table 4.2 Emission data of the dyes recorded in various solvents.

Dye	λ_{em} (nm)						Stokes shift (cm^{-1})				
	TOL	THF	DCM	ACN	DMF	$\Delta f_{max,}$ (TOL-DMF)	TOL	THF	DCM	ACN	DMF
14	500	508	513	518	523	23	4752	5129	5632	6336	5942
15	437	456	478	524	522	85	5526	6399	8065	10242	9296
16	433	440	470	509	500	67	5074	5284	7295	9089	8249
17	482	492	493	498	501	19	5026	5922	5178	6874	6218

Table 4.3 Emission data of the dyes recorded in various solvents

Dye	λ_{em} (nm)											$\Delta\lambda$ ($\lambda_{TOL}-\lambda_{DMF}$) (nm)
	TOL	THF	DCM	ACN	DCB	BuEt	EtOAc	TCE	TEA	DEE	DMF	
21	509	510	515	524	511	505	510	509	498	507	528	19
23	592	613	628	660	611	578	606	603	575	589	659	67
22	605	611	610	615	608	600	606	603	603	604	617	12
24	565	572	582	599	576	554	567	567	552	558	602	37

Table 4.4 Stokes shift data of the dyes recorded in various solvents

Dye	Stokes shift (cm^{-1})										
	TOL	THF	DCM	ACN	DCB	BuEt	EtOAc	TCE	TEA	DEE	DMF
21	5354	5268	5835	5916	5061	5012	5518	4984	4550	5152	6186
23	4340	5100	5353	6540	4554	4066	5143	4381	3931	4481	6239
22	3921	4210	4225	4704	3796	3825	4160	3741	3741	4062	4411
24	4573	4889	5090	5981	4617	4271	5009	4586	4306	4500	5627

To further understand the relationship between the excited state properties and the solvent polarity, the dipole moment of the excited state (μ_e) was estimated using Lippert–Mataga relation. (Figure 4.7) The dyes **14, 15, 16, 17** have shown linear trends with positive slope, which indicate a general dye-solvent interaction in the excited state. However, the lateral benzimidazole substituted dyes **21-24** exhibited non-linear relationship between Stokes shift and solvent polarity. The dyes exhibited the dipole moment μ_e of 9.56-13.75 Debye in low polar solvents indicate a LE-state dominated character, while the μ_e of 26.4-35.2 Debye in high

polar solvents can be attributed to CT-state. This analysis holds the consideration over the concept of intercrossing and the coexistence of LE and CT components, which facilitate the HLCT state in medium polarity solvents for the dyes. [193, 194]

Furthermore, the transient PL decay curves of these materials in toluene exhibit a single-exponential fluorescence decay process with a lifetime of 3.72, 4.6, 6.27 and 7.27 ns for **21, 22, 23** and **24** respectively. No delayed fluorescence was observed from the transient PL decay curves, suggesting these compounds are not TADF emitters.

With the combination of the PLQY in toluene, radiative rate constants were estimated and found to be in the order **21> 22 > 23~24.** The dyes **21** and **22** containing electron withdrawing group at C4 and C7 positions, possess larger radiative rates k_r (18.8-16.9 $\times$ 10^7 sec^{-1}), than the donor substituted derivatives **23** and **24** (7.0-7.1 $\times$ 10^7 sec^{-1}). However, the non-radiative rate constant of the dyes follows the order **22 <24 <21<23** which presumably due to the twist regulated donor-acceptor interaction. This suggests that the higher Φ_f values for **21, 22** when compared to **23** and **24,** resulted from the promotion of the radiative process along with the suppression of the non-radiative process in the former. Similarly, the benzimidazole functionalized dyes (**14-17**) showed large non radiative decay constant for the lateral substituted dyes **15** and **16** when compared to the linear substituted dyes (**14, 17**). Therefore the lateral substituted dyes possess higher radiationless relaxation providing low Φ_f values when compared to the linearly substituted dyes by following the order **17>14>15>16.**

The emission spectra recorded for the drop-cast thin films of the dyes are displayed in Figure 4.9.The compounds (**15**, **16, 17, 21**, **23** and **24**) in thin film showed hypsochromic shift with 15-36 nm than those recorded in dichloromethane solution. However dye **22** exhibited similar profile in thin film as in dichloromethane solution with λ_{max} of 610 nm. Moreover, PL spectra of **21, 22, 23** and **24** dyes showed close resemblance to those observed in TOL solutions. This result highlights the importance of lateral benzimidazole unit in inhibiting aggregation in solid state.
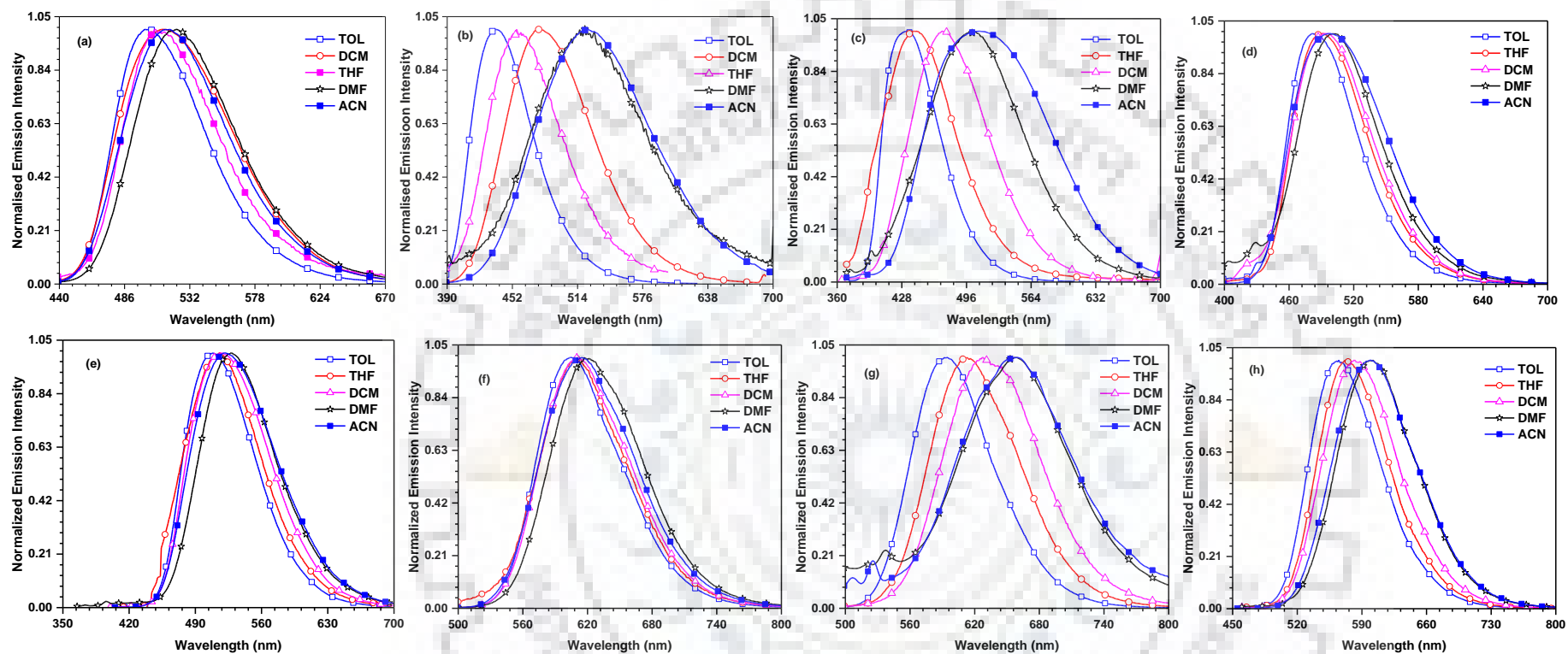
Figure 4.6. Normalized emission spectra of the dyes recorded in different solvents a) **14** b) **15** c) **16** d) **17** e) **21** f) **22** g) **23** and h) **24**
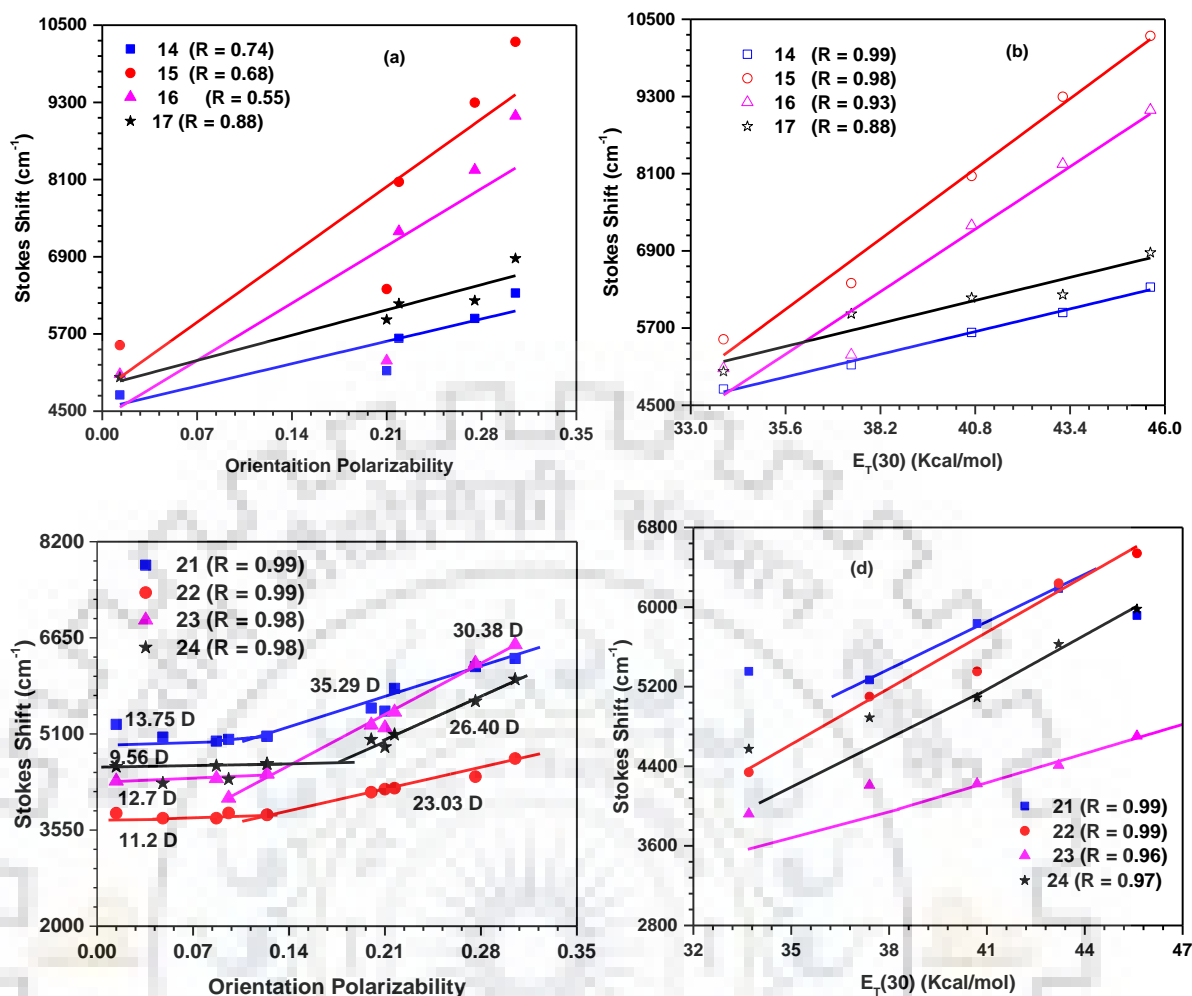
Figure 4.7 Correlation between the Stokes shift and solvent parameter, correlation plot of *v vs* Δ*f* (a and c) $E_T(30)$ (b and d).
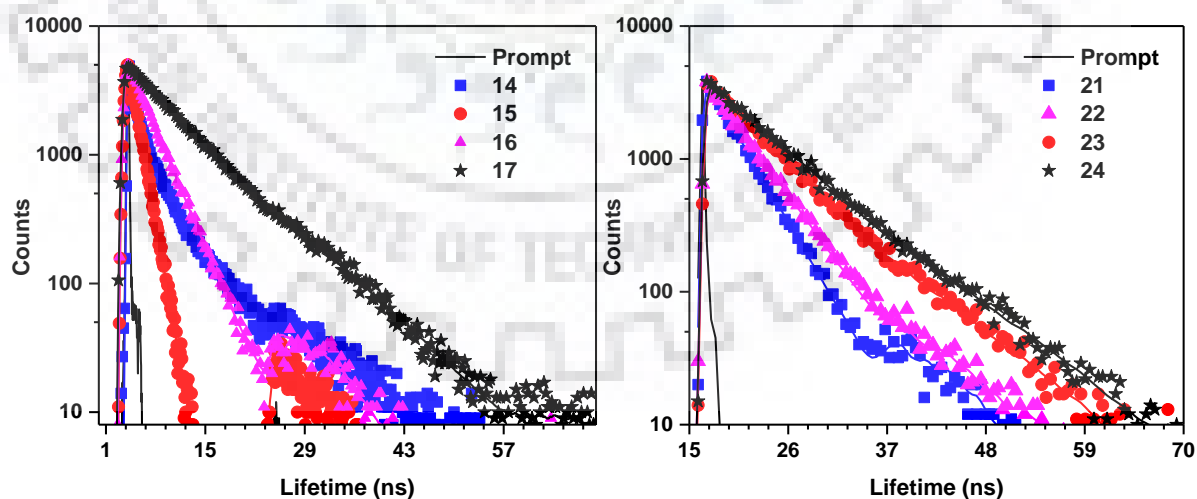
Figure 4.8 Time-resolved fluorescence decay profiles for the dyes

119
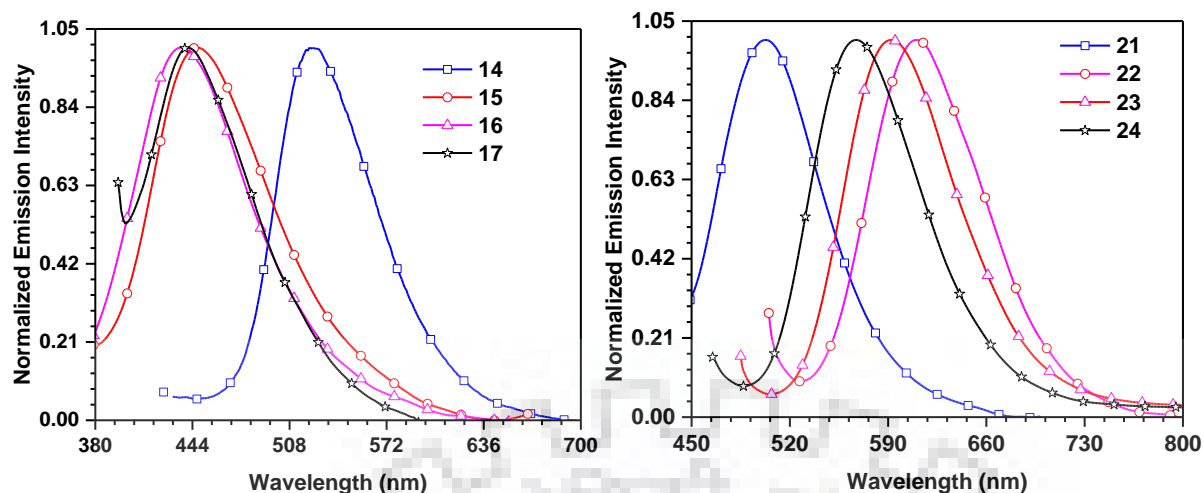
Figure 4.9 Emission spectra of the drop-cast thin films of the dyes

Table 4.5 Photophysical properties of the dyes

Dye	τ^a (ns)	$\Phi_F{}^b$	$k_r{}^c$ (10^7 s^{-1})	$k_{nr}{}^d$ (10^7 s^{-1})
14	4.7	0.55	11.5	9.4
15	1.3	0.30	22.7	53.0
16	3.2	0.25	7.6	22.9
17	5.9	0.58	9.8	7.1
21	3.7	0.70	18.8	8.0
22	4.6	0.78	16.9	4.7
23	6.2	0.44	07.0	8.9
24	7.2	0.52	7.1	6.6

$^a\tau$ = fluorescence lifetime decay ^{b}Absolute quantum yields determined with a calibrated integrating sphere system. ^{c} Radiative decay rates (k_r) calculated using Φ_F/τ. ^{d}Non-radiative decay rate (k_{nr}) calculated using $\Phi_F = k_r/(k_r + k_{nr})$.

4.2.3 Thermal properties

Thermal stability of the compounds was analysed by thermogravimetric analysis (Figure 4.10) under a nitrogen atmosphere at a heating rate of 10 °C/min, and pertinent data compiled in Table 4.5. All dyes exhibited excellent thermal stability with thermal decomposition temperature (T_d) ranging from 418 to 516 °C. The onset decomposition temperatures corresponding to the 10% weight loss (T_{onset}) are above 418 °C. The linear isomer dye **14** exhibit higher thermal decomposition temperature than lateral substituted **15** dye attributed to geometrical orientation. Similarly, the **23-24** dyes exhibited higher decomposition temperature than linear benzimidazole containing dyes (**21-22**). As triphenylamine and carbazole units helps to achieve ordered structure in solid state. The compounds containing planar fragments are reported to exhibit pronounced thermal stability. [195, 196, 197] Furthermore on comparison with non-methylated benzothiadiazole derivatives (**L2**), all dyes showed superior thermal

stability this suggests influential role of lateral benzimidazole on the thermal stability of molecules.
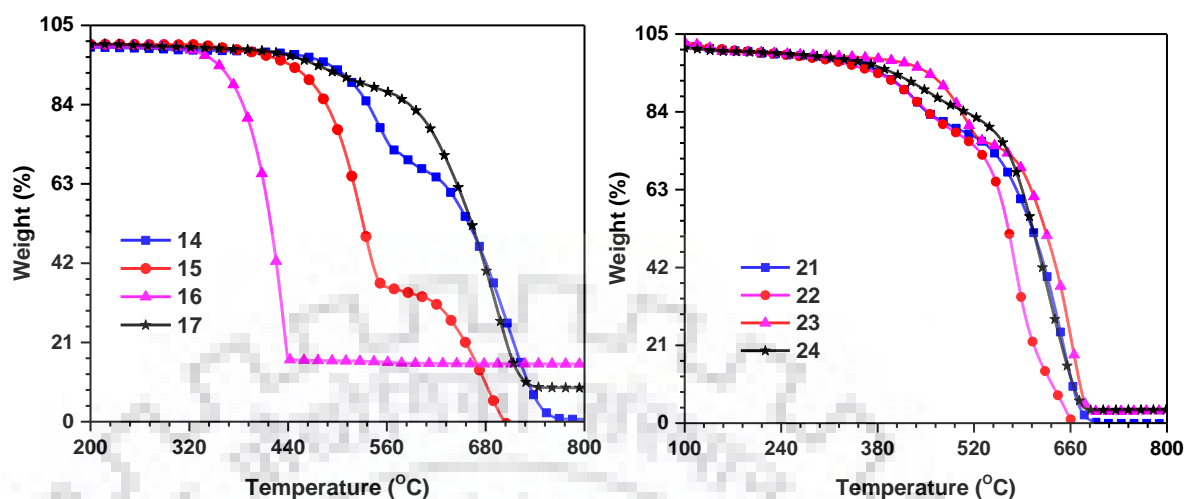
Figure 4.10 Thermogravimetric plots of the dyes

4.2.4 Electrochemical properties

Electrochemical analysis of the dyes was carried out using cyclic voltammetry (CV) and differential pulse voltammetry (DPV) measurements and the relevant spectra are presented in Figure 4.11 and the results are summarized in Table 4.6. The dyes **23** and **24** showed a quasi-reversible oxidation and the oxidation potential of the dye **23** are lower when compared to other dyes **24** attributed to involvement of electron rich triphenylamine in oxidation. However **14, 15, 16, 17, 21** and **22** dyes showed reduction potential attributed to benzimidazole and benzothiadiazole units. The **21** and **22** exhibited lower reduction potential this probably due to increase in electron deficient unit when compared to other benzimidazole compounds (**14, 15, 16, 17**). The HOMO and LUMO energy levels of the materials are very crucial parameters for the understanding of charge transport kinetics in the molecular layers. The HOMO energy levels of the compounds (Table 4.3) were calculated using oxidation and reduction potential of the dyes and referencing to ferrocene HOMO energy (4.8 eV) which falls in the narrow range −5.32 - 6.83 eV. Compound **14, 15, 16, 17, 21-2** possessed the low-lying HOMO among the compounds owing to the absence of trivial donor. Whereas, among the dyes **23-24**, the triphenylamine containing dye (**23**) exhibited high lying HOMO when compared to carbazole derivative **24.** The energies of lowest unoccupied molecular orbital (LUMO) deduced from the reduction potentials where the dyes **14, 15, 16, 17, 21, 22** showed low lying LUMO when compared to **23** and **24** dyes. These alternations are consistent with the electron richness and electron deficiency of the respective compounds. [198, 199] The band gaps of the compounds

121

were obtained from the optical edge. The small band gap ($E_{0–0}$) observed in the dyes **22** and **23** which presumably benefits the conjugation and eventually corresponds to red shift in absorption profile. (*vide supra*).

Table 4.6 Thermal and electrochemical data of the dyes.

Dye	T_{onset} (°C)	E_{ox} (V)[b]	E_{red} (V)[b]	HOMO (eV)[c]	LUMO (eV)[d]	E_{0-0} (eV)[e]
14	516	-	-1.17, -1.79	-6.33	-3.63	2.70
15	467	-	-1.18, -1.90	-6.65	-3.62	3.03
16	-	-	-1.11, -1.89	-6.83	-3.69	3.14
17	-	-	-1.11, -1.78	-6.64	-3.69	2.95
21	419	1.12	-1.51	-6.05	-3.29	2.76
23	479	1.08	-	-5.32	-3.03	2.29
22	418	0.78, 1.11	-1.46	-5.59	-3.34	2.25
24	429	0.75, 1.04	-	-5.55	-3.10	2.45
L10	518	0.52	-	-5.32	-2.53	2.79

[a] Temperature corresponding to 10% weight loss. [b] Measured for 0.1 mM dichloromethane solutions and the potentials are quoted with reference to ferrocene internal standard. [c] HOMO = -(4.8 + E_{ox}). [d] LUMO = HOMO – $E_{0–0}$. [e] Optical band gap obtained from the intersection of absorption and emission spectra
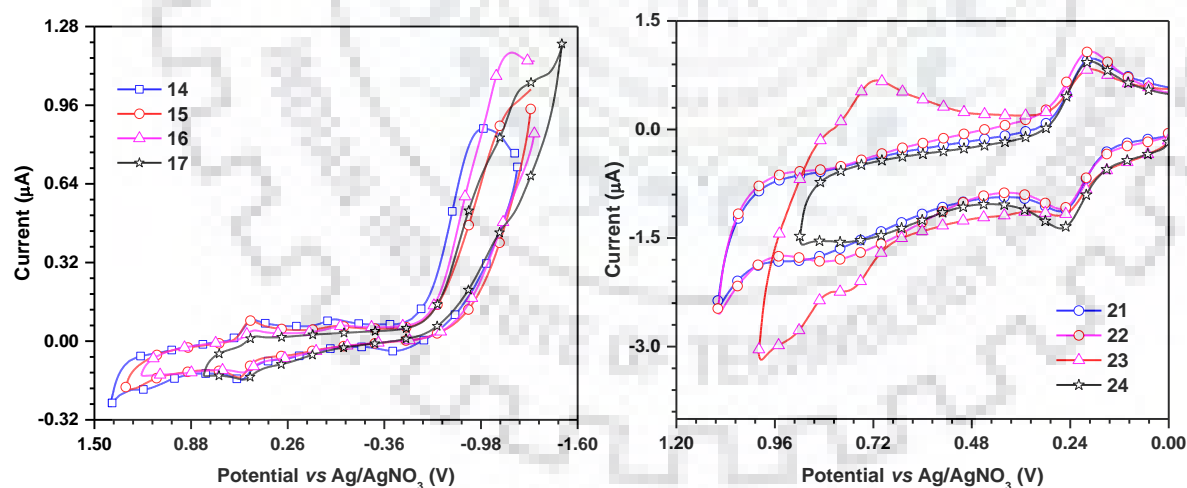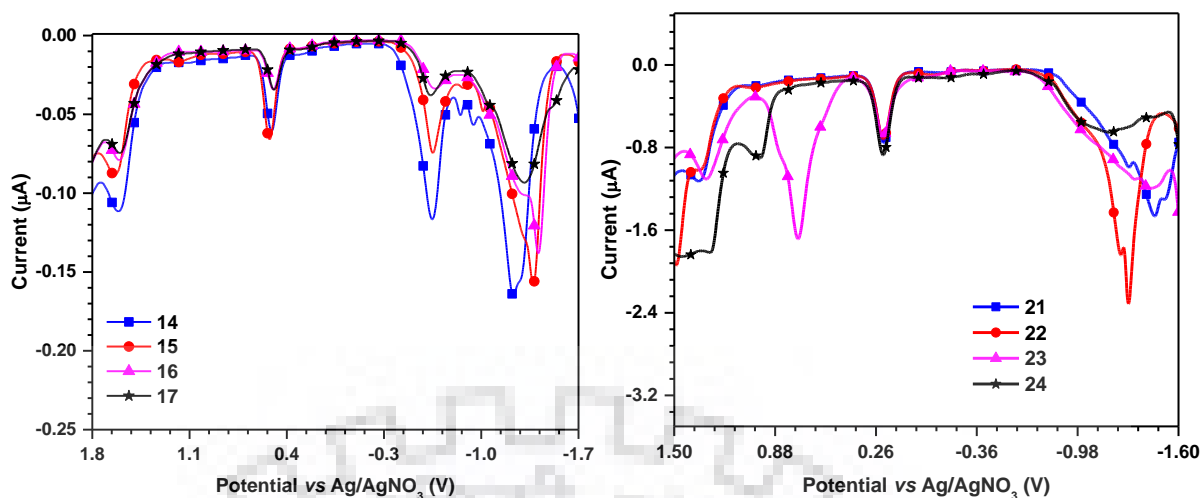
Figure 4.11 Cyclic voltammograms and Differential pulse voltammogram of the dyes recorded in DCM

4.2.5 Theoretical investigations

To further understand the photophysical and redox behaviours of the dyes, density functional theory at B3LYP/6-31g(d,p) level were performed. The respective highest occupied molecular orbitals (HOMOs) and lowest unoccupied molecular orbitals (LUMOs) for the dyes are displayed in Figures 4.12 and 4.13. For the linear substituted dyes **14** and **17** the HOMO electrons is delocalized over the entire molecule, except the *N*-phenyl of *N*-phenylbenzimidazole. Similar distributions of electrons are observed for the lateral substituted dyes **15** and **16.** Moreover, for dyes **21-22** and **23-24** the π electrons in HOMO orbitals are delocalized over entire molecule except the laterally substituted phenyl benzimidazole unit. (Figure 4.12) While the LUMOs electrons are mostly localized over benzothiadiazole nuclei and partly to adjacent phenyl unit.
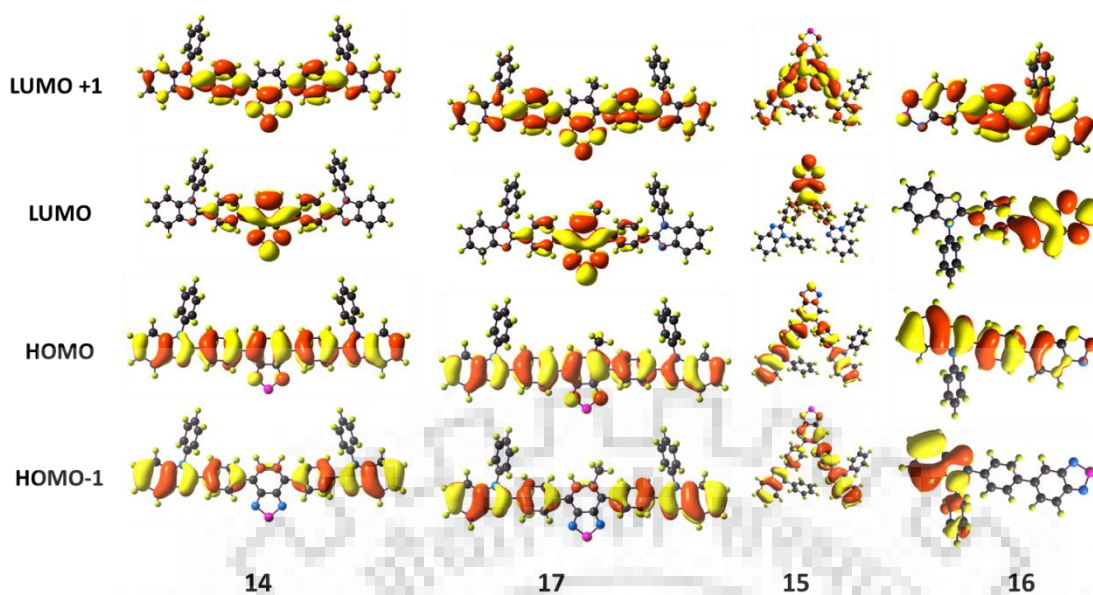
Figure 4.12 Composition of frontier molecular orbitals of the compounds **14-17.**
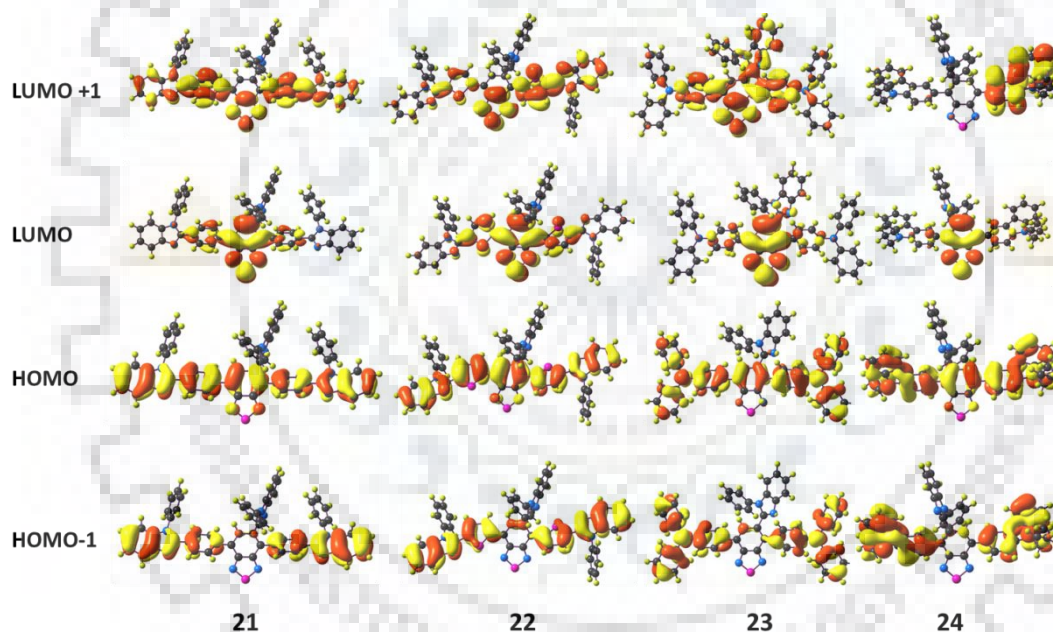
Figure 4.13 Composition of frontier molecular orbitals of the compounds **21-24.**

The charge migrations over the molecules are contributed by triphenylamine, carbazole, *N*-phenyl benzimidazole to HOMO and benzothiadiazole nuclei to LUMO. The HOMO-1 is mainly restricted to arms of all the compounds which are composed of phenyl benzimidazole, carbazole and triphenylamine chromophores. However, the LUMO+1 for the dyes (**21, 22, 14 and 17**, **15** and **16**) are mainly localized on the arms and thiadiazole ring of benzothiadiazole unit. However, for dyes **23** LUMO+1 predominantly restricted to the benzothiadiazole unit and distributed to phenyl linker and the lateral benzimidazole group. For the dye **24**, LUMO+1 electrons are mainly localized on one arm of carbazole.[200] The energies of the HOMO and

124

LUMO levels and HOMO−LUMO energy gap values computed for the dyes are listed in Table. The computed HOMO and LUMO energy levels fall in the narrow ranges of 6.3-7.12 and 2.42-1.91 eV, respectively. The band gap (HOMO−LUMO) of the dyes is in the range of 4.23−5.30 eV.

Table 4.7 Computed absorption wavelengths and their oscillator strengths (f) of dyes.

Dye	λ_{abs} (nm)	f	Assignment (%)
14	395.4	1.19	HOMO→LUMO (86%), HOMO-4→LUMO+0 (10%)
	295.1	1.46	HOMO→LUMO+1 (61%), HOMO-1→LUMO+2 (15%), HOMO-1→LUMO (15%).
15	323.0	1.0284	HOMO→LUMO+1 (64%), HOMO-5→LUMO (18%), HOMO-1→LUMO (7%).
	290.1	0.7458	HOMO→LUMO+1 (46%), HOMO-4→LUMO (18%), HOMO-1→LUMO (17%).
	276.1	0.5970	HOMO-1→LUMO+1 (44%), HOMO→LUMO+2 (22%), HOMO-5→LUMO (11%).
17	374.6	1.0256	HOMO→LUMO (82%), HOMO-4→LUMO (13%),
	291.0	1.4782	HOMO→LUMO+1 (51%), HOMO-1→LUMO+2(19%), HOMO-4→LUMO (17%).
16	411.4	0.24	HOMO→LUMO (99%)
	307.1	0.88	HOMO→LUMO+1 (93%)
21	382.6	1.0336	HOMO→LUMO+1 (81%), HOMO-6→LUMO (15%),
	292.3	0.5657	HOMO-4→LUMO (54%), HOMO→LUMO+1(19%), HOMO-1→LUMO+2(7%), HOMO-6→LUMO (6%)
	289.7	0.7030	HOMO→LUMO+1 (28%), HOMO-4→LUMO (24%), HOMO-5→LUMO (14%), HOMO-6→LUMO (13%), HOMO-1→LUMO+2 (9%)
22	484.5	1.3373	HOMO→LUMO (93%)
	325.7	1.0229	HOMO→LUMO+1 (67%), HOMO-1→LUMO+2 (10%), HOMO→LUMO+2 (6%), HOMO-6→LUMO (5%)
23	446.3	0.7014	HOMO→LUMO (87%), HOMO-2→LUMO (5%),
	304.8	0.5371	HOMO-4→LUMO (31%), HOMO→LUMO+1(25%), HOMO→LUMO+2 (8%), HOMO-3→LUMO (7%),
24	415.1	0.5693	HOMO→LUMO (89%), HOMO-6→LUMO (6%),

4.2.5 Electroluminescence Characteristics

Further to evaluate the electroluminescence performance of compounds solution processed multilayered OLED devices were fabricated (Device 1 and Device 2). The configuration of device 1 and device 2 are ITO/PEDOT:PSS/ (**21** or **22** or **23** or **24)** /TPBi/LiF/Al and ITO/PEDOT:PSS/(CBP: **14 or 15 or 21** or **22** or **23** or **24)**/TPBi/LiF/Al respectively. In device 2 the compounds were employed as emitting dopant in 4,4′-bis(*N*-carbazolyl)-1,1′-biphenyl (CBP) host with different concentrations of 1, 5 and 10 wt %. Here ITO and LiF/Al act as the

anode and the cathode, respectively. The poly(3,4-ethylenedioxythiophene)-poly(styrenesulfonate) (PEDOT:PSS) served as hole injection layer, 1,3,5-tris(*N*-phenylbenzimidazol-2-yl)-benzene (TPBi) functioned as electron transporting layer (ETM) and hole blocking layer; and CBP was used as the host material as it possessed suitable HOMO and LUMO to ensure efficient charge trapping by new dyes to construct the emitting layer (EML).[201] The energy levels of compounds of the materials used in the fabrication of the devices are depicted in Figure 4.14.
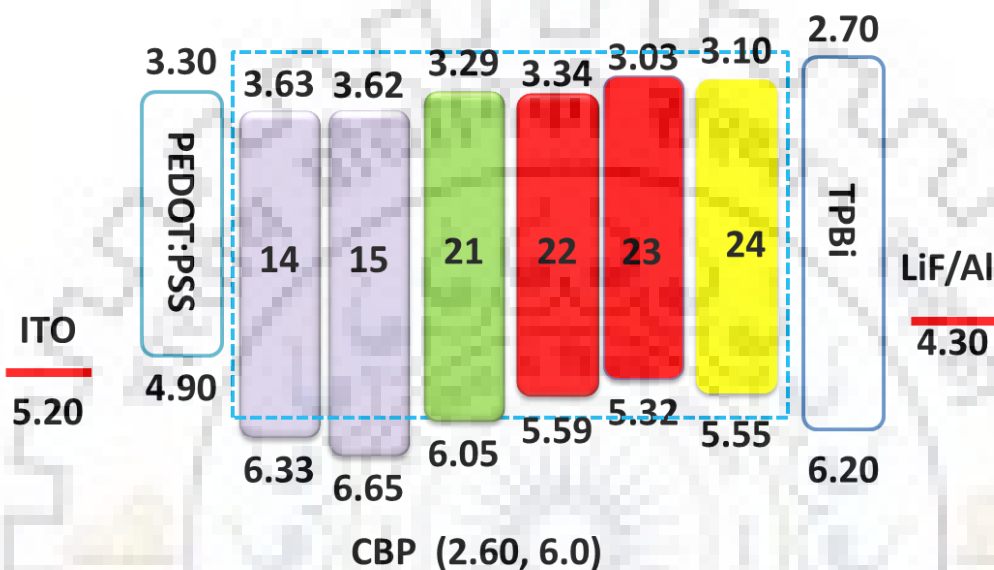
Figure 4.14 Energy-level diagram of the materials used for the fabrication of OLED devices (all values are in eV with respect to vacuum level).

The dyes **21, 22**, **23** and **24** showed poor electroluminescent characteristics when applied as non-doped emitting layer (EL) in device 1. Among the devices, the one fabricated with **23** exhibited reddish-orange electroluminescence with EQE of 0.8 % CIE coordinates (0.59, 0.41), current efficiency (η_c) 0.9 cd A^{-1}, power efficiency (η_P) 0.6 lm W^{-1}. However, the devices where dyes are employed as emitting dopants in CBP host showed improved electroluminescent characteristics. The dyes **14, 15, 22, 23,** and **24** with 5% or 10% dopant concentration and **21** with 1% dopant concentration showed satisfactory results. The device 1 showed red shifted electroluminescence when compared to the device 2 probably due to aggregation in the neat films.

Current density–voltage–luminescence (I–V–L) plots of the diodes are shown in Figures 4.15 and 4.16 and the data listed in Table 4.8. The dyes with phenyl-benzimidazole unit at C4 and C7 positions (**21** and **22**) exhibited high current densities and low operating voltages when compared to **23** and **24** dyes possesing donor unit. Similar trend was observed for lateral substituted benzimidazole dye **15** when compared to linear substituted benzimidazole dye **14.**

This suggests the effective injection of charge carriers in the molecular layer, is facilitated by suitable HOMO-LUMO levels from the adjacent electron transport layer (ETL) and hole transport layer, respectively. [202]
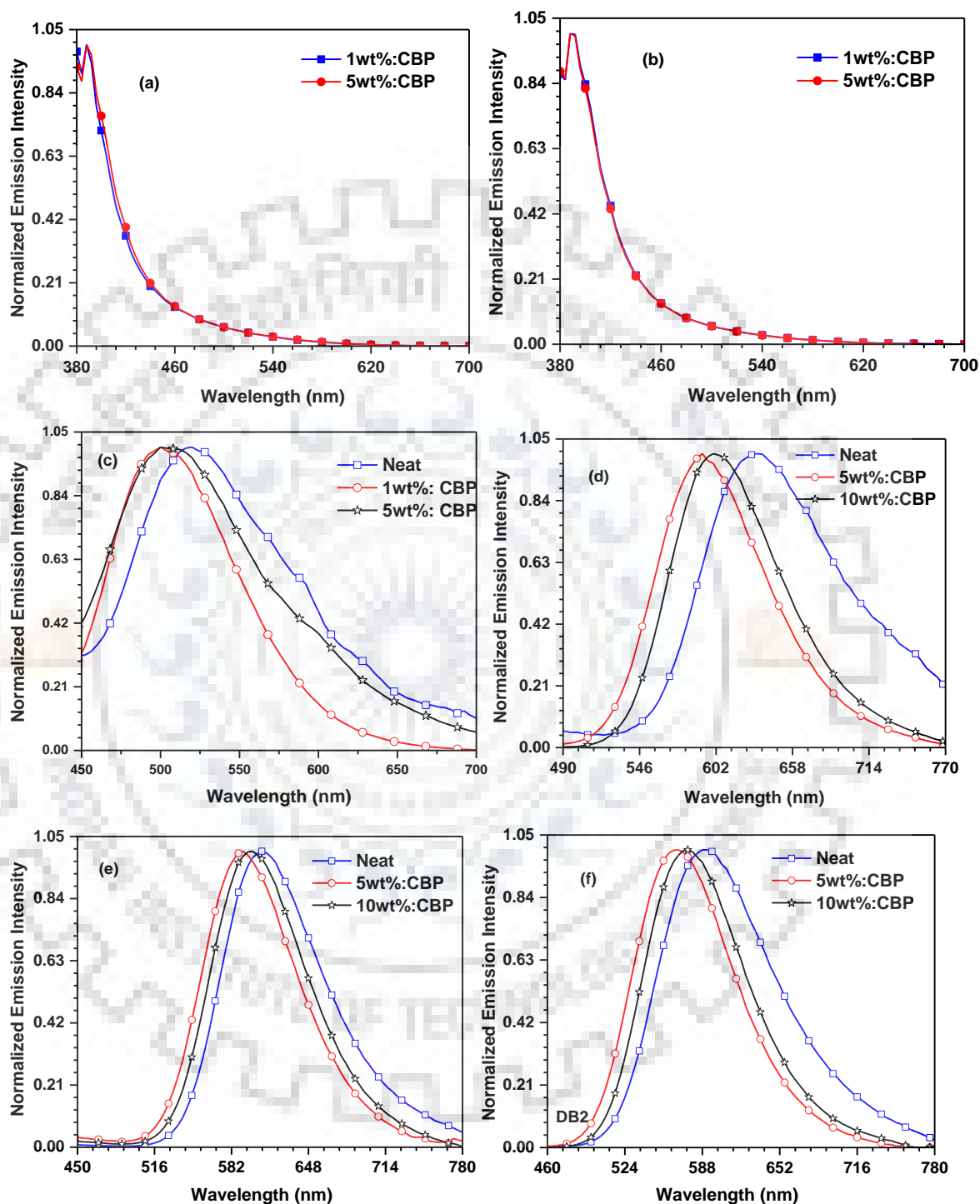
Figure 4.15 EL spectra of the diodes in different doping concentrations: (a) **14** (b) **15** (c) **21** (d) **22** (e) **23** and (e) **24**
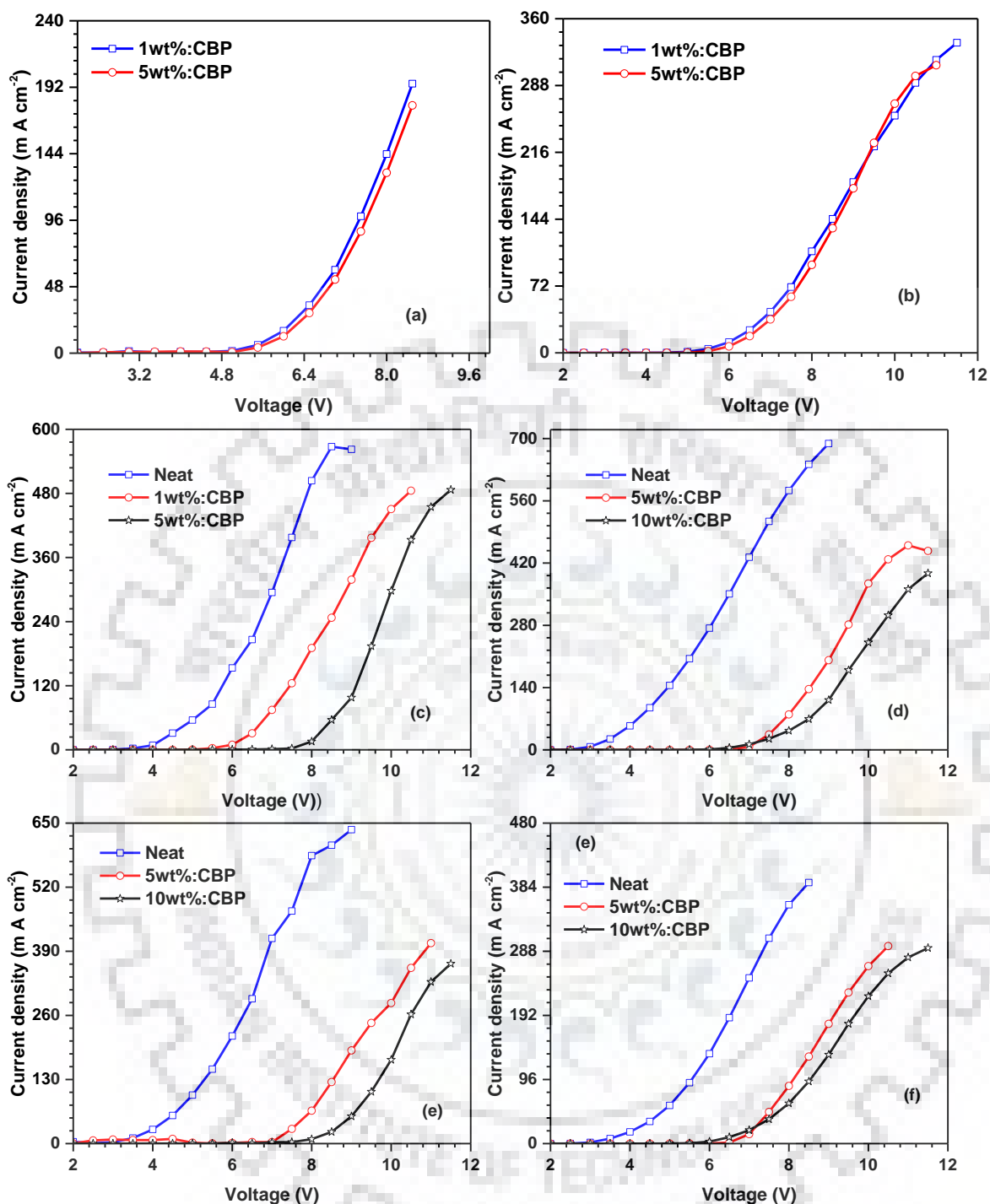
Figure 4.16 Current density–voltage (I–V) plots of the diodes of (a) **14** (b) **15** (c) **21** (d) **22** (e) **23** and (f) **24**

Furthermore, the device made with 5 wt% doped dyes in CBP exhibited high luminance characteristics, reflecting the balanced confinement of charge carriers in the emitting layer and effective capturing of electronically generated excitons in the CBP host matrix. [203]
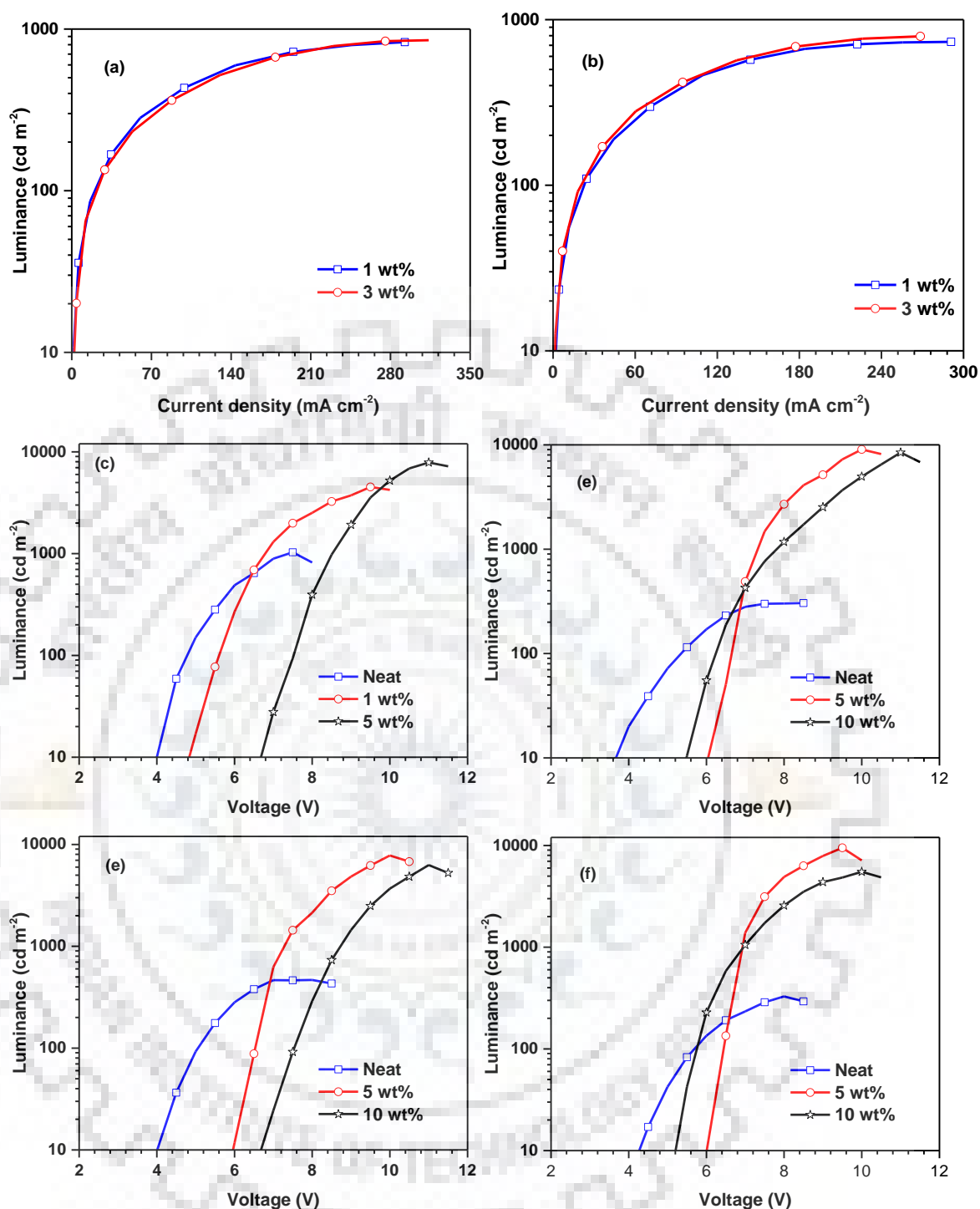
Figure 4.17 Luminance–current density (L–I) and luminance–voltage (L–V) plots of the diodes of (a) **14** (b) **15** (c) **21** (d) **22** (e) **23** and (f) **24**

All the devices with 5% dopant concentration showed varied electroluminescence (EL) spectra, the bright green emission for the device (**21**) with peaks centered at 500 nm and CIE of (0.21, 0.41). For the devices doped with **22** and **23**, reddish orange and orange emission was observed at the wavelength maxima of 592 and 592 nm, respectively, with CIE coordinates of (0.57, 0.42) and (0.51, 0.45). Similarly, yellow emission observed for device doped with **24** with peaks centred at 568 nm with CIE coordinates of (0.45, 0.52).[204] The EL spectra of the

diodes (**21-22** and **23-24**) resemble the photoluminescence (PL) spectra of the materials as thin film. These results suggest that the obtained electroluminescence from the doped devices is result of recombination in the desired emitting layer (EML) and also showed absence of aggregate formation in the solid state. However, the blue emission observed for the device (**14** and **15**) is not from the compound but from CBP host material (~390 nm).[205] This suggests the tri-substitution on benzothiadiazole nuclei facilitates the balanced recombination of exciton in the emitting layer.

Overall, the device with 5 wt% dopant concentration of **22** exhibited excellent performance in the series with maximum luminance of 9032 cdm^{-2}, maximum current efficiency of 8.5 cdA^{-1}, maximum power efficiency of 5.1 lmW^{-1}, CIE coordinates of (0.55, 0.44) and EQE of 9.1%. This is attributed to the utilization of both energies of LE and CT excitons (i.e., hybridized local and charge transfer (HLCT)). The efficiencies are among the highest for orange/red HLCT-based devices reported.[182, 206]

Table 4.8 Electroluminescence characteristics of the dyes.

Dye	Conc. (wt%)[a]	Power Efficiency[b] (lm W^{-1})	Current Efficiency[b] (cd A^{-1})	EQE[b] (%)	CIE[b]	Max. luminescence (cd m^{-2})	EL max. (nm)
14	1	6.1	0.3	1.4	(0.17, 0.11)	830	388
	5	6.2	0.3	1.7	(0.17, 0.11)	924	388
15	1	6.3	0.2	1.3	(0.17, 0.10)	734	388
	5	6.5	0.2	1.4	(0.17, 0.10)	830	388
21	Neat	0.2/0.3	0.4/0.5	0.3/0.4	(0.31, 0.45)	1038	520
	1	4.2/3.5/5.7	5.8/5.1/6.8	7.1/3.7/8.9	(0.21, 0.41)	3720	500
	5	2.3/2.1/2.4	4.0/3.9/4.4	2.9/1.9/3.3	(0.23, 0.43)	7862	500
22	Neat	0.1/0.1	0.1/0.1	0.1/0.1	(0.60, 0.38)	305	632
	5	5/4.5/5.1	8.2/7.6/8.5	8.7/5.8/9.1	(0.55,0.44)	9032	592
	10	4.5/3.2/4.7	6.8/4.9/7.9	5.2/4.4/5.8	(0.57,0.42)	8438	600
23	Neat	0.4/0.6	0.8/0.9	0.6/0.8	(0.59, 0.41)	431	608
	5	4.3/4.4/4.5	8.8/6.9/7.0	3.3/2.5/3.4	(0.51,0.45)	7804	592
	10	5/4.1/5.4	7.5/6.1/7.9	4.9/3.5/5.2	(0.56,0.43)	6281	600
24	Neat	1.2/0.8	1.7/1.7	0.5/0.5	(0.53, 0.46	1675	588
	5	2.9/3.6/3.8	5.9/7.9/8.5	2.3/2.6/2.8	(0.45, 0.52)	9500	568
	10	6.4/4.4/6.6	9.9/7.3/10	4.6/3.8/5.2	(0.48, 0.51)	5513	576

[a] concentration of dye for doped devices (device II) [b] value at 100/1000 cd/m^2

4.3. Conclusions

In conclusion, we have synthesized two set of a series containing benzimidazole-benzothiadiazole conjugates by Suzuki/Stille coupling and condensation reaction condition protocol. The Type1 derivatives feature phenyl-benzimidazole substitution at different functionalization of benzothiadiazole moiety and Type 2 derivatives contains lateral benzimidazole unit at C5 position of BTD nuclei appended by acceptor and donor unit at C4 and C7 positions. The structure-function relationships of the dyes were studied systematically and compared with BTD derivatives (**L8**, **L9** and **L10**). Interestingly, the linear benzimidazole derivative **14** showed bathochromic shift when compared to its 'V' shaped regioisomer **15** suggesting the perturbation of conjugation in 'V' shaped isomer. However the lateral substituted BI chromophore derivative **21** showed red shift compared to **14,** which suggests the active participation of lateral substitution in extending the conjugation. The absorption profiles of the dyes are insensitive to the solvent polarity suggestive of non-polar ground state. However, the dyes exhibited positive solvatochromism in emission indicating a polar excited state involving significant structural and electronic reorganizations. Electrochemical studies showed HOMO/LUMO shift to high level in **23** and **24** while **21** and **22** showed low lying LUMO in series. Further, the dyes were applied in solution processable multilayer OLEDs either as dopant emitters. The doped devices exhibited gamut of emission electroluminescence with CIE of $0.21 \leq x \leq 0.59$, $0.41 \leq y \leq 0.52$ and superior luminance. The device fabricated with isomer **22** exhibited better performance in the series attributable to well-aligned energy levels which resulted in EQE of 9.1% (8.5 A^{-1}) and L_{max} of 9032 cd m^{-2} with 5 wt% dopant concentration.

4.4. Experimental Section

4.4.1 Synthesis

4,4'-(Benzo[*c*][1,2,5]thiadiazole-5,6-diyl)dibenzaldehyde (13b). A mixture of 5,6-dibromobenzo[*c*][1,2,5]thiadiazole (0.40 g, 1.36 mmol), 4-formylphenyl)boronic acid (0.51 g, 3.4 mmol) K_2CO_3 (1.12 g, 8.16 mmol), $Pd(PPh_3)_4$ (6 mol%) and THF:H_2O (3:1) 80°C under nitrogen atmosphere. After completion of the reaction, it was poured into ice water and extracted with chloroform. The combined organic layer was thoroughly washed with water and dried over anhydrous Na_2SO_4, filtered organic extract was evaporated to obtain orange residue, which was purified by column chromatography on silica gel using hexanes/dichloromethane (1:4) as eluant. Yellow Solid (0.31 g, 67 %); mp 196-199 °C; IR (KBr, cm^{-1}) 1660 ($v_{C=O}$);^{1}H

NMR (400 MHz, CDCl$_3$, δ ppm): 10.12 (s, 2 H), 8.45 (s, 1H), 7.97-7.80 (m, 5H), 7.63-7.60 (m, 4H);^{13}C NMR (100 MHz, CDCl$_3$, δ ppm):):19.6, 154.2, 145.8, 141.7, 135.2, 130.4, 122.6; HRMS (ESI-TOF) *m/z*: [M]$^+$ Calcd for C$_{20}$H$_{12}$N$_2$O$_2$S 344.0619, found 344.0621.

4-(Benzo[*c*][1,2,5]thiadiazol-5-yl)benzaldehyde (13c). It was obtained from 5-bromobenzo[*c*][1,2,5]thiadiazole (0.23 g, 1 mmol), 4-formylphenyl)boronic acid (0.35 g, 0.2 mmol) by following the procedure described above for **13b**. Green Solid (0.18 g, 78 %); mp 120-123 °C; IR (KBr, cm^{-1}) 1660 ($v_{C=O}$);^{1}H NMR (400 MHz, CDCl$_3$, δ ppm): 10.1 (s, 1H), 8.25 (s, 1H), 8.12 (d, *J* = 8 Hz, 1H), 8.04-8.02 (m, 2H), 7.91-7.86 (m, 3H);^{13}C NMR (100 MHz, CDCl$_3$, δ ppm):191.6, 155.0, 154.4, 145.4, 141.0, 136.0, 130.4, 129.5, 128.1, 128.0, 122.0, 119.0; HRMS (ESI-TOF) *m/z*: [M]$^+$ Calcd for C$_{13}$H$_8$N$_2$OS 240.0357, found 240.0347.

4,4'-(5-Methylbenzo[*c*][1,2,5]thiadiazole-4,7-diyl)dibenzaldehyde (13d) It was obtained from 4,7-dibromo-5-methylbenzo[*c*][1,2,5]thiadiazole (0.23 g, 0.74 mmol), 4-formylphenyl)boronic acid (0.33 g, 0.18 mmol) by following the procedure described above for **13b**. Green Solid (0.19 g, 72 %); mp 220-223 °C IR (KBr, cm^{-1}) 1660 ($v_{C=O}$);^{1}H NMR (400 MHz, CDCl$_3$, δ ppm): 10.1 (d, *J* = 4 Hz, 2H), 8.17 (d, *J* = 8 Hz, 2H), 8.06-8.09 (m, 4H), 7.76 (s, 1H), 7.67 (d, *J* = 8 Hz, 2H) 2.5 (s, 3H); ^{13}C NMR (100 MHz, CDCl$_3$, δ ppm):191.8, 155.4, 152.0, 143.0, 136.8, 136.0, 135.8, 132.6, 131.8, 131.6, 130.9, 129.9, 129.8, 129.7, 20.2; HRMS (ESI-TOF) *m/z*: [M+H]$^+$ Calcd for C$_{21}$H$_{15}$N$_2$O$_2$S 359.0776, found 359.0780.

5,6-Bis(4-(1-phenyl-1H-benzo[*d*]imidazol-2-yl)phenyl)benzo[*c*][1,2,5]thiadiazole (15). A mixture of **13b** (0.32, 0.43 mmol), *N1*-phenylbenzene-1,2-diamine (0.29 mg, 1.0 mmol) and sodiumthiosulfate (0.49 mg, 2.5 mmol) were dissolved in DMF and the resultant mixture was heated at 95 °C for 8 h. After completion of the reaction, it was poured into ice water and filtered. Further was recrystallized to be used in further reaction using hexane and chloroform. Off white solid (0.58 g, 87 %); mp 235-237 °C ^{1}H NMR (400 MHz, CDCl$_3$, δ ppm): 8.03 (s, 2H), 7.88 (d, *J* = 8Hz, 2H), 7.40-7.48 (m, 8H), 7.32-7.36 (t, *J* = 8 Hz, 2H), 7.22-7.25 (m, 8H), 7.07 (d, *J* = 8Hz, 4H);^{13}C NMR (100 MHz, CDCl$_3$, δ ppm): 154.2, 151.5, 142.8, 142.4, 140.8, 137.0, 136.6, 130.0, 129.6, 129.0, 128.9, 128.5, 127.2, 123.4, 123.0, 121.9, 119.8, 110.0; HRMS (ESI-TOF) *m/z*: [M+H]$^+$ Calcd for C$_{44}$H$_{29}$N$_6$S 673.2096, found 673.2100.

4,7-Bis(4-(1-phenyl-1H-benzo[*d*]imidazol-2-yl)phenyl)benzo[*c*][1,2,5]thiadiazole.(14)

It was obtained from **4,4'-(benzo[*c*][1,2,5]thiadiazole-4,7-diyl)dibenzaldehyde** (0.32 g, 0.43 mmol), *N1*-phenylbenzene-1,2-diamine (0.29 g, 1 mmol) by following the procedure described above for **15**. Pale yellow Solid (0.24 g, 85 %); mp 303-305 °C;^{1}H NMR (400 MHz, CDCl$_3$, δ ppm): 7.90-7.96 (m , 6H), 7.74-7.78 (m, 6H), 7.47-7.52 (m, 6H), 7.33-7.40 (m, 6H), 7.23-7.30 (m, 5H);^{13}C NMR (100 MHz, CDCl$_3$, δ ppm): 154.0, 151.6, 142.6, 138.2, 137.2, 136.8, 132.5,

130.0, 129.5, 129.1, 128.8, 128.2, 127.5, 123.6, 123.2, 119.7, 110.5; HRMS (ESI-TOF) *m/z*: [M+H]$^+$ Calcd for C$_{44}$H$_{29}$N$_6$S 673.2096, found 673.2100.

5-(4-(1-Phenyl-1*H*-benzo[d]imidazol-2-yl)phenyl)benzo[*c*][1,2,5]thiadiazole (16). It was obtained from **13c** (0.15 g, 0.62 mmol), *N1*-phenylbenzene-1,2-diamine (0.25 g, 1.36 mmol) by following the procedure described above for **15**. Pale yellow Solid (0.22 g, 90 %); mp 176-177 °C;^{1}H NMR (400 MHz, CDCl$_3$, δ ppm): 8.16 (s, 1H), 8.04 (d, *J* = 4 Hz, 1H),), 7.90 ((d, *J* = 8 Hz, 1H), 7.85-7.87 (m, 1H), 7.63-7.72 (m, 4H), 7.48-7.55 (m, 1H), 7.33-7.37 (m, 3H), 7.27-7.31 (m, 2H);^{13}C NMR (100 MHz, CDCl$_3$, δ ppm): 155.3, 154.3, 151.6, 142.8, 141.4, 140.4, 137.3, 137.0, 130.0, 129.7, 128.8, 127.4, 127.3, 123.6, 123.2, 121.6, 119.8, 118.7, 110.5; HRMS (ESI-TOF) *m/z*: [M]$^+$ Calcd for C$_{25}$H$_{16}$N$_4$S 404.1096, found 404.1200.

5-Methyl-4,7-bis(4-(1-phenyl-1*H*-benzo[d]imidazol-2yl)phenyl)benzo[*c*][1,2,5]thiadiazole (17). It was obtained from **13d** (0.12 g, 0.33 mmol), *N1*-phenylbenzene-1,2-diamine (0.13 g, 0.72 mmol) by following the procedure described above for **15**. Green Solid (0.17 g, 75 %); mp 283-285 °C;^{1}H NMR (400 MHz, CDCl$_3$, δ ppm): 7.90-7.96 (m, 4H), 7.74-7.77 (m , 4H), 7.6 (s, 1H), 7.50-7.55 (m, 6H), 7.37-7.43 (m, 8H), 7.28-7.35 (m, 4H), 2.41 (s, 1H); ^{13}C NMR (100 MHz, CDCl$_3$, δ ppm): 155.6, 152.1, 151.9, 143.0, 137.0, 132.2, 130.2, 129.9, 129.2, 129.0, 128.7, 127.6, 127.5, 123.4, 123.0, 119.8, 110.5, 20.34; HRMS (ESI-TOF) *m/z*: [M+H]$^+$ Calcd for C$_{45}$H$_{30}$N$_6$S 687.2253, found 687.2250.

4,7-Dibromo-5-(1-phenyl-1*H*-benzo[d]imidazol-2-yl)benzo[*c*][1,2,5]thiadiazole (19). It was obtained from 4,7-dibromobenzo[*c*][1,2,5]thiadiazole-5-carbaldehyde (0.30 mg, 0.93 mmol), *N1*-phenylbenzene-1,2-diamine (0.18 mg, 1.02 mmol) by following the procedure described above for **15**. Dirty yellow solid (0.40 g, 90 %); mp 206-208 °C; ^{1}H NMR (400 MHz, CDCl$_3$, δ ppm): 7.94-8.01 (m, 3H), 7.38-7.44 (m, 6H), 7.30-7.37 (m, 2H); ^{13}C NMR (100 MHz, CDCl$_3$, δ ppm): 154.57, 152.05, 151.88, 139.95, 133.70, 132.76, 131.23, 128.88, 125.80, 113.22; 34.83, 31.38, 23.04; HRMS (ESI-TOF) *m/z*: [M+H]$^+$ Calcd for C$_{19}$H$_{10}$Br$_2$N$_4$S 483.8993, found 472.8970.

4,4'-(5-(1-Phenyl-1*H*-benzo[d]imidazol-2-yl)benzo[*c*][1,2,5]thiadiazole-4,7-diyl)dibenzaldehyde (20a). It was obtained from 4,7-dibromo-5-(1-phenyl-1*H*-benzo[d]imidazol-2-yl)benzo[*c*][1,2,5]thiadiazole (0.10 g, 0.20 mmol), (4-formylphenyl)boronic acid (0.75 g , 0.50 mmol) by following the procedure described above for **13a.** Pale yellow solid (0.73 g, 68 %); mp 142-145 °C; IR (KBr, cm^{-1}) 1664 ($v_{C=O}$); ^{1}H NMR (400 MHz, CDCl$_3$, δ ppm): 10.14 (s, 1H), 10.00 (s, 1H), 8.41 (s, 1H), 8.28 (d, *J* = 4Hz, 2H), 8.09 (d, *J* = 4Hz, 2H), 7.96 (d, *J* = 4Hz, 2H), 7.66 (d, *J* = 4Hz, 2H), 7.28 - 7.43 (m, 4 H), 7.12-7.24 (m, 4H), 6.56 (d, *J* = 4Hz, 2H); ^{13}C NMR (100 MHz, CDCl$_3$, δ ppm): 135.1, 130.8,

129.9, 129.4, 129.2, 128.9, 128.7, 128.4, 127.5, 127.4, 125.5, 125.3, 12.3, 110.7, 110.5; HRMS (ESI-TOF) *m/z*: [M+H]$^+$ Calcd for $C_{33}H_{20}N_4O_2S$ 536.1307, found 536.1280.

5,5'-(5-(1-Phenyl-1*H*-benzo[d]imidazol-2-yl)benzo[*c*][1,2,5]thiadiazole-4,7-diyl)bis(thiophene-2-carbaldehyde) (20b). A mixture of (5-(1,3-dioxolan-2-yl)thiophen-2-yl)tributylstannane (0.88 mmol), 4,7-dibromo-5-(1-phenyl-1*H*-benzo[d]imidazol-2-yl)benzo[*c*][1,2,5]thiadiazole (0.21 g, 0.44 mmol), Pd(PPh₃)₂Cl₂ (2 mol %) and dry DMF (5 mL) was heated at 80 °C under nitrogen atmosphere. On completion of the reaction, the mixture was poured into water and extracted with chloroform. The organic layer was washed with brine solution followed by water and dried over anhydrous Na₂SO₄. The volatiles were removed to obtain a solid residue. It was dissolved in glacial acetic acid (5 mL) and heated to 60°C. After 30 min, it was treated with 10 mL of water and continued the heating for a further 6 h. The cooled solution was extracted with chloroform. The chloroform layer was washed with water and dried over anhydrous Na₂SO₄. On removal of solvent, the obtained dark residue was purified by column chromatography on silica gel using hexanes/chloroform (1:1) as eluant. Red solid; yield 0.38 g, 52%; mp 158-160°C; IR (KBr, cm^{-1}) 1660 ($\upsilon_{C=O}$); ^{1}H NMR (400 MHz, CDCl₃, δ ppm): 10.01 (s, 1H), 9.85 (s, 1H), 8.50 (s, 1H), 8.36 (s, 1H), 7.97-8.0 (m, 4H), 7.89(s, 1H), 7.52-7.87 (m, 6H), 6.70-6.87 (m, 3H); ^{13}C NMR (100 MHz, CDCl₃, δ ppm): 190.9, 188.6, 184.8, 168.0, 160.8, 160.8, 159.8, 151.8, 150.3, 149.9, 145.4, 130.3, 130.1, 129.6, 129.6, 129.5, 128.5, 128.4, 128.2, 125.4, 125.3, 123.8, 123.7, 123.6, 123.5, 123.2, 122.5, 122.4, 120.6, 120.55, 120.4, 120.2, 110.8, 100.6, 100.2, 97.8, 89.3, 89.2, 86.9, 77.3, 77.00, 76.6; HRMS (ESI-TOF) *m/z*: [M+H]$^+$ Calcd for $C_{29}H_{16}N_4O_2S$ 548.0435, found 548.0440.

5-(1-Phenyl-1*H*-benzo[d]imidazol-2-yl)-4,7-bis(4-(1-phenyl-1*H*-benzo[d]imidazol-2-yl)phenyl)benzo[*c*][1,2,5]thiadiazole (21). It was obtained from **20a** (0.10 g, 0.20 mmol), *N1*-phenylbenzene-1,2-diamine (0.80 g, 0.44 mmol) by following the procedure described above for **15**. Green Solid (0.16 g, 93 %); mp 140-142 °C; ^{1}H NMR (400 MHz, CDCl₃, δ ppm): 8.27 (s, 1H) 8.06 (d, *J* = 8.0 Hz, 2H), 7.88-7.92 (m, 3H), 7.76 (d, *J* = 8.0 Hz, 2H), 7.43-7.55 (m, 4H), 7.35-7.41 (m, 15 H), 7.28-7.33 (m, 3H), 7.09-7.30 (m, 4 H), 6.92 (d, *J* = 8Hz, 2 H), 6.51 (d, *J* = 8Hz, 2 H);^{13}C NMR (100 MHz, CDCl₃, δ ppm):142.7, 142.2, 137.4, 130.0, 129.9, 129.6, 129.2, 127.5, 124.0, 110.5; HRMS (ESI-TOF) *m/z*: [M+H]$^+$ Calcd for $C_{57}H_{36}N_8S$ 864.2784, found 864.2780.

5-(1-Phenyl-1*H*-benzo[d]imidazol-2-yl)-4,7-bis(5-(1-phenyl-1*H*-benzo[d]imidazol-2-yl)thiophen-2-yl)benzo[*c*][1,2,5]thiadiazole (22). It was obtained from **20b** (0.11g, 0.20 mmol), *N1*-phenylbenzene-1,2-diamine (0.04 mg, 0.22 mmol) by following the procedure described above for **15**. Red Solid (0.14 g, 80 %); mp 285-287 °C; ^{1}H NMR (400 MHz, CDCl₃,

δ ppm): 8.26 (s, 1H), 7.96 (d, J = 8.0 Hz, 2H), 7.91(d, J = 4 Hz, 2H), 7.81-7.87 (m, 2H), 7.61-7.65 (m, 3H), 7.39-7.49(m, 6H), 7.20-7.31 (m, 9H), 7.09-7.14 (m, 3 H), 6.99 (d, J = 8 Hz, 1H), 6.89 (d, J = 4Hz, 1H), 6.83 (d, J = 8 Hz, 1H), 6.68 (d, J = 8Hz, 2H), 6.63 (d, J = 4 Hz, 1H); ^{13}C NMR (100 MHz, CDCl$_3$, δ ppm):173.2, 166.9, 163.0, 152.1, 150.7, 146.9, 143.3, 142.8, 140.7, 138.6, 137.8, 136.3, 135.8, 135.6, 135.0, 130.2, 130.1, 129.3, 128.5, 128.3, 125.8, 125.5, 123.9, 123.6, 123.2, 120.4, 119.6, 119.3, 110.7, 110.5, 110.3; HRMS (ESI-TOF) *m/z*: [M+H]$^+$ Calcd for C$_{53}$H$_{32}$N$_8$S$_3$ 876.1912, found 876.1918.

4,4'-(5-(1-Phenyl-1H-benzo[*d*]imidazol-2-yl)benzo[*c*][1,2,5]thiadiazole-4,7-diyl)bis(*N,N*-diphenylaniline) (23). It was obtained from **19** (0.5 g, 1 mmol), (4-(diphenylamino)phenyl)boronic acid (0.6 g, 2.1mmol) by following the procedure described above for **13a**. Red solid (0.62 g, 77%); mp 150-152 °C; ^{1}H NMR (400 MHz, CDCl$_3$, δ ppm): 8.20 (s, 1H), 7.98 (d, J = 8.0 Hz, 2H), 7.91 (d, J = 8 Hz, 1H), 7.81-7.87 (m, 2H), 7.25-7.31 (m, 9H), 7.17-7.21 (m, 9 H), 7.02-7.12 (m, 10 H), 6.71-6.87 (m, 6H); ^{13}C NMR (100 MHz, CDCl$_3$, δ ppm):147.6, 147.5, 131.2, 130.1, 129.4, 129.3, 129.1 ,128.7, 127.5, 125.8, 125.0, 123.6, 123.5, 123.4, 122.9, 121.9, 117.9, 115.8, 115.7,114.5, 111.4, 110.4; HRMS (ESI-TOF) *m/z*: [M+H]$^+$ Calcd for C$_{55}$H$_{38}$N$_6$S 814.2879, found 814.2880.

4,7-Bis(9-butyl-9*H*-carbazol-3-yl)-5-(1-phenyl-1*H*-benzo[*d*]imidazol-2 yl)benzo[*c*][1,2,5]thiadiazole (24). It was obtained from **19** (0.15 g, 0.30 mmol), (9-butyl-9*H*-carbazol-3-yl)boronic acid (0.24 g, 0.92 mmol) by following the procedure described above for **13a**. Red solid (0.18 g, 77%); mp 148-150 °C; ^{1}H NMR (400 MHz, CDCl$_3$, δ ppm): 8.85 (s, 1H), 8.22-8.29 (dd, J =4Hz, 2H), 7.9 (d, J = 4.0 Hz, 1H), 7.8 (d, J = 4.0 Hz, 1H), 7.25-7.63 (m, 8H), 7.04-7.19 (m, 5H), 6.87 (d, J = 4.0 Hz, 2H), 6.41 (d, J = 4.0 Hz, 2H), 4.22-4.40 (m, 4H), 1.80-1.96 (m, 4H), 1.36-1.45(m, 4H), 0.92-1.03 (m, 6H); ^{13}C NMR (100 MHz, CDCl$_3$, δ ppm): 152.6, 143.4, 143.3, 140.9, 140.6, 140.0, 139.5, 135.5, 135.3, 135.1, 131.3, 131.1, 129.4, 129.2, 128.9, 127.8, 127.1, 125.6, 124.7, 123.3, 122.9, 121.5, 120.7, 120.5, 119.1, 118.9, 110.4, 110.2, 109.0, 108.9, 108.6, 108.5, 108.2, 108.1, 108.0; HRMS (ESI-TOF) *m/z*: [M+H]$^+$ Calcd for C$_{51}$H$_{42}$N$_6$S 770.3192, found 770.3192.
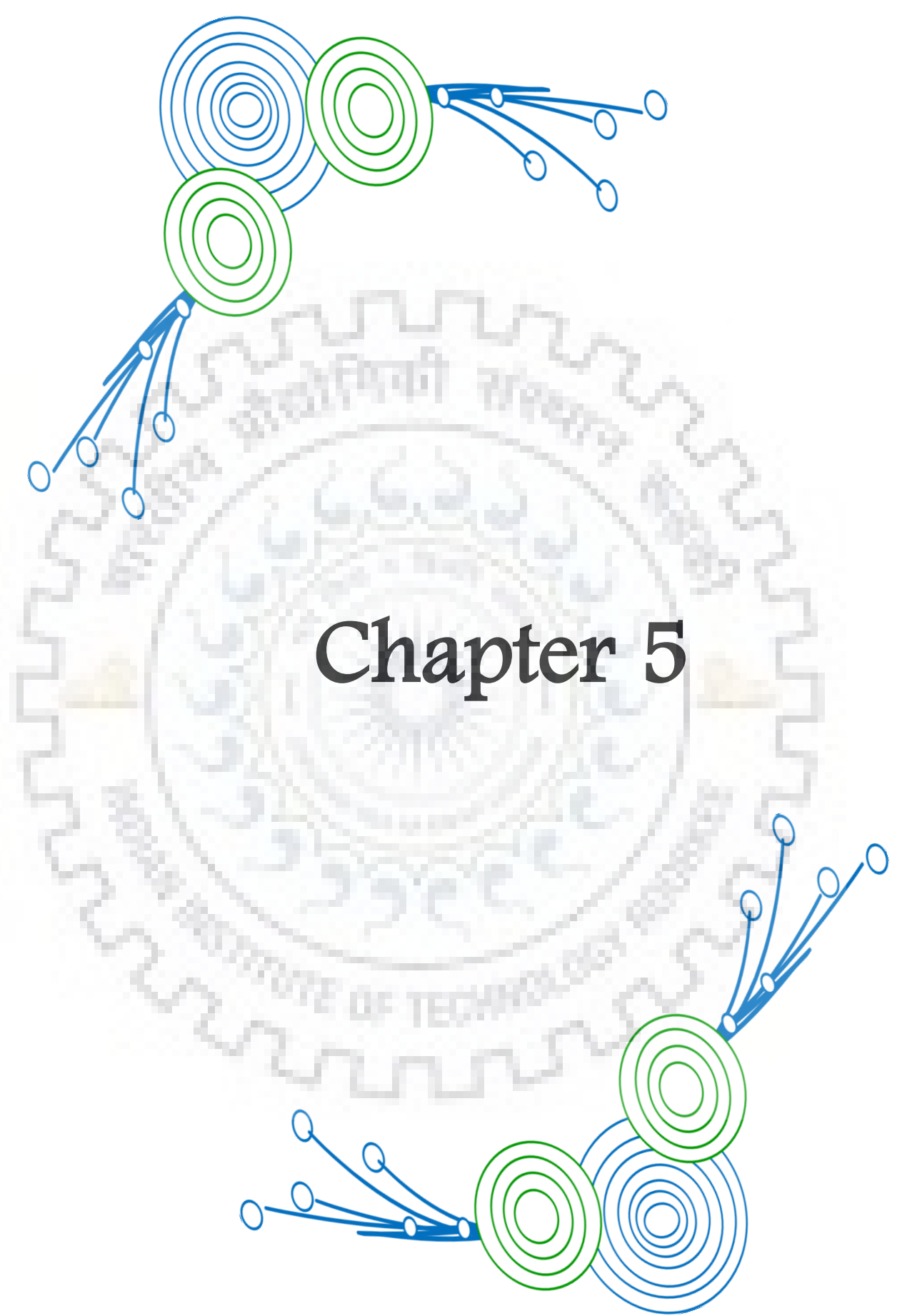
Chapter 5

Chapter 5

Modulation of Donor-Acceptor Interaction by Methyl Substitution in Benzothiadiazole Dyes: Effect on Absorption and Photovoltaic Properties
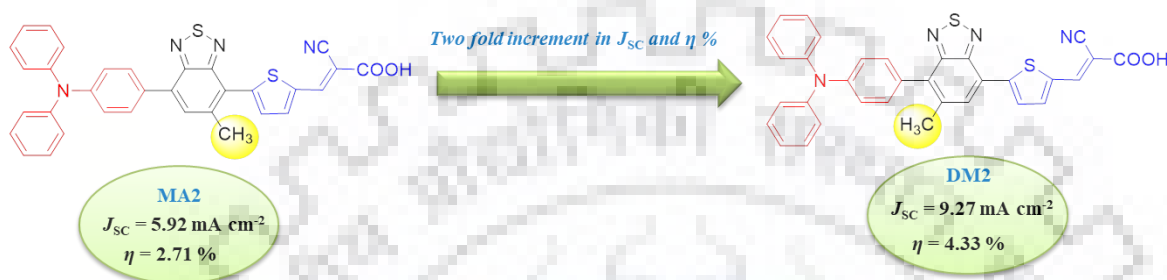
5.1 Introduction

The scientific community has paid extensive attention toward the dye-sensitized solar cells (DSSCs) in last two decades after the exciting demonstration by Grätzel and co-workers that ruthenium complexes adsorbed on nanocrystalline titanium dioxide can effectively convert light energy into electrical energy in the presence of a suitable electrode. [207, 208, 209] Later, organic dyes, porphyrin derivatives were also found to effectively act as sensitizer in DSSCs. The sensitizer is one of the most important components in DSSC and to date ruthenium polypyridyl complexes as sensitizers have achieved power conversion efficiency (η) over 10-11% under standard conditions (1.5 AM). Moreover, the zinc porphyrin sensitized DSSCs have reached the efficiency of over 12%. [210] However, the rarity and high cost of the inorganic metal may impede their further development for large-scale applications. On the other hand metal-free organic sensitizers have drawn a significant interest from scientific community due to their low cost of production, easy availability, high molar extinction coefficients, environmental friendliness and wide structural diversity to tune the optical and photovoltaic properties. [211, 212, 213] Moreover, organic dyes are compound of donors and acceptors (D-π-A) which ensure charge separation at the molecular level. Till date several modifications have been made on traditional D-π-A architecture in order to optimize the performance of organic dyes such as D–A′–π–A, [214-219] D–D–π–A, [220] D–π–D–π–A, [221] D–π–A–π–A, [222-224] (A–π–)$_2$D[46, 66] and (D–π-)$_2$A. [225] Recently, it has been observed that the

presence of auxiliary acceptors (D–A′–π–A) is beneficial for the efficient charge transfer, which contributes to the enhancement in device efficiency. Consequently many auxiliary acceptors have been used such as squaraine, [226-229] 2,1,3-benzothiadiazole, [95-98, 230] benzotriazole, [231, 232] quinoxaline, [233-236] phthalimide [237] and diketopyrrolopyrrole. [238-241] Among them, benzothiadiazole is found to be a beneficial nucleus for the DSSCs application Zhu et al, [26] used the idea of evolution of D-π-A configuration to D-A-π-A by introducing benzothiadiazole where the benzothiadiazole worked as charge trapper which favorly participates in charge separation and facilitates the electron migration to cyanoacetic acid unit. Further, Chou et al [69] & Chen et al [72] found that incorporation of alkoxy group on BTD nucleus prevents dye-aggregation. Such incorporation reported to have increase in V_{OC} which results good photovoltaic performances. [242-244]

It is also important to understand the structure – performance relationship of dyes. It is expected that the incorporation of a unit might influence the geometrical configuration of the dyes on the TiO_2 films, affecting the performance of the device. Chaurasia et al [75] reported the dyes where benzene unit have been replaced by pyridine unit leading to new auxiliary group pyridal[2,1,3]thiadiazole (**PyT**) based on D–A′–π–A molecular configuration. Due to the asymmetric nature of pyridine ring in **PyT** allows the formation of two isomers (Figure 5.1). The dye with pyridine nitrogen on the donor side (**L14**) exhibited high efficiency (1.16%) than the isomeric dye containing pyridine nitrogen facing the acceptor side (**L15**, $\eta = 0.78\%$). The high electron affinity of pyridal[2,1,3]thiadiazole than benzothiadiazole may emphasize the increased charge trapping behavior which would probably lowers the charge injection, thus resulting poor performances.

In this chapter, we demonstrate the variation of properties by changing the position of methyl group with respect to spacer. We introduced methyl group at C5 or C6 position, which leads to synthesis of two types of isomeric dyes, Type 1 named as **DM** where methyl is near donor group at C6 (**27** & **28**). Type 2 named as **MA** where methyl is near acceptor unit at C5 (**31** & **32**). In this configuration triphenylamine (TPA) incorporated as donor, cooperate in reducing charge recombination and in preventing aggregation due to its non-planar structure. [245-249]
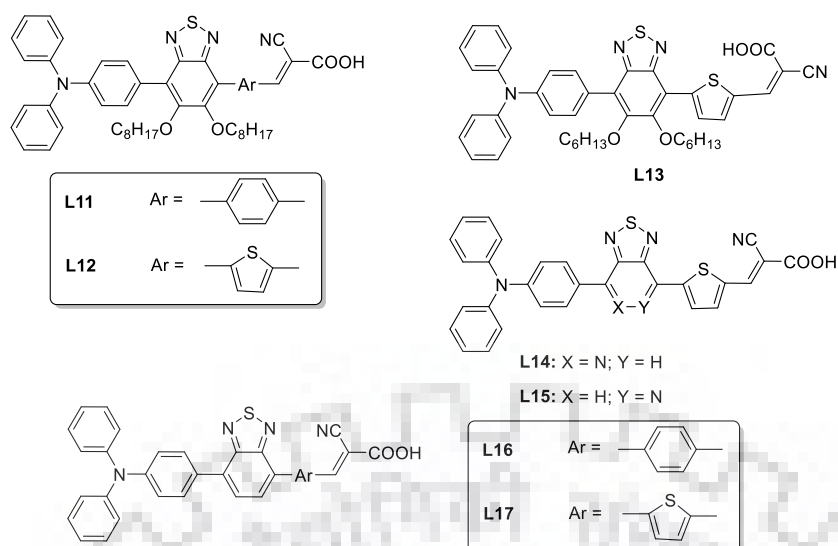
Figure 5.1. Reported lateral substituted benzothiadiazole derivatives.
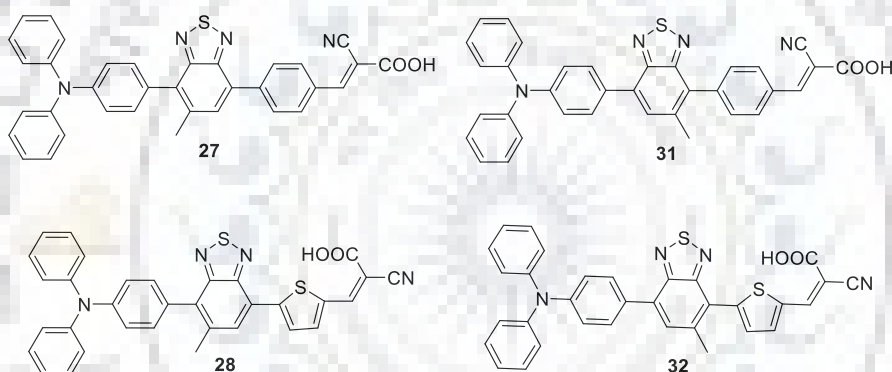
Figure 5.2. Chemical structures of the dyes **27-28** and **31-32.**

This followed by benzene or thiophene as spacer which modulates the electronic communication, influencing light harvesting and in turn efficiency. [150] These showed significant variation in photophysical and electrochemical properties attributable to methyl group position. It was further attested by the TD-DFT computational studies and photovoltaic performances, which have shown that R_{rec} is enhanced in **DM** dyes compared to that of **MA** dyes contrarily the R_{ct2} is reduced for **MA** dyes, Consequently, the **DM** dyes exhibited better performance than MA dyes in DSSC

5.2. Results and Discussion

5.2.1. Synthesis and characterization

The syntheses of the isomeric organic sensitizers (**27**, **28**, **31** and **32**) were accomplished by two-step protocol as illustrated in Schemes 5.1 and 5.2. In the first step, triphenylamine or aryl

aldehyde unit was introduced on the sterically less demanding region by Suzuki or Stille coupling reaction to obtain the monofunctionalized benzothiadiazole derivatives **25a**, **25b** and **29**. The regioselective reaction on C4 of benzothiadiazole was earlier demonstrated in chapter 3. The required donor-acceptor framework was achieved by an additional Suzuki/Stille coupling reaction of **25a, 25b** & **29** with suitable boronic acid or Stannylene reagents. Finally, the target dyes **27**, **28, 31** and **32** were synthesized by following the Knoevenagel condensation of cyanoacetic acid with the aldehydes **26a, 26b, 30a** and **30b** in the presence of ammonium acetate. All the dyes are moderately soluble in solvents such as TOL, DCM, THF, ACN, DMF and partially soluble in MeOH. The structures of the dyes were found to be consistent with ^{1}H, ^{13}C NMR, HRMS spectra and elemental analyses data.
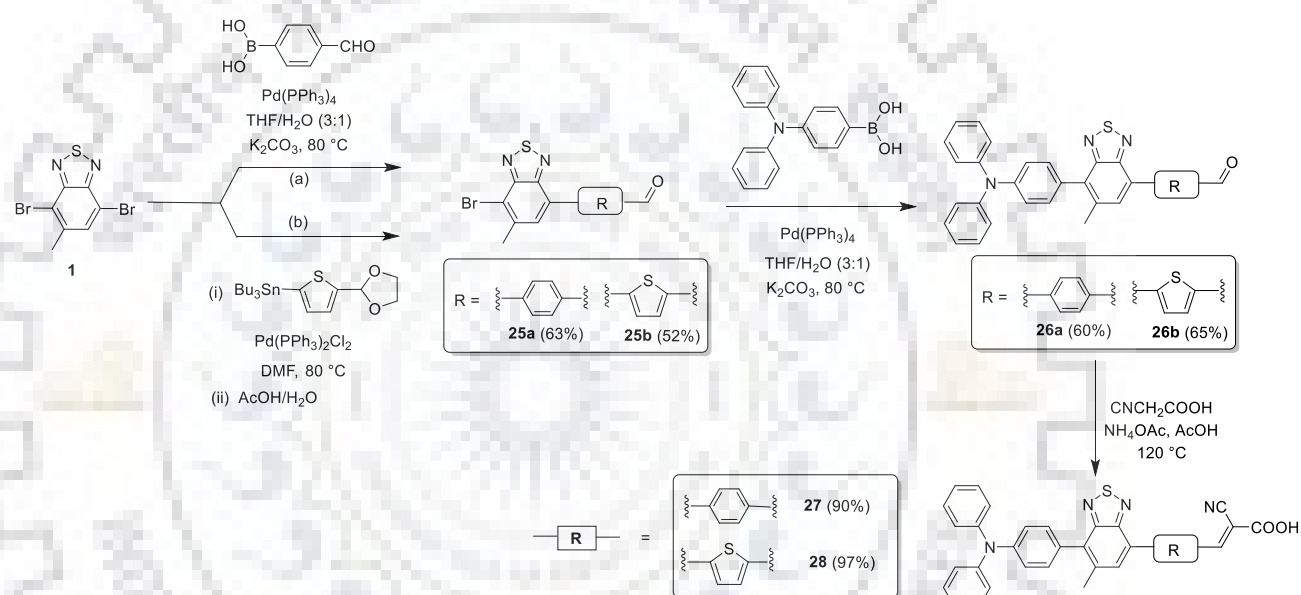
Scheme 5.1 Synthetic protocol of Type 1 dyes, **27** and **28.**
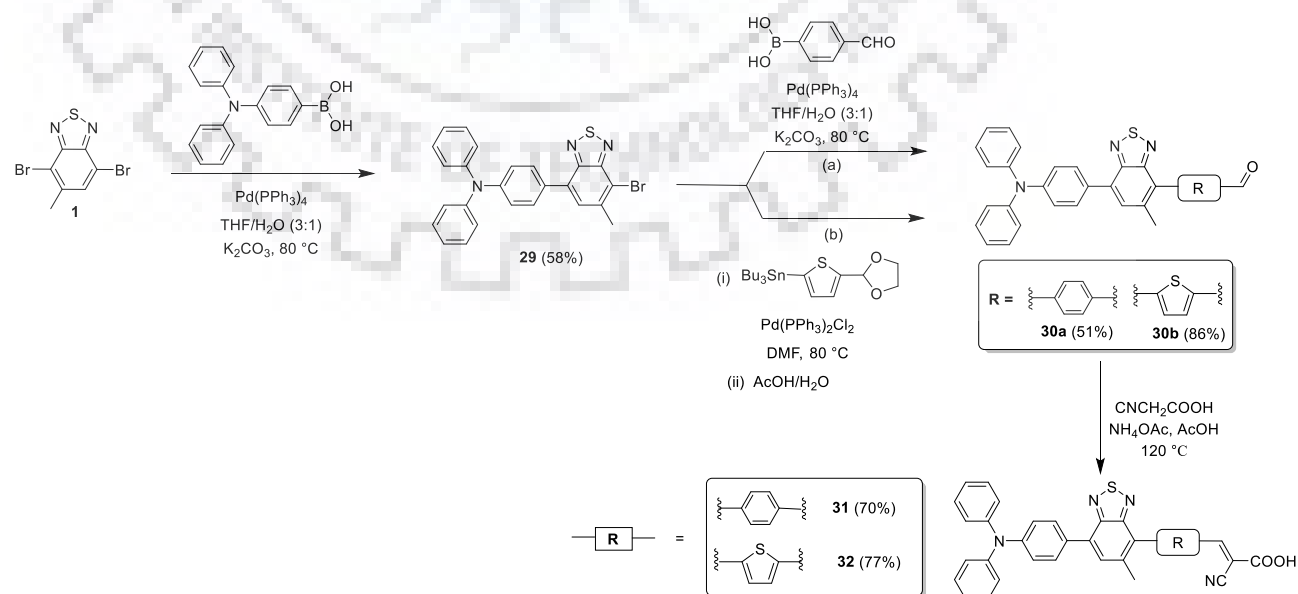
Scheme 5.2 Synthetic protocol of Type 2 dyes, **31** and **32.**

141

5.2.2. Theoretical investigations

To gain deep insight into the effect of methyl group on the electronic structure of the dyes, we performed density functional theoretical (DFT) calculations using the Gaussian 09 program package. The presence of methyl group on benzothiadiazole leads to significant geometrical changes in the dyes. The interplanar angles between the BTD and the aryl linker on the methyl side displayed a tilting ca 20° attributable to the steric effect of methyl unit, this illustrates the conjugation and donor-acceptor interaction. Further, on comparing optimized structures of non-methylated BTD dyes to **MA** and **DM** dyes, it is found that **DM** dyes show planarity at similar angles between BTD and acceptor while the **MA** dyes show appreciable twisting attributable to methyl on BTD which cause non-planarity between BTD and acceptor segment . Interestingly, twisting between BTD and donor segment is increased in **DM** dyes. Such perturbation in the structure due to methyl group is expected to affect the photophysical and photovoltaic properties appreciably.
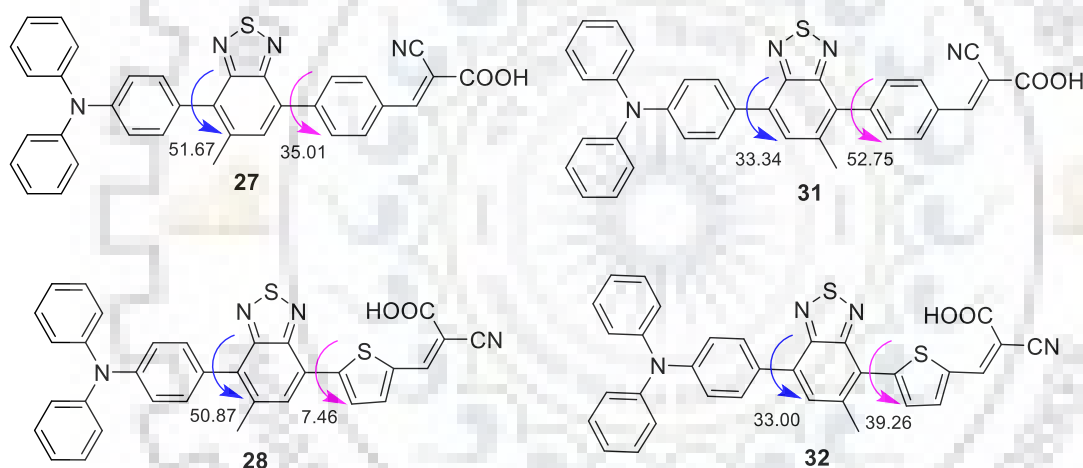
Figure 5.3. Computed interplanar angles between the different aryl groups in the dyes

Furthermore, the HOMO/LUMO values were estimated, (Table 5.2) where the HOMO value remained constant ~ 6.2 eV, while the LUMO varied in accordance with the effect of spacer thiophene and phenyl. [101] The electronic distribution in the frontier molecular orbitals for sensitizers shown in Figure 5.4. The HOMO orbitals of the dyes are mainly localized on TPA whereas LUMO orbitals are predominantly showed on benzothiadiazole, spacer and anchoring group. The presence of such well separated frontier molecular orbitals can facilitate charge migration on electronic excitation involving HOMO and LUMO orbitals. However, contrary to good overlap the PCE varied (*vide infra*) to large extent attributable to the presence of methyl group on BTD nucleus

Table 5.1. Calculated vertical transition energies and their oscillator strengths and configurations for the dyes.

Dye	λabs (nm)	f	Assignment (%)
27	413	0.88	HOMO → LUMO (64%), HOMO-1→LUMO (18%),
	341	0.48	HOMO-1→LUMO (69%), HOMO→LUMO+1(+12%), HOMO→LUMO (9%)
28	464	1.09	HOMO→LUMO (66%), HOMO-1→LUMO (28%)
	382	0.19	HOMO-1→LUMO (65%), HOMO→LUMO (22%), HOMO→LUMO+1(6%)
	339	0.11	HOMO-1→LUMO+1(46%), HOMO→LUMO+1(40%), HOMO→LUMO (5%)
31	416	0.90	HOMO→LUMO (62%), HOMO→LUMO+1(19%), HOMO-1→LUMO (12%)
	335	0.31	HOMO→LUMO+1(53%), HOMO-1→LUMO (20%), HOMO-1→LUMO+1(11%), HOMO→LUMO (6%)
	323	0.08	HOMO-1→LUMO (49%), HOMO→LUMO (21%), HOMO-1→LUMO+1(16%)
32	451	1.12	HOMO→LUMO (70%), HOMO-1→LUMO (19%), HOMO→LUMO+1(7%)
	364	0.25	HOMO-1→LUMO (52%), HOMO→LUMO+1(29%), HOMO-1→LUMO+1(7%)
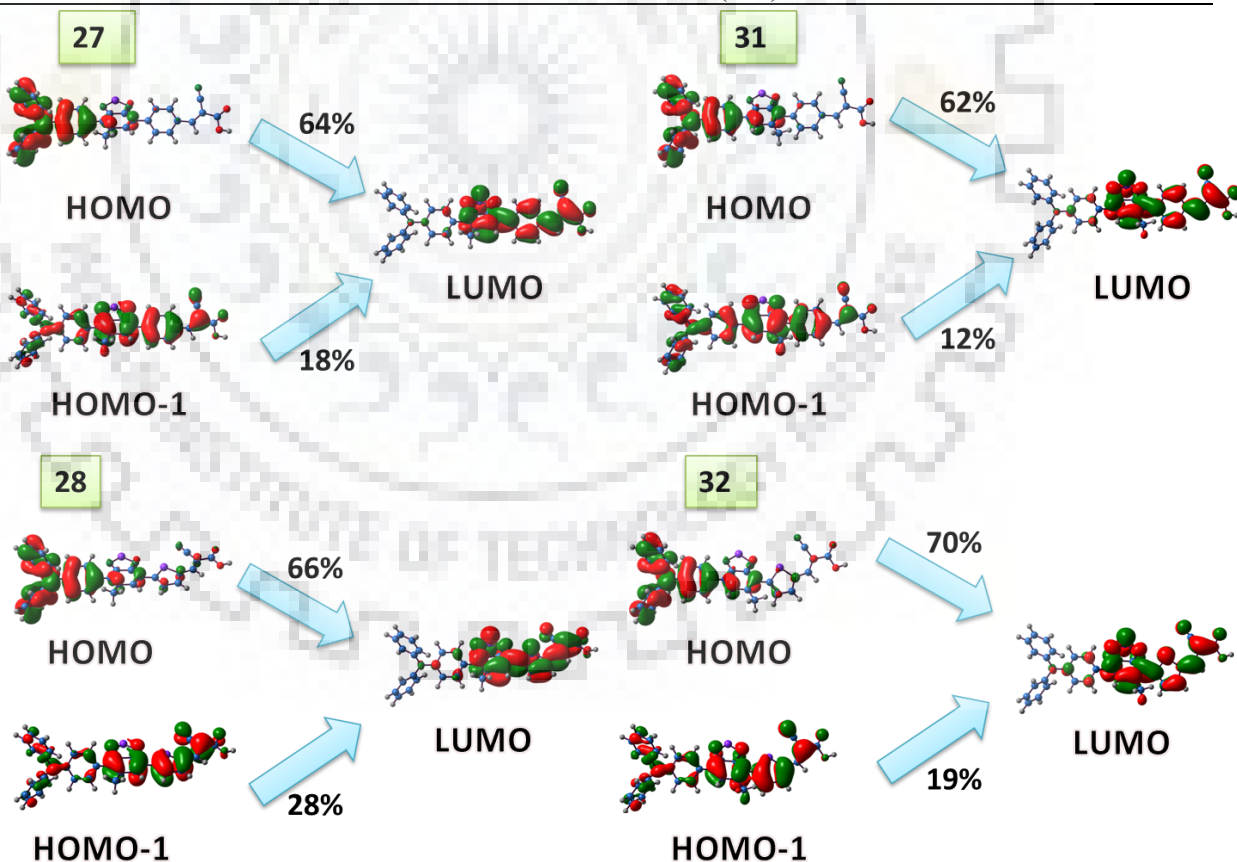
Figure 5.4. Electronic distribution observed in the frontier wavelength orbitals of the dyes involved in absorption

. As in the **MA** dyes, the LUMO electronic distribution is more concentrated on BTD unit than the spacer, this may be rationalized by charge trapping behavior of BTD [250] which is facilitated by the presence of methyl at C5. This behavior hampers electronic injection from the sensitizer to the TiO$_2$ which may lead to low J_{sc} and perhaps affects the cell performance. This points that **DM** dyes possess favorable structure for efficient photovoltaic dyes. The prominent absorption of the compound has contribution of electronic interaction from HOMO & HOMO-1 to LUMO (Table 5.2). Since, the HOMO-1 is organized with a major contribution for BTD, spacer and acceptor, the major absorption may be attributed to the contribution of donor to acceptor charge transfer and localized absorption within acceptor.

Table 5.2. Computed energy states of the dyes.

Dye	HOMO (eV)	LUMO (eV)	E$_{0-0}$ (eV)
27	-6.23	-1.96	4.27
28	-6.23	-2.21	4.01
31	-6.21	-1.87	4.33
32	-6.21	-2.07	4.13

5.2.3. Optical properties

Figure 5.5a shows the electronic absorption spectra of the dyes collected in DCM and the pertinent data available in Table 5.3. All the dyes showed two or three prominent absorption bands in the range of ~280 -580 nm. The highest energy band appearing at ~350 nm corresponds to the localized π–π* electronic transitions of aromatic segments. The lower energy transition showing absorption maximum above 380 nm corresponds to π–π* transitions originated from the thiophene/phenyl unit to cyanoacrylic acid segment that is merged with intramolecular charge transfer (ICT) bands from the triphenylamine donor to the cyanoacrylic acid acceptor unit, which resulted in broad absorption peaks. Introduction of triphenylamine to **25b,** triggers a red shift and broadening of longer wavelength absorption in **26b**. This suggests the presence of CT and localized absorption. Similar observations are possible on comparing **29** and **30b**, the CT between donor to BTD is present in **29** which is supposed to undergo further red shifted on introduction of thiophene aldehyde moiety in **5b**. But due to methyl unit the donor acceptor interaction perturbed. (Figure 5b) To illustrate further, the effect of methyl unit comparison were made with reported sensitizers, for example Zhu et al [26] introduced non-methylated congeners (**L16** and **L17**) where the present dyes exhibit higher molar extinction coefficient and blue shift to former reported dyes which suggests the methyl unit jeopardized the donor-acceptor interaction due to twisting. Similarly, on comparing the alkoxy substituted derivatives, **L11** showed similar absorption profile as of **31 and 27** dyes. However, **L12**

showed bathochromic shift to **32** & **28** but the present dyes showed higher molar extinction coefficient inducing better light harvesting property

Table 5.3. Optical and electrochemical properties of the dyes recorded in DCM solutions.

Dye	λ_{abs} (nm ($\varepsilon_{max} \times 10^3$ M^{-1} cm^{-1})) [a]	E_{ox} (V) (ΔEp, (mV)) [b]	HOMO (eV) [c]	LUMO (eV) [d]	E_{0-0} (eV) [e]	E_{ox} (eV) (vs NHE)	E_{ox}^{*} (eV) [f]
27	311 (83.68), 361 (45.48), 428 (25.94)	0.51 (70)	-5.31	-2.84	2.47	1.28	− 1.19
28	307 (59.78), 453 (br)	0.51 (69)	-5.31	-2.92	2.30	1.28	− 1.02
31	312 (48.49), 428 (14.87)	0.48 (64)	-5.28	-2.84	2.44	1.25	− 1.19
32	311 (53.77), 376 (24.54), 452 (29.16)	0.51 (62)	-5.31	-3.00	2.32	1.27	− 1.05
L11	423 (7.6)	-	-	-	2.49	0.99	-1.50
L12	468 (16.1)	-	-	-	2.23	1.01	-1.22
L13	466 (20.1), 408 (13.7), 307 (22.6)	-	-5.71	-3.42	2.29	-	-
L16	455 (16.10)	-	-	-	2.27	0.95	-1.32
L17	497 (13.00)	-	-	-	2.11	0.95	-1.16

[a]absorption maxima recorded in dichloromethane solution. [b]Redox potentials are reported with reference to the ferrocene internal standard. [c]Deduced from the oxidation potential using the formula HOMO = 4.8 + E_{ox}. [d]Obtained from the optical band gap and the electrochemically deduced HOMO value. [e]Calculated from optical edge. [f]Excited state oxidation potential *versus* NHE.

Further among Type1 and Type 2 dyes both showed similar absorption maxima with respect to their isomers and also exhibited prominent increment in molar extinction coefficient, which follows the order **28** > **32** > **27** > **31**. However, when we compare absorption maxima of the dyes with respect to spacer (thiophene, phenyl) it follows the order **28** > **27** and **32** > **31**. This corroborates that thiophene substituted isomers exhibit longer wavelength absorption spectra compared to phenyl congeners due to its planar framework that emphasizes the decrement in steric congestion which possibly improves the facile electronic communication compared to their analogs (*vide supra*). It is interesting to compare isomers **28** and **32** where the dye **28** showed broad peak probably due to merging of π–π* and charge transfer peak this results in increase in light harvesting property and showed 1.25 folds higher molar extinction coefficient compared to its congeners which further supports for its high J_{SC}. Thus, all these observations

suggest that Type 2 dyes showed an efficient delocalization which may influence photovoltaic performance, as suggested above through theoretical calculation and later in the chapter.
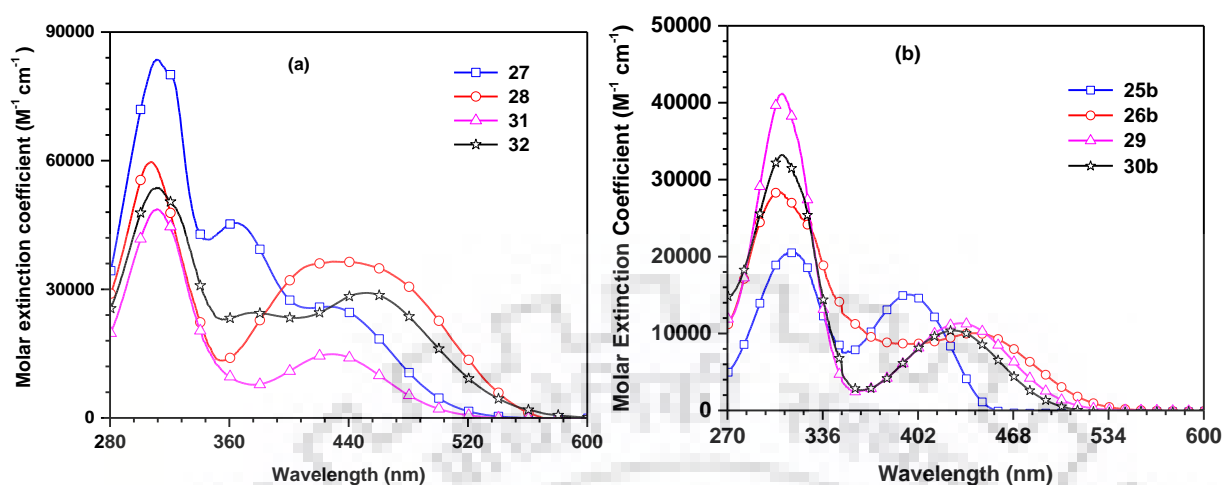
Figure 5.5. Absorption spectra of the a) **27**, **28**, **31** and **32** b) **25b**, **26b**, **29** and **30b** dyes recorded in dichloromethane solution

The absorption spectra of the dyes recorded on thin TiO_2 film are shown in Figure 5.6. The absorption maxima of the dyes on the TiO_2 film shows broadening and a red-shift compared to those observed in solution. This may be due to *J*-aggregation of dyes at the TiO_2 surface. However, it is observed that dye **31** showed blue shift emission when compared to other dyes, this probably due to deprotonation of the carboxylic acid [251, 252] or *H* –aggregation of the dye. [253, 254] Interestingly, the dyes **27**, **28** and **32** showed longer wavelength region light harvesting and eventually favorable photocurrent response.

To investigate the effect of polarity on ICT absorption peak we have recorded solvatochromism of dyes in different solvents such as DCM, TOL, THF, DMF and ACN. The pertinent data are compiled in Table 5.4 and the absorption spectra recorded for **32** in different solvents shown in Figure 5.7.It shows a blue shift in absorption on gradual increment of polarity attributed to the effective solvation of the dyes. But an unusual red shift observed for DCM due to instant stabilization induced by fast rearrangement of polarizable electron during excitation as has been recognized for ionic dyes. [255]
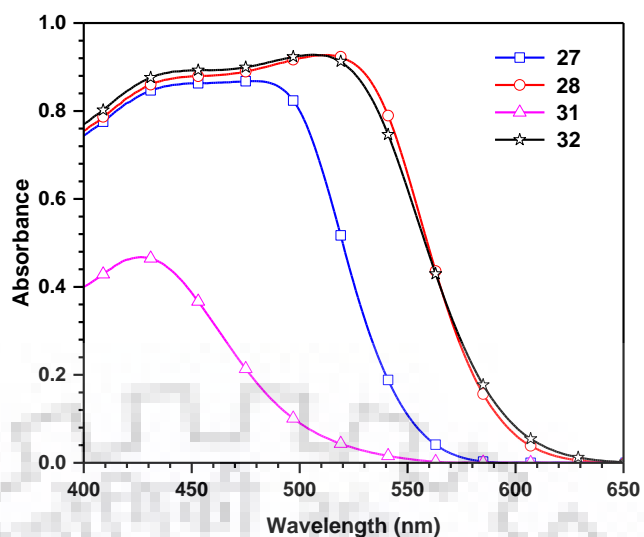
Figure 5.6. Absorption spectra of the dyes recorded on thin TiO$_2$ film.
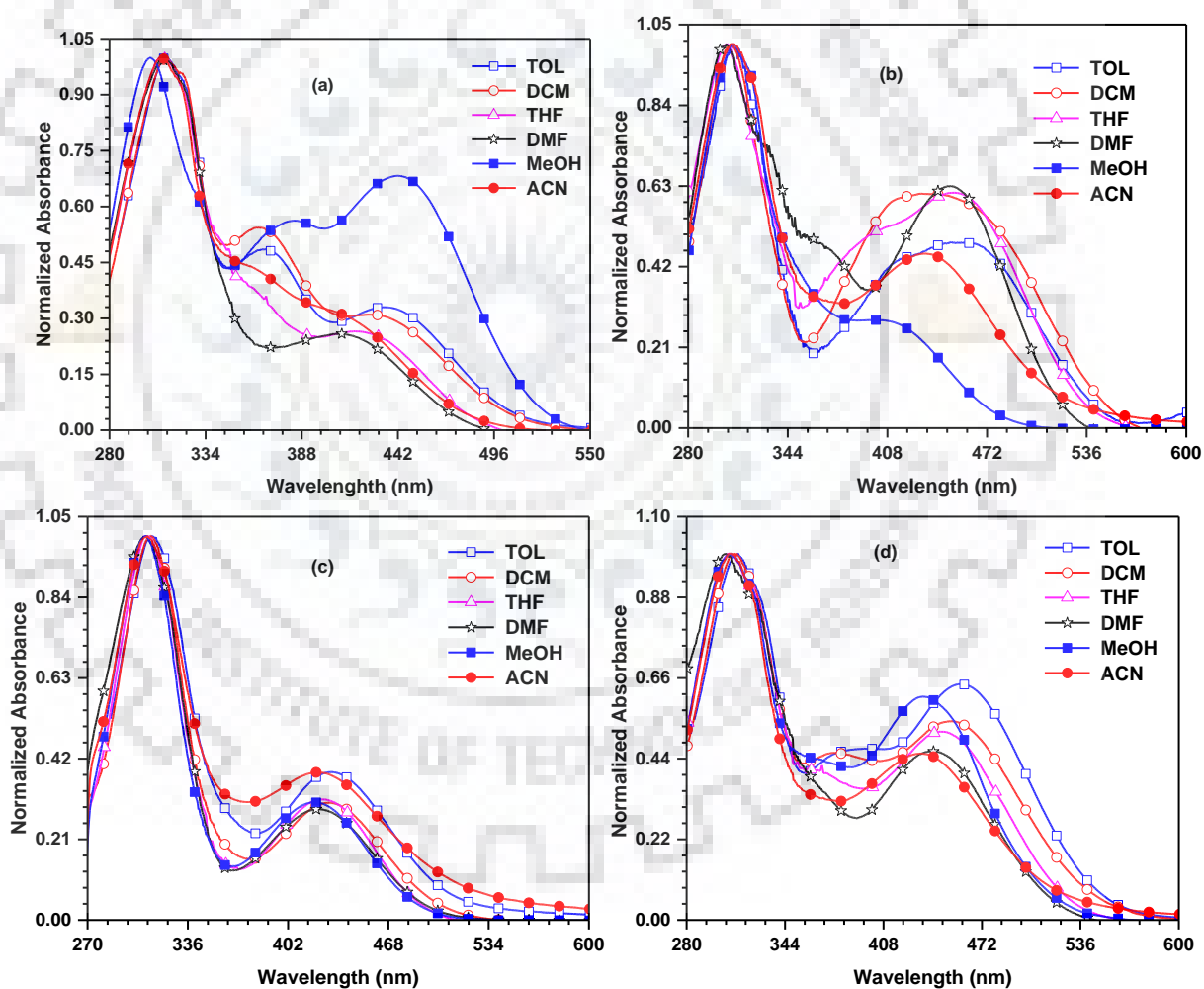
Figure 5.7. Normalized Absorption spectra of dyes recorded in different solvents a) **27** b) **28** c) **31** and d) **32**
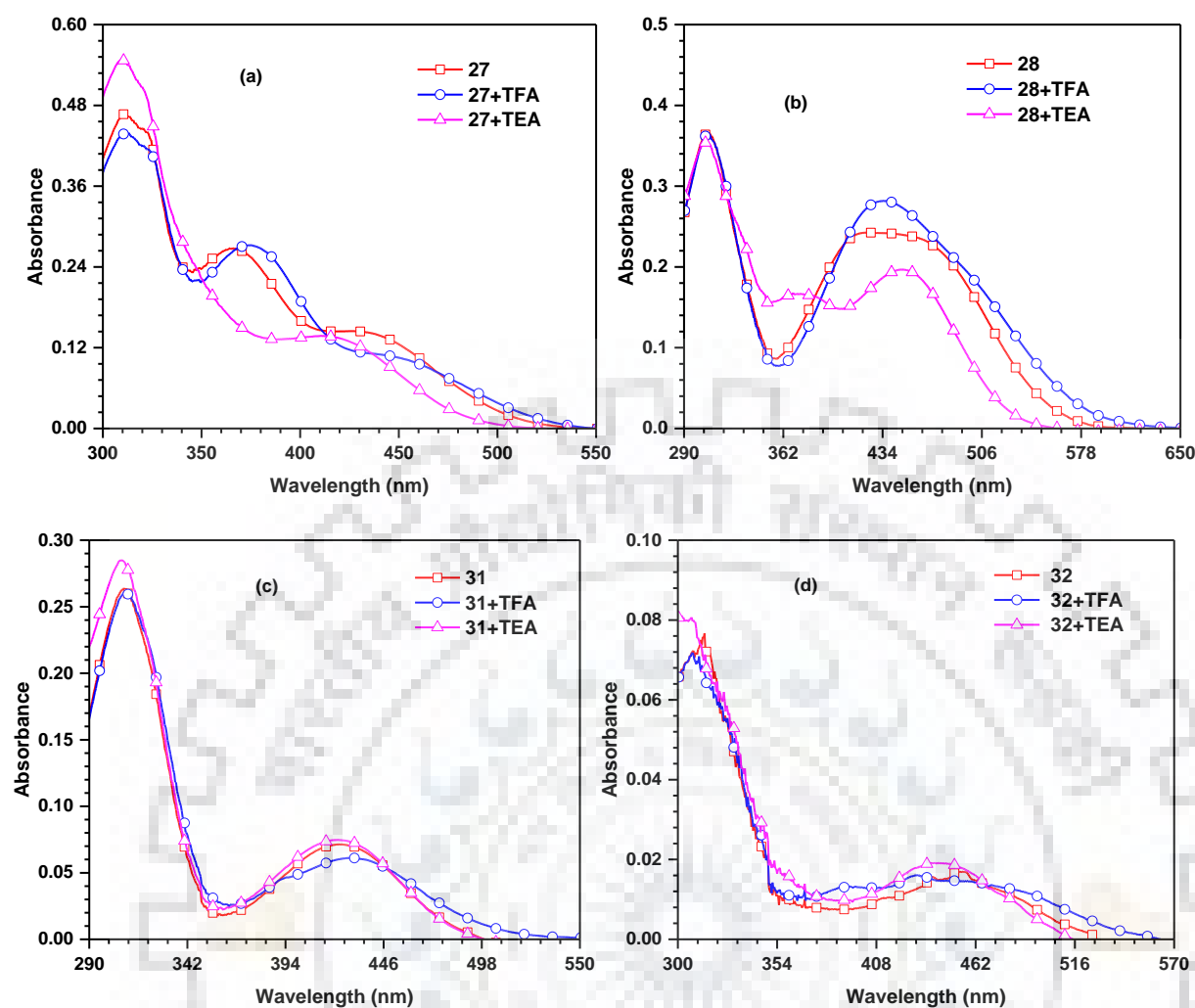
Figure 5.8. Absorption spectra of the dyes a) **27** b) **28** c) **31** d) **32** recorded in DCM, after the addition of TFA and TEA.

Table 5.4 Absorption wavelength of dyes in different solvents

Dye	TOL	THF	DCM	DMF	ACN	MeOH
27	433	428	429	411	410	442
28	456	451	453(br)	449	432	404
31	431	423	429	423	421	421
32	460	444	452	439	432	434

Further to confirm the presence of intramolecular charge transfer (ICT) from TPA donor to cyanoacrylic acid acceptor, acid base equilibrium studies were performed. This ICT was confirmed by addition of a small amount of trifluoroacetic acid (TFA) or triethylamine (TEA) to the dye. Generally, the dye exists in acid-base equilibrium in solution, whereas in polar solvent, the dyes are present in deprotanated form. Thus on addition of TFA, the dyes exhibit bathochromic shift, as the equilibrium shifts to protonated form, pronouncing the ICT effect,

while TEA caused a minor blue-shift due to deprotonation of carboxylic acid which lessens the acceptor strength and thus weakens donor-acceptor interaction. Interestingly in DMF, the absorption maxima of the dyes closely matched with those observed in the presence of TEA, probably due to basic nature of DMF which caused deprotonation of carboxylic acid and this will reduce the donor-acceptor interaction. It clearly indicates that the dyes are in the deprotonated state in DMF.
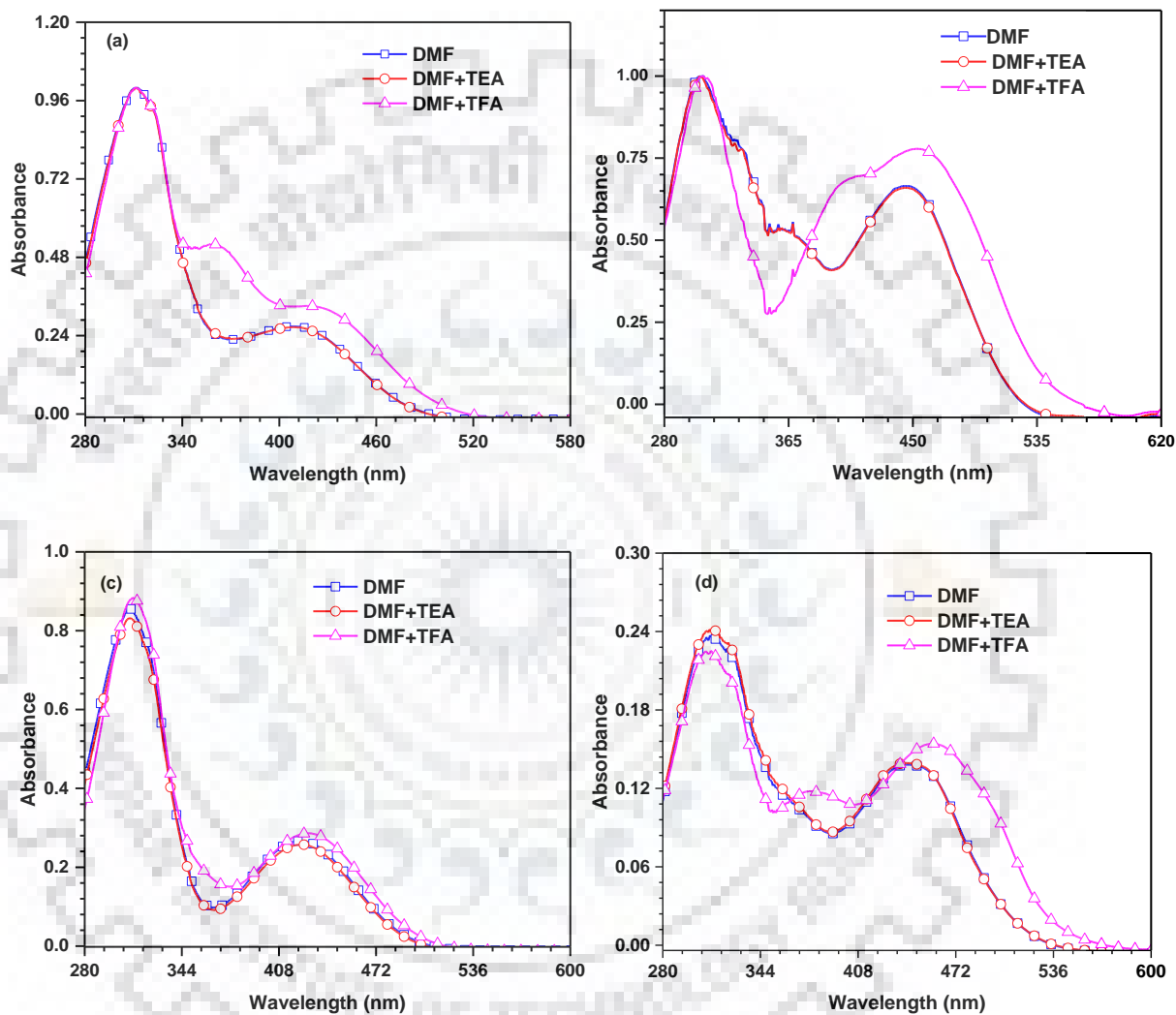
Figure 5.9 Absorption spectra of the dye a) **27** b) **28** c) **31** d) **32** recorded in DMF, after the addition of TFA and TEA.
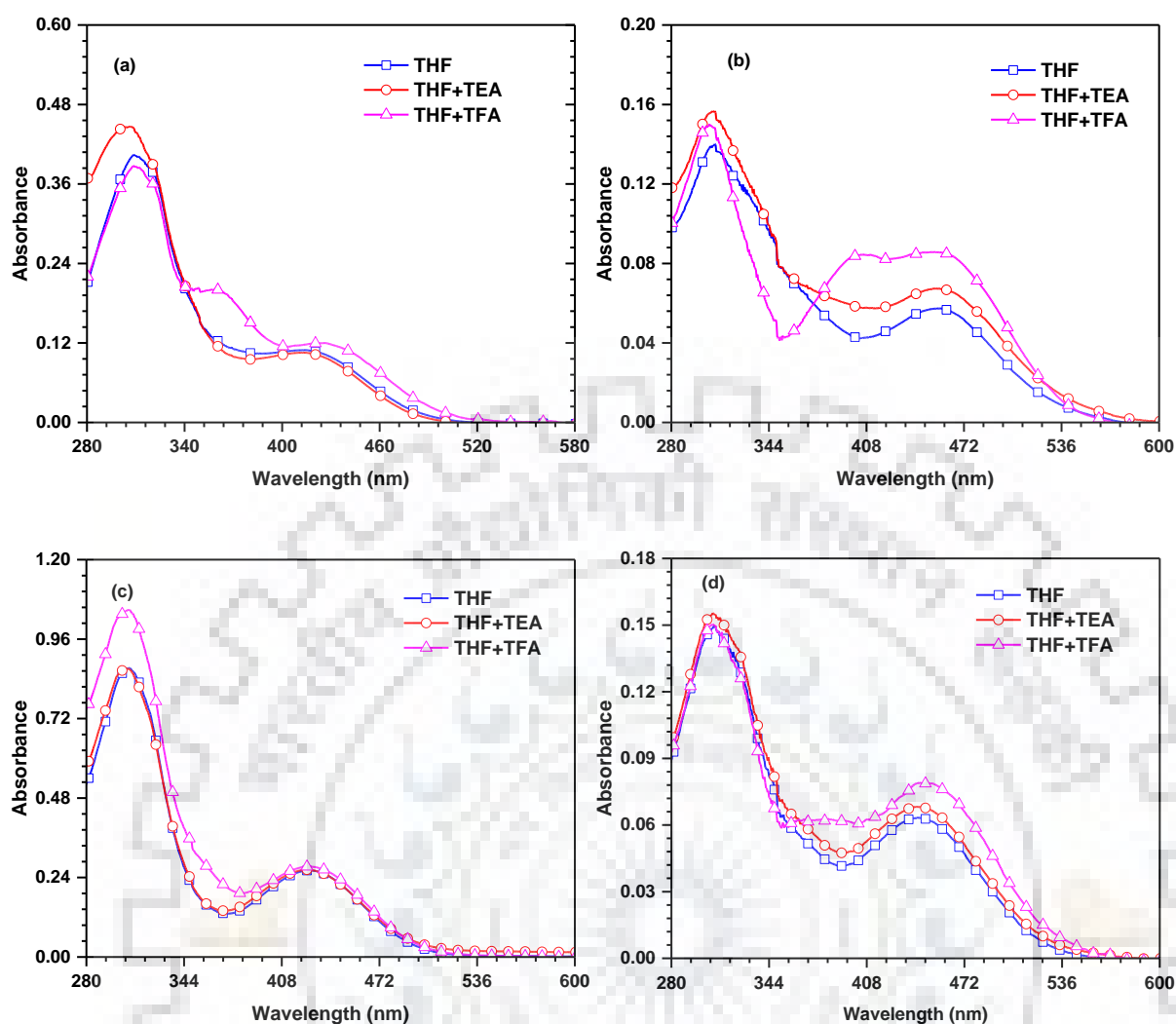
Figure 5.10. Absorption spectra of the dye a) **27** b) **28** c) **31** d) **32** recorded in THF, after the addition of TFA and TEA.

5.2.4 Electrochemical properties

For the investigation of electrochemical properties, cyclic voltammetry was recorded for the dyes in DCM and the corresponding electrochemical data compiled in Table 5.3 Figure.5.11 displays the cyclic voltammograms of the dyes. All the dyes displayed a quasi-reversible oxidation couple with positive oxidation potential than the internal ferrocene standard. This originates due to the removal of electron from the TPA unit. The oxidation potential for the Type1 is lower than the Type2 dyes, which may be attributed to the positional effect of methyl unit. The insertion of methyl unit near the TPA donor interrupted the planarity between TPA and BTD units, which reduces the effective electron delocalization leading to high oxidation potential for Type2. Further, we have evaluated the thermodynamic driving force for electron injection into the conduction band of TiO_2 and regeneration feasibility of the oxidized dyes by

150

electrolyte (Figure.5.12). The positions of HOMO for **27, 28, 31** and **32** dyes are located similarly at 1.28, 1.28, 1.25 and 1.27 V *vs.* the normal hydrogen electrode (NHE), respectively. These values suggest that all of the four sensitizers can provide sufficient driving force for regeneration of dye by I^-/I_3^- redox electrolyte (0.4 V vs. NHE). The LUMO values of the dyes **27, 28, 31** and **32** are –1.19, –1.02, –1.19 and –1.05 V vs. NHE, respectively, which are more negative than CB of TiO_2 (–0.5 V *vs.* NHE). These values suggest an energetically favorable electron injection from the excited dye molecules into the CB of TiO_2

In general, ΔG_{inj} closer to 0.5 eV is kinetically favorable for electron injection. Therefore, if we compare phenyl and thiophene spacer derivatives dyes, the thiophene (**28** and **32**) observed to have ~ 0.52- 0.55 eV, the kinetically more favorable for injection of electron into the CB of TiO_2 when compared to **27** and **31** (~0.69 eV).
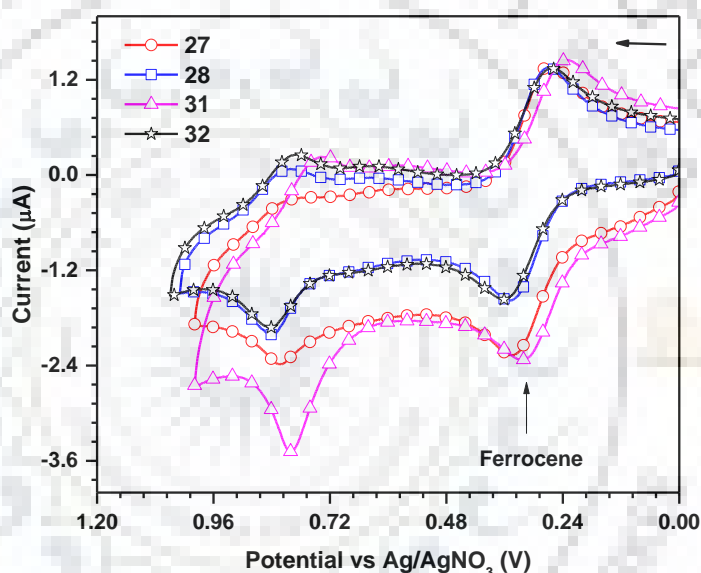
Figure 5.11. Cyclic voltammograms of the dyes recorded in DCM solutions
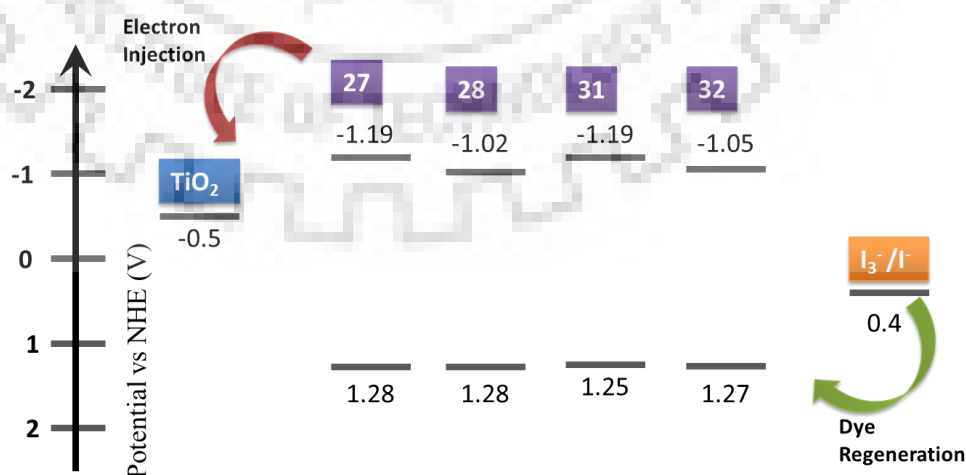
Figure 5.12 Ground state and excited state oxidation potentials of the dyes with respect to NHE.

5.2.5 Photovoltaic Performance

To evaluate the solar energy to power conversion efficiency (η) of the synthesized dyes, we employed them as sensitizers in nanocrystalline TiO$_2$-based DSSC. The incident photon-to-current conversion efficiency (IPCE) curves and current-voltage (*I-V*) characteristics observed for the device under simulated solar light irradiation are displayed in Figure 5.13 and relevant photovoltaic parameters compiled in Table 5.5. The **28** dye exhibited relatively higher η of 4.33 % in the series, attributable to high photocurrent density, J_{SC} (9.27 mA cm^{-2}) and enhanced V_{OC} (0.70 V) compared to its congener **32** showing lower η of 2.71 % (J_{SC} = 5.92 mA cm^{-2}, V_{OC} = 0.64 V). The J_{SC} and efficiency for the devices follows the order of **28 > 27 > 32 > 31**. In general, the J_{SC} corresponds to intense light absorption capability of dye over wide region of light which correlates to broad spectra of IPCE curve. However, the IPCE plots relates to the molar extinction coefficient of the dyes. Consequently, the **DM** dyes has a higher J_{SC} values compared to their respective **MA** analogue as a result of higher IPCE value.

IPCE measured against the wavelengths displays the response of absorption propensity at different wavelengths. All the dyes exhibited exceptional IPCE in the wavelength region from 400 to 600 nm. The dyes **27** and **28** showed very high IPCE in the 400−500 nm region when compared to dyes **31** and **32** which is complementary to the ruthenium-based organometallic dyes such as **N719** and ascribed to the high molar extinction coefficients observed for the dyes in that region. According to formula,

IPCE (λ) $=$ LHE (λ) $*$ Φinj $*$ Φc,

where, LHE (λ) is the light-harvesting efficiency, Φ_{inj} is the electron injection efficiency, Φ_c is the charge collection efficiency, since all the dye isomers have similar HOMO and LUMO energy levels, the different IPCE values for the organic dyes may have resulted from their different charge injection efficiencies. The lower IPCE value of **MA** dyes probably relates to charge trapping behavior as discussed above that would be hampering electronic migration toward CB of TiO$_2$ and also supported by higher ΔG_{inj} which resulted in reduced electron injection efficiency compared to **DM** dyes.

Table 5.5. Performance Parameters of the DSSCs Fabricated Using the Dyes

Dye	η (%)	V_{OC} (V)	J_{SC} (mA cm^{-2})	τ_e (ms)	R_{ct2} (ohm)	R_{rec} (ohm)	FF
27	3.94	0.70	8.28	10.23	26.87	33.08	0.68
28	4.33	0.67	9.27	8.69	25.01	26.18	0.70
31	0.68	0.57	1.77	0.76	54.20	15.03	0.67
32	2.71	0.64	5.92	2.01	36.35	19.19	0.71
N719	8.14	0.79	14.69	16.67	17.15	90.62	0.71
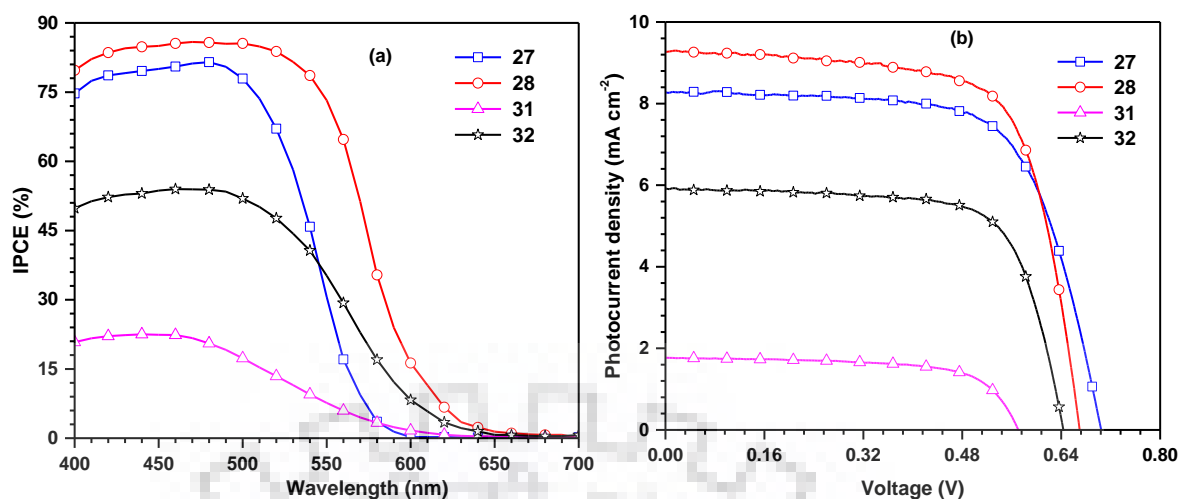
Figure 5.13. IPCE plot (a) and *I−V* curves (b) of the DSSCs fabricated using the dyes.

From the data in Table 5.5 we can find that in the series V_{OC} follows the order, **27** >**28** >**32** > **31**. The larger V_{OC} observed in **27** (0.70 V), **28** (0.67 V) compared to their isomers due to the methyl unit substitution near donor has possibly reduced the charge recombination by retarding the approach of triodide (I_3^-) at the TiO_2 surface than dyes **31** (0.57 V), **32** (0.64 V) which has shown lower V_{OC}. The other performance parameter and the higher V_{OC} values for the DSSCs based **DM** dyes can be explained by their different charge recombination rates.

5.2.6. Electrochemical Impedance Spectroscopy

To elucidate further the outcome of the positioning effect of methyl group in **DM** and **MA** dyes on the performance of DSSC, electrochemical impedance spectroscopy (EIS) were conducted. The Nyquist plots of the DSSC measured under dark and illumination conditions are displayed in Figure 5.14. Figure 5.14(a), which corresponds to dark conditions, exhibits three semicircles and each semicircle, corresponds to the TiO_2/dye/electrolyte interfacial electron recombination kinetics. The larger semicircle corresponds to the recombination resistance (R_{rec}) at TiO_2/electrolyte interface and the radius of this semicircle follows the order **27** > **28** > **32** > **31**. R_{rec} value gives the knowledge of electronic recombination resistance i.e. the larger the radius of the semicircle, the smaller is the rate for electron recombination at the interface, which results in high V_{OC}. The R_{rec} for the device follow the order **27** > **28** > **32** > **31**, pointing that the methyl at C6 position is beneficial to block the approach of I_3^- ion to TiO_2. The enhanced electron recombination rate is attributed to the dye characteristics such as aggregation and complex formation with iodide in the electrolyte. [256] Smaller R_{rec} for **MA** dyes indicates high recombination rate compared to **DM** dyes .On this basis, one would expect comparatively high V_{OC} for the **DM** dyes. The relatively large amount of electrons in the conduction band of TiO_2 could also give rise to high V_{OC}. The electron density in the

153

conduction band of TiO_2 may be a result of better charge collection efficiency in the corresponding device. To elucidate the charge transfer rates in the devices, EIS were measured under illumination conditions (Figure 5.14(b). The charge transport resistance (Rct2) is small for **27** and **28** dyes relative to their analogues (**31** and **32**). This suggests an effective electron collection for the **DM** dyes. This observation is in agreement with the larger J_{SC} values observed for the **DM** dyes. Additionally, The electron lifetime ($\tau_e = 1/\omega_{min} = 1/2\pi f_{max}$, where f_{max} is the maximum frequency of the low-frequency peak) in the Bode phase plot (Figure 5.15) is highest for **27** (**27** > **28** > **32** > **31**) The highest τ_e observed for **27** is suggestive of effective suppression of back reaction of injected electrons with I_3^- ions in the electrolyte, which leads to improvement of V_{OC}. The EIS study evidenced the performances of dyes on account of position of methyl unit where methyl at C6 positions has the better performance attributable to their comparatively good light-harvesting properties, the favorable electron injection, and the effective retardation of electron recombination.
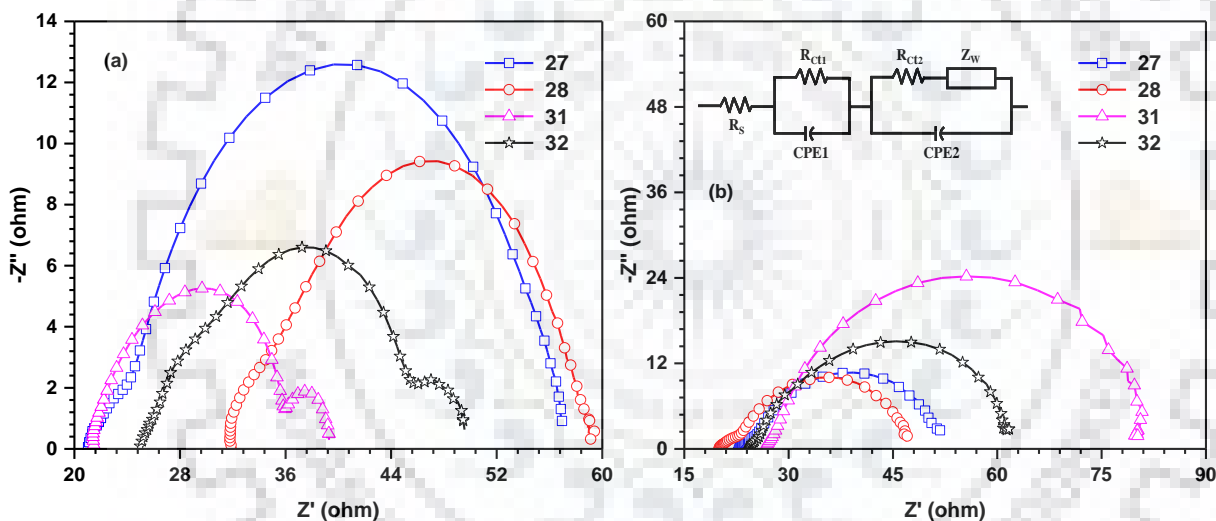
Figure 5.14. Nyquist plots observed for the DSSCs measured under (a) dark and (b) illumination conditions.
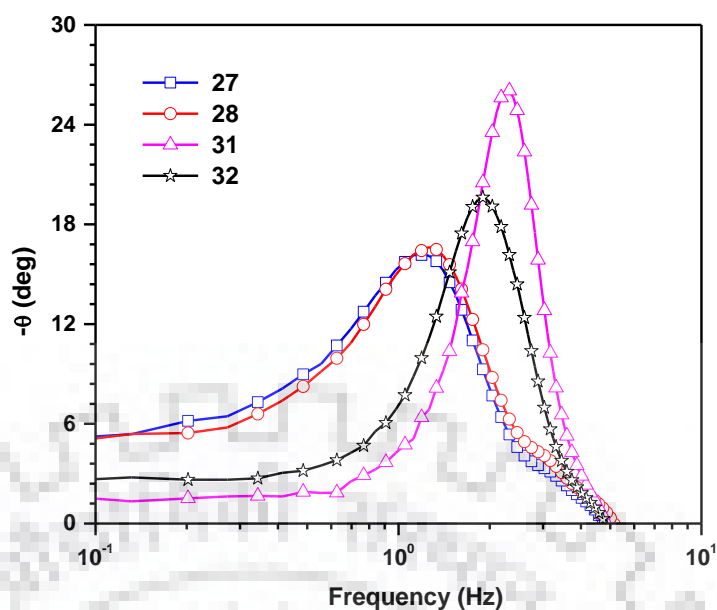
Figure 5.15. Bode phase plots of the DSSCs under illumination condition.

5.3. Conclusions

We have designed and synthesized four isomeric dyes (**27, 31, 28** and **32**) containing methyl benzothiadiazole as auxiliary acceptor using Suzuki/Stille coupling reaction condition. Further, the structural effects of incorporation of methyl unit on BTD nucleus have been studied by photophysical and electrochemical properties and TD-DFT calculations. The results indicate that positional effect of methyl has appreciable effect on photophysical and electrochemical properties. Interestingly, the Type 1 dyes showed 1.25 folds higher molar extinction coefficient, strong light harvesting ability compared to their Type 2 congeners. Moreover, the dyes showed significant impact in form of aggregation, electron injection and light harvesting ability, thus leading to distinctive photovoltaic performance. Consequently, the dyes were used as sensitizers in DSSC and found to result efficiency in the range of 0.68- 4.33% attributable to their isomeric constitution. The Type 1 builds as promising design for the retardation of electron recombination where R_{rec} follows the order **27** > **28** > **32** > **31**, showing Type 1 are more resistent to recombination, surplusing the increment in V_{OC}. The dye **28** exhibited the highest efficiency (4.33%) among the isomeric dyes attributed to high J_{SC} (9.27 mA cm^{-2}) and V_{OC} (0.67 V) values compared to its isomer **32**. This poor performance of Type 2 dyes is attributed to significant dye aggregation and charge trapping effects which hampers the electron injection. Overall, this work demonstrated the positional effect of methyl group on benzothiadiazole nucleus and the ability for design of efficient sensitizers for DSSC.

5.4. DSSCs Fabrication and Measurements

A fluorine-doped SnO_2 conducting glass electrode (FTO, 7 Ω sq^{-1}, transmittance *ca.* 80%) was first cleaned with a neutral cleaner and then washed with deionized water, acetone, and isopropyl alcohol, sequentially. The conducting surface of the FTO was treated with a solution of titanium tetraisopropoxide (1 g) in 2-methoxyethanol (3 g) to obtain a good mechanical contact between the conducting glass and TiO_2 film, as well as to isolate the conducting glass surface from the electrolyte. TiO_2 pastes were coated onto the treated conducting glass by using the doctor blade technique. To coat each TiO_2 layer, the dried TiO_2 film was gradually heated to 450 °C under an oxygen atmosphere and subsequently sintered at that temperature for 30 min. The TiO_2 photoanodes of the DSSCs employed in the experiments were composed of a 12 μm thickness and 20 nm particle size TiO_2 layer/4 μm scattering TiO_2 layer. After sintering at 450 °C and cooling to 80 °C, the TiO_2 film was immersed in a 3×10^{-4} M solution of dye at room temperature for 24 h. The standard ruthenium complex, **N719**, was dissolved in acetonitrile and tert-butyl alcohol (1:1) to make a reference dye solution. Various organic dye solutions were prepared in a mixing solvent containing MeCN/*tert*-BuOH/DMSO (3.5:3.5:3 v/v). Then, the prepared TiO_2/dye electrode was placed on a platinum-sputtered conducting glass electrode (ITO, 7 Ω sq^{-1}), thus keeping the two electrodes separated by a 25 μm thick Surlyn. The two electrodes were then sealed by heating. A mixture of 0.1M GuSCN, 1.2M 1-propyl-2,3-dimethylimidazolium iodide (DMPII), 0.035 M I2, and 0.5 M tertbutylpyridine (TBP) in ACN/3-methoxypropionitrile (MPN) (8:2) was used as the electrolyte. The electrolyte was injected into the gap between the electrodes by capillary; the electrolyte-injecting hole was previously made in the counter electrode with a drilling machine, and the hole was sealed with hot-melt glue after the injection of the electrolyte. The surface of the DSSC was covered by a mask with a light illuminated area of 0.16 cm^2 and then illuminated by a class A quality solar simulator. Incident light intensity (100 mW cm^{-2}) was calibrated with a standard silicon cell. Photocurrent−voltage curves of the DSSCs were obtained with a potentiostat/galvanostat. The thickness of the TiO_2 film was judged by scanning electron microscopic images (SEM). For UV absorption spectra, dye molecules were coated on the TiO_2 films, and the corresponding spectra were obtained by using an UV/vis spectrophotometer equipped with an integrating sphere. Electrochemical impedance spectra (EIS) were obtained from the potentiostat/galvanostat, equipped with a FRA2 module, under a constant light illumination of 100 mWcm^{-2}. The frequency range explored was 10 MHz to 65 kHz. The applied bias voltage was set at the open-circuit voltage of the DSSC between the ITO-Pt counter electrode and the

FTO-TiO$_2$ dye working electrode, starting from the short-circuit condition; the corresponding alternating current (AC) amplitude was 10 mV. The impedance spectra were analyzed by using an equivalent circuit model. IPCE curves were obtained under short-circuit conditions. The light source was a class A quality solar simulator (PEC-L11, AM 1.5 G); light was focused through a monochromator onto the photovoltaic cell. The monochromator was incremented through the visible spectrum to generate the IPCE (λ) as defined by IPCE (λ) = 1240 (J_{SC}/ϕ), where λ is the wavelength, J_{SC} is the short-circuit photocurrent density (mA cm^{-2}) recorded with a potentiostat/galvanostat, and ϕ is the incident radiative flux (Wm^{-2}) measured with an optical detector and a power meter.

5.5. Experimental section

5.5.1. General Materials and Methods

The precursors, 4,7- dibromo-5- methylbenzo[*c*][1,2,5]thiadiazole required for the synthesis of the dyes were synthesized according to literature procedures.[28] All other chemicals were bought commericially and used as received without further purification. All prerequisite reactions were carried out under N$_2$ in standard inert atmosphere. Solvents were dried using suitable drying agent by standard procedures. All column chromatography for synthetically obtained compounds was performed with the use of 100-200 mesh silica gel as the stationary phase in a column. NMR spectral data (^{1}H and ^{13}C) were recorded in NMR spectrometers operating at 400.00 or 500.13 MHz for ^{1}H NMR and 100.00 or 125.77 MHz for ^{13}C NMR. The chemical shifts were calibrated from the residual peaks observed for the deuterated solvents such as chloroform (CDCl$_3$) and dimethyl sulfoxide (DMSO-*d6*) at δ 7.26 and 2.52 ppm for ^{1}H and 77.0 and 39.5 ppm for ^{13}C, respectively. Mass spectral (HRMS) data were collected on a Bruker ESI TOF high resolution mass spectrometer in positive ion mode. Elemental analyses for carbon, hydrogen and nitrogen were performed on a Vario EL III microanalyzer. By using Carey 100 UV-vis spectrophotometer, optical absorption spectra of freshly prepared solutions of the dyes were measured. The IR spectra were recorded by using a FT-IR spectrometer. The cyclic voltammemetric experiments were carried out by following the conventional procedure which includes three-electrode configuration consisting of a glassy carbon working electrode, a platinum wire auxiliary electrode, and a non-aqueous Ag/AgNO$_3$ reference electrode. The $E_{1/2}$ values were determined as 1/2($E_p^a + E_p^c$), where E_p^a and E_p^c are the anodic and cathodic peak potentials, respectively. The potentials are standardized against the ferrocene internal standard.

The measurements were performed at room temperature in DCM using 0.1 M tetrabutylammonium perchlorate as a supporting electrolyte.

5.5.2. Synthesis

4-(7-Bromo-6-methylbenzo[*c*][1,2,5]thiadiazol-4-yl)benzaldehyde (25a). A mixture of 4,7-Dibromo-5- methylbenzo[*c*][1,2,5]thiadiazole (0.49 g, 1.60 mmol), 4-Formylphenylboronic acid (0.24 g, 1.60 mmol), K_2CO_3 (0.66 g, 4.80 mmol), PPh_3 (0.008 g, 2 mol%), $Pd(PPh_3)_2Cl_2$ (0.011 g, 1 mol%) and 30 mL $DMF:H_2O$ (3:1) was heated at 80 °C under nitrogen atmosphere. The progress of the reaction was monitored by TLC. After completion of the reaction, the reaction was quenched by the addition of water. The organic product was extracted with chloroform. The collected organic layer was thoroughly washed with brine solution and dried over anhydrous Na_2SO_4. The volatiles were removed to obtain a pale yellow residue, which was purified by column chromatography on silica gel using hexanes/ chloroform (1:3) as eluant. Pale yellow solid; yield 0.33 g, 63%; mp 179-182 °C; IR (KBr, cm^{-1}) 1655 ($v_{C=O}$); ^1H NMR (400 MHz, CDCl$_3$, δ ppm): 10.1 (s, 1H), 8.08 (d, *J* = 8 Hz, 2H), 8.03 (d, *J* = 4 Hz, 2H), 7.68 (s, 1H), 2.55 (s, 1H); ^{13}C NMR (100 MHz, CDCl$_3$, δ ppm): 191.7, 154.5, 151.4, 142.3, 139.8, 135.9, 132, 131.1, 129.9, 129.7, 114.9, 22.9; HRMS (ESI-TOF) m/z: [M+Na]$^+$ Calcd for $C_{14}H_9BrN_2OSNa$ 354.9511, Found 354.9516; Anal. Calcd for $C_{14}H_9BrN_2OS$: C, 50.46; H, 2.72; N, 8.41; S, 9.62. Found: C, 50.33; H, 2.66; N, 8.22; S, 9.54.

5-(7-Bromo-6-methylbenzo[*c*][1,2,5]thiadiazol-4-yl)thiophene-2-carbaldehyde (25b). A mixture of (5-(1,3-Dioxolan-2-yl)thiophen-2-yl)tributylstannane (2.16 mmol), 4,7- Dibromo-5-methylbenzo[*c*][1,2,5]thiadiazole (0.99 g, 3.24 mmol), $Pd(PPh_3)_2Cl_2$ (1 mol %) and dry DMF (5 mL) was heated at 80 °C under nitrogen atmosphere. On completion of the reaction, the mixture was poured into water and extracted with chloroform. The organic layer was washed with brine solution followed by water and dried over anhydrous Na_2SO_4. The volatiles were removed to obtain a solid residue. It was dissolved in glacial acetic acid (5 mL) and heated to 60°C. After 30 min, it was treated with 10 mL of water and continued the heating for a further 6 h. The cooled solution was extracted with chloroform. The chloroform layer was washed with water and dried over anhydrous Na_2SO_4. On removal of solvent, the obtained dark residue was purified by column chromatography on silica gel using hexanes/chloroform (1:1) as eluant. Pale yellow solid; yield 0.38 g, 52%; mp 194-199 °C; IR (KBr, cm^{-1}) 1660 ($v_{C=O}$); ^1H NMR (400 MHz, CDCl$_3$, δ ppm): 9.97 (s, 1H), 8.18 (d, *J* = 4Hz, 1H), 7.87 (s, 1H), 7.84 (d, *J* = 4Hz, 1H), 2.93 (s, 3H); ^{13}C NMR (100 MHz, CDCl$_3$, δ ppm): 183.5, 154.4, 150.1, 147.7, 139.8, 136.7, 130.4, 128.7, 124.4, 115.6, 23;. HRMS (ESI-TOF) m/z: [M]$^+$ Calcd for $C_{12}H_7BrN_2OS_2$

337.9178, Found 337.9176; Anal. Calcd for $C_{12}H_7BrN_2OS_2$: C, 42.49; H, 2.08; 55; N, 8.26; S, 18.90. Found: C, 42.30; H, 2.08; N, 7.98; S, 18.90.

4-(7-(4-(Diphenylamino) phenyl)-6-methylbenzo[*c*][1,2,5]thiadiazol-4-yl)benzaldehyde (26a). A mixture of 4-(7-Bromo-6-methylbenzo[*c*][1,2,5]thiadiazol-4-yl)benzaldehyde (0.30 g, 0.90 mmol), 4 (Diphenylamino)phenylboronic acid (0.31 mg ,1.08 mmol), K_2CO_3 (0.37 mg, 2.70 mmol) and 20 mL THF:H_2O (3:1), Pd(PPh$_3$)$_4$ (31 mg, 3 mol%) was heated at 80 °C under nitrogen atmosphere for 12 h. On completion of the reaction, the mixture was poured into water and extracted with chloroform. The organic layer was washed with brine solution followed by water and dried over anhydrous Na_2SO_4. The volatiles were removed to obtain a pale yellow residue, which was purified by column chromatography on silica gel using hexanes/ chloroform (1:1) as eluant. Yellow solid; yield 0.26 g, 60%; mp 209-215°C; IR (KBr, cm^{-1}) 1690 ($\upsilon_{C=O}$); ^{1}H NMR (400 MHz, CDCl$_3$, δ ppm): 10.1 (s, 1H), 8.16 (d, J = 8 Hz, 2H), 8.05 (d, J = 8 Hz, 2H), 7.75 (s, 1H), 7.34-7.29 (m, 7H), 7.23-7.05(m, 8H), 2.55 (s, 3H); ^{13}C NMR (100 MHz, CDCl$_3$, δ ppm): 191.9, 155.9, 152.1, 147.5, 147.4, 143.3, 136.6, 135.7, 13, 132.8, 130.9, 130.5, 129.9, 129.7, 129.3, 125.0, 123.3, 122.1, 20.6; HRMS (ESI-TOF) m/z: [M+Na]$^+$ Calcd for $C_{32}H_{23}N_3OSNa$ 552.1352, Found 552.1353; Anal. Calcd for $C_{32}H_{23}N_3OS$: C, 77.24; H, 4.66; N, 8.44; S, 6.44. Found: C, 77.00; H, 4.61; N, 8.34; S, 6.21.

5-(7-(4-(Diphenylamino)phenyl)-6-methylbenzo[*c*][1,2,5]thiadiazol-4-yl)thiophene-2-carbaldehyde (26b). It was obtained from **25b** (0.40 g, 1.23 mmol) by following a procedure described above for **26a**. Orange solid; yield 0.40 g, 65%; mp 218- 222 °C; IR (KBr, cm^{-1}) 1665 ($\upsilon_{C=O}$); ^{1}H NMR (400 MHz, CDCl$_3$, δ ppm): 9.98 (s, 1H), 8.23 (d, J = 4Hz, 1H), 7.95 (s, 1H), 7.85 (d, J = 4Hz, 1H), 7.35-7.29 (m, 6H), 7.22 - 7.06 (m, 8H), 2.54 (s, 3H). ^{13}C NMR (125.77 MHz, CDCl$_3$, δ ppm): 180.0, 155.8, 150.9, 148.7, 147.6, 147.4, 136.8,136.5, 133.5, 131.5, 130.8, 129.4, 129.3, 128.2, 127.9, 125.5, 125.2, 124.9, 123.8, 123.2, 122.2, 121.8, 20.6; HRMS (ESI-TOF) m/z: [M+Na]$^+$ Calcd for $C_{30}H_{21}N_3OS_2Na$ 526.1019, Found 526.1019; Anal. Calcd for $C_{30}H_{21}N_3OS_2$: C, 71.54; H, 4.20; N, 8.34; S, 12.73. Found: C, 71.33; H, 4.20; N, 8.23; S, 12.50.

4-(7-Bromo-6-methylbenzo[c][1,2,5]thiadiazol-4-yl)-*N,N*-diphenylaniline (29). It is obtained from mixture of 4, 7-Dibromo-5-methylbenzo[*c*][1,2,5]thiadiazole (0.50 g, 1.62 mmol), 4-(Diphenylamino)phenylboronic acid (0.70 g, 2.43 mmol) by following a procedure described above for **26a**. Orange solid; yield 0.40 g, 58%; mp 187-191 °C; ^{1}H NMR (400 MHz, CDCl$_3$, δ ppm): 7.79 (d, J = 6 Hz, 2H), 7.56 (s, 1H), 7.29- 7.24 (m, 4H), 7.19 - 7.03 (m, 8H), 2.65 (s, 3H); ^{13}C NMR (100 MHz, CDCl$_3$, δ ppm): 154.5, 151.8, 148.3, 147.3, 139.8, 132.1, 130.5, 129.8, 129.7, 129.3, 124.9, 123.4, 122.7, 112.6, 22.9; HRMS (ESI-TOF) m/z: [M+H]$^+$

Calcd for $C_{25}H_{19}BrN_3S$ 472.0399, Found 472.0403; Anal. Calcd for $C_{25}H_{18}BrN_3S$: C, 63.56; H, 3.84; N, 8.90; S, 6.79. Found: C 63.50; H, 3.79; N, 8.80; S, 6.69.

5-(7-(4-(Diphenylamino)phenyl)-5-methylbenzo[c][1,2,5]thiadiazol-4-yl)phenyl-2-carbaldehyde (30a) It was obtained from **29** (0.60 g, 1.27 mmol) by following a procedure described above for **29**. Pale yellow solid; yield 0.32 g, 51%; mp 208-212°C; IR (KBr, cm^{-1}) 1666 ($v_{C=O}$); ^{1}H NMR (400 MHz, DMSO-d_6, δ ppm): 10.01 (s, 1H) 8.06 (d, J = 8 Hz, 2H), 7.98 (d, J = 8.4 Hz, 2H), 7.88 (s, 1 H), 7.74 (d, J = 8.4 Hz, 2H), 7.38-7.34 (m, 4H), 7.12-7.07 (m, 8 H) 2.44 (s, 3H); ^{13}C NMR (100 MHz, DMSO-d_6, δ ppm): 187.2, 150.8, 147.5, 143.5, 142.6, 138.6, 130.9, 128.1, 126.3, 125.6, 125.2, 124.9, 124.6, 120.2, 118.6, 118, 15.6; HRMS (ESI-TOF) m/z: $[M+Na]^+$ Calcd for $C_{32}H_{23}N_3OSNa$ 552.1352, Found 552.1353; Anal. Calcd for $C_{32}H_{23}N_3OS$: C, 77.24; H, 4.66; N, 8.44; S, 6.44. Found: C, 77.00; H, 4.60; N, 8.40; S, 6.20.

5-(7-(4-(Diphenylamino)phenyl)-5-methylbenzo[c][1,2,5]thiadiazol-4-yl)thiophene-2-carbaldehyde (30b). It is obtained from mixture of (5-(1,3-Dioxolan-2-yl)thiophen-2-yl)tributylstannane (0.93 mmol), **26a** (0.40 g, 0.84 mmol) by following procedure described above for **25b.** Pale yellow solid; yield 0.35 g, 86%; mp 216-220°C; IR (KBr, cm^{-1}) 1660 ($v_{C=O}$); ^{1}H NMR (400 MHz, DMSO-d_6, δ ppm): 10.00 (s, 1H) 8.15 (s, 1H), 7.98 (d, J = 8.4 Hz, 2 H), 7.88 (s, 1H), 7.61 (d, J = 8 Hz, 2H), 7.38-7.33 (m, 4H), 7.13-7.08 (m, 8 H); ^{13}C NMR (100 MHz, DMSO-d_6, δ ppm): 182.8, 155.1, 152.0, 148.3, 147.1, 144.1, 138.7, 136.8, 135.9, 135.5, 130.9, 130.2, 129.8, 129.7, 129.3, 126.3, 124.1, 123.0, 122.4, 122.3, 21.1; HRMS (ESI-TOF) m/z: $[M+Na]^+$ Calcd for $C_{30}H_{21}N_3OS_2Na$ 526.1019, Found 526.1019; Anal. Calcd for $C_{30}H_{21}N_3OS_2$: C, 71.54; H, 4.20; N, 8.34; S, 12.73. Found: C, 71.48; H, 3.96; N, 7.90; S, 12.58.

(*E*)-2-Cyano-3-(4-(7-(4-(diphenylamino)phenyl)-6-methylbenzo[c][1,2,5]thiadiazol-4-yl)phenyl)acrylic acid (27). A mixture of 4-(7-Bromo-6-methylbenzo[c][1,2,5]thiadiazol-4-yl)benzaldehyde (0.13 g, 0.25 mmol) **26a,** Cyanoacetic acid (0.02 g, 0.32 mmol), NH$_4$OAc (0.009 g, 0.10 mmol) and CH$_3$COOH (10 mL) was refluxed. The progress of the reaction was monitored by TLC. After 24 h, the starting materials disappeared indicating the completion of the reaction, then washed with water, followed by filteration and dried. Reddish brown solid; yield 0.13 g, 90%; mp 257-261 °C; IR (KBr, cm^{-1}) 2223 ($v_{C\equiv N}$); ^{1}H NMR (400 MHz, DMSO-d_6, δ ppm): 8.34 (s, 1H), 8.27 (d, J = 8 Hz, 2H), 8.22 (d, J = 8 Hz, 2H), 8.04 (s, 1H), 7.44-7.35 (m, 6H), 7.14 - 7.08 (m, 8H), 2.51 (s, 3H); ^{13}C NMR (100 MHz, DMSO-d_6, δ ppm): 172.1, 163.3, 155.3, 153.7, 151.4, 147.0, 141.0, 136.6, 133.0, 131.9, 131.4, 131.1, 130.8, 129.7, 129.6, 128.4, 124.5, 123.5, 121.8, 116.3, 103.8, 20.2; HRMS (ESI-TOF) m/z: $[M+H]^+$ Calcd for $C_{35}H_{25}N_4O_2S$ 565.1693, Found 565.1698; Anal. Calcd for $C_{35}H_{24}N_4O_2S$: C, 74.45; H, 4.28; N, 9.92; S, 5.68. Found: C, 74.33; H, 4.24; N, 9.86; S, 5.20.

(Z)-2-Cyano-3-(5-(7-(4-(diphenylamino)phenyl)-6-methylbenzo[c][1,2,5]thiadiazol-4-yl)thiophen-2-yl)acrylic acid (28). It was obtained from **26b** (0.20 g, 0.40 mmol) by following a procedure described above for **27**. Brown solid; yield 0.22 g, 97%; mp 305-310°C; IR (KBr, cm^{-1}) 2225 ($\upsilon_{C\equiv N}$); ^{1}H NMR (400 MHz, DMSO-d_6, δ ppm): 8.55 (s, 1H), 8.32-8.30 (m, 3H), 8.1 (d, $J = 4$ Hz, 1H), 7.44-7.35 (m, 5H), 7.14-7.07 (m, 8H), 2.51(s, 3H); ^{13}C NMR (100 MHz, DMSO-d_6, δ ppm): 163.6, 155.0, 150.1, 147.3, 146.9, 146.5, 139.8, 136.6, 136.6, 132.6, 131.5, 129.7, 129.4, 127.8, 124.5, 123.6, 122.8, 121.7, 116.5, 98.9, 20.2; HRMS (ESI-TOF) m/z: [M+H]$^+$ Calcd for C$_{33}$H$_{23}$N$_4$O$_2$S$_2$ 571.1257, Found 571.1257; Anal. Calcd for C$_{33}$H$_{22}$N$_4$O$_2$S$_2$: C, 69.45; H, 3.89; N, 9.82; S, 11.24. Found: C, 69.31; H, 3.86; N, 9.43; S, 11.00.

(E)-2-Cyano-3-(4-(7-(4-(diphenylamino)phenyl)-5-methylbenzo[c][1,2,5]thiadiazol-4-yl)phenyl)acrylic acid (31). It was obtained from **30a** (0.15 g, 0.30 mmol) by following a procedure described above for **27**. Brown solid; yield 0.11 g, 70%; mp 252-257 °C; IR (KBr, cm^{-1}) 2216 ($\upsilon_{C\equiv N}$); ^{1}H NMR (400 MHz, DMSO-d_6, δ ppm): 8.36 (s, 1H), 8.16 (d, $J = 8$Hz, 1H), 7.97 (d, $J = 8$ Hz, 2 H), 7.87 (s, 1H), 7,70 (d, $J = 8$ Hz, 1H), 7.32-7.38 (m, 4H), 7.12-7.10 (m, 10H), 2.46 (s, 3H); ^{13}C NMR (100 MHz, DMSO-d_6, δ ppm): 155.8, 152.1, 147.9, 147.4, 132,1, 131.9, 130.8, 130.6, 130.2, 127.6, 124.9, 124.0, 122.8, 119.2, 20.5; HRMS (ESI-TOF) m/z: [M+H]$^+$ Calcd for C$_{35}$H$_{25}$N$_4$O$_2$S 565.1693, Found 565.1698; Anal. Calcd for C$_{35}$H$_{24}$N$_4$O$_2$S: C, 74.45; H, 4.28; N, 9.92; S, 5.68. Found: C, 74.20; H, 4.24; N, 9.80; S, 5.18.

(Z)-2-Cyano-3-(5-(7-(4-(diphenylamino)phenyl)-5-methylbenzo[c][1,2,5]thiadiazol-4-yl)thiophen-2-yl)acrylic acid (32). It was obtained from **30b** (0.12 g, 0.24 mmol) by following a procedure described above for **27**. Brown solid; yield 0.10 g, 77%; mp 287-291°C; IR (KBr, cm^{-1}) 2213 ($\upsilon_{C\equiv N}$); 1H NMR (400 MHz, DMSO-d_6, δ ppm): 8.33 (s, 1H), 7.96-7.98 (m, 4 H), 7.93 (d, $J=3$Hz, 1H), 7.89 (s, 1 H), 7.54 (d, $J = 3$Hz, 1H), 7.36 (t, $J = 8$ Hz, 4 H), 7.12-7.08 (m, 10 H), 2.61 (s, 3H). ^{13}C NMR (100 MHz, DMSO-d_6, δ ppm): δ 155.2, 148.2, 147.3, 139.4, 132.6, 131.8, 131.1, 130.9, 130.2, 125.1, 124.2, 122.6, 21.4; HRMS (ESI-TOF) m/z: [M+H]$^+$ Calcd for C$_{33}$H$_{23}$N$_4$O$_2$S$_2$ 571.1257, Found 571.1257; Anal. Calcd for C$_{33}$H$_{22}$N$_4$O$_2$S$_2$: C, 69.45; H, 3.89; N, 9.82; S, 11.24. Found: C, 69.28; H, 3.73; N, 9.43; S, 11.00.
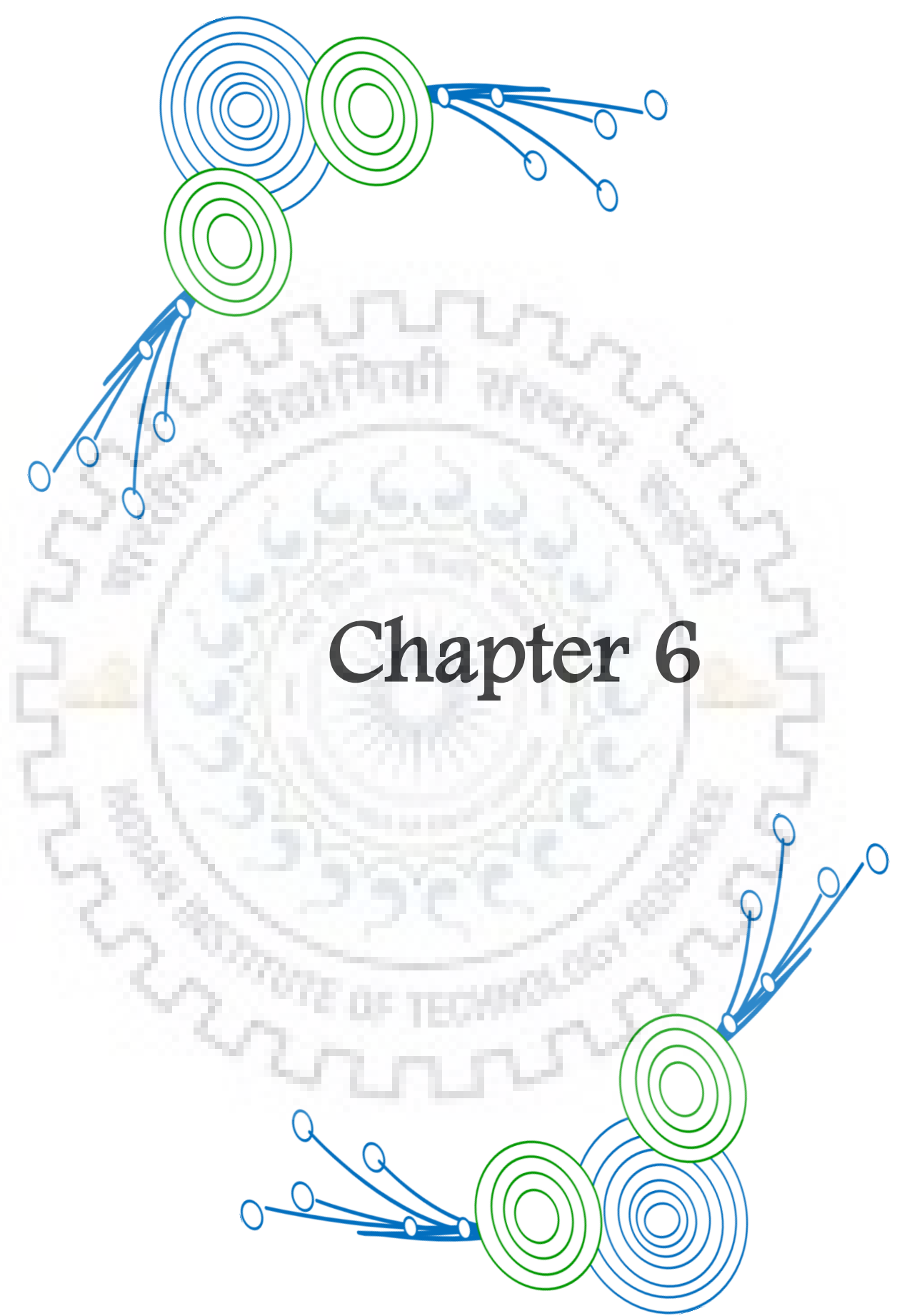
Chapter 6

Chapter 6

Topological Influence of Lateral Substituted Benzothiadiazole Hybrids on Photophysical and Electrochemical and Electroluminescence Properties
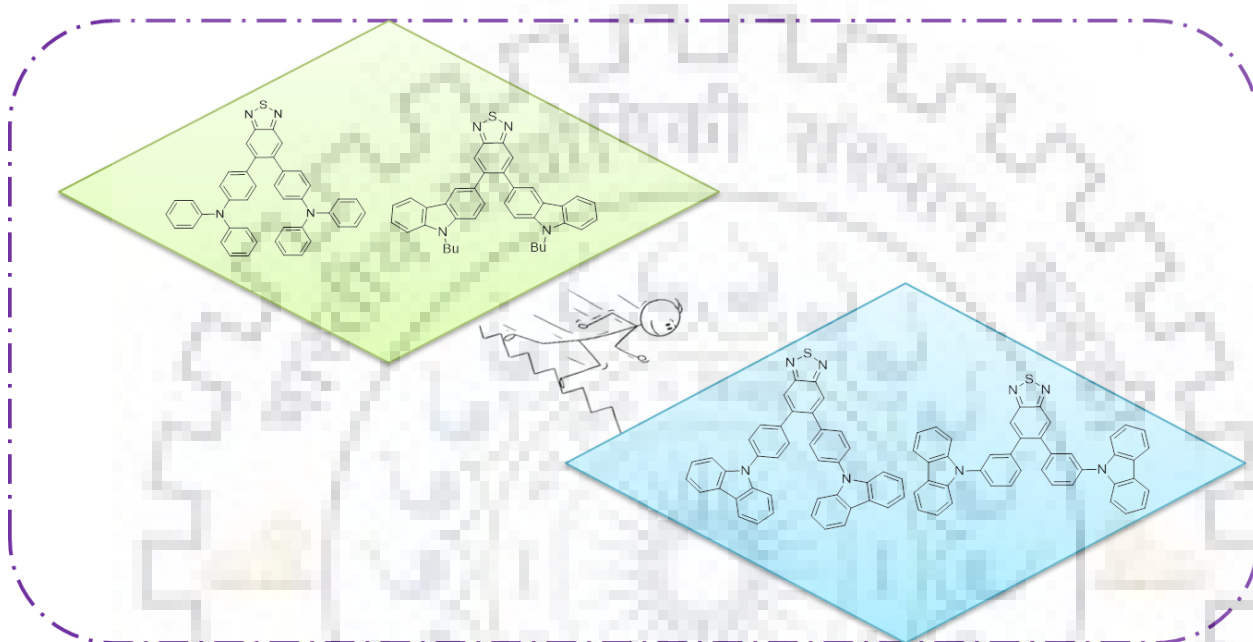
6.1 Introduction

The π-conjugates are beneficial for various application of organic electronic, such as organic light emitting diodes (OLEDs) [257, 258], organic photovoltaics (OPVs) [259, 260], organic field effect transistors (OFETs) [261, 262], nonlinear optics [263, 264], and molecular sensors [265]. Moreover, organic light-emitting diode (OLED) attracted the immense attention of organic chemistry is presumably due to its imminent role of lower power consumption towards lightings and full-color display applications. The development of red and green emitting materials have been standardized, however the blue OLED lags behind due intrinsically wider energy gaps which often cause unbalanced charge injection and unfavourable electrical properties. The quality of the OLED often depends on the structural and functional properties of organic materials. [266, 267] Eventually, an organized structural framework proves to be beneficial for balanced charge transport character, high fluorescence quantum yield, high thermal stability and amorphous morphology, suitable for solution processable devices which tune the performance of OLED. [268]

The π-conjugation effectively reduces the energy band gap between the highest occupied molecular orbital (HOMO) and lowest unoccupied molecular orbital (LUMO) and beneficially extends absorption profiles of the dyes to the visible region. [269,270] Therefore, the conjugative building blocks help to optimize the functional properties of materials by tethering diverse chromophores by simple chemical modifications. Likewise, topological connectivity of donor and acceptor via a linker influence greatly the physicochemical, thermal, and carrier transport properties. [271] Moreover, substituting phenyl as linker, interestingly provides different positional linkage via *ortho-*, *meta-* and *para* substitution, which provides more pathway for functional tuning. Therefore, the systematic studies of linking topology received more attention as a measure to improve the characteristics functional materials used in light-emitting devices [268, 272]

Benzothiadiazole molecule is well known in the literature due to its effective electronic conjugation and capacity to reduce the LUMO energy level, thus finding wide variety of applications. [200] Furthermore, its 4,7 nuclear positions has been well explored and has been employed as red and green emitters in OLED device.[20, 117] However, benzothiadiazole moiety has never been employed as blue emitter in OLEDs. In this pursuit, here in this chapter we aim to investigate photophysical, thermal and electrochemical properties of "V" shaped benzothiadiazole derivatives exploring C5 and C6 nuclear positions. (Figure 6.2) The substitution of different electron donating unit such as triphenylamine, carbazole, *N*-phenyl carbazole and *N*-phenyl phenothiazine units has been accounted as well crafted moieties for increasing conjugation and molecular rigidity, leading to amorphous materials with pronounced morphological and thermal stability. [273, 274, 275] Thus, to better understand the impact of the conjugation, the study of the hybrid dye is carried out by comparing photophysical properties of its linear molecular structures as well as parent phenyl phenothiazine (**L19**) [276] and phenyl carbazole (**L18**) [277] chromophores. (Figure 6.1). Interestingly, among 5 % doped dyes (CBP), the dye **33** exhibited better device performance with external quantum efficiency of 1.7%, maximum luminance of 1906 cd m^{-2} when employed as green emitter with CIE coordinates (0.2 0.4). Extensively, to the best of our knowledge the strategical introduction of the *N*-phenylcarbazole has resulted first benzothiadiazole based blue emitter with maximum luminance of 1464 cd m^{-2}, CIE coordinates (0.16, 0.19). Thus, the topological differences significantly altered the photophysical, electrochemical and electroluminescence performances.[110, 278, 279]
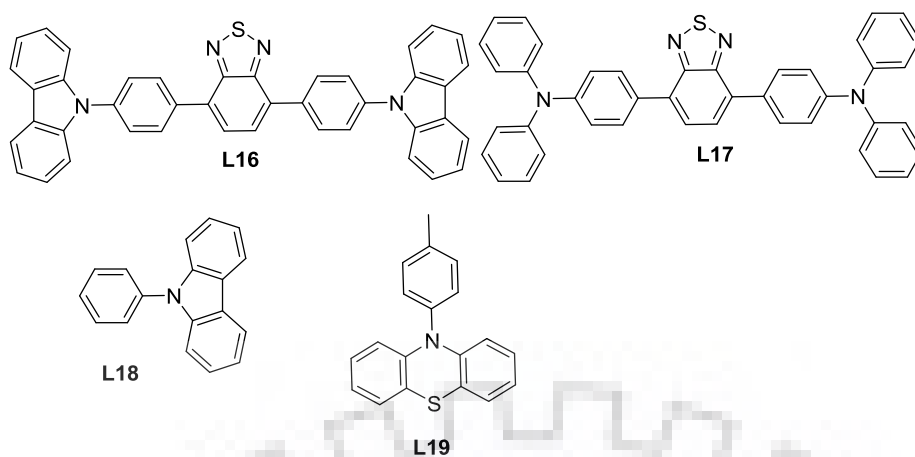
Figure 6.1 Structures of the related dyes.
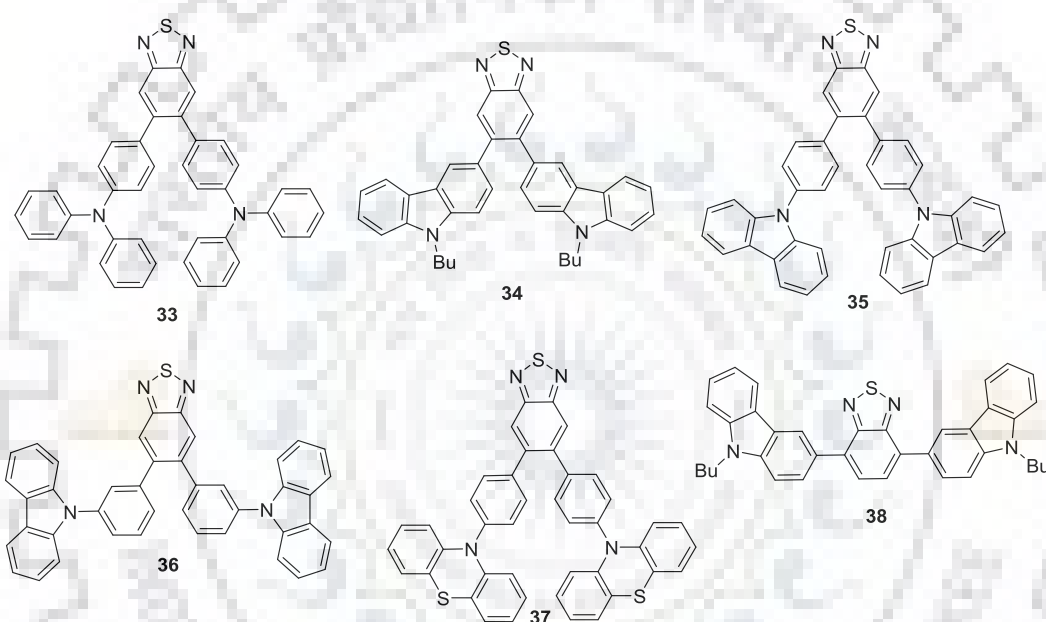
Figure 6.2. Structures of the target dyes.
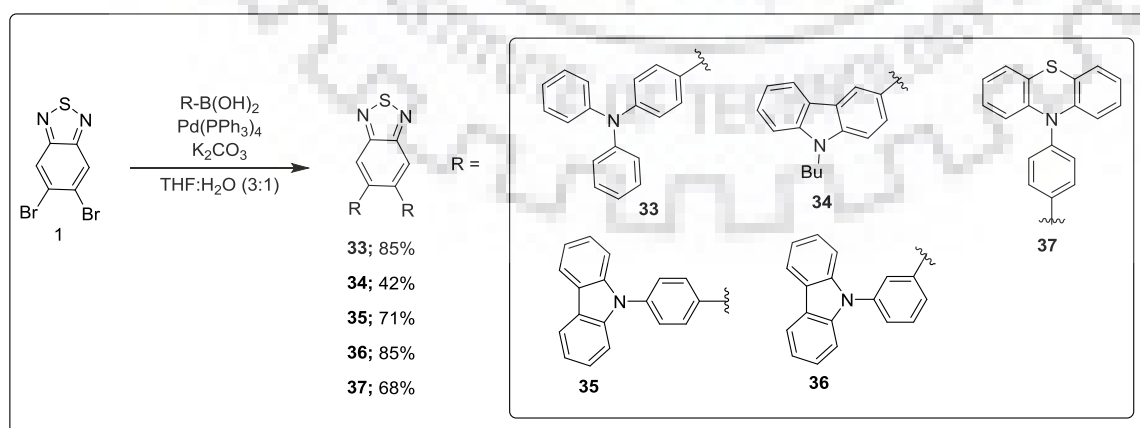
Scheme 6.1 Synthetic protocol of the dyes **33-34** and **34-36.**

6.2 Results and Discussion

6.2.1 Synthesis and Characterization

In this work, we have synthesized six new organic compounds (**33, 34, 35, 36**, **37** and **38**) containing benzothiadiazole nuclei which is laterally substituted with different chromophores by following single step Suzuki coupling reaction as shown in Scheme 6.1. The precursor lateral 5,6 dibromo-benzothiadiazole is prepared by following the reported literature procedure. The final dyes **33, 34, 35, 36, 37** and **38** were prepared by palladium catalysed Suzuki coupling reactions in the presence of potassium carbonate. All the dyes appear pale yellow in color and soluble in most common organic solvents such as TOL, DCM, THF and DMF. All these new compounds were thoroughly analysed by NMR (^{1}H & ^{13}C) spectroscopy and high resolution mass spectrometry (HRMS) and the data found consistent with the proposed structures.

6.2.2 Photophysical Properties

The photophysical spectra for the dyes were recorded in dichloromethane and displayed in Figure 6.3 and the corresponding data is tabulated in Table 6.1. All the dyes showed absorption profile in the range of 230-530 nm. The higher energy wavelength assigned to π-π* localized transition originating from the chromophores such as benzothiadiazole, carbazole, phenothiazine and benzene. However, the longer wavelength absorption ~340-440 nm is attributed to π-π* delocalized transition of the entire molecule. The lateral benzothiadiazole derivatives (**33, 34, 35, 36** and **37**) in absorption profile follow the trend **33 > 34 > 37> 35 > 36** which reflects the increasing electron donating character of appended chromophores (triphenylamine, carbazole , *N*- phenylphenothiazine, *N*-phenyl carbazole). Interestingly, among the carbazole substituted BTD derivatives (**34, 35, 36**), the directly linked carbazole showed high molar extinction coefficient with bathochromic shift when compared to its *N*-phenyl carbazole derivatives (**35** and **36**). This is attributed to the extended electronic conjugation in the former whereas the non-planar *N* phenyl linkage in later reduces the conjugation. [280, 281] Likewise, the *para* linked dye **35** showed bathochromic shift when compared to *meta* linked dye **36**, attributed to facile electronic conjugation of *para* compared to *meta* linked dyes. Interestingly, the absorption maxima of **L18** dye (Figure 6.1) and **36** is same (~340 nm), this suggests the dyes are not in facile conjugation and *N*-phenyl carbazole unit is playing the major role for characteristic absorption maxima of the dye **36**. However, the dye **35** exhibited the red shift proclaiming the extension of conjugation. Similarly, the dye **37** has showed bathochromic shift compared to **L19** dye, (Figure 6.1) confirming the *para* linkage

helps in extending the conjugation. Further, on comparing the present dyes with the linearly substituted chromophores on BTD nuclei as reported in literature (**L16, L17** and **37**) has shown bathochromic shift compared to lateral (C5 and C6) substituted benzothiadiazole derivatives, **L17 > 33, L16 > 35** and **37 > 34**.
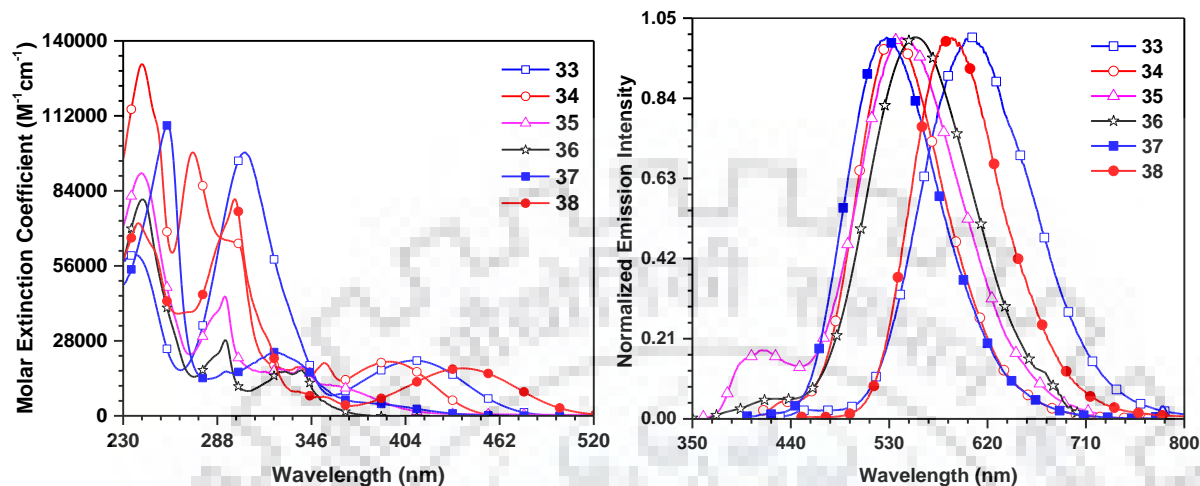
Figure 6.3 Absorption and Emission spectra of the dyes recorded in DCM.

Table 6.1 Optical properties of the dyes

Dye	λ_{abs} (nm) ($\varepsilon_{max} \times 10^3$ (M^{-1} cm^{-1}))[a]	λ_{em} (nm)[a] (Φ_f)[b]	Stokes shift (cm^{-1})	λ_{em} (nm)[c]
33	414 (20.57), 305 (98.51), 237 (60.13)	609 (0.68)	7734	424
34	394 (20.21), 339 (18.20), 300 (sh), 273 (98.47), 242 (131.35).	535 (0.65)	6689	512
35	361 (11.24), 340 (18.48), 293 (44.67), 241 (90.65)	542 (0.45)	9251	440
36	340 (17.13), 293 (28.49), 241 (80.89)	554 (0.30)	11361	447
37	390 (4.27), 322 (23.84), 257 (108.40)	528 (0.47)	6702	421
38	440 (17.73), 299 (81.06), 240 (71.87)	583	5575	-
L16	408 (13.68)	542	6060	-
L17	464 (16.54)	624	5530	-
L18	242 , 293, 341	363	1777	-
L19	257, 320	443	8677	-

[a] Measured in DCM solution. [b] Absolute quantum yields determined using a calibrated integrated sphere system. [c] Measured for spin cast film from TOL.
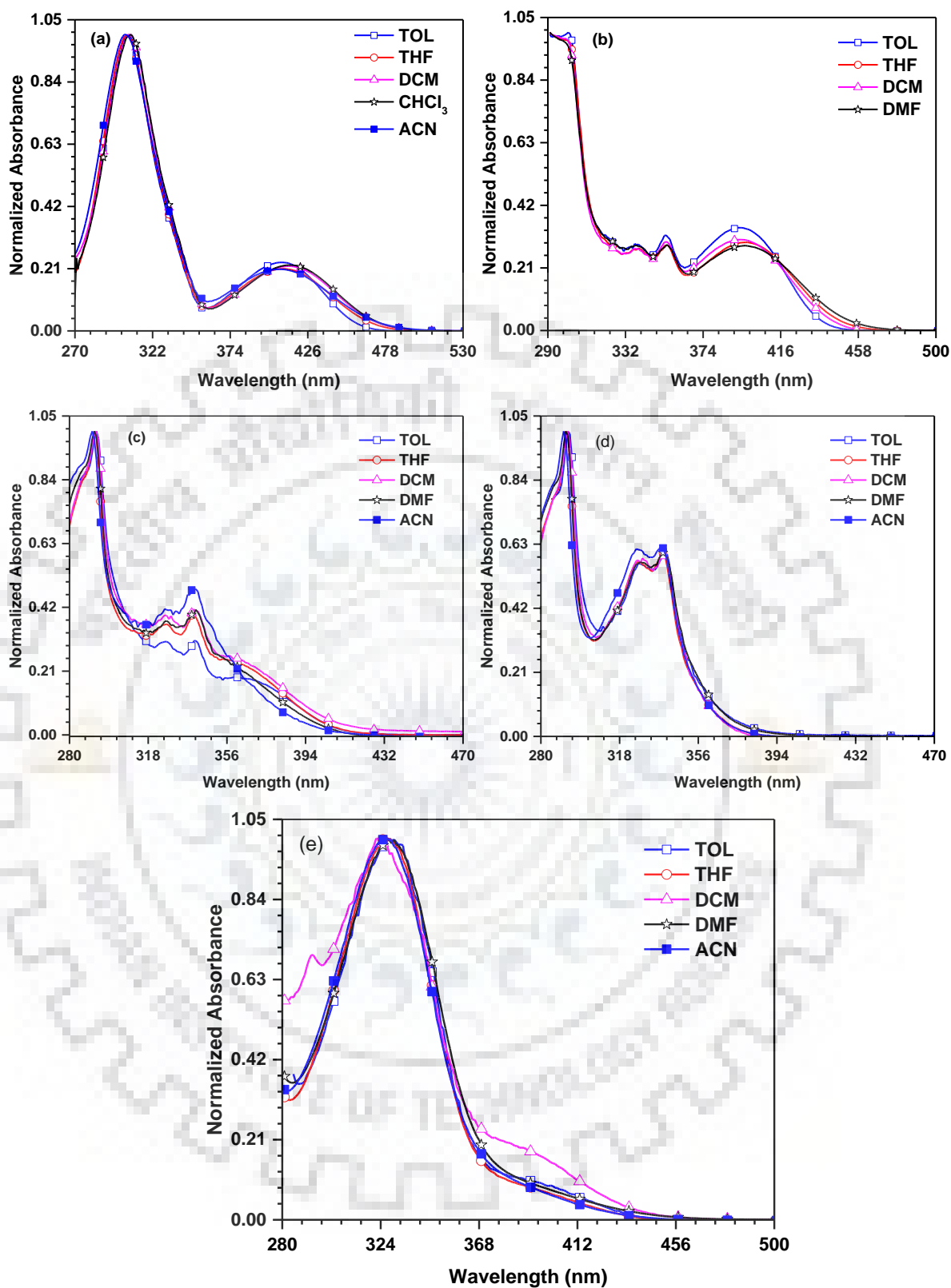
Figure 6.4. Absorption spectra of the dyes recorded in different solvents a) **33** b) **34** c) **35** d) **36** and e) **37**

All the dyes showed blue-shifted absorption suggestive of positional effects and non-planarity of sterically twisted chromophores such as carbazole, *N*-phenyl carbazole, triphenylamine on benzothiadiazole at C5 and C6 positions. [282]

The emission spectra of the dyes recorded in DCM are shown in Figure 6.3 where all the dyes exhibited featureless emission profile ranged from 433 to 609 nm. The emission maxima of the dyes follows the trend, **34** (433 nm) < **37** (528 nm) < **35** (542 nm) < **36** (554 nm) < **33** (609 nm) which is contrary to the trend observed in absorption spectra. The carbazole derivatives showed the reverse trend in emission profile compared to absorption in the order **36** > **35** > **34**. This suggests that dye **36** probably undergoing more structural reorganization in the excited state.[283, 284] This structural reorganization can be measured by Stokes shift which calculates the degree of structural deformation in the excited state and it follows the order as **34** (6689 cm^{-1}) < **35** (9251 cm^{-1}) < **36** (11361 cm^{-1}). Conversely, on comparing the literature reported linear substituted dyes with present lateral derivatives, the emission profile follows the similar trend **L17** > **33,** and **38** > **34.** Where, the dye **L16** and **35** showed similar emission maxima of 542 nm, this probably ascertains that the lateral and linear *N*-phenyl carbazole substituted dye emission originating from similar electronic state.

Furthermore, the effect of the solvents on electronic structure was studied by measuring photophysical properties in solvents of different polarities. (Figure 6.4 and 6.5) In absorption, these dyes showed insensitiveness towards the increasing solvent polarity which reveals a non-polar ground state. The dyes **33** and **34** displayed positive emission solvatochromism ascribed to dipolar relaxation of the molecule in the excited state. In contrast, the dye **37** gave hypsochromic shift toward increasing the polarity suggesting different structural perturbation by solvent polarity. [285, 286] However, the dye **35** and **36** showed structureless emission with positive interaction towards non-polar to mediocre polar solvents (TOL, THF, DCM), but showed structured blue shift emission in high polar solvents (DMF and ACN). This behaviour suggests perturbation of donor-acceptor (D-A) interaction with the polar solvents in the excited state which is further investigated through concentration dependent emission studies in DMF solvents as shown in Figure 6.6. The dye **35** showed structured emission which gradually collapse to dual emission on increasing the concentration from 1×10^{-6} M to 1×10^{-4} M. [287,288] Moreover, the dyes exhibits dual emission in high concentration where the bands at the longer wavelength could be assigned as ICT emission while the shorter band to local excited state (LE). Such shift suggests that the D-A interaction increases on increasing the concentration due to strong dipolar interaction with the polar solvent in the excited state. [289]
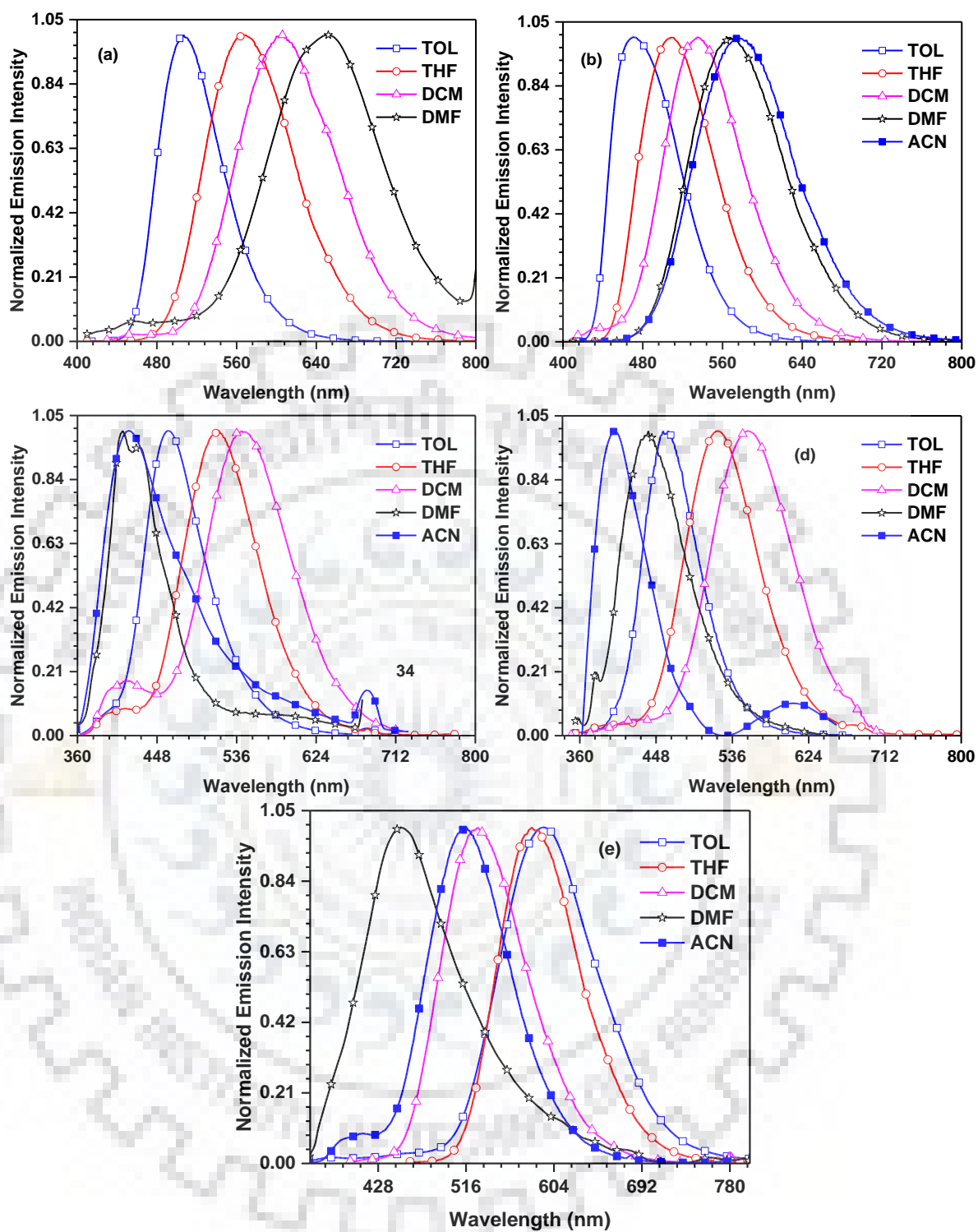
Figure 6.5 Emission spectra of the dyes recorded in different solvents a) **33** b) **34** c) **35** d) **36** and e) **37**
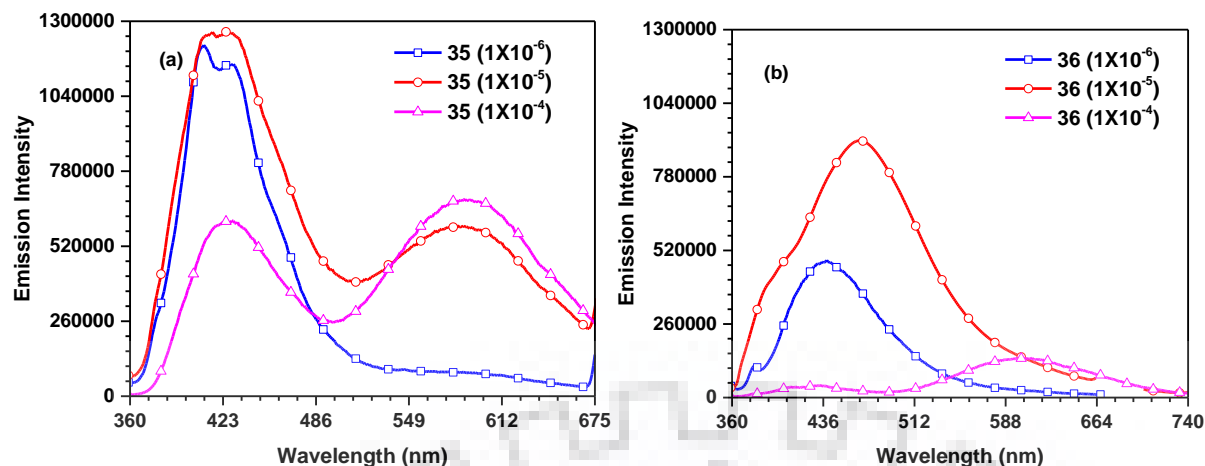
Figure 6.6. Concentration dependent emission spectra of (a) **35** and (b) **36**

Furthermore, to prove the behaviours of the dyes, they were recorded in water–DMF solvent compositions. (Figure 6.7). The emission maxima exhibited a gradual decrease of intensity on addition of water from 0% to 70% into DMF which on further addition of 90% water showed dual emission bands considered to be originated due to LE and ICT state as stated above. [290] The dual emission merge to red shifted emission ascribing charge transfer shift (ICT), this may be due to formation of aggregates.
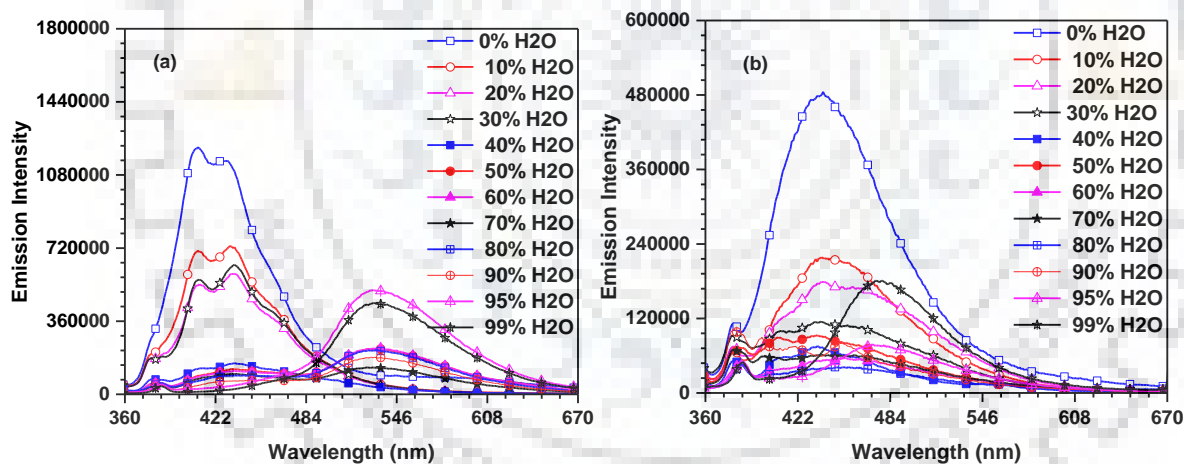
Figure 6.7. Emission spectra recorded in water–DMF mixtures for (a) **35** and (b) **36**
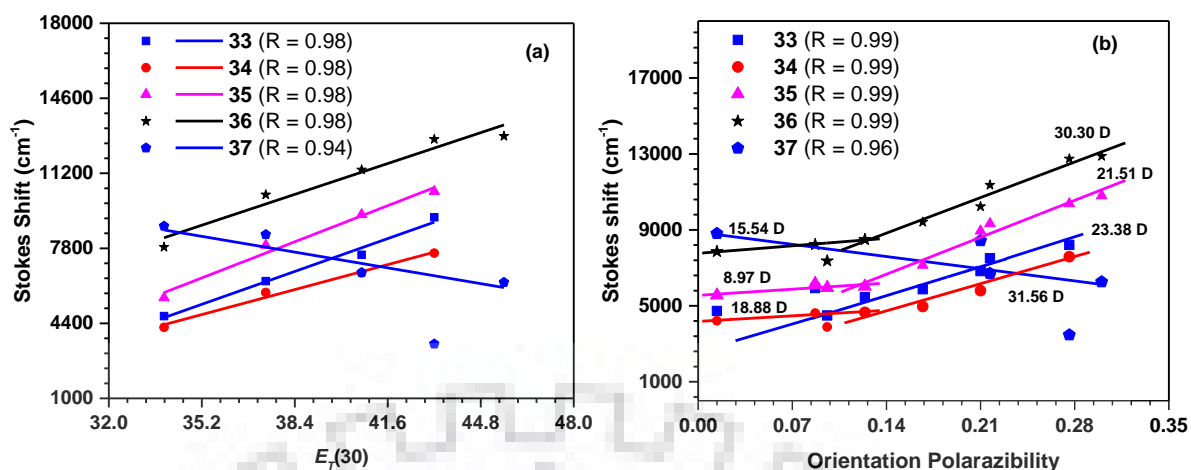
Figure 6.8 Correlation between the Stokes shift and solvent parameter, $E_T(30)$ (a) and correlation plot of v *vs* Δf (b)

To further unravel the nature of the excited state in the compounds, the trend of Stokes shift versus the orientation polarizability (Δf) has been studied. The dyes **34, 35** and **36** exhibited two fitted lines attributable to two different excited states in high- and low-polarity solvents. The dipole moment were calculated to be 18.8, 8.9, 15.5 Debye in low polarity solvent and 31.56, 21.51 and 30.30 D in high polarity solvent for dyes **34, 35** and **36**, respectively. Moreover, the μ_e are slightly larger in low polarity than that of the usual LE excited state, implying the emissive state of dyes is a LE like state involving a slight CT component. However, the triphenylamine substituted dye (**33**) exhibited a single straight line corresponds to one indistinguishable μe of 23.38 D, implies that the LE and CT components are well hybridized. [291, 292, 293] On the other hand, carbazole containing dyes (**34, 35** and **36**) demonstrated typical LE-dominated property.The dyes **33, 34, 35** and **36** exhibited monoexponential lifetime of 4.5, 2.2, 1.9 and 1.17 ns, respectively which is attributed to a single emissive state with hybridized LE and CT components of the HLCT state

To obtain further insight into the relationship between the structure and photophysical properties, we determined the fluorescence lifetimes (τ_f) with the time-correlated single photon counting method and calculated the radiative (k_r) and nonradiative (k_{nr}) decay constants from the singlet excited state, based on the equations $k_r = \Phi_f/\tau_f$ and $k_{nr} = (1 - \Phi_f)/\tau_f$. The calculation showed the carbazole derivative exhibited comparable radiative rate, however by contrast the orthogonal configured phenyl linked carbazole may possibly cause the vibrational non radiative deactivation of the excitons, resulting in a large $k$nr~ 5.9×10^8 sec^{-1} for meta-linked when compared to para linked derivative as strengthen by comparably large oscillator strength from the extended conjugation and more overlap of the frontier molecular orbitals.

173

The emission spectra recorded for the dyes in film is displayed in Figure 6.10 where all the dyes exhibited hypsochromic shift when compared to the corresponding spectra recorded in toluene attributable to the *H*-type aggregation.[294] However, the carbazole derivative dye **34** showed red shift of 41 nm attributed to *J*-aggregation of the molecules in the solid state. The dyes showed the trend **34 > 36~35 > 33~37,** where the triphenylamine and phenyl phenothiazine derivative showed blue shift when compared to other dyes following the reverse trend than in solution, highlights the importance of the present design in inhibiting the aggregation.
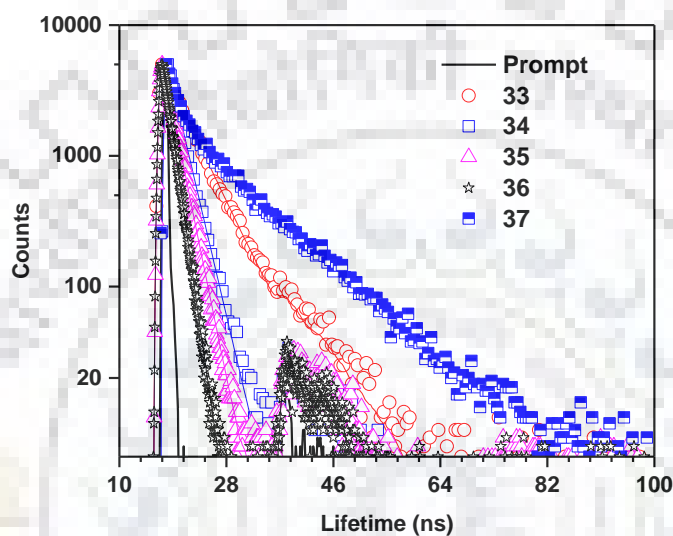
Figure 6.9 Time-resolved fluorescence decay profiles for the dyes in dichloromethane solution
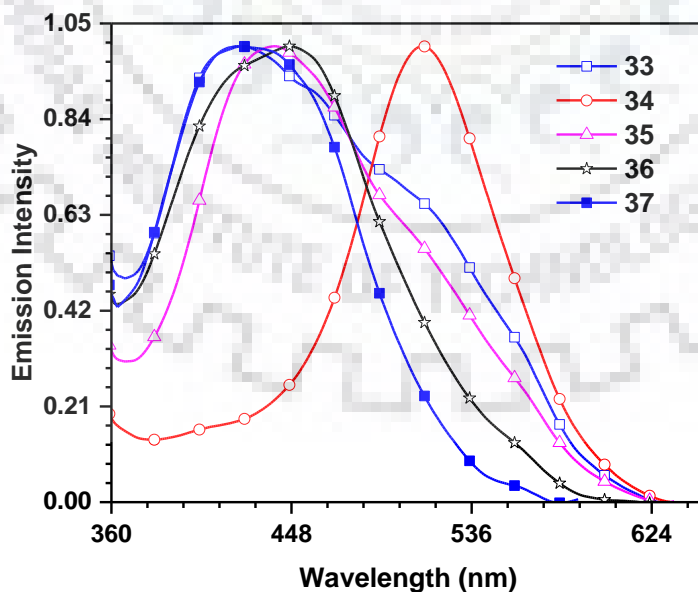
Figure 6.10. Emission spectra of the drop-cast thin films of the dyes.

Table 6.2. Absorption data of the dyes recorded in various solvents

	TOL	TCE	BUET	DEE	DCB	THF	DCM	ACN	DMF
33	409	402	405	402	414	417	417	410	407
34	393	397	391	389	400	393	394	397	397
35	367	368	363	370	369	366	360	360	361
36	339	340	338	337	340	339	340	340	340
37	390	399	397	399	404	390	390	390	390

Table 6.3. Emission data of the dyes recorded in various solvents

Dye	λ_{em}(nm)									$\Delta\lambda$,
	TOL	TCE	BUET	DEE	DCB	THF	DCM	ACN	DMF	$(\lambda_{TOL}-\lambda_{DMF})$ (nm)
33	507	528	495	515	547	566	607	-	651	144
34	471	486	461	475	499	509	535	575	568	97
35	461	476	463	476	501	516	542	417	422, 585	124
36	462	472	450	472	500	519	554	400,605	442, 600	138
37	594	433	576	401	435	581	528	516	451	-

Table 6.4. Stokes shift data of the dyes recorded in various solvents

	Stokes Shift (cm^{-1})								
	TOL	THF	DCM	TCE	BUET	DEE	DCB	ACN	DMF
33	4726	6313	7506	5936	4489	5458	5873	-	9209
34	4214	5799	6689	4613	3883	4654	4960	7798	7583
35	5556	7943	9328	6166	5950	6019	7140	3792	3776, 10379
36	7854	10231	11361	8225	7364	8487	9412	4412, 12883	6768, 12745
37	8806	8429	6702	1968	7828	125	1764	6261	3468

Table 6.5 Photophysical properties of the dyes

Dye	τ^{a} (ns)	Φ_F^{b}	k_r^{c} (10^8s^{-1})	k_{nr}^{d} (10^8s^{-1})
33	4.55	0.68	1.5	0.7
34	2.23	0.65	2.9	1.6
35	1.91	0.45	2.3	2.8
36	1.17	0.30	2.5	5.9
37	1.37	0.47	3.4	3.9

$^{a}\tau$ = fluorescence lifetime decay ^{b}Absolute quantum yields determined with a calibrated integrating sphere system. ^{c} Radiative decay rates (k_r) calculated using Φ_F/τ. ^{d}Non-radiative decay rate (k_{nr}) calculated using $\Phi_F = k_r/(k_r + k_{nr})$.

6.2.3 Thermal properties

The thermal stability of the dyes were investigated by thermogravimetric analysis (TGA) at a heating rate of 10 °C/min under nitrogen atmosphere. All the dyes exhibited reasonable thermally stability with the onset temperature corresponding to 10% weight loss falling in the range of 390-446 °C (Figure 6.11). The thermal stability of the compounds varies with the respect of topological effect of the substituents. [294] The carbazole-containing derivative (**34, 35** and **36**) showed remarkable thermal stability in the order **34 < 35 < 36** attributed to its increasing twisting (non-planar nature) which resulted in higher thermal decomposition temperature. [41]
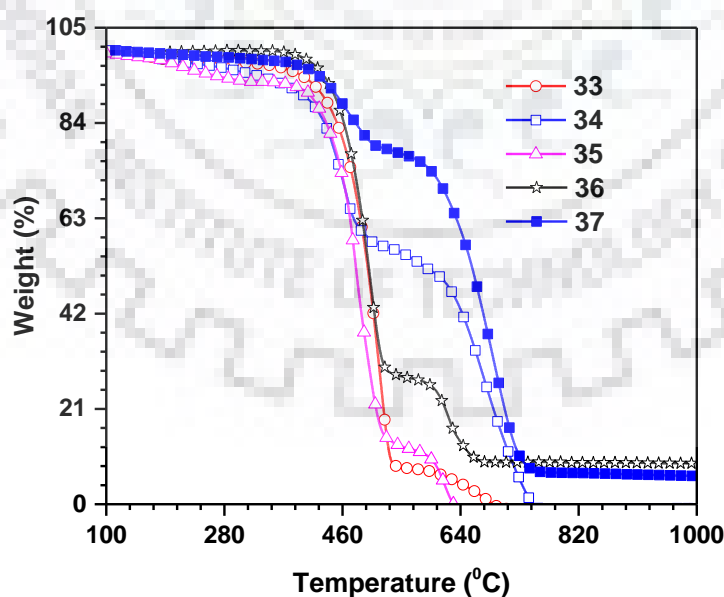
Figure 6.11. Thermogravimetric plots of the dyes.

Table 6.6 Thermal and electrochemical data of the dyes

Dye	T_{onset} (°C)[a]	E_{ox} (V)[b]	HOMO (eV)[c]	LUMO (eV)[d]	E_{0-0} (eV)[e]
33	425	0.54	-5.34	-2.71	2.63
34	391	0.71, 0.86	-5.49	-2.71	2.78
35	404	0.87	-5.67	-2.43	3.24
36	445	0.40, 0.85	-5.65	-2.21	3.44
37	446	0.28	-5.08	-2.16	2.92
L16	509	0.57	-5.67	-3.02	2.65
L17	268	0.38	-5.48	-3.11	2.37
L18	-	0.81	-5.61	-2.05	3.05
L19	-	0.54	-5.34	-2.71	2.63

[a] Temperature corresponding to 10% weight loss. [b] Measured for 0.1 mM dichloromethane solutions and the potentials are quoted with reference to ferrocene internal standard. [c] HOMO = 4.8 + E_{ox}. [d] LUMO = HOMO – E_{0-0}. [e] Optical band gap obtained from the intersection of absorption and emission spectra

6.2.4 Electrochemical properties

To investigate the oxidation propensity of molecules, cyclic voltammetry (Figure. 6.12) and differential pulse voltammetry (Figure. 6.13) experiment were carried out in DCM solution using ferrocene as an internal standard. The triphenylamine containing dye (**33**) exhibits quasi reversible oxidation couple while other dyes (**34, 35, 36, 37**) displayed irreversible oxidation wave. The oxidation propensity of the dyes increased with increasing electron donating unit, therefore triphenylamine and phenothiazine substituted dyes (**33, 37**) showed higher oxidation propensity when compared to carbazole substituted derivatives (**34, 35, 36**). The feasibility of removal of electron from electron donating unit leads to the oxidation in the compounds. Consequently, the triphenylamine and phenothiazine substituted dyes (**33, 37**) exhibits lower oxidation potential when compared to carbazole substituted derivatives (**34, 35, 36**). The HOMO energies of the dyes are in the small range of -5.08 to -5.67 eV while the LUMO showed wide variation from -2.16 to -2.71 eV. The dyes **33** and **34**, exhibit relatively low band gap, with simultaneous lowering of LUMO and upward HOMO shift. The *N*-phenyl carbazole derivatives (**35** and **36**) being less electron rich exhibited wide band gap.[295] Thus, conjures the blue shift in absorption spectra.
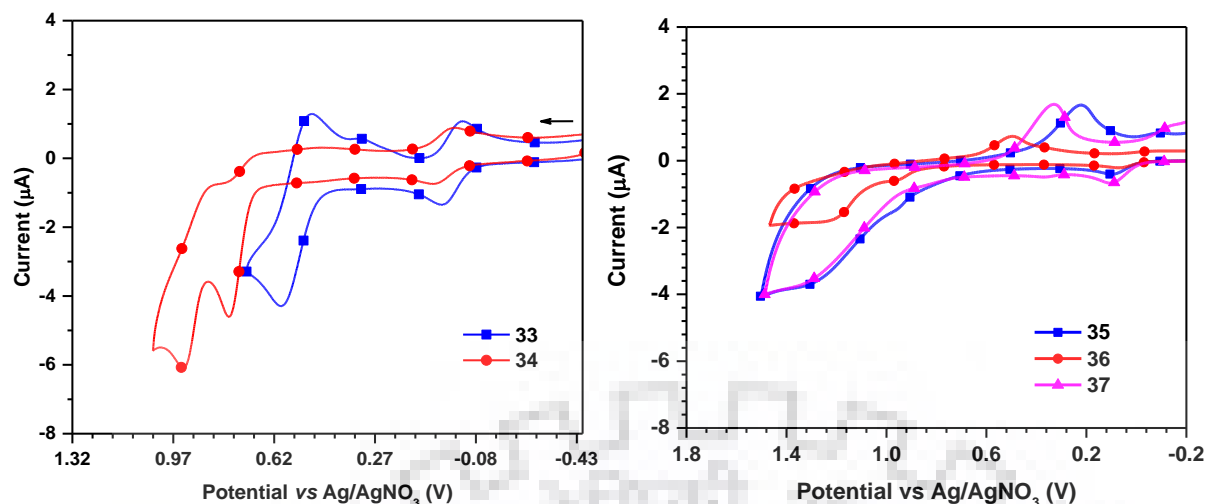
Figure 6.12. Cyclic voltammograms of the dyes recorded in DCM a) **33** and **34** b) **35**, **36** and **37**
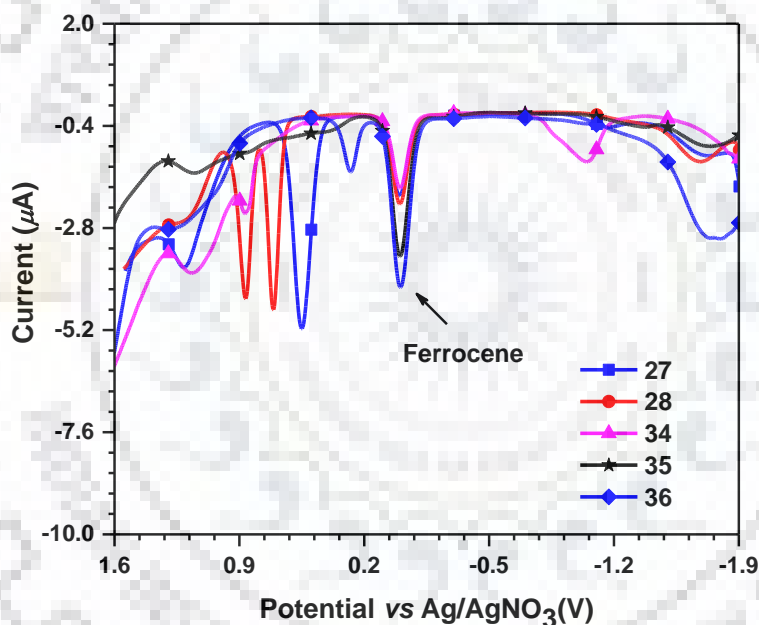
Figure 6.13. Differential Pulse Voltammogram of the dyes recorded in DCM

6.2.5 Theoretical Properties

Furthermore, computational studies were performed to understand the redox behaviors of the dyes. The structures for the dyes were optimized using density functional theory (DFT) with the Becke's three-parameter functional that was hybridized with the Lee−Yang−Parr correlation functional and 6-31 G(d,p) basis set.[159] The frontier molecular orbitals of the dyes displaying the electronic distributions are showed in Figure 6.14. The highest occupied molecular orbitals (HOMO) of the dyes are mainly constituted by the donor unit (*N*-phenyl carbazole, carbazole, triphenylamine unit and *N*-phenyl phenothiazine unit) substituted at

	LUMO+1	LUMO	HOMO	HOMO-1
33				
34				
35				
36				
37				
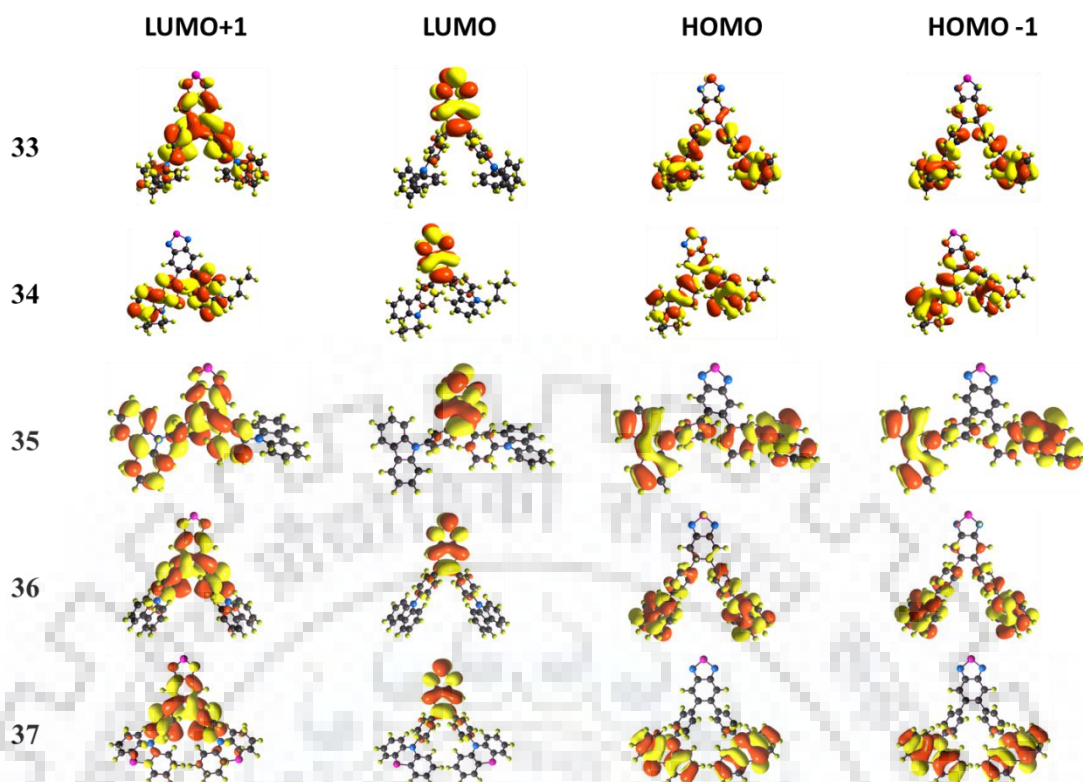
Figure 6.14. Composition of frontier molecular orbitals of the compounds.

Table 6.7 Computed absorption wavelengths and their oscillator strengths (*f*) of dyes.

Dye	λ_{abs} (nm)	*f*	Assignment (%)
33	376	0.5598	HOMO→LUMO (88%) HOMO-3→LUMO (7%)
34	360	0.5113	HOMO→LUMO (88%) HOMO-5→LUMO (5%)
35	332	0.5953	HOMO→LUMO (74%), HOMO-5→LUMO (20%),
	298	0.1695	HOMO-4→LUMO (49%), HOMO-1→LUMO (34%), HOMO-10→LUMO (5%)
	265	0.6109	HOMO-1→LUMO+1 (59%), HOMO→LUMO+4 (18%), HOMO→LUMO (7%)
36	324	0.0720	HOMO→LUMO (54%), HOMO-4→LUMO (21%), HOMO-5→LUMO (12%), HOMO-1→LUMO (9%),
	298	0.4654	HOMO-5→LUMO (73%), HOMO→LUMO (10%), HOMO-11→LUMO (6%)
37	304	0.7246	HOMO-4→LUMO (86%), HOMO-12→LUMO (6%),
38	424	0.6559	HOMO→LUMO (91%) HOMO-4→LUMO (5%)
	268	1.3438	HOMO→LUMO+3 (50%), HOMO-4→LUMO (22%), HOMO-2→LUMO+2 (6%),

lateral position. However, lowest unoccupied molecular orbitals (LUMOs) are mainly present on benzothiadiazole core. The large dihedral angle > 51° between BTD and donor unit with *N*-phenyl spacer (**35, 36** and **37**) twisted the chromophore out of the plane restricting the orbital overlap resulting well separated HOMO and LUMO orbitals. This suggests a weak ICT from electron rich donor units to benzothiadiazole acceptor. Interestingly this structural orientation imparts good morphology and high thermal stability for the materials. However, in the dyes 33

and 34 the HOMO is located on triphenylamine and carbazole respectively and also contributed by BTD unit exerts better donor-acceptor interaction compared to other dyes, due to strong electron donating nature.

6.2.6 Electroluminescence Characteristics

The thermal robustness, redox properties helps to fine tune the electroluminescent characteristics of the compounds **33, 34, 35** and **36** which were investigated by employing them as dopant in solution processed multilayered OLED devices. The configuration of device I and device II are ITO/PEDOT:PSS/ **33, 34** /TPBI/LiF/Al and ITO/PEDOT:PSS/CBP: **33, 34, 35** or **36** (5 or 10%)/TPBI/LiF/Al. The ITO and LiF/Al respectively works as anode and cathode. The poly(3,4-ethylene-dioxythiophene)epoly (styrenesulfonate) (PEDOT:PSS) served as a hole-injection layer and 1,3,5-tris(*N*-phenylbenzimidazol-2-yl)benzene (TPBI) as an electron-transporting layer. The dyes were doped in 4,4-bis(9*H*-carbazol-9-yl)biphenyl (CBP) which possessed suitable HOMO and LUMO to ensure efficient charge trapping by new dyes to construct the emitting layer (EML). The energy levels alignment of the materials used in the fabrication of the devices are depicted in Figure 6.15.
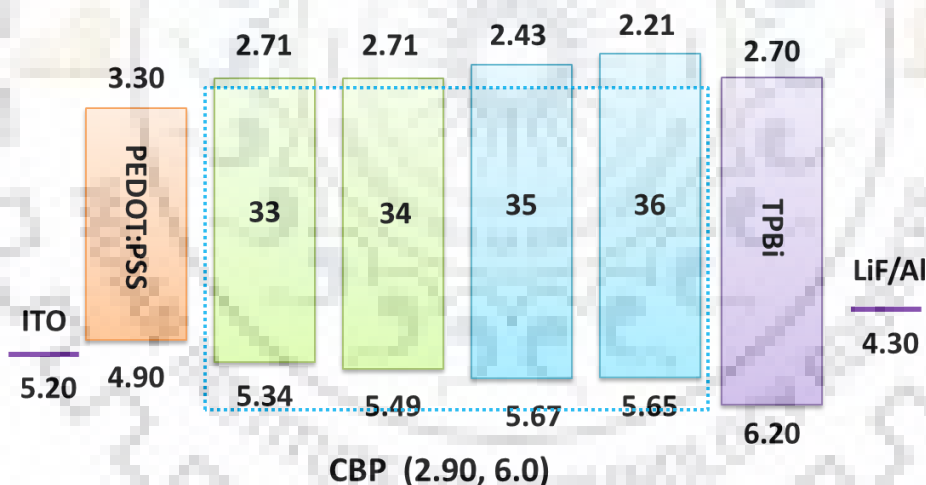
Figure 6.15 Energy-level diagram of the materials used for the fabrication of OLED devices (all values are in eV with respect to vacuum level).

The EL of device I showed red-shifted emission when compared to the corresponding dyes in device II, indicates an aggregation induced emission shift in device I. (Figure 6.16) Where on dilution in CBP, aggregation was reduced, however, when dopant concentration was increased to 5% or 10% red shift was observed, this point out that dilution is required to control the aggregation. Furthermore, in device doped with 1 wt% of **33** and **34** shoulder peak at 400 nm observed because of the residual emission from the CBP host. Similar shoulder peak

observed for **35** and **36** with 5 wt%. This was attributed to incomplete energy transfer, thus CBP layer favours the well recombination of electronically generated exciton within the layer.[191]
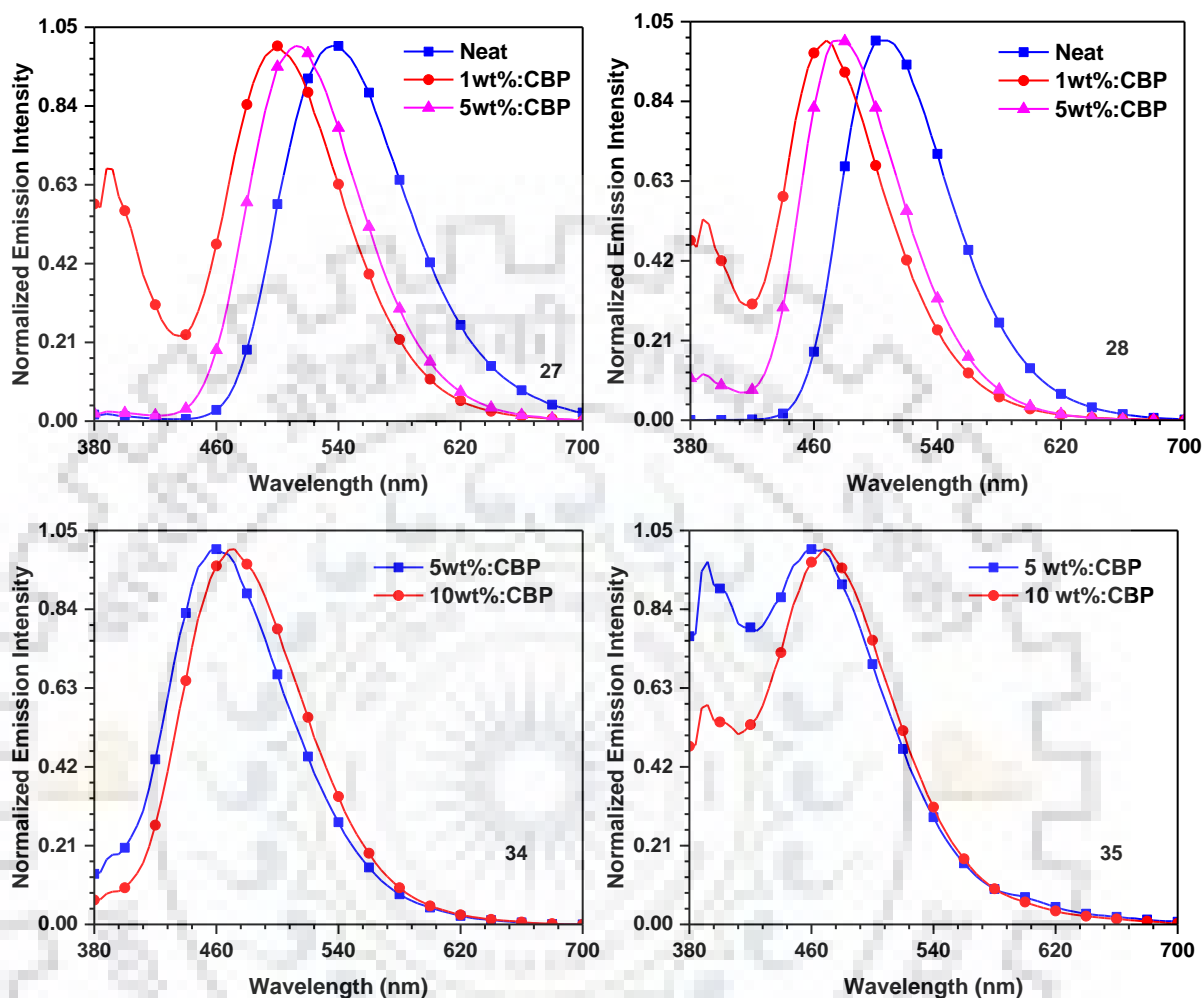
Figure 6.16 EL spectra of the diodes in different doping concentrations of (a) **33**(b) **34** (c) **35** and (d) **36**

Moreover, the energy level alignment for the devices (Figure 6.15) of **33** and **34** predicts an effective hole and electron injection compared to other dyes due to small hole and electron injection barrier at the HTM/dye and ETM/dye interface ie ~0.01 eV and 0.44-0.59 eV, respectively. However the *N*-pheny carbazole substituted dyes (**35** and **36**) displayed significant barrier (0.27-0.49 eV) (0.75-0.77) which may hinder the electron flow into the dye layer. Thus, we can assume that on varying the donor strength will produce diverse electroluminescence characteristics. The current density−voltage−luminance (I−V−L) plots of the devices are displayed in Figure 6.17, and pertinent data are listed in Table 6.6. The dyes **33** , **34** and **34** ,**35** with 5 wt % and 10 wt% dopant respectively exhibited high current densities and high luminance, this is because of the balanced confinement of charge carriers in the emitting layer

and effective capturing of electronically generated excitons in the CBP host matrix in the series. When the dyes are applied as 5 % dopant in CBP, the dye **33** and **34** exhibited green electroluminescence with high luminance of 1906/1152 cd m^{-2}), Commission International de l'Éclairage coordinates (CIE) coordinates (0.2 0.4)/(0.15, 0.19), current density of 3.8/1.6 cd A^{-1}, power efficiency of 2.3/0.9 lm W^{-1} and EQE of 1.7/ 1.3%. Interestingly, the dyes **35** and **36** exhibited blue electroluminescence with maximum luminance of 1464/966 cd m^{-2} with CIE coordinates (0.16 0.19), which are among first blue emitters to be reported with benzothiadiazole core.
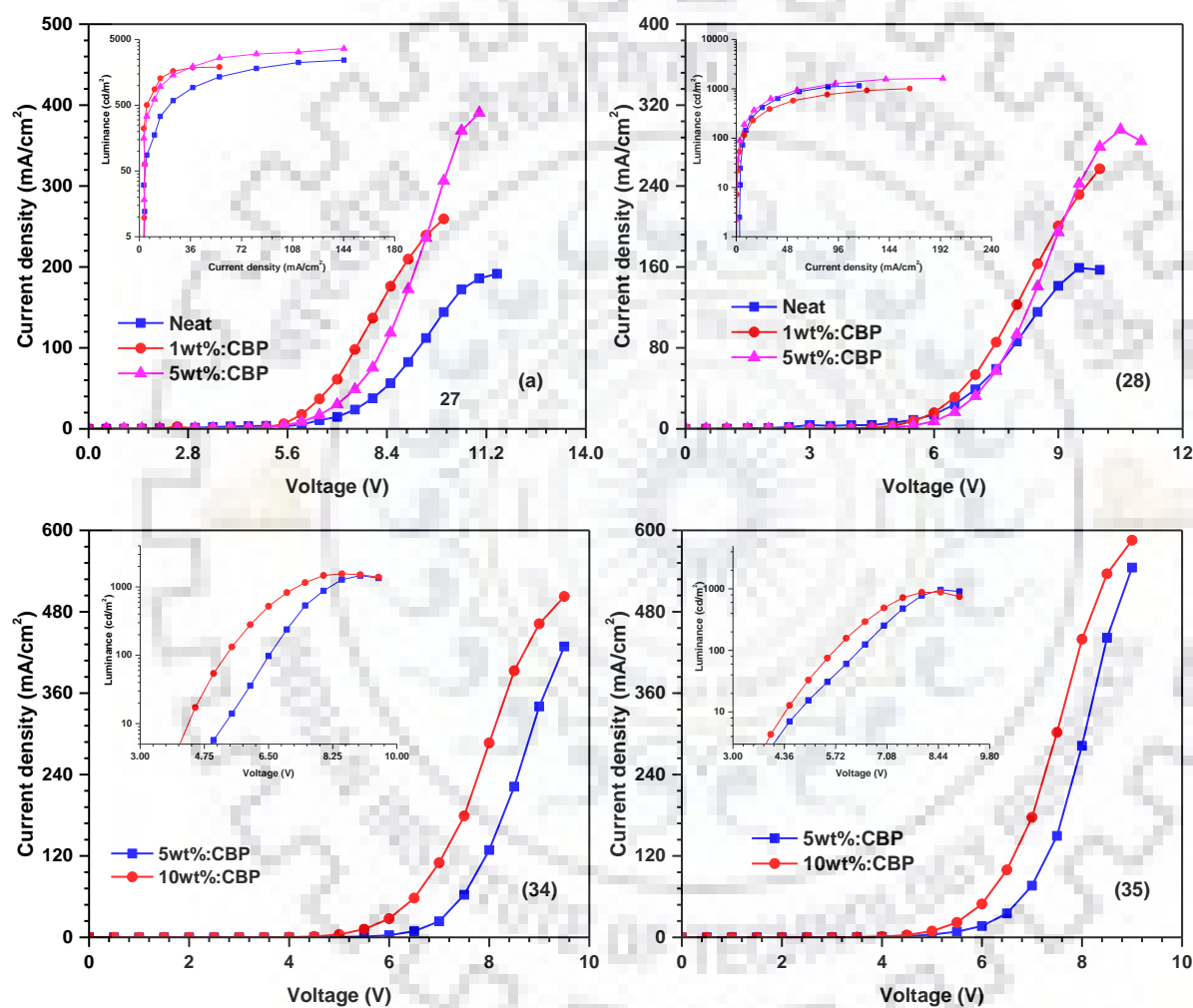
Figure 6.17 Current density–voltage- Luminance (I–V-L) plots of the diodes of (a) **33**(b) **34** (c) **35** and (d) **36**

Table 6.8 Electroluminescence characteristics of the dyes

Dye	Conc.(wt%)[a]	Turn on voltage (V)	Power Efficiency[b] (lm W^{-1})	Current Efficiency[b] (cd A^{-1})	EQE[b] (%)	CIE[b]	Max. luminescence (cd m^{-2})	EL max. (nm)
33	Neat	6.1/ 8.1	0.9/ 1.0	1.7/ 2.5	0.5/-	(0.35, 0.57)/-	2435	540
	1	5.1/ 6.7	2.3/ 1.1	3.8/ 2.3	1.7/ 1.2/-	(0.2, 0.4)/ (0.2, 0.36)	1906	500
	5	5.2/ 7.0	2.4/ 1.4	4.0/ 3.2	1.3/ 1.1/-	(0.24, 0.53)/ (0.23, 0.5)	3661	512
34	Neat	5.2/ 7.8	0.8/ 0.6	1.4/ 1.4	0.5/ -/-	(0.23, 0.52)/-	1152	500
	1	5.4/ 8.4	0.9/ 0.2	1.6/ 0.6	1.3/-/-	(0.15, 0.19)/-	1012	468
	5	5.6/ 7.6	1.5/ 0.7	2.7/ 1.6/	1.5/ -/-	(0.15, 0.27)/-	1632	476
35	5	5.1	0.5/-/1.6	1.6/-/1.9	0.7/-/1.9	(0.16, 0.19)	1464	460
	10	4.2	0.7/-/1.6	1.2/-/1.7	0.7/-/0.8	(0.16, 0.23)	1557	472
36	5	4.7	0.2/-/0.2	0.4/-/0.4	0.3/-/0.3	(0.17, 0.19)	966	460
	10	4.3	0.2/-/0.2	0.3/-/0.4	0.2/-/0.3	(0.16, 0.21)	893	468

100/1,000 /max cd/m^2

6.3. Conclusions

We have designed and synthesized a series of "V" shaped green-blue emitters containing triphenylamine, carbazole and *N*-phenylcarbazole unit on the benzothiadiazole core by employing Suzuki coupling reaction. The lateral substitution at C5 and C6 position of benzothiadiazole nucleus influenced the photophysical and electroluminescent properties significantly. The compound containing triphenylamine substitution (**33**) exhibited bathochromic shift in absorption spectra when compared to other derivatives. Among the carbazole containing dyes, simple modification of attachment with phenyl spacer (*para* and *meta*) *para* linked *N*-phenyl carbazole compound exhibited red shift in absorption and emission spectra due to extended π-conjugation. The rigid nature of triphenylamine and carbazole contributed the high thermal stabile compounds. The electroluminescent device using **33** as dopant in CBP host exhibited high luminance of 1906 cd m^{-2}, current efficiency (3.8 cd/A) and external quantum efficiency (1.7%), with CIE coordinates (0.2 0.4) corresponding to green emission at 100 cd/m^{-2} luminance. However, the *N*-phenylcarbazole substituted materials realized to achieve CIE coordinates (0.16 0.19), which is first report for BTD derivatives being employed as blue emitter to the best of our knowledge.

6.4. Experimental Section

6.4.5. Synthesis

5,6-Bis(9-butyl-9H-carbazol-3-yl)benzo[*c*][1,2,5]thiadiazole (**34**) A mixture of 5,6-dibromobenzo[*c*][1,2,5]thiadiazole (0.29 g, 1 mmol), (9-butyl-9*H*-carbazol-3-yl)boronic acid (0.66 g, 2.5 mmol), K$_2$CO$_3$ (0.82 g, 6.0 mmol), Pd(PPh$_3$)$_4$ (0.018 g, 6 mol%) and 20 mL THF:H$_2$O (3:1) was heated at 80 °C under nitrogen atmosphere. The progress of the reaction was monitored by TLC. After completion of the reaction, the reaction was quenched by the addition of water. The organic product was extracted with chloroform. The collected organic layer was thoroughly washed with brine solution and dried over anhydrous Na$_2$SO$_4$. The volatiles were removed to obtain a light yellow residue, which was purified by column chromatography on silica gel using hexanes/ chloroform (1:3) as eluant. Pale green Solid; yield 0.24 g, 42%; mp 192-194°C; ^{1}H NMR (400 MHz, CDCl$_3$, δ ppm):8.17 (s, 2H), 8.14 (s, 2H), 7.9(d, *J* = 4Hz, 2H), 7.37-7.46 (m, 4H), 7.15-7.21 (m, 4H), 7.10-7.13 (m, 4H), 1.47-1.4 (m, 4H), 1.25-1.36 (m, 4H), 0.8-0.9 (m, 4H); ^{13}C NMR (100 MHz, CDCl$_3$, δ ppm):154.4, 145.0,

140.6, 139.6, 131.3, 127.9, 125.6, 122.6, 121.8, 121.4, 120.3, 118.8, 108.7, 42.8, 31.0, 20.4, 13.8. HRMS (ESI-TOF) m/z: [M]$^+$ Calcd for $C_{38}H_{34}N_4S$ 578.2498, Found 578.2480.

4,4'-(Benzo[*c*][1,2,5]thiadiazole-5,6-diyl)bis(*N,N*-diphenylaniline) (33)

It is obtained from mixture of 5,6-dibromobenzo[*c*][1,2,5]thiadiazole (0.29 g, 1 mmol), (4-(diphenylamino)phenyl)boronic acid (0.66 g, 2.5 mmol) by following a procedure described above for **34**. Pale yellow solid; yield 0.45 g, 85%; mp 193-195 °C; ^{1}H NMR (400 MHz, CDCl$_3$, δ ppm):7.9 (s, 2H), 7.24(t, *J* = 8Hz, 8H), 7.08-7.10 (d, *J* = 8Hz, 8H), 7.0-7.03 (m, 8H), 6.96 (d, *J* = 4Hz, 4H); ^{13}C NMR (100 MHz, CDCl$_3$, δ ppm):147.2, 140.1, 139.9, 136.5, 126.8, 123.4, 122.1, 117.4, 115.9, 115.3, 113.9.;HRMS (ESI-TOF) m/z: [M]$^+$ Calcd for $C_{42}H_{30}N_4S$ 622.2185, Found 622.2176;

5,6-Bis(4-(9*H*-carbazol-9-yl)phenyl)benzo[*c*][1,2,5]thiadiazole (35)

It is obtained from mixture of 5,6-dibromobenzo[*c*][1,2,5]thiadiazole (0.2 g, mmol), (4-(9*H*-carbazol-9-yl)phenyl)boronic acid (0.42 g, 1.5 mmol) by following a procedure described above for **34**. Pale green solid; yield 0.30 g, 71%; mp 336-338 °C; ^{1}H NMR (400 MHz, CDCl$_3$, δ ppm):8.25(s, 2H); 8.15(d, *J* = 8 Hz, 4H);7.50-7.56 (m, 8H); 7.40-7.42 (d, *J* = 8Hz, 2H); 7.28-7.37 (m, 10H); ^{13}C NMR (100 MHz, CDCl$_3$, δ ppm): 154.2; 142.8; 140.6 139.1; 137.1; 131.3; 126.7; 126.1; 123.5; 122.1; 120.4; 120.1; 109.5; HRMS (ESI-TOF) m/z: [M+1]$^+$ Calcd for $C_{42}H_{26}N_4S$ 619.1951, Found 619.1947

5,6-Bis(3-(9*H*-carbazol-9-yl)phenyl)benzo[*c*][1,2,5]thiadiazole (36) It is obtained from mixture of 5,6-dibromobenzo[*c*][1,2,5]thiadiazole (0.2 g, mmol), (3-(9*H*-carbazol-9-yl)phenyl)boronic acid (0.53 g, 1.86 mmol) by following a procedure described above for **34**. Pale green; yield 0.34 g, 85%; mp 410-413 °C; ^{1}H NMR (400 MHz, CDCl$_3$, δ ppm):8.15(s, 2H); 8.07(d, *J* = 8 Hz, 4H);7.75-7.79 (m, 2H); 7.68 (d, *J* = 8Hz, 2H), 7.59 (d, *J* = 8Hz, 2H), 7.41 (s, 2 H), 7.18-7.24 (m, 8 H), 6.96 (d, *J* = 8 Hz, 4 H); ^{13}C NMR (100 MHz, CDCl$_3$, δ ppm): 154.2, 142.2, 140.4, 137.8, 130.5, 128.7, 128.3, 126, 125.9,123.3, 122.8, 120.2, 120, 109.5; HRMS (ESI-TOF) m/z: [M+1]$^+$ Calcd for $C_{42}H_{26}N_4S$ 619.1951, Found 619.1947

5,6-Bis(4-(10*H*-phenothiazin-10-yl)phenyl)benzo[*c*][1,2,5]thiadiazole (37) It is obtained from mixture of 5,6-dibromobenzo[*c*][1,2,5]thiadiazole (0.2 g, mmol), (4-(10*H*-phenothiazin-10-yl)phenyl)boronic acid (0.53 g, 1.86 mmol) by following a procedure described above for **34**. Yellow solid; yield 0.31 g, 68%; mp 260-263 °C; ^{1}H NMR (400 MHz, CDCl$_3$, δ ppm):8.24 (s, 2H); 8.14 (d, *J* = 8 Hz, 4H), 7.55-7.57 (m, 4H),7.48-7.51(m, 4 H), 7.39-7.41 (m, 4H), 732-7.36 (m, 4H), 7.28-7.29 (m, 4 H); ^{13}C NMR (100 MHz, CDCl$_3$, δ ppm): 154.2, 143.7, 142.7, 140.7,139.5, 132.2, 129.4, 127, 126.9, 122.8, 121.8, 121.3, 116.6; HRMS (ESI-TOF) m/z: [M+1]$^+$ Calcd for $C_{42}H_{26}N_4S_3$ 682.1314, 682.1295
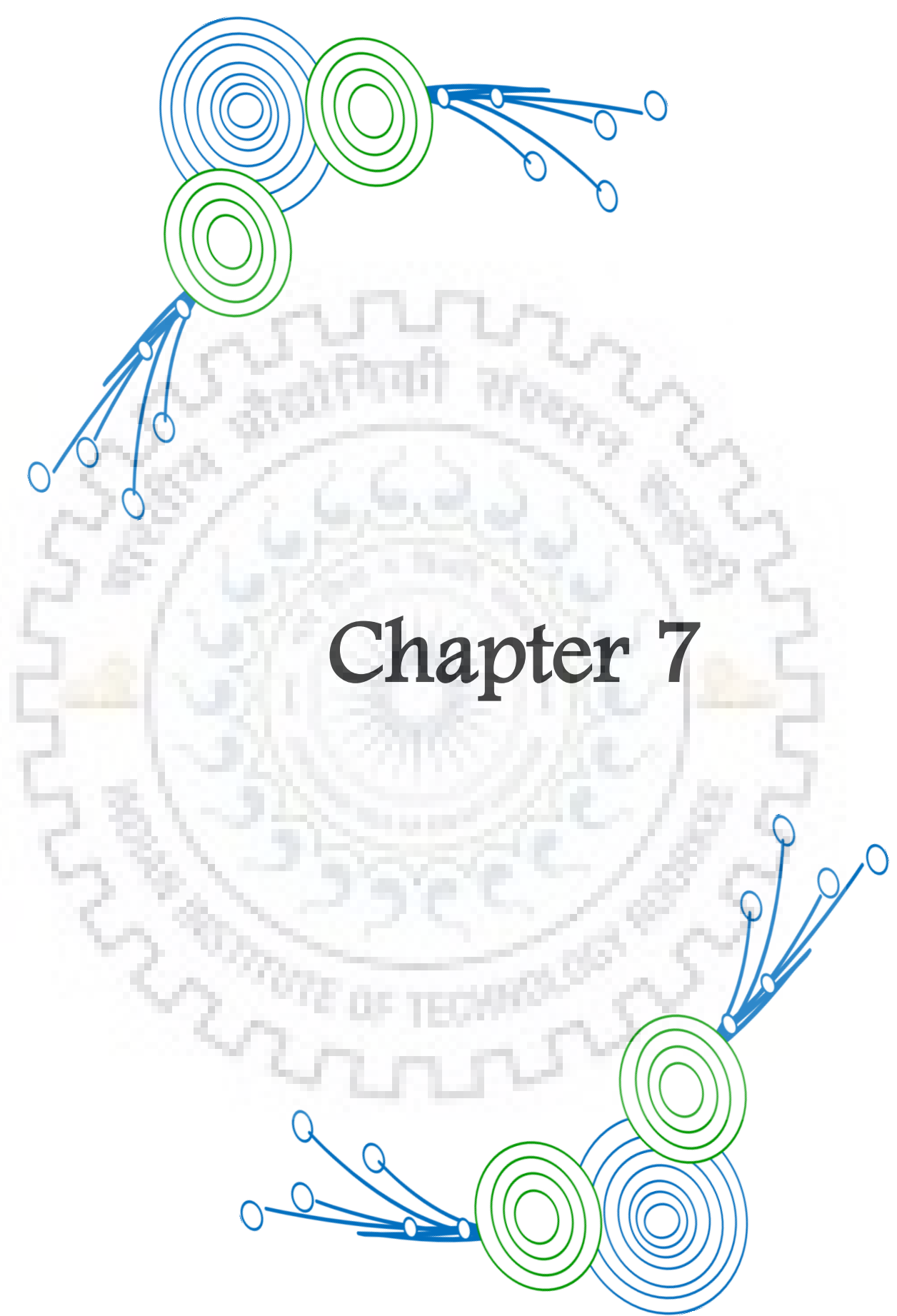
Chapter 7

Chapter 7

Summary

In this thesis we have pictured the different functionalization of benzothiadiazole unit and further characterized to build the structure-property relationship for them. The materials were synthesized by following different palladium catalyzed coupling (Suzuki, Stille) and condensation protocols. The synthesized dyes showed the decisive role of benzothiadiazole-based compound and also unraveled the significant progress related to physicochemical, thermal, electrochemical characterization electronic applications of benzothiadiazole-based compound used in DSSCs and luminescent materials in OLEDs

Chapter 3

- ✓ Here, a series of 5-methylbenzo[*d*][1,2,3]thiadiazole based derivatives have been synthesized using palladium catalyzed selective Suzuki-Miyaura coupling reaction resulted in eight regioisomers.

- ✓ The effect of methyl substitution on electronic absorption, emission, thermal, electrochemical and electroluminescent characteristics was studied in detailed.

- ✓ The dyes containing methyl unit near *tert*-butylpheny showed red-shifted absorption when compared to its regioisomer due to interrupted π-conjugation between triphenylamine/ *N*-phenylcarbazole and benzothiadiazole probably twisted and affected the conjugative delocalization of the π-electron which inferred to blue shift.

- ✓ The geometrical changes in the ground (non-planar) and excited (more planar) states manifested in the absorption and emission properties.

- ✓ The dyes displayed positive solvatochromism in the emission spectra indicative of more pronounced intramolecular charge transfer in the excited state.

- ✓ The compound containing disubstituted triphenylamine exhibited high lying HOMO in the series while the LUMO is stabilized in *tert*-butylpheny substituted compound.

- ✓ The electronic structure correlations are supported by density functional calculations..

- ✓ All of the compounds exhibited exceptional thermal stability attributable to the rigid (MBTD) building block.

✓ Solution processed multi-layered OLED device were fabricated employing these compounds either as host emitters or dopant emitters in suitable host matrix and exhibited green/yellowish green electroluminescence

Chapter 4

✓ Here, we demonstrate two sets of benzimidazole-benzothiadiazole conjugates to tune the optical, electrochemical and electroluminescent properties.

✓ The benzothiadiaozle unit recognized as rational electron accepting core to produce the extensive gamut of emitters from blue to red region, in virtue of its bulky conjugated structure and excellent electron-accepting ability.

✓ The one set of compounds deals with different functionalization of benzimidazole unit on benzothiadiazole nuclei. Whereas, the other set of series contains dyes where benzimidazole unit is substituted at lateral position followed by substitution of triphenylamine, carbazole and phenyl-benzimidazole chromophores at C4 and C7 positions of benzothiadiazole nuclei.

✓ The introduction of *N*-phenylbenzimidazole unit considered to impart rigidity to molecule and helps in reducing aggregation propensity. Also thrives electron-transporting ability to the resulting materials and facilitate electron injection.

✓ The different substitution pattern showed its intense impact on photophysical, thermal, electrochemical and electroluminescent characteristics.

✓ The tri- benzimidazole substituted chromophore showed red shift compared to substituted at C4 and C7, this suggests the lateral substitution may be participating in extending the conjugation.

✓ The dye containing lateral benzimidazole exhibits distinct HLCT nature with moderate quantum yield of 25-75%. The device with 5% dopant concentration exhibited satisfactorily performance with violet, green, yellow and orange-red emission.

✓ The thiophene based compound as orange-red emitter exhibited excellent performance in the series which is attributed to the utilization of both energies of LE and CT excitons (i.e., hybridized local and charge transfer (HLCT))

Chapter 5

✓ Here, we have designed and synthesized a series of compound based on 5-methyl benzothiadiazole to demonstrate the variation of properties by changing the position of methyl group with respect to spacer for dye sensitized solar cell application.
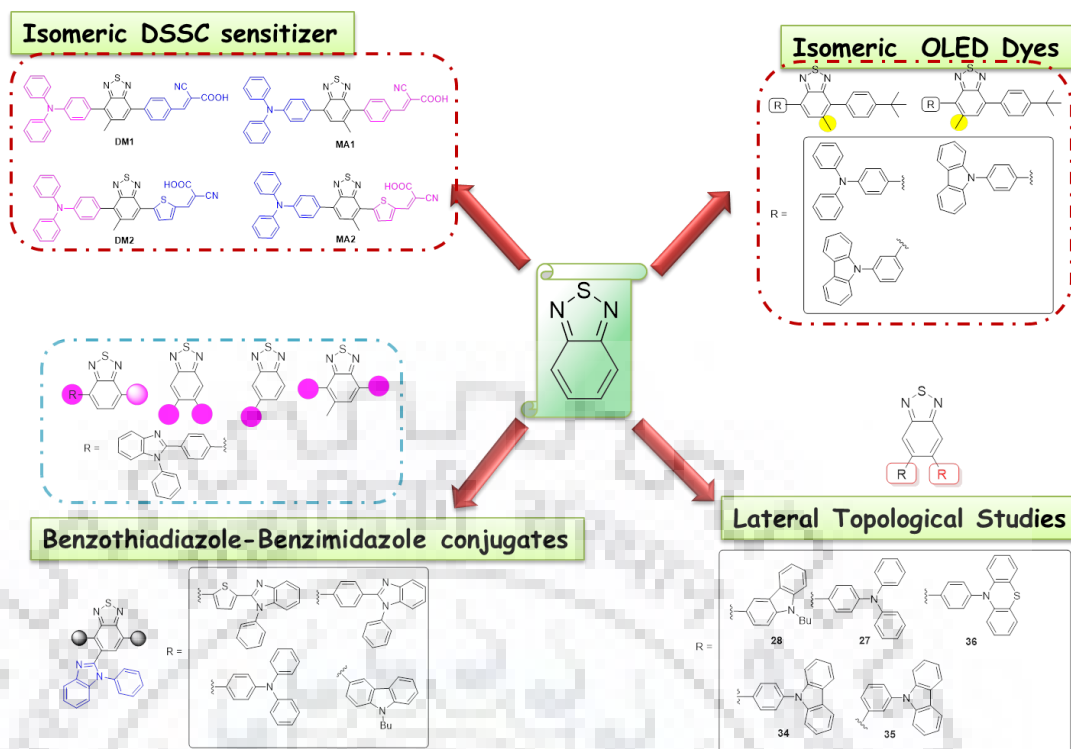
- ✓ The compound containing methyl unit substituted near donor exhibited high molar extinction coefficient, strong light harvesting ability, and better photovoltaic performances compared to their congeners where methyl unit positioned near acceptor.
- ✓ The compounds tethered with benzene or thiophene as spacer modulates the electronic communication, influencing light harvesting and in turn efficiency.
- ✓ Consequently, investigation of DSSCs performances under standard global AM 1.5 solar conditions, the dyes containing methyl unit substituted near donor with thiophene as spacer exhibited two fold increment in power conversion efficiency (PCE) value upto 4.33% compared to its congener (2.71%).

Chapter 6

- ✓ Here, a series of lateral substituted benzothiadiazole hybrids are presented.
- ✓ The substitution at C5 and C6 position of benzothiadiazole nuclei have been analysed by photophysical, electrochemical, thermal and electroluminescence properties.
- ✓ The compound containing triphenylamine substitution exhibited bathochromic shift in absorption spectra compared to other derivatives.
- ✓ Among the carbazole containing dyes, simple modification of attachment with phenyl unit (*para* and *meta*) *para* linked *N*-phenyl carbazole compound exhibited red shift absorption and emission spectra with extended π-conjugation.
- ✓ This work provides the photophysical, electrocluminescence insight into lateral functionalization with classical donor-acceptor energy pair in comparison with linear isomers.

Isomeric DSSC sensitizer

Isomeric OLED Dyes

Benzothiadiazole-Benzimidazole conjugates

**Lateral Topological Studies**

Future Perspectives

Moreover, by looking into the literature, the scope for benzothiadiazole-based blue OLED is still required to be investigated. Thus we proposed to design the dye using phenyl unit which being non-planar will restricts the conjugation and cyano and pyrene unit favours to be .use as blue emitters. It may also can be promising design for HLCT, as lateral position may extensively allow partial orbital overlapping.
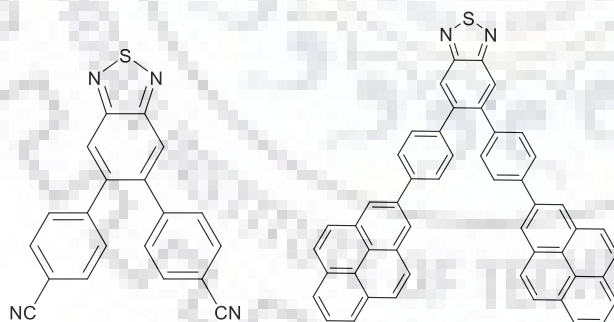
Interestingly, we can introduce benzothiadiazole-based covalent organic framework (COF) materials for optoelectronic applications. The introduction of covalent organic frameworks (COF) diversified the field for chemist, which deals with stable, porous organic crystalline framework. Interestingly, exploration of BTD in new materials, as promisingly tune the band gap and improve the charge separation and adjoins the conjugation. So the idea to introduce both donor and acceptor, providing amvbipolar electron and hole transport which suggest the good phtocoonductivity according to charge carrier probability. The idea to synthesize this COF, adopts hexagonal skeletton

191
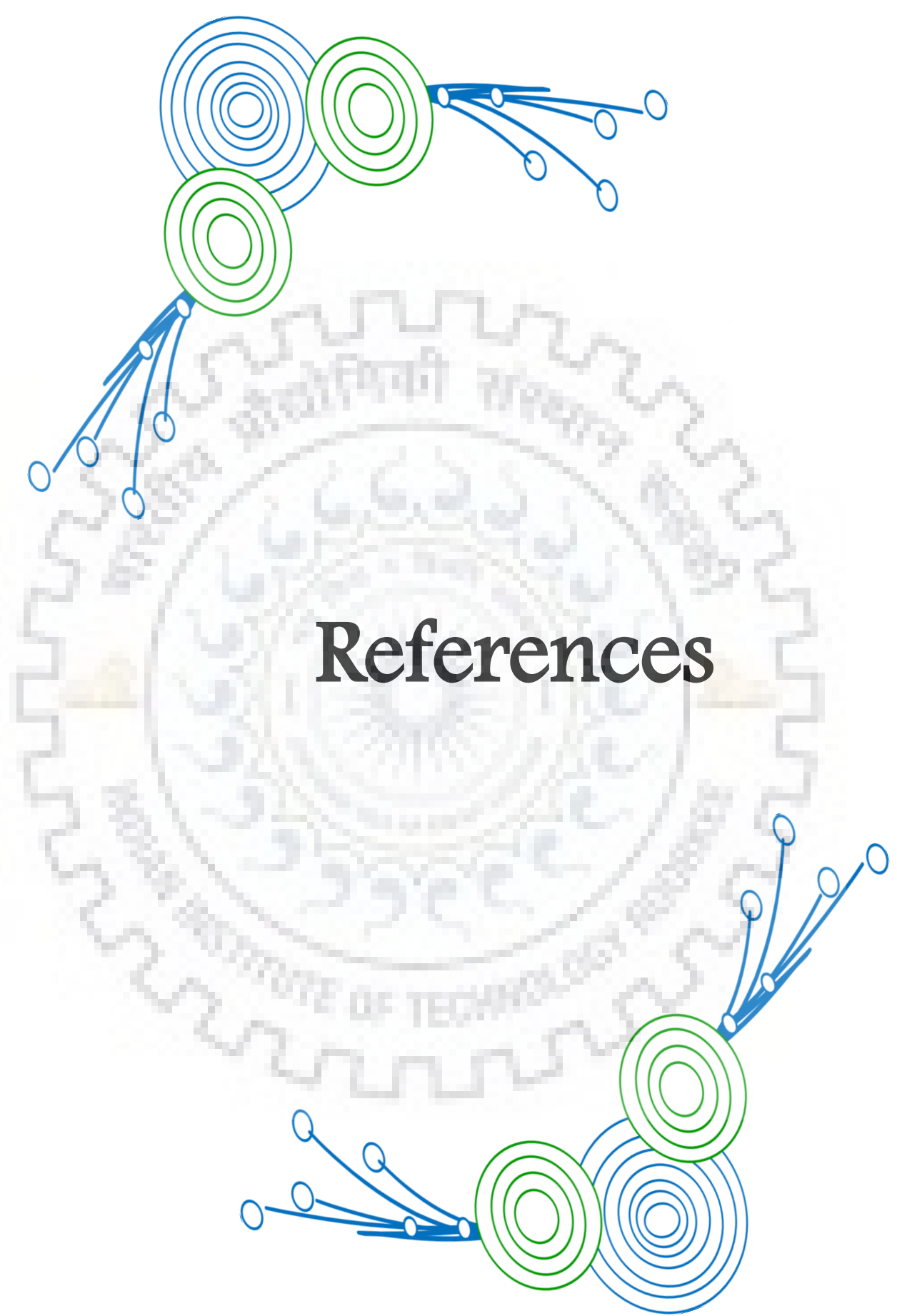
References

REFERENCES

[1]   Shirota, Y. Organic materials for electronic and optoelectronic devices. *J. Mater. Chem.* **2000**, *10*, 1-25.

[2]   Tang, C. W.; Vanslyke, S. A. Organic Electroluminescent Diodes. *Appl. Phys. Lett.* **1987**, *51*, 913–915.

[3]   Tang, C. W.; Vanslyke, S. A.; Chen, C. H. Electroluminescence of Doped Organic Thin Films. *J. Appl. Phys.* **1989**, *65*, 3610–3616.

[4]   Anthony, J. E. Small-Molecule, Nonfullerene Acceptors for Polymer Bulk Heterojunction Organic Photovoltaics. *Chem. Mater.* **2011**, *23*, 583–590.

[5]   Mei, J.; Diao, Y.; Appleton, A. L.; Fang, L.; Bao, Z. Integrated Materials Design of Organic Semiconductors for Field-Effect Transistors. *J. Am. Chem. Soc.* **2013**, *135*, 6724–6746.

[6]   Klikar, M.; Le Poul, P.; Ružička, A.; Pytela, O.; Barsella, A.; Dorkenoo, K. D.; Robin-Le Guen, F.; Bureš, F.; Achelle, S. Dipolar NLO Chromophores Bearing Diazine Rings as π-Conjugated Linkers. *J. Org. Chem.* **2017**, *82*, 9435–9451.

[7]   Organic Semiconductors for Biological Sensing. *J. Mater. Chem. C* **2019**, *7*, 1111–1130.

[8]   Ni, W.; Wan, X.; Li, M.; Wang, Y.; Chen, Y. A-D-A Small Molecules for Solution-Processed Organic Photovoltaic Cells. *Chem. Commun.* **2015**, *51*, 4936–4950.

[9]   Clifford, J. N.; Martínez-Ferrero, E.; Viterisi, A.; Palomares, E. Sensitizer Molecular Structure-Device Efficiency Relationship in Dye Sensitized Solar Cells. *Chem. Soc. Rev.* **2011**, *40*, 1635–1646.

[10]   Ren, X.; Jiang, S.; Cha, M.; Zhou, G.; Wang, Z. S. Thiophene-Bridged Double D-π-A Dye for Efficient Dye-Sensitized Solar Cell. *Chem. Mater.* **2012**, *24*, 3493–3499.

[11]   Choi, H.; Baik, C.; Kang, S. O.; Ko, J.; Kang, M. S.; Nazeeruddin, M. K.; Grätzel, M. Highly Efficient and Thermally Stable Organic Sensitizers for Solvent-Free Dye-Sensitized Solar Cells. *Angew. Chem Int. Ed.* **2008**, *47*, 327–330.

[12]   Okumoto, K.; Kanno, H.; Hamada, Y.; Takahashi, H.; Shibata, K. High Efficiency Red Organic Light-Emitting Devices Using Tetraphenyldibenzoperiflanthene-Doped Rubrene as an Emitting Layer. *Appl. Phys. Lett.* **2006**, *89*, 1–4.

[13]   Reineke, S.; Lindner, F.; Schwartz, G.; Seidler, N.; Walzer, K.; Lüssem, B.; Leo, K. White Organic Light-Emitting Diodes with Fluorescent Tube Efficiency. *Nature* **2009**, *459*, 234–238.

References

[14]   Tyagi, P.; Venkateswarao, A.; Thomas, K. R. J. Solution Processable Indoloquinoxaline Derivatives Containing Bulky Polyaromatic Hydrocarbons: Synthesis, Optical Spectra, and Electroluminescence. *J. Org. Chem.* **2011**, *76*, 4571.

[15]   Raimundo, J. M.; Blanchard, P.; Brisset, H.; Akoudand, S.; Roncali, J. Proquinoid acceptors as building blocks for the design of efficient π-conjugated fluorophores with high electron affinity. *Chem. Commun.* **2000**, 939.

[16]   Neto, B. A. D.; Lapis, A. A. M.; Da Silva Júnior, E. N.; Dupont, J. 2,1,3-Benzothiadiazole and Derivatives: Synthesis, Properties, Reactions, and Applications in Light Technology of Small Molecules. *European J. Org. Chem.* **2013**, *2*, 228–255

[17]   Li, Y.; Li, A.-Y.; Li, B.-X.; Huang, J.; Zhao, L.; Wang, B.-Z.; Li, J.-W.; Zhu, X.-H.; Peng, J.; Cao, Y.; Ma, D.-G.; Roncali, J. Asymmetrically 4,7-Disubstituted Benzothiadiazoles as Efficient Non-doped Solution-Processable Green Fluorescent Emitters. *Org. Lett.,* **2009**, *11*, 5318

[18]   Cho, N.; Song, K.; Lee, J. K.; Ko, J. Facile Synthesis of Fluorine-Substituted Benzothiadiazole-Based Organic Semiconductors and Their Use in Solution-Processed Small-Molecule Organic Solar Cells. *Chem. Asian Eur. J.* **2012**, *18*, 11433–11439.

[19]   Cho, N.; Han, J.; Song, K.; Kang, M. S.; Jun, M. J.; Kang, Y.; Ko, J. Substituent Effect of Fluorine Atom on Benzothiadiazole Bridging Unit in Dye Sensitized Solar Cells. *Tetrahedron* **2014**, *70*, 427–433.

[20]   D. P. Hagberg , T. Marinado , K. M. Karlsson , K. Nonomura, P. Qin , G. Boschloo , T. Brinck , A. Hagfeldt , L. Sun, Tuning the HOMO and LUMO energy levels of organic chromophores for dye sensitized solar cells, *J. Org. Chem.* **2007**, *72*, 9550-9556

[21]   Thangthong, A.; Prachumrak, N.; Saengsuwan, S.; Namuangruk, S.; Keawin, T.; Jungsuttiwong, S.; Sudyoadsuka, T.; Promarak, V. Multi-triphenylamine-substituted bis(thiophenyl)benzothiadiazoles as highly efficient solution-processed non-doped red light-emitters for OLEDs. *J. Mater. Chem. C*, **2015**, *3*, 3081

[22]   Chou, H.-H.; Chen, Y.-C.; Huang, H.-J.; Lee, T.-H.; Lin, J. T.; Tsaic, C.; Chen, K. High-performance dye-sensitized solar cells based on 5,6-bis-hexyloxy-benzo[2,1,3]thiadiazole, *J. Mater. Chem.* **2012**, *22*, 10929-10938

[23]   Kono, T.; Kumaki, D.; Nishida, J.-i.; Sakanoue, T.; Kakita, M.; Tada, H.; Tokito, S.; Yamashita, Y. High-Performance and Light-Emitting *n*-Type Organic Field-Effect Transistors Based on Dithienylbenzothiadiazole and Related Heterocycles. *Chem. Mater.* **2007**, *19*, 1218

[24]   Du, J.; Biewer, M. C.; Stefan, M. C. Benzothiadiazole Building Units in Solution-Processable Small Molecules for Organic Photovoltaics. *J. Mater. Chem. A* **2016**, *4*, 15771–15787

[25]   Jiang, J.; Hu, D.; Hanif, M.; Li, X.; Su, S.; Xie, Z.; Liu, L.; Zhang, S.; Yang, B.; Ma, Y. Twist Angle and Rotation Freedom Effects on Luminescent Donor–Acceptor Materials: Crystal Structures, Photophysical Properties, and OLED Application. *Adv. Optical Mater*. **2016**, *4, * 2109.

[26]   Zhu, W.; Wu, Y.; Wang, S.; Li, W.; Li, X.; Chen, J.; Wang, Z. S.; Tian, H. Organic D-A-π-A Solar Cell Sensitizers with Improved Stability and Spectral Response. *Adv. Funct. Mater.* **2011**, *21,* 756–763.

[27]   Jiang, D.; Chen, S.; Xue, Z.; Li, Y.; Liu, H.; Yang, W.; Li, Y. Donor-Acceptor Molecules Based on Benzothiadiazole: Synthesis, X-Ray Crystal Structures, Linear and Third-Order Nonlinear Optical Properties. *Dyes Pigments* **2016**, *125*, 100–105.

[28]   Pilgram, K.; Zupan, M.; Skiles, R. Bromination of 2,1,3-benzothiadiazoles. *J. Hetrocycl. Chem.* **1970**, *7*, 629.

[29]   Cai, J.; Liu, L.; Hong, K. H.; Wang, P.; Li, L.; Cao, M.; Sun, C.; Wu, X.; Zong, X.; Chen, J.; et al. Discovery of Phenoxybutanoic Acid Derivatives as Potent Endothelin Antagonists with Antihypertensive Activity. *Bioorganic Med. Chem.* **2015**, *23*, 657–667.

[30]   Huang, Y.; Ye, L.; Wu, F.; Mei, S.; Chen, H.; Tan, S. Synthesis and Photovoltaic Properties of Two-Dimensional Copolymers Based on Novel Benzothiadiazole and Quinoxaline Acceptors with Conjugated Dithienylbenzothiadiazole Pendants. *J. Polym. Sci. Part A Polym. Chem.* **2016**, *54*, 668–677.

[31]   Zhang, Q.; Zhang, J.; Zuo, H.; Wang, C.; Shen, Y. A Novel Colorimetric and Fluorescent Sensor for Cyanide Anions Detection Based on Triphenylamine and Benzothiadiazole. *Tetrahedron* **2016**, *72*, 1244–1248.

[32]   Zhang, Q.; Zhang, J.; Zuo, H.; Wang, C.; Shen, Y. A Novel Near-Infrared Chemosensor for Mercury Ion Detection Based on D-A Structure of Triphenylamine and Benzothiadiazole. *Tetrahedron* **2017**, *73*, 2824–2830.

[33]   Nazeeruddin, M.K.; Kay, A.; Rodicio, I.; Humphrybaker, R.; Muller, E.; Liska, P.; Vlachopoulos, N.; Grätzel, M., Conversion of light to electricity by cis-X2bis(2,2'-bipyridyl-4,4'-dicarboxylate)ruthenium(II) charge-transfer sensitizers (X = Cl-, Br-, I-, CN-, and SCN-) on nanocrystalline titanium dioxide electrodes, *J. Am. Chem. Soc*. **1993**, *115*, 6382–6390.

References

[34] Wangdong, Z.; Yiming, C.; Yu, B.; Yinghui, W.; Yushuai, S.; Min, Z.; Fangfang, W.; Chunyue, P.; Peng, W., Efficient dye-sensitized solar cells with an organic photosensitizer featuring orderly conjugated ethylenedioxythiophene and dithienosilole blocks. *Chem. Mater.* **2010**, *22*, 1915−1925.

[35] Zhang, G.; Bala, H.; Cheng, Y.; Shi, D.; Lv, X.; Yu, Q.; Wang, P., High efficiency and stable dye-sensitized solar cells with an organic chromophore featuring a binary π-conjugated spacer, *Chem. Commun.* **2009**, 2198-2200.

[36] Cai, S.; Tian, G.; Li, X.; Su, J.; Tian, H. Efficient and Stable DSSC Sensitizers Based on Substituted Dihydroindolo[2,3-*b*]Carbazole Donors with High Molar Extinction Coefficients. *J. Mater. Chem. A* **2013**, *1*, 11295−11305.

[37] Wang, X.; Yang, J.; Yu, H.; Li, F.; Fan, L.; Sun, W.; Liu, Y.; Koh, Z. Y.; Pan, J.; Yim, W. L.; et al. A Benzothiazole–Cyclopentadithiophene Bridged D–A−π–A Sensitizer with Enhanced Light Absorption for High Efficiency Dye-Sensitized Solar Cells. *Chem. Commun.* **2014**, *50*, 3965−3968.

[38] Ning, Z.; Zhang, Q.; Pei, H.; Luan, J.; Lu, C.; Cui, Y.; Tian, H. Photovoltage Improvement for Dye-Sensitized Solar Cells via Cone-Shaped Structural Design. *J. Phys. Chem. C* **2009**, *113*, 10307−10313.

[39] Fan, W. J.; Cai, J. W.; Yang, G. J.; Chi, J. W.; Zhou, D.; Tan, D. Z.; Zhang, R. Q. Aggregation of Metal-Free Organic Sensitizers on TiO$_2$(1 0 1) Surface for Use in Dye-Sensitized Solar Cells: A Computational Investigation. *Comput. Theor. Chem.* **2016**, *1093*, 1−8.

[40] Xie, Y.; Wu, W.; Zhu, H.; Liu, J.; Zhang, W.; Tian, H.; Zhu, W. H. Unprecedentedly Targeted Customization of Molecular Energy Levels with Auxiliary-Groups in Organic Solar Cell Sensitizers. *Chem. Sci.* **2016**, *7*, 544−549.

[41] Duan, T.; Hsiao, T. Y.; Chi, Y.; Chen, X.; He, Y.; Zhong, C. End-Capped "Thiophene-Free" Organic Dye for Dye-Sensitized Solar Cell: Optimized Donor, Broadened Spectra and Enhanced Open-Circuit Voltage. *Dyes Pigments* **2016**, *124*, 45−52.

[42] Yan, R.; Qian, X.; Jiang, Y.; He, Y.; Hang, Y.; Hou, L. Ethynylene-Linked Planar Rigid Organic Dyes Based on Indeno[1,2-*b*]Indole for Efficient Dye-Sensitized Solar Cells. *Dyes Pigments* **2017**, *141*, 93−102.

[43] Eom, Y. K.; Hong, J. Y.; Kim, J.; Kim, H. K. Triphenylamine-Based Organic Sensitizers with π-Spacer Structural Engineering for Dye-Sensitized Solar Cells: Synthesis, Theoretical Calculations, Molecular Spectroscopy and Structure-Property-Performance Relationships. *Dyes Pigments* **2017**, *136*, 496−504.

[44] Liu, Z.; Duan, K.; Guo, H.; Deng, Y.; Huang, H.; Yi, X.; Chen, H.; Tan, S. The Enhancement of Photovoltaic Properties of the DSSCs Based on D−A−π−A Organic Dyes via Tuning Auxiliary Acceptor. *Dyes Pigments* **2017**, *140*, 312–319.

[45] Huang, L.; Ma, P.; Deng, G.; Zhang, K.; Ou, T.; Lin, Y.; Wong, M. S. Novel Electron-Deficient Quinoxalinedithienothiophene and Phenazinedithienothiophene-Based Photosensitizers: The Effect of Conjugation Expansion on DSSC Performance. *Dyes. Pigments.* **2018**, *159*, 107–114.

[46] Lee, D. H.; Lee, M. J.; Song, H. M.; Song, B. J.; Seo, K. D.; Pastore, M.; Anselmi, C.; Fantacci, S.; De Angelis, F.; Nazeeruddin, M. K.; et al. Organic Dyes Incorporating Low-Band-Gap Chromophores Based on π-Extended Benzothiadiazole for Dye-Sensitized Solar Cells. *Dyes Pigments* **2011**, *91*, 192–198.

[47] Yigit, M. Z.; Bilgili, H.; Sefer, E.; Demic, S.; Zafer, C.; Can, M.; Koyuncu, S. Effect of a π-Bridging Unit in Triphenylamine-Benzothiadiazole Based Donor Acceptor Chromophores for Dye-Sensitized Solar Cells. *Electrochemica. Acta* **2014**, *147*, 617–625.

[48] Huang, Z.-S.; Zang, X.F.; Hua, T.; Wang, L.; Meier, H.; Cao, D., 2,3-Dipentyldithieno[3,2-*f*:2′,3′-*h*]quinoxalineBased Organic Dyes for Efficient Dye-Sensitized Solar Cells: Effect of π-Bridges and Electron Donors on Solar Cell Performance *ACS Appl. Mater. Interfaces* **2015**, *7*, 20418−20429.

[49] Li, F.; Chen, Y.; Zong, X.; Qiao, W.; Fan, H.; Liang, M.; Xue, S. New Benzothiadiazole Based Dyes Incorporating Dithieno[3,2-*b*:2′,3′-*d*]Pyrrole (DTP) π-Linker for Dye-Sensitized Solar Cells with Different Electrolytes. *J. Power Sources* **2016**, *332*, 345–354.

[50] Jia, H. L.; Zhang, M. D.; Yan, W.; Ju, X. H.; Zheng, H. G. Effects of Structural Optimization on the Performance of Dye-Sensitized Solar Cells: Spirobifluorene as a Promising Building Block to Enhance V_{OC}. *J. Mater. Chem. A* **2016**, *4*, 11782–11788.

[51] Zhu, W.; Wu, Y.; Wang, S.; Li, W.; Li, X.; Chen, J.; Wang, Z. S.; Tian, H. Organic D-A-π-A Solar Cell Sensitizers with Improved Stability and Spectral Response. *Adv. Funct. Mater.* **2011**, *21*, 756–763.

[52] Seo, K. D.; Choi, I. T.; Kim, H. K. Organic Dyes with Well-Defined Structures for Highly Efficient Dye-Sensitised Solar Cells Based on a Cobalt Electrolyte. *Chem. Eur. J.* **2015**, *21*, 14804–14811.

References

[53] Seo, K. D.; Choi, I. T.; Park, Y. G.; Kang, S.; Lee, J. Y.; Kim, H. K. Novel D-A-π-A Coumarin Dyes Containing Low Band-Gap Chromophores for Dye-Sensitised Solar Cells. *Dyes Pigments* **2012**, *94*, 469–474.

[54] Fernandes, S. S. M.; Pereira, A.; Ivanou, D.; Mendes, A.; Raposo, M. M. M. Benzothiadiazole Derivatives Functionalized with Two Different (Hetero)Aromatic Donor Groups: Synthesis and Evaluation as TiO_2 Sensitizers for DSSCs. *Dyes Pigments* **2018**, *151*, 89–94.

[55] Dall'Agnese, C.; Komatsu, K.; Koshika, M.; Morikawa, D.; Moineau-Chane Ching, K. I.; Mori, S. Enhancement of Quantum Efficiency by Co-Adsorbing Small Julolidine Dye and Bulky Triphenylamine Dye in Dye-Sensitized Solar Cells. *J. Photochem. Photobiol. A Chem.* **2018**, *356*, 403–410.

[56] Keerthi, A.; Sriramulu, D.; Liu, Y.; Yuan Timothy, C. T.; Wang, Q.; Valiyaveettil, S. Architectural Influence of Carbazole Push-Pull-Pull Dyes on Dye Sensitized Solar Cells. *Dyes Pigments* **2013**, *99*, 787–797.

[57] Velusamy, M.; Thomas, K. R. J.; Lin, J. T.; Hsu, Y. C.; Ho, K. C. Organic Dyes Incorporating Low-Band-Gap Chromophores for Dye-Sensitized Solar Cells. *Org. Lett.*, **2005**, 7, 1899–1902.

[58] Feng, Q.; Jia, X.; Zhou, G.; Wang, Z. S. Embedding an Electron Donor or Acceptor into Naphtho[2,1-*b*:3,4-*b*′] Dithiophene Based Organic Sensitizers for Dye-Sensitized Solar Cells. *Chem. Commun.* **2013**, *49*, 7445–7447.

[59] Gao, Y.; Li, X.; Hu, Y.; Fan, Y.; Yuan, J.; Robertson, N.; Hua, J.; Marder, S. R. Effect of an Auxiliary Acceptor on D-A-π-A Sensitizers for Highly Efficient and Stable Dye-Sensitized Solar Cells. *J. Mater. Chem. A* **2016**, *4*, 12865–12877.

[60] Han, M. L.; Zhu, Y. Z.; Liu, S.; Liu, Q. L.; Ye, D.; Wang, B.; Zheng, J. Y., The Improved Photovoltaic Performance of Phenothiazine-Dithienopyrrole Based Dyes with Auxiliary Acceptors. *J. Power Sources* **2018**, *387*, 117–125.

[61] Liang, M.; Chen, J., Arylamine Organic Dyes for Dye-Sensitized Solar Cells; *Chem. Soc. Rev.*, **2013**, *42*, 3453-3488

[62] Koumura, N.; Wang, Z.-S.; Mori, S.; Miyashita, M.; Suzuki, E.; Hara, K., Alkyl-functionalized organic dyes for efficient molecular photovoltaics *J. Am. Chem. Soc.* **2006**; *128*:14256-14257.

[63] Kim, J. J.; Choi, H.; Lee, J. W.; Kang, M. S.; Song, K.; Kang, S. O.; Ko, J. A Polymer Gel Electrolyte to Achieve ≥6% Power Conversion Efficiency with a Novel Organic

Dye Incorporating a Low-Band-Gap Chromophore. *J. Mater. Chem.* **2008**, *18*, 5223–5229.

[64]   Cho, N.; Han, J.; Song, K.; Kang, M. S.; Jun, M. J.; Kang, Y.; Ko, J. Substituent Effect of Fluorine Atom on Benzothiadiazole Bridging Unit in Dye Sensitized Solar Cells. *Tetrahedron* **2014**, *70*, 427–433.

[65]   Huang, H.; Chen, H.; Long, J.; Wang, G.; Tan, S. Novel D–A–π–A Organic Dyes Based on 3-Dimensional Triarylamine and Benzothiadiazole Derivatives for High-Performance Dye-Sensitized Solar Cells. *J. Power Sources* **2016**, *326*, 438–446.

[66]   Tang, Z. M.; Lei, T.; Jiang, K. J.; Song, Y. L.; Pei, J. Benzothiadiazole Containing D-π-A Conjugated Compounds for Dye-Sensitized Solar Cells: Synthesis, Properties, and Photovoltaic Performances. *Chem. Asian J.* **2010**, *5*, 1911–1917.

[67]   Wu, Y.; Zhang, X.; Li, W.; Wang, Z. S.; Tian, H.; Zhu, W. Hexylthiophene-Featured D-A-π-a Structural Indoline Chromophores for Coadsorbent-Free and Panchromatic Dye-Sensitized Solar Cells. *Adv. Energy Mater.* **2012**, *2*, 149–156.

[68]   Wu, Y.; Marszalek, M.; Zakeeruddin, S. M.; Zhang, Q.; Tian, H.; Grätzel, M.; Zhu, W. High-Conversion-Efficiency Organic Dye-Sensitized Solar Cells: Molecular Engineering on D-A-π-A Featured Organic Indoline Dyes. *Energy Environ. Sci.* **2012**, *5*, 8261–8272.

[69]   Chou, H. H.; Chen, Y. C.; Huang, H. J.; Lee, T. H.; Lin, J. T.; Tsai, C.; Chen, K. High-Performance Dye-Sensitized Solar Cells Based on 5,6-Bis-Hexyloxy-Benzo[2,1,3]Thiadiazole. *J. Mater. Chem.* **2012**, *22*, 10929–10938.

[70]   Hu, X.; Cai, S.; Tian, G.; Li, X.; Su, J.; Li, J. Rigid Triarylamine-Based D-A-π-A Structural Organic Sensitizers for Solar Cells: The Significant Enhancement of Open-Circuit Photovoltage with a Long Alkyl Group. *RSC Adv.* **2013**, *3*, 22544–22553.

[71]   Wang, C.; Fang, Y.; Cao, Z.; Huang, H.; Zhao, B.; Li, H.; Liu, Y.; Tan, S. Synthesis and Photovoltaic Properties of New Branchlike Organic Dyes Containing Benzothiadiazole or Triphenylamine-Linked Consecutive Vinylenes Units. *Dyes Pigments* **2013**, *97*, 405–411.

[72]   Chen, L.; Li, X.; Ying, W.; Zhang, X.; Guo, F.; Li, J.; Hua, J. 5,6-Bis(Octyloxy)Benzo[*c*][1,2,5]Thiadiazole-Bridged Dyes for Dye-Sensitized Solar Cells With High Open-Circuit Voltage Performance, *Eur. J. Org. Chem.* **2013**, *9*, 1770–1780.

[73]   Zhang, X.; Chen, L.; Li, X.; Mao, J.; Wu, W.; Ågren, H.; Hua, J. Photovoltaic Properties of Bis(Octyloxy)Benzo-[*c*][1,2,5]Thiadiazole Sensitizers Based on an *N,N*-Diphenylthiophen-2-Amine Donor. *J. Mater. Chem. C* **2014**, *2*, 4063–4072.

References

[74] Grisorio, R.; De Marco, L.; Giannuzzi, R.; Gigli, G.; Suranna, G. P. Molecular Engineering of Largely π-Extended Metal-Free Sensitizers Containing Benzothiadiazole Units: Approaching 10% Efficiency Dye-Sensitized Solar Cells Using Iodine-Based Electrolytes. *Dyes Pigments* **2016**, *131*, 282–292.

[75] Chaurasia, S.; Hsu, C. Y.; Chou, H. H.; Lin, J. T. Synthesis, Optical and Electrochemical Properties of Pyridal[2,1,3] Thiadiazole Based Organic Dyes for Dye Sensitized Solar Cells. *Org. Electron.* **2014**, *15*, 378–390.

[76] Song, X.; Zhang, W.; Li, X.; Jiang, H.; Shen, C.; Zhu, W. H. Influence of Ethynyl Position on Benzothiadiazole Based D-A-π-A Dye-Sensitized Solar Cells: Spectral Response and Photovoltage Performance. *J. Mater. Chem. C* **2016**, *4*, 9203–9211.

[77] Yum, J. H.; Baranoff, E.; Wenger, S.; Nazeeruddin, M. K.; Grätzel, M. Panchromatic Engineering for Dye-Sensitized Solar Cells. *Energy Environ. Sci.* **2011**, *4 (3)*, 842

[78] Kim, S.; Lee, J. K.; Kang, S. O.; Ko, J.; Yum, J. H.; Fantacci, S.; De Angelis, F.; Di Censo, D.; Nazeeruddin, K.; Grätzel, M. Molecular Engineering of Organic Sensitizers for Solar Cell Applications. *J. Am. Chem. Soc.* **2006**, *128*, 16701–16707.

[79] Murali, M. G.; Wang, X.; Wang, Q.; Valiyaveettil, S., New Banana Shaped A–D–π–D–A Type Organic Dyes Containing Two Anchoring Groups for High Performance Dye-Sensitized Solar Cells. *Dyes Pigments* **2016**, *134*, 375–381.

[80] Mikroyannidis, J. A.; Suresh, P.; Roy, M. S.; Sharma, G. D. Triphenylamine- and Benzothiadiazole-Based Dyes with Multiple Acceptors for Application in Dye-Sensitized Solar Cells. *J. Power Sources* **2010**, *195*, 3002–3010.

[81] Shah, S. A. A.; Sayyad, M. H.; Wahab, F.; Khan, K. A.; Munawar, M. A.; Elbohy, H.; Qiao, Q., Synthesis, Modeling and Photovoltaic Properties of a Benzothiadiazole Based Molecule for Dye-Sensitized Solar Cells. *J. Mater. Sci: Mater. Electron.* **2016**, *27*, 4501–4507.

[82] Haid, S.; Marszalek, M.; Mishra, A.; Wielopolski, M.; Teuscher, J.; Moser, J. E.; Humphry-Baker, R.; Zakeeruddin, S. M.; Grätzel, M.; Bäuerle, P. Significant Improvement of Dye-Sensitized Solar Cell Performance by Small Structural Modification in π-Conjugated Donor-Acceptor Dyes. *Adv. Funct. Mater.* **2012**, *22*, 1291–1302.

[83] Lin, L. Y.; Tsai, C. H.; Lin, F.; Huang, T. W.; Chou, S. H.; Wu, C. C.; Wong, K. T. 2,1,3-Benzothiadiazole-Containing Donor-Acceptor-Acceptor Dyes for Dye-Sensitized Solar Cells. *Tetrahedron* **2012**, *68*, 7509–7516.

[84] Han, L.; Zu, X.; Cui, Y.; Wu, H.; Ye, Q.; Gao, J. Novel D-A-π-A Carbazole Dyes Containing Benzothiadiazole Chromophores for Dye-Sensitized Solar Cells. *Org. Electron.* **2014**, *15*, 1536–1544.

[85] Elmorsy, M. R.; Su, R.; Fadda, A. A.; Etman, H. A.; Tawfik, E. H.; El-Shafei, A. Molecular Engineering and Synthesis of Novel Metal-Free Organic Sensitizers with D-π-A-π-A Architecture for DSSC Applications: The Effect of the Anchoring Group. *Dyes Pigments* **2018**, *158*, 121–130.

[86] Stalder, R.; Xie, D.; Islam, A. l.; Han, L.; Reynolds, J. R.; Schanze, K. S., Panchromatic Donor−Acceptor−Donor Conjugated Oligomers for Dye-Sensitized Solar Cell Applications, *ACS Appl. Mater. Interfaces* **2014**, *6*, 8715−8722.

[87] Islam, A.; Akhtaruzzaman, M.; Chowdhury, T. H.; Qin, C.; Han, L.; Bedja, I. M.; Stalder, R.; Schanze, K. S.; Reynolds, J. R., Enhanced Photovoltaic Performances of Dye-Sensitized Solar Cells by Co-Sensitization of Benzothiadiazole and Squaraine-Based Dyes, *ACS Appl. Mater. Interfaces* **2016**, *8*, 4616−4623.

[88] Wu, Z.; Li, X.; Li, J.; Hua, J.; Agren, H.; Tian, H. Influence of the Auxiliary Acceptor on the Absorption Response and Photovoltaic Performance of Dye-Sensitized Solar Cells. *Chem. Asian J.* **2014**, *9*, 3549–3557.

[89] Kunić, S.; Šego, Z. OLED Technology and Displays. *ELMAR, 2012 Proc. 12-14 Sept.* **2012**, No. September, 31–35. 54th International Symposium ELMAR-2012, 12-14 September 2012, Zadar, Croatia

[90] Burrows, P. E.; Gu, G.; Bulovi, V.; Shen, Z.; Forrest, S. R.; Thompson, M. E. Achieving Full-Color Organic LEDs for Lightweight, Flat-Panel Displays-P. E. Burrows. *IEEE Trans. Electron Devices* **1997**, *44*, 1188–1203.

[91] Zhang, M.; Xue, S.; Dong, W.; Wang, Q.; Fei, T.; Gu, C.; Ma, Y. Highly-Efficient Solution-Processed OLEDs Based on New Bipolar Emitters. *Chem. Commun.* **2010**, *46*, 3923–3925.

[92] Chen, C. T. Evolution of Red Organic Light-Emitting Diodes: Materials and Devices. *Chem. Mater.* **2004**, *16*, 4389–4400.

[93] Thomas, K. R. J.; Lin, J. T.; Velusamy, M.; Tao, Y.-T.; Chuen, C.-H. Color Tuning in Benzo[1,2,5]Thiadiazole-Based Small Molecules by Amino Conjugation/Deconjugation: Bright Red-Light-Emitting Diodes. *Adv. Funct. Mater.* **2004**, *14*, 83–90.

[94] Huang, J.; Li, C.; Xia, Y.-J.; Zhu, X.-H.; Peng, J.; Cao, Y. Amorphous Fluorescent Organic Emitter for Efficient Soln-Processed Pure Red Electroluminescence LED:

References

Synth, Purification, Morphology, Solid-State Photoluminescence. *J. Org. Chem.* **2007**, *72*, 8580–8583.

[95] Huang, J.; Qiao, X.; Xia, Y.; Zhu, X.; Ma, D.; Cao, Y.; Roncali, J., A Dithienylbenzothiadiazole Pure Red Molecular Emitter with Electron Transport and Exciton Self-Confinement for Nondoped Organic Red-Light-Emitting Diodes. *Adv. Mater.* **2008**, *20*, 4172–4175.

[96] Huang, J.; Liu, Q.; Zou, J. H.; Zhu, X. H.; Li, A. Y.; Li, J. W.; Wu, S.; Peng, J.; Cao, Y.; Xia, R.; Electroluminescence and Laser Emission of Soluble Pure Red Fluorescent Molecular Glasses Based on Dithienylbenzothiadiazole. *Adv. Funct. Mater.* **2009**, *19*, 2978–2986.

[97] Chen, L.; Zhang, B.; Cheng, Y.; Xie, Z.; Wang, L.; Jing, X.; Wang, F. Pure and Saturated Red Electroluminescent Polyfluorenes with Dopant/Host System and PLED Efficiency/Color Purity Trade-Offs, *Adv. Funct. Mater.* **2010**, *20*, 3143–3153.

[98] Ni, F.; Wu, Z.; Zhu, Z.; Chen, T.; Wu, K.; Zhong, C.; An, K.; Wei, D.; Ma, D.; Yang, C. Teaching an Old Acceptor New Tricks: Rationally Employing 2,1,3-Benzothiadiazole as Input to Design a Highly Efficient Red Thermally Activated Delayed Fluorescence Emitter. *J. Mater. Chem. C* **2017**, *5* (6), 1363–1368.

[99] Zhang, M.; Xue, S.; Dong, W.; Wang, Q.; Fei, T.; Gu, C.; Ma, Y. Highly-Efficient Solution-Processed OLEDs Based on New Bipolar Emitters. *Chem. Commun.* **2010**, *46* (22), 3923–3925.

[100] Wang, Z.; Lu, P.; Xue, S.; Gu, C.; Lv, Y.; Zhu, Q.; Wang, H.; Ma, Y. A Solution-Processable Deep Red Molecular Emitter for Non-Doped Organic Red-Light-Emitting Diodes. *Dyes Pigments* **2011**, *91*, 356–363.

[101] Zhang, J.; Yang, Y.; He, C.; Li, Y. Red-Emission Organic Light-Emitting Diodes Based on Solution-Processable Molecules with Triphenylamine Core and Benzothiadiazole-Thiophene Arms. *Sci. China Chem.* **2011**, *54*, 695–698.

[102] Zhao, Z.; Deng, C.; Chen, S.; Lam, J. W. Y.; Qin, W.; Lu, P.; Wang, Z.; Kwok, H. S.; Ma, Y.; Qiu, H.; et al. Full Emission Color Tuning in Luminogens Constructed from Tetraphenylethene, Benzo-2,1,3-Thiadiazole and Thiophene Building Blocks, *Chem. Commun.* **2011**, *47*, 8847–8849.

[103] Zhao, Z.; Geng, J.; Chang, Z.; Chen, S.; Deng, C.; Jiang, T.; Qin, W.; Lam, J. W. Y.; Kwok, H. S.; Qiu, H., A Tetraphenylethene-Based Red Luminophor for an Efficient Non-Doped Electroluminescence Device and Cellular Imaging. *J. Mater. Chem.* **2012**, *22*, 11018–11021.

[104] Thangthong, A.; Prachumrak, N.; Sudyoadsuk, T.; Namuangruk, S.; Keawin, T.; Jungsuttiwong, S.; Kungwan, N.; Promarak, V. Multi-Triphenylamine-Functionalized Dithienylbenzothiadiazoles as Hole-Transporting Non-Doped Red Emitters for Efficient Simple Solution Processed Pure Red Organic Light-Emitting Diodes. *Org. Electron.* **2015**, *21*, 117–125.

[105] Thelakkat, M. Star-Shaped, Dendrimeric and Polymeric Triarylamines as Photoconductors and Hole Transport Materials for Electro-Optical Applications. *Macromol. Mater. Eng.* **2002**, *287*, 442–461.

[106] Wang, J. L.; Zhou, Y.; Li, Y.; Pei, J. Solution-Processable Gradient Red-Emitting π-Conjugated Dendrimers Based on Benzothiadiazole as Core: Synthesis, Characterization, and Device Performances. *J. Org. Chem.* **2009**, *74*, 7449–7456.

[107] Khanasa, T.; Prachumrak, N.; Rattanawan, R.; Jungsuttiwong, S.; Keawin, T.; Sudyoadsuk, T.; Tuntulani, T.; Promarak, V. An Efficient Solution Processed Non-Doped Red Emitter Based on Carbazole-Triphenylamine End-Capped Di(Thiophen-2-yl)Benzothiadiazole for Pure Red Organic Light-Emitting Diodes. *Chem. Commun.* **2013**, *49*, 3401–3403.

[108] Khanasa, T.; Prachumrak, N.; Rattanawan, R.; Jungsuttiwong, S.; Keawin, T.; Sudyoadsuk, T.; Tuntulani, T.; Promarak, V. Bis(carbazol-9-ylphenyl)aniline End-Capped Oligoarylenes as Solution-Processed Nondoped Emitters for Full-Emission Color Tuning Organic Light-Emitting Diodes. *J. Org. Chem.*, 2013, *78*, 6702–6713.

[109] Prachumrak, N.; Pojanasopa, S.; Namuangruk, S.; Kaewin, T.; Jungsuttiwong, S.; Sudyoadsuk, T.; Promarak, V. Novel Bis[5-(fluoren-2-yl)thiophen-2-yl]benzothiadiazole End- Capped with Carbazole Dendrons as Highly Efficient Solution- Processed Nondoped Red Emitters for Organic Light-Emitting Diodes. *ACS Appl. Mater. Interfaces,* **2013**, *5*, 8694

[110] Sudyoadsuk, T.; Moonsin, P.; Prachumrak, N.; Namuangruk, S.; Jungsuttiwong, S.; Keawin, T.; Promarak, V. Carbazole Dendrimers Containing Oligoarylfluorene Cores as Solution-Processed Hole-Transporting Non-Doped Emitters for Efficient Pure Red, Green, Blue and White Organic Light-Emitting Diodes. *Polym. Chem.* **2014**, *5*, 3982–3993.

[111] Wang, Y. K.; Huang, C. C.; Kumar, S.; Li, S. H.; Dong, Z. L.; Fung, M. K.; Jiang, Z. Q.; Liao, L. S. Thermally Activated Delayed Fluorescence Sensitizer for D-A-A Type Emitters with Orange-Red Light Emission. *J. Mater. Chem. C* **2018**, *6*, 10030–10035.

References

[112] Omer, K. M.; Ku, S.; Wong, K.; Bard, A. J. Green Electrogenerated Chemiluminescence of Highly Fluorescent Benzothiadiazole and Fluorene Derivatives *J. Am. Chem. Soc.* **2009**, *2*, 10733–10741.

[113] Ku, S. Y.; Chi, L. C.; Hung, W. Y.; Yang, S. W.; Tsai, T. C.; Wong, K. T.; Chen, Y. H.; Wu, C. I. High-Luminescence Non-Doped Green OLEDs Based on a 9,9-Diarylfluorene- Terminated 2,1,3-Benzothiadiazole Derivative. *J. Mater. Chem.* **2009**, *19*, 773–780.

[114] Li, Y.; Li, B. X.; Tan, W. Y.; Liu, Y.; Zhu, X. H.; Xie, F. Y.; Chen, J.; Ma, D. G.; Peng, J.; Cao, Y.; et al. Structure-Properties Relationships in Solution-Processable Single-Material Molecular Emitters for Efficient Green Organic Light-Emitting Diodes. *Org. Electron.* **2012**, *13*, 1092–1099.

[115] Findlay, N. J.; Breig, B.; Forbes, C.; Inigo, A. R.; Kanibolotsky, A. L.; Skabara, P. J. High Brightness Solution-Processed OLEDs Employing Linear, Small Molecule Emitters. *J. Mater. Chem. C* **2016**, *4*, 3774–3780.

[116] Wang, C.; Li, X.; Pan, Y.; Zhang, S.; Yao, L.; Bai, Q.; Li, W.; Lu, P.; Yang, B.; Su, S.; Ma, Y., Highly Efficient Nondoped Green Organic Light-Emitting Diodes with Combination of High Photoluminescence and High Exciton Utilization. *ACS Appl. Mater. Interfaces* **2016**, *8*, 3041−3049

[117] Moonsin, P.; Prachumrak, N.; Namuangruk, S.; Jungsuttiwong, S.; Keawin, T.; Sudyoadsuk, T.; Promarak, V. Novel Bis(Fluorenyl)Benzothiadiazole-Cored Carbazole Dendrimers as Highly Efficient Solution-Processed Non-Doped Green Emitters for Organic Light-Emitting Diodes. *Chem. Commun.* **2013**, *49*, 6388–6390.

[118] Wang, Z.; Liu, Q.; Chen, T.; Wang, Y.; Yuan, J.; Zheng, C.; Chen, R.; Huang, W. Molecular Rearrangement at Charged States: Intrinsic Effects upon Photo and Electroluminescence. *Dyes Pigments* **2015**, *113*, 529–535.

[119] Mróz, W.; Villafiorita-Monteleone, F.; Pasini, M.; Grisci, G.; Paolino, M.; Razzano, V.; Cappelli, A.; Botta, C. π-Stacked Polybenzofulvene Derivatives as Hosts for Yellow and Red Emitting OLEDs. *Mater. Lett.* **2015**, *142*, 197–200.

[120] Wu, Y.-C. M.; Molaire, M. F.; Weiss, D. S.; Angel, F. A.; De Blase, C. R.; Fors, B. P., Synthesis of Amorphous Monomeric Glass Mixtures for Organic Electronic Applications, *J. Org. Chem.* **2015**, *80*, 12740−12745.

[121] Jiang, J.; Hu, D.; Hanif, M.; Li, X.; Su, S.; Xie, Z.; Liu, L.; Zhang, S.; Yang, B.; Ma, Y. Twist Angle and Rotation Freedom Effects on Luminescent Donor−Acceptor Materials:

Crystal Structures, Photophysical Properties, and OLED Application. *Adv. Opt. Mater.* **2016**, *4*, 2109–2118.

[122] Cho, Y. J.; Chin, B. D.; Jeon, S. Y.; Lee, J. Y. 20% External Quantum Efficiency in Solution-Processed Blue Thermally Activated Delayed Fluorescent Devices *Adv. Funct. Mater.* **2015**, *25*, 6786.

[123] Zhu, X. H.; Peng, J.; Cao, Y.; Roncali, J. Solution-processable single-material molecular emitters for organic light-emitting devices. *Chem. Soc. Rev*. **2011**, *40*, 3509.

[124] Du, J.; Biewer, M. C.; Stefan, M. C. Benzothiadiazole building units in solution processable small molecules for organic photovoltaics. *J. Mater. Chem. A*, **2016**, *4*, 15771.

[125] Lin, Y.; Li, Y.; Zhan, X. Small molecule semiconductors for high-efficiency organic photovoltaics. *Chem. Soc. Rev.,* **2012**, *41*, 4245.

[126] Hales, J. M.; Barlow, S.; Kim, H.; Mukhopadhyay, S.; Bredas, J. C.; Perry, J. W.; Marder, S. R. Design of Organic Chromophores for All-Optical Signal Processing Applications. *Chem. Mater.,* **2014**, *26*, 549.

[127] Aldakov, D.; Palacios, M. A.; Anzenbacher, P. Benzothiadiazoles and Dipyrrolyl Quinoxalines with Extended Conjugated Chromophores-Fluorophores and Anion Sensors. *Chem. Mater.*, **2005**, *17*, 5238.

[128] Duan, L.; Hou, L.; Lee, T. W.; Qiao, J.; Zhang, D.; Dong, G.; Wang, L.; Qiu, Y. Solution Processable Small Molecules for Organic Light-Emitting Diodes. *J. Mater. Chem.* **2010**, *20*, 6392–6407

[129] Ishii, T.; Ikeda, K.; Ogawaa, M.; Kusakaki, Y. Light-emitting properties of donor–acceptor and donor–acceptor–donor dyes in solution, solid, and aggregated states: structure–property relationship of emission behavior. *RSC Adv.,* **2015**, *5*, 89171.

[130] Zhang, M.; Xue, S.; Dong, W.; Wang, Q.; Fei, T.; Gu, C.; Ma, Y. Highly-efficient solution-processed OLEDs based on new bipolar emitters. *Chem. Commun*. **2010**, *46*, 3923.

[131] Kajjam, A. B.; Kumar, P. S. V.; Subramanian, V.; Vaidyanathan, S. Triphenylamine Based Yellowish-Orange Light Emitting Organic Dyes (Donor-π-Acceptor) for Hybrid WLEDs and OLEDs: Synthesis, Characterization and Theoretical Study. *Phys. Chem. Chem. Phys.,* **2018**, *20*, 4490

[132] Cui, L.-S.; Nomura, H.; Geng, Y.; Kim, J. U.; Nakanotani, H.; Adachi, C. Controlling Singlet–Triplet Energy Splitting for Deep-Blue Thermally Activated Delayed Fluorescence Emitters. *Angew. Chem. Int. Ed*. **2017**, *56*, 1571.

References

[133] Zeng, W.; Lai, H. Y.; Lee, W. K.; Jiao, M.; Shiu, Y. J.; Zhong, C.; Gong, S.; Zhou, T.; Xie, G.; Sharma, M.;. Achieving Nearly 30% External Quantum Efficiency for Orange–Red Organic Light Emitting Diodes by Employing Thermally Activated Delayed Fluorescence Emitters Composed of 1,8-Naphthalimide-Acridine Hybrids. *Adv. Mater.* **2018**, *30*, 1–8.

[134] Tydlität, J.; Fecková, M.; le Poul, P.; Pytela, O.; Klikar, M.; Rodríguez-López, J.; Robin-le Guen, F.; Achelle, S. Influence of Donor-Substituents on Triphenylamine Chromophores Bearing Pyridine Fragments. *European J. Org. Chem.* **2019**, *2019*, 1921–1930.

[135] Swamy. C. A.; Thilagar P. Effect of substituent position on optical properties of boron-dipyrromethane isomers *Inorganica Chimica Acta* **2014**, *411*, 97–101

[136] Mukherjee, S.; Thilagar, P. Recent advances in purely organic phosphorescent materials *Chem. Commun.*, **2015**, *51*, 10988

[137] Chen, K. W.; Lin, L. Y.; Li, Y. H.; Li, Y. Z.; Nguyen, T. P.; Biring, S.; Liu, S. W.; Wong, K. T. Fluorination Effects of A-D-A-Type Small Molecules on Physical Property and the Performance of Organic Solar Cell. *Org. Electron.* **2018**, *52*, 342–349.

[138] Tagare, J.; Kumar, D.; Jou, J.; Vaidyanathan, S. Dyes and Pigments Synthesis , Photophysical , Theoretical and Electroluminescence Study of Triphenylamine-Imidazole Based Blue Fluorophores for Solution-Processed Organic Light Emitting Diodes. *Dyes Pigments.* **2019**, *160,* 944–956.

[139] Ding, J.; Zhang, B.; Lü, J.; Xie, Z.; Wang, L.; Jing, X.; Wang, F. Solution-Processable Carbazole-Based Conjugated Dendritic Hosts for Power-Efficient Blue-Electrophosphorescent Devices. *Adv. Mater.* **2009**, *21*, 4983–4986

[140] Miyaura, N.; Yamada, K.; Suzuki, A., A new stereospecific cross-coupling by the palladium-catalyzed reaction of 1-alkenylboranes with 1-alkenyl or 1-alkynyl halides. *Tetrahedron Lett.* **1979**, *20*, 3437.

[141] Bodedla, G. B.; Thomas, K. R. J.; Fan, M.-S.; Ho, K.-C. Benzimidazole-Branched Isomeric Dyes: Effect of Molecular Constitution on Photophysical, Electrochemical, and Photovoltaic Properties. *J. Org. Chem.* **2016**, *81*, 640.

[142] Almond-Thynne, J.; Blakemore, D. C.; Pryde, D. C.; Spivey, A. C. Site-selective Suzuki–Miyaura coupling of heteroaryl halides understanding the trends for pharmaceutically important classes. *Chem. Sci.* **2017**, *8*, 40.

[143] Tanaka, H.; Shizu, K.; Nakanotani, H.; Adachi, C. Twisted Intramolecular Charge Transfer State for Long-Wavelength Thermally Activated Delayed Fluorescence. *Chem. Mater.* **2013**, *25*, 3766−3771

[144] Popli, C.; Patil, Y.; Misra, R. Design and Synthesis of *N* -Phenylcarbazole-Substituted Diketopyrrolopyrrole-Based Monomers and Dimers : *Phys. Chem. Chem. Phys* **2018**, 6474–6481.

[145] Wang, X.; Wang, S.; Ma, Z.; Ding, J.; Wang, L.; Jing, X.; Wang, F. Solution-Processible 2,2′-Dimethyl-Biphenyl Cored Carbazole Dendrimers as Universal Hosts for Efficient Blue, Green, and Red Phosphorescent OLEDs. *Adv. Funct. Mater.* **2014**, *24* (22), 3413–3421.

[146] Hong, M.; Ravva, M. K.; Winget, P.; Brédas, J. L. Effect of Substituents on the Electronic Structure and Degradation Process in Carbazole Derivatives for Blue OLED Host Materials. *Chem. Mater.* **2016**, *28* (16), 5791–5798.

[147] Guo, J.; Li, X.-L.; Nie, H.; Luo, W.; Hu, R.; Qin, A.; Zhao, Z.; Su, S.-J.; Tang, B. Z. Robust Luminescent Materials with Prominent Aggregation-Induced Emission and Thermally Activated Delayed Fluorescence for High- Performance Organic Light-Emitting Diodes. *Chem. Mater.* 2017, **29**, 3623.

[148] Konidena, R. K.; Thomas, K. R. J.; Kumar, S.; Wang, Y.-C.; Li, C.-J.; Jou, J.-H. Phenothiazine Decorated Carbazoles: Effect of Substitution Pattern on the Optical and Electroluminescent Characteristics. *J. Org. Chem.* **2015**, *80*, 5812

[149] Reichardt, C. Solvatochromic Dyes as Solvent Polarity Indicators. *Chem. Rev*. **1994**, *94*, 2319.

[150] Bhim R. T.; Vaghasiya J.V.; Afroz M.A.; Soni S.S.; Iyer P.K. Twisted donor substituted simple thiophene dyes retard the dye aggregation and charge recombination in dye-sensitized solar cells. *Org. Electron.* **2017**, *50*, 25-32.

[151] Qiu, Y.; Wei, P.; Zhang, D. Q.; Qiao, J.; Duan, L.; Yi, Y. K.; Gao, Y. D.; Zhang, L. D. Novel Naphtho[2,3-*c*][1,2,5]thiadiazole Derivative for Non-doped Small Molecular Organic Red-Light-Emitting Diodes. *Adv. Mater.* **2006**, *18*, 1607.

[152] Zhou, Y.; He, Q.; Yang, Y.; Zhong, H.; He, C.; Sang, G.; Liu, W.; Yang, C.; Bai, F.; Li, Y. Binaphthyl-Containing Green- and Red-Emitting Molecules for Solution-Processable Organic Light-Emitting Diodes. *Adv. Funct. Mater.* **2008**, *18*, 3299

[153] Frisch, M. J.; Trucks, G. W.; Schlegel, H. B.; Scuseria, G. E.; Robb, M. A.; Cheeseman, J. R.; Scalmani, G.; Barone, V.; Mennucci, B.; Petersson, G. A.; Nakatsuji, H.; Caricato, M.; Li, X.; Hratchian, H. P.; Izmaylov, A. F.; Bloino, J.; Zheng, G.;

Sonnenberg, J. L.; Hada, M.; Ehara, M.; Toyota, K.; Fukuda, R.; Hasegawa, J.; Ishida, M.; Nakajima, T.; Honda, Y.; Kitao, O.; Nakai, H.; Vreven, T.; Montgomery, Jr., J. A.; Peralta, J. E.; Ogliaro, F.; Bearpark, M.; Heyd, J. J.; Brothers, E.; Kudin, K. N.; Staroverov, V. N.; Kobayashi, R.; Normand, J.; Raghavachari, K.; Rendell, A.; Burant, J. C.; Iyengar, S. S.; Tomasi, J.; Cossi, M.; Rega, N.; Millam, J. M.; Klene, M.; Knox, J. E.; Cross, J. B.; Bakken, V.; Adamo, C.; Jaramillo, J.; Gomperts, R.; Stratmann, R. E.; Yazyev, O.; Austin, A. J.; Cammi, R.; Pomelli, C.; Ochterski, J. W.; Martin, R. L.; Morokuma, K.; Zakrzewski, V. G.; Voth, G. A.; Salvador, P.; Dannenberg, J. J.; Dapprich, S.; Daniels, A. D.; Farkas, O.; Foresman, J. B.; Ortiz, J. V.; Cioslowski, J.; Fox, D. J. *Gaussian 09,* Revision A.02, Gaussian Inc., Wallingford CT, **2009**.

[154] Thomas, K. R. J.; Lin, J.T.; Tao, Y.-T.; Ko, C.-W. New Star-Shaped Luminescent Triarylamines:Synthesis, Thermal, Photophysical, and Electroluminescent Characteristics *Chem. Mater.* 2002, **14**, 1354.

[155] Konidena, R. K.; Thomas, K. R. J.; Singh, M.; Jou, J.-H. Thienylphenothiazine integrated pyrenes: an account on the influence of substitution patterns on their optical and electroluminescenceproperties. ***J. Mater. Chem. C*** 2016, *4*, 4246.

[156] Tutiš, E.; Bussac, M. N.; Masenelli, B.; Carrard, M.; Zuppiroli, L. Numerical model for organic light-emitting diodes. *J. Appl. Phys.,* **2001**, *89*, 430.

[157] Thomas, K. R. J.; Lin, J.T.; Tao, Y.-T.; Ko, C.-W. Light-Emitting Carbazole Derivatives: Potential Electroluminescent Materials. *J. Am. Chem. Soc.* 2001**, 123**, 9404.

[158] Becke, A. D. A New Mixing of Hartree-Fock and Local Density-Functional Theories. *J. Chem. Phys.* **1993**, *98* (2), 1372–1377.

[159] Lee, C.; Yang, W.; Parr, G. Development of the Colle-Salvetti correlation-energy formula into a functional of the electron density. *Phys. Rev. B.* **1988**, *37*, 785-789.

[160] Lynch, B. J.; Fast, P. I.; Harris, M.; Truhlar, D. G. Adiabatic Connection for Kinetics. *J. Phys. Chem. A* **2000**, *104*, 4811.

[161] Gómez-Bombarelli, R.; Aguilera-Iparraguirre, J.; Hirzel, T. D.; Duvenaud, D.; Maclaurin, D.; Blood-Forsythe, M. A.; Chae, H. S.; Einzinger, M.; Ha, D. G.; Wu, T.; et al. Design of Efficient Molecular Organic Light-Emitting Diodes by a High-Throughput Virtual Screening and Experimental Approach. *Nat. Mater.* **2016**, *15* (10), 1120–1127.

[162] Uoyama, H.; Goushi, K.; Shizu, K.; Nomura, H.; Adachi, C. Highly Efficient Organic Light-Emitting Diodes from Delayed Fluorescence. *Nature* **2012**, *492*, 234–238.

[163] Kwon, O. K.; Park, J.; Kim, D. W.; Park, S. K.; Park, S. Y. An All-Small-Molecule Organic Solar Cell with High Efficiency Nonfullerene Acceptor. *Adv. Mater.* **2015**, *27*, 1951–1956.

[164] Karuppuswamy, P.; Chen, H. C.; Wang, P. C.; Hsu, C. P.; Wong, K. T.; Chu, C. W. The 3 D Structure of Twisted Benzo[Ghi]Perylene-Triimide Dimer as a Non-Fullerene Acceptor for Inverted Perovskite Solar Cells. *ChemSusChem* **2018**, *11*, 415–423

[165] Chen, K. W.; Lin, L. Y.; Li, Y. H.; Li, Y. Z.; Nguyen, T. P.; Biring, S.; Liu, S. W.; Wong, K. T. Fluorination Effects of A-D-A-Type Small Molecules on Physical Property and the Performance of Organic Solar Cell. *Org. Electron.* **2018**, *52*, 342–349.

[166] Cho, I.; Park, S. K.; Kang, B.; Chung, J. W.; Kim, J. H.; Yoon, W. S.; Cho, K.; Park, S. Y. Dicyanovinyl-Substituted Indolo[3,2-*b*]Indole Derivatives: Low-Band-Gap π-Conjugated Molecules for a Single-Component Ambipolar Organic Field-Effect Transistor. **2016**, 9460–9468.

[167] Dalton, L. R.; Sullivan, P. A.; Bale, D. H. Electric Field Poled Organic Electro-optic Materials: State of the Art and Future Prospects. *Chem. Rev.* **2010**, *110*, 25–55.

[168] Li, M.; Zhang, H.; Zhang, Y.; Hou, B.; Li, C.; Wang, X.; Zhang, J.; Xiao, L.; Cui, Z.; Ao, Y. Facile Synthesis of Benzothiadiazole-Based Chromophores for Enhanced Performance of Second-Order Nonlinear Optical Materials. *J. Mater. Chem. C* **2016**, *4*, 9094–9102.

[169] Jiang, D.; Chen, S.; Xue, Z.; Li, Y.; Liu, H.; Yang, W.; Li, Y. Donor-Acceptor Molecules Based on Benzothiadiazole: Synthesis, X-Ray Crystal Structures, Linear and Third-Order Nonlinear Optical Properties. *Dyes Pigments.* **2016**, *125*, 100–105.

[170] Burroughes, J. H.; Bradley, D. D. C.; Brown, A. R.; Marks, R. N.; Mackay, K.; Friend, R. H.; Burns, P. L.; Holmes, A. B. Light-Emitting Diodes Based on Conjugated Polymers. *Nature* **1990**, *347*, 539–541

[171] Su, W. M.; Li, W. L.; Xin, Q.; Su, Z. S.; Chu, B.; Bi, D. F.; He, H.; Niu, J. H. Effect of Acceptor on Efficiencies of Exciplex-Type Organic Light Emitting Diodes. *Appl. Phys. Lett.* **2007**, *91*, 28–31.

[172] Li, Y.; Chen, T.; Huang, M.; Gu, Y.; Gong, S.; Xie, G.; Yang, C. Tuning the Twist Angle of Thermally Activated Delayed Fluorescence Molecules via a Dendronization Strategy: High-Efficiency Solution-Processed Non-Doped OLEDs. *J. Mater. Chem. C* **2017**, *5*, 3480–3487.

[173] Li, J.; Nakagawa, T.; Macdonald, J.; Zhang, Q.; Nomura, H.; Miyazaki, H.; Adachi, C. Highly Efficient Organic Light-Emitting Diode Based on a Hidden Thermally Activated

References

Delayed Fluorescence Channel in a Heptazine Derivative. *Adv. Mater.* **2013**, *25*, 3319–3323.

[174] Cho, Y. J.; Jeon, S. K.; Chin, B. D.; Yu, E.; Lee, J. Y. The Design of Dual Emitting Cores for Green Thermally Activated Delayed Fluorescent Materials. *Angew. Chem. Int. Ed.* **2015**, *54*, 5201–5204.

[175] Data, P.; Pander, P.; Okazaki, M.; Takeda, Y.; Minakata, S.; Monkman, A. P. Dibenzo[*a,j*]Phenazine-Cored Donor-Acceptor-Donor Compounds as Green-to-Red/NIR Thermally Activated Delayed Fluorescence Organic Light Emitters. *Angew. Chem. Int. Ed.* **2016**, *55*, 5739–5744.

[176] Kulhánek, J.; Bureš, F. Imidazole as a Parent Π-Conjugated Backbone in Charge-Transfer Chromophores. *Beilstein J. Org. Chem.* **2012**, *8*, 25–49.

[177] Tanaka, H.; Shizu, K.; Nakanotani, H.; Adachi, C. Twisted Intramolecular Charge Transfer State for Long-Wavelength Thermally Activated Delayed Fluorescence. *Chem. Mater.* **2013**, *25* , 3766–3771.

[178] Wang, C.; Li, X.; Pan, Y.; Zhang, S.; Yao, L.; Bai, Q.; Li, W.; Lu, P.; Yang, B.; Su, S.; et al. Highly Efficient Nondoped Green Organic Light-Emitting Diodes with Combination of High Photoluminescence and High Exciton Utilization. *ACS Appl. Mater. Interfaces* **2016**, *8*, 3041–3049.

[179] Han, X.; Bai, Q.; Yao, L.; Liu, H.; Gao, Y.; Li, J.; Liu, L.; Liu, Y.; Li, X.; Lu, P.; et al. Highly Efficient Solid-State Near-Infrared Emitting Material Based on Triphenylamine and Diphenylfumaronitrile with an EQE of 2.58% in Nondoped Organic Light-Emitting Diode. *Adv. Funct. Mater.* **2015**, *25* (48), 7521–7529.

[180] Luo, S.; Lin, J.; Zhou, J.; Wang, Y.; Liu, X.; Huang, Y.; Lu, Z.; Hu, C. Novel 1,8-Naphthalimide Derivatives for Standard-Red Organic Light-Emitting Device Applications. *J. Mater. Chem. C* **2015**, *3* (20), 5259–5267.

[181] Yu, T.; Liu, L.; Xie, Z.; Ma, Y. Progress in Small-Molecule Luminescent Materials for Organic Light-Emitting Diodes. *Sci. China Chem.* **2015**, *58* (6), 907–915.

[182] Li, W.; Pan, Y.; Xiao, R.; Peng, Q.; Zhang, S.; Ma, D.; Li, F.; Shen, F.; Wang, Y.; Yang, B.; et al. Employing ∼100% Excitons in OLEDs by Utilizing a Fluorescent Molecule with Hybridized Local and Charge-Transfer Excited State. *Adv. Funct. Mater.* **2014**, *24*, 1609–1614.

[183] Li, X.; Yan, T.; Bin, H.; Han, G.; Xue, L.; Liu, F.; Yi, Y.; Zhang, Z. G.; Russell, T. P.; Li, Y. Insertion of Double Bond π-Bridges of A-D-A Acceptors for High Performance near-Infrared Polymer Solar Cells. *J. Mater. Chem. A* **2017**, *5* (43), 22588–22597.

[184] Tydlitát, J.; Fecková, M.; le Poul, P.; Pytela, O.; Klikar, M.; Rodríguez-López, J.; Robin-le Guen, F.; Achelle, S. Influence of Donor-Substituents on Triphenylamine Chromophores Bearing Pyridine Fragments. *European J. Org. Chem.* **2019**, *2019* (9), 1921–1930.

[185] Badgujar, S.; Lee, G. Y.; Park, T.; Song, C. E.; Park, S.; Oh, S.; Shin, W. S.; Moon, S. J.; Lee, J. C.; Lee, S. K. High-Performance Small Molecule via Tailoring Intermolecular Interactions and Its Application in Large-Area Organic Photovoltaic Modules. *Adv. Energy Mater.* **2016**, *6* (12)

[186] Grabowski, Z. R.; Rotkiewicz, K.; Rettig, W. Structural Changes Accompanying Intramolecular Electron Transfer: Focus on Twisted Intramolecular Charge-Transfer States and Structures. *Chem. Rev.* **2003**, *103* (10), 3899–4032.

[187] Pathak, A.; Justin Thomas, K. R.; Singh, M.; Jou, J. H. Fine-Tuning of Photophysical and Electroluminescence Properties of Benzothiadiazole-Based Emitters by Methyl Substitution. *J. Org. Chem.* **2017**, *82*, 11512–11523.

[188] Etherington, M. K.; Franchello, F.; Gibson, J.; Northey, T.; Santos, J.; Ward, J. S.; Higginbotham, H. F.; Data, P.; Kurowska, A.; Dos Santos, P. L.; et al. Regio-A Nd Conformational Isomerization Critical to Design of Efficient Thermally-Activated Delayed Fluorescence Emitters. *Nat. Commun.* **2017**, *8*, 1–11.

[189] Zhao, C. H.; Zhao, Y. H.; Pan, H.; Fu, G. L. Highly Solid-State Emissive Para-Terphenyls Laterally Substituted with a Diphenylamino Group. *Chem. Commun.* **2011**, *47*, 5518–5520.

[190] Joseph, V.; Thomas, K. R. J.; Singh, M.; Sahoo, S.; Jou, J. H. Manipulation of Donor–Acceptor Interactions in Carbazole-Based Emitters by Chromophore Choice To Achieve Near-UV Emission. *European J. Org. Chem.* **2017**, *2017*, 6660–6670.

[191] Konidena, R. K.; Thomas, K. R. J. Star-Shaped Asymmetrically Substituted Blue Emitting Carbazoles: Synthesis, Photophyscial, Electrochemical and Theoretical Investigations. *Chem. Select* **2017**, *2*, 7514–7524.

[192] Shen, Y.; Li, J.; Chen, S.; Wan, J.; Zhao, Y.; Lu, Z. H.; Li, M.; Yang, L.; Yu, X.; Chen, D.; et al. Novel Benzimidazole-Containing Heterocyclic Compounds: Synthesis, Physical Properties and OLED Application. *Chem. Select* **2017**, *2*, 11206–11210.

References

[193] Thanikachalam, V.; Jeeva, P.; Jayabharathi, J. Highly Efficient Non-Doped Blue Organic Light Emitting Diodes Based on a D-π-A Chromophore with Different Donor Moieties. *RSC Adv.* **2017**, *7*, 13604–13614.

[194] Chen, W. C.; Yuan, Y.; Ni, S. F.; Zhu, Z. L.; Zhang, J.; Jiang, Z. Q.; Liao, L. S.; Wong, F. L.; Lee, C. S. Highly Efficient Deep-Blue Electroluminescence from a Charge-Transfer Emitter with Stable Donor Skeleton. *ACS Appl. Mater. Interfaces* **2017**, *9*, 7331–7338.

[195] Totsatitpaisan, P.; Nunes, S. P.; Tashiro, K.; Chirachanchai, S. Investigation of the Role of Benzimidazole-Based Model Compounds on Thermal Stability and Anhydrous Proton Conductivity of Sulfonated Poly(Ether Ether Ketone). *Solid State Ionics* **2009**, *180*, 738–745.

[196] Liang, X.; Tu, Z. L.; Zheng, Y. X. Thermally Activated Delayed Fluorescence Materials: Towards Realization of High Efficiency through Strategic Small Molecular Design. *Chem. Eur. J.* **2019**, *25*, 5623–5642.

[197] Kochapradist, P.; Prachumrak, N.; Tarsang, R.; Keawin, T.; Jungsuttiwong, S.; Sudyoadsuk, T.; Promarak, V. Multi-Triphenylamine-Substituted Carbazoles: Synthesis, Characterization, Properties, and Applications as Hole-Transporting Materials. *Tetrahedron Lett.* **2013**, *54*, 3683–3687.

[198] Cho, N.; Han, J.; Song, K.; Kang, M. S.; Jun, M. J.; Kang, Y.; Ko, J. Substituent Effect of Fluorine Atom on Benzothiadiazole Bridging Unit in Dye Sensitized Solar Cells. *Tetrahedron* **2014**, *70*, 427–433.

[199] Hirata, S.; Sakai, Y.; Masui, K.; Tanaka, H.; Lee, S. Y.; Nomura, H.; Nakamura, N.; Yasumatsu, M.; Nakanotani, H.; Zhang, Q.; et al. Highly Efficient Blue Electroluminescence Based on Thermally Activated Delayed Fluorescence. *Nat. Mater.* **2015**, *14*, 330–336.

[200] Gautam, P.; Misra, R. Tuning of the HOMO–LUMO gap of donor substituted symmetrical and unsymmetrical benzothiadiazoles. *Org. Biomol. Chem.*, **2014**, *12*, 5448.

[201] Jou, J. H.; Kumar, S.; Fang, P. H.; Venkateswararao, A.; Thomas, K. R. J.; Shyue, J. J.; Wang, Y. C.; Li, T. H.; Yu, H. H. Highly Efficient Ultra-Deep Blue Organic Light-Emitting Diodes with a Wet- and Dry-Process Feasible Cyanofluorene Acetylene Based Emitter. *J. Mater. Chem. C* **2015**, *3* (10), 2182–2194.

[202] Thelakkat, M.; Schmidt, H. W. Low Molecular Weight and Polymeric Heterocyclics as Electron Transport/ Hole-Blocking Materials in Organic Light-Emitting Diodes. *Polym. Adv. Technol.* **1998**, *9* (7), 429–442

[203] Chen, W. C.; Yuan, Y.; Ni, S. F.; Tong, Q. X.; Wong, F. L.; Lee, C. S. Achieving Efficient Violet-Blue Electroluminescence with CIE:Y <0.06 and EQE >6% from Naphthyl-Linked Phenanthroimidazole-Carbazole Hybrid Fluorophores. *Chem. Sci.* **2017**, *8* (5), 3599–3608.

[204] Tagare, J.; Ulla, H.; Kajjam, B.; Satyanarayan, M. N. Star-Shaped Phenanthroimidazole-Triphenylamine-Based Yellow Organic Emitter for Organic Light Emitting Diodes. *Chem. Select* **2017**, *2*, 2611–2620

[205] Zhang, T.; Liang, Y.; Cheng, J.; Li, J. A CBP Derivative as Bipolar Host for Performance Enhancement in Phosphorescent Organic Light-Emitting Diodes. *J. Mater. Chem. C* **2013**, *1*, 757–764.

[206] Gao, Y.; Zhang, S.; Pan, Y.; Yao, L.; Liu, H.; Guo, Y.; Gu, Q.; Yang, B.; Ma, Y. Hybridization and De-Hybridization between the Locally-Excited (LE) State and the Charge-Transfer (CT) State: A Combined Experimental and Theoretical Study. *Phys. Chem. Chem. Phys.* **2016**, *18*, 24176–24184.

[207] O'Regan, B.; Grätzel, M. A low-cost, high-efficiency solar cell based on dye-sensitized colloidal TiO_2 films. *Nature*, **1991**, *353*, 737.

208. Nazeeruddin, M. K.; Angelis, F. D.; Fantacci, S.; Selloni, A.; Viscardi, G.; Liska, P.; Ito, S.; Bessho, T.; Grätzel, M., Combined experimental and dft-tddft computational study of photoelectrochemical cell ruthenium sensitizers. *J. Am. Chem. Soc*. **2005**, 127, 16835–16847.

[209] Nazeeruddin, M. K., Pechy, P., Renouard, T.; Zakeeruddin, S. M.; Humphry-Baker, R., Comte, P.; Liska, P.; Cevey, L.; Costa, E.; Shklover, V.; Spiccia, L.; Deacon, G. B.; Bignozzi, C. A.; Grätzel, M., Engineering of Efficient Panchromatic Sensitizers for Nanocrystalline TiO_2-Based Solar Cells, *J. Am. Chem. Soc*. **2001**, *123*, 1613–1624.

[210] Yella, A.; Lee, H-W., Tsao, H. N.; Yi, C.; Chandiran, A. K.; Nazeeruddin, M. K.; Diau, E. W-G, Yeh, C.-Y.; Zakeeruddin, S. M.; Grätzel, M., Porphyrin-sensitized solar cells with cobalt (II/III)-based redox electrolyte exceed 12 percent efficiency. *Science* **2011**, *334*, 629−634.

[211] Mishra A.; Fischer M. K. R.; Bäuerle P. Metal-free organic dyes for dye-sensitized solar cells: From structure: Property relationships to design rules. *Angew. Chem. Int. Ed.* **2009**, *48*, 2474-99.

References

[212] Anandan, S. Recent Improvements and Arising Challenges in Dye-Sensitized Solar Cells. *Sol. Energy Mater. Sol. Cells* **2007**, *91* (9), 843–846.

[213] Haid, S.; Marszalek, M.; Mishra, A.; Wielopolski, M.; Teuscher, J.; Moser, J.-E.; Humphry-Baker, R.; Zakeeruddin, S. M.; Gratzel, M.; Bauerle, P. Significant Improvement of Dye- Sensitized Solar Cell Performance by Small Structural Modification in π- Conjugated Donor–Acceptor Dyes, *Adv. Funct. Mater*. **2012,** *22*, 1291–1302.

[214] Narayanaswamy, K.; Swetha, T.; Kapil, G.; Pandey, S. S.; Hayase, S.; Singh, S. P., Simple metal-free dyes derived from triphenylamine for DSSC: A comparative study of two different anchoring group. *Electrochimica Acta* **2015**, *169*, 256–263.

[215] Wu Y.; Zhu W. Organic sensitizers from D-π-A to D-A-π-A: effect of the internal electron-withdrawing units on molecular absorption, energy levels and photovoltaic performances. *Chem. Soc. Rev.*, **2013**, *42*, 2039

[216] Chaurasia, S., Hung, W.-I., Chou, H.-H., Lin, J. T., Incorporating a new 2*H*-[1,2,3]Triazolo[4,5-*c*]pyridine moiety to construct D−A−π−A organic sensitizers for high performance solar cells, *Org. Lett*., **2014**, *16*, 3052-3055.

[217] Lin, R. Y.-Y.; Lee, C.-P.; Chen, Y.-C.; Peng, J.-D.; Chu, T.-C.; Chou, H.-H.; Yang, H.-M.; Lin, J. T.; Ho, K.-C., Benzothiadiazole-containing donor–acceptor–acceptor type organic sensitizers for solar cells with ZnO photoanodes. *Chem. Commun*. **2012**, *48*, 12071−12073.

[218] Zhu, W.; Wu, Y.; Wang, S.; Li, W.; Li, X. Chen, J.; Wang, Z.-S.; Tian, H.; Organic D-A-π-A Solar Cell Sensitizers with Improved Stability and Spectral Response. *Adv. Funct. Mater*. **2011,** *21*, 756–763.

[219] Wu, Y.; Marszalek, M.; Zakeeruddin, S. M.; Zhang, Q.; Tian, H.; Grätzel, M.; Zhu, W., High-conversion-efficiency organic dye-sensitized solar cells: molecular engineering on D–A–π-A featured organic indoline dyes. *Energy Environ. Sci*. **2012**, *5*, 8261–8272.

[220] Hu, W.; Zhang, Z.; Shen, W.; Li, M.; He, R., Cyclopentadithiophene bridged organic sensitizers with different auxiliary acceptor for high performance dye-sensitized solar cells. *Dyes Pigments* **2017**, *137*, 165-173.

[221] Mao, J.; Zhang, X.; Liu, S.-H.; Shen, Z.; Li, X.; Wu, W.; Chou, P.-T.; Hua, J., Molecular engineering of D-A-π-A dyes with 2-(1,1-dicyanomethylene)rhodanine as an electron-accepting and anchoring group for dye-sensitized solar cells. *Electrochimica Acta* **2015**,*179*,179–186.

[222] Sudyoadsuk, T.; Pansay, S.; Morada, S.; Rattanawan, R.; Namuangruk, S.; Kaewin, T., Synthesis and characterization of D-D-π-A type organic dyes bearing carbazole – carbazole as a donor moiety (D-D) for efficient dye sensitized solar cells. *Eur. J. Org. Chem.* **2013**, *2013*, 5051‑5063.

[223] Murali, M.G.; Wang, X.; Wang, Q.; Valiyaveettil, S., New banana shaped A–D–π–D–A type organic dyes containing two anchoring groups for high performance dye-sensitized solar cells, *Dyes Pigments* **2016***, 134*, 375-381.

[224] Khanasa, T.; Prachumrak, N.; Kochapradist, P.; Namuangruk, S.; Keawin, T.; Jungsuttiwong, S., The design, synthesis, and characterization of D-π-A-π-A type organic dyes as sensitizers for dye-sensitized solar cells (DSSCs), *Tetrahedron Lett.***2014**, *55*, 3244-3248.

[225] Ning, Z.; Zhang, Q.; Wu, W.; Pei, H.; Liu, B.; Tian, H.; Starburst triarylamine based dyes for efficient dye-sensitized solar cells, *J. Org. Chem.* **2008**, *73*, 3791-3797.

[226] Tang, J.; Wu, W.; J. Hua, J. Li , X. Li , Tian, H.; Starburst triphenylamine-based cyanine dye for efficient quasi-solid-state dye-sensitized solar cells, *Energy Environ. Sci.* **2009***, 2*, 982-990.

[227] Qian, X.; Lan, X.; Yan, R.; He, Y.; Huang, J.; Hou, L.; T-shaped (D)2–A–π–A type sensitizers incorporating indoloquinoxaline and triphenylamine for organic dye-sensitized solar cells, *Electrochimica Acta* **2017**, *232*, 377–386.

[228] Kumar, M. H.; Mathews, N.; Boix, P. P.; Nonomura, K.; Powar, S.; Ming, L. Y.; Grätzel, M.; Mhaisalkar, S. G.; Decoupling light absorption and charge transport properties in near IR sensitized Fe_2O_3 regenerative cells, ***Energy Environ. Sci. 2013, 6,*** 3280-3285.

[229] Yum, J.-H.; Walter, P.; Huber, S.; Rentsch, D.; Geiger, T.; Nüesch, F.; Angelis, F.D.; Grätzel, M.; Nazeeruddin, M.K.; Efficient far red sensitization of nanocrystalline TiO_2 films by an unsymmetrical squaraine dye, *J. Am. Chem. Soc.* **2007**, *129*, 10320-10321.

[230] Pati, P.B.; Zade, S.S.; New panchromatic dyes comprising benzothiadiazole units within a donor-acceptor π-conjugated spacer Synthesis and photophysical properties, *Tetrahedron* **2013**, *69*, 2167-2174.

[231] Yigitsoy, B.; A.Karim, S.M.; Balan, A.; Baran, D.; Toppare, L.; Multichromic polymers of benzotriazole derivatives: Effect of benzyl substitution, *Electrochimica Acta* **2011**, 56, 2263–2268.

[232] Mao, J.; Guo, F.; Ying, W.; Wu, W.; Li, J.; Hua, J.; Benzotriazole‐ bridged sensitizers containing a furan moiety for dye‐ sensitized solar cells with high open‐ circuit voltage performance. *Chem Asian J.* **2012**, *7*, 982-991.

References

[233] Tyagi, P.; Venkateswarao, A.; Thomas, K. R. J.; Solution processable indoloquinoxaline derivatives containing bulky polyaromatic hydrocarbons: synthesis, optical spectra, and electroluminescence, *J. Org. Chem.* **2011**, *76*, 4571-4581.

[234] Chang, D. W.; Lee, H. J.; Kim, J. H.; S.Y. Park, S. M Park, L. Dai, Novel quinoxaline-based organic sensitizers for dye-sensitized solar cells, *Org Lett.* **2011**, *13*, 3880-3883.

[235] Pei, K.; Wu, Y.; Wu, W.; Zhang, Q.; Chen, Tian, H.; Constructing organic D–A–π-A- featured sensitizers with a quinoxaline unit for high- efficiency solar cells: The effect of an auxiliary acceptor on the absorption and the energy level alignment, *Chem A Eur J.* **2012**, *18*, 8190-200.

[236] Park, J. M.; Jung, C. Y.; Wang, Y.; Choi, H. D.; Park, S. J.; Ou, P.; Jang, W.D.; Jaung, J. Y.; Effect of regioisomeric substitution patterns on the performance of quinoxaline-based dye-sensitized solar cells, *Electrochimica Acta* **2019**, *298*, 650-662.

[237] Saini, A.; Thomas, K. R. J.; Donor–acceptor–acceptor (D–A–A) type 1,8-naphthalimides as non-fullerene small molecule acceptors for bulk heterojunction solar cells, *RSC Adv.* **2016**, *6*, 2017-2024.

[238] Yuan, C.; Liu, W.; Shi, M.; Li, S.; Wang, Y.; Chen, H.; Li, C.-Z.; Chen, H.; A non-fullerene electron acceptor with a spirobifluorene core and four diketopyrrolopyrrole arms end capped by 4-fluorobenzene, *Dyes Pigments.* **2017**, *143*, 217-222.

[239] Qu, S.; Tian, H.; Diketopyrrolopyrrole (DPP)-based materials for organic photovoltaics, *Chem.Commun.* **2012**, *48*, 3039-3051.

[240] Qu, S.; Wu, W.; Hua, J.; Kong, C.; Long, Y.; Tian, H.; New Diketopyrrolopyrrole (DPP) Dyes for Efficient Dye-Sensitized Solar Cells, *J. Phys. Chem. C* **2010**, *114*, 1343-1349.

[241] Qu, S.; Qin, C.; Islam, A.; Wu, Y.; Zhu, W.; Hua, J.; Tian, H.; Han, L.; A novel D–A-π-A organic sensitizer containing a diketopyrrolopyrrole unit with a branched alkylchain for highly efficient and stable dye-sensitized solar cells, *Chem. Commun.* **2012**, *48*, 6972-6974.

[242] Gao, P.; Tsao, H. N.; Grätzel, M.; Nazeeruddin, M. K.; Fine-tuning the electronic structure of organic dyes for dye-sensitized solar cells, *Org. Lett.* **2012**, *14*, 4330–4333.

[243] Lu, X.; Jia, X.; Wang, Z.; Zhou, G.; X-shaped organic dyes with a quinoxaline bridge for use in dye-sensitized solar cells, *J. Mater. Chem. A* **2013**, *1*, 9697–9706.

[244] Kim, S.; Lee, J. K.; Kang, S. O.; Ko, J.; Yum, J. H.; Fantacci, S.; Angelis, F. De; Censo, D. Di; Nazeeruddin, M. K.; Grätzel , M.; Molecular engineering of organic sensitizers for solar cell applications, *J. Am. Chem. Soc.* **2006**, *128*, 16701-16707.

[245] Wang, M.; Xu, M.; Shi, D.; Li, R.; Gao, F.; Zhang, G.; Yi, Z.; Humphry-Baker, R.; Wang , P.; Zakeeruddin, S. M.; Gräzel, M.; High- performance liquid and solid dye-sensitized solar cells based on a novel metal- free organic sensitizer, *Adv. Mater.* **2008**, *20*, 4460-4463.

[246] Yigit, M. Z.; Bilgili, H.; Sefer, E.; Demic, S; Zafer, C.; Can , M.; Koyuncu, S.; Effect of a pi-bridging unit in triphenylamine-benzothiadiazole based donor acceptor chromophores for dye-sensitized solar cells, *Electrochimica Acta* **2014**, *147*, 617–625.

[247] Liu, W. H.; Wu, I. C.; Lai, C. H.; Lai, C. H.; Chou, P. T.; Li, Y. T.; Y. T. Chen, Y. T.; Hsu, Y. Y.; Chi, Y.; Simple organic molecules bearing a 3,4-ethylenedioxythiophene linker for efficient dye-sensitized solar cells, *Chem. Commun.* **2008,** 5152-5154.

[248] Yum, J.-H.; Hagberg, D. P.; Moon, S.-J.; Karlsson, K. M.; Marinado, T.; Sun , L.; Hagfeldt, A.; Nazeeruddin, M. K.; Grätzel, M.; A light-resistant organic sensitizer for solar-cell applications, *Angew. Chem. Int. Ed.* **2009**, 48, 1576-1580.

[249] Ning, Z. J.; Tian, H.; Triarylamine: a promising core unit for efficient photovoltaic materials, *Chem. Commun.* **2009**, 5483-5495.

[250] Huang, S.-T.; Hsu, Y.-C.; Yen, Y.-S.; Chou, H. H.; Lin, J.T.; Chang, C.-W.; Hsu, C.-P.; Tsai, C.; Yin, D.-J.; Organic dyes containing a cyanovinyl entity in the spacer for solar cells applications, *J. Phys. Chem. C* **2008***, 112*, 19739–19747.

[251] Hagberg, D. P.; Edvinsson, T.; Marinado, T.; Boschloo, G.; Hagfeldt, A.; Sun, L.; A novel organic chromophore for dye-sensitized nanostructured solar cells, *Chem. Commun.* **2006**, 2245-2247.

[252] Hara, K.; Wang, Z.-S; Sato, T.; Furube, A.; Katoh, R.; Sugihara, H.; Dan-oh, Y.; Kasada, C.; Shinpo, A.; Suga, S.; Oligothiophene-containing coumarin dyes for efficient dye-sensitized solar cells, *J. Phys. Chem. B* **2005**, *109,* 15476-15482.

[253] Li, S.-L.; Jiang, K.-J.; Shao, K.-F.; Yang, L.M.; Novel organic dyes for efficient dye-sensitized solar cells, *Chem. Commun.* **2006**, 2792-2794.

[254] Kim, S.; Choi, H.; Kim, D.; Song, K.; Kang, S.O.; Ko, J.; Novel conjugated organic dyes containing bis-dimethylfluorenyl amino phenyl thiophene for efficient solar cell, *Tetrahedron* **2007**, *63*, 9206-9212.

[255] Baheti, A.; Thomas, K. R. J.; Li, C-T.; Lee, C-P.; Ho, K.-C.; Fluorene-based sensitizers with a phenothiazine donor: effect of mode of donor tethering on the performance of dye-sensitized solar cells, *ACS Appl. Mater. Interfaces* **2015**, *7* 2249−2262.

[256] Wielopolski, M.; Kim, J-H.; Jung, Y-S.; Yu, Y-J.; Kay, K.-Y.; Holcombe, T. W.; Zakeeruddin, S. M.; Grätzel, M.; Mose, J-E.; Position-dependent extension of

References

π-conjugation in D-π-A dye sensitizers and the impact on the charge-transfer properties, *J. Phys. Chem. C* **2013**, *117*, 13805−13815.

[257] Zeng, W.; Lai, H. Y.; Lee, W. K.; Jiao, M.; Shiu, Y. J.; Zhong, C.; Gong, S.; Zhou, T.; Xie, G.; Sharma, M.;. Achieving Nearly 30% External Quantum Efficiency for Orange–Red Organic Light Emitting Diodes by Employing Thermally Activated Delayed Fluorescence Emitters Composed of 1,8-Naphthalimide-Acridine Hybrids. *Adv. Mater.* **2018**, *30* (5), 1–8.

[258] Goes, M.; Verhoeven, J. W.; Hofstraat, H.; Brunner, K. OLED and PLED Devices Employing Electrogen- Cence. *Chemphyschem A Eur. J. Chem. Phys. Phys. Chem.* **2003**, *4* (4), 349–358.

[259] Yu G.; Gao, J.; Hummelen J.C.; Wudl, F.; Heeger A. J. Polymer photovoltaic cells: Enhanced via a network of internal donor-acceptor heterojunctions. *Science*, **1995**, *270*, 1789.

[260] Zeng, W.; Cao, Y.; Bai, Y.; Wang, Y.; Shi, Y.; Zhang, M.; Wang, F.; Pan, C.; Wang, P. Efficient Dye-Sensitized Solar Cells with an Organic Photosensitizer Featuring Orderly Conjugated Ethylenedioxythiophene and Dithienosilole Blocks, *Chem. Mater.* **2010** *22*, 1915-1925.

[261] Kim, M.; Park, W. T.; Park, S. A.; Park, C. W.; Ryu, S. U.; Lee, D. H.; Noh, Y. Y.; Park, T. Controlling Ambipolar Charge Transport in Isoindigo-Based Conjugated Polymers by Altering Fluorine Substitution Position for High-Performance Organic Field-Effect Transistors. *Adv. Funct. Mater.* **2019**, *29* (10), 1–8.

[262] Meijer, E. J.; De Leeuw, D. M.; Setayesh, S.; Van Veenendaal, E.; Huisman, B. H.; Blom, P. W. M.; Hummelen, J. C.; Scherf, U.; Klapwijk, T. M. Solution-Processed Ambipolar Organic Field-Effect Transistors and Inverters. *Nat. Mater.* **2003**, *2* (10),

[263] Misra, R.; Maragani, R.; Pathak, B.; Gautam, P. Star Shaped Ferrocenyl Substituted. RSC Advances **2015**, 71046–71051.

[264] Dalton, L. R.; Sullivan, P. A.; Bale, D. H. Electric Field Poled Organic Electro-optic Materials: State of the Art and Future Prospects. *Chem. Rev.* **2010**, *110*, 25–55

[265] Mukherj S.; Thilagar, P. Molecular Flexibility Tuned Emission in '"V"' Shaped Naphthalimides: Hg(II) detection and aggregation induced emission enhancement (AIEE) *Chem. Commun.,* **2013**, *49*, 7292–7294.

[266] Thelakkat, M.; Schmidt, H. W. Low Molecular Weight and Polymeric Heterocyclics as Electron Transport/ Hole-Blocking Materials in Organic Light-Emitting Diodes. *Polym. Adv. Technol.* **1998**, *9* (7), 429–442

[267] Mukherjee, S.; Thilagar, P. Fine-Tuning Solid-State Luminescence in NPIs (1,8-Naphthalimides): Impact of the Molecular Environment and Cumulative Interactions. *Phys.Chem.Chem.Phys.,* **2014**, 16, 20866–20877.

[268] Jou, J. H.; Kumar, S.; Agrawal, A.; Li, T. H.; Sahoo, S. Approaches for Fabricating High Efficiency Organic Light Emitting Diodes. *J. Mater. Chem. C* **2015**, *3* (13), 2974–3002.

[269] Steckler, T. T.; Zhang, X.; Hwang, J.; Honeyager, R.; Ohira, S.; Zhang, X. H.; Grant, A.; Ellinger, S.; Odom, S. A.; Sweat, D.; et al. A Spray-Processable, Low Bandgap, and Ambipolar Donor - Acceptor Conjugatedpolymer. *J. Am. Chem. Soc.* **2009**, *131* (8), 2824–2826.

[270] Heeney, M.; Zhang, W.; Crouch, D. J.; Chabinyc, M. L.; Gordeyev, S.; Hamilton, R.; Higgins, S. J.; McCulloch, I.; Skabara, P. J.; Sparrowe, D.; et al. Regioregular Poly(3-Hexyl)Selenophene: A Low Band Gap Organic Hole Transporting Polymer. *Chem. Commun.* **2007**, No. 47, 5061–5063.

[271] Bizzarri, C.; Spuling, E.; Knoll, D. M.; Volz, D.; Bräse, S. Sustainable Metal Complexes for Organic Light-Emitting Diodes (OLEDs). *Coord. Chem. Rev.* **2018**, *373*, 49–82.

[272] Romain, M.; Thiery, S.; Shirinskaya, A.; Declairieux, C.; Tondelier, D.; Geffroy, B.; Jeannin, O.; Rault-Berthelot, J.; Métivier, R.; Poriel, C. Ortho-, Meta-, and Para-Dihydroindenofluorene Derivatives as Host Materials for Phosphorescent OLEDs. *Angew. Chem. Int. Ed.* **2015**, *54* (4), 1176–1180

[273] Wagner, D.; Rothmann, M.; Strohriegl, P.; Lennartz, C.; Münster, I.; Wagenblast, G.; Schildknecht, C. Host Materials for Blue Phosphorescent OLEDs. *Org. Light Emit. Mater. Devices XVI* **2012**, *8476*, 84761O.

[274] Elmorsy, M. R.; Su, R.; Fadda, A. A.; Etman, H. A.; Tawfik, E. H.; El-Shafei, A. Molecular Engineering and Synthesis of Novel Metal-Free Organic Sensitizers with D-π-A-π-A Architecture for DSSC Applications: The Effect of the Anchoring Group. *Dye. Pigment.* **2018**, *158* (March), 121–130.

[275] Patil, Y.; Misra, R.; Chen, F. C.; Sharma, G. D. "Small molecule based *N*-phenyl carbazole substituted diketopyrrolopyrroles as donors for solution-processed bulk heterojunction organic solar cells" *Phys. Chem. Chem. Phys.* **2016**, *18*, 22999

[276] Liu, T.; Wei, Y. G.; Yuan, Y. Q.; Guo, Q. X. Charge Transfer in Excited Donor-Acceptor Phenothiazine Derivatives. *Chinese J. Chem.* **2005**, *23* (10), 1430–1436.

References

[277] Ding, J.; Zhang, B.; Lü, J.; Xie, Z.; Wang, L.; Jing, X.; Wang, F. Solution-Processable Carbazole-Based Conjugated Dendritic Hosts for Power-Efficient Blue-Electrophosphorescent Devices. *Adv. Mater.* **2009**, *21* (48), 4983–4986.

[278] Sarma, M.; Wong, K. T. Development of Materials for Blue Organic Light Emitting Devices. *Chem. Rec.* **2019**, 1–27.

[279] Tagare, J.; Ulla, H.; Satyanarayan, M. N.; Vaidyanathan, S. Journal of Photochemistry and Photobiology A : Chemistry Ef Fi Cient Non-Doped Bluish-Green Organic Light Emitting Devices Based on N 1 Functionalized Star-Shaped Phenanthroimidazole Fl Uorophores. *"Journal Photochem. Photobiol. A Chem.* **2018**, *353*, 53–64.

[280] Li, W.; Li, J.; Liu, D.; Wang, F.; Zhang, S. Bipolar Host Materials for High-Efficiency Blue Phosphorescent and Delayed-Fluorescence OLEDs. *J. Mater. Chem. C* **2015**, *3*, 12529–12538.

[281] Chen, B.; Ding, Y.; Li, X.; Zhu, W.; Hill, J. P.; Ariga, K.; Xie, Y. Steric Hindrance-Enforced Distortion as a General Strategy for the Design of Fluorescence "Turn-on" Cyanide Probes. *Chem. Commun.* **2013**, *49* (86), 10136–10138.

[282] Rosspeintner, A.; Vauthey, E. Bimolecular Photoinduced Electron Transfer Reactions in Liquids under the Gaze of Ultrafast Spectroscopy. *Phys. Chem. Chem. Phys.* **2014**, *16*, 25741–25754.

[283] Konidena, R. K.; Justin Thomas, K. R.; Singh, M.; Jou, J. H. Thienylphenothiazine Integrated Pyrenes: An Account on the Influence of Substitution Patterns on Their Optical and Electroluminescence Properties. *J. Mater. Chem. C* **2016**, *4* (19), 4246–4258.

[284] Karthik, D.; Thomas, K. R. J.; Jou, J. H.; Chen, Y. L. Synthesis, Characterization and Electroluminescence of Carbazole-Benzimidazole Hybrids with Thiophene/Phenyl Linker. *Dye. Pigment.* **2016**, *133*, 132–142.

[285] Carlotti, B.; Benassi, E.; Spalletti, A.; Fortuna, C. G.; Elisei, F.; Barone, V. Photoinduced Symmetry-Breaking Intramolecular Charge Transfer in a Quadrupolar Pyridinium Derivative. *Phys. Chem. Chem. Phys.* **2014**, *16*, 13984–13994.

[286] Carlotti, B.; Consiglio, G.; Elisei, F.; Fortuna, C. G.; Mazzucato, U.; Spalletti, A. Intramolecular Charge Transfer of Push-Pull Pyridinium Salts in the Triplet Manifold. *J. Phys. Chem. A* **2014**, *118*, 7782–7787.

[287] Singh, A.; Pati, A. K.; Mishra, A. K. Photoinduced Intramolecular Charge Transfer in a Cross-Conjugated Push-Pull Enediyne: Implications toward Photoreaction. *Phys. Chem. Chem. Phys.* **2018**, *20*, 14889–14898.

[288] Singh, A.; Pati, A. K.; Mishra, A. K. Photophysical Impact of Diacetylenic Conjugation on Classical Donor-Acceptor Electronic Energy Pair. *J. Phys. Chem. A* **2019**, *123*, 443–453.

[289] Pati, A. K.; Mohapatra, M.; Ghosh, P.; Gharpure, S. J.; Mishra, A. K., Deciphering the Photophysical Role of Conjugated Diyne in Butadiynyl Fluorophores: Synthesis, Photophysical and Theoretical Study. *J. Phys. Chem. A* **2013**, *117*, 6548−6560

[290] Pati, A. K.; Gharpure, S. J.; Mishra, A. K. On the Photophysics of Butadiyne Bridged Pyrene-Phenyl Molecular Conjugates: Multiple Emissive Pathways through Locally Excited, Intramolecular Charge Transfer and Excimer States. *Faraday Discuss.* **2015**, *177*, 213–235.

[291] Rajendiran, N.; Venkatesh, G.; Sankaranarayanan, R. K. Dual Fluorescence of Omeprazole: Effect of Solvents and PH. *Phys. Chem. Liq.* **2014**, *52* (6), 738–750.

[292] Klymchenko, A. S.; Kenfack, C.; Duportail, G.; Mély, Y. Effects of Polar Protic Solvents on Dual Emissions of 3-Hydroxychromones. *J. Chem. Sci.* **2007**, *119* (2), 83–89.

[293] Vuram, P. K.; Subuddhi, U.; Krishnaji, S. T.; Chadha, A.; Mishra, A. K. Synthesis and Aggregation Properties of Dansylated Glycerol-Based Amphiphilic Polyether Dendrons. *European J. Org. Chem.* **2010**, *26*, 5030–5040

[294] Liu, Y.; Guo, J.; Yue, H.; Luo, T.; Tan, R.; Li, X. Enhancement of Thermal Stability and Photoluminescent Performance of Blue Light Emitting Material by Incorporating Adamantane Moieties into Carbazole System. *J. Macromol. Sci. Part A Pure Appl. Chem.* **2018**, *55* (2), 176–182.

[295] Collado-Fregoso, E.; Boufflet, P.; Fei, Z.; Gann, E.; Ashraf, S.; Li, Z.; McNeill, C. R.; Durrant, J. R.; Heeney, M. Increased Exciton Dipole Moment Translates into Charge-Transfer Excitons in Thiophene-Fluorinated Low-Bandgap Polymers for Organic Photovoltaic Applications. *Chem. Mater.* **2015**, *27* (23), 7934–7944.
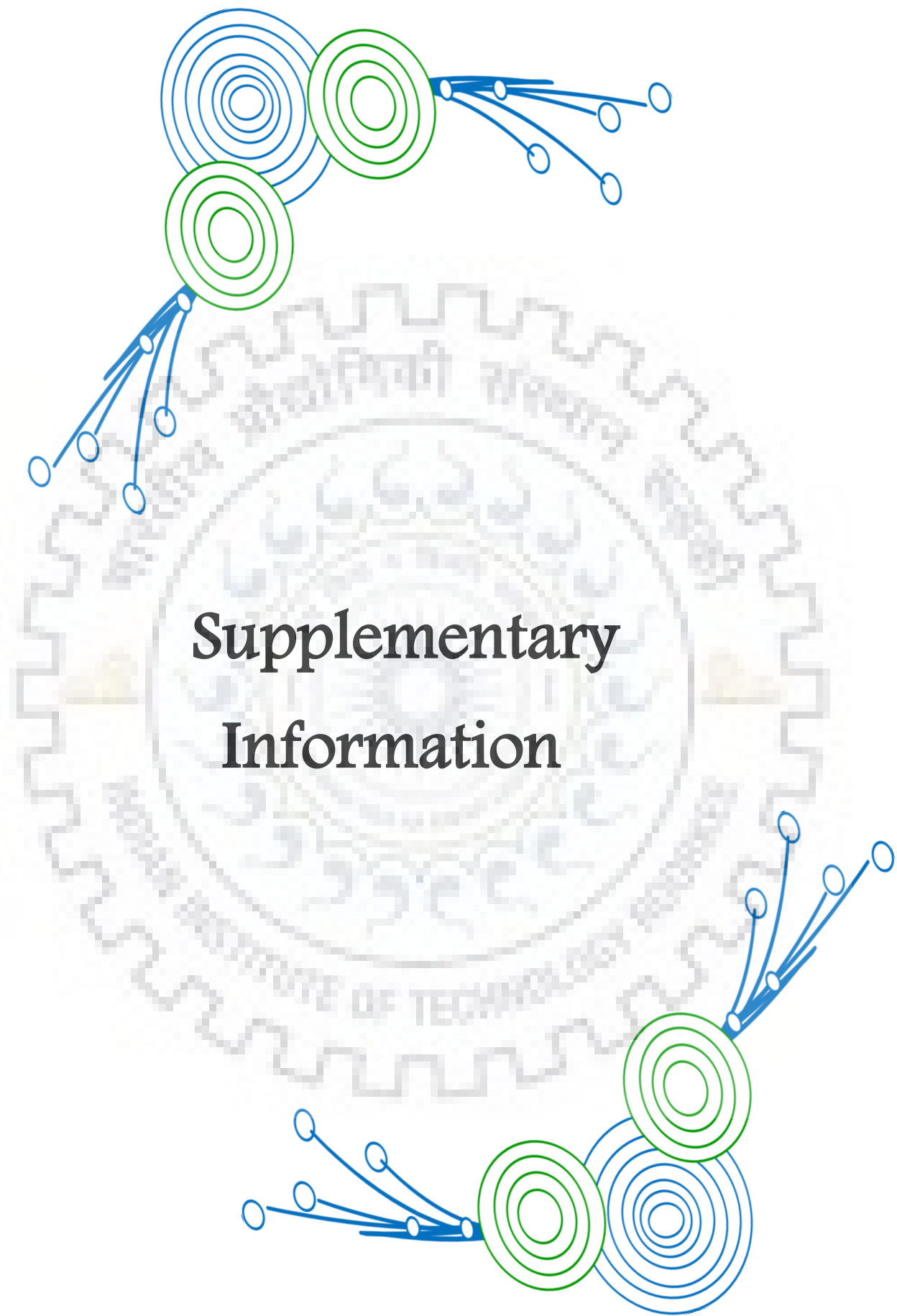
Supplementary Information

Supplementary Information

(¹H and ¹³C NMR spectra of unpublished compounds)
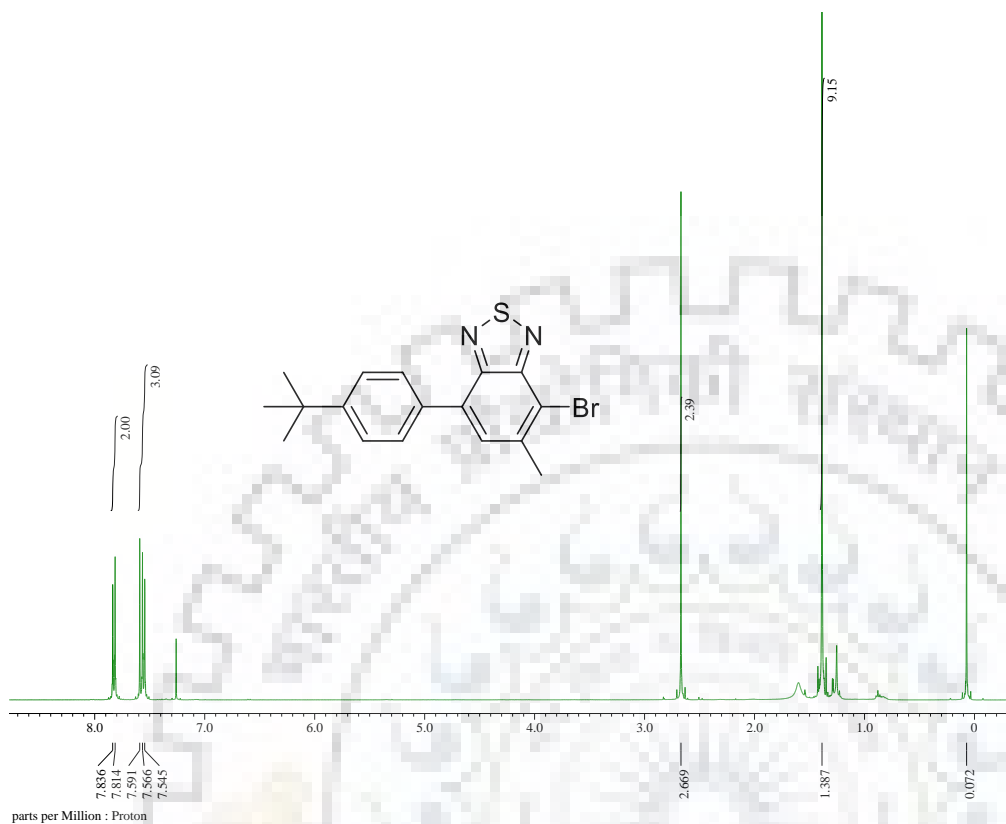
Figure S1 ¹H NMR spectra of **2a** recorded in CDCl₃.
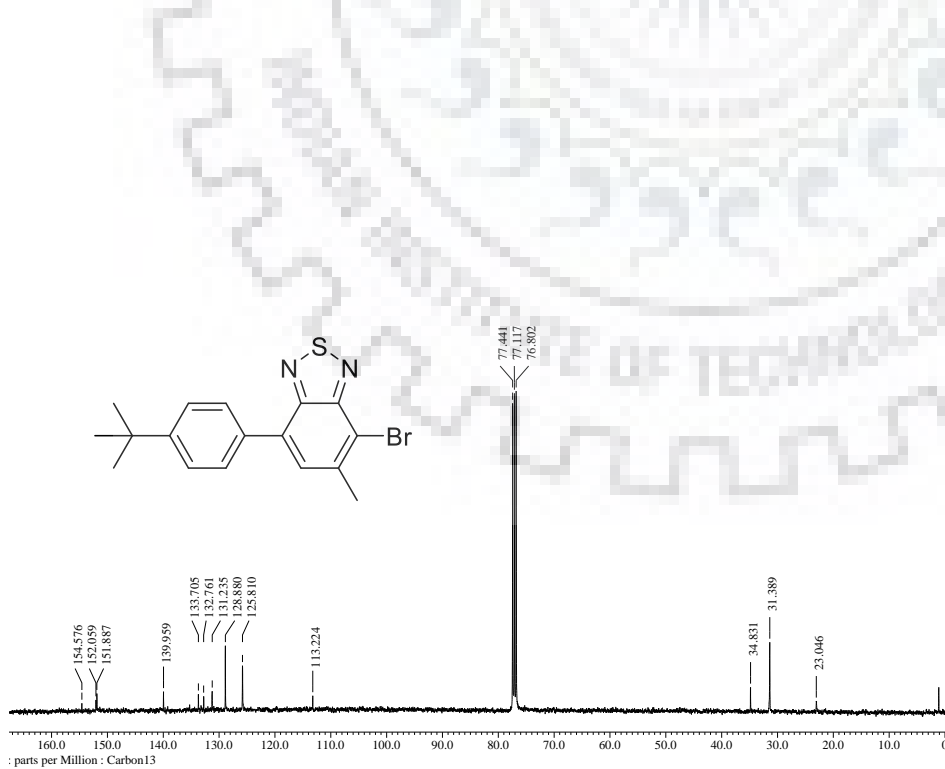
Figure S2 ¹³C NMR spectra of **2a** recorded in CDCl₃.

224
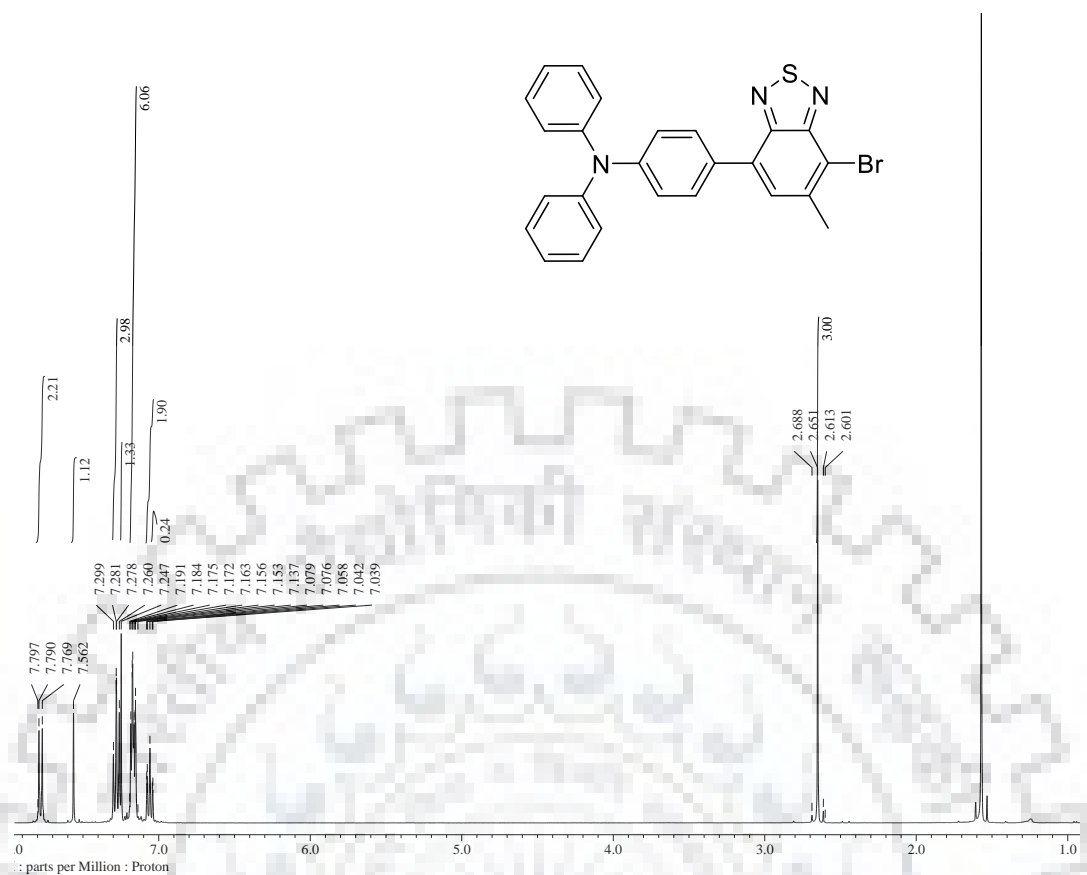
Figure S3 ¹H NMR spectra of **2b** recorded in CDCl₃.
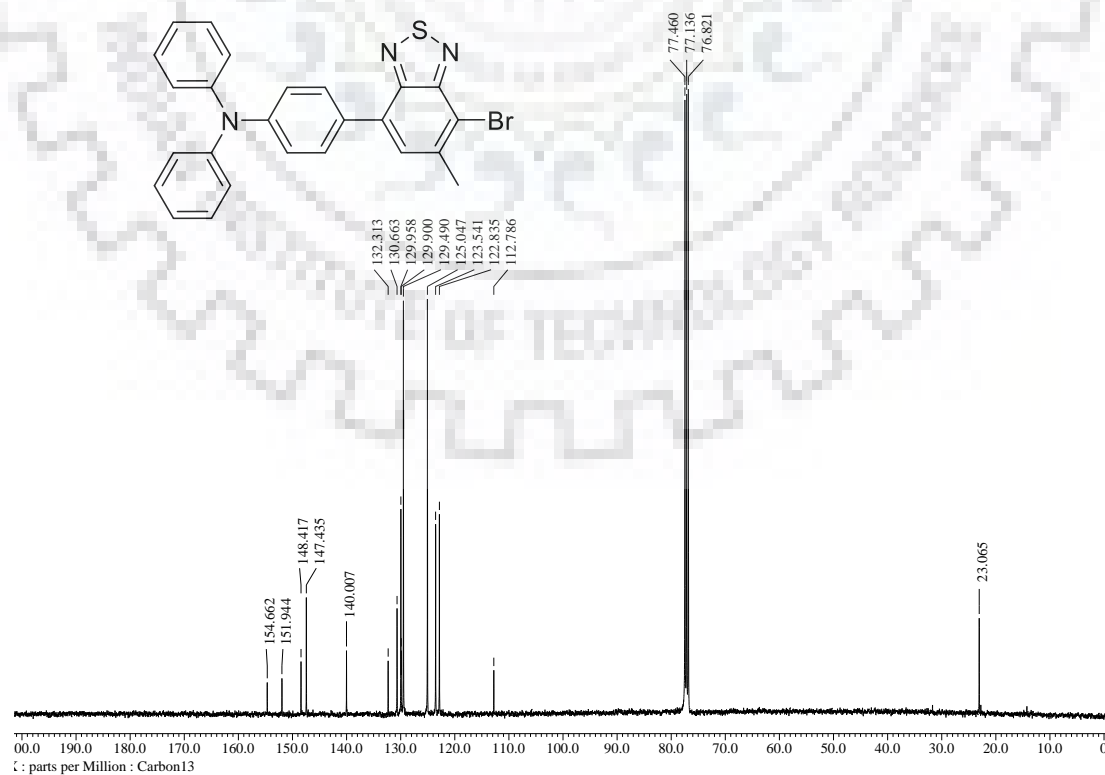
Figure S4 ¹³C NMR spectra of **2b** recorded in CDCl₃.

225
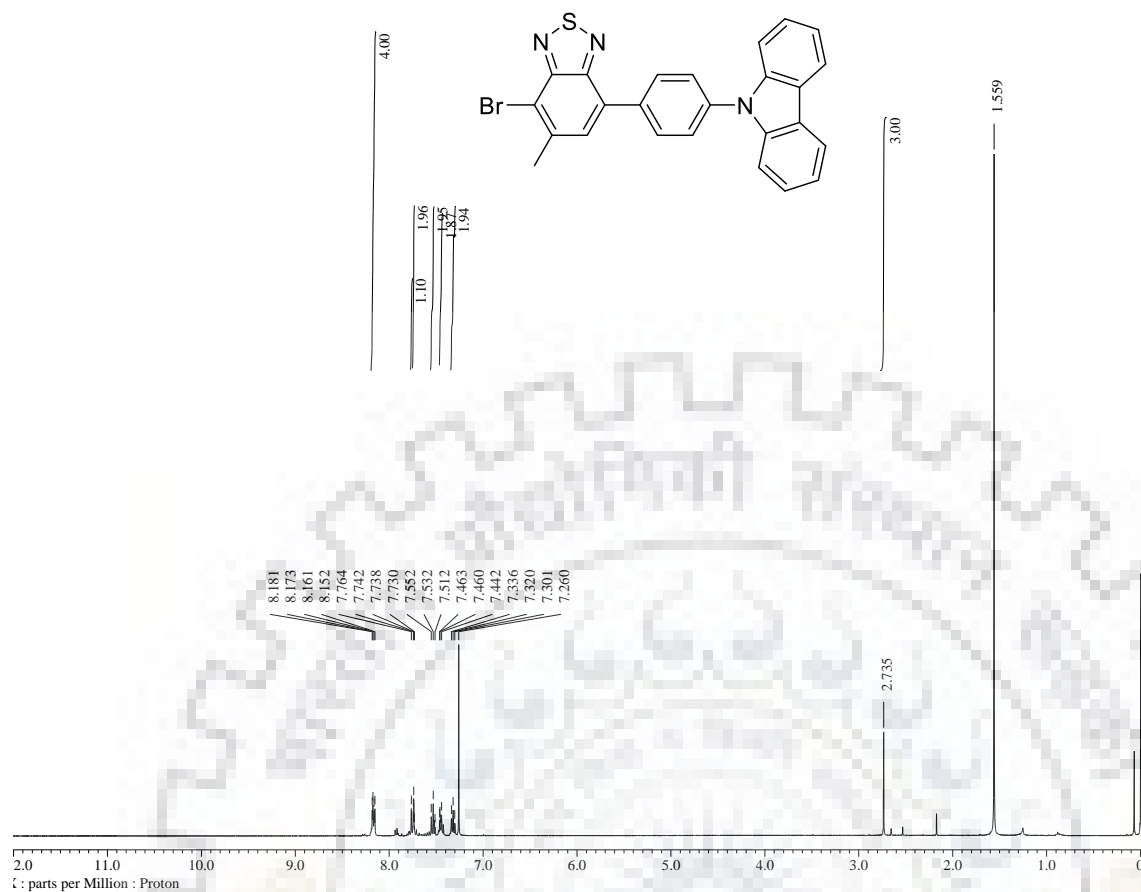
Figure S5. ^{1}H NMR spectra of **7a** recorded in CDCl$_3$
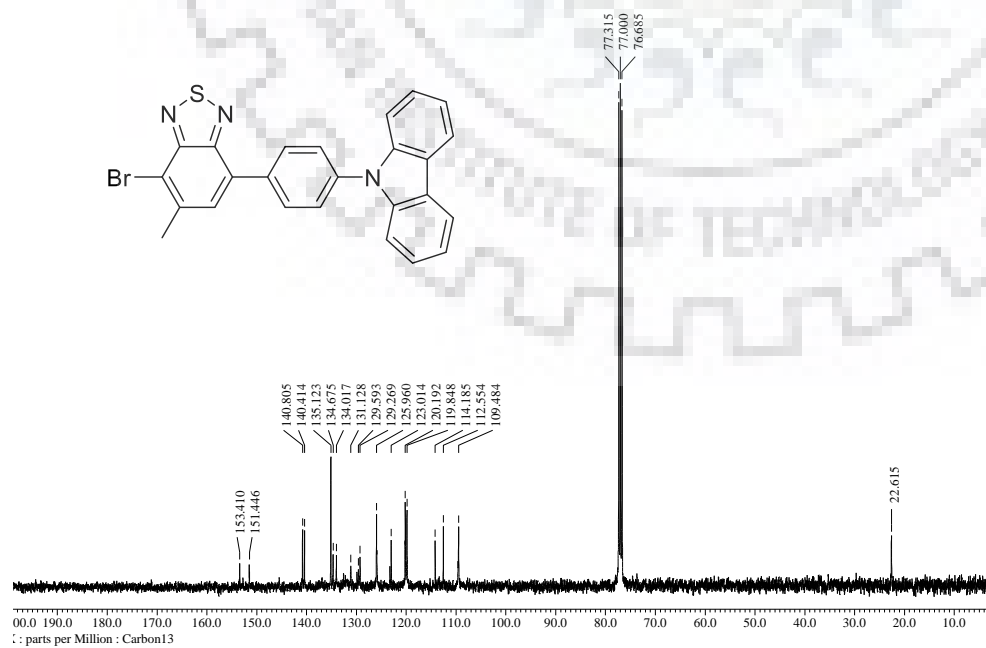
Figure S6. ^{13}C NMR spectra of **7a** recorded in CDCl$_3$
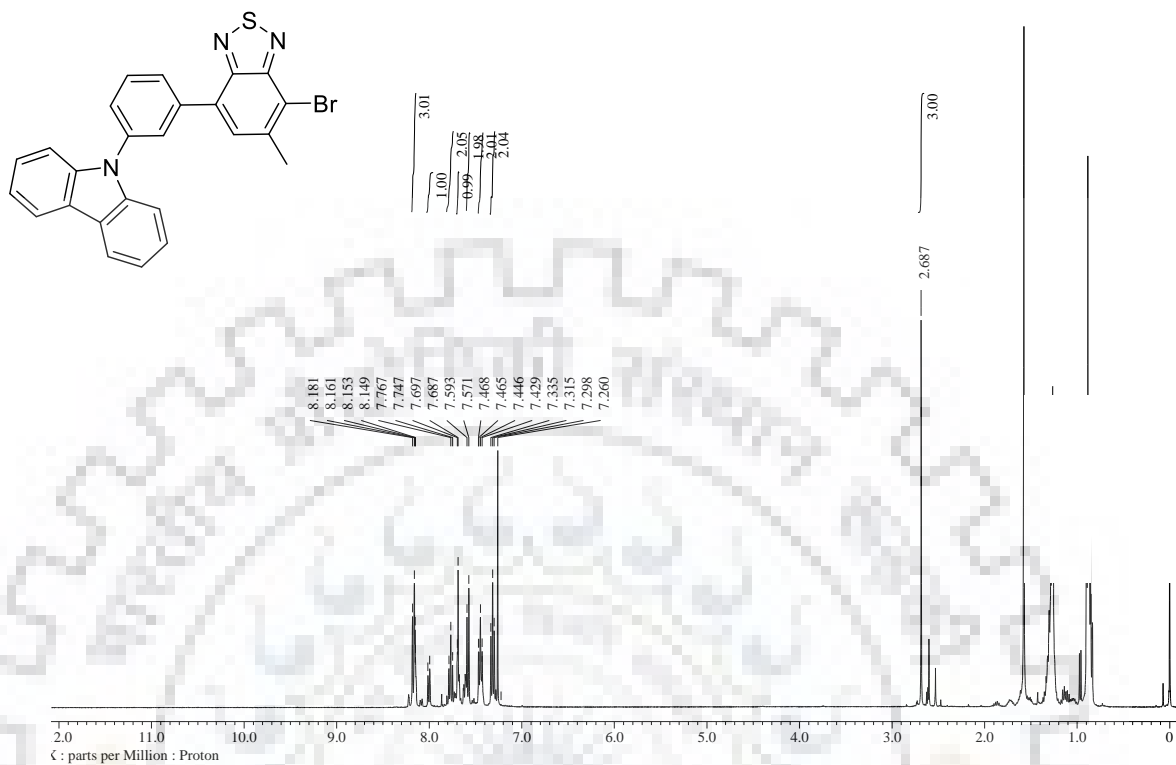
Figure S7. ^{1}H NMR spectra of **7b** recorded in CDCl$_3$
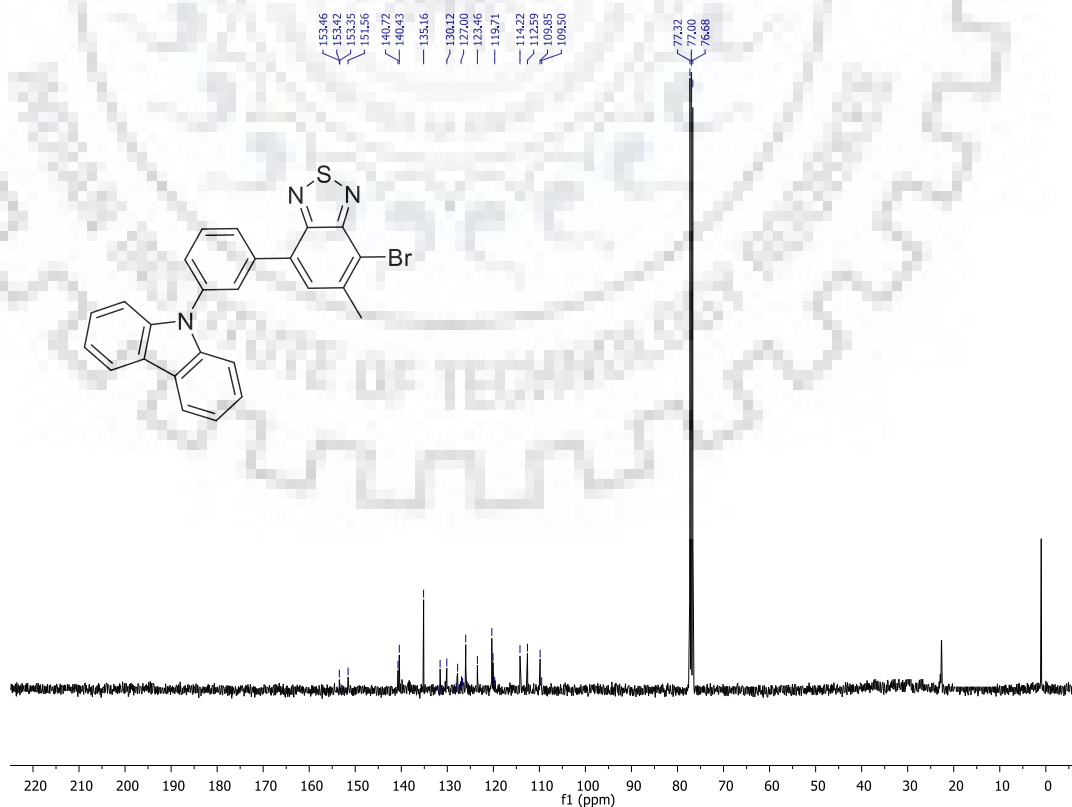
Figure S8. ^{13}C NMR spectra of **7b** recorded in CDCl$_3$
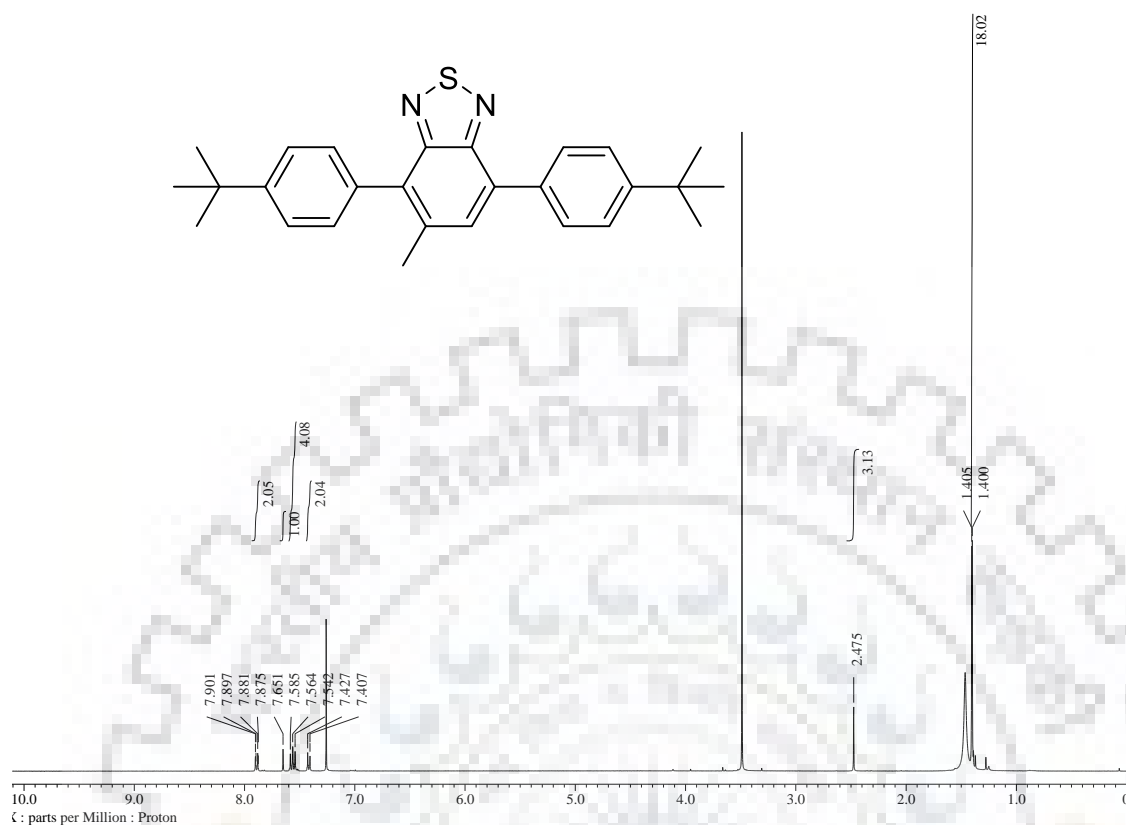
Figure S9 ^{1}H NMR spectra of **3** recorded in CDCl$_3$.
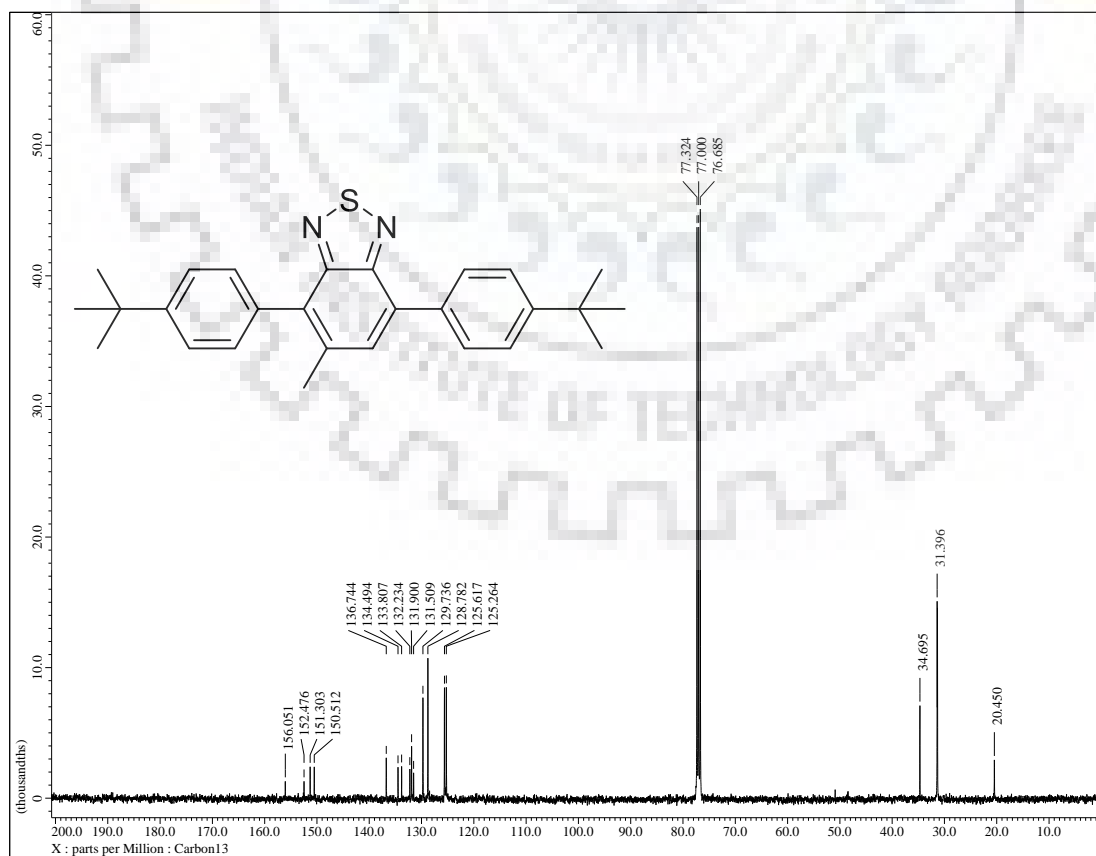
Figure S10 ^{13}C NMR spectra of **3** recorded in CDCl$_3$.
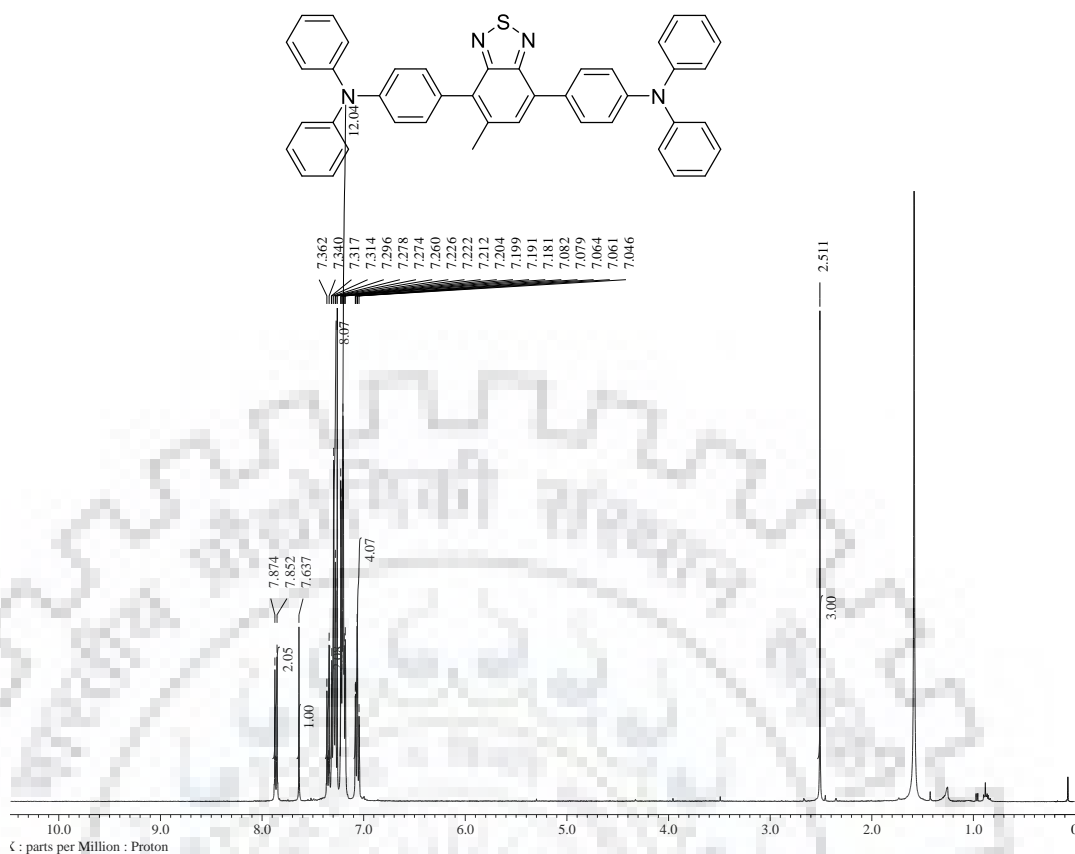
Figure S11 ^{1}H NMR spectra of **4** recorded in CDCl$_3$.
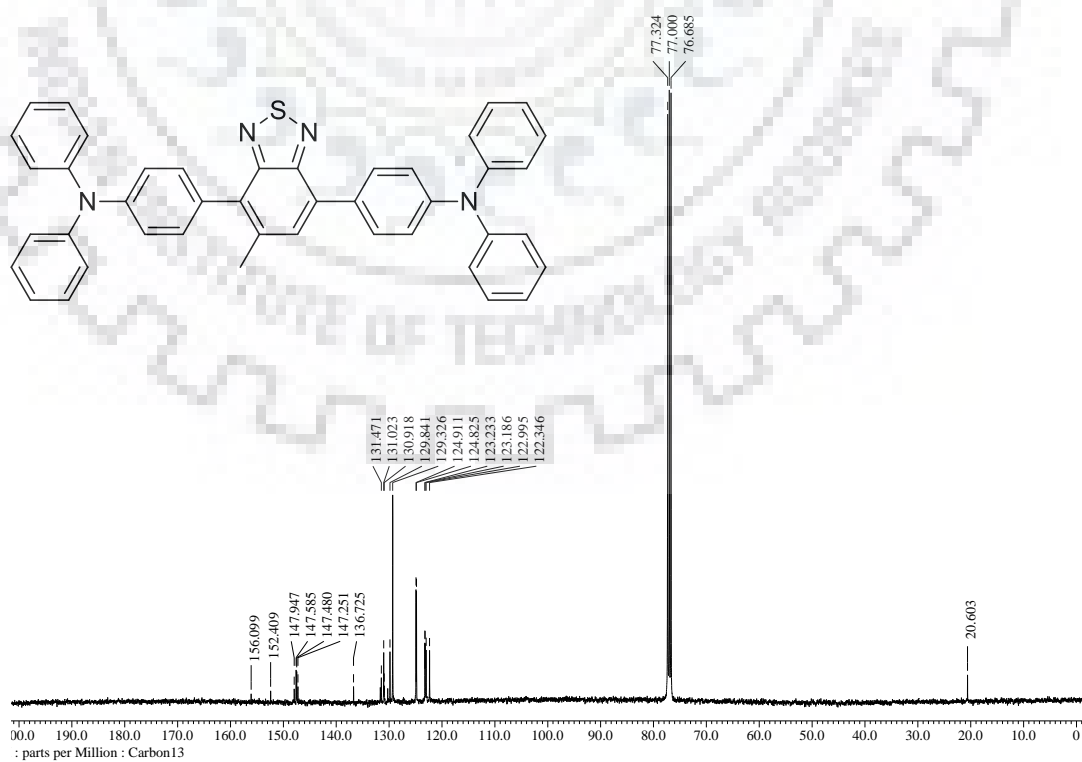
Figure S12 ^{13}C NMR spectra of **4** recorded in CDCl$_3$.

229
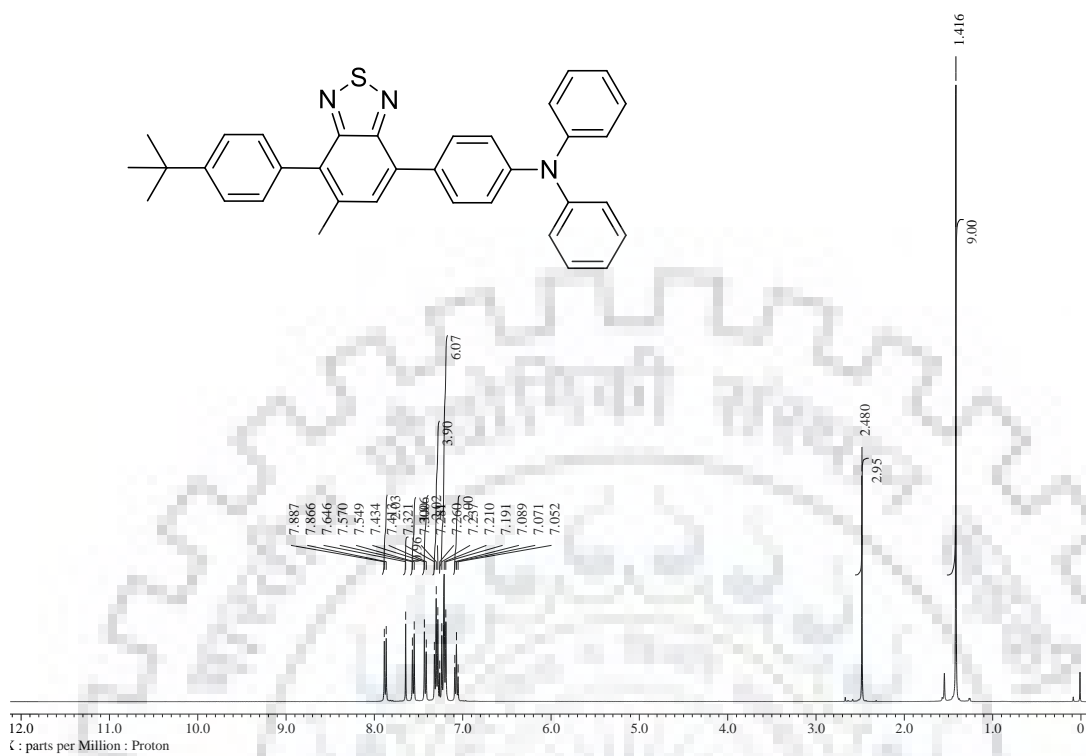
Figure S13 ^{1}H NMR spectra of **5** recorded in CDCl$_3$.

Figure S14 ^{13}C NMR spectra of **5** recorded in CDCl$_3$.
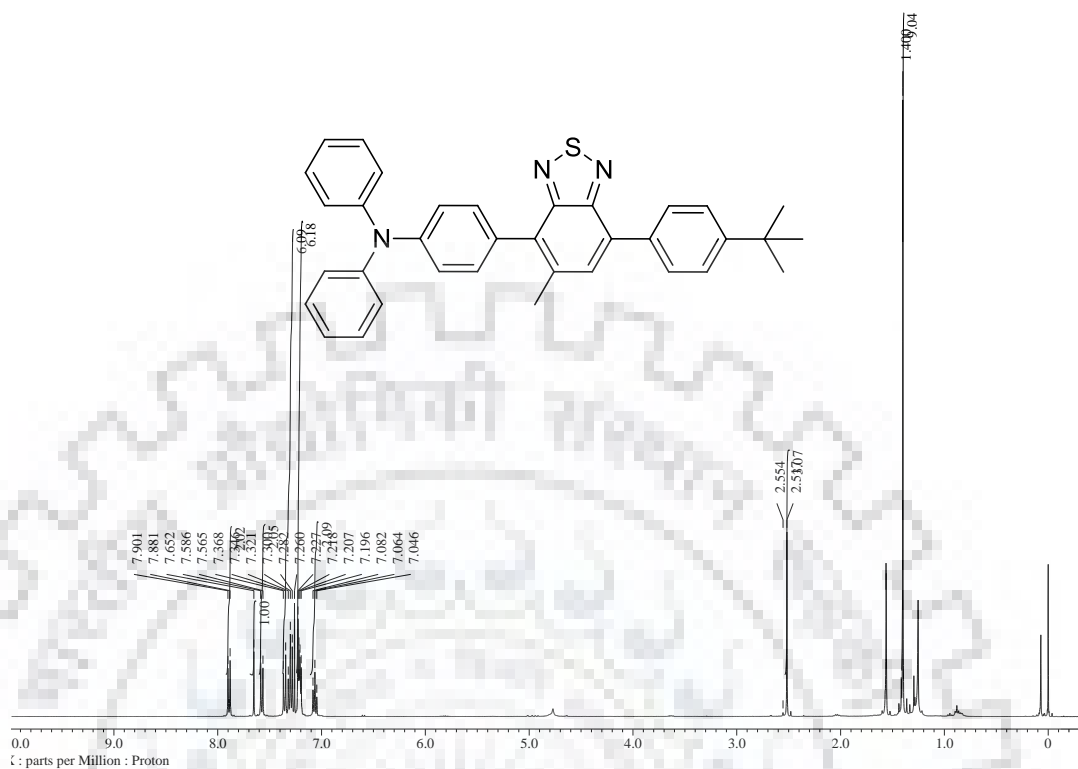
Figure S15 ^{1}H NMR spectra of **6** recorded in CDCl$_3$.
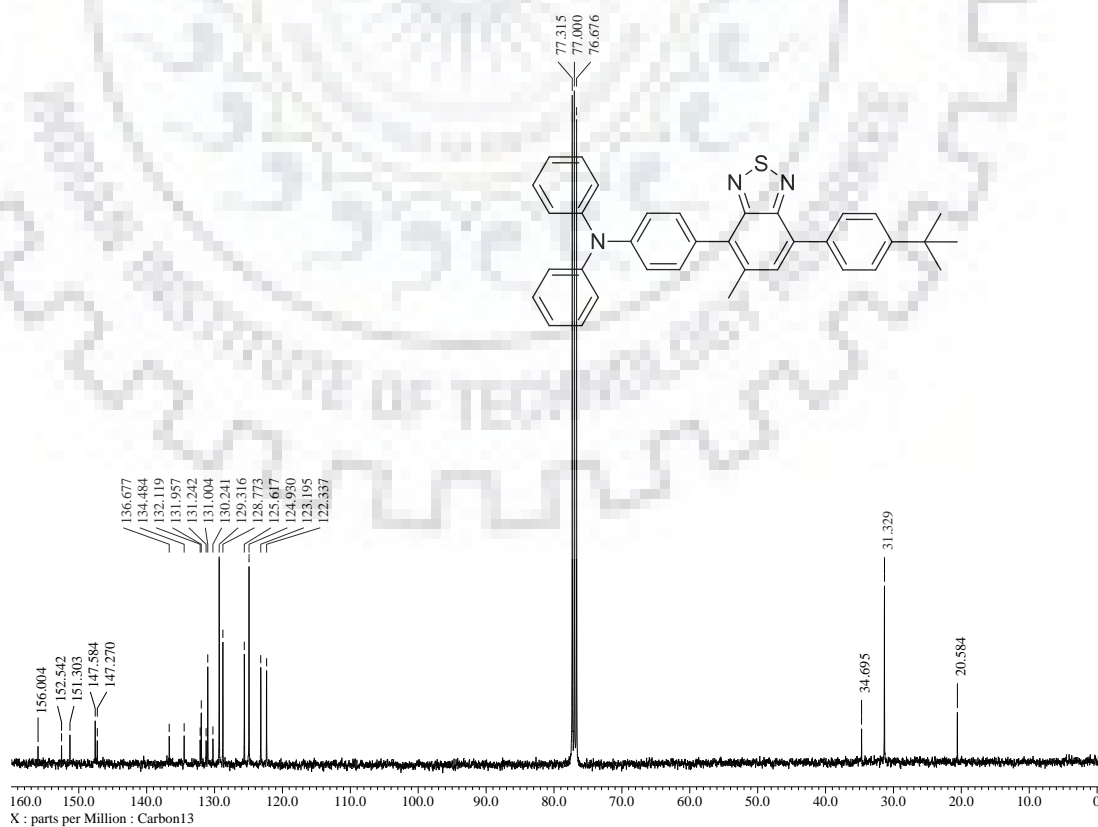
Figure S16 ^{13}C NMR spectra of **6** recorded in CDCl$_3$.

231
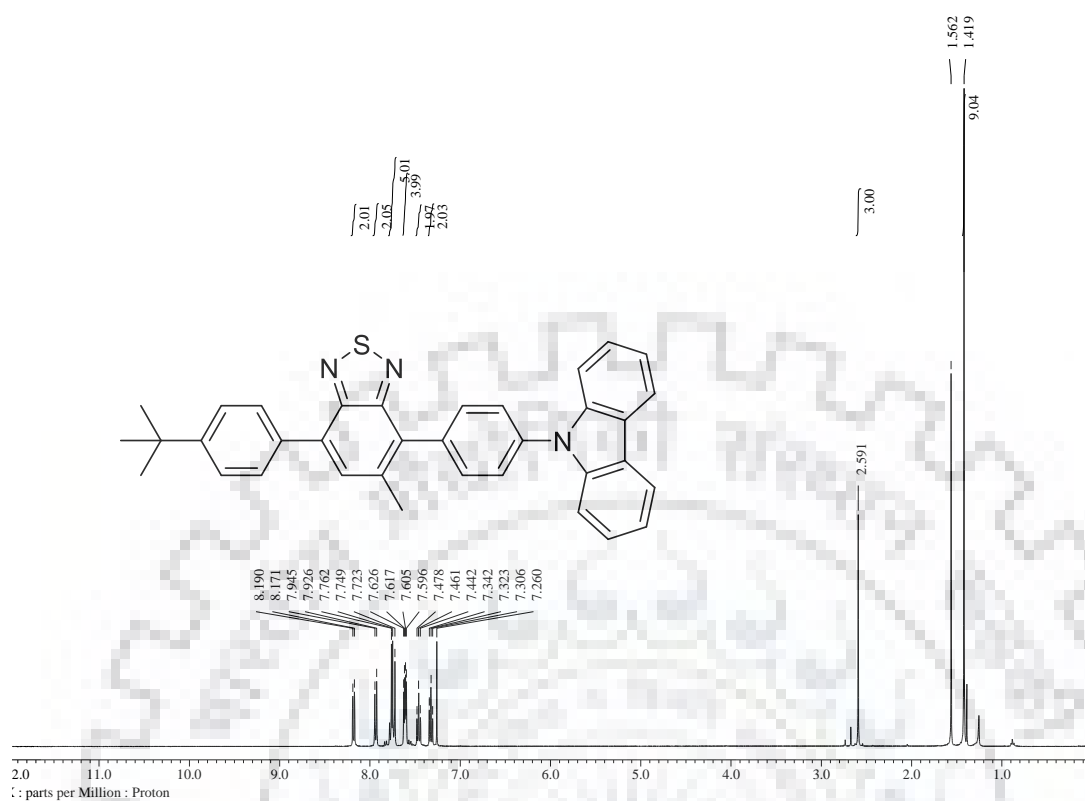
Figure S17. ^{1}H NMR spectra of **8** recorded in CDCl$_3$
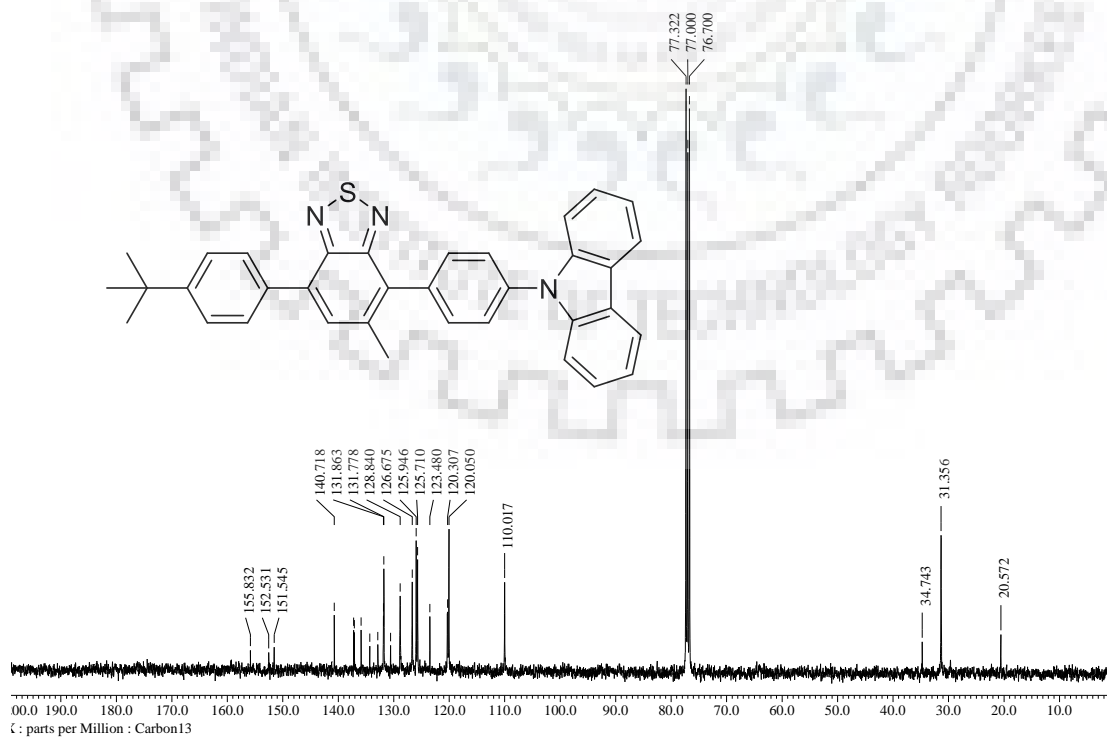
Figure S18. ^{13}C NMR spectra of **8** recorded in CDCl$_3$
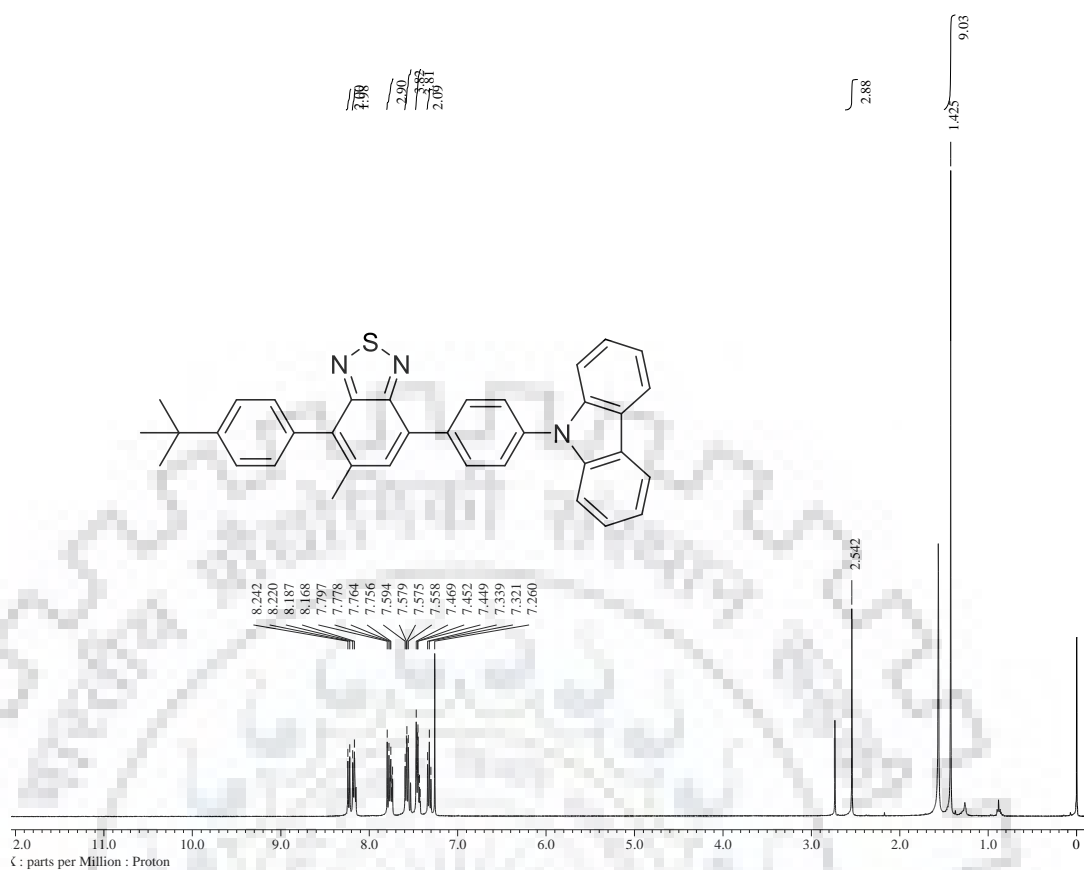
Figure S19. ^{1}H NMR spectra of **9** recorded in CDCl$_3$
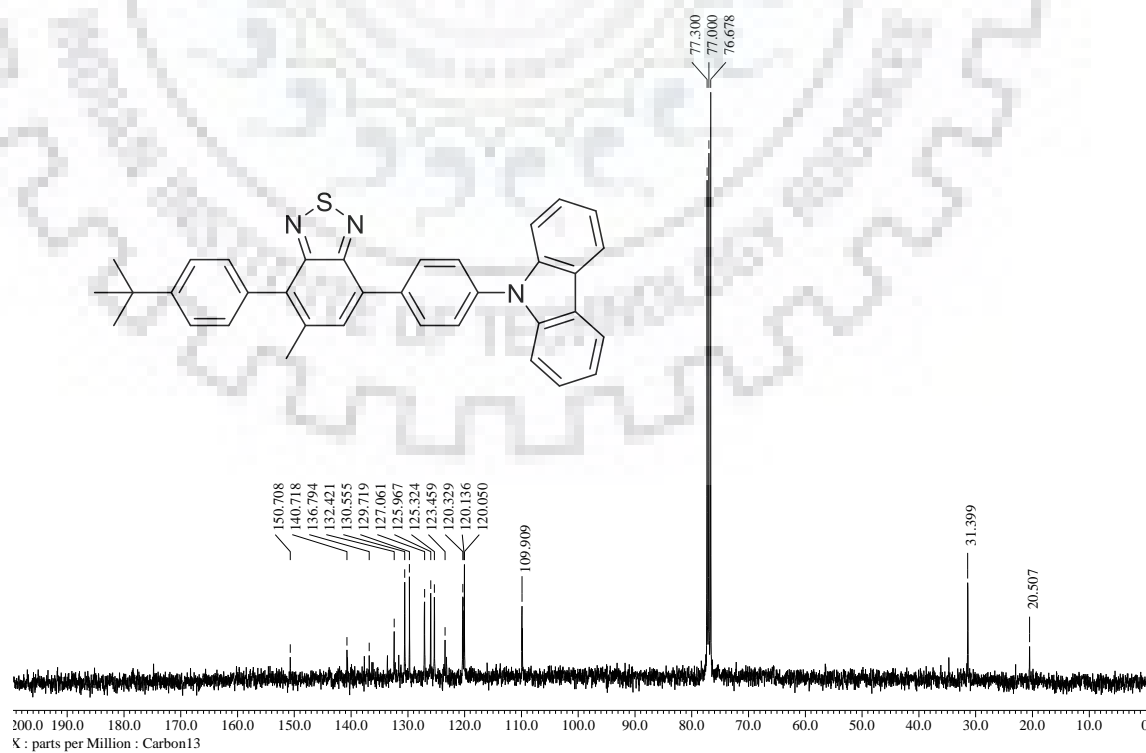
Figure S20. ^{13}C NMR spectra of **9** recorded in CDCl$_3$

233

Figure S21. ^{1}H NMR spectra of **10** recorded in CDCl$_3$

Figure S22 ^{13}C NMR spectra of **10** recorded in CDCl$_3$

234
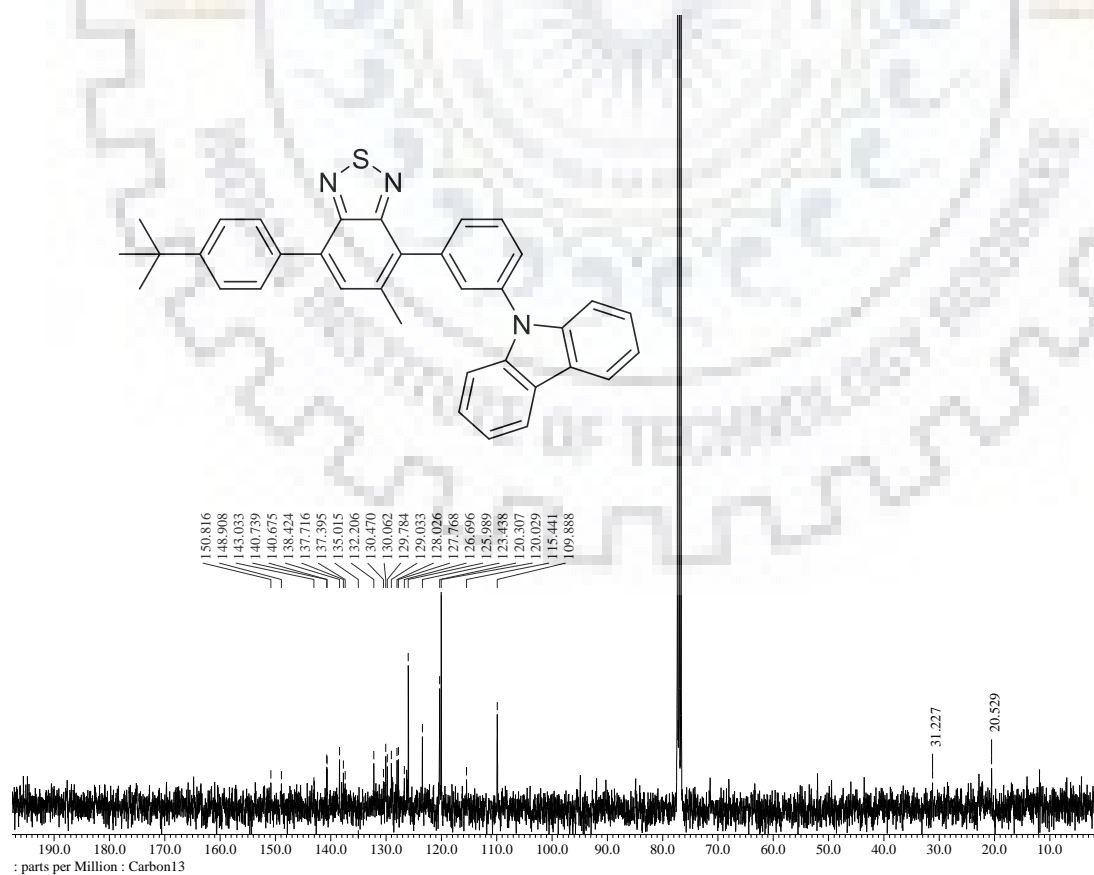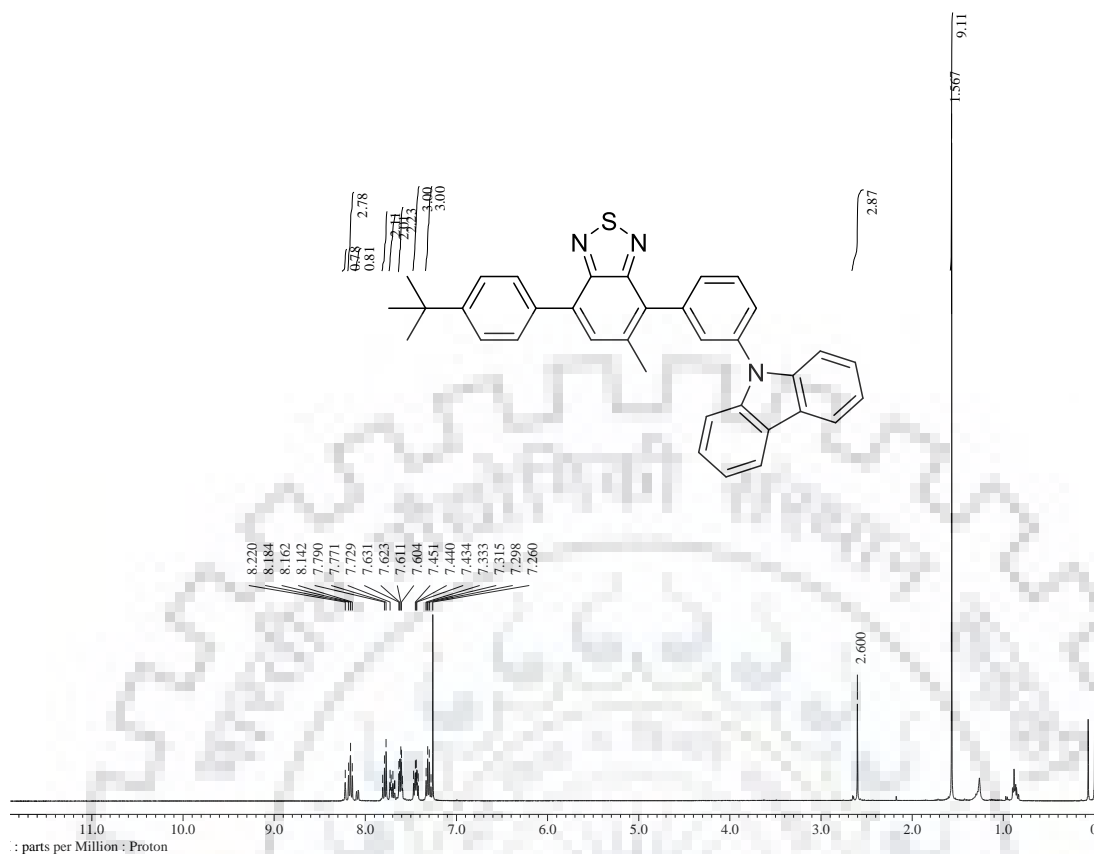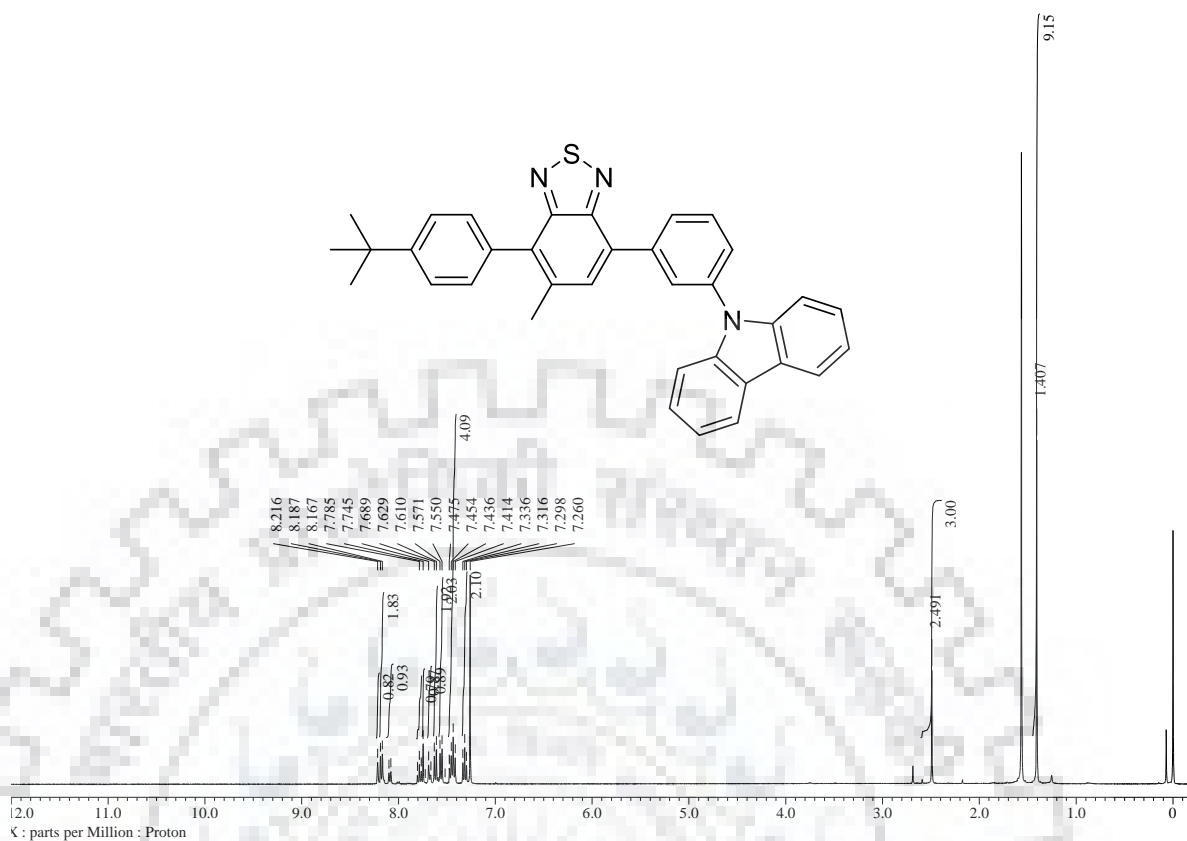
Figure S23. ^{1}H NMR spectra of **11** recorded in CDCl$_3$
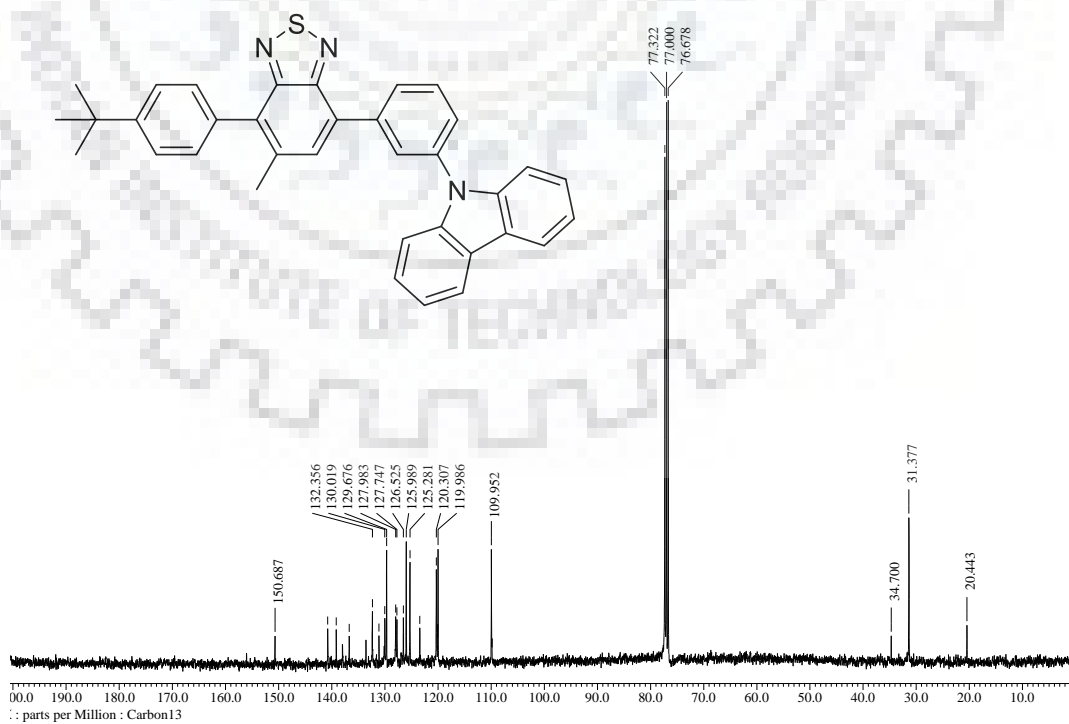
Figure S24. ^{13}C NMR spectra of **11** recorded in CDCl$_3$

235
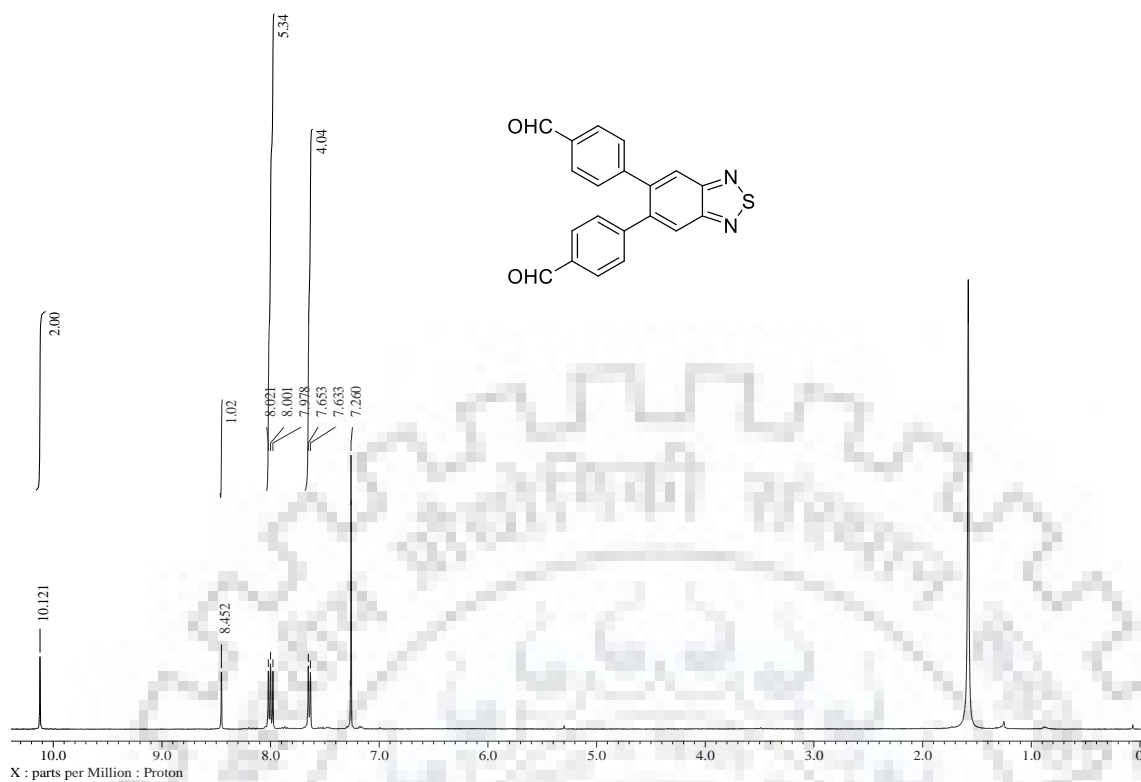
Figure S25. ^{1}H NMR spectra of **13b** recorded in CDCl$_3$
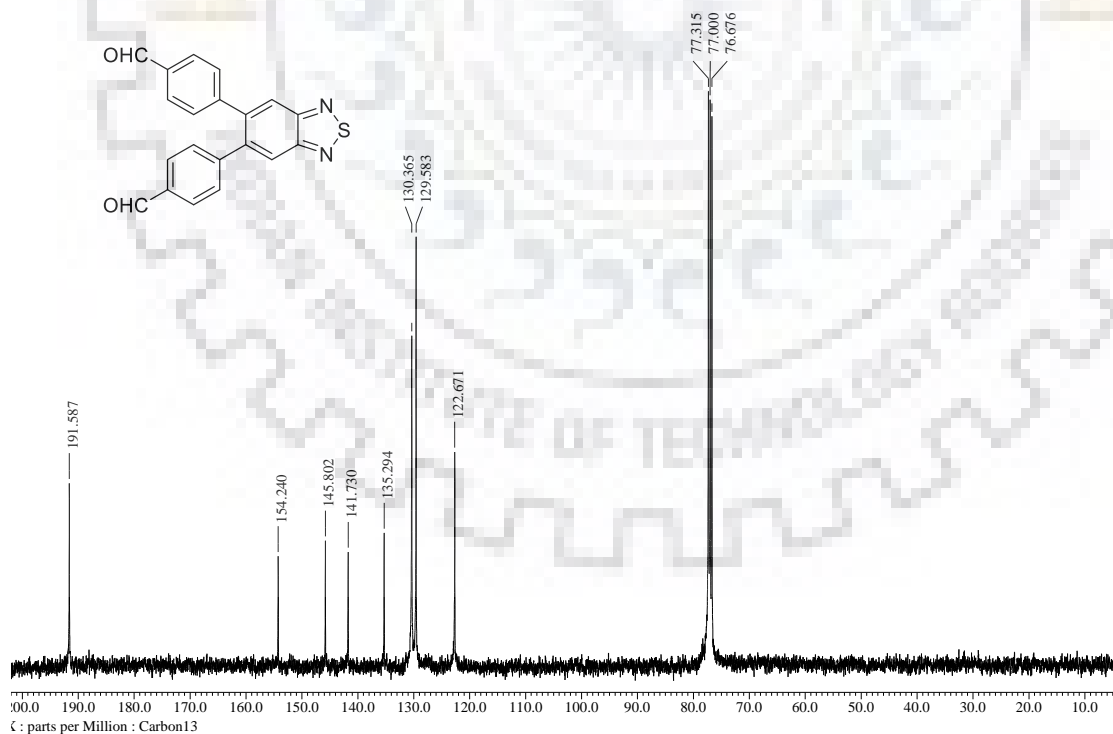
Figure S26. ^{13}C NMR spectra of **13b** recorded in CDCl$_3$
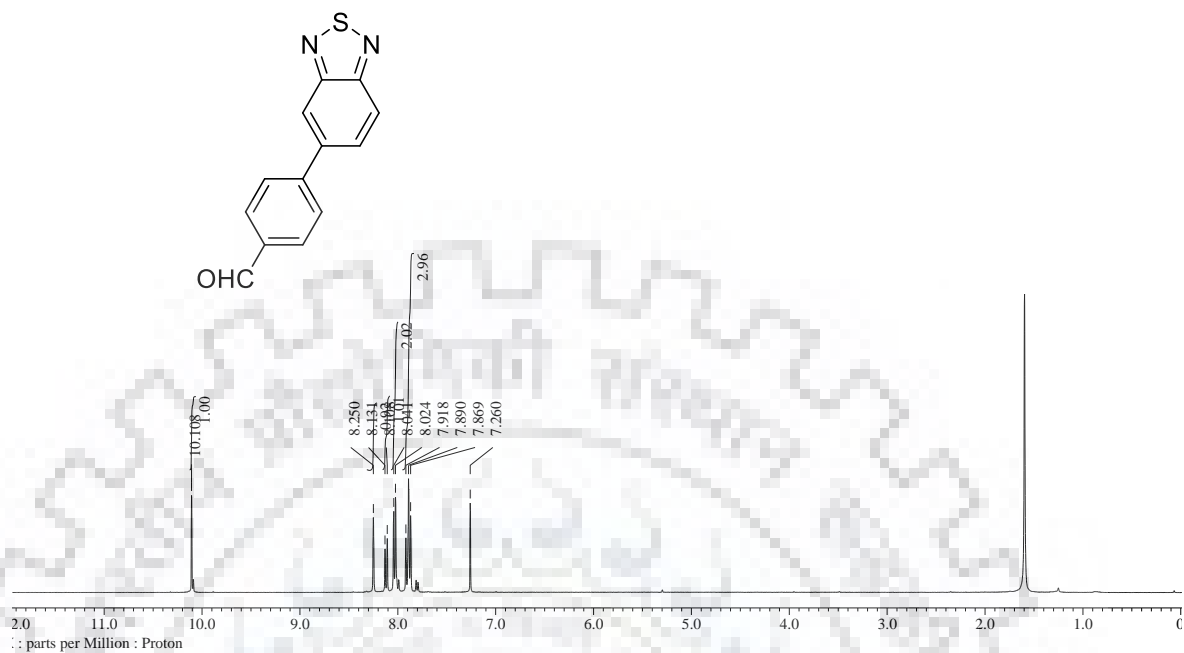
Figure S27. ^{1}H NMR spectra of **13c** recorded in CDCl$_3$
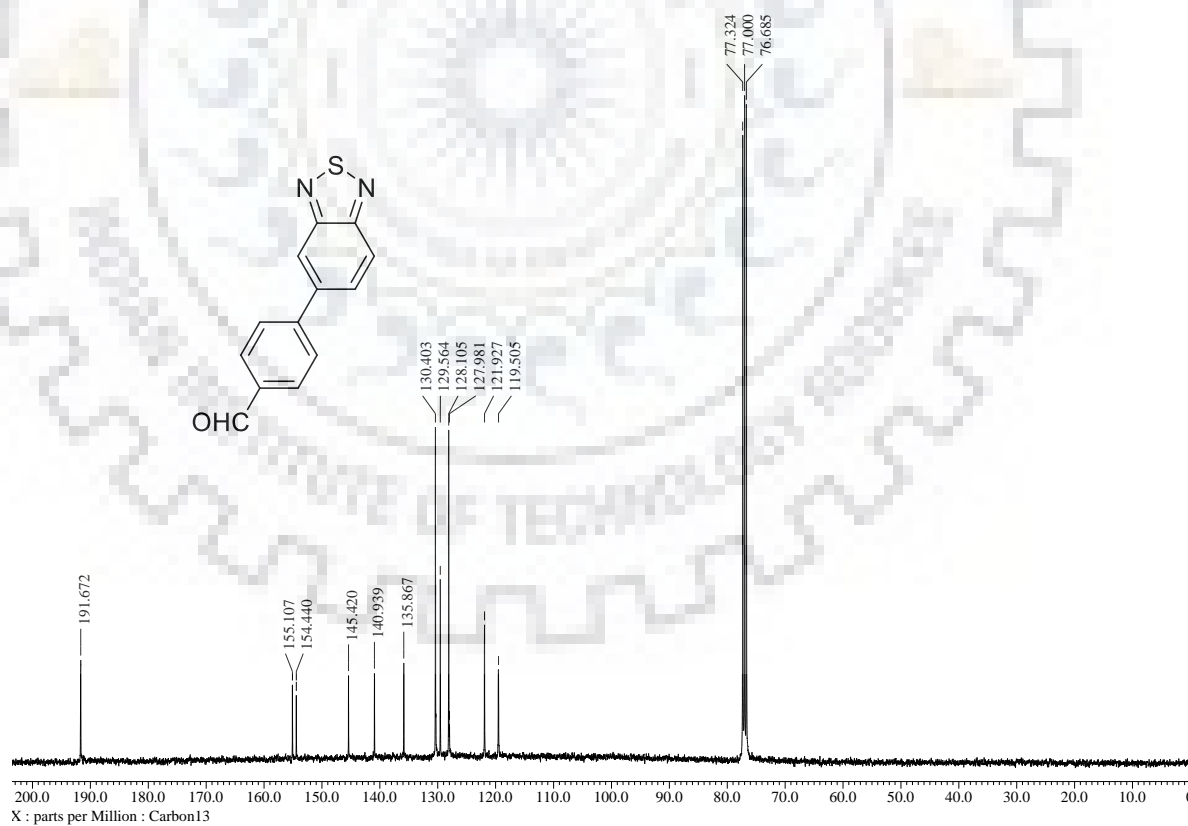
Figure S28. ^{13}C NMR spectra of **13c** recorded in CDCl$_3$

Figure S29. ¹H NMR spectra of **13d** recorded in CDCl₃
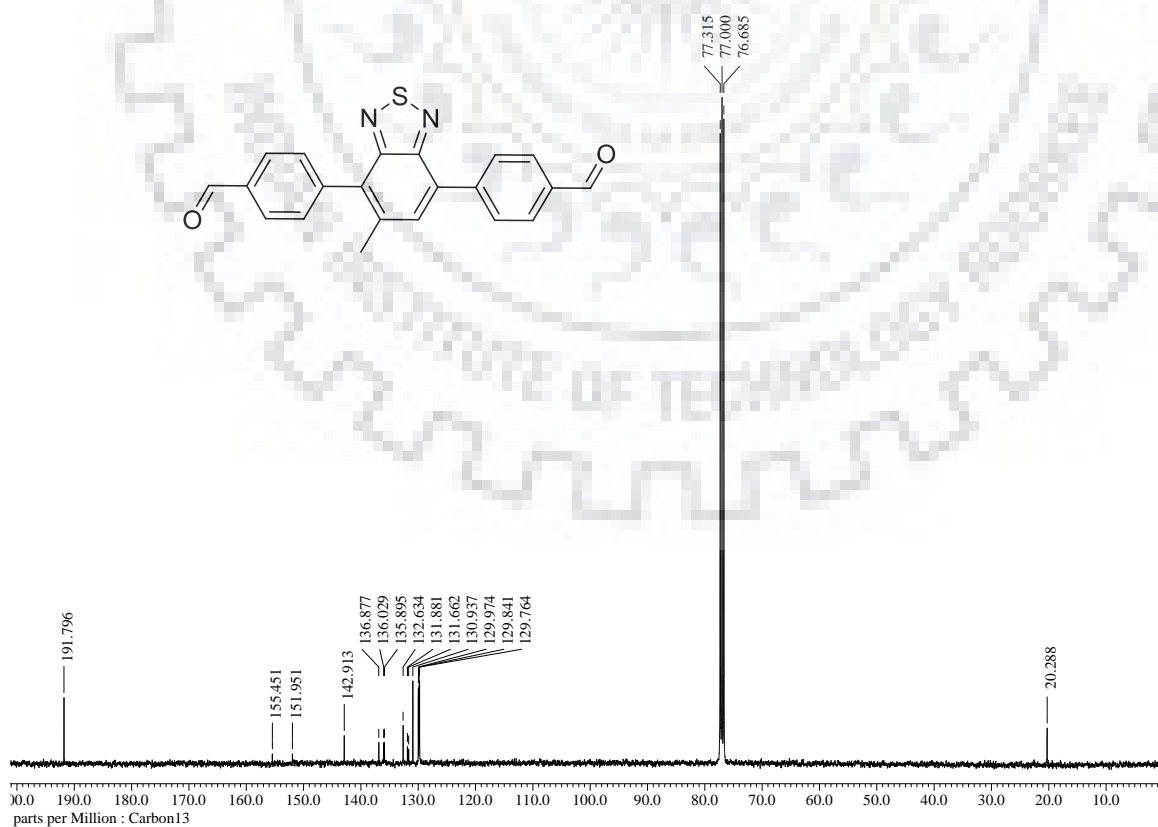
Figure S30. ¹³C NMR spectra of **13d** recorded in CDCl₃

238
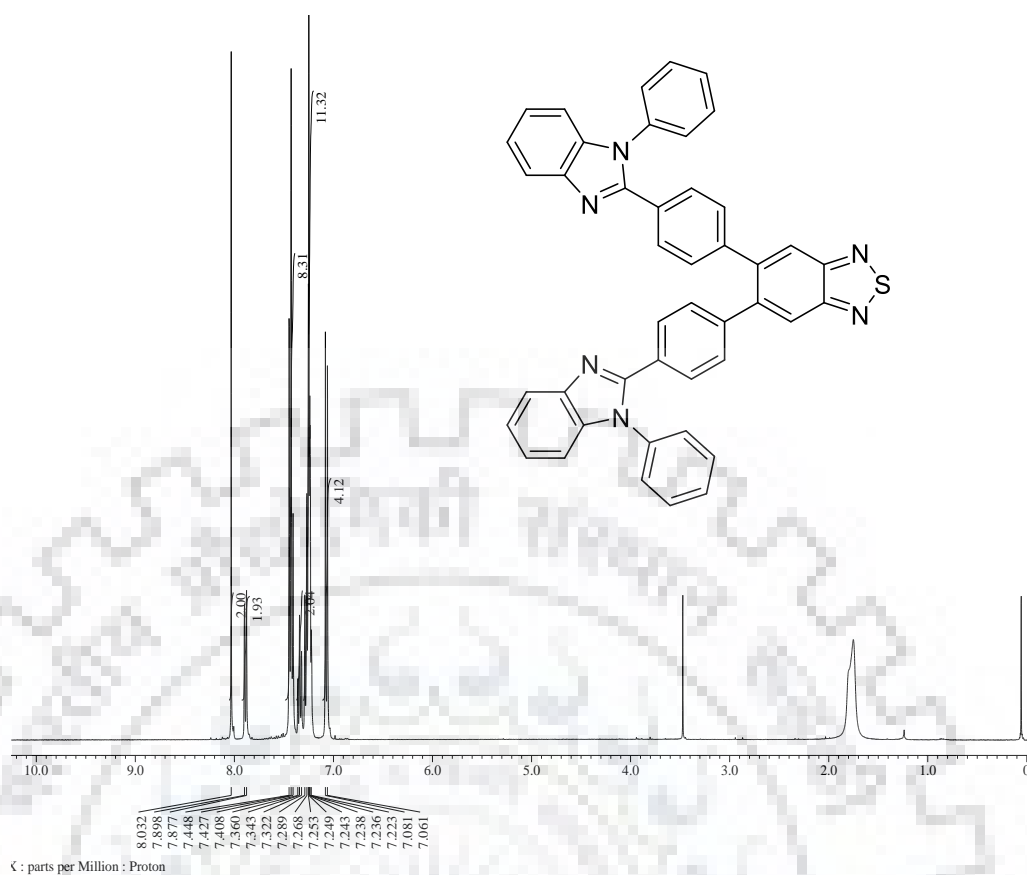
Figure S31. ^{1}H NMR spectra of **15** recorded in CDCl$_3$
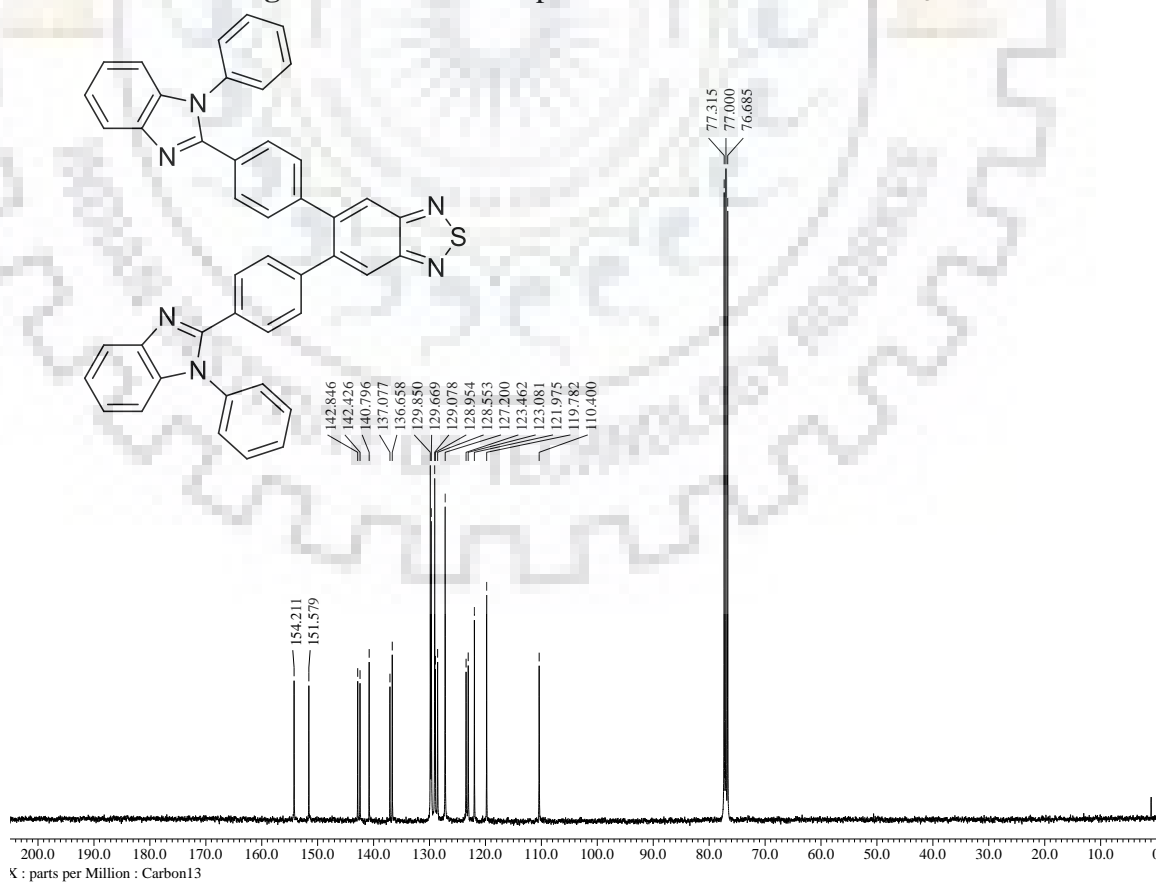
Figure S32. ^{13}C NMR spectra of **15** recorded in CDCl$_3$

239
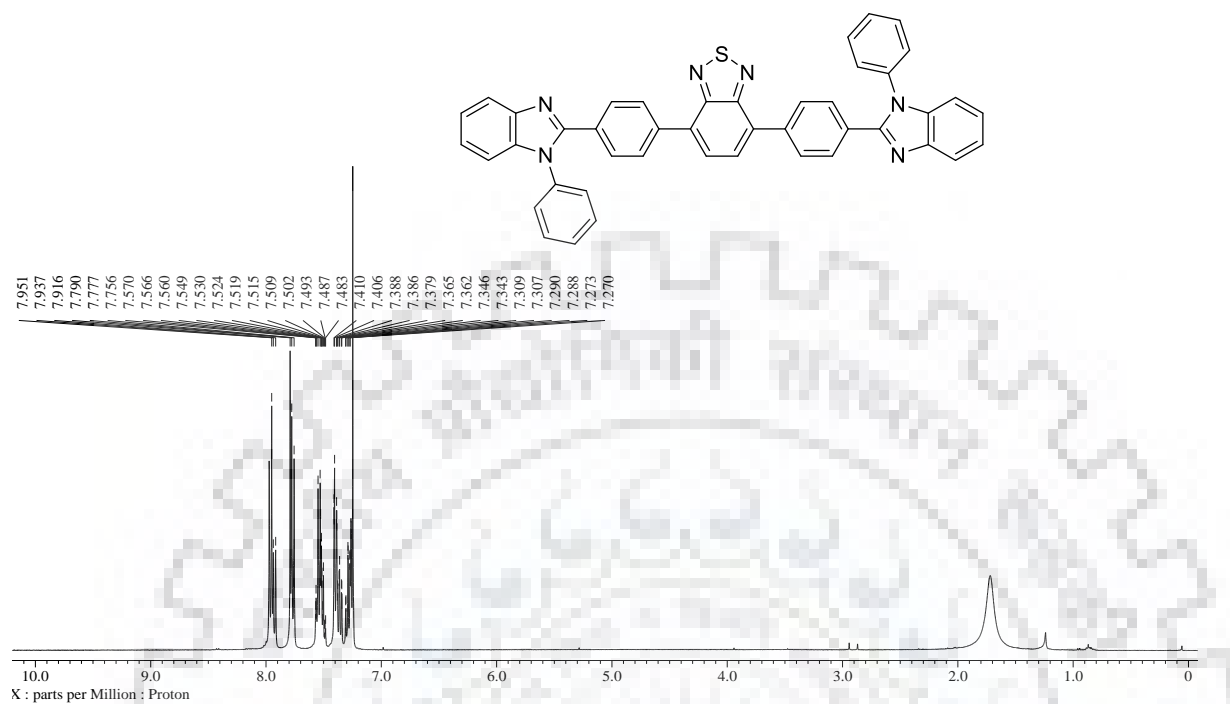
Figure S33. ^{1}H NMR spectra of **14** recorded in CDCl$_3$
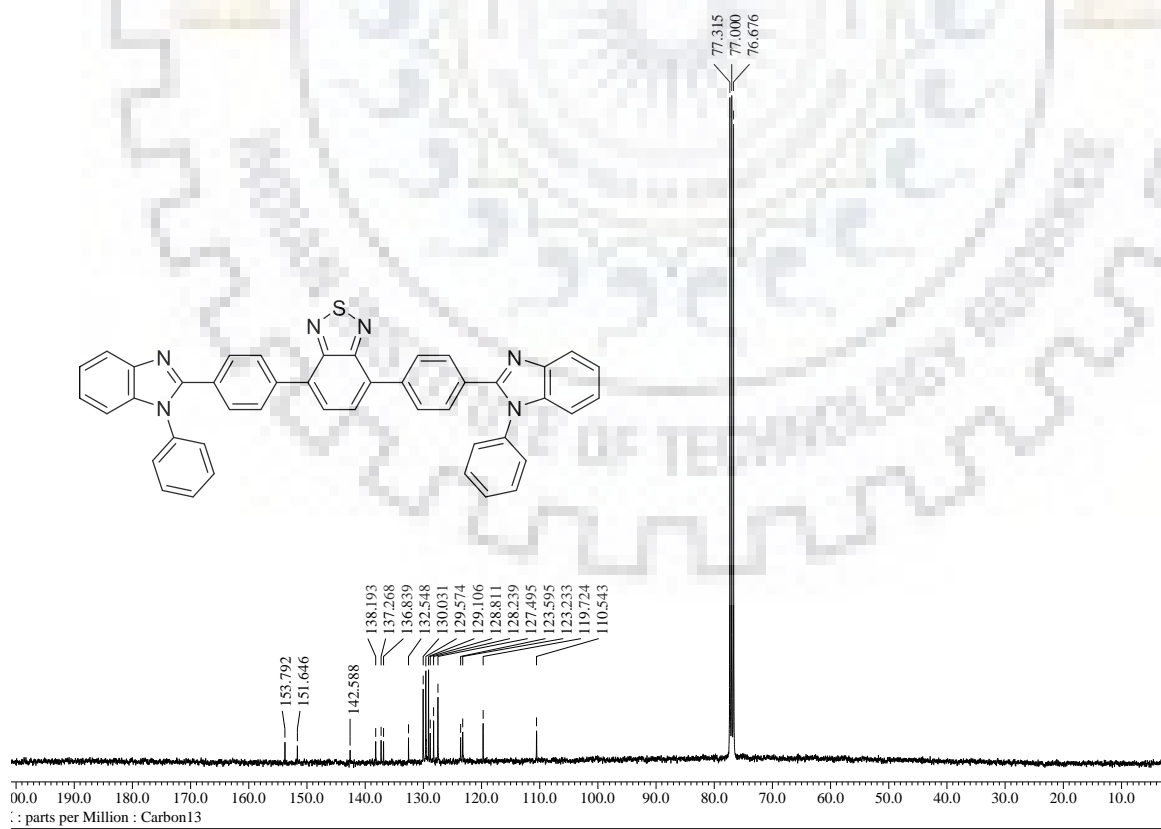
Figure S34. ^{13}C NMR spectra of **14** recorded in CDCl$_3$

Figure S35. ^{1}H NMR spectra of 16 recorded in CDCl$_3$
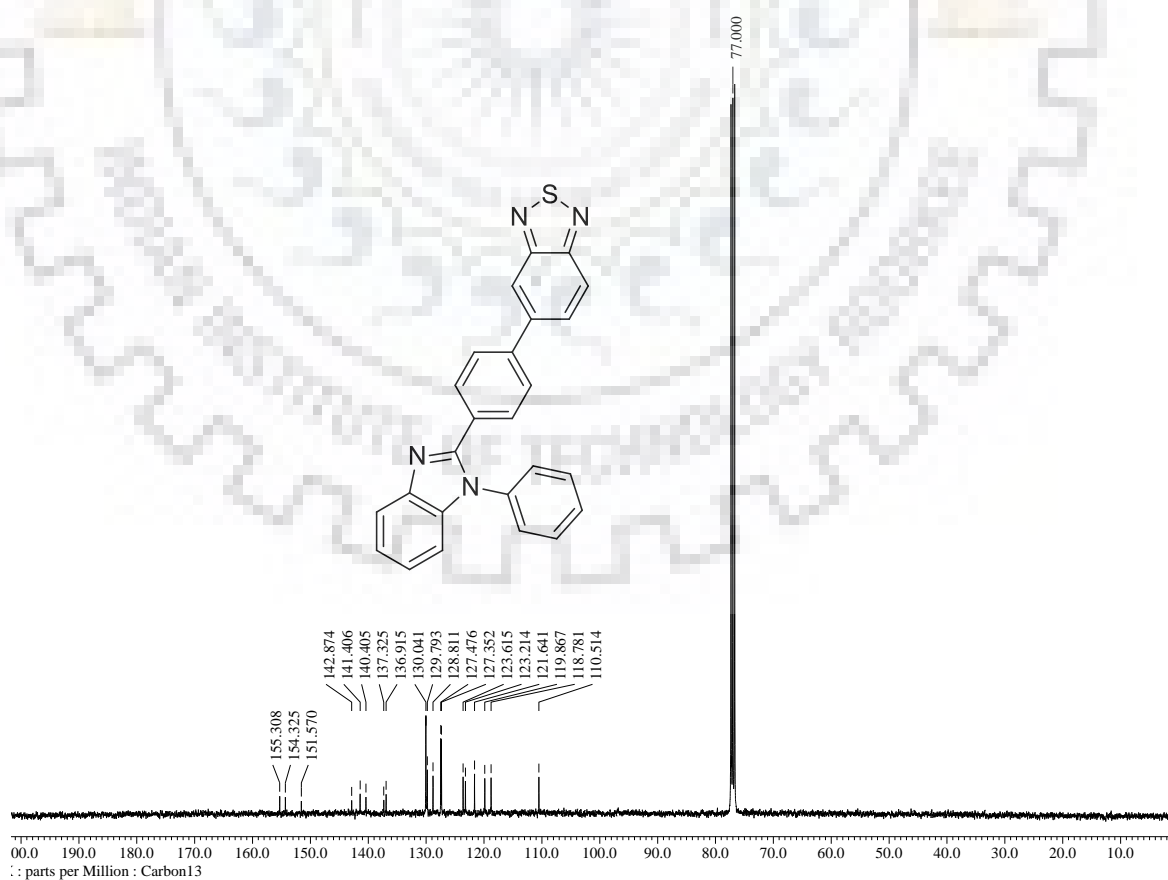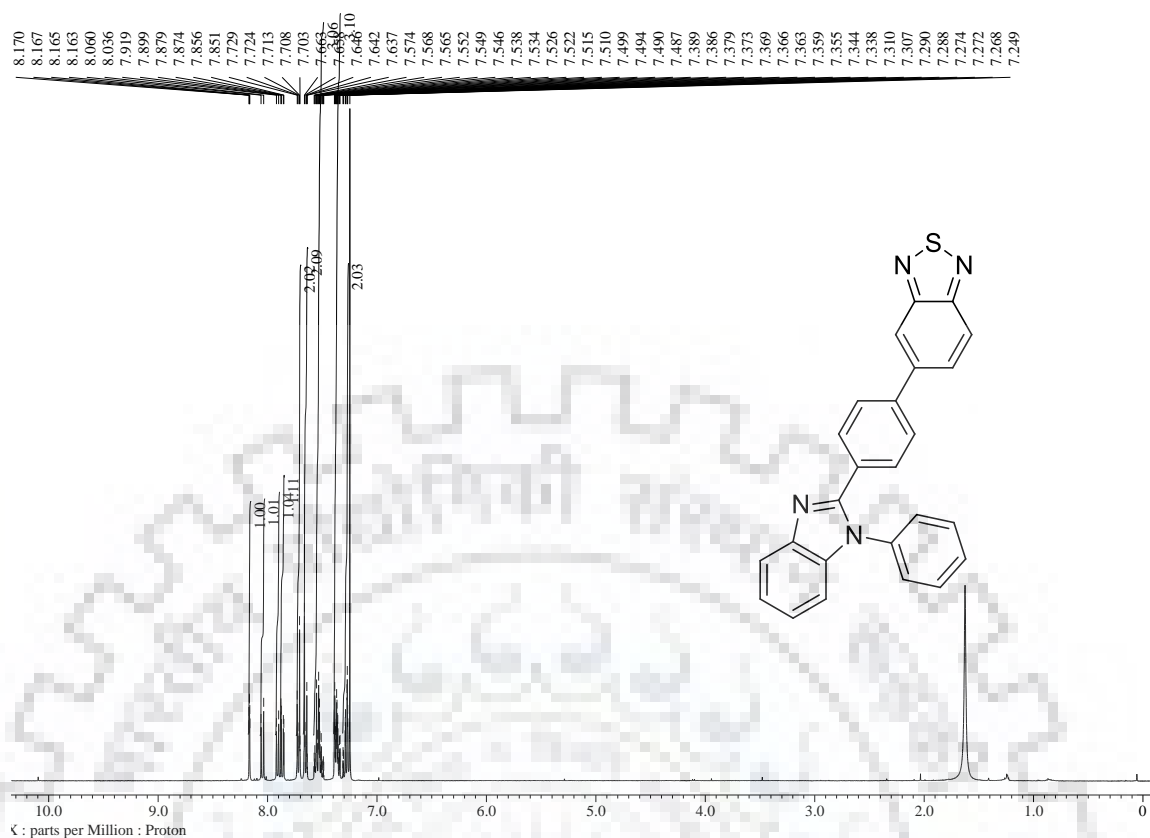
Figure S36. ^{13}C NMR spectra of 16 recorded in CDCl$_3$
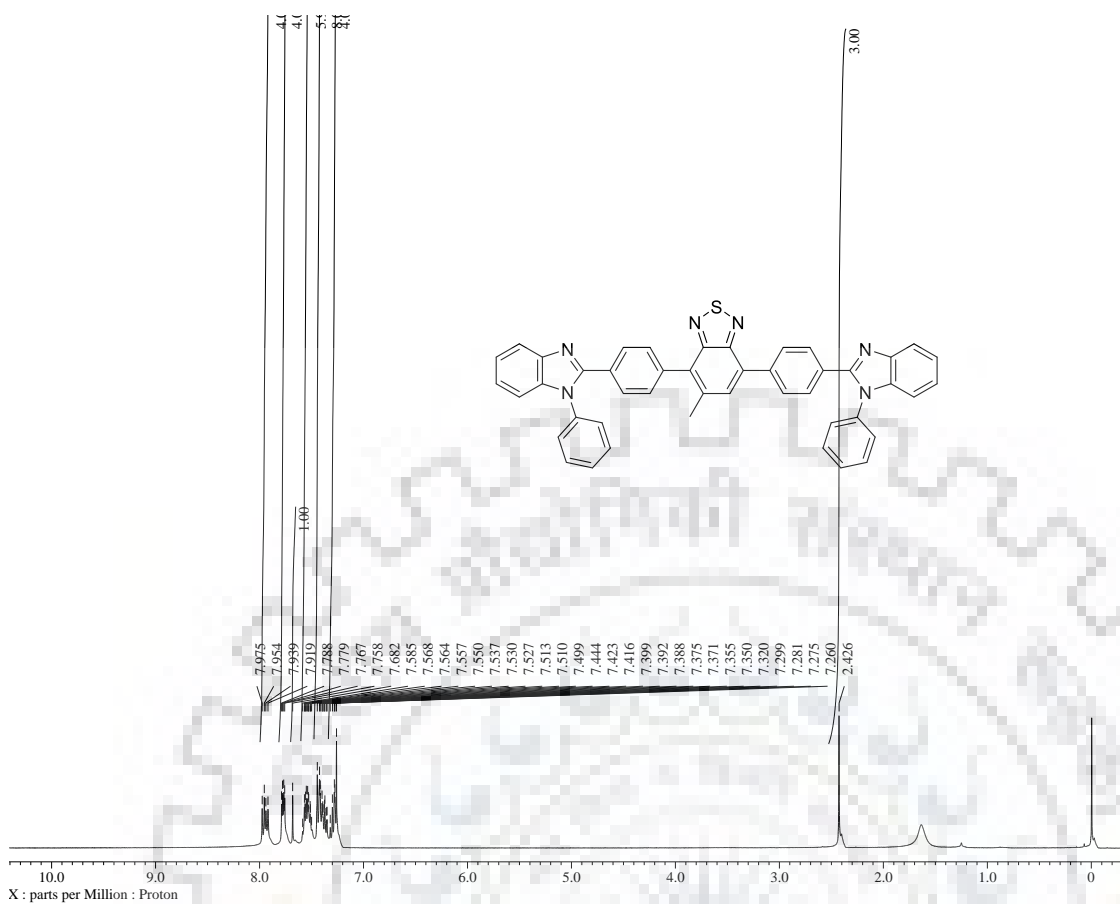
Figure S37. ¹H NMR spectra of 17 recorded in CDCl₃
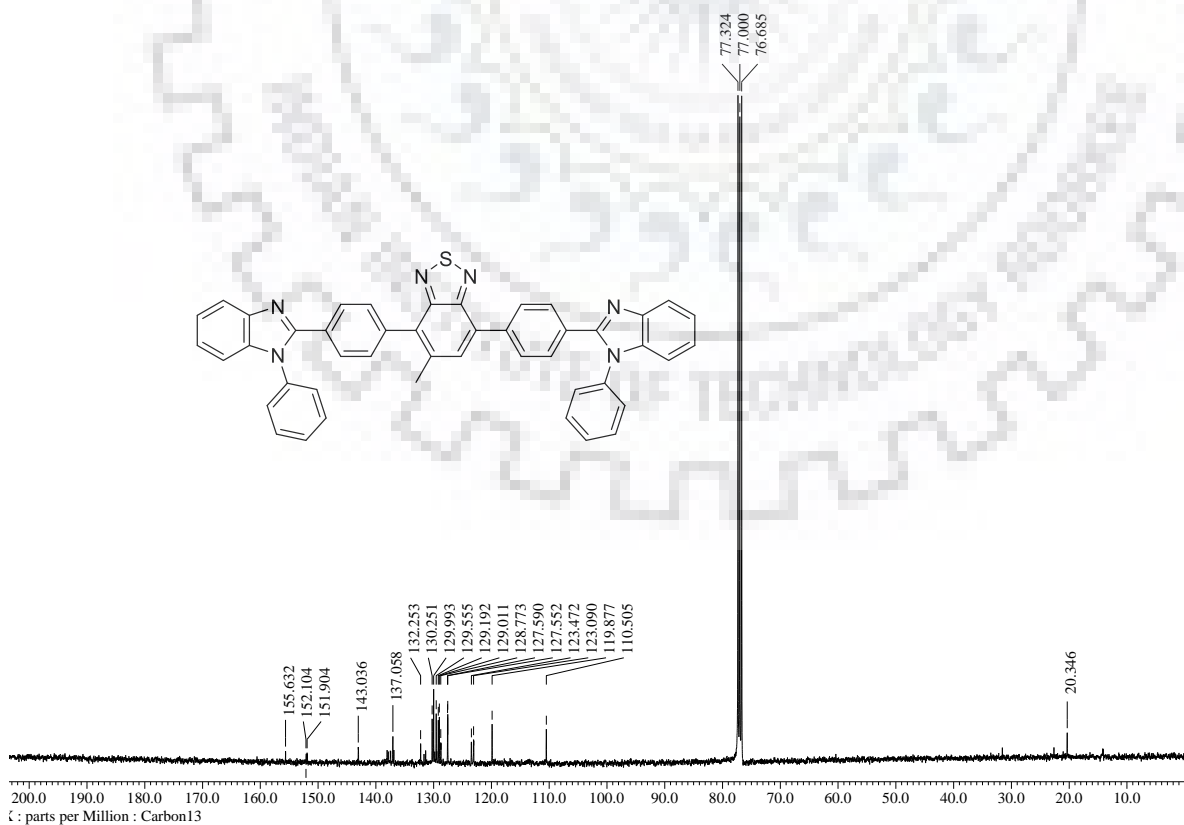
Figure S38. ¹³C NMR spectra of 17 recorded in CDCl₃

242
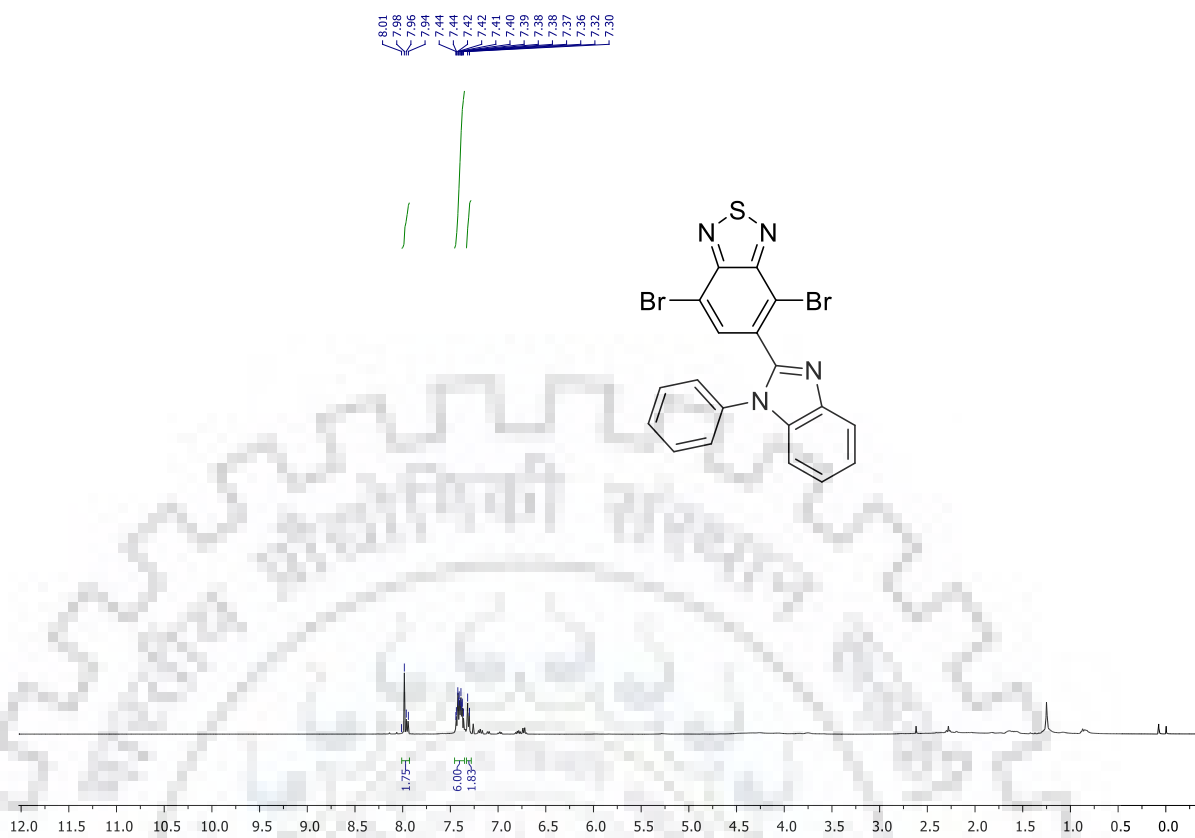
Figure S39. ^{1}H NMR spectra of **19** recorded in CDCl$_3$
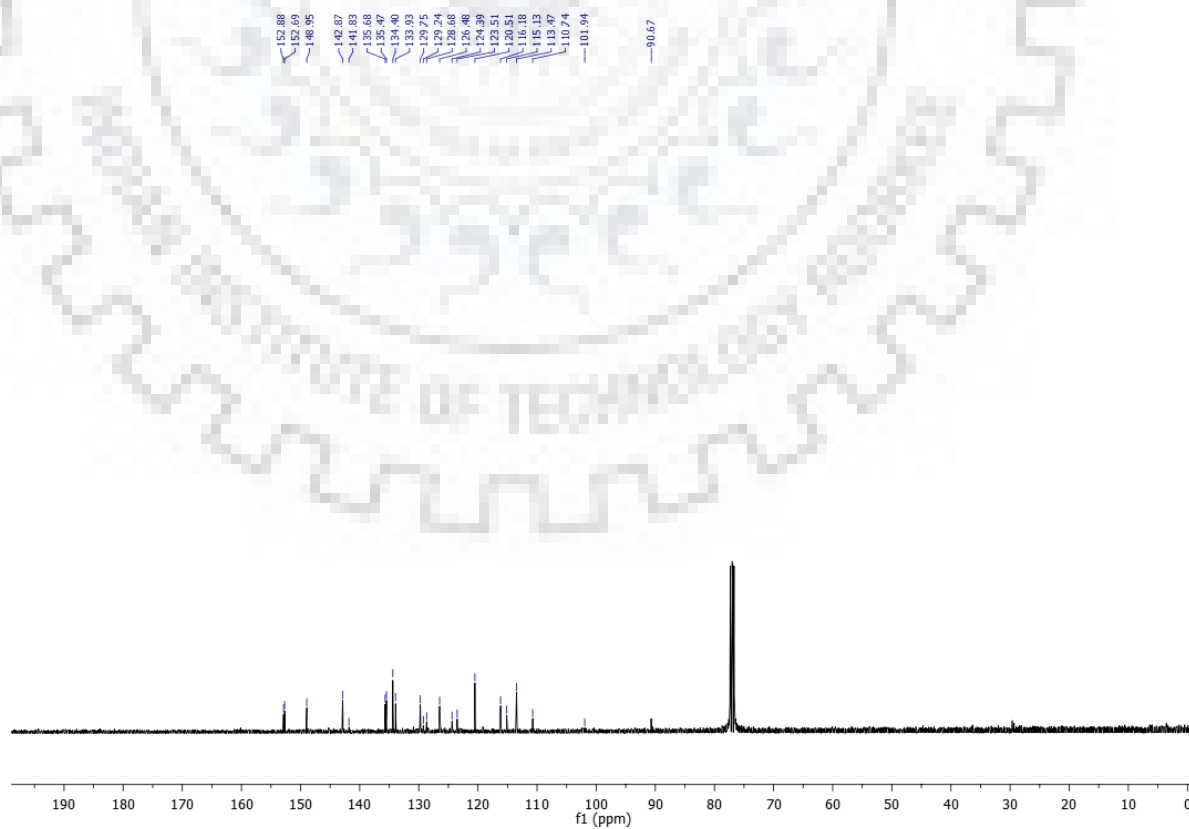
Figure S40. ^{13}C NMR spectra of **19** recorded in CDCl$_3$

243
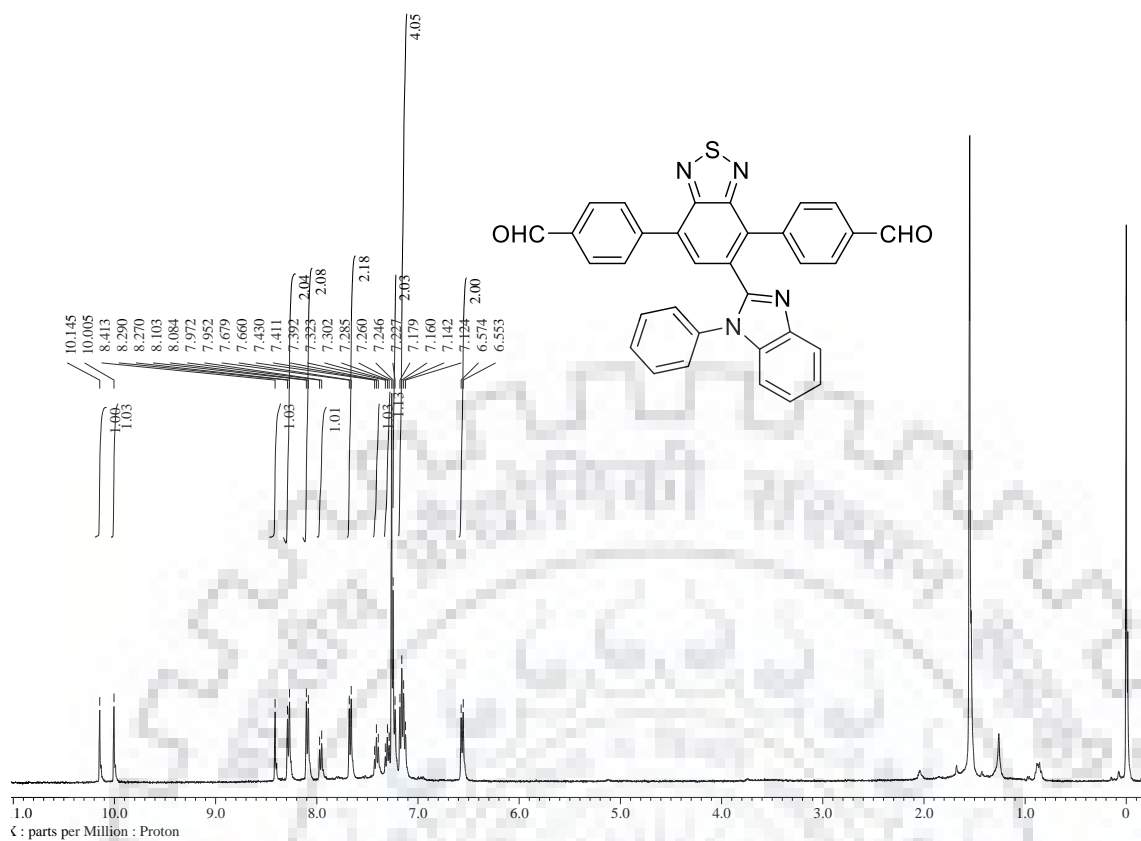
Figure S41. ^{1}H NMR spectra of **20a** recorded in CDCl$_3$
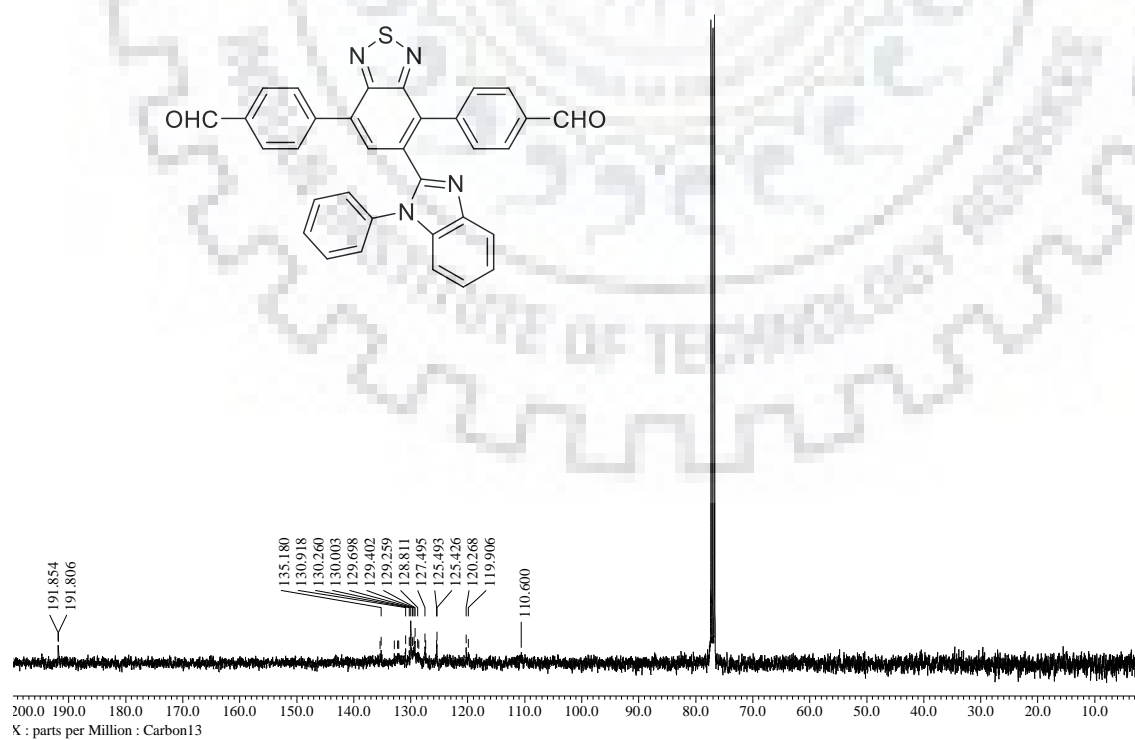
Figure S42. ^{13}C NMR spectra of 20a recorded in CDCl$_3$

Figure S43. ^{1}H NMR spectra of 20b recorded in CDCl$_3$

Figure S44. ^{13}C NMR spectra of **20b** recorded in CDCl$_3$
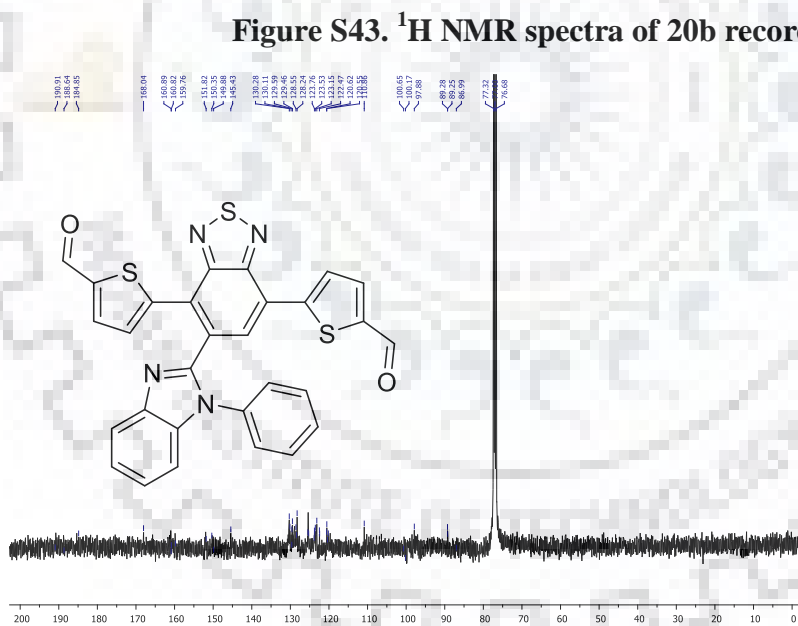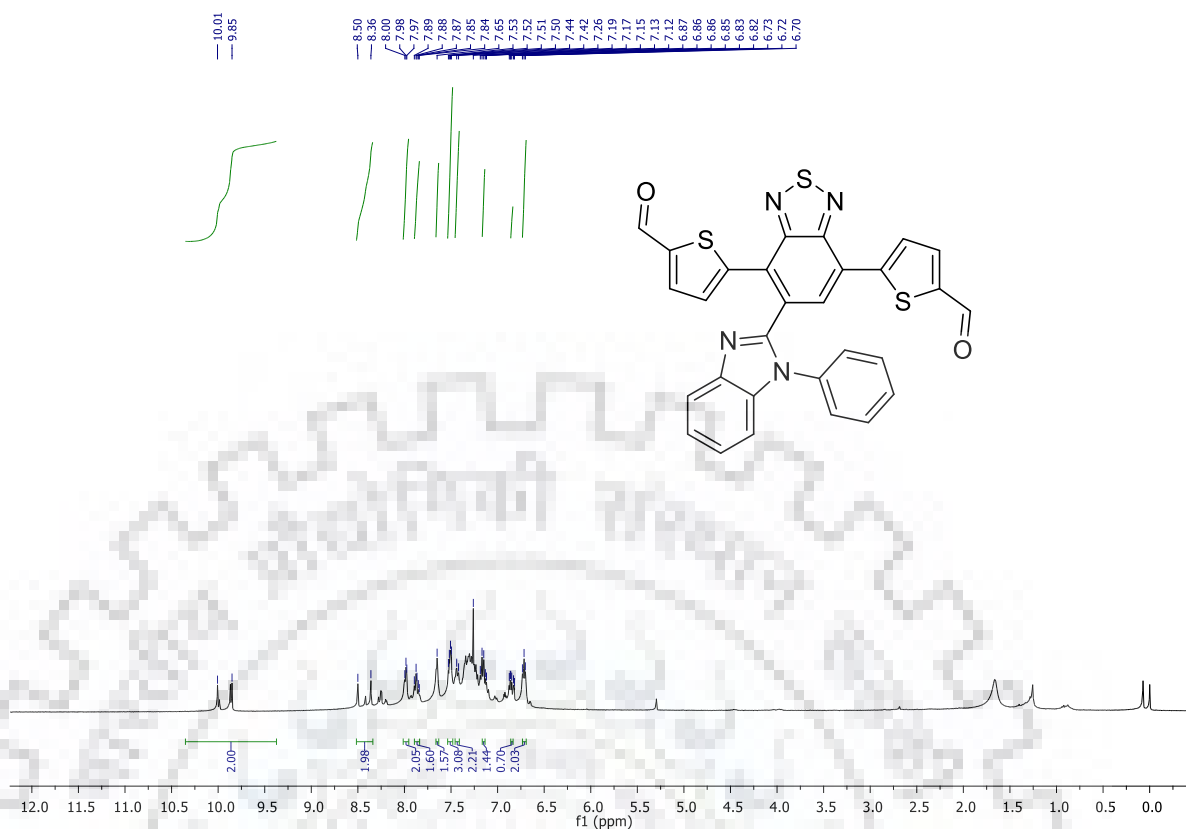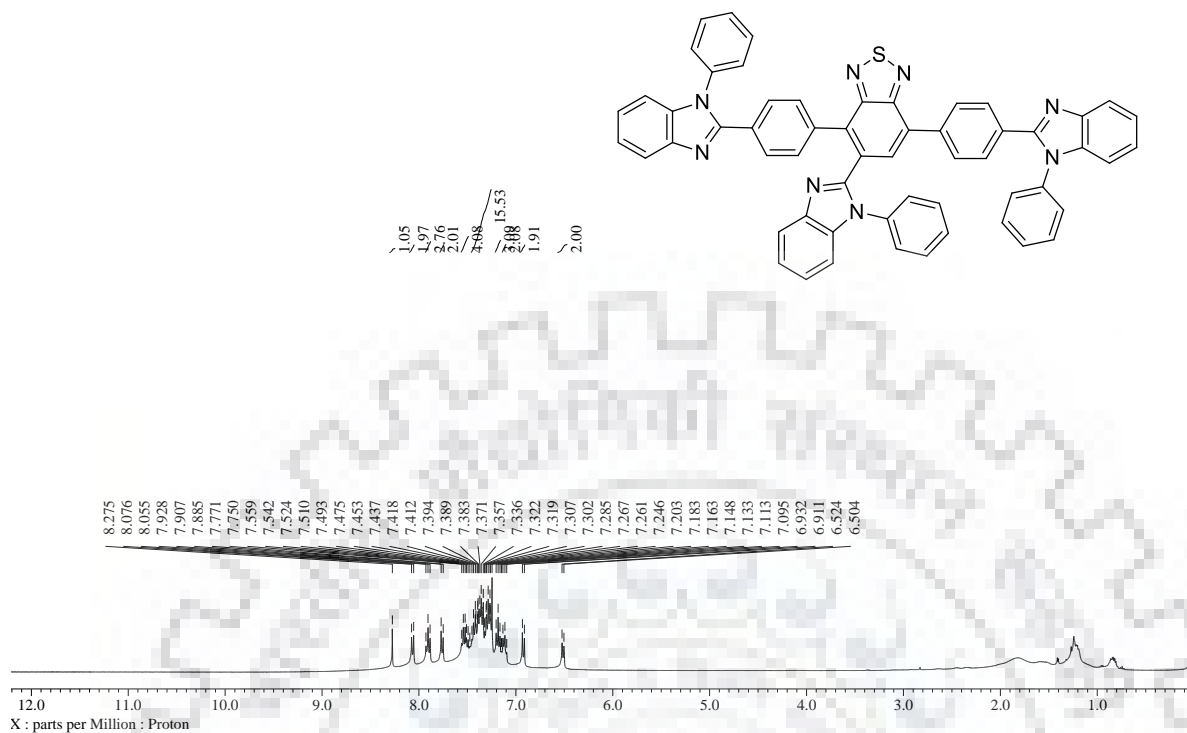
Figure S45. ^{1}H NMR spectra of **21** recorded in CDCl$_3$
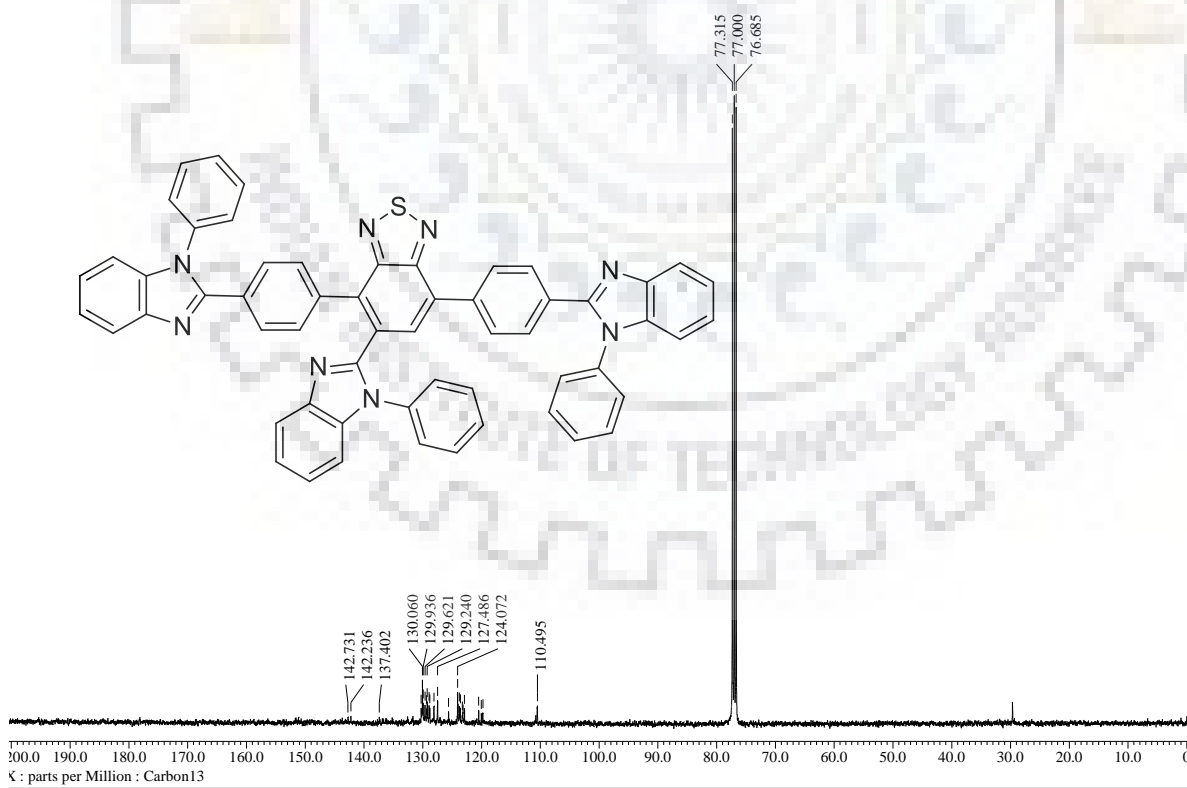
Figure S46. ^{13}C NMR spectra of **21** recorded in CDCl$_3$

246
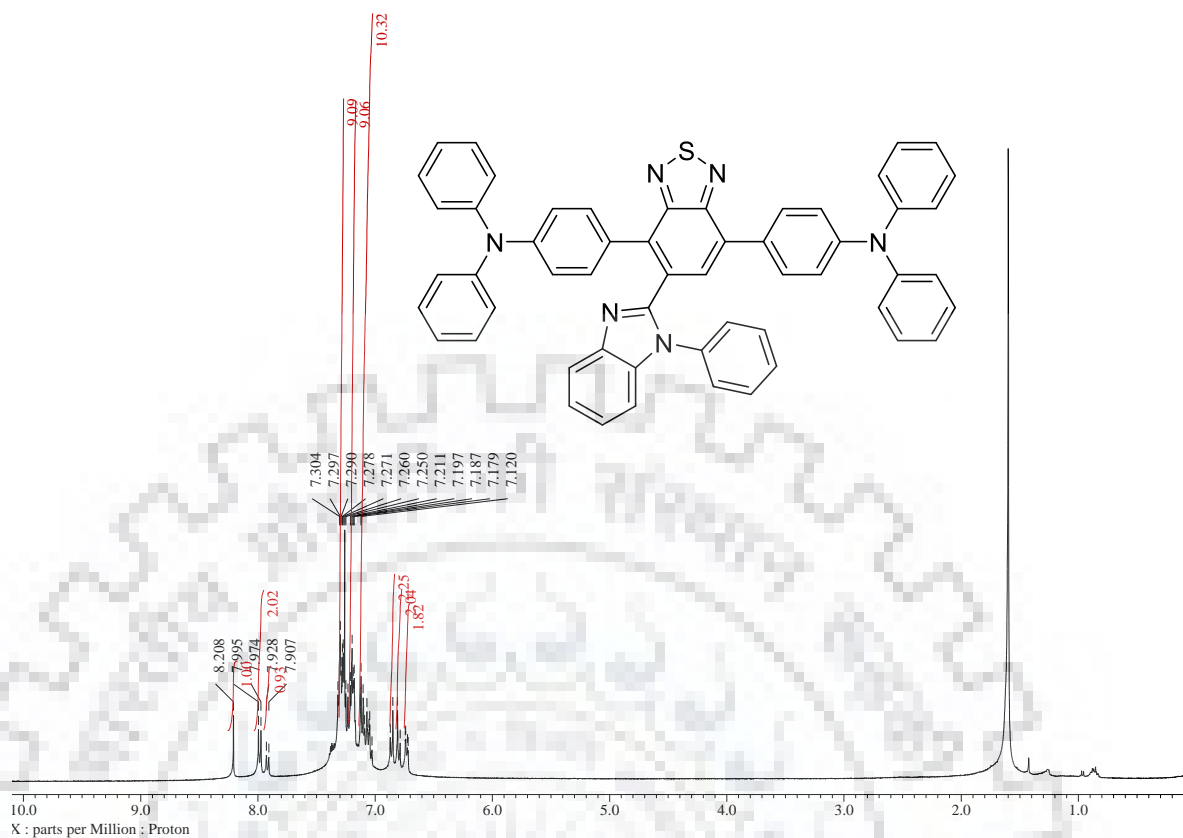
Figure S47. ^{1}H NMR spectra of **23** recorded in CDCl$_3$
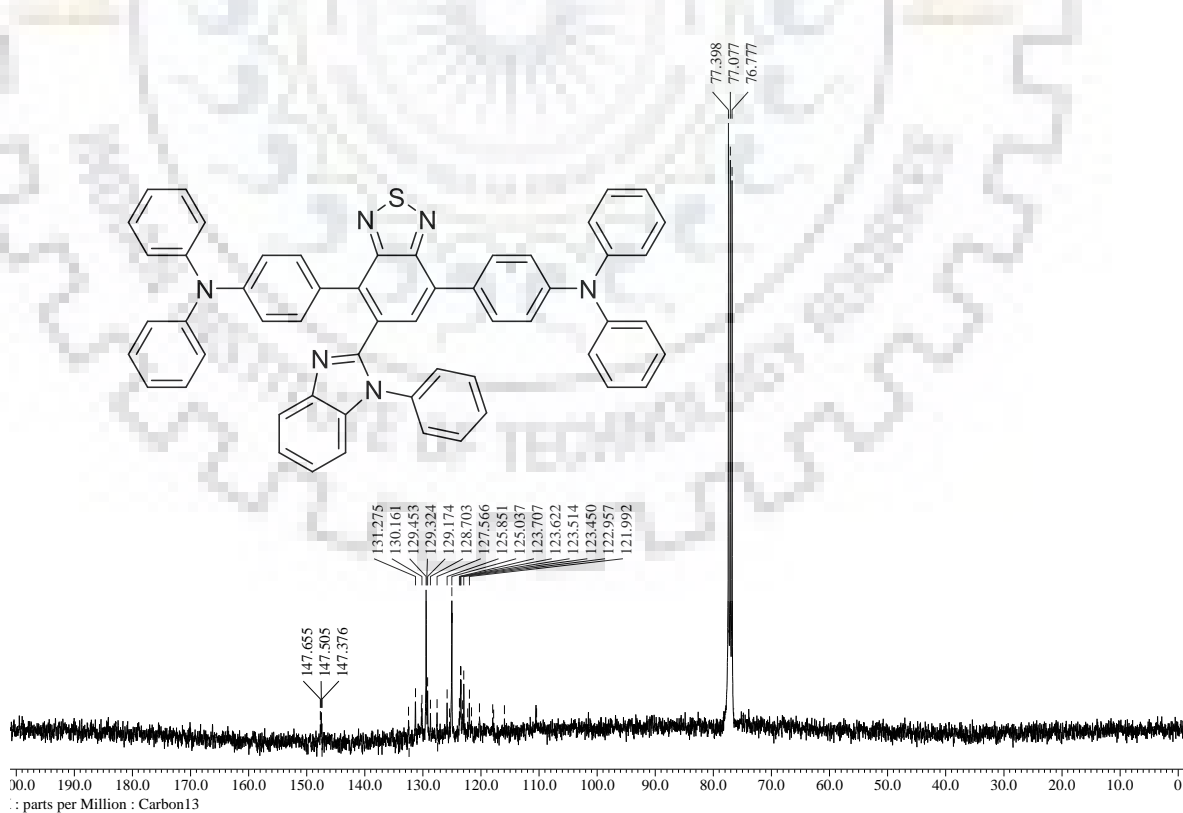
Figure S48. ^{13}C NMR spectra of **23** recorded in CDCl$_3$
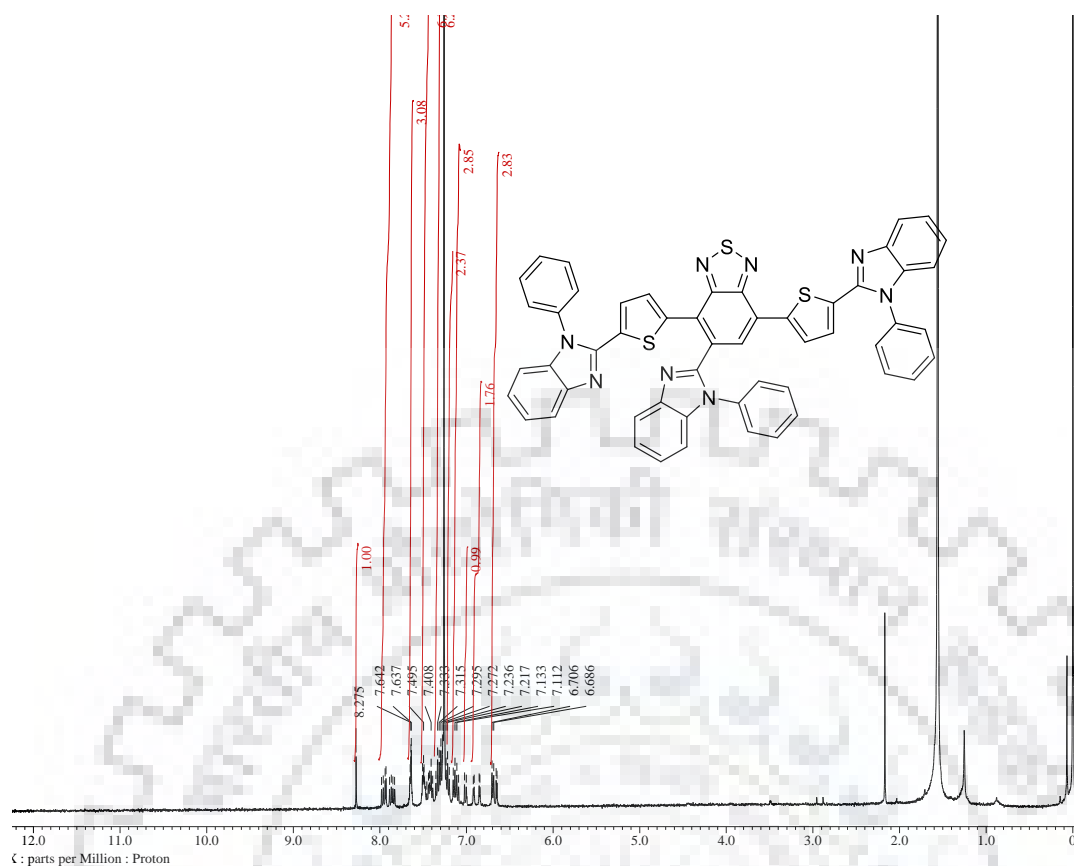
Figure S49. ¹HNMR spectra of 22 recorded in CDCl₃
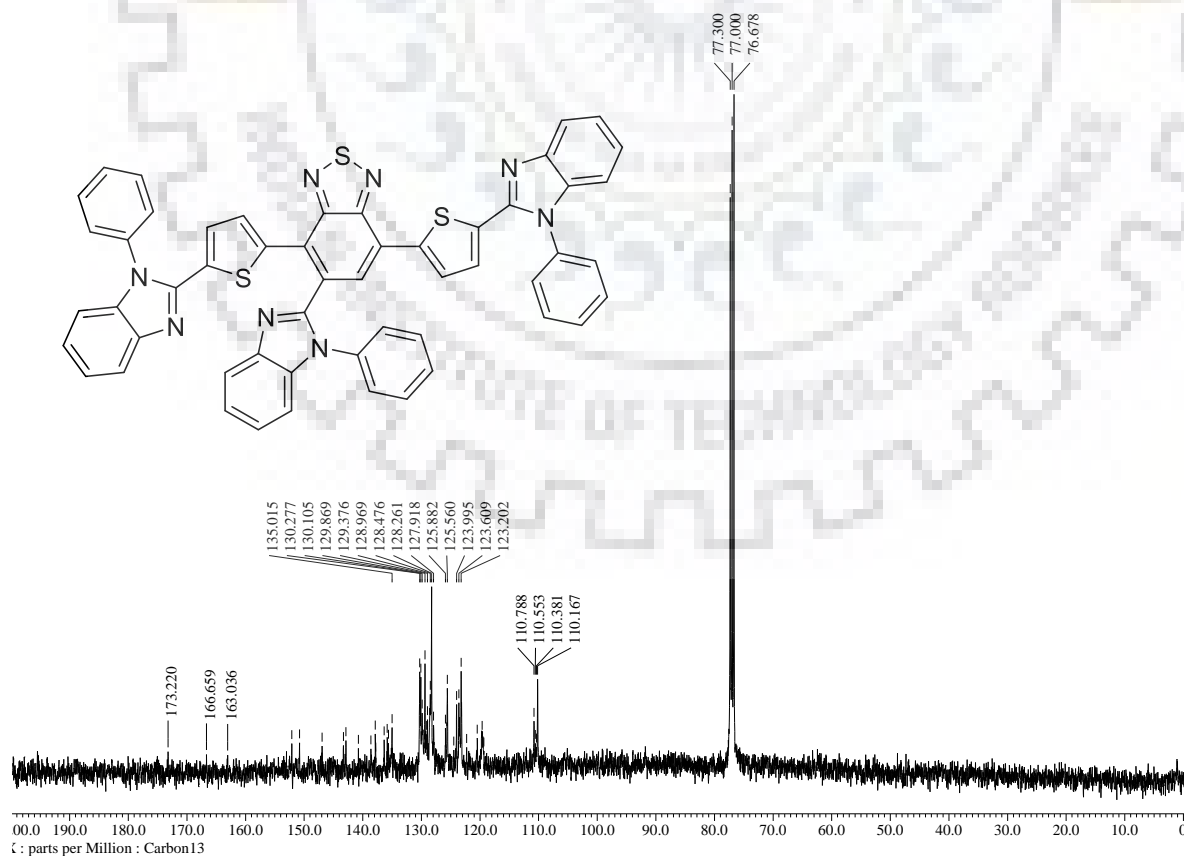
Figure S50. ¹³C NMR spectra of 22 recorded in CDCl₃

248
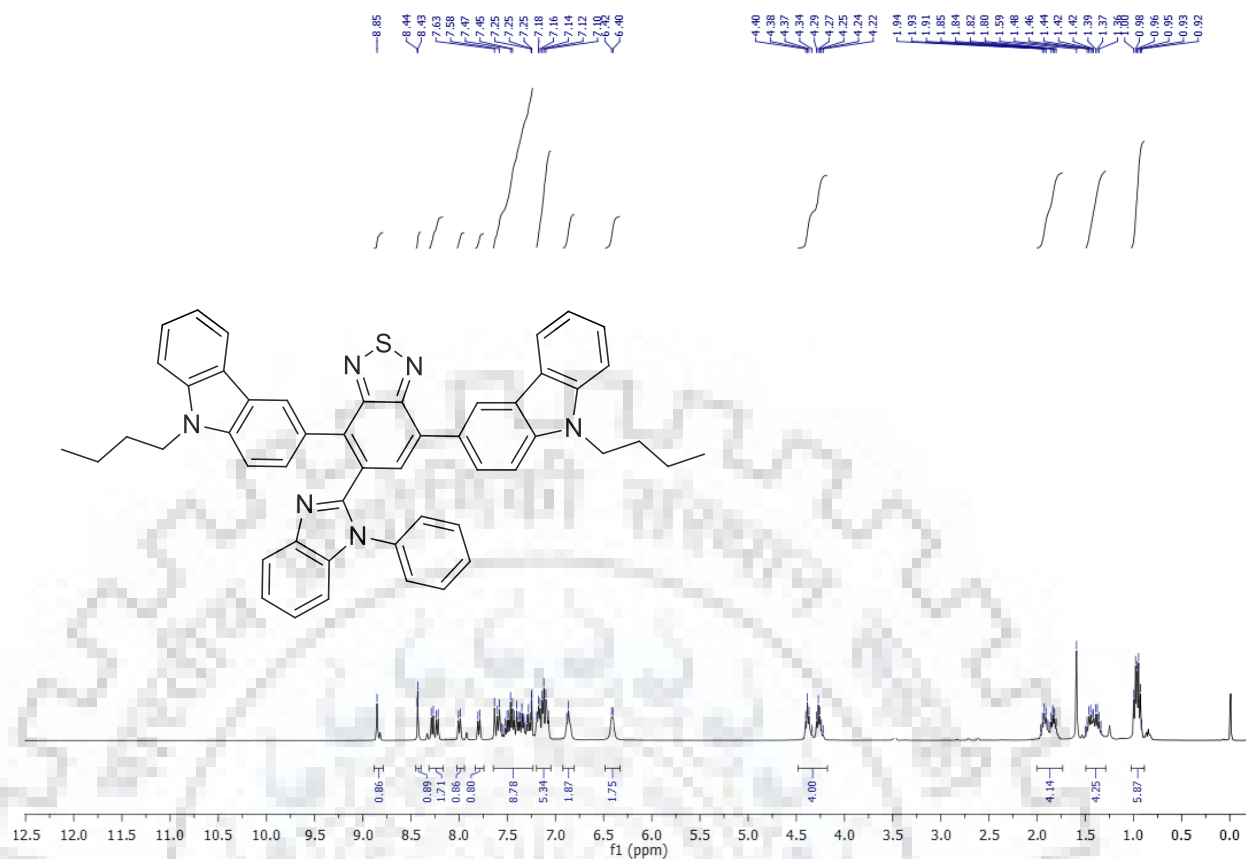
Figure S51. ^{1}H NMR spectra of 24 recorded in CDCl$_3$
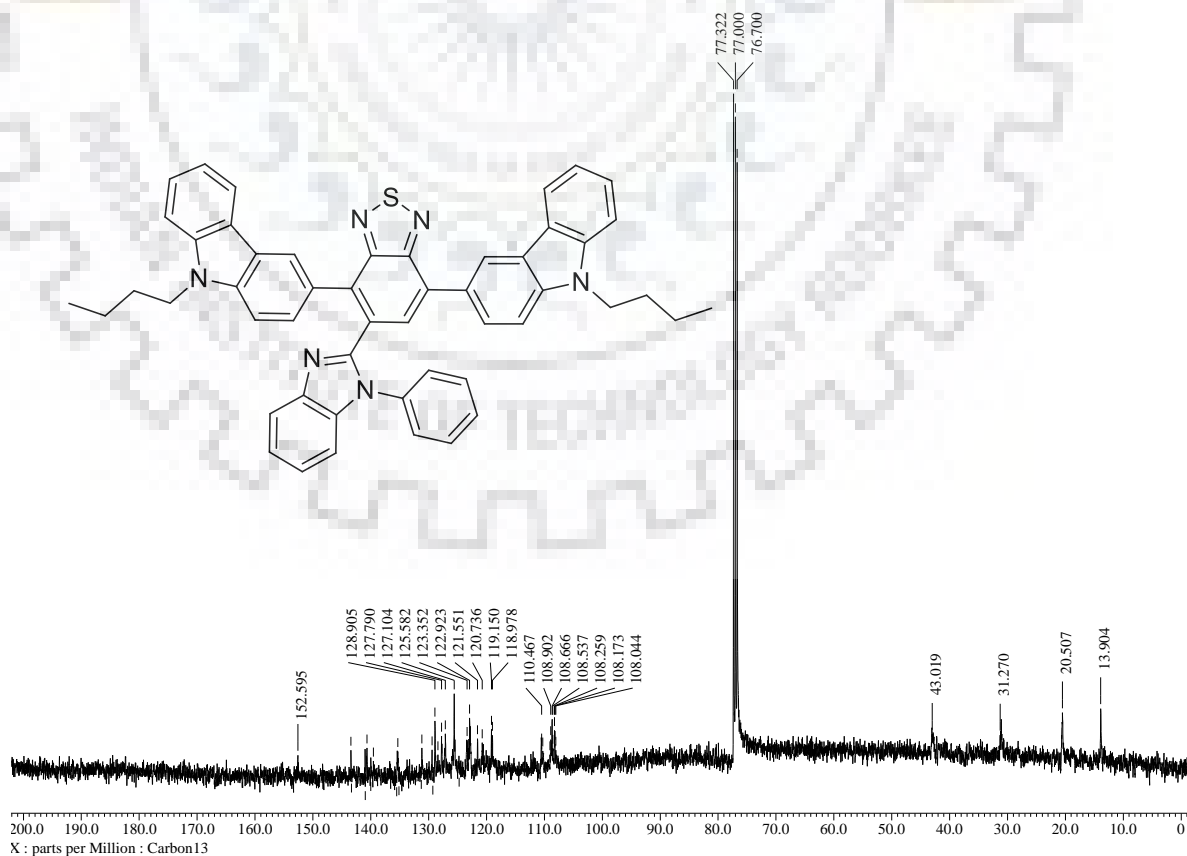
Figure S52. ^{13}C NMR spectra of 24 recorded in CDCl$_3$
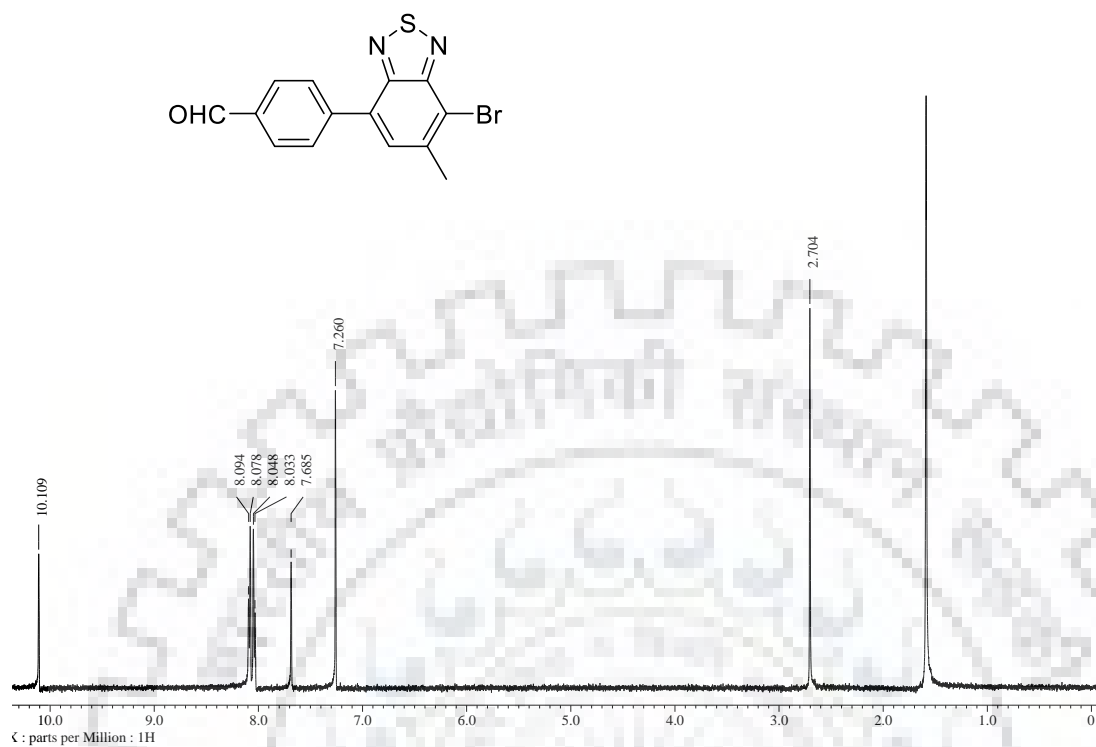
Figure S53. ^{1}H NMR spectrum of 25a recorded in CDCl$_3$
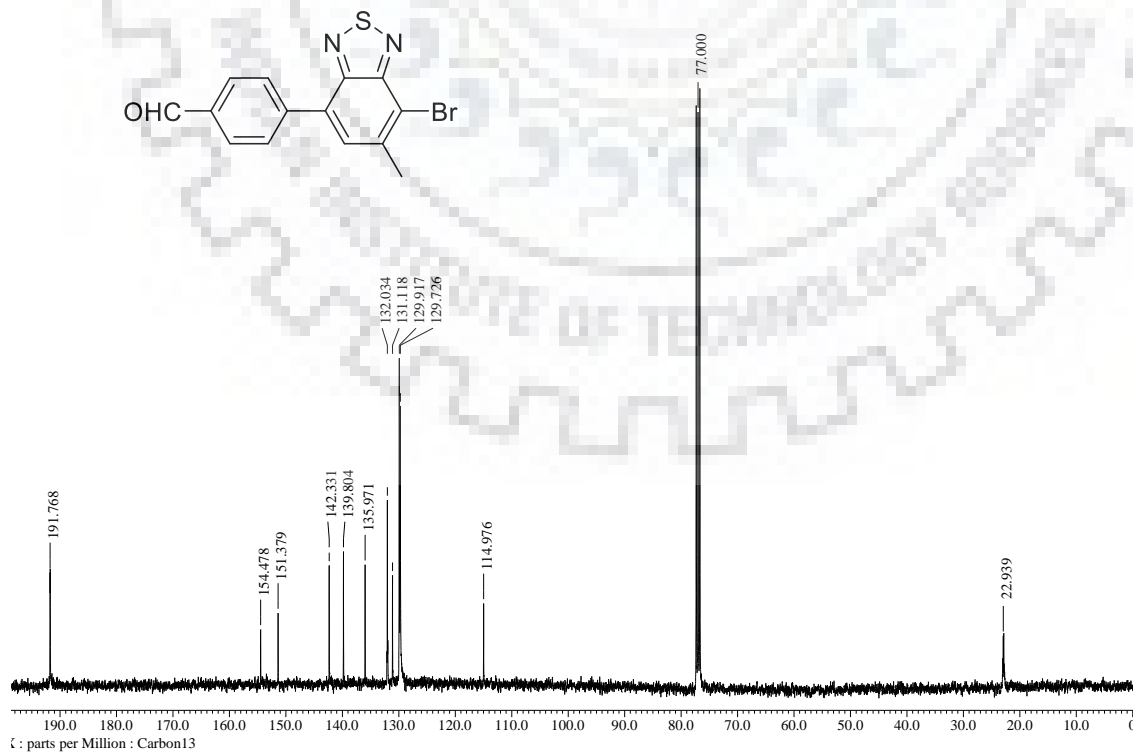
Figure S54. ^{13}C NMR spectrum of 25a recorded in CDCl$_3$
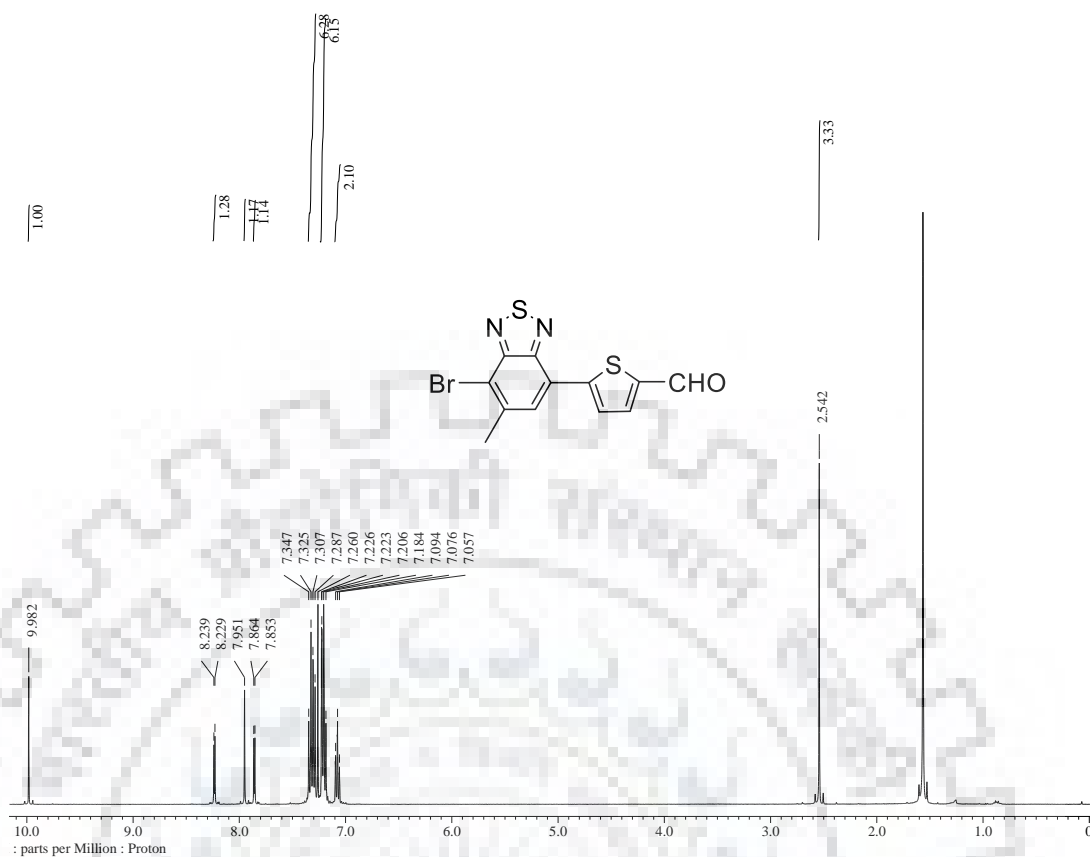
Figure S55. ^{1}H NMR spectrum of **25b** recorded in CDCl$_3$
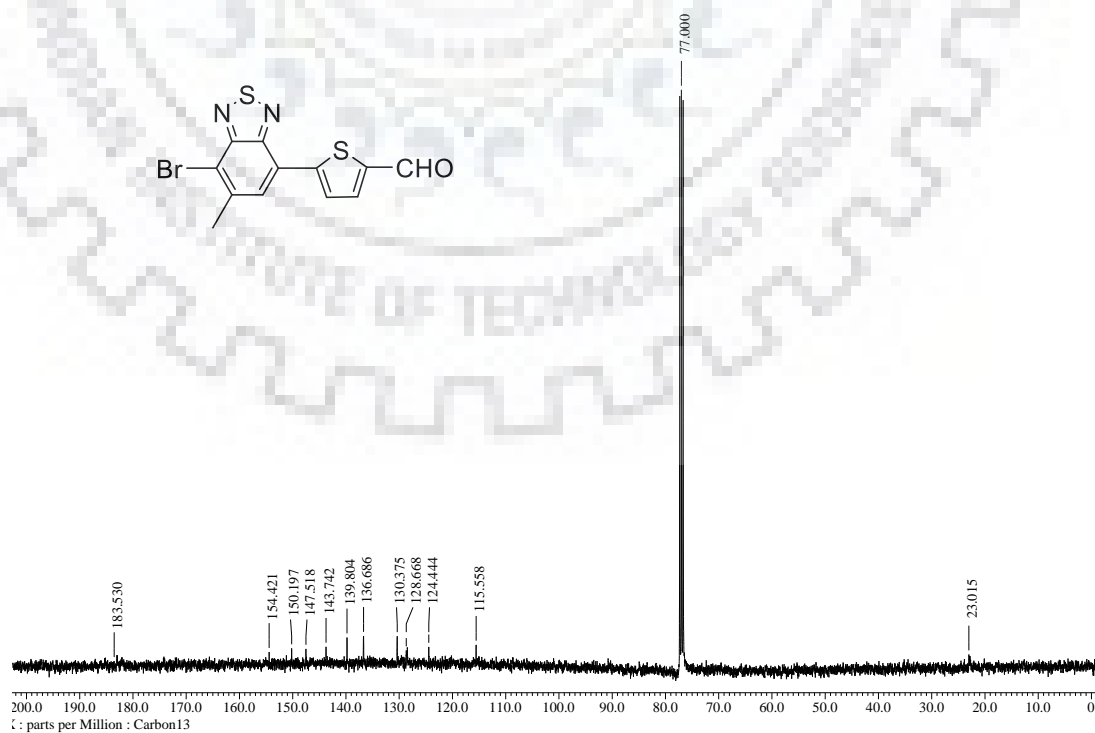
Figure S56. ^{13}C NMR spectrum of **25b** recorded in CDCl$_3$
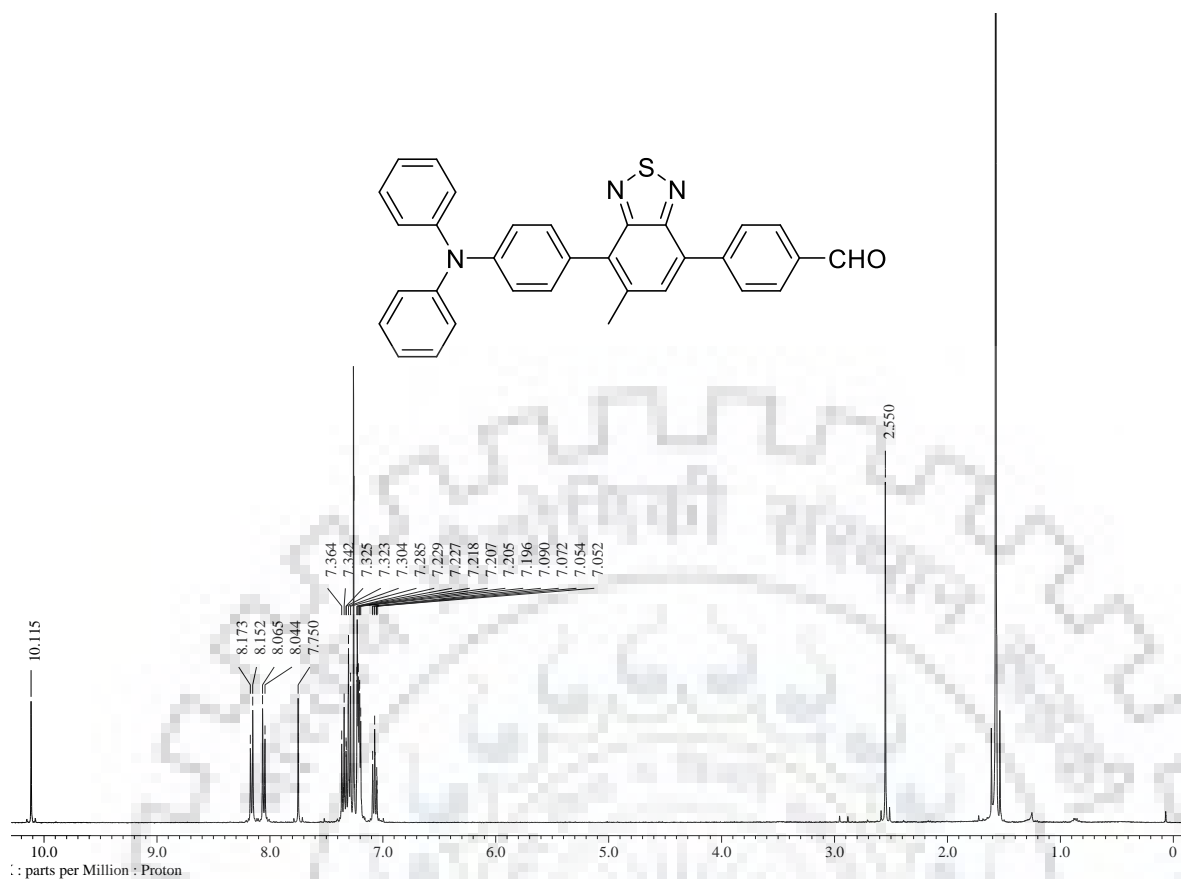
Figure S57. ^{1}H NMR spectrum of **26a** recorded in CDCl$_3$
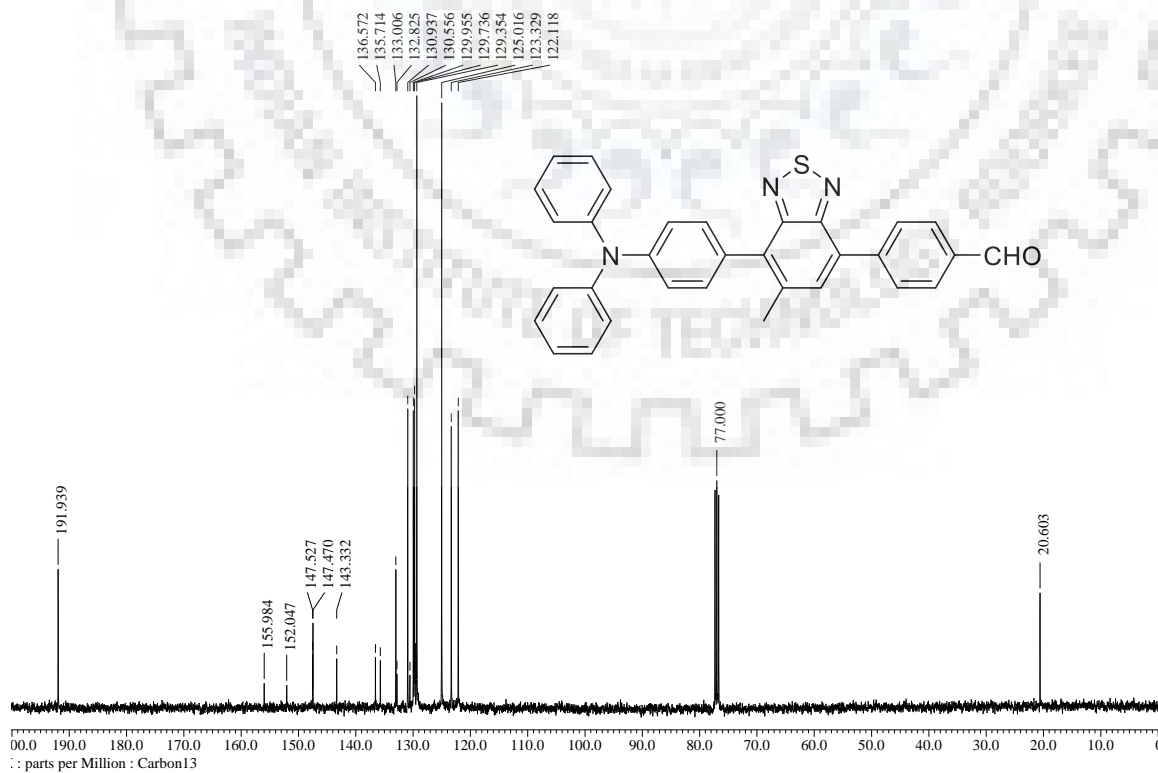
Figure S58. ^{13}C NMR spectrum of **26a** recorded in CDCl$_3$
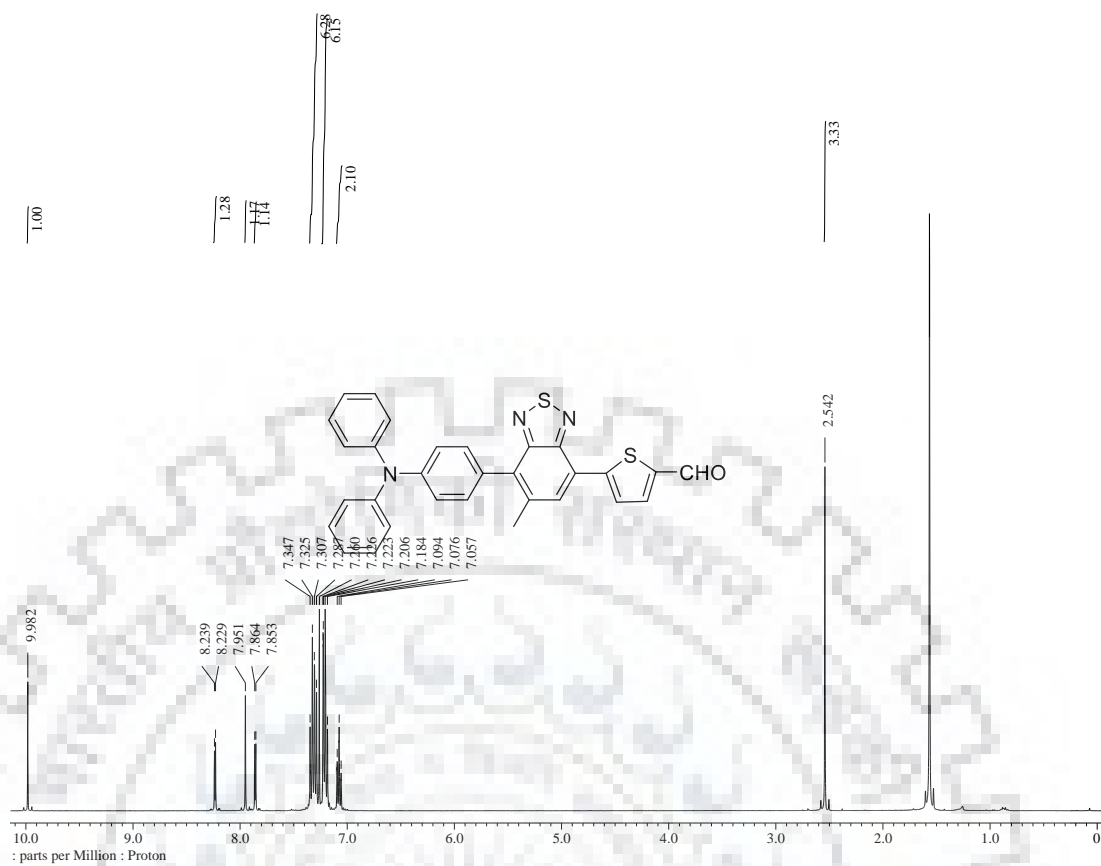
Figure S59. ^{1}H NMR spectrum of **26b** recorded in CDCl$_3$
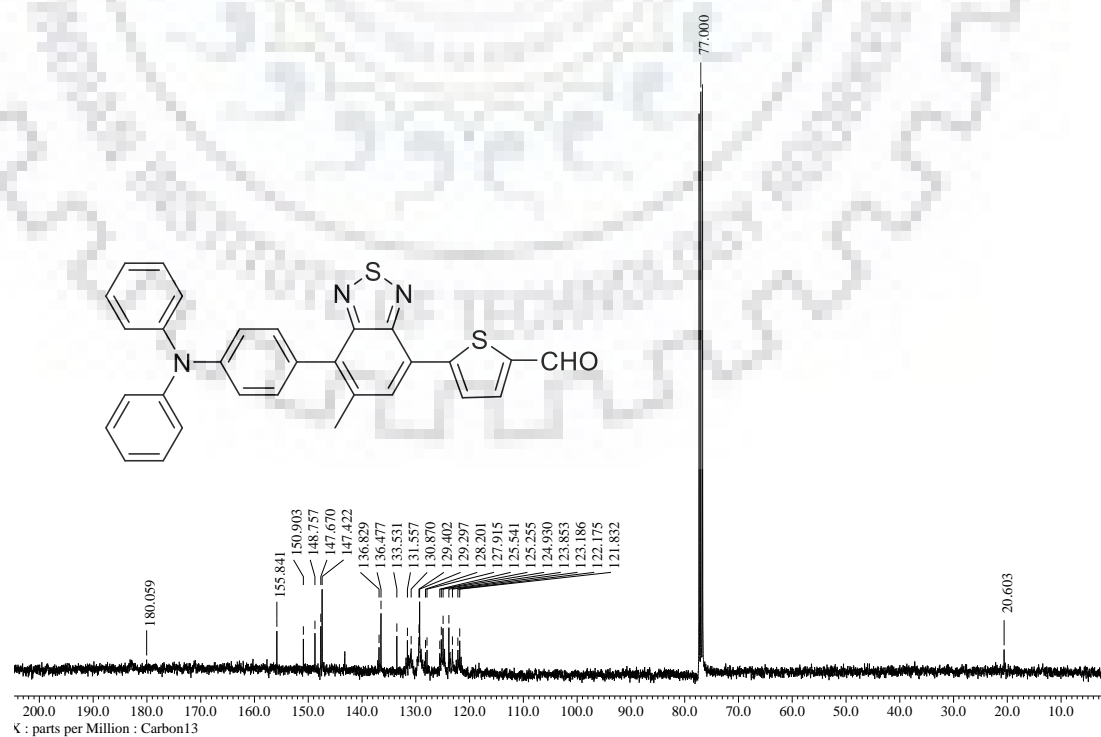
Figure S60. ^{13}C NMR spectrum of **26b** recorded in CDCl$_3$.
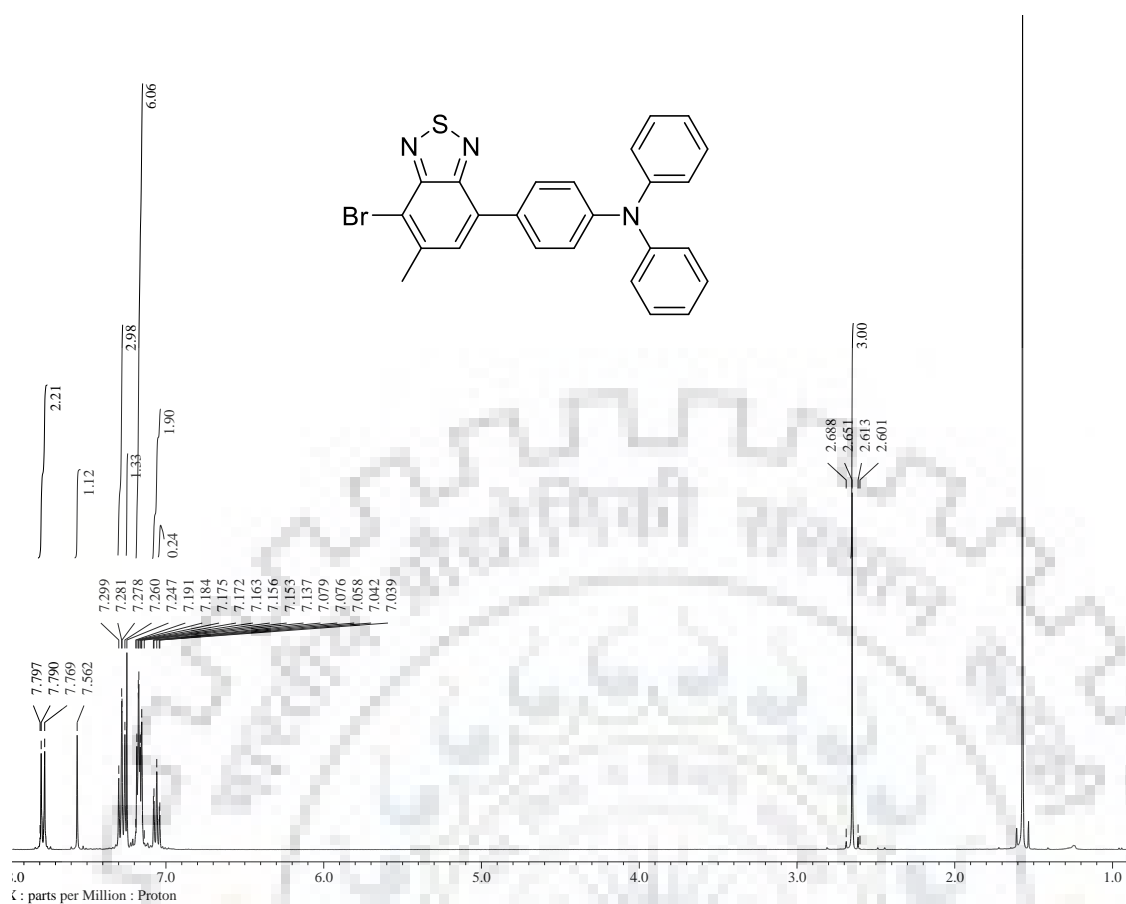
Figure S61. ^{1}H NMR spectrum of **29** recorded in CDCl$_3$
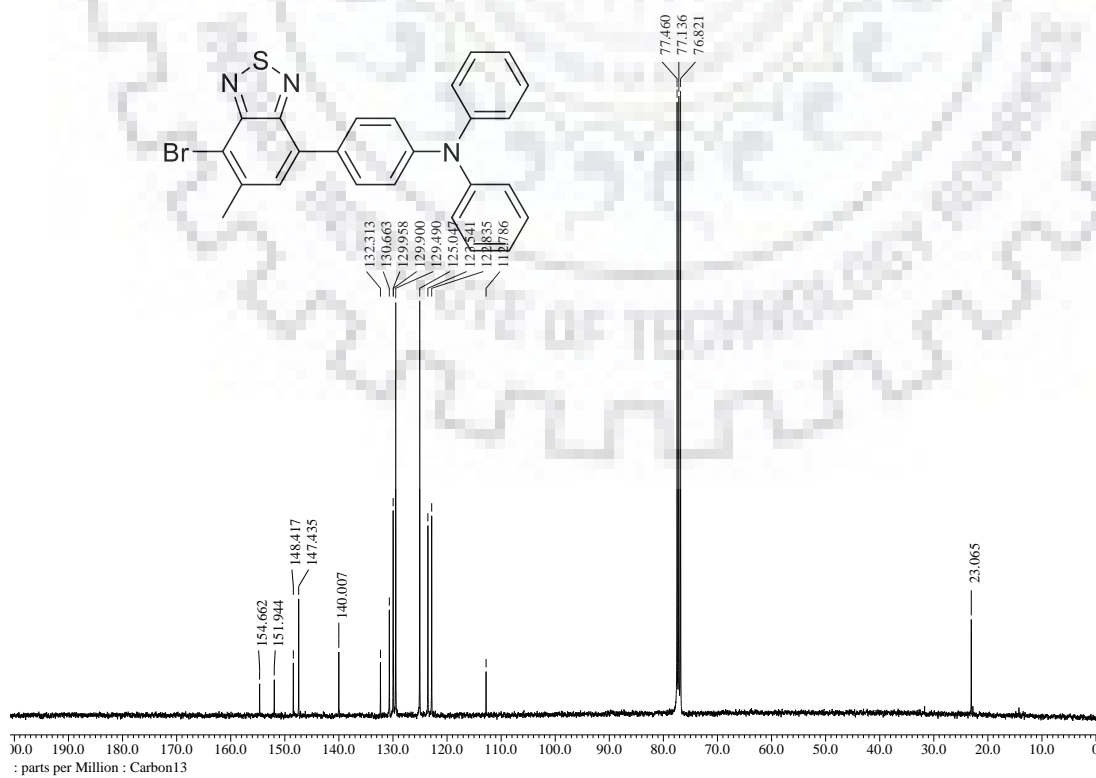
Figure S62. ^{13}C NMR spectrum of **29** recorded in CDCl$_3$.
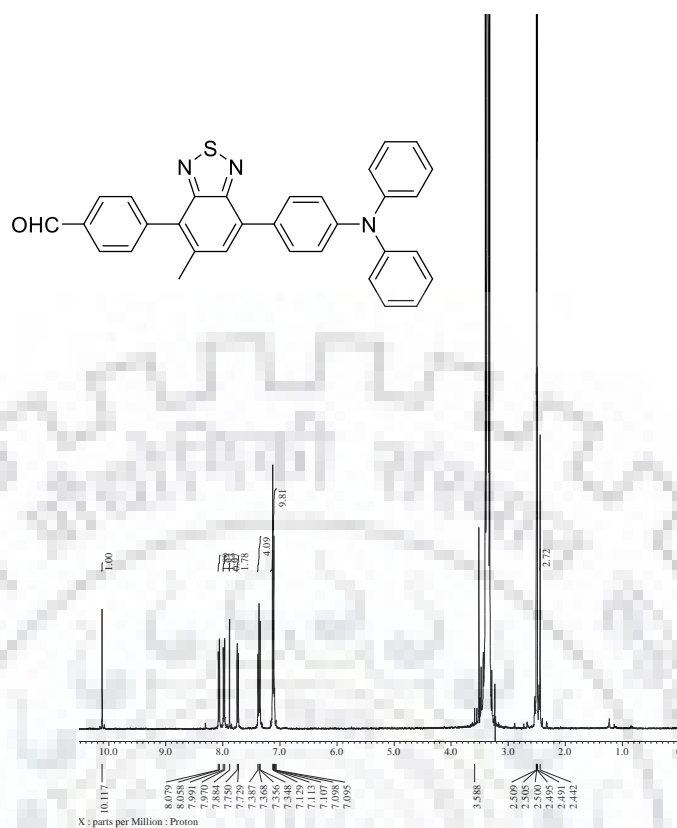
Figure S63. ^{1}H NMR spectrum of **30a** recorded in DMSO-*d*6
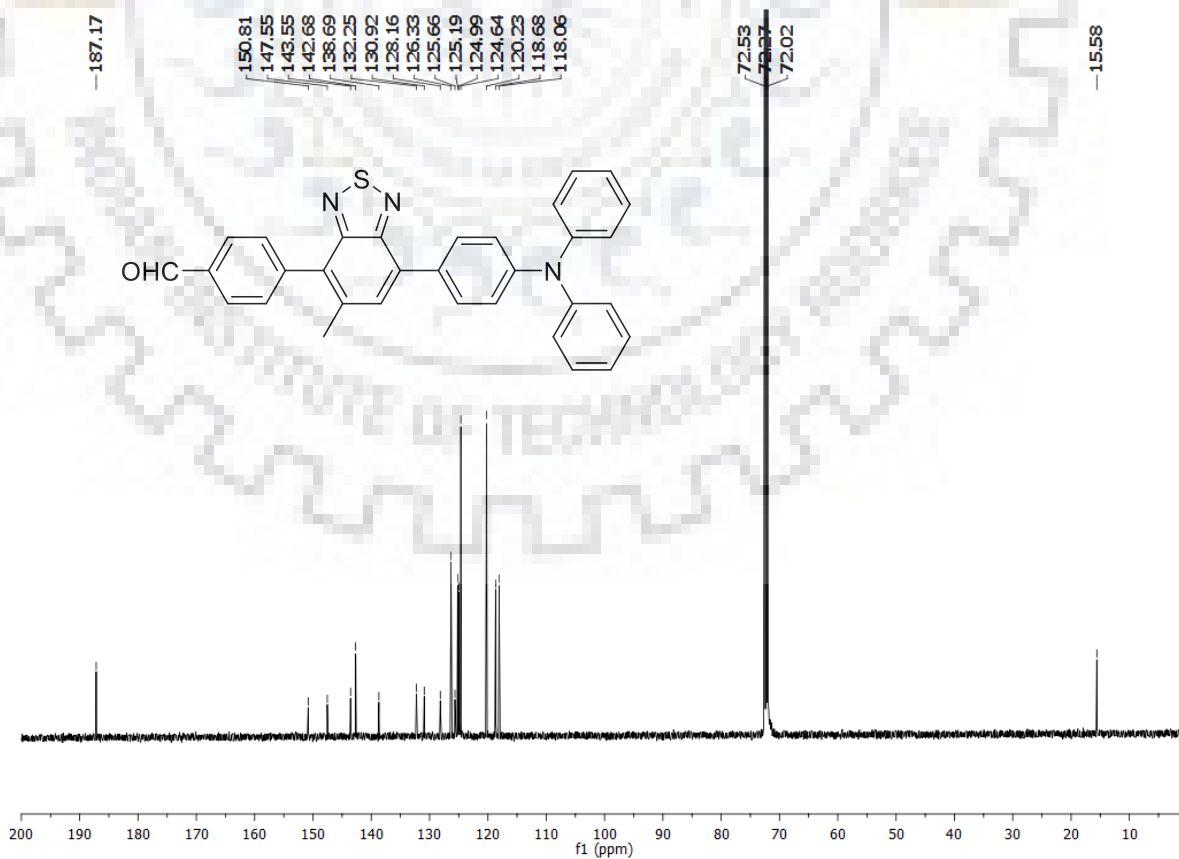
Figure S64. ^{13}C NMR spectrum of **30a** recorded in CDCl$_3$.

Figure S65. ^{1}H NMR spectrum of **30b** recorded in DMSO-*d*6

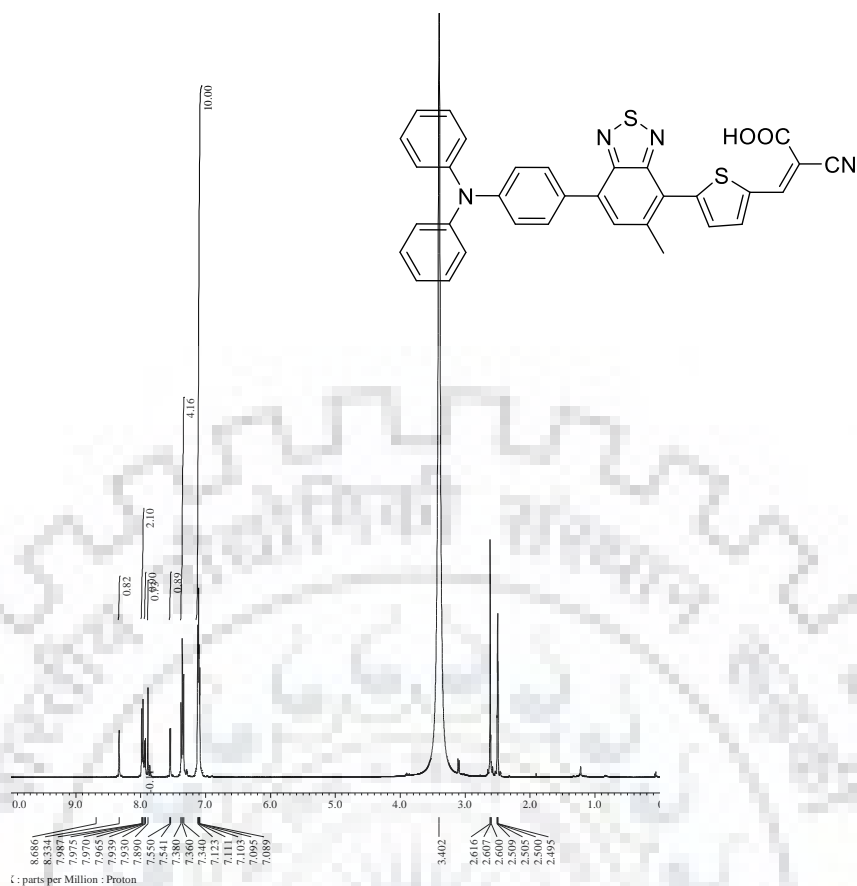**Figure S66.** ^{13}C NMR spectrum of **30b** recorded in CDCl$_3$.
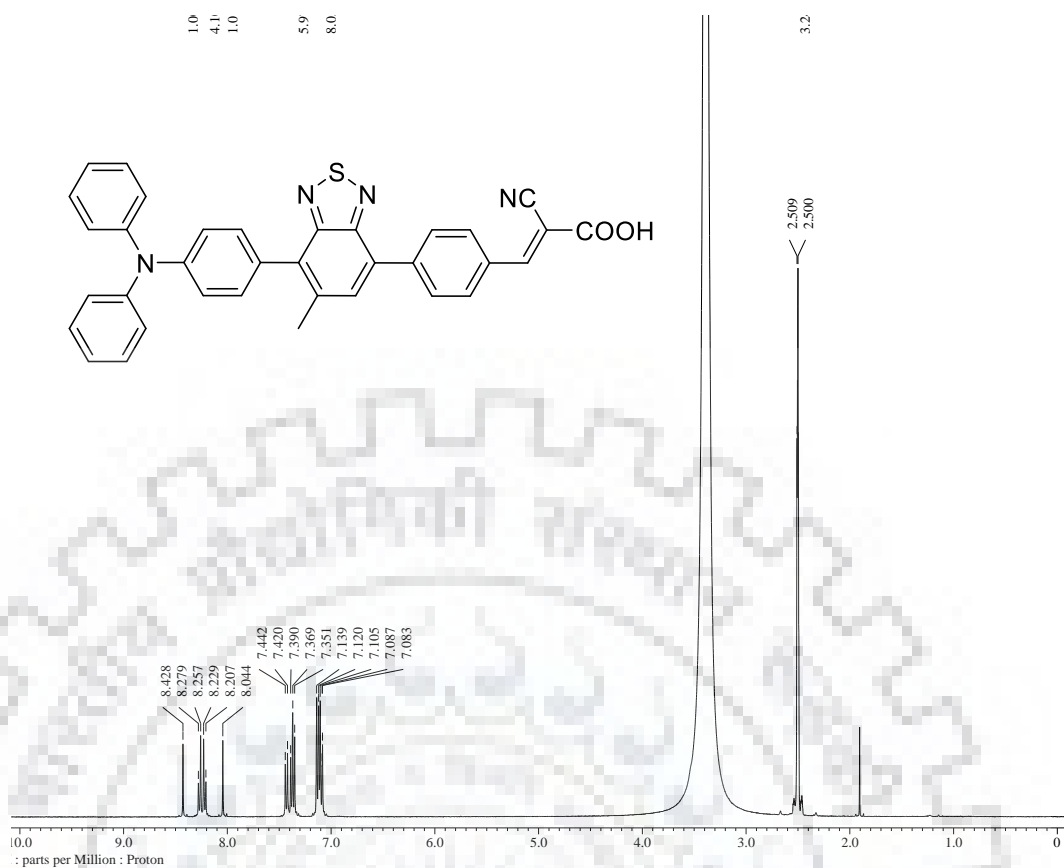
Figure S67. ^{1}H NMR spectrum of **27** recorded in DMSO-*d*6
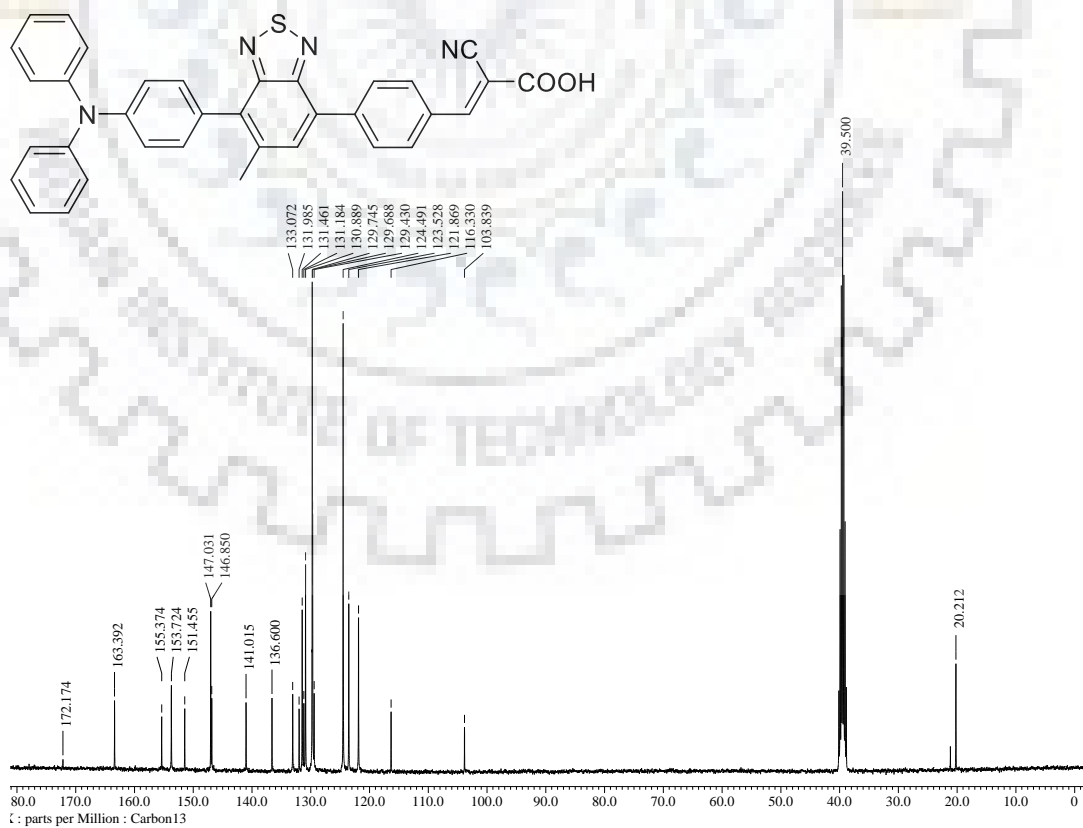
Figure S68. ^{13}C NMR spectrum of **27** recorded in DMSO-*d*6
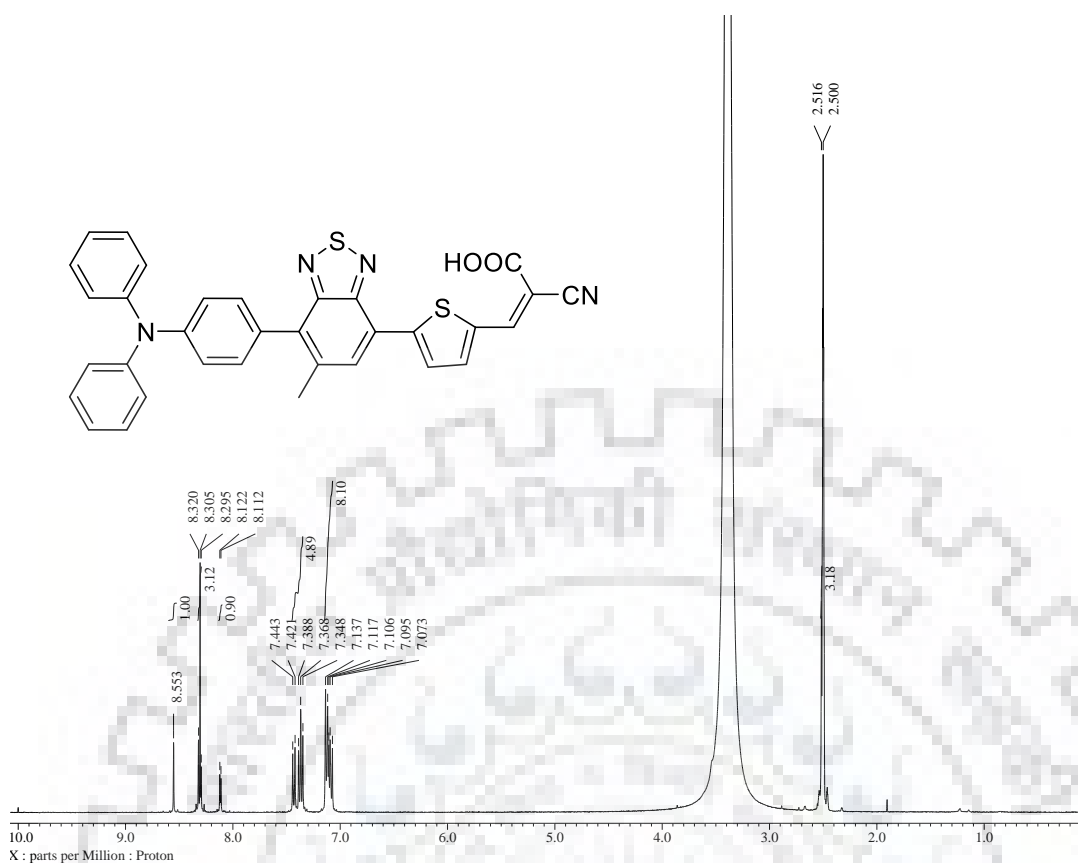
Figure S69. ^{1}H NMR spectrum of **28** recorded in DMSO-*d*6
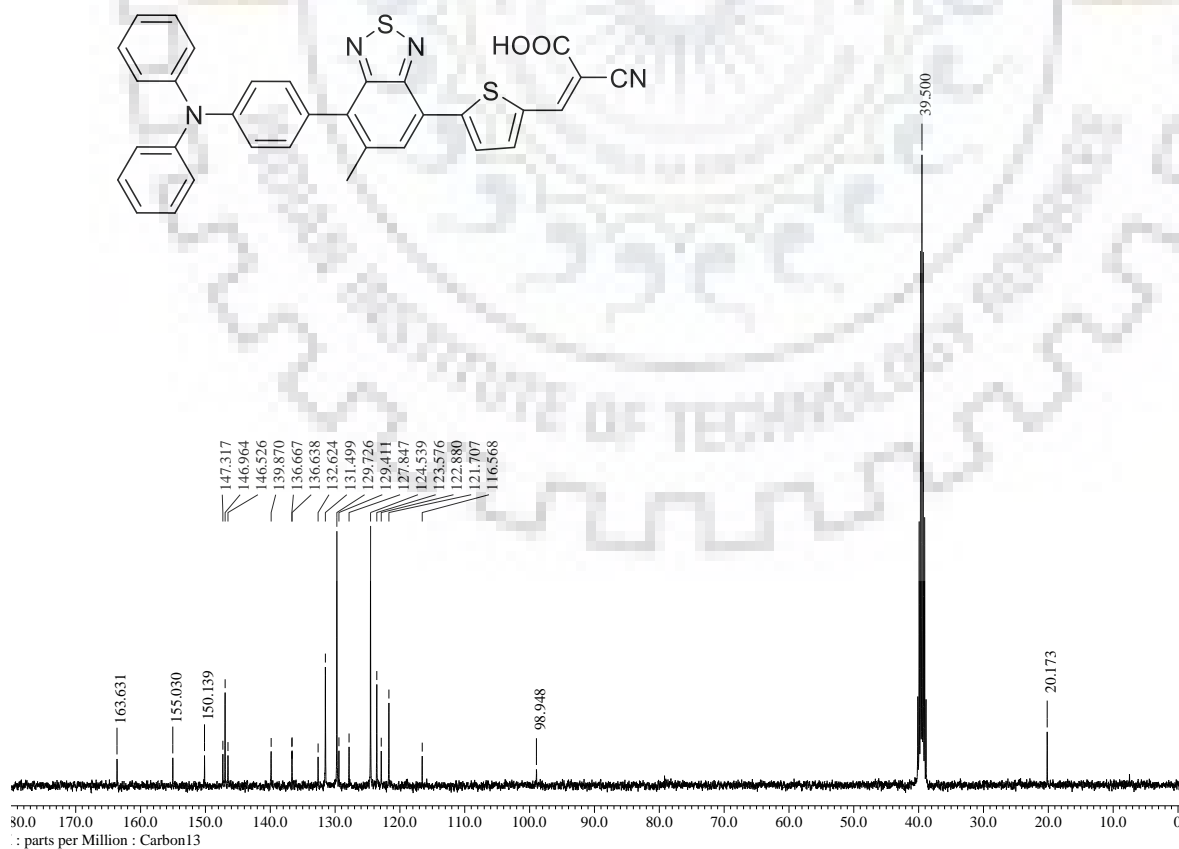
Figure S70. ^{13}C NMR spectrum of **28** recorded in DMSO-*d*6

258
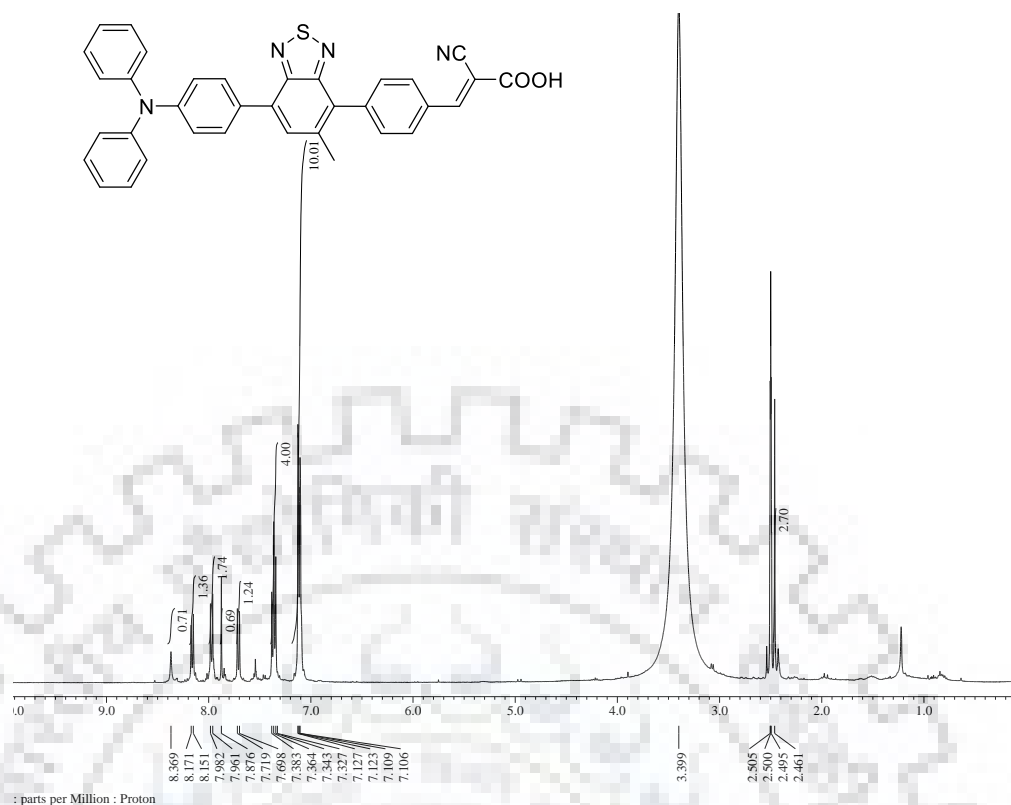
Figure S71. ^{1}H NMR spectrum of **31** recorded in DMSO-*d*6
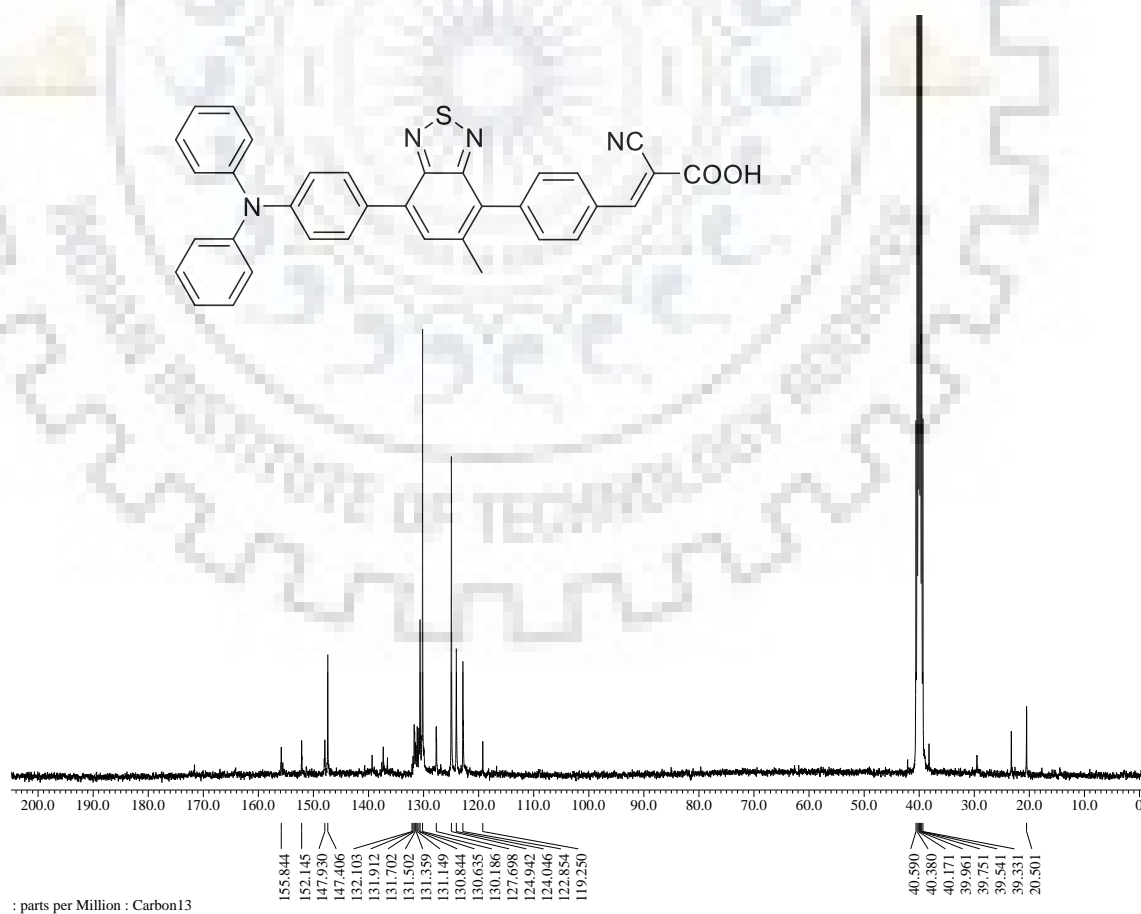
Figure S72. ^{13}C NMR spectrum of **31** recorded in DMSO-*d*6

Figure S73. ^{1}H NMR spectrum of **32** recorded in DMSO-*d*6

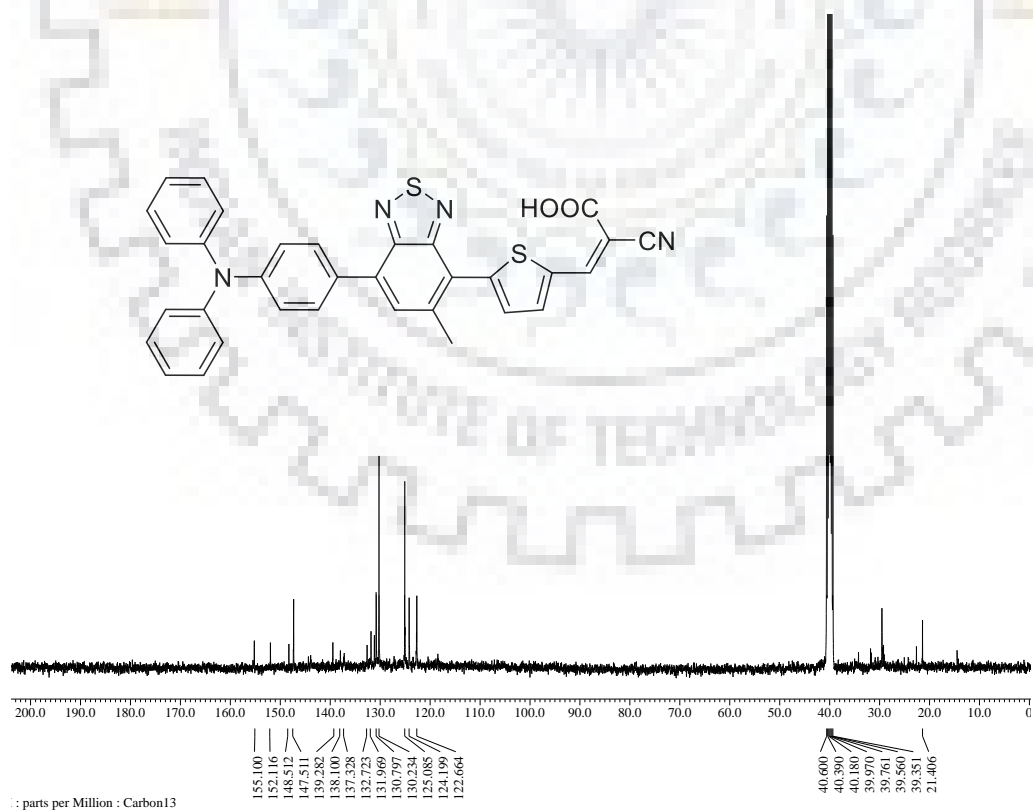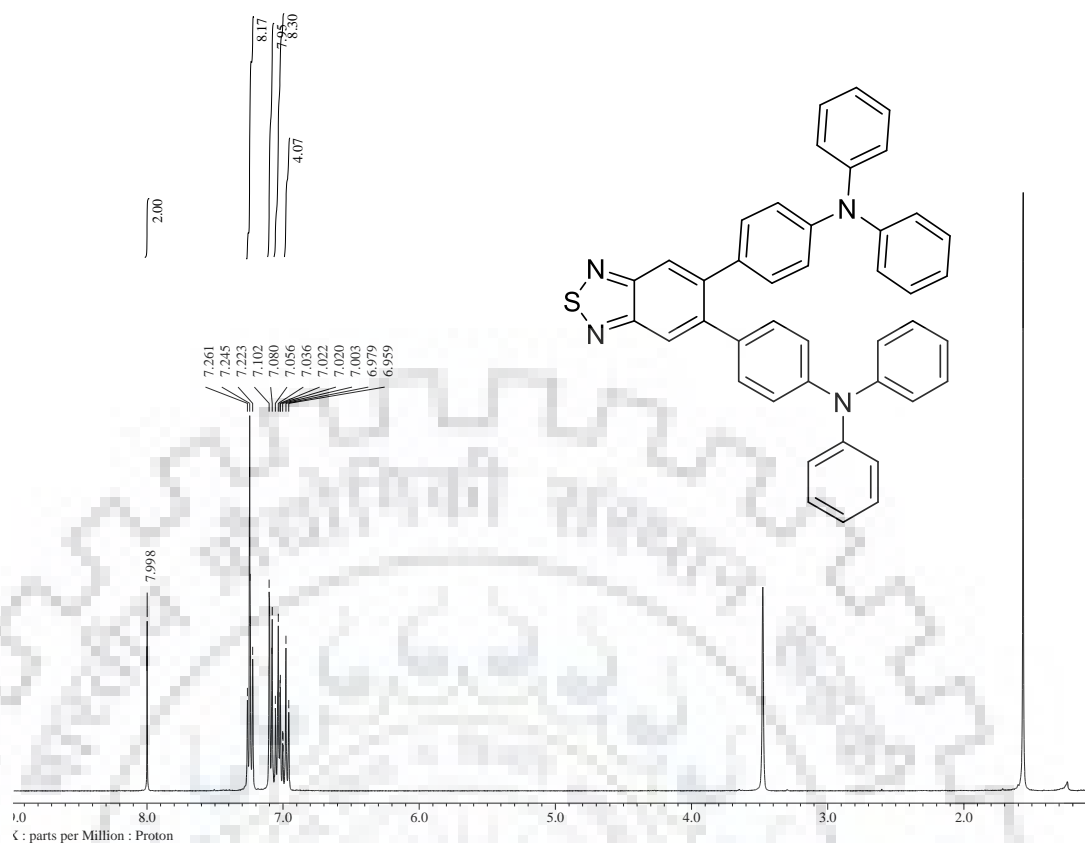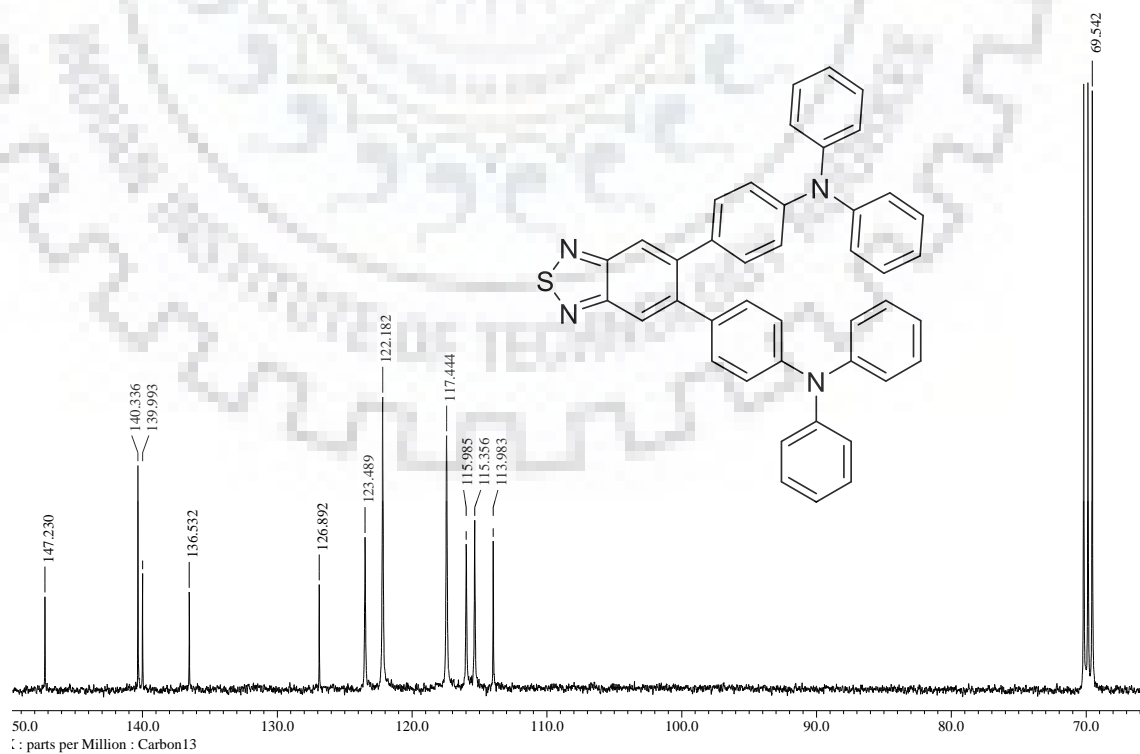**Figure S74.** ^{13}C NMR spectrum of **32** recorded in DMSO-*d*6

Figure S75. ^{1}HNMR spectrum of **33** recorded in CDCl$_3$.

Figure S76. ^{13}C NMR spectrum of **33** recorded in CDCl$_3$.

261

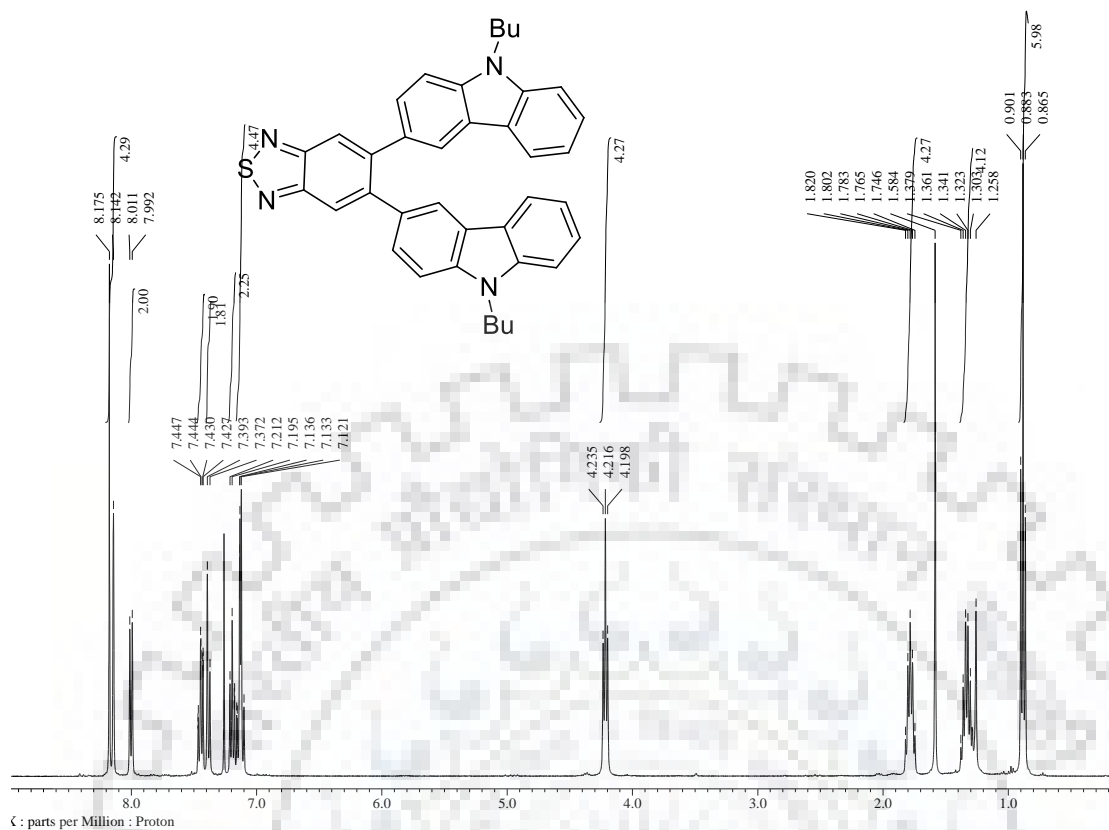**Figure S77.** ^{1}H NMR spectrum of **34** recorded in CDCl$_3$.
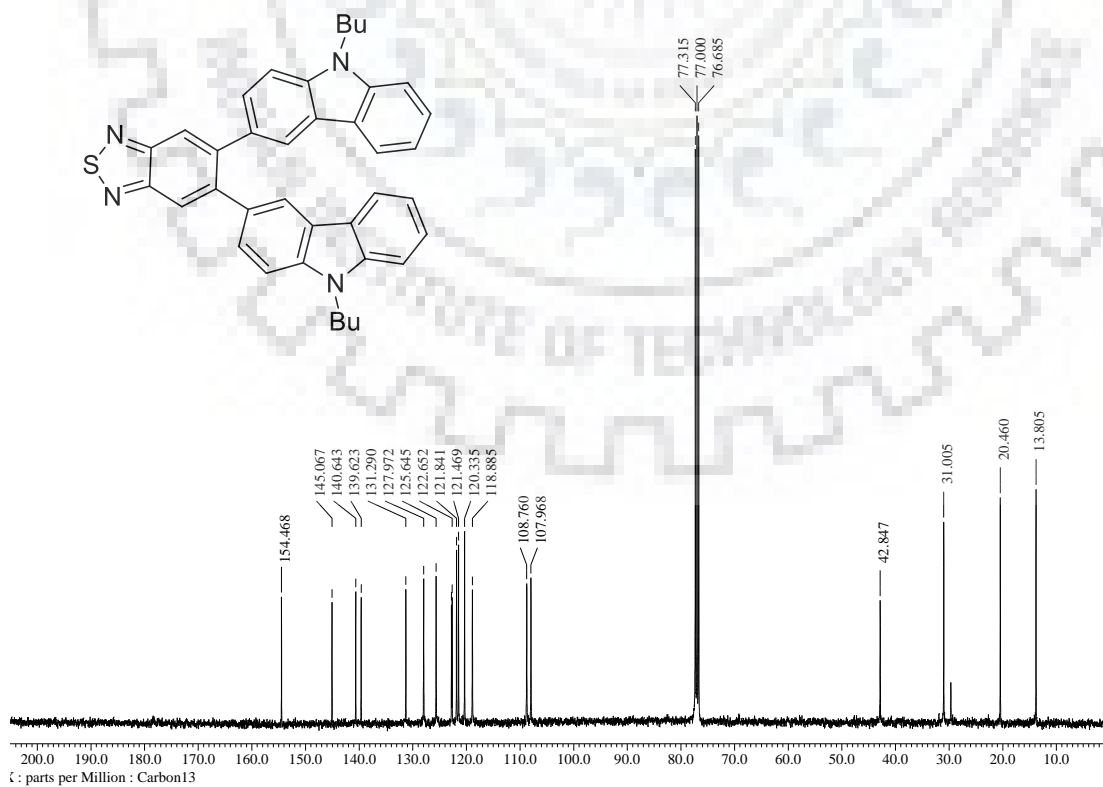
Figure S78. ^{13}C NMR spectrum of **34** recorded in CDCl$_3$.

Figure S79. [^1]H NMR spectrum of **35** recorded in CDCl₃.

Figure S80. [^13]C NMR spectrum of **35** recorded in CDCl₃.

Figure S81. ^{1}H NMR spectrum of **36** recorded in CDCl$_3$.

Figure S82. ^{13}C NMR spectrum of 36 recorded in CDCl$_3$.

Figure S823. ^{1}H NMR spectrum of **37** recorded in CDCl$_3$.

Figure S84. ^{13}C NMR spectrum of **37** recorded in CDCl$_3$.